An investigation towards passive treatment solutions for the oxidation of sulphide and subsequent removal of sulphur from acid mine water

Neehal Mooruth

August 2013

University of Cape Town

Thesis presented for the Degree of DOCTOR OF PHILOSOPHY

In the Department of Chemical Engineering



The copyright of this thesis vests in the author. No quotation from it or information derived from it is to be published without full acknowledgement of the source. The thesis is to be used for private study or non-commercial research purposes only.

Published by the University of Cape Town (UCT) in terms of the non-exclusive license granted to UCT by the author.

University of Cape Town

Abstract

Mine wastewaters are presently generated at working and abandoned mining operations, both within South Africa and internationally. Currently, active treatment systems are being utilised to treat the voluminous quantities of acid rock drainage that are being generated within South Africa, largely as a result of groundwater rebound through abandoned workings. However these technologies are not economically viable for the treatment of smaller discharges from diffuse sources, such as coal spoil heaps, overburden and waste rock dumps, over a long period of time. In addition, they are questionable from a sustainability perspective. The Integrated managed passive (IMPI) treatment system is a semi-passive biological process, which was developed for the treatment of sulphate-laden mine water discharges. The system consists of modular sulphate reduction and sulphide oxidation units. A demonstration-scale plant was constructed at BHP Billiton's Middelburg Colliery, however the sulphide oxidation unit, the linear flow channel reactor (LFCR) did not perform efficiently. This study was conducted to develop a greater understanding of the physical, chemical and biological processes occurring within the reactor.

Data generated during previous studies were critically evaluated and a number of unsubstantiated assumptions and experimental deficiencies were identified. An improved linear flow channel reactor, with multiple sampling ports and feed/effluent ports, was designed. Three LFCRs, made from Perspex to allow observation of sub-surface phenomena, were built and used to conduct hydrodynamic and chemical and biological sulphide oxidation experiments. A linear flow channel reactor was constructed from perspex with multiple sampling ports and inlet/outlet ports to conduct the various chemical and biological sulphide oxidation experiments. Additional batch-reactor studies were conducted to investigate chemical sulphide oxidation. Analytical techniques to quantify polysulphides were developed and optimised and allowed the sulphur balance across the experiments to be closed. Packed bed sulphate reduction columns were utilised to generate the required sulphide feed. The preparation, operation and performance of the columns were investigated in greater detail once it was confirmed that LFCR performance was dependent on consistent feed composition. Additional batch-reactor tests were performed to investigate the hydrolysis of complex organic substrates and how this would impact the performance of a biological sulphate reduction unit.

A hydrodynamic study confirmed that the assumption of plug flow in the LFCR was incorrect. Flow within the reactor was shown to be laminar, with significant vertical stratification. The reactor configuration was changed to prevent influent bypassing the reaction zone. Furthermore, the study showed that the relative density difference between the feed and bulk liquid was critical and affected the hydraulic regime. Therefore, optimal

University of Cape Town

LFCR performance was dependent on a consistent feed from the the upstream biological sulphate reduction reactor.

The abiotic sulphide oxidation study revealed that the primary products of sulphide oxidation were thiosulphate, polysulphides and a small amount of colloidal sulphur, and that pH played a critical role in determining reaction chemistry. The maximum sulphide removal in an abiotic LFCR was 24-32%. The primary products formed in the biologically catalysed system were sulphur and sulphate, which together with the significantly higher conversion, indicated that biological rather than chemical sulphide conversion dominated. The initial biological LFCR experiments revealed carbon substrate limitation, resulting in incomplete or structurally unsound floating sulphur biofilm (FSB) formation and a microbial community dominated by photoautotrophic organisms.

The subsequent LFCR experiments were supplemented with acetate, which improved the overall reactor performance and FSB development. The microbial community showed greater diversity, with a substantial number of heterotrophic species, including sulphur oxidisers, identified. The minimum organic loading was determined to be 0.1 g acetate/L. The sulphide oxidation rate was highest shortly after complete biofilm formation and decreased with time, reaching a minimum after approximately four residence times. This was related to reduced oxygen mass transfer as the biofilm matured and sulphur deposition increased. The optimum residence time was 1-2 days, yielding the greatest sulphur recovery and FSB structural development ideal for sulphur accumulation. At this residence time the FSB should be harvested every 3-4 residence times, which will ensure an average maximum sulphide oxidation rate of 3.0-4.7 mmol/L.day and a sulphur yield within the range of 75-92%. Detailed dissolved oxygen and oxygen mass transfer studies were conducted, confirming that the sulphide oxidation rate was mass transfer controlled. However it was greatly dependent on the porosity of the FSB, rather than the thickness of the biofilm, had a greater impact on the rate. The oxygen mass transfer coefficient ($D_f < 3.940 \times 10^{-10}$ m^2/s) through the FSB was significantly lower, by an order of magnitude, than through attached biofilms due to sulphur accumulation.

The sulphate reduction column studies showed that lignocellulosic substrates were not able to sustain the steady release of organic carbon substrates necessary to support sulphate reduction, even with molasses supplementation. Additional batch studies showed that biological sulphate reduction was only inhibited in the presence of high (1 g/L) concentrations of low molecular weight phenolics, indicating their liberation from lignin biodegradation would not affect sulphate reduction in the packed columns.

The research confirmed that the LFCR is a viable process unit for the remediation of sulphide wastes, provided it is operated within the recommended range with respect to the important process parameters. The composition of the feed to the LFCR is critical and the research suggests that packed bed reactors, loaded with lignocellulosic material, are not able generate feed of a suitable quality over the medium to long term. The potential for recovery of sulphur is good and this may prove a valuable by-product.

University of Cape Town

Publications & Presentations

1. Mooruth, N. and van Hille, R.P. (2011) Characterisation of sulphide oxidation in a passive acid rock drainage (ARD) treatment system. 50th International Conference of Metallurgists 2011 (COM 2011). Montreal, Canada.

2. Mooruth, N (2011) Passive treatment of acid mine drainage via a linear flow channel reactor utilising a floating sulphur biofilm. 11th International Mine Water Association Congress (IMWA 2011), pp. 411-415. Aachen, Germany

3. van Hille, R.P, van Wyk, N., Motleleng, L. and Mooruth, N. (2011) Lessons in passive treatment: Towards efficient operation of a sulphate reduction and sulphide oxidation system. 11th International Mine Water Association Congress (IMWA 2011), pp. 491-495. Aachen, Germany

4. van Hille, R.P. and Mooruth, N (2011) Investigation of sulphide oxidation kinetics and impact of reactor design during passive treatment of mine water. Research Report (WRC) – ISBN: 978-1-4312-0102-0.

5. van Hille, R.P, Mooruth N, Raja S, Heath RA (2012) Towards passive treatment solutions for the oxidation of sulphide and subsequent sulphur removal from acid mine water. Research Report (WRC) - ISBN: 978-1-4312-0249-2

6. Mooruth, N. and van Hille, R.P. (2012). Optimisation of a floating sulphur biofilm reactor in a passive acid mine drainage treatment system. 12th International Mine Water Association Symposium (IMWA 2012), pp 723. Bunbury, Australia

University of Cape Town

Presentations

1. Mooruth, N and van Hille, R.P. (2011) Application of a biofilm to remove sulphide in acid mine drainage (AMD) via a linear flow channel reactor. 2nd Regional conference of the Southern African Young Water Professionals (YWP 2011). Pretoria, South Africa

2. Mooruth, N and van Hille, R.P. (2011) Passive treatment of acid mine drainage via a linear flow channel reactor utilising a floating sulphur biofilm. Mineral Processing Conference 2011. Cape Town, South Africa.

3. Mooruth, N and van Hille, R.P. (2012) An overview of the Integrated Managed Passive treatment system for the treatment of ARD. Mineral Processing Conference 2012. Cape Town, South Africa.

Acknowledgements

I would like to thank God for seeing me through the past three years, such that I have finally arrived at this stage.

As a token of my appreciation, I would like to acknowledge those who not only aided me in the completion of this thesis, but also supported me throughout my years as a postgraduate:

- My most profound graditude goes to my parents, Ashwin & Nadira Mooruth, who continually guided and supported me through the hard and stressful times of not only this thesis, but my undergraduate studies as well. It would not have been possible without you.
- Thanks to my sister for the support over the past four years.
- Dr. Rob van Hille, I am truly grateful for the opportunity you provided me in being able to work on this industrial project. I also deeply appreciate your help, guidance and support in being my supervisor and mentor. I will also not forget the fun and memorable moments in Aachen, Germany.
- Fran, you were always willing to help with regard to lab purchases or equipment, and for that I am indebted to you.
- Thanks to the Water Research Commission & Golder Associates Africa for the generous funding of this project, which enabled me to conduct the various experiments to make this dream come true.
- Thanks to Dr. Jo Burgess, Dr. Ralph Heath, Dr. Sashnee Raja and Ritva Muhlbauer for their assistance and support as industrial collaborators, throughout the duration of this project.
- Thanks to the David & Elaine Potter Foundation for awarding me the prestigious David & Elaine Potter Fellowship for 2012 and 2013. I am extremely grateful for the financial assistance you provided me for my doctoral studies.
- Thanks to UCT post-graduate funding office and CeBER for the partial funding of my conference travels and 2010/2011 academic year respectively.
- Thanks to the National Research Foundation (NRF) for awarding me an NRF Innovation scholarship for my doctoral studies.
- Sincere thanks to Miranda Waldron at the electron microscope unit (UCT), for the numerous hours spent with me analysing my biofilm samples.

University of Cape Town

- Wynand and Theo thanks for your friendship, support and help in the lab, as well as the many hilarious and entertaining times in and outside the lab.
- Fernal, Kyle, Thaabit and Craig thanks for being legendary friends and supportive through the tough times. Moreover, to Kyle & Thaabit for the fun and enjoyable TED sessions.
- Olga and Cindy-Jade thanks for your help and teachings in the lab during my first year.
- Thanks to Nathan van Wyk for his assistance, guidance and teachings in the field of molecular biology.
- Nikita and Katie Mann (aka crazy Katie) thanks for entertaining me in the lab, thus making things seem much more manageable, especially during the final stressful months.
- Finally thanks to my friends Neil, Aliya, Yastil, Yousef, Rashed, Naadia, Linus, Remi, Warren and Howard for your encouragement and understanding.

University of Cape Town

Contents

1 Background **1**

2 Introduction and preliminary studies at GARL **8**

2.1 Background 8

2.2 Reactor design and construction 9

2.2.1 Linear Flow Channel Reactor 9

2.2.2 Degrading Packed Bed Reactor 9

2.2.3 Reactor operation 10

2.2.4 Experimental design 11

2.3 LFCR - Preliminary performance study 12

2.3.1 Run 1 - 33 L/day 12

2.3.2 Run 2 - 66 L/day 12

2.3.3 Run 3 - 132 L/day 12

2.4 Floating sulphur biofilm harvesting study 15

2.4.1 No harvesting 15

2.4.2 FSB inter-harvest period study 18

2.5 Conclusions 21

2.6 Final interpretations & shortcomings of GARL study 22

3 Literature Review **24**

3.1 Industrial effluents 24

3.1.1 Generation of Acid Rock Drainage 24

3.1.1.1 Effects on human health 27

3.1.1.2 Effects on the environment 28

3.1.2 Treatment Technologies 29

3.1.3 Active treatment technologies 30

3.1.3.1 Chemical treatment 30

3.1.3.2 Ion-Exchange 30

University of Cape Town

3.1.3.3 Membrane technology 31
3.1.3.4 Biological Sulphate Reduction 32
3.1.4 Passive Treatment Technologies 35
3.1.4.1 Anoxic Limestone Drains 36
3.1.4.2 Aerobic wetlands 37
3.1.4.3 Anaerobic wetlands 37
3.1.4.4 Open limestone channels 38
3.1.4.5 Sulphate reduction bioreactors (SRBRs) 38
3.1.5 Wheal Jane passive treatment plant 39
3.2 Sulphide Chemistry 40
3.3 Chemical sulphide oxidation 41
3.3.1 Influence of pH 41
3.3.2 Influence of temperature 42
3.4 Biological sulphide oxidation 42
3.4.1 Biological sulphur cycle 42
3.4.2 Ratio of sulphide to oxygen 44
3.4.3 Effect of chemical sulphide oxidation on biological sulphide oxidation 44
3.4.4 Biologically produced sulphur 45
3.5 Polysulphide formation and its impact on sulphide oxidation 45
3.5.1 Redox potential 47
3.6 Biofilms 48
3.6.1 Biofilm structure 49
3.6.1.1 Extracellular polymeric substance 50
3.6.1.2 Floating biofilms - Formation theory 51
3.6.2 Mass transport and mass transfer limitations 53
3.7 Microbial ecology 55
3.7.1 Sulphur oxidising Prokaryotes 55
3.8 Research motivation 57
3.9 Research Strategy 60
3.10 Research hypotheses 61

University of Cape Town

4 Reactor design & Analytical methods development 63

4.1 Introduction . . . 63

4.2 Linear Flow Channel Reactor Design (LFCR) . . . 63

4.3 Polysulphides Assay development . . . 68

4.3.1 Introduction . . . 68

4.3.2 Standard synthesis - K_2S_5 . . . 69

4.3.2.1 Experimental Procedure . . . 69

4.3.3 Standard Synthesis - K_2S_3 . . . 72

4.3.3.1 Experimental Procedure . . . 72

4.3.4 Polysulphide Standards . . . 72

4.4 Conclusion . . . 75

5 Materials & Methods 76

5.1 Experimental Setup . . . 76

5.1.1 Degrading Packed Bed Reactor Column . . . 76

5.1.2 Linear Flow Channel Reactor . . . 77

5.1.2.1 Sampling Layout . . . 77

5.2 Analytical Methods . . . 78

5.2.1 Chemical Oxygen Demand (COD) . . . 78

5.2.1.1 Low concentration range (100 - 1500 mg/L) . . . 78

5.2.1.2 High concentration range (1500 - 10000 mg/L) . . . 78

5.2.1.3 COD - Sulphur . . . 78

5.2.2 pH . . . 78

5.2.3 Redox . . . 79

5.2.4 Phenolics - Assay . . . 79

5.2.4.1 Catechol . . . 79

5.2.4.2 Gallic Acid . . . 79

5.2.5 Hydrogen sulphide assay . . . 79

5.2.6 Sulphate assay . . . 80

5.2.7 Sulphur assay . . . 80

5.2.8 Thiosulphate assay . . . 81

University of Cape Town

5.2.9 Volatile Fatty Acids (VFAs) assay 81
5.2.10 Polysulphides Assay - S_X (x = 2 - 11) 81
5.3 Error analysis 82
5.4 Scanning Electron Microscopy (SEM) 83
5.4.1 Top-view 83
5.4.2 Bottom-view 83
5.4.3 Cross-sectional Biofilm analysis 83
5.5 Floating sulphur biofilm - Elemental analysis 84
5.5.1 Sulphur analysis 84
5.5.2 Carbon and inorganic analysis 84
5.6 Microsensor measurement 85
5.6.1 Dissolved Oxygen 85
5.6.2 Redox 85
5.7 Floating sulphur biofilm harvesting 85
5.8 Molecular Methods 86
5.8.1 Nucleic acid extraction 86
5.8.2 Polymerase chain reaction 86
5.8.3 Agarose gel electrophoresis 87
5.8.4 Denaturing gradient gel electrophoresis 87
5.8.5 DNA gel extraction 88
5.8.6 Ligation 88
5.8.7 Transformation 88
5.8.8 Plasmid extraction 88
5.8.9 Sequencing 89
5.8.10 Quantitative real-time polymerase chain reaction 89

6 Fluid dynamics within the LFCR **90**
6.1 Introduction 90
6.2 Bypass study 90
6.2.1 Test conditions 90
6.2.2 Results and discussion 91

University of Cape Town

6.3 Dye tracer study 92
6.3.1 Experimental method 92
6.3.2 Test conditions 93
6.3.2.1 Phenolphthalein tracer 93
6.3.2.2 Potassium dichromate tracer 93
6.3.2.3 Food colouring tracer 93
6.3.2.4 Sulphide tracer 93
6.4 Results 95
6.4.1 Phenolphthalein Test 95
6.4.1.1 Test 1 95
6.4.1.2 Test 2 95
6.4.1.3 Test 3 95
6.4.1.4 Test 4 99
6.4.2 Potassium Dichromate dye tracer - Test 5 99
6.4.3 Green dye tracer - Test 6 99
6.4.4 Sulphide tracer - Test 7 99
6.5 Discussion 102
6.6 Hydraulic density study 107
6.6.1 Test conditions 107
6.6.2 Results & discussion 107
6.7 Conclusion 113

7 Abiotic sulphide oxidation and Initial biotic studies 115

7.1 Introduction 115
7.2 Abiotic sulphide oxidation - Batch reactor study 116
7.2.1 Experimental 116
7.2.2 Results & discussion 116
7.2.2.1 Experimental run 1 - pH = 11.6 116
7.2.2.2 Experimental run 2 - 11.6 > pH > 6.5 117
7.2.2.3 Experimental run 3 - pH = 7.0 120
7.2.2.4 Rate constant 120

University of Cape Town

7.2.3 Conclusion . . . 121
7.3 Abiotic sulphide oxidation - LFCR study . . . 123
7.3.1 Experimental . . . 123
7.3.2 Results . . . 123
7.3.2.1 Experimental run 4 - Five day R.T. and pH 11.6 . . . 123
7.3.2.2 Experimental run 5 - Two day R.T. - pH = 7.0 . . . 124
7.4 Biological sulphide oxidation - Initial LFCR study . . . 129
7.4.1 Experimental . . . 129
7.4.2 Results and discussion . . . 129
7.4.2.1 Experimental run 6 - Five Day R.T. - No acetate addition 130
7.4.2.2 Experimental run 7 - Five day R.T. - No acetate addition . 131
7.5 Final conclusions . . . 139

8 Biological LFCR experiments 141

8.1 Introduction . . . 141
8.2 Experimental Conditions . . . 142
8.3 Pseudo-steady-state . . . 143
8.3.1 Sulphide depth/length profiling . . . 143
8.4 Results - Sulphur species material balance . . . 146
8.4.1 Sulphide removal efficiency and oxidation rate . . . 149
8.4.2 Effect of pH and colloidal sulphur . . . 152
8.4.2.1 Experimental run 11 - 2 day R.T. - 0.99 g/L acetate loading152
8.4.2.2 Experimental run 12 - 2 day R.T. - 2.26 g/L acetate loading153
8.4.3 Sulphur yield vs. residence time . . . 158
8.4.4 Sulphate production minimisation . . . 161
8.4.5 Reasons for poor LFCR performance . . . 162
8.4.5.1 Floating sulphur biofilm collapse . . . 162
8.4.5.2 Effect of a short residence time - 0.5 day . . . 166
8.4.5.3 Poor harvesting method - Experimental run 16 - (1) - 1.5 day R.T. . . . 169
8.4.5.4 Effect of green sulphur bacteria (GSB) . . . 172

University of Cape Town

8.5 Carbon species material balance . . . 174
8.5.1 Results . . . 174
8.5.2 Discussion . . . 175
8.6 Floating sulphur biofilm analysis . . . 179
8.6.1 Compositional analysis . . . 179
8.6.2 EPS, strand networks and FSB thickness . . . 182
8.6.3 Conduits and pores . . . 187
8.6.4 Spherical and oval-shaped pod macrostructures . . . 189
8.6.5 Discussion . . . 190
8.7 Results - Dissolved oxygen profiling - LFCR experimental runs . . . 196
8.7.1 Introduction . . . 196
8.7.2 Floating sulphur biofilm structural heterogeneity . . . 196
8.7.3 Effect of FSB age . . . 197
8.7.4 The oxygen mass transfer coefficient in the FSB . . . 199
8.7.4.1 Experimental . . . 199
8.7.4.2 Results & discussion . . . 200
8.7.5 Conclusions - Dissolved oxygen profiling . . . 204
8.8 Microbial ecology . . . 204
8.8.1 Introduction . . . 204
8.8.2 Experimental . . . 205
8.8.3 Results - Comparison of microbial populations . . . 207
8.9 Final discussion & conclusions . . . 211

9 Packed bed column studies 215

9.1 Background - Research motivation . . . 215
9.2 Introduction - Biological sulphate reduction . . . 215
9.2.1 Sulphate reduction bioreactor configurations . . . 216
9.3 Effect of pH, redox potential and temperature on BSR process . . . 218
9.4 Direct organic substrates . . . 219
9.5 Indirect organic substrates . . . 220
9.5.1 Characterisation of organic wastes . . . 220

University of Cape Town

9.5.2 Indirect substrate - Hydrolysis 221
9.5.2.1 Organic wastes - Sewage sludge / manure 221
9.5.2.2 Lignocellulosic wastes - Wood chips / grass / leaves 223
9.6 Sulphate reducing prokaryotes 224
9.7 Objectives 227
9.8 Initial BSR column studies 227
9.8.1 Introduction 227
9.8.2 Experimental 228
9.8.3 Preliminary results and discussion 229
9.9 DPBR column study 231
9.9.1 Introduction 231
9.9.2 Experimental setup 231
9.9.2.1 Characterisation of packing materials 231
9.9.2.2 Packing regime 232
9.9.2.3 Inoculation protocol 233
9.9.2.4 Methane inhibition 233
9.9.2.5 Feed stream composition 233
9.9.3 Hydraulic residence time (HRT) 233
9.9.4 Unsteady-state 234
9.9.5 Results & discussion 234
9.9.5.1 Characterisation of packing materials 234
9.9.5.2 Packed bed reactor column performance 235
9.9.5.3 Relationship between pH and sulphur speciation 241
9.9.5.4 Hydrolysis of organic packing to volatile fatty acids 242
9.9.6 Conclusions 245
9.10 VFA release study 247
9.10.1 Experimental Procedure 247
9.10.2 Results & Discussion 248
9.11 Effect of phenolic compounds on sulphate-reducing process 253
9.11.1 Introduction 253

University of Cape Town

9.11.2 Experimental procedure . . . 253
9.11.3 Results and Discussion - Catechol . . . 254
9.11.4 Results and discussion - Gallic acid . . . 254
9.12 Final conclusions . . . 257

10 Conclusions & recommendations 259

A Analytical methods 266
A.1 Polysulphides assay protocol . . . 266
A.1.1 Experimental Apparatus . . . 266
A.2 Hydrogen sulphide assay . . . 267
A.2.1 Reagent preparation . . . 267
A.2.1.1 N,N-dimethyl-p-phenylene diamine dihydrochloride solution 267
A.2.1.2 Ferric chloride solution . . . 267
A.2.2 Hydrogen sulphide standard curve . . . 267
A.3 Sulphate assay . . . 268
A.3.1 Mobile phase preparation . . . 268
A.3.1.1 Sodium Borate-Gluconate stock solution (1L) . . . 268
A.3.1.2 Moblie phase solution (1L) . . . 268
A.3.2 Sulphate standard curve . . . 268
A.4 Sulphur assay standard curve . . . 269
A.5 Thiosulphate assay standard curve . . . 270
A.6 Volatile Fatty acids (VFAs) assay . . . 270
A.6.1 VFAs chromatogram . . . 274
A.7 Error analysis . . . 275
A.8 Molecular methods . . . 276
A.8.1 50X TAE Buffer . . . 276
A.9 Sulphur material balance formula . . . 276

B Microbial community structure study 277

Bibliography 281

University of Cape Town

List of Figures

1.1 Map of Witwatersrand basin goldfields and the approximate quantities of gold in each area (Superior Mining) 3

1.2 Process flow diagram for the three integrated processes for the treatment of acid mine water. The high density sludge (HDS) process, the Rhodes BioSURE Process and the Ancor sewage treatment plant at Grootvlei Gold mine (South Africa). (Adapted from (Neba et al., 2007)) 5

1.3 Original process flow diagram of the Integrated Managed Passive (IMPI) treatment system ((Coetser et al., 2005; Mack et al., 2009)) 6

2.1 Eight Channel laboratory-scale LFCR constructed at GARL 9

2.2 Schematic representation of the LFCR, where 1, 4 and 8 represent channel number. The stars represent the inter-connections between channels causing alternating flow directions. 10

2.3 Arrangement of packing material inside the 250 L DPBR 11

2.4 Experimental data of run 1 at Golder Associates Research Laboratories (GARL) 13

2.5 Images of the floating sulphur biofilms for experimental runs 2 and 3 at GARL 13

2.6 Experimental data of run 2 and 3 at Golder Associates Research Laboratories (GARL) 14

2.7 Observations of the FSB progression over a 21 day period with no harvesting 17

2.8 Profile of influent and effluent sulphide concentrations over the 21 day period the reactor was operated with no active harvesting 18

2.9 Sticky FSB (a) attached to the side of the reactor, (b) hindering elemental sulphur recovery 18

2.10 Profiles of sulphide concentration in the reactor feed (C1 in) and the exit points of the individual channels 19

2.11 LFCR channels during the 24 hour inter-harvest period (a) prior to harvesting and (b) five minutes after harvesting 19

2.12 Profiles of sulphide concentration in the reactor feed (C1 in) and the exit points of the individual channels the 36 hour inter-harvest period. 20

University of Cape Town

2.13 Profiles of sulphide concentration in the reactor feed (C1 in) and the exit points of the individual channels for a 48 hour inter-harvest period 21

3.1 Process flow diagram of SULFATEQ™ treatment process (Paques, 2013) . 34

3.2 Schematic representation of Thiopaq Process ((Benschop et al., 2004)) . . 35

3.3 Flow chart enabling the selection of passive treatment technology flow chart (Adapted from (The International Network for Acid Prevention, 2009)) 36

3.4 The sulphur cycle (Robertson and Kuenen, 1992) 43

3.5 Potential-pH diagram for a sulphur/water system at 298.15K 47

3.6 Occurrence of a floating sulphur biofilm on a high-organic load sulphidic tannery pond in Wellington, South Africa (Molwantwa, 2007) 51

3.7 Simplified schematic diagram of the LFCR with an FSB and air penetrating the FSB (left-hand side). The right-hand side is an expanded view of the air-liquid interface, rotated 90 degrees to the right. Depicted is the bulk gas layer, laminar gas film, FSB layer and bulk liquid layer. Additionally the change in dissolved oxygen concentration gradient across all layers is shown. The diagram is not to scale and neither is the dissolved oxygen concentration profile. 54

3.8 Illustration of the research strategy adopted in this work 62

4.1 Floor plan view of the LFCR unit with the entire length being drawn as three separate sections showing the necessary lengths and spacings of the cylindrical holes for baffle placement 64

4.2 Floor plan view of section 2 of the LFCR unit showing the necessary lengths and spacings of the cylindrical holes for baffle placement 65

4.3 Schematic drawing of the front and rear wall of the LFCR with 3 liquid inlet/outlets (Top inlet = Inlet 1) and a gas inlet/outlet; additionally two cylindrical baffles represented. 66

4.4 Schematic drawing of 15 sampling ports on the sampling side wall of the LFCR 67

4.5 Diagrammatical representation of the polysulphide standard synthesis apparatus 70

4.6 Photograph of the polysulphide standard synthesis apparatus 70

4.7 Polysulphide sample standard curves for chain length 2 & 3, for a 0%, 25%, 50% and 75% dilution. The S2 50% dilution data point was taken as an outlier. 73

University of Cape Town

4.8 Polysulphide sample standard curves for chain length 5-9, for a 0%, 25%, 50% and 75% dilution 74

4.9 Linear trend between polysulphide of chain length (2 - 11) and retention time 75

5.1 Schematic diagram of LFCR front wall with the 15 sampling ports being highlighted & numbered accordingly 77

6.1 Inlet and outlet sulphide concentrations (mM) which were observed during the (LFCR - demonstration-scale plant design) hydraulic regime study . 91

6.2 Contour map of the sulphide concentration (mM) within the LFCR on day 2, illustrating the hydraulic regime within the original LFCR demonstration-scale plant design 92

6.3 Illustration depicting the original LFCR design as per the demonstration-scale plant (a) and the improved LFCR design with the effluent port at the liquid surface (b) 92

6.4 The fluid flow path of hydrochloric acid (0.042 M), pumped in at a volumetric flow rate of 120 L/day. Cylindrical baffles (10 mm) were utilised to induce mixing (test 1). All photographs were taken in cross-sectional view of the reactor. 96

6.5 The fluid flow path of hydrochloric acid (0.40 M), pumped in at a volumetric flow rate of 120 L/day. Cylindrical baffles (10 mm) were utilised to induce mixing (test 2). All photographs were taken in cross-sectional view of the reactor. 97

6.6 The fluid flow path of hydrochloric acid (0.420 M) within the reactor, which was pumped in at a volumetric flow rate of 120 L/day. Cylindrical baffles (30 mm) were utilised to induce mixing (test 3). All photographs were taken in cross-sectional view of the reactor. 98

6.7 Hydrochloric acid path within the reactor with no cylindrical baffles (test 4) 100

6.8 The fluid flow path of $K_2Cr_2O_7$ (ρ = 1.0004 g/cm^3), pumped in at a volumetric flow rate of 120 L/day. Cylindrical baffles (10 mm) were utilised to induce mixing (test 5). The yellow layer volume occupied was 0.00695 m^3. All photographs were taken in cross-sectional view of the reactor. . . 101

6.9 The fluid flow path of green dye (ρ = 0.99991 g/cm^3), pumped in at a volumetric flow rate of 120 L/day, through inlet port 2. Cylindrical baffles (30 mm) were utilised to induce mixing (test 6). All photographs were taken in cross-sectional view of the reactor. 101

University of Cape Town

6.10 Concentration profile of the reactor in the y & z-direction with time. Ports number 1-4 are the top row (1.1 - 4.1), ports number 5-8 (1.2 - 4.2) and 9-12 (1.3 - 4.3) are the second and third rows respectively. 102

6.11 Schematic representation of fluid flow regime in the LFCR with various types of flow being displayed accordingly. The sinking influent (green arrows), entrance dead zone (red arrows), laminar parabolic flow (black arrows) and back corner dead zone (orange, maroon, blue arrows) are displayed. The smaller pink arrows represent the movement of fluid in the y-direction due to diffusion. 103

6.12 Photograph (a) and illustration (b) depicting Couette flow between parallel plates 104

6.13 Schematic diagram of the flow regime within the LFCR. The incoming influent continually sinks to the bottom thus displacing the previous laminar layer (orange plane) upwards. This happens until that particular plane reaches the top and exits (green arrow) out the LFCR. The FSB floats on top of the liquid surface (blue layer) with the headspace above containing air. 106

6.14 Photographs depicting the flow of HCl into the dead-zone (back-corner) of the LFCR 109

6.15 Graph of the relationship between linear fluid velocity and relative density difference. Data point 0.287 mm/s was classified as an outlier and ignored due to back-mixing and the hydraulic regime not being observed. 109

6.16 Photographs of the clear laminar layer and pink layer interface, depicting the effects of transverse dispersion by increased diffusive transport 111

6.17 Photograph depicting the retardation of fluid flow in the LFCR by 30 mm cylindrical baffles. Additionally, the recirculation and significant increase in mixing and dispersion is clearly illustrated by the uneven clear-pink interface. (Test no. 3, HCl (0.42 M)) 112

7.1 Sulphide concentration and pH vs. time for experimental batch-reactor runs 1(a), 2 (b) & 3 (c) 118

7.2 Sulphur species concentration profiles measured during experimental runs 1 (pH = 11.6), 2 (11.6 > pH > 6.5) and 3 (pH = 7) 119

7.3 Plot of linearised sulphide concentrations as a function of time for constant-volume batch reactor runs 1 (a), 2 (b) & 3 (c). Plots show a first-order relationship 122

7.4 Influent an effluent sulphide concentration and pH profile of the LFCR (experimental run 4) 125

University of Cape Town

7.5 Sulphide concentration (mM) contour map of the LFCR on day 1 (experimental run 4). Depth 1 represents the top layer of sample ports and Length 1 the ports closest to the inlet (refer to Figure 5.1) 125

7.6 Sulphide concentration (mM) contour map of the LFCR on day 5 (experimental run 4) 126

7.7 Evidence of colloidal sulphur formation during pH-controlled abiotic experimental run 5 (Day 1) 127

7.8 pH profiles of influent and effluent of LFCR experimental run 5. The feed pH was controlled within the optimal range of pH 7-8.3. The LFCR bulk-liquid pH was not controlled. 127

7.9 Sulphide and thiosulphate inlet and outlet concentrations measured over the duration of LFCR experimental run 5 128

7.10 Dissolved oxygen concentration profile through the liquid surface for experimental run 5 (pH = 7.0) on day 4. 128

7.11 Elemental sulphur formation in the LFCR. Both the floating sulphur biofilm and colloidal sulphur particles are visible. 131

7.12 Influent and effluent concentration profiles for measured sulphur species in experimental run 6 of the LFCR 132

7.13 Contour plot showing the distribution of colloidal sulphur (mM) through the LFCR on day 2 of experimental run 6 133

7.14 Contour plot showing distribution of colloidal sulpur (mM) through the LFCR on day 12 133

7.15 Influent and effluent concentration profiles for measured sulphur species in experimental run 7 of the LFCR 135

7.16 Light microscope image at 100X magnification depicting the planktonic population 136

7.17 Sulphide concentration (mM) contour plot for experimental run 7 on day 10, representing the 'floating' of sulphide. 136

7.18 Sulphur (a) and sulphate (b) concentration (mM) contour plots for experimental run 7 on day 9 137

7.19 Sulphide (a) and sulphate (b) concentration (mM) contour plots for experimental run 7 on day 12 138

8.1 Sulphide concentration contour maps of LFCR experimental runs 7 and 10, depicting the sulphide concentration profiles at unsteady-state and pseudo-steady-state respectively. 145

University of Cape Town

8.2 Sulphide concentration (mM) contour map of the bulk liquid in the LFCR in experimental run 11 (day 10) 145

8.3 Influent and effluent sulphide, colloidal sulphur and sulphate concentrations (mM) throughout the duration of experimental run 11 146

8.4 Representing the daily sulphide oxidation rate in the LFCR. Experimental run 8 and 9 were conducted at a four day residence time and average sulphide loading of 33.56 and 29.69 mmol/day. Annotated with the unsteady-state phase. 150

8.5 Sulphide oxidation rate profiles for experimental runs 10 - 16-(2), except run 15. 151

8.6 Influent and effluent pH profiles for experimental run 11 153

8.7 Contour plot of sulphide concentration (mM) in the LFCR on day 5 (experimental run 11) 154

8.8 Contour plots of concentration distributions in the LFCR on day 12, illustrating the production of polysulphides (Experimental run 12) 156

8.9 Influent and effluent sulphide and colloidal sulphur concentrations (mM) throughout the duration of experimental run 12. The spike of colloidal sulphur on day 12 was due to an inconsistency in the upstream DPBR.. . 157

8.10 Sulphate concentrations (mM) and the associated pH profile of the influent and effluent stream throughout the duration of experimental run 12. . . . 157

8.11 Influent and effluent sulphide, colloidal sulphur and sulphate concentrations (mM) throughout the duration of experimental run 10 159

8.12 Influent and effluent sulphide and colloidal sulphur concentrations (mM) throughout the duration of experimental run 14 160

8.13 Sulphate concentrations (mM) and the associated pH profile of the influent and effluent stream throughout the duration of experimental run 14 . . . 160

8.14 Linear relationship between sulphur recovered in the FSB and residence time. Two points were identified as outliers at a sulphur yield of 225.8 and 122.14 mmol. Data from experimental runs 6 - 16-(2). 161

8.15 Parabolic relationship between sulphate production and residence time. The percentage of sulphate produced does not incorporate the oxidation of influent colloidal sulphur. Data from experimental runs 6 - 16-(2) . . . 162

8.16 Plot of influent and effluent sulphide concentrations and pH over the duration of experimental run 8 163

University of Cape Town

8.17 Plot of influent and effluent sulphate and colloidal sulphur concentrations over the duration of experimental run 8 164

8.18 Partially broken spongy biofilm grown at a flow rate of 6.25 L/day which, is heavily laden with sulphur particles (Experiment 8, Day 8) 164

8.19 Contour plots of sulphide and sulphur concentrations in the LFCR for experimental run 8. Depicting the consequences of FSB collapse. 165

8.20 Influent and effluent sulphide and colloidal sulphur concentrations (mM) throughout the duration of experimental run 15 167

8.21 Sulphate concentrations (mM) and the associated pH profile of the influent and effluent stream throughout the duration of experimental run 15 . . . 167

8.22 Contour plots of sulphur species profiles in the LFCR in experimental run 15 ($\frac{1}{2}$ day R.T.). Illustrating the oxidation of colloidal sulphur due to tearing of the FSB. 168

8.23 Photographs of the FSB (side-view) depicting the tearing of the lower layers due to a high flow rate. (Experimental run 15, 0.5 day R.T.) 169

8.24 Sulphate and colloidal sulphur concentrations (mM) of the influent and effluent stream throughout the duration of experimental run 16, phases 1-3 170

8.25 Photograph of the LFCR showing the pieces of FSB which, fell to the reactor floor during harvesting in phase one (Experimental run 16). . . . 171

8.26 Thin white skin layer representing initial biofilm growth four hours after harvesting the previous FSB (Experimental run 16, day 7) 171

8.27 Photograph of the underside of the FSB and the EPS strand networks which, are attached to the reactor floor, side walls and other parts of the FSB. Green sulphur bacteria are also present on the wall of the reactor as small green colonies. Additionally, the bulk fluid was a green colour due to the presence of GSB (Day 14, experimental run 16, phase two). 173

8.28 Photographs of the top of the FSB of experimental run 16 - phase 3 . . . 174

8.29 Relationship between residence time and acetate utilisation within the LFCR for biological experimental runs. Experimental run 12 and 14 were ignored with regard to the linear plot, due to the higher organic loading rate. 176

8.30 Concentration of acetate used for LFCR experimental runs 11 - 16-(2). The scatter-plot shows that the average consumption rate of acetate in the FSB is a constant. 176

8.32 Acetate concentration contour plot showing no accumulation of acetate in the dead-zones of the LFCR (Experimental run 12, day 5) 177

University of Cape Town

8.31 Daily acetate utilised for biological LFCR experimental runs 11 - 14. . . . 178

8.33 Compositional breakdown of the floating sulphur biofilm from experimental runs 8 - 16-(2). 180

8.34 Scanning electron microscopy images of inorganic matter in the FSB structure 181

8.35 Scanning electron microscopy images of sulphur deposits formed within the FSB matrix. 183

8.36 Photographs and SEM images illustrating the presence of EPS strand networks, anchoring, increasing the surface area and joining layers of the biofilm. 184

8.37 Scanning electron microscopy images of FSB samples (4 and 2 day residence time) in cross-sectional view. Each image is annotated with the measured thickness of the FSB. 185

8.38 Scanning electron microscopy images of FSB samples in cross-sectional view. Each image is annotated with the measured thickness of the FSB. . 186

8.39 Scanning electron microscopy images of FSB samples in cross-sectional view. Each image is annotated with the measured thickness of the FSB. The bright white zones are high concentrations of sulphur. 186

8.40 Relationship between FSB thickness and residence time, with the maximum thickness being reached at a residence time of 1-2 days. The FSB thickness at a 0.5 and 1.5 day R.T. were classified as outliers. 187

8.41 Scanning electron microscopy image depicting a conduit within the the FSB structure (cross-sectional view), with a cell cluster in the centre to possibly receive the incoming nutrients. (Experimental run 10) 188

8.42 Scanning electron microscopy images of the internal and top surface of the FSB from experimental run 13 188

8.43 Scanning electron microscopy image of a pore, showing no sharp broken edges, hence a true structural feature of the FSB. 189

8.44 Scanning electron microscopy image of the top-side of the floating sulphur biofilm (experimental run 12). Illustrating the formation of large spherical pod structures. An enlarged image of the central pod is displayed in the red box in the top left-hand corner. 190

8.45 Scanning electron microscopy images of the FSB in experimental run 11 and 13 depicting the diverse microbial population and cell clusters within the FSB 191

University of Cape Town

8.46 Scanning electron microscopy image of the top-side of the floating sulphur biofilm (experimental run 12). Illustrating the topography of the FSB and a spherical pod in the lower half of the image. In the upper half (red box) the density image of the same position clearly showing the presence of sulphur particles within the central spherical pod as well as other pods which are concealed by the EPS layers. 191

8.47 Day one of FSB growth (0 - 12 hours) is depicted in step 1. Illustration depicting the colloidal sulphur layer that forms in the bulk liquid at the air-liquid interface. Just below this layer is an EPS layer which forms the framework of the biofilm. On the right-side is a photograph of the colloidal sulphur layer. Day two to three of FSB growth (step 2). A thick (yellow/orange) sulphur layer develops on the top surface of the FSB, due to deposition of sulphur. In addition to the sulphur there are other inorganic precipitates such as magnesium and calcium sulphate close to the entrance of the LFCR. These are formed by evaporative crystallisation. The newly formed biofilm (blue) layer contains the sulphur-oxidising consortia, sulphur deposits and metal sulphide precipitates. The underside of the FSB which sits in the bulk liquid (faded orange) layer, is enlarged below. The light blue/purple layer is the structural matrix of the FSB. Attached below it is a newly formed EPS strand network containing sulphide-oxidising bacteria, EPS producers and sulphur deposits produced both chemically and biologically. This will form the new scaffolding for the subsequent biofilm layer. 194

8.48 Photographs and SEM images illustrating the different stages of FSB development from day 1 - 5 for a one day residence time study. 195

8.49 Dissolved oxygen concentration profiles through a FSB grown at an one day and half day residence time. 198

8.50 Dissolved oxygen profiles through the FSB grown at a 1 day residence time and measured on days 1-5. 202

8.51 Calculated diffusional coefficient of oxygen in the FSB for experimental runs 11 - 16-(2). 203

8.53 A 30 to 80% gradient denaturing gradient gel showing separation of various bands for samples 1-8. Similar bands were identified across the samples. . 206

8.54 A 30 to 60% gradient denaturing gradient gel of showing separation of various bands for samples 1-6. Due to the feint nature of the bands they are not all clearly visible in the photograph. 206

8.52 A 30 to 80% gradient denaturing gradient gel showing separation of four bands (A-D) from sample no. 9. 206

University of Cape Town

8.55 Overall Phylogenetic tree relating the rumen fluid and LFCR inoculum sample (9,10) sequences to known species from the National Centre for Biotechnology Information database. 209

8.56 Phylogenetic tree of sample 11 from a non-acetate supplemented LFCR experiment (6). The sequences were compared to known species from the National Centre for Biotechnology Information database. This tree represents an overall picture of the populations present prior to LFCR acetate supplementation and post inoculation. 209

8.57 Overall Phylogenetic tree relating the floating sulphur biofilm sample (1-7, 11) sequences to known species from the National Centre for Biotechnology Information database. This tree includes isolates for the study and represents an overall picture of the populations present during LFCR acetate supplementation. Sample 8 was DPBR 2 effluent liquid. The inoculation samples were not included (9, 10). 210

9.1 Effluent sulphide concentration (mM) of DPBR columns A & B 230

9.2 pH of DPBR columns A & B effluent stream 230

9.3 Layout of organic packing materials with respective masses within DPBR columns 1 & 2, including column dimensions and inlet/outlet configuration 232

9.4 pH data of DPBR columns 1 and 2 effluent 235

9.5 DPBR Column 1 redox & sulphide concentration (mM) data over a period of 359 days 236

9.6 Sulphate removal efficiency for DPBR columns 1 and 2, based on measurement of effluent sulphate concentration. 237

9.7 Effluent sulphate concentrations from DPBR column 1 and 2 237

9.8 DPBR Column 2 redox & sulphide concentration (mM) data over a period of 233 days. 240

9.9 Volatile fatty acids concentrations in DPBR column 1 effluent stream. No VFAs were detected after day 120 (data not shown). 240

9.10 Volatile fatty acids concentrations in DPBR column 2 effluent stream (1 - 137 day). No VFAs were detected in the effluent stream after day 137 (data not shown). 241

9.11 Sulphide concentration (mM) and pH data for DPBR column 1 over a period of 75 days. Depicting the relationship between pH and sulphide concentration. 242

University of Cape Town

9.12 Colloidal sulphur concentration (mM) in effluent samples from DPBR columns 1 & 2, over the period of 241 days (69 - 310 days). 243

9.13 The required theoretical amount of acetic acid for given sulphate reduction in DPBR column 1 244

9.14 The required theoretical amount of acetic acid for given sulphate reduction in DPBR column 2 245

9.15 Chemical oxygen demand concentrations (mg COD/L) of DPBR column 1 & 2 effluent over the period Jan - April 2012. Filtered and unfiltered samples were analysed. 246

9.16 DPBR column 1 effluent COD concentrations (mg/L) over approximately a one month time period (285 - 312 days). 246

9.17 Volatile fatty acids cumulative concentration within bioreactor 1 containing 20 g of wood chips 250

9.18 Volatile fatty acids cumulative concentration within bioreactor 2 containing 20 g of grass 250

9.19 Volatile fatty acids cumulative concentration within bioreactor 3 containing 20 g of dry sewage sludge 251

9.20 Volatile fatty acids cumulative concentration within bioreactor 4 containing 20 g of spent brew malt 251

9.21 pH data of batch bioreactors in VFA liberation kinetics study 252

9.22 Batch bioreactors 1 - 5, with 1 being the control and the rest dosed with catechol at varying concentrations and run for a period of eight days. . . 255

9.23 Batch bioreactors 1 - 5, with 1 being the control and the rest dosed with gallic acid at varying concentrations and run for a period of four days. . . 256

10.1 Simplified process flow diagram of an optimised Integrated managed passive treatment system. The sulphate conversion efficiency of the first unit (SRBR column) is 80%, with the generation of sulphate within the second unit (LFCR). Hence, the overall sulphate conversion efficiency was 79.5%, with a maximum removal of sulphur species from the ARD being 66%. S_c: Colloidal sulphur, S_c-SO_4^{2-}: Colloidal sulphur which was oxidised to sulphate within the LFCR. 265

A.1 High performance liquid chromatography analysis of polysulphide standard, illustrating species of chain length 3-11 and the internal standard at a retention time of 54 minutes. 266

A.2 Hydrogen sulphide standard curve for the concentration range 0 - 1 mg/L 267

University of Cape Town

A.3 Sulphate standard curve for the concentration range 0-10 mM 269

A.4 Sulphur standard curve for the concentration range 0 - 7.516 mM 269

A.5 Thiosulphate standard curve for the concentration range 0-0.1 mM 270

A.6 Lactic acid standard curve for the concentration range 0 - 1000 mg/L . . 271

A.7 Acetic acid standard curve for the concentration range 0 - 1000 mg/L . . 271

A.8 Propionic acid standard curve for the concentration range 0 - 1000 mg/L 272

A.9 Iso-butyric acid standard curve for the concentration range 0 - 1000 mg/L 272

A.10 Butyric acid standard curve for the concentration range 0 - 1000 mg/L. . 273

A.11 Iso-valeric acid standard curve for the concentration range 0 - 1000 mg/L 273

A.12 Valeric acid standard curve for the concentration range 0 - 1000 mg/L . . 274

A.13 High performance liquid chromatography chromatogram of volatile fatty acid compounds 275

A.14 HPLC sulphur concentration standard curve, for a set of standards at the start (1) and end (2) of an analytical run. The error between the two standards is 0.1 %. 275

B.1 A 0.8% agarose gel showing 586bp amplified polymerase chain reaction products of samples 1-4 at three different temperatures 55 (lanes 1-4), 60 (5-8) and 65°C (9-12). 277

University of Cape Town

List of Tables

2.1 Residence time experiments conducted at GARL. The residence time refers to the entire system, not each individual channel. 11

2.2 Summary of results from preliminary LFCR study 14

3.1 Allowable sulphate concentrations in potable water as per domestic water use legislation standards ((USDA, 2004), (WHO, 2004)). 27

3.2 Guidelines for drinking-water quality of various chemicals (WHO, 2003). 28

3.3 Toxicological data of hydrogen sulphide gas for humans and the associated durations of maximum exposure and respective symptoms 33

3.4 Summary of various sulphur oxidising prokaryotes, both photoautotrophs and chemolithotrophs. (Dworkin et al., 2006a; Imhoff, 2004; Lens et al., 2000) 56

3.5 Performance of different biological sulphide oxidising systems reported in literature 59

4.1 Retention time of each methylated polysulphide species from n = 2 - 11 . 74

5.1 Synthetic AMD feed based on Landau colliery effluent after neutralisation with lime. Feed pH was adjusted to pH 6.1 - 6.5. 76

5.2 High performance liquid chromatography elution protocol for the polysulphides assay 82

5.3 Touch-down programme used for PCR amplification (40 cycles) 87

6.1 Tables of experimental parameters used in the hydrodynamic study to improve mixing within the LFCR. 94

6.2 Results of hydrodynamic experiment tests no. 1 -4. Average velocities, respective reynolds numbers and clear layer volumes are presented. 95

6.3 Hydraulic density study results showing the relative density difference and influent fluid velocities, Reynolds numbers (Re) and Peclet numbers (Pe), as well as the respective measured residence times. 108

7.1 Results of sulphide oxidation and sulphur species formed within the constant-volume batch reactor study at various pH values 116

University of Cape Town

7.2 Summary of operating conditions in the abiotic sulphide oxidation LFCR study. The pH in the LFCRs was not controlled, however the feed pH was maintained in the optimum range for run 5. 123

7.3 Sulphur species balance of abiotic sulphide oxidation LFCR experiments 4 - 5 123

7.4 Experimental parameters for initial LFCR biological sulphide oxidation study (experimental run 6, 7). 129

7.5 Sulphur species balance across initial biological experimental runs 6 & 7. Biofilm sulphur refers to sulphur in the floating biofilm. 129

8.1 Summary of experimental conditions throughout all biological LFCR experimental runs 8 -16 144

8.2 Sulphur species balance across experimental runs 8 - 16. Solids refers to sulphur recovered from collapsed biofilm, while biofilm refers to sulphur in the floating biofilm. 148

8.3 The measured amount of colloidal sulphur which was consumed over the period of day 2 - 5, the effluent concentration of polysulphides and the equivalent colloidal sulphur (S_x^{2-}-S_8) that reacted with bisulphide ions to form polysulphides (experimental run 11). 153

8.4 Acetate material balance across the LFCR for biological experimental runs 11 - 16-(2) 174

8.5 Elemental compositional analysis of the FSB from experimental runs 8 - 16-(2). The mass of organic carbon (C) and inorganic matter (I) (excluding solid sulphur recovered) is presented. The mass of sulphur recovered is presented as FSB-S*. The compositional break-down of the inorganic fraction is presented as weight percent. The sulphur (%) is due to sulphate salts. Analyses conducted using SEM-EDS. 180

8.6 Exponential functions which were fitted to the dissolved oxygen concentration data for days 1 - 5. Additionally the goodness of fit and the respective functions' derivatives is presented. The calculated diffusion and local mass transfer coefficient of oxygen in the FSB is presented as well. 201

8.7 Extracted DNA concentrations from various sampling points of the LFCR FSB for experimental runs 14, 15, 16-(2) and 16-(3). DPBR 2 effluent and the DPBR inoculum - Rumen fluid was analysed. The LFCR stock culture inoculum from the demonstration-scale plant and LFCR experimental run 6 FSB was analysed as well. 205

University of Cape Town

9.1 Comparison of active and passive sulphate reduction bioreactor systems. 217

9.2 Morphological features of cellulolytic bacteria (Lynd et al., 2002; Roman, 2004) 224

9.3 Morphological and physiological properties of the genera of sulphate reducing bacteria (Adapted from(Dworkin et al., 2006a)) 226

9.4 Void volume and hydraulic residence times of DPBR columns 1 and 2 . . 234

9.5 Chemical oxygen demand of each organic packing material 235

9.6 Summary of DPBR column 1 & 2 study findings, with regard to sulphate removal and VFA liberation 247

9.7 Inoculation and experimental protocol followed in setting up a batch bioreactor 248

9.8 Summary of the results from VFA liberation kinetics study. Total VFA and soluble COD data represent final values at the end of the experiment. 248

9.9 Individual components of the batch bioreactor mixture to determine the effect of a phenolic compound on the BSR process. 254

A.1 Elution times of all seven volatile fatty acid compounds. 274

B.1 Summary of the floating sulphur biofilm samples from experimental runs 14 and 15, identified in the National Centre for Biotechnology Information database. Showing the sample number, clone number, family, genus and the one/two closest species identified and associated percentage similarities to isolate. The percentages given are the percentage homology between the sequence sent in for BLAST and the actual species listed on the NCBI database.. 278

B.2 Summary of the floating sulphur biofilm samples from experimental runs 16-(2) and 16-(3), identified in the National Centre for Biotechnology Information database. Showing the sample number, clone number, family, genus and the one/two most likely species identified and associated percentage similarities to isolate. 279

B.3 Summary of the LFCR stock culture inoculum and experimental run 6 FSB samples, identified in the National Centre for Biotechnology Information database. Showing the sample number, clone number, and the most likely species identified and associated percentage similarities to isolate. 280

University of Cape Town

List of Abbreviations

ALD	Anoxic limestone drain
AMD	Acid mine drainage
ARD	Acid rock drainage
ATP	Adenosine triphosphate
BSR	Biological sulphate reduction
COD	Chemical oxygen demand
CSTR	Continuous stirred tank reactor
D.O.	Dissolved oxygen
DOC	Dissolved organic carbon
DPBR	Degrading packed bed reactor
EBRU	Environmental biotechnology research unit
EPA	Environmental protection agency
EPS	Extracellular polymeric substance
FSB	Floating sulphur biofilm
GAA	Golder Associates Africa
GARL	Golder Associates research laboratories
HPLC	High performance liquid chromatography
KZN	Kwazulu-Natal
LFCR	Linear flow channel reactor
MIW	Mining influenced water
ORP	Oxidation reduction potential
PCR	Polymerase chain reaction
PSS	Pseudo-steady-state
RDD	Relative density difference
RO	Reverse osmosis
RT	Residence time
SCOD	Soluble COD
SEM	Scanning electron microscopy
SSRU	Secondary sulphate reduction reactor
SRBR	Sulphate reduction bioreactor
SRP	Sulphate reducing prokaryotes
UASB	Upflow anartobic sludge blanket
VFA	Volatile fatty acid
WCW	Water care works
XRD	X-ray diffraction

University of Cape Town

Nomenclature

D_f	Diffusion coefficient of oxygen in the floating sulphur biofilm
D_m	Molecular diffusion coefficient of proton (H^+)
F_{depth}	Depth in the FSB over which the change in concentration was measured.
k_f	Local mass transfer coefficient of oxygen in the floating sulphur biofilm
mM	Millimolar (mmol/L)
N_{O_2}	Molar flux of oxygen (mol/m^2.s)
ϕ	Confinement ratio - ratio between the channel width and cylinder diameter
Pe	Peclet number
Re	Reynolds number
$S^{\%}$	Percent (error) difference between measured sulphide converted and the sum of sulphur species products from sulphide oxidation.
τ_C	Transverse diffusion time
τ_D	Advection time
$V_{reactor}$	Reactor volume
$\dot{V}_{S_8}$	Volumetric rate of sulphur production (mmol/L.day)

University of Cape Town

Chapter 1

Background

The world is currently facing a serious challenge, one which is critical for human development and survival; that of ensuring water security. "Water security is the gossamer that links together the web of food, energy, climate, economic growth, and human security challenges, that the world economy faces over the next two decades" (The World Economic Forum Water Initiative, 2011). Therefore, it is crucial that water be regarded as a valuable commodity, rather than a readily available resource that is underpriced, wasted and overused. As the global economy continues to grow so does the demand for water, which is further exacerbated by the inexorable increase in world population. As a result humanity will demand more food, energy and ultimately water resources to meet its needs. Global demand for meat is projected to increase by 50% by 2025, which will also drive a 42% increase in grain demand (The World Economic Forum Water Initiative, 2011). The International Energy Agency (2009) has forecast that the world economy will demand at least 40% more energy by 2030 than is currently being used. Between 1990 and 2000, while the world's population grew by a factor of four, freshwater withdrawals grew by a factor of nine. This implies that withdrawals of water through to 2030 will increase much faster than the global population, as people get wealthier and consumption patterns rise. Recent analysis suggests that the world could face a 40% shortfall between water demand and available freshwater supply by 2030 (McKinsey & Company, 2009). If current trends continue, approximately two thirds of the world's population will be living in areas of high water stress by 2030, whilst one third will have their livelihood seriously affected (The World Economic Forum Water Initiative, 2011).

University of Cape Town

While the management of water resources must be dealt with locally, regional water scarcity has the potential for global impact. In 2010 Russia experienced a heat-wave that led to water shortages and fears of shortages in grain supply. This caused considerable anxiety in the global commodity markets, which led to an increase in food prices around the world. This incident clearly illustrated the need for water security and new management and conservation regimes at local and regional levels. However, certain countries are already facing water scarcity and challenges associated with water security. One such country is South Africa.

Drought is a recurrent feature of the South African climate, with drought spells lasting an average of 3 to 24 months (Rouault & Richard, 2003). The average annual rainfall in South Africa varies from 300 to 500 mm, with approximately 21% of the country receiving less than 200 mm per annum (WeatherSA, 2012). South Africa is the 29th driest country

in the world, with an estimated 1110 m^3 of potable water per person in 2005 (Muller, 2009). An analysis conducted by the Water Resources Group has forecasted that by 2030 the water supply-demand deficit will be 2.7 billion m^3, representing approximately 17% of the country's overall demand (The Water Resources Group 2030, 2012). Therefore, South Africa will have to improve its water conservation strategies and management measures in order to close the 17% gap. Approximately 45% of the water demand will be consumed by agricultural irrigation, with the remainder being industrial, commercial and households. Therefore, a shortfall will have significant impact on the agricultural industry. Approximately 90% of the water supplied will be from surface streams, lakes or dams, whilst the remainder is ground water. However, this analysis has not accounted for South Africa's current and worsening acid mine drainage problem.

Mining influenced water (MIW) is defined as any water whose chemical composition has been affected by mining or mineral processing (Wildeman & Schmiermund, 2006). The term 'acid mine drainage' (AMD) is generally used to describe acidic waters that are generated as a result of water flowing from adits or shafts, which have a mineral acidity due to the oxidation of exposed sulphide minerals (typically pyrite or pyrrhotite) in the presence of oxygen and water (Wildeman & Schmiermund, 2006). Acid rock drainage (ARD) on the other hand is a natural process whereby rock (sulphide bearing material) is weathered and oxidised to form an acidic run off water. This process has been taking place for millions of years and will continue long into the future. The exposure of sulphide bearing material occurs naturally, but the amount has been increased by orders of magnitude through anthropogenic activities, such as mining. Acidic waters generated from waste rock piles, pit walls, overburden and coal spoil heaps are also termed ARD. Additionally, mineral processing waters which have a circumneutral pH (pH $\approx$ 7), alkalinity and soluble anions such as arsenate, selenate and iron/copper cyanide complexes are also termed ARD. As a result acidic mine waters will be referred to as ARD, in order to encapsulate the different ways in which these form and the different chemistry of these MIWs (Downing & Mills, 2012; Wildeman & Schmiermund, 2006; The International Network for Acid Prevention, 2009).

Acid rock drainage is a significant problem associated with the mining and industrial sectors of South Africa. It has been reported in a number of areas within South Africa, including the Witwatersrand gold fields, Mpumalanga and KZN coal fields and the OKiep copper district. The nature and arrangement of the gold deposits in the Witwatersrand has led to the development of large complexes of interconnected mines, which are often referred to as 'basins' (Ramontja et al., 2010). The priority areas are the western (West Rand), central (Johannesburg area) and eastern basins (Springs-Nigel (East Rand) area). Since the beginning of mining in these particular areas, the inflow of underground water into the mines has been a problem. Therefore water was pumped out from the mines in order to access the gold reserves. When individual mines ceased operations, due to resource depletion or economic constraints, pumping ceased allowing the underground workings to

University of Cape Town

flood. As a result, neighbouring mines either became flooded or had to increase their pumping capacity due to the underground interconnections facilitating easy movement of water. Over time more mines closed and the burden of pumping became too great, causing the last mine to stop pumping. On the East and Central Rand pumping ceased in 2008, prior to which approximately 64.5 and 36 ML/day respectively was extracted (Ramontja et al., 2010; Scott, 1995).

Flooding of underground mine shafts has resulted in AMD decanting to the surface at an average rate of 15 - 20 ML/day. The central basin water level has been rising at an average rate of 0.59 m/day and at the end of November 2010 the mine water level was 510 m below the surface. In the eastern basin, pumping at the Grootvlei Mine at a rate of 75 – 105 ML/day, has ensured that the mine water level is kept at an acceptable level (Ramontja et al., 2010). The government's current strategy, is to resume pumping from all three basins and treat the water by high density sludge (HDS) for neutralisation and metal removal. This will ensure there is no decanting of AMD to the surface, but will result in the discharge of partially treated water, heavily laden with sulphate.

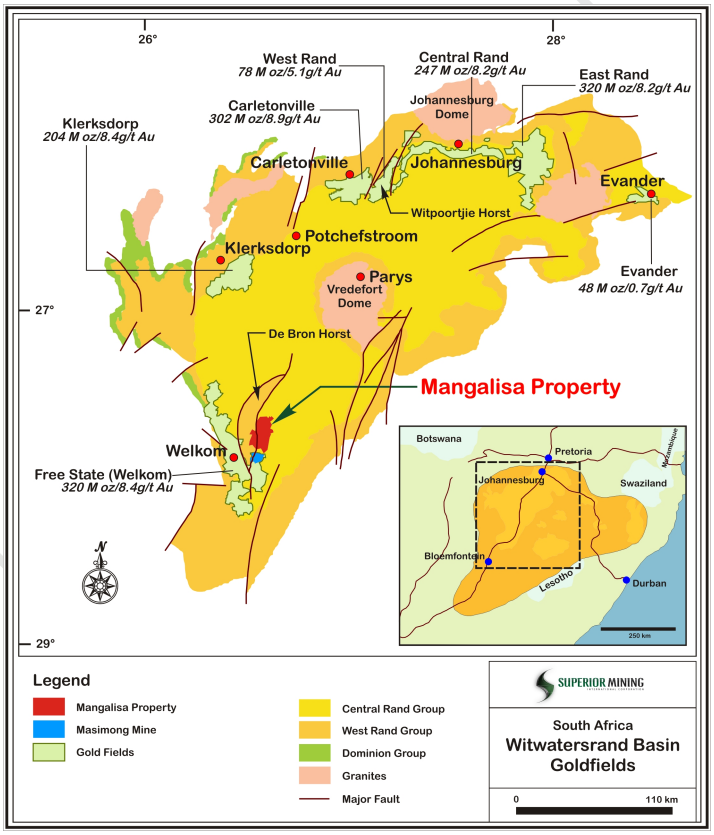


Figure 1.1: Map of Witwatersrand basin goldfields and the approximate quantities of gold in each area (Superior Mining)

The second class of ARD is primarily associated with the coal mining industry, especially within the Witbank coalfield area. Mining operations originally began in 1908 at the Middelburg colliery. The ARD currently being generated is a result of the percolation

of rainwater down to the underground workings, as well as the flooding of (abandoned) underground workings due to groundwater rebound. The second major source of ARD at the mining site is associated with the two spoil heaps (approximately 56 000 and 66 000 m^2 in size). Seepage of water from these heaps has caused significant environmental damage to the surrounding environment and Blesbokspruit water catchment system. The pH of the water has been lowered to below pH 3 and the sulphate (> 2000 mg/L) and metal concentrations increased beyond environmental limits (Bell et al., 2001). This scenario is playing out across the country's coal fields. Therefore, ARD treatment and management measures are required in order to address these crises.

Various treatment technologies have been implemented to deal with the large volumes of AMD currently being generated, the most successful of which is the eMalahleni water reclamation plant. The treatment plant is a joint initiative between BHP Billiton and Anglo Coal. Water is reclaimed essentially by the process of reverse osmosis (RO). The eMalahleni water reclamation plant is able to treat up to 25 000 m^3/day of mine water, with an average sulphate loading of 3000 mg/L and pH of 2.7. The process is based on the high recovery precipitating reverse osmosis (HiPRO), whereby mine water is firstly neutralised by the addition of lime in neutralisation reactors (Hutton et al., 2009). Thereafter the sludge is separated by clarifiers and the processed water is sent to the primary RO plant. RO reject from this plant is subsequently passed down onto secondary and tertiary RO plants. The sludge from each step is sent to a series of clarifiers for dewatering in order to produce a gypsum sludge cake. The plant produces approximately 150 - 200 tons/day of solid gypsum waste and 60 - 100 m^3/day of brine (from the tertiary RO plant). Solid waste (sludge) is disposed of in a landfill site on top of a coal discards facility and the brine is disposed of in a lined pond (Anglo Coal, 2009). The plant is able to achieve 99% water recovery and is able to reduce the sulphate concentration to below 200 mg/L. However, it is a costly process as limestone costs approximately $10 - 15 / ton and the energy consumption is approximately 2.5 kW/m^3. Additionally, the cost of replacing or refurbishing the RO membranes due to scaling or fouling is also a costly process (Anglo Coal, 2009). The life cycle of the plant was predicted to be 20 years with capital and operational expenditures being calculated over this time frame (Gunther & Mey, 2006). Beneficiation of the gypsum that is formed during the dewatering processes is performed, to recover solid gypsum at a grade of 30% and 86% after the primary and secondary RO steps respectively. These by-products are sold at approximately R450 and R4000/ton respectively. The recovered water is also sold back to the local municipality (eMalahleni), but the process is not financially sustainable and has to be subsidised by the mining companies. Such a technology will not address the long-term challenge of ARD. A potentially more sustainable option is the Rhodes BioSURE Process®, developed at Rhodes University, in an effort to treat sulphate-rich mine wastewaters. It used primary sewage sludge as the carbon source and electron donor for biological sulphate reduction (Neba et al., 2007). Over a period of 12 years the Rhodes BioSURE Process® was investigated

University of Cape Town

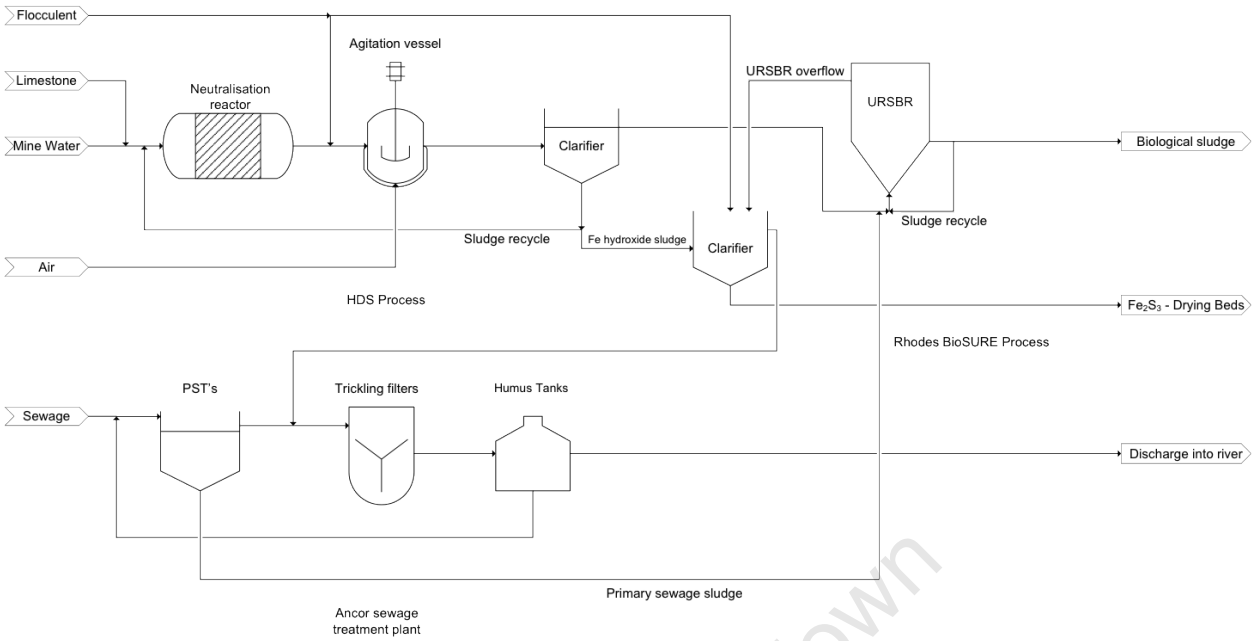


Figure 1.2: Process flow diagram for the three integrated processes for the treatment of acid mine water. The high density sludge (HDS) process, the Rhodes BioSURE Process and the Ancor sewage treatment plant at Grootvlei Gold mine (South Africa). (Adapted from (Neba et al., 2007))

University of Cape Town

and continuously improved. A full-scale plant was constructed in 2005 at the East Rand Water Care company's (ERWAT) Ancor sewage treatment plant. The plant was designed to treat up to 10 000 m^3/day of partially treated water from the Grootvlei Gold mine. The overall process essentially comprised three linked but independent processes (Figure 1.2).

The raw mine water was treated using the high density sludge (HDS) process to neutralise the acidity and precipitate most of the metal load. The partially treated mine water, with an average pH of 7.3 - 7.5, was then pumped to the Ancor works. The sulphate reduction occurred in eight Upflow Recycle Sludge Blanket Reactors (URSBR). The URSBRs were fed primary sewage and humus sludge from the Ancor sewage treatment works. This particular unit was designed to reduce the sulphate concentration to below 250 mg/L, whilst operating at a COD/SO_4^{2-} ratio of 1.15. The sludge from the URSBR was removed from the reactor to prevent accumulation, although some was recycled to promote flocculation and biomass retention. The overflow from the URSBR was mixed with the HDS ferric hydroxide sludge and flocculant to promote iron sulphide precipitation and achieve sulphide removal. Thereafter a clarifier was utilised to remove the sludge which was subsequently sent to drying beds. The clarifier overflow was sent back to Ancor sewage treatment works to remove the residual organic material and ammonia (nitrogen) compounds (Whittington-Jones et al., 2002; Neba et al., 2007; Rose, 2013). The Rhodes BioSURE Process® is a more sustainable and economical solution to AMD treatment, but still requires a large amount of lime and energy in the pre-treatment HDS process. More

significantly, it has to be linked to the existing municipal treatment works, to provide the necessary electron donor. It is therefore, not suitable for remote locations.

While the active processes described above have been used with some success to treat AMD from discrete point sources, there is still a need for systems to address the issue, of persistent lower volume, dispersed discharges associated with operating mines and legacy sites. These need to be low cost and low maintenance. The Integrated Managed Passive (IMPI) treatment process was developed concurrently at the Environmental Biotechnology Research Unit (EBRU) at Rhodes University in conjunction with Pulles, Howard & de Lange Inc. to address such discharges. The treatment system is semi-passive process comprised of essentially four unit operations (Figure 1.3). Biological sulphate reduction and biological sulphide oxidation are carried out to recover solid sulphur and effluent water with a reduced sulphate concentration. The first unit, the degrading packed bed reactor (DPBR) receives the raw mine water. The DPBR consists of a packed bed reactor with multiple layers of selected carbon sources (electron donors) to provide the necessary substrates for biological sulphate reduction (BSR). In addition, liquid molasses is added to provide readily available carbon for the biological processes. The DPBR is typically packed with lignocellulosic materials such as hay, grass, straw and wood chips, with smaller amounts of organic waste materials such as manure, sewage sludge and chicken litter. Therefore, the rapid hydrolysis of the complex organic layers is crucial for the production of volatile fatty acids (VFAs) to sustain BSR. The effluent from the DPBR is then partially oxidised in the primary sulphide oxidising bioreactor (PSOBR) to recover solid sulphur from the dissolved sulphides. The effluent is passed down to a secondary sulphate reducing unit (SSRU) for further biological sulphate reduction and subsequently oxidised in a secondary sulphide oxidising bioreactor (SSOBR) or oxidation cascade. The effluent is sent to a final aerobic wetland to remove any residual sulphide or COD(Coetser et al., 2005).

University of Cape Town

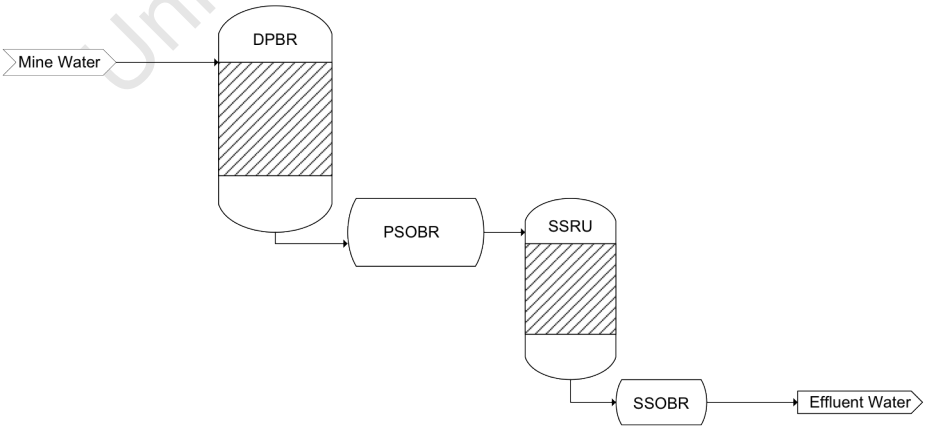


Figure 1.3: Original process flow diagram of the Integrated Managed Passive (IMPI) treatment system ((Coetser et al., 2005; Mack et al., 2009))

The primary sulphide oxidising bioreactor was only selected toward the end of the process

development. The unit consisted of a linear flow channel reactor (LFCR), in which the dissolved sulphides were oxidised via a floating sulphur biofilm (FSB). Initial studies into the the nature of the biofilm and the microbial ecology of the system were conducted at Rhodes University. Molwantwa et al. (2007); Molwantwa (2008) showed that the LFCR had the potential for the treatment of sulphidic wastewaters as part of the passive (IMPI) treatment system. An average sulphide removal of 65% and sulphur recovery of 56% was achieved. Ideally, further investigation and optimisation of the LFCR should have been performed prior to scale-up. However, limited fundamental investigations were performed prior to construction of a demonstration-scale plant at BHP Billiton's Middelburg coal mine (Mpumalanga, South Africa) in 2009. A 200 m^3/day DPBR and 20 m^3/day LFCR was constructed in order to treat mine water on site (Mack et al., 2009). However, the plant's LFCR unit did not meet designed performance levels.

In an attempt to address the shortcomings preliminary work into the fundamental biological and chemical processes occurring within the LFCR was conducted at Golder Associates Research Laboratories (GARL). The results from this study will be discussed in Chapter 2 in conjunction with the motivation for the research presented in this particular thesis.

University of Cape Town

Chapter 2

Introduction and preliminary studies at GARL

2.1 Background

The larger, passive treatment project was a collaboration between Golder Associates Africa (GAA), BHP Billiton, Coaltech and Anglocoal, resulted in the construction of the demonstration plant. However, the Linear Flow Channel Reactor (LFCR) was only designed to treat 10% of the daily flow (20 m^3/day) (Muhlbauer et al., 2010). The fundamental microbiology and reaction chemistry of biological sulphide oxidation is relatively well understood, but the integration of this information with fundamental engineering principles in the context of a treatment system required further work, particularly for the LFCR. In an attempt to achieve this a laboratory scale unit was built at Golder Associates Research Laboratories (GARL). The outcomes from this study provided the initial motivation for the work presented in this thesis and informed the experimental programme. The results are discussed below to provide the necessary context. All experiments were conducted by GARL personnel and not by the author, however, final interpretations are the author's conclusions.

The primary aims of the laboratory studies at GARL were:

1. To develop and refine a single linear flow sulphide oxidation reactor unit, for the optimisation of the pilot scale unit to be built as part of the Middelburg mine passive water treatment demonstration plant.

2. To carry out the optimisation of flow rate for maximum sulphide oxidation and sulphur recovery to inform the operation of the pilot scale reactor on the mine.

3. To refine the harvesting and inter-harvest recovery periods for maximum sulphide removal and sulphur recovery and use the results to make necessary changes to pilot scale operations.

4. To refine the settling and drying of the harvested sulphur for maximum sulphur recovery.

5. To develop operation and design guidelines for the removal of sulphide and sulphur from semi-treated AMD (exiting the upstream DPBR), using this system.

University of Cape Town

In addition to the LFCR a pilot scale degrading packed bed reactor (DPBR) was constructed to provide feed for the LFCR. The following data sets or similar are not readily available, due to the novel and unique nature of the reactors and their arrangement. Hence, the following results will provide context and background to the research the author conducted, which will be presented in the subsequent chapters.

2.2 Reactor design and construction

2.2.1 Linear Flow Channel Reactor

The laboratory-scale reactor was constructed from brick with smooth-plastered internal walls coated in seven coats of waterproofing paint (COPROX™) (Figure 2.1). Initially the intention was to mimic the demonstration-scale reactor, comprising a single long channel separated by baffles. However, due to space constraints at GARL the configuration shown in Figure 2.2, with eight parallel channels was adopted. Each channel was 2.5 m long, with a width of 0.1 m. The internal dimensions of each channel resulted in a liquid surface area of 0.25 m^2, with a maximum liquid depth of 0.1 m. The channels were connected by a slot cut into the bottom of the channel wall at the end of each channel and the effluent drained from the bottom of each channel. The reactor was designed in such a way that a number of operating parameters could be adjusted.



Figure 2.1: Eight Channel laboratory-scale LFCR constructed at GARL

2.2.2 Degrading Packed Bed Reactor

The sulphide-rich feed required by the LFCR was generated in a Degrading packed bed reactor (DPBR) commissioned at the laboratory. A 250 L tank was cleaned and modified

University of Cape Town

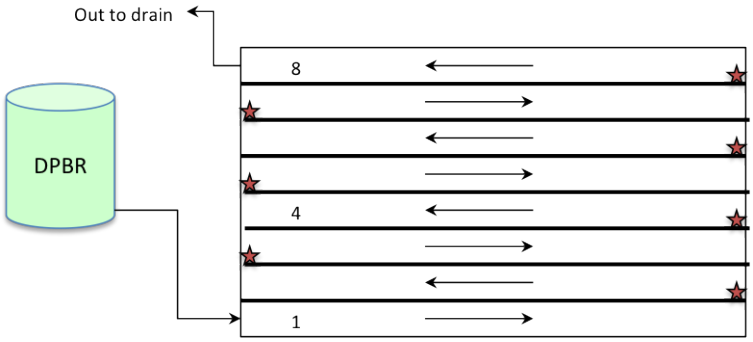


Figure 2.2: Schematic representation of the LFCR, where 1, 4 and 8 represent channel number. The stars represent the inter-connections between channels causing alternating flow directions.

to include inlet/outlet points at the top and bottom. This tank was then packed, as shown in Figure 2.3, with three lignocellulosic carbon sources, each with a different degree of recalcitrance to degradation. These were black wattle (Acacia sp.) wood chips, bluegum (Eucalyptus sp.) wood chips and grass cuttings. In total, approximately 7.5 kg of wattle chips and the equivalent mass of bluegum chips were used. The base of the reactor was filled with inert beads to minimise blockages, as a result of carbon-source compaction, and channeling of the inlet fluid. Once the reactor was packed to the height of the top outlet point, 25 L of primary sewage sludge (ERWAT WCW, Olifantsfontein) was poured over the packing material, followed by 50 L of effluent collected from smaller DPBRs already active in the laboratory. After addition of the sludge and effluent, the DPBR was left to pre-acclimatise for seven days before feeding was started. Upon commencement of the feeding regime, a flow rate of 60 L/day was used which equated to an empty bed retention time of 4.2 days. This flow rate was subsequently decreased for the initial LFCR experiment.

University of Cape Town

2.2.3 Reactor operation

The intention of the DPBR was to provide an adequate and consistent supply of sulphide to the LFCRs. Once a relatively stable effluent sulphide concentration was achieved, the effects of altering the feed flow rate to the LFCR (i.e.. changing the residence time (RT)) could be determined. The liquid volume of each channel was 25 L. The effluent line of the DPBR was then connected to channel 1 to provide feed to the reactor. The outflow of the reactor was at channel 8. The inflow and outflow were sampled on a daily basis for pH, redox potential, sulphide (iodometric method) and sulphate (ion chromatography). During specific experimental runs liquid samples were taken at approximately 10 mm below the surface from individual channels. At the end of each experiment the entire reactor was drained and the biofilm layer recovered and dried for five days in an oven at 50°C. These samples were subsequently sent to the Agricultural Research Council for total sulphur analysis. The solid layer consisted of a combination of various sulphur compounds,

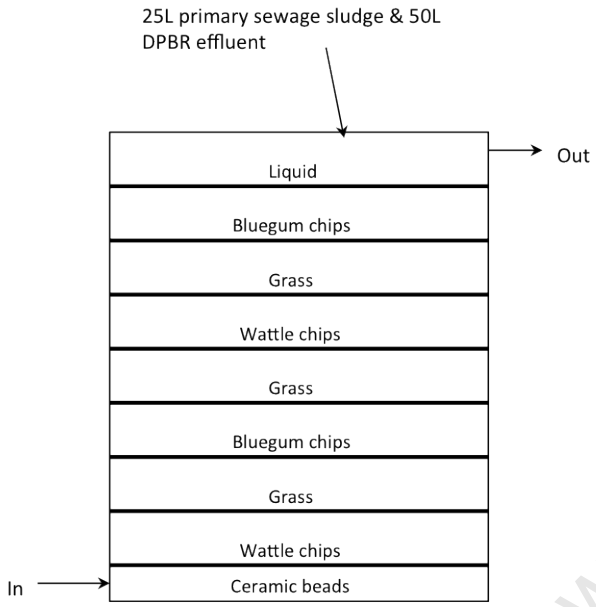


Figure 2.3: Arrangement of packing material inside the 250 L DPBR

including elemental sulphur and precipitated sulphides. The analytical methods required to determine the intermediate sulphur compounds were not available so only total sulphur analysis was carried out. The methods for intermediate sulphur species analysis were developed at UCT and are described in Chapter 4.

2.2.4 Experimental design

The experiments were conducted at three different feed rates in order to investigate the effect of residence time (Table 2.1).

Table 2.1: Residence time experiments conducted at GARL. The residence time refers to the entire system, not each individual channel.

Run No.	Flow rate (L/day)	Residence time (days)	Run time (days)	No. of channels used
1	33	6	13	8
2	66	1.5	7	4
3	132	1.5	9	8

University of Cape Town

2.3 LFCR - Preliminary performance study

2.3.1 Run 1 - 33 L/day

The first experiment was run over a 13 day period. The hydraulic retention time was 6 days with an average inflow sulphide concentration of 6.97 mM (230 mg/L), while the average outflow sulphide concentration was 0 mM (Figure 2.4). This suggested a 100% sulphide removal (Table 2.2). Furthermore, it was noted that the sulphide concentration had been reduced to 0 mM by channel 4, implying that complete sulphide removal occurred in the first four channels of the LFCRs. The presence of elemental sulphur was determined visually for all experiments Figure 2.5 as a solid layer floating on the surface of the channels. These results were consistent with the observation made by Molwantwa (2007) who described a white floating layer on the surface of a LFCR treating sulphide containing water. The presence of elemental sulphur in the floating layer was confirmed using HPLC analysis.

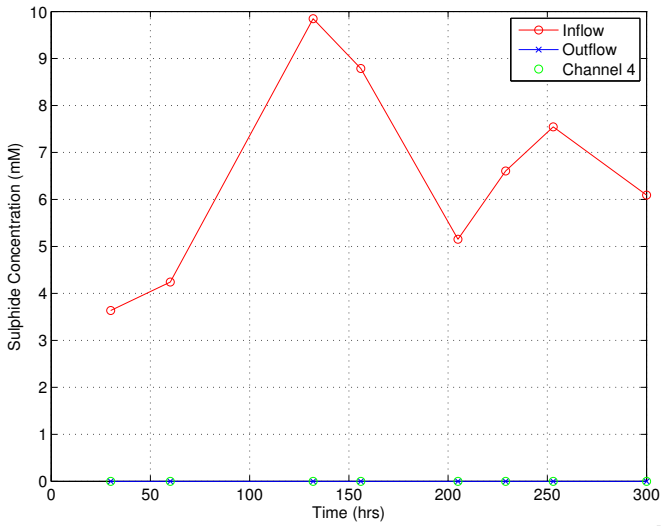
2.3.2 Run 2 - 66 L/day

On completion of the 33 L/day flow rate experiment, the feed rate to the DPBR was increased to 66 L/day. After a four day acclimation period the DPBR outflow was connected to the LFCRs. The 66 L/day flow rate experiment was run using only four channels, as the previous experiment suggested that all the sulphide was removed in the first four channels. The hydraulic residence time was 1.5 days, with an average sulphide concentration in the feed of 8.33 mM (275 mg/L) and an average concentration near the outlet of 1.33 mM (44 mg/L). Therefore the average sulphide conversion was 80%. However the effluent sulphide concentration did not decrease to 0 mM. Two possible reasons were suggested for this result (i) at the shorter R.T. of 1.5 days, four channels did not provide sufficient surface area to enable oxidation of all the sulphide in solution, (ii) at the higher flow rate the sulphate load to the DPBR is increased resulting in a higher sulphide concentration in the LFCR influent. Figure 2.5a shows the sulphur layer floating on the surface of the channels. It was noted that the layers were whiter in colour than those observed at a six day RT. Furthermore, the layers appeared to be thinner and more brittle than the sulphur layers found at the lower flow rate. This observation was confirmed when the sulphur was harvested on completion of the experiment and the sulphur samples compared on drying.

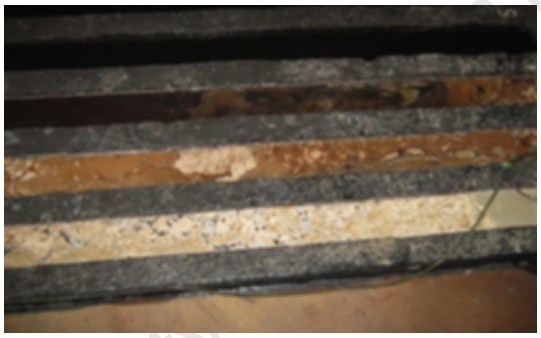
2.3.3 Run 3 - 132 L/day

The final study was carried out at a flow rate of 132 L/day. Based on the results of the second flow rate experiment, all eight LFCR channels were used. The retention time and sulphide loading rate were 1.5 days and 516 mmol/day respectively. The average outflow

University of Cape Town



(a) Influent and effluent sulphide concentrations at a flow rate of 33 L/day



(b) Photograph of floating sulphur biofilm

Figure 2.4: Experimental data of run 1 at Golder Associates Research Laboratories (GARL)



(a) Image of floating sulphur biofilms on all four channels



(b) Image of floating sulphur biofilms on all eight channels

Figure 2.5: Images of the floating sulphur biofilms for experimental runs 2 and 3 at GARL

University of Cape Town

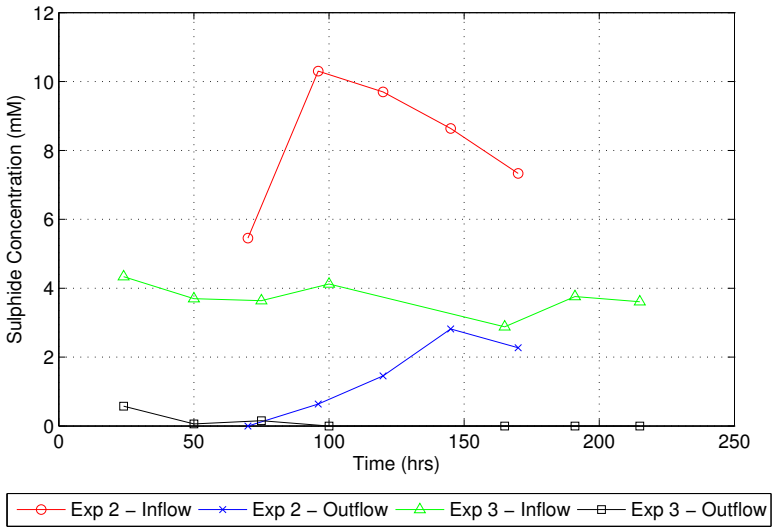


Figure 2.6: Experimental data of run 2 and 3 at Golder Associates Research Laboratories (GARL)

Table 2.2: Summary of results from preliminary LFCR study

Run No.	Run Time (days)	Channels used	Flow rate (L/day)	Sulphide removed (%)	Sulphide loading mg/L.day	Solids recovered (g)	Sulpur recovery (%)
1	13	8	33	100	37.95	23.3	25
2	7	4	66	80	181.43	16.4	15
3	9	8	132	90	85.16	24.5	16

concentration was 0.12 mM (3.96 mg/L) (Figure 2.6) which, equated to a 90% sulphide removal in the reactor, albeit at a significantly lower feed sulphide concentration. The sulphide concentration of the LFCR inflow was almost half that of the two previous experiments, suggesting the feed rate to the DPBR exceeded kinetic capacity of the sulphate reducers. This may be an indication of reduced DPBR performance. Figure 2.5b shows the sulphur layer floating on the surface of the LFCR channels. The colour of the floating sulphur layer was similar to the sulphur layer formed during experiment 2. It is possible that the differences between the colour and consistency of the floating layers at the different flow rates were due to changes in the ratio of sulphur to organic matter. The lower linear flow velocity through the channels at the slower flow rate (run 1) could enhance biofilm growth. This was further supported by the sticky consistency of the floating layer which is normally associated with a high concentration of EPS.

The solids yield was highest at the slowest flow rate (33 L/day) and decreased on increasing the flow rate (Table 2.2). Maintaining a constant R.T. of 1.5 days while increasing the flow rate from 66 to 132 L/day resulted in a similar solids yields. The surface area utilised in run 2 (66 L/day) was half that used in run 3 (132 L/day). Furthermore the inflow sulphide concentration in run 3 was almost half that observed in run 2. These results offer an insight into the effect of surface area and sulphide load on the overall extent

University of Cape Town

of sulphide oxidation. Reducing the surface area resulted in reduced biofilm formation, reduced available oxygen and thus a decrease in the total sulphide oxidised to elemental sulphur. The reduced sulphide load observed in run 3, as compared to run 2, resulted in an equally low yield due to run 3 having a higher flow rate. Molwantwa (2008) demonstrated an 80% sulphide removal using a similar reactor setup. The author used an average inflow sulphide concentration of 4.03 mM. Thus the results compare favourably. Furthermore, the data obtained at the higher flow rates in this study showed no significant decline in sulphide removal provided sufficient surface area is available. The amount of sulphide oxidised did not correlate with the amount of sulpur recovered via the floating sulphur biofilm. A 100% sulphide conversion was achieved in experiment 1, which equates to 95.68 g of sulphur being produced, however only 23.3 g were recovered. Therefore, there was a discrepancy in sulphide removal and sulphur recovery. Due to the lack of analytical tools, no other sulphur species were measured as possible by-products. Moreover, it was suspected that there was stratification within the channel, with a higher concentration of sulphide occurring along the floor of the reactor. Hence the sulphide measurements would have been inaccurate, as the samples were taken 1 cm below the liquid surface. Therefore a more robust analysis of the sulphide oxidation reaction products and sulphur species mass balance was necessary.

University of Cape Town

2.4 Floating sulphur biofilm harvesting study

The FSB that forms on the surface of the channels needs to be harvested at regular intervals. The inter-harvest period is a key operational parameter and is also a means to recover the elemental sulphur product from the system. Since harvesting results in disruption of the FSB, it is important to optimise the harvesting process without compromising the sulphide oxidation kinetics within the reactor. If the FSB is not harvested it becomes thick and may hinder oxygen diffusion and reduce the sulphide oxidation rate. If the FSB is harvested too early, the production of by-products is increased due to the fact, that sulphates and/or polysulphides may be produced as a result of more complete oxidation, during the early stages of FSB development. The aim of this preliminary study was to determine the ideal inter-harvest period taking into account all these limitations. The flow rate (66 L/day) and residence time (1.5 days, 4 channels) were kept constant during the course of the study while the harvesting regime was varied. Unfortunately it was not possible to keep the sulphide concentration constant as the LFCRs were fed directly by a DPBR.

2.4.1 No harvesting

The nature of the FSB, in the absence of harvesting, was observed over a 3 week period. Photographs were taken every 3 days (Figure 2.7). The sulphide concentration in the

inflow and outflow were measured daily. Figure 2.7a shows the LFCRs on day one, when no distinct biofilm was visible on any of the channels. On day four (Figure 2.7b) a brittle FSB was observed on channel 1 with a thin, transparent and diffuse FSB visible on channel 2. On Day seven (Figure 2.7c) the FSB on channel 1 was thicker and a thin more distinct FSB was visible on channel 2. Furthermore, channel 3 started to show signs of biofilm development. Golder associates research laboratories proposed that due to the lack of harvesting, the FSB on channel 1 increased in thickness to the point where sulphide oxidation was limited by reduced oxygen diffusion. As a result, the biofilm in channels 2 and 3 may have started to develop due to more sulphide being available. On day 8 (Figure 2.7d) the FSB on channel 1 started to collapse at the channel inlet. On day 11 (Figure 2.7e) most of the FSB on channel 1 had fallen to the base of the reactor while three days later (Figure 2.7f) the FSB had regenerated and was already thick, brittle and white in colour. This FSB was thicker than the one formed three days after the start of the experiment indicating a faster rate of FSB development. This may be because when the biofilm settles a thin layer of extracellular polymeric substance (EPS) remains on the channel surface which forms the base for the next FSB enabling faster and better FSB growth. Four days later (Figure 2.7g) the FSB in channel 1 started settling. On day 21 (Figure 2.7h) both channels 1 and 2 exhibited a thick, brittle FSB, however the inflow sulphide concentration at this time had increased to 3 mM so this may have influenced the increase in thickness of the FSB on channel 2. The influent sulphide concentration fluctuated significantly, due to non-steady state performance of the DPBR (Figure 2.8), but for the duration of the experiment no sulphide was detected in the effluent stream.

It was concluded from this experiment that if the LFCR is not harvested regularly, the FSB becomes thick enough that it collapses and settles on its own. However, allowing the FSB to become thick and sticky may limit the sulphide oxidation rate, possibly due to a reduction in oxygen diffusion from the atmosphere to the air-water interface. Furthermore, the stickiness of the older FSB resulted in incomplete settling in some cases possibly disrupting the liquid flow (Figure 2.9a). Thus even though the FSB eventually drops on its own, a phenomenon that could reduce the required intervention, it is important to note that the capacity of the system to oxidise sulphide may be compromised and recovery of the elemental sulphur may become more difficult (Figure 2.9b). This is explored in more detail in Chapter 8.

University of Cape Town

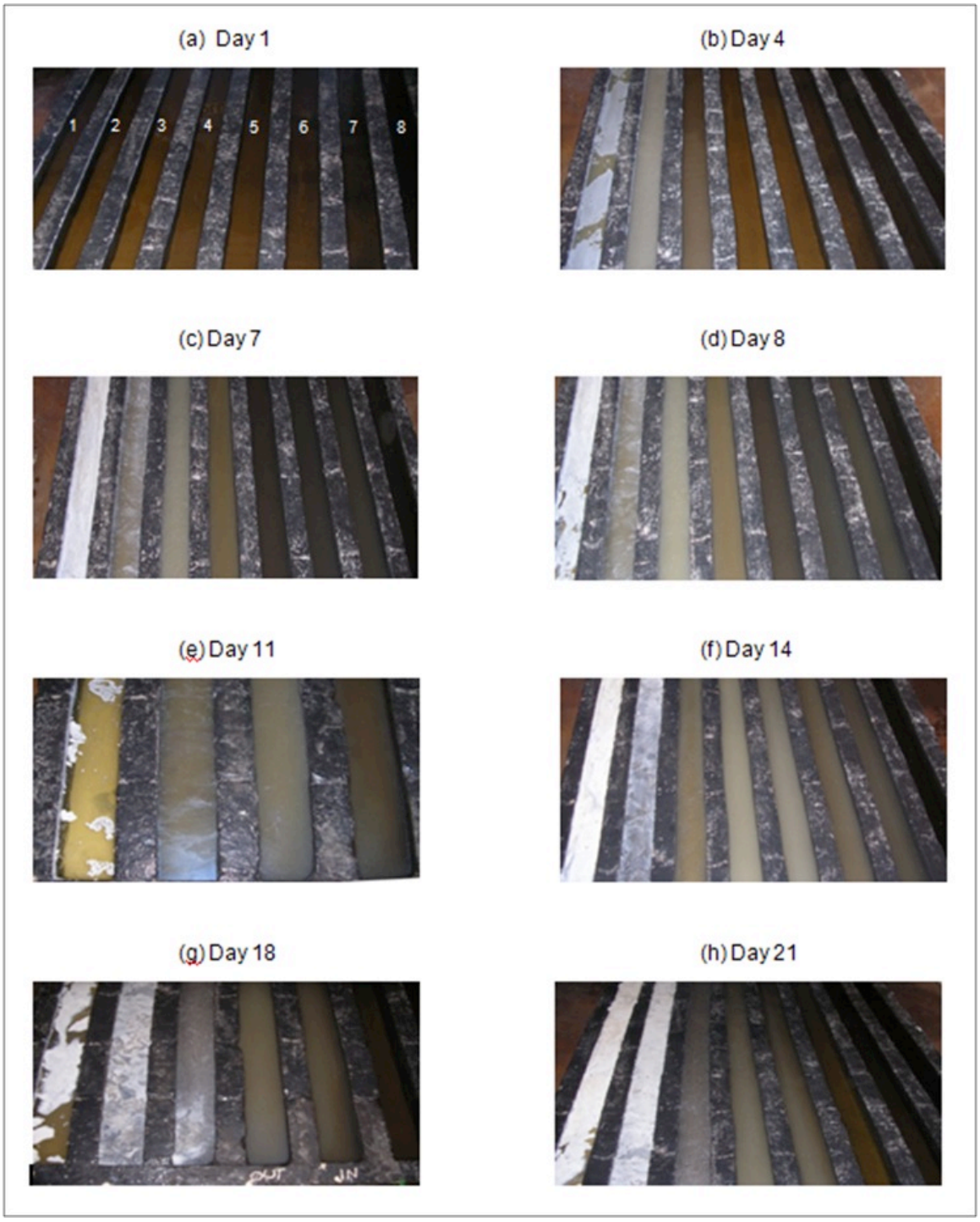


Figure 2.7: Observations of the FSB progression over a 21 day period with no harvesting

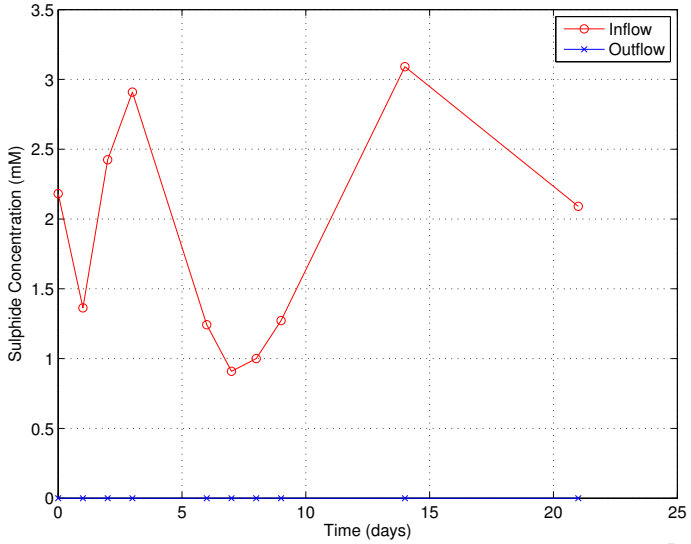


Figure 2.8: Profile of influent and effluent sulphide concentrations over the 21 day period the reactor was operated with no active harvesting



Figure 2.9: Sticky FSB (a) attached to the side of the reactor, (b) hindering elemental sulphur recovery

2.4.2 FSB inter-harvest period study

The channels were operated at a feed rate of 66 L/day, utilising four channels and varying the harvesting regime over a 24, 36 and 48 hour inter-harvest period. The harvesting of the FSB was performed by spraying the surface with water. This caused a disturbance in the water surface tension, hence the FSB collapsed. The FSB was allowed to sink and was collected at the end of the respective inter-harvest period. The 24 hour inter-harvest period study was run for four days. The LFCR inflow sulphide concentration varied between 3 and 6.06 mM in the first inter-harvest period. Figure 2.10 shows the concentrations in each respective channel of the 24 hour inter-harvest period. Channel 1 had a sulphide oxidation of 0.61 - 1.51 mmol/L.day whilst channel 2 was higher at an average 2.42 mmol/L.day. Sulphide oxidation in channels 3 and 4 was significantly lower due to the respective lower inlet concentrations.

University of Cape Town

Figure 2.11a shows the LFCR channels prior to harvesting on day 2 of the 24 hour inter-harvest period experiment. Biofilm is visible on the first three channels. The FSB in the first two channels appeared cream in colour and brittle when sprayed. The FSB in the third channel was brown in colour with a sticky consistency. The difference in colour of the channels is attributed to the difference in the amount of sulphur in the FSB. Furthermore channel 3 and 4 are a dark brown colour due to the lower sulphur content. Channel 4 was devoid of biofilm. Figure 2.11b shows channel 1 and 2 after harvesting. All of the FSB in channel 1 settled immediately due to its brittle nature while some sticky biofilm present in channel 2 remained after harvesting. This is due to channel 1 being composed primarily of sulphur whilst, channel 2 had a greater proportion of organic material relative to sulphur.

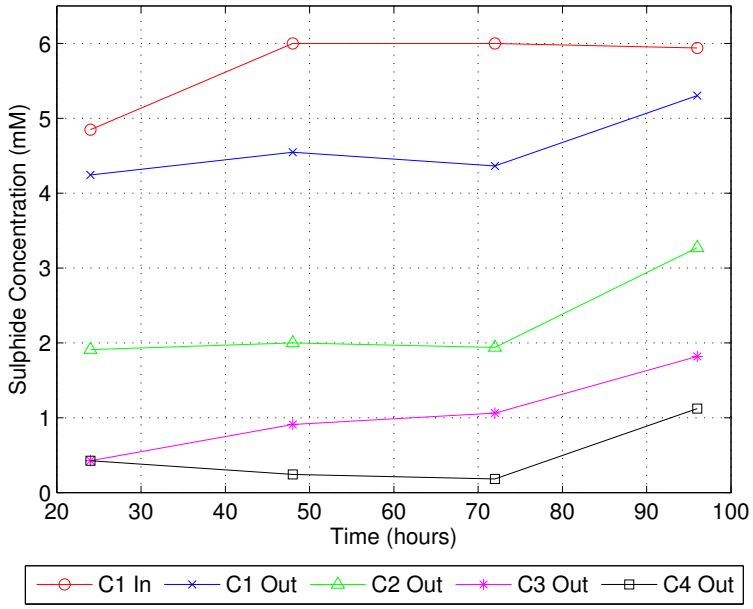


Figure 2.10: Profiles of sulphide concentration in the reactor feed (C1 in) and the exit points of the individual channels

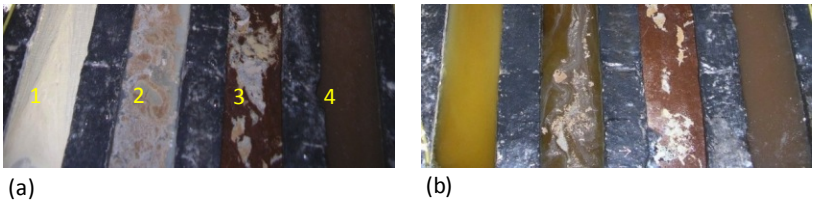


Figure 2.11: LFCR channels during the 24 hour inter-harvest period (a) prior to harvesting and (b) five minutes after harvesting

The thirty-six hour inter-harvest study was run for the 11 days and the channels were harvested every 36 hours. Complete sulphide removal was achieved over the four channels,

however at a lower inlet sulphide concentration (Figure 2.12). No significant change was seen in sulphide removal as the harvesting regime was changed and, as expected, the percentage sulphide removed remained closely linked to the inflow sulphide concentration for each channel. It is possible that at low sulphide concentrations, 36-hour harvesting has no significant effect on the efficiency of the reactor. Golder Associates Africa proposed that these experiments be repeated at higher inflow sulphide concentrations to determine the efficiency of the LFCRs.

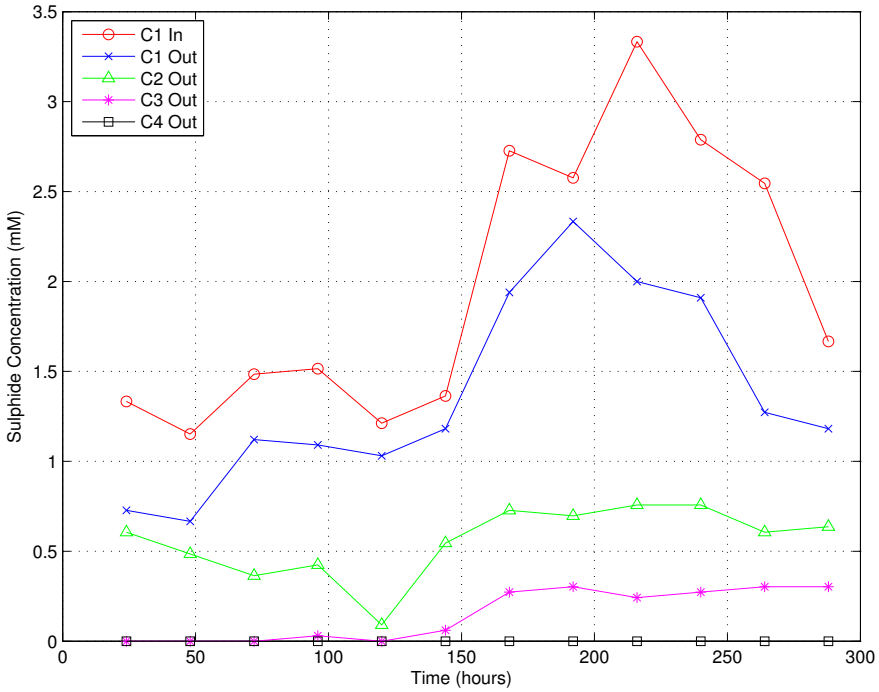


Figure 2.12: Profiles of sulphide concentration in the reactor feed (C1 in) and the exit points of the individual channels the 36 hour inter-harvest period.

The final experiment was run at a 48 hour inter-harvest period for nine days. The FSBs on channels 2 and 3 were cream and brittle to sticky while channel 4 had a brown, sticky FSB. No biofilm was visible on channel 4 during the 24 hour inter-harvest period but increasing the harvesting period to 48 hours resulted in biofilm formation on channel 4. It is possible that because the FSB in channels 1-3 were not harvested after 24 hours, this reduced oxygen diffusion into these three channels, resulting in a greater surface area required for sulphide oxidation, which may explain why a FSB was established on channel 4. A sulphide removal efficiency of 81.2% was attained, which was lower compared to the 24-hour inter-harvest period (91.3%). A greater proportion of sulphide was oxidised within the first three channels as compared to channel 4 (Figure 2.13).

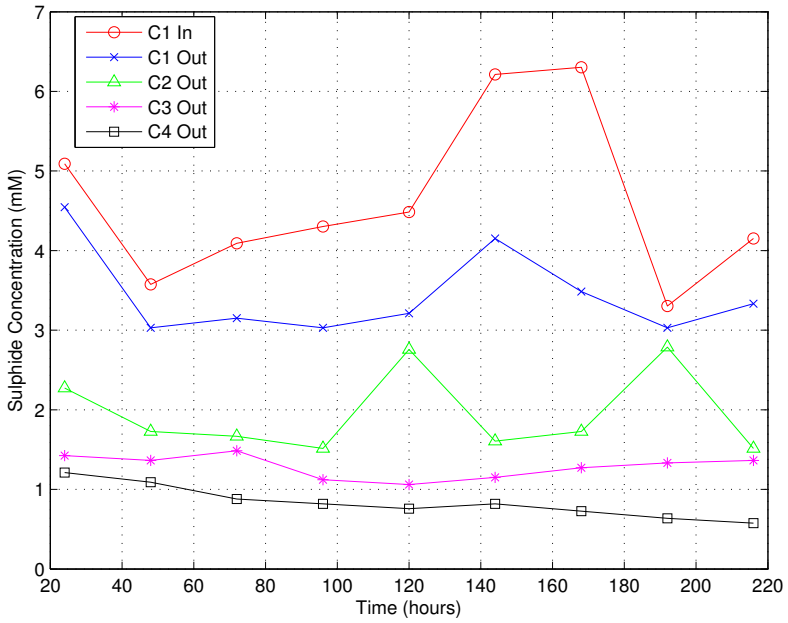


Figure 2.13: Profiles of sulphide concentration in the reactor feed (C1 in) and the exit points of the individual channels for a 48 hour inter-harvest period

2.5 Conclusions

Several conclusions were reached during the course of this component of the study by GAA personnel.

- A thick, brittle FSB is required before successful harvesting can occur.
- The inter-harvest period is dependent on the concentration of sulphide in the inflow as this affects the thickness and consistency of the FSB.
- The optimal inter-harvest period may be as short as 24 hours; however the post-harvest settling time is increased. Furthermore, frequent harvesting may affect the efficiency of the system and the ability of the biofilm to regenerate. Additionally if there is not sufficient sulphur within the film it will not beneficial to harvest.
- A long inter-harvest period will cause the FSB to become sticky and successful harvesting becomes more difficult. Furthermore, the thick, sticky FSB may reduce oxygen diffusion into the channel thus affecting the sulphide oxidation rate.
- When the sulphide concentration is very low, no FSB forms. Instead the channel becomes cloudy with what appears to be colloidal sulphur particles. This phenomenon will hinder sulphur recovery and the suspended particles will be lost

University of Cape Town

through the outflow. The chemistry and mechanisms associated with colloidal sulphur formation are discussed in greater detail in Chapter 7.

- Under the conditions prevalent in the laboratory-scale reactor at GARL, 24 hours was chosen as the best inter-harvest period. The highest sulphide removal efficiency was attained and the FSB was able to reform every 24 hours.

2.6 Final interpretations & shortcomings of GARL study

The LFCR channels at GARL were only sampled from the liquid surface (1 cm below the surface), due to costs and logistical issues. Therefore no samples were able to be taken from lower down in the reactor volume. Furthermore, due to the nature of the construction of the LFCRs, it was not possible to see below the liquid surface. It was suspected that the incoming sulphide feed bypassed the reaction zone at the FSB as the inlet and outlet were at the base of each channel of the reactor. This was suspected as a possible explanation for the discrepancy between the observed sulphide oxidation and sulphur recovered via the FSB. The sulphide feed could have crept along the floor of the reactor to the outlet point. Furthermore, the final outlet sample was also taken from the top surface of the respective channel, therefore this value would have been considerably inaccurate if bypassing was present. Therefore, a more superior and sophisticated design of a LFCR is necessary to allow for samples to be taken along the length and depth of the channel. Additionally, if the channel is transparent it will also allow visual observations of the bulk liquid colour and underside of the FSB.

A hydrodynamic tracer study is also necessary in order to conclusively determine if short-circuiting occurred or if the assumption of plug flow in the LFCR was justified. This information will prove crucial with regard to the scale-up design and industrial scale designs. Additionally, this in conjunction with the multiple sampling ports will also provide information on the vertical sulphide gradient within the LFCR, as it was suspected that there was significant stratification. The hydrodynamic study will be discussed in Chapter 6.

There was a change in FSB colour as the experiments progressed as well as difference in colour amongst experimental runs one, two and three. It is suspected that the FSB was more organic in nature at the lower flow rate and became more sulphur laden at 66 L/day. However, in experiment three, channels three to eight had a more brown coloured FSB whilst, one and two were white. It is suspected that this change in colour was due to the increase in molasses dosing to the DPBR upstream. Consequently, the increase in organic dosing and shortened residence time of the DPBR resulted in the LFCRs being heavily dosed with soluble organics. Therefore organic biofilm development was most likely promoted and a lower quantity of sulphur was seen in the FSB. For this reason a detailed study between residence time, organic loading rate and sulphur yield is necessary in order

University of Cape Town

to determine the operational parameters of the LFCR. This will ensure that an adequate FSB is formed every time and able to retain the maximum amount of sulphur therefore ensuring sustained optimal efficiency of the LFCR. These parameters will be covered in Chapter 8, whilst the shortcomings of the DPBR will be investigated in Chapter 9.

Lastly, the harvesting period of the FSB was investigated. However, if the flow rate, organic loading rate and sulphide oxidation is not at an optimum then this will inevitably change and be influenced by these operational parameters. Therefore it's crucial these parameters be determined first and then the optimal harvesting regime. Finally, an effort to understand the mass flux of oxygen into the floating sulphur biofilm and the required surface area for 100% sulphide removal is necessary. Due to the nature of the FSB and its ability to grow in thickness and sulphur content, it is crucial that the oxygen penetration through the FSB be understood, to achieve maximum sulphide oxidation to sulphur continuously. Moreover, this information will be pertinent in the optimisation and management of a large-scale system and will be discussed in Chapter 8.

University of Cape Town

Chapter 3

Literature Review

3.1 Industrial effluents

Industrial wastewater continues to be a significant problem within the sector, not only in South Africa but globally. As the global population continues to grow, industrial activity is rapidly increasing resulting in a greater generation of wastewaters. These wastewaters pose a threat to the surrounding ecosystems and habitats within which we reside. Major industries responsible for the generation of these effluents are chemical, tanning, metallurgical and mining. The effluents from the above-mentioned industries are generally rich in sulphates, sulphides and dissolved metals. However, the biggest contributor of metal and sulphate containing effluent is the mining industry, through acid rock drainage which is significantly affecting the quality and pH of surface water, as well as the surrounding aquatic environments. As a result the mitigation and treatment of ARD warrants considerable attention and management.

3.1.1 Generation of Acid Rock Drainage

Acid rock drainage is caused by the exposure of sulphidic minerals to both oxygen and water as a consequence of mining and processing of metal ores and coals (Johnson & Hallberg, 2005a). Acid rock drainage can be generated abiotically in the presence of oxygen and moisture (Reactions 3.1-3.2), but the process kinetics are significantly increased in the presence of iron and sulphur oxidising microorganisms(Reaction 3.3) (Akcil & Koldas, 2006).

$$FeS_2 + \frac{7}{2}O_2 + H_2O \rightarrow Fe^{2+} + 2SO_4^{2-} + 2H^+ \tag{3.1}$$

$$Fe^{3+} + 3H_2O \rightarrow Fe(OH)_3 \downarrow + 3H^+ \tag{3.2}$$

$$FeS_2 + 14Fe^{3+} + 8H_2O \rightarrow 15Fe^{2+} + 2SO_4^{2-} + 16H^+ \tag{3.3}$$

$$Fe^{2+} + \frac{1}{4}O_2 + H^+ \rightarrow Fe^{3+} + \frac{1}{2}H_2O \tag{3.4}$$

University of Cape Town

Pyrite (FeS_2) is the most abundant sulphide mineral and is the primary mineral responsible for ARD generation (Oyekola, 2008). The process is initiated due to its weathering and oxidation (reaction 3.1) at a neutral pH. Reaction 3.1 is abiotic and while reaction 3.4 can occur abiotically the kinetics are slow, particularly in acidic waters (pH $<$ 4). The generation of ARD is further amplified when reaction 3.4 is catalysed by aerobic, iron-oxidising microorganisms (Zagury et al., 2007; Johnson & Hallberg, 2003).

These particular organisms are characterised as being acidophilic, aerobic chemoautotrophic species which are most active at pH 1.0 - 3.5. They are capable of increasing the rate of Fe^{2+} oxidation (reaction 3.4) by several orders of magnitude (Gazea et al., 1996). Ferric iron has low solubility and if the pH is higher than 2.3 - 3.5, it precipitates as ferric hydroxide releasing H^+ and therefore lowers the pH as per reaction 3.2 (Zagury et al., 2007). The ferric hydroxide precipitate gives water a red-orange colour, which is a common characteristic of ARD discharge. On the other hand the ferric ions may react with more pyrite (reaction 3.3), producing more ferrous iron to drive reaction 3.4. In the presence of sufficient dissolved oxygen, a continuous cycle is maintained (Johnson & Hallberg, 2003). This process is complementary seeing that as the pH continues to decrease, ferric iron will remain in solution and will be reduced by pyrite. This will generate additional ferrous iron and acidity until all the pyrite is depleted.

A second group of microorganisms, which are responsible for the oxidation of reduced sulphur species, are typically found within the mineral ore environment. They are most typically chemoautotrophic and use inorganic electron-donors as their energy supply, although some are mixotrophic or heterotrophic. *Acidithiobacillus thiooxidans* and *At. caldus* are the most common mineral degrading acidophiles which utilise sulphur species as electron donors to produce sulphate in conjunction with H^+ ions. As a result, the dissolution of acid-labile minerals leads to further release of heavy metals and ions contributing to salinity (Wolkersdorfer, 2008).

Acid mine drainage can be formed actively during mining operations, as the excavation of target mineral ores often means penetrating the local shallow water table. Hence, if the country rock has a high hydraulic conductivity then there is a large amount of underground water ingress into the mine pit or shaft. Various options are possible to manage the water inflows, either by dewatering, diversion or sealing. It is advantageous to target actual groundwater flows in order to minimise the formation of AMD (Morton, 1993).

On the other hand ARD is generally formed via the weathering of waste rock dump piles or the flooding of underground abandoned mines. The closure of underground mines also poses a serious threat in terms of uncontrolled ARD formation. These workings generally would have intersected the water table, requiring active dewatering schemes during operation. However, after mine closure the dewatering processes are terminated allowing for the rebound of groundwater back in to the various mine shafts. Rebound not only results in a repositioning of the water table and surface discharges, but can also have a profound effect on the water quality. During dewatering water passes through

University of Cape Town

workings along discrete flow-paths which are well washed and as such any soluble minerals are flushed from them. When the workings are left to flood all the void spaces come into contact with water. Underground water essentially flows along the pathways created during the mining process. Such is the case in the Pennsylvanian Anthracite fields in USA. More than 95% of the open voids were flooded. When the water table rose, the mine water became enriched with contaminants and discharged through several points causing surrounding nearby homes to be flooded (Wolkersdorfer, 2008).

A similar occurrence has been observed at the Middelburg Colliery in the Witbank Coalfield, South Africa. Mining operations originally began at the mine in 1908 and the coal was worked by the bord and pillar method. In the late 1930s and early 1940s pillar robbing began in order to improve the overall coal extraction ratio from 60% to 90% (Bell et al., 2001). In the bord and pillar method of mining, pillars of coal are left in place to support the roof. Therefore, the pillars have to sustain the load attributable to the overburden, however slow deterioration or failure of pillars might take place once mining operations have ceased. Consequently, the roof rock may collapse giving rise to crownholes at the surface or subsidence may occur. This has occurred at Middelburg Colliery, where the roof strata has collapsed totally into the old workings, resulting in voids 15 - 20 m deep and crownholes with diameters between 5 - 10 m. Surface subsidence has also caused tension cracks and several crownholes extending downwards to the mine level, allowing for free passage of air and water down into the the old mine workings (Bell et al., 2001). As a result the remaining coal in the mine has undergone spontaneous combustion for the past 50 years and approximately 150 - 200 ha has been affected by the burning. Furthermore, the burning of pillars also exacerbates the strain taken by the remaining pillars, resulting in further roof collapse and introduction of air. Analysis of the coal revealed it was a low-rank bituminous coal with an average pyrite content of 2% or more, which would enhance the combustion process and formation of ARD. There is availability of carbonates and other aluminosilicates which could provide some buffering capacity, however it is not sufficient for long-term neutralisation (Pinetown et al., 2007). Various attempts to extinguish the burning coal have been made, including water injection and flooding of the mine. However, due to the many open voids and absence of cut-off trenches, the water inevitably drains off resulting in the fire not being completely extinguished. As a result, ARD is promoted and sulphurous steam is created which exits to the surface via the crownholes and tension cracks (Bell et al., 2001).

The second major source of ARD is the two spoil heaps (approximately 56 000 and 66 000 m^2 in size). These old heaps contain a significant amount of coal (20 - 30%) and due to the heaps being formed by tipping, there has been very little compaction. Consequently, the heaps are highly permeable allowing for significant penetration of air and rainfall, promoting spontaneous combustion and ARD formation. Seepage of water from these heaps as well as the underground workings into the ground water has led to severe contamination of the Blesbokspruit catchment. Analysis of the seepage water,

University of Cape Town

Blesbokspruit waters as well as acid mine water from drill holes sunk at adjacent collieries was conducted by Bell and co-workers (2001). The pH was extremely low at an average of 2.2, 2.7 and 2.8 respectively across various sampling points. The sulphate concentrations also exceeded environmental standards and were approximately 2200 mg/L, 1250 mg/L and 2330 mg/L respectively. Likewise, there was an observed increase in heavy metal concentrations (Fe, Mn and Al), with iron being the highest at 167 mg/L, 40 mg/L and 256 mg/L respectively.

Therefore, these discharges need to managed correctly and treated accordingly to avoid further contamination of other surface streams and catchments. These discharges pose a serious health risk and need to be monitored according to the appropriate standards.

3.1.1.1 Effects on human health

The acceptable water quality standards set by the U.S. Environmental Protection Agency (EPA) stipulates a maximum dissolved sulphate concentration of 250 mg/l or less. This is based primarily on taste considerations. However, potable water generally has a sulphate concentration of 0 - 200 mg/L (DWAF, 1996). There is no set guideline with regard to acceptable sulphate concentration within potable water according to The World Health Organisation, primarily due to the fact that there is no conclusive evidence linking sulphate concentration and diarrhoea within human individuals (WHO, 2004). This is partly due to the fact that each individual's body has a different tolerance for sulphate (USDA, 2004). However, the World Health Organisation does recommend that the relevant authorities be notified if the sulphate concentration exceeds 500 mg/L.

Table 3.1: Allowable sulphate concentrations in potable water as per domestic water use legislation standards ((USDA, 2004), (WHO, 2004)).

Sulphate Range (mg/l)	Effects
0 - 250	No health or aesthetic effects are experienced
	No foul taste is detectable
250 - 500	Diarrhoea is possible in certain individuals.
	Definite salty or bitter taste
500 - 1000	Diarrhoea in most individuals. User-adaptation does not occur.
	Pronounced salty or bitter taste.
> 1000	Diarrhoea in all individuals or slight change in stool mass.
	Very strong salty and bitter taste.

From Table 3.1 it is evident that a sulphate concentration exceeding 200 mg/L can have adverse effects on the human body. ARD is not only harmful due to the high sulphate loading, but also various heavy metals and hydrogen sulphide (Table 3.2).

University of Cape Town

Table 3.2: Guidelines for drinking-water quality of various chemicals (WHO, 2003).

Compound	Guideline Value (mg/L)
Copper	2
Hydrogen sulphide	0-0.05
Iron	2
Lead	0.01
Manganese	0.4
Zinc	3

3.1.1.2 Effects on the environment

Acid rock drainage has a substantial impact on the aquatic ecosystems of affected environments. It has been shown that the low pH of ARD run off is a continuous environmental problem at many active or abandoned sulphide mineral and coal mine sites. Firstly, the most common problem with ARD is the iron oxyhydroxide precipitates which form within the contaminated water. Often called "ochre", as it is a mixture of crystalline and amorphous iron precipitates with a yellow to orange-red colour. It can exist as a gelatinous flocculant or suspended solid (Wolkersdorfer, 2008; Hogsden & Harding, 2012). This can cause discolouration or high turbidity of streams, on the other hand exceptionally clear water could result due to sedimentation (Bae et al., 2010). It has been shown that these metal precipitates or oxyhydroxides are of specific concern to the health of all aquatic wildlife, namely benthic macro/micro invertebrates and vertebrates (fish and amphibians). The suspension of these chemical species are more harmful than the deposition of them along the sediment of a water body. This is due to the increased conductivity and uptake of the heavy metals by the organisms (Nicola & Stapleton, 2002; Azrina et al., 2006).

Many studies have been conducted at mining affected sites across the world. MacCausland & McTammany (2007) showed that the low pH and high aluminium and metal concentration eliminated most macro-invertebrate taxa within the surface streams that were measured. There was a strong correlation between dissolved metal concentration and specific conductance, which was negatively correlated with macroinvertebrate density and richness. Hence, at these particular sites toxic concentrations of metals led to a decrease in macro-invertebrate density and richness. Furthermore, Keinanen et al. (2004) showed that acidity and heavy metals have an adverse effect on the early developmental phases of roach (*Rutilus rutilus*) and pike fish (*Esox lucius*). Glover & Hogstrand (2003) and Cooper et al. (2006) showed that dissolved metals affect the metabolic processes of certain freshwater fish.

In South Africa, the Olifants River in Mpumalanga has been detrimentally affected by anthropogenic activities. Investigations were conducted on the Moses and Olifants Rivers

University of Cape Town

as well as Loskop Dam and the lower catchment Lake Flag Boshielo (Ashton & Dabrowski, 2011). The concentration of Al (3.3 mg/L), As (0.058 mg/L), Cu (16 mg/L) in the Moses and Olifants river was above the guideline values as stipulated by the WHO (2003). However, in the downstream catchment of Lake Flag Boshielo the levels of heavy metals within the lake sediment were extraordinarily high, with concentrations of Al (105.9 g/kg sediment), Cu (0.08 g/kg), Fe (67.2 g/kg) Mn (1.7 g/kg) and Ti (2.4 g/kg) recorded. These levels suggest that a significant proposition of dissolved metals or colloid metal precipitates are washing downstream into Lake Flag Boshielo. However, there was no arsenic present within the lake sediment (Ashton & Dabrowski, 2011). Numerous surveys and research studies (University of Johannesburg) were conducted on the bioaccumulation of trace metals within several fish species. These studies showed that trace metals were accumulating to harmful concentrations that posed a health risk to anyone who might consume the fish. This led to the death of a large number (>170) of Nile crocodiles in 2009 due to pansteatitis, which they may have contracted due to consuming toxic fish (Ashton & Dabrowski, 2011; Heath et al., 2010).

Therefore anthropogenic acidity and metal contamination has a negative effect, not only on the water, but on individual animal species and the food web structures. Furthermore, this has a negative social impact, as people are unable to utilise the river or the fish species for consumption or recreation due to the current toxicity levels. Hence, treatment systems are required in order to treat these industrial wastewaters which are entering these natural surface waters.

University of Cape Town

3.1.2 Treatment Technologies

There are a variety of technologies that have been developed for the treatment of ARD. The established methods are generally targeted at acid neutralisation, sulphate and metal removal. The most appropriate treatment depends on the volume of effluent, concentration, type of contaminants and pH of the water (Gazea et al., 1996). ARD treatment can essentially be arranged into two categories viz. active and passive treatment. Active treatment generally entails the installation of agitated reactors or similar units which require constant energy input. Furthermore, the addition of alkaline chemicals and reagents to treat the acidic effluent can become costly, given that the drainage will be either generated in voluminous quantities or will occur on many decommissioned mine sites (Gazea et al., 1996). There is a diverse range of active treatment technologies such as chemical precipitation, ion-exchange, membrane technology and biological sulphate reduction.

3.1.3 Active treatment technologies

3.1.3.1 Chemical treatment

The most common chemical treatment method is the addition of an alkaline material to raise the pH, precipitate heavy metals and accelerate the rate of chemical oxidation of ferrous iron (for which aeration is necessary). Traditionally ARD is neutralised with lime resulting in the concomitant precipitation of iron and other metal hydroxides. The most common reagents are lime ($Ca(OH)_2$), slaked lime, limestone ($CaCO_3$), sodium carbonate (Na_2CO_3) or sodium hydroxide (NaOH). However, each compound varies in cost and effectiveness. The chosen compound is generally limestone or calcium oxide due to economic concerns (Johnson & Hallberg, 2005a). Liming as a treatment process is effective in the removal of sulphate to below the saturation level of gypsum ($CaSO_4.2H_2O$) and neutralization of acidity (reaction 3.5). Furthermore, it removes most dissolved metals to form metal hydroxides. However, the resulting sludge (gypsum and metal hydroxides) is unstable at a low pH leading to re-solubilisation of the metal hydroxides (reaction 3.7) (Lorax-International, 2003). The major disadvantage of this treatment process is the production and disposal of the sludge and the high cost of chemicals (Lorax-International, 2003; Johnson & Hallberg, 2005a).

$$Ca(OH)_2 + H_2SO_4 \leftrightarrow CaSO_4.2H_2O \downarrow \tag{3.5}$$

$$CaCO_3 + H_2O + H_2SO_4 \leftrightarrow CaSO_4.2H_2O + CO_2 \tag{3.6}$$

$$Ca(OH)_2 + H_2SO_4 + Me^{2+} \leftrightarrow 2H^+ + CaSO_4 \downarrow + Me(OH)_2 \downarrow \tag{3.7}$$

A common process for the treatment of ARD via lime addition is the High Density Sludge (HDS) process. This process has its advantages, as there is a substantial reduction in sludge volume and increase in sludge stability (chemically and physically). The ARD effluent is firstly mixed in a tank with limestone and sludge recycle, which ensures neutralisation and precipitation of metals. Thereafter, it is agitated and aerated aggressively to ensure optimum process chemistry. Lastly flocculant is added and sent to the clarifier for solid-liquid separation where 95 - 99% of the liquid is recovered. Some of the sludge is recycled in order to promote flocculation of the precipitates after neutralisation (The International Network for Acid Prevention, 2009).

3.1.3.2 Ion-Exchange

Ion-exchange processes are widely used to remove ions from industrial wastewaters. The main advantage of ion-exchange is the high treatment capacity, high removal efficiency and

University of Cape Town

fast kinetics (Fu & Wang, 2011). Selected ions are removed from solution by transferring them to a solid material (ion-exchange resin) by adsorption and an equivalent number of desirable ions, stored on the resin, are released into solution by desorption. Anions such as sulphate can be removed through anion exchange via an anionic resin (R-OH). This is best represented by the following reaction(Haghsheno et al., 2009):

$$2R - OH + SO_4^{2-} \underset{k_2}{\overset{k_1}{\rightleftharpoons}} R_2SO_4 + 2OH^- \tag{3.8}$$

Where 'R' is the ion exchange radical and k_1 and k_2 are the forward and reverse reaction rate constants respectively (Haghsheno et al., 2009). One such industrial process is GYP-CIX process, demonstrated at the Grootvlei Proprietary Mines Ltd site (South Africa). This process is able to reduce the feed sulphate concentration by 94%, with an annual operating cost of 0.6 USD/m^3 and total annual cost of 8.6 million USD/m^3 (Haghsheno et al., 2009). Additionally synthetic ion-exchange resins can be utilised in the removal of heavy metals from solution. The most common cation exchange resins are strongly acidic due to the sulfonic acid group (SO_3H) or, weakly acidic due to a carboxylic acid group (COOH) (Fu & Wang, 2011).

$$nR - SO_3H + M^{n+} \rightarrow (R - SO_3^-)_n + nH^+ \tag{3.9}$$

$$nR - COOH + M^{n+} \rightarrow (R - COO^-)_n M^{n+} + nH^+ \tag{3.10}$$

Generally the affinity is greatest for large ions with a high valency and follows the following sequence: $Mn^{2+} < Cu^{2+} < Zn^{2+} < Al^{3+} < Fe^{3+}$. An alternative to synthetic resins are natural zeolites (clinoptotile), which have gained interest mainly because their sorption properties provide a combination of ion exchange and molecular sieve properties; with a metal removal efficiency of 80 - 99% (Motsi et al., 2009).

3.1.3.3 Membrane technology

The two commercial technologies which utilise membranes in water treatment are reverse osmosis and electrodialysis. In reverse osmosis (RO) a brine solution is placed on one side of a semi-permeable membrane and water is placed on the other side. There is a natural tendency for the pure water to diffuse through the membrane to the solute side until an equilibrium osmotic pressure is achieved. However, in RO pressure greater than the osmotic potential is applied to the solute side, causing water to diffuse from the solution through the membrane to the fresh water side. This results in a concentrate stream containing the impurities and a high purity water stream (permeate) (Kim, 2011). The membranes are typically made of cellulose acetate, aromatic polyamide, polyamide or thin film composites. These membranes have salt rejection rates of 94-97% and a long service life, provided the

University of Cape Town

waste stream is free of particulate matter and species ($CaCO_3$, $CaSO_4$) which may cause scaling or fouling of the membrane (Kim, 2011; Perez-Gonzalez et al., 2012). Therefore, pre-treatment is critical for successful use of RO membranes. RO processes are relatively inexpensive to install, operate and maintain. However, the pre-treatment systems and disposal of the concentrated negatively affect the economic viability.

The eMalahleni water reclamation plant is able to obtain a 99% water recovery whilst, reducing the sulphate concentration below 200 mg/L. However, it generates approximately 150 - 200 tons/day of solid gypsum waste and 60 - 100 m^3/day of concentrated brine (Anglo Coal, 2009).

The alternative to RO is electrodialysis which involves an electrical potential being utilised to move dissolved ions through a selectively permeable membrane. Electrodialysis consists of a large number of cells alternately contained within anion-exchange and cation-exchange membranes and arranged between an anode and a cathode (Lorax-International, 2003; Kim, 2011). The process is at least as expensive as RO and would not be economical for low concentration solutions. However, if used in conjunction with a reverse osmosis plant, it can be utilised to treat the concentrated brine discharge. This is due to the fact that reverse osmosis processes are generally able to handle solutions with a TDS concentration range of 0 - 100 000 ppm. Whilst electrodialysis is best suited for concentrated brines within a TDS range of 100 000 - 150 000 ppm.

University of Cape Town

3.1.3.4 Biological Sulphate Reduction

Biological sulphate removal has the potential to be an economically viable alternative to the costly chemical processes discussed earlier. Sulphate-reducing prokaryotes (SRP) are either heterotrophic or autotrophic organisms and reduce sulphate to sulphide via a dissimilatory process. The sulphate reduction is catalysed by bacteria, and the sulphate acts as the electron acceptor whilst the organic substrate undergoes oxidation (electron donor) (reaction 3.11) (Zagury et al., 2007). Ethanol, hydrocarbons, volatile fatty acids, primary sewage sludge and lignocellulosic materials may be utilised as electron donors, however this is contingent on availability and cost of the substrate. In most cases the use of ethanol or hydrocarbons is not possible due to prohibitive costs, in the treatment of an invaluable waste stream.

$$2CH_2O + SO_4^{2-} \rightarrow 2HCO_3^- + H_2S \tag{3.11}$$

Whilst the sulphate is reduced to sulphide there is a reduction in acidity, as a strong acid (H_2SO_4) is transformed into a weaker acid (H_2S). The following products of the reduction process viz. HS^-, $HCO_3{}^-$. This also has a propitious effect as toxic metals are immobilised from the ARD (reaction 3.12) (Johnson & Hallberg, 2005a).

Table 3.3: Toxicological data of hydrogen sulphide gas for humans and the associated durations of maximum exposure and respective symptoms

Concentration (ppm)	Max. duration	Effect / Observation
0.1	24 hrs[a]	Airborne concentration below which, it is believed that nearly all individuals could be exposed up to 24 hours without experiencing transient adverse health effects or perceiving a clearly defined objectionable odour.
0.1 - 10	8hrs/day[b]	Occupational exposure, clearly defined objectionable odour.
11 - 20	4 hrs[c]	Airborne concentration at which it is predicted that the general population, including susceptible individuals, could experience irreversible or other serious, long lasting adverse health effects or an impaired ability to escape. Serious adverse effects include eye irritation, headaches and nausea.
21 - 50	10 mins[b,d]	Airborne concentrations at which it is predicted that the general population, including susceptible individuals could experience life-threatening health effects resulting in death. Adverse health effects include headaches, nausea, vomiting, dizziness and breathing difficulties
50 - 100	< 10 mins[b,d]	Immediately dangerous to life and health

a) (WHO, 2000)b)(OSHA, 2006; NIOSH, 2005)c)(NRC, 2010)d)(EPA, 2003)

$$Me^{2+} + H_2S \rightarrow MeS \downarrow +2H^+ \tag{3.12}$$

(Me is a cationic metal such as Cd, Cu, Fe, Mn, Ni, Zn).

The precipitates are formed fairly rapidly even at a low pH and are less soluble than hydroxide equivalents (Stumm & Morgan, 1996). Sulphate reduction produces harmful sulphides, therefore a hydrogen sulphide removal step is necessary. Hydrogen sulphide is a gas and the major route of exposure is inhalation. Hydrogen sulphide is an extremely toxic, hazardous, corrosive and flammable gas. It is not only toxic to humans but to animals and other organisms as well (Table 3.3) . It has been postulated that the underlying mechanism of toxicity of hydrogen sulphide is that it causes direct inhibition of cellular enzymes (Deng, 1992; Beauchamp et al., 1984). In particular, cytochrome oxidase, an enzyme involved in cellular oxidative processes and energy production. Inhibition of this enzyme is believed to cause a disruption in the electron transport chain inevitably impairing oxidative cell metabolism, causing anaerobic metabolism to occur. Consequently, ATP production and cellular energy generation is decreased, with increased generation of lactic acid. Nervous and cardiac tissue have the highest oxygen demand and the smallest disruption in the oxidative metabolism may result in death due to respiratory arrest (ATSDR, 2006). Therefore it's imperative that gaseous hydrogen sulphide concentrations be kept to a minimum.

Paques (bv.) have developed an active treatment system known as SULFATEQ™ that is capable of dealing with an influent sulphate concentration in the range of 1 - 25 g/L across a pH range of 2 - 8. It essentially consists of a sulphate reduction bioreactor followed by a metal precipitation unit and then a sulphide oxidation unit (Figure 3.1).

University of Cape Town

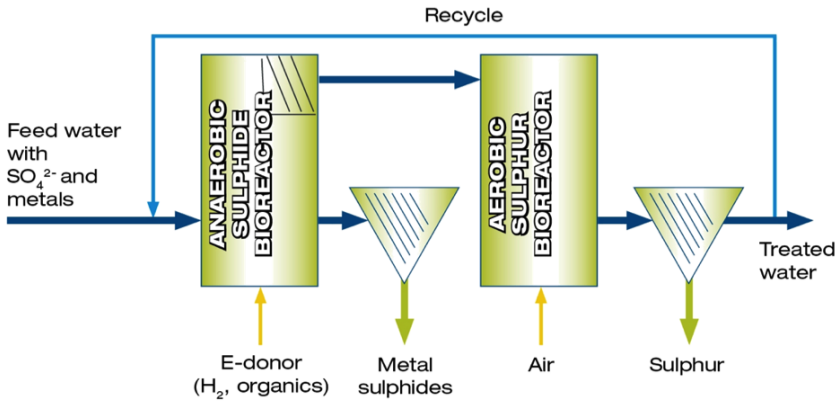


Figure 3.1: Process flow diagram of SULFATEQ™ treatment process (Paques, 2013)

The bioprocess uses an energy source such as hydrogen or ethanol. The recovery of metals in the form of metal sulphides and the sulphur species as solid elemental sulphur is possible (Paques, 2013). Paques also developed a gas desulfurization system similar to the sulphide oxidation unit within SULFATEQ™. The Thiopaq™ gas desulfurization process is capable of removing H_2S from gas streams by biological sulphide oxidation. The working principle of the Thiopaq system is shown in Figure 3.2. The sulphide-containing sour gas enters the absorption section and is passed through an alkaline scrubbing liquid, which absorbs the sulphide. The sulphide-free biogas then exits the top of the absorber. The sulphide-containing liquid flows into the bioreactor, where bacteria oxidise the sulphide, in the presence of oxygen, to form elemental sulphur. Air is blown into the reactor at 1 bar and the pH of the reactor solution is maintained between pH 8.2 - 9. The reactor is either a bubble tank or gas-lift loop reactor. The sulphur is then removed via a settler and the sulphide-free scrubber liquid is returned to the absorber ((Benschop et al., 2004)). Passive technologies on the other hand are utilised in order to treat ARD in a cost-effective manner.

University of Cape Town

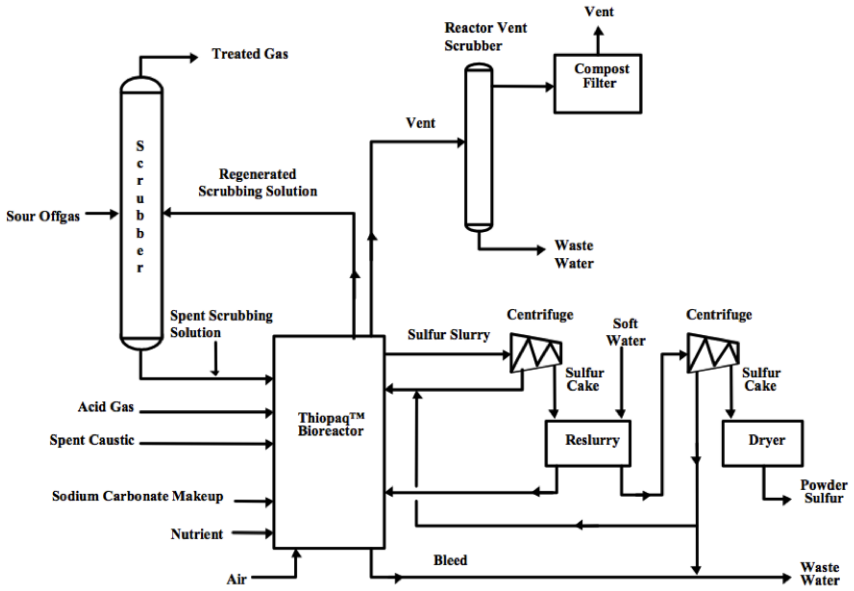


Figure 3.2: Schematic representation of Thiopaq Process ((Benschop et al., 2004))

3.1.4 Passive Treatment Technologies

Passive treatment technologies do not require regular human intervention, operations or maintenance. They should preferably employ natural construction materials (e.g., soils, clays and plant residues such as straw, wood chips, manure, and compost) and promote the growth of natural vegetation. Passive treatment systems normally use gravity flow for water movement instead of pumping. A truly passive system is able to function without electrical power and is able to operate for many years (> 5 years). There are various treatment systems, which occur in numerous configurations within industry, but there are essentially five types.

1. Anoxic Limestone drains
2. Aerobic wetlands
3. Anaerobic wetlands
4. Limestone channels / permeable barriers
5. Sulphate reducing bioreactors

Figure 3.3 is a flow diagram and is a basic summary of the methodology behind the selection process, for the most appropriate and effective system for passive treatment.

University of Cape Town

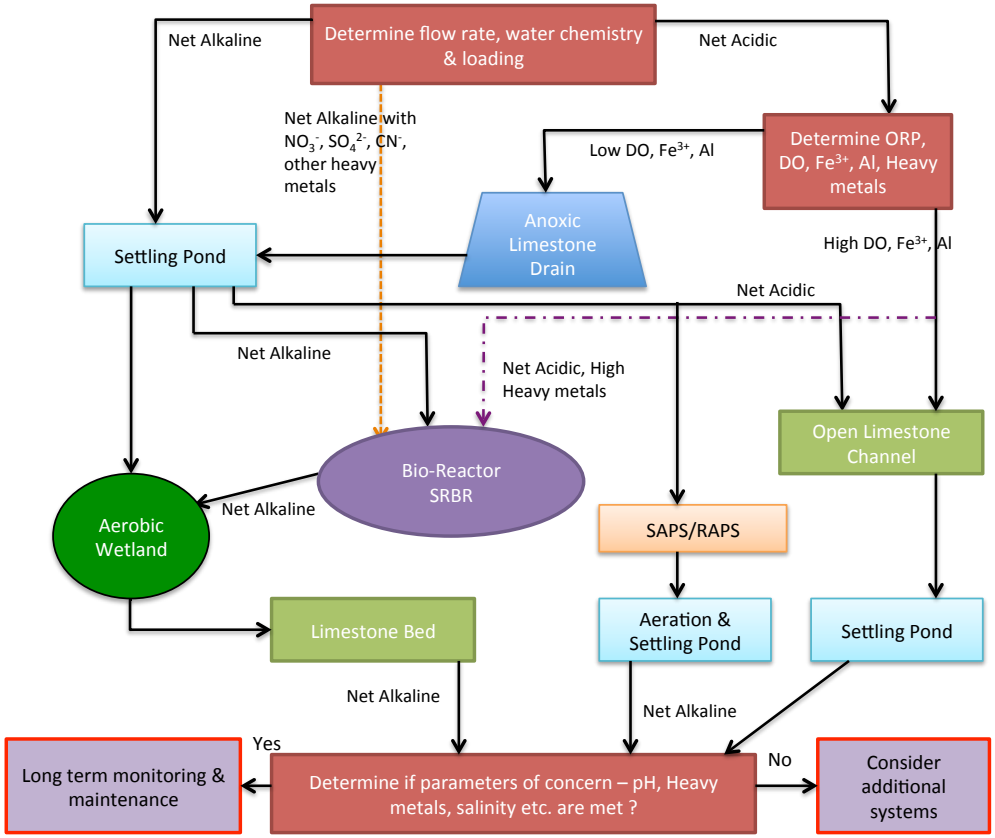


Figure 3.3: Flow chart enabling the selection of passive treatment technology flow chart (Adapted from (The International Network for Acid Prevention, 2009))

3.1.4.1 Anoxic Limestone Drains

Anoxic limestone drains are an alternative method of adding alkalinity to ARD and form one component of a passive treatment system. An ALD is buried under several metres of clay and a plastic liner is placed as an additional gas barrier between the limestone and the clay soil. Hence the ALD is almost entirely sealed from atmospheric oxygen and the accumulation of CO_2 is promoted. The ARD water is then directed downwards via a well to the limestone whilst minimising the amount of exposure to the atmosphere (Gazea et al., 1996). It's imperative that the ferrous iron remain in its reduced form otherwise, if oxidised, it would lead to the precipitation of ferric hydroxide on the limestone. This is known as armouring and considerably reduces the effectiveness of the limestone and its ability to dissolve. Furthermore the accumulation of carbon dioxide is encouraged as it accelerates the rate of limestone dissolution. Therefore, in order for an ALD to be an effective treatment method the acidic water should have a low ferric iron (Fe^{3+}< 2 mg/l) or aluminium concentration (Al^{3+} < 2 mg/l) and a low dissolved oxygen concentration (DO < 1 mg/l) (Gazea et al., 1996; Johnson & Hallberg, 2005a). Additionally, the residence (contact) time, initial carbon dioxide partial pressure, limestone particle size and concentration of calcium carbonate within the limestone will also be a factor in the

liberation of alkalinity in the ALD (Watzlaf et al., 2000). The design criteria for ALDs is a residence time greater than 15 hours. However, Ziemkiewicz et al. (2003) showed that the most efficient ALDs had an acidity removal rate of 380 - 675.2 g/(day.t), with a residence time in the range of 2-6 hours. Under certain circumstances, the heavy metal precipitates do not settle and remain as colloidal particles. Therefore, a wetland would be required to treat ALD effluent in order to capture all contaminants.

3.1.4.2 Aerobic wetlands

Aerobic (oxidising) wetlands are predominantly used to treat net alkaline waters and consist of *Typha* and other wetland vegetation planted in shallow sediment (< 30 cm). The sediment is normally comprised of soil, clay or mine spoil. Aerobic wetlands are designed to provide sufficient residence time to allow metal oxidation and hydrolysis, thereby causing precipitation, adsorption or ion exchange in order to retain the metal hydroxides (Ziemkiewicz et al., 2003; Sheoran & Sheoran, 2006). Ideally ARD is firstly neutralised via an anoxic limestone drain and thereafter sent to an aerobic wetland to remove all metal hydroxides. Hedin et al. (1994) showed that wetlands receiving net alkaline waters would be able to remove up to 20 g/(m^2.day) for iron. Skousen & Ziemkiewicz (2005) reviewed the performance of six aerobic wetlands with regard to removal efficiency of acidity. The results were highly variable with the wetlands removing between 0.1 to 27 t/yr of acid and costing between USD \$23 to $>$ \$7000 /(t.yr). To operate an optimally performing cost effective wetland it is critically important that the wetland is sized correctly to handle a particular flow rate. Furthermore, the precipitation and retention of metal hydroxides is important to ensure acidity and metal removal. However, aerobic wetlands are also capable of absorption/uptake of heavy metals, provided the correct plants (macrophytes) are used. The main route of heavy metal uptake is through the roots, or leaves in the case of plants with completely submerged leaves. Submerged rooted plants are capable of extracting metals from sediments as well as the water (Sheoran & Sheoran, 2006). Cheng et al. (2002) showed that *Cyperus alternifolius* was more efficient at removing copper as it accumulated 75% as much copper as the sand. Furthermore, it was able to remove up to 6.72% of zinc from the polluted water. Hence, the correct selection of soils/sand materials and plants to perform the necessary removal of contaminants from wastewater is especially important.

3.1.4.3 Anaerobic wetlands

Alternatively an anaerobic wetland may be utilised to treat ARD which has not been neutralised upstream by an anoxic limestone drain. Anaerobic wetlands require rich organic substrates to generate reducing conditions and produce alkalinity via the process of biological sulphate reduction. This results in the concomitant removal of sulphates and heavy metals as metal sulphides, which precipitate and become immobilised within the

sand/organic matrix of the wetland. Ziemkiewicz and co-workers (2003) reported that the performance of anaerobic wetlands varied greatly in terms of acid removal from 0 to 67.9 t/yr and treatment costs from USD $ 341/(t.yr) to $4762/(t.yr). Hallberg and Johnson (2005b) and Sinicrope et al. (1992) showed the reduction of heavy metals to non-mobile forms by bacterial activity. However, the performance of a wetland treatment system depends on the input water quality and the mechanism by which metals and other contaminants are removed. If the primary mechanism is anaerobic biological sulphate reduction, then it is vital that there are readily available organic substrates and heavy metals to precipitate dissolved sulphides to prevent sulphur cycling within the wetland. The principal cause of sulphur cycling is the movement of sulphide species from the anoxic to oxic zone, leading to the oxidation of sulphide to sulphur or sulphate, that is later reduced to sulphide (Wu et al., 2012). An alternative source of oxygen for sulphide oxidation is the release of oxygen from the roots of helophytes (Wiessner et al., 2010).

Therefore, the design of a particular wetland requires attention to every specific detail in order to achieve the required removal efficiency within the given process constraints.

3.1.4.4 Open limestone channels

Open limestone channels operate aerobically, allowing for the precipitation of metal hydroxides within the channel. However, the channel must be designed along the slope of a hill, in order to have a high flow velocity to scour settled solids off the limestone rocks, which would otherwise inhibit the process (The International Network for Acid Prevention, 2009). Skousen and Ziemkiewicz (2005) showed that an open limestone channel was able to remove up to 121 g acidity/(day.t) of ARD with a low cost efficiency of USD $ 26/(t.yr). Open limestone channels are best suited for net acidic waters with a large concentration of heavy metals.

3.1.4.5 Sulphate reduction bioreactors (SRBRs)

Sulphate reduction bioreactors (SRBRs) are generally operated as active systems with very few studies on passive SRBRs. There are several problems associated with passive SRBRs, such as compacting, overloading, inconsistent flow patterns and carbon limitation, which lead to problems with stability and ultimately failure of a SRBR. Cheong et al. (1998) were able to maintain a SRBR for 56 days, effectively removing metals and reducing acidity. However, after 118 days the reactor failed due to substrate compaction and clogging of the influent pipes by metal hydroxides. Tsukamoto and Miller (1999) also operated a pilot-scale SRBR that was packed with horse manure and sand. However, it was only able to reduce the influent sulphate concentration by less than 10%, primarily due to organic substrate limitation. Likewise, Hallberg and Johnson (2005a; 2005b) found that there was an increase in ferric iron in the effluent of an SRBR. Furthermore, it was identified that microbial acclimatisation was essential to optimal performance of the SRBR. In their study the

SRBR was packed with a large amount of materials recalcitrant to biodegradation (sawdust and hay). Very little information could be gathered regarding the substrate dynamics in a SRBR. Therefore, additional studies are required to understand the microbial dynamics, substrate hydrolysis and utilisation within an SRBR, to assess whether a suitable packing configuration exists.

The choice of passive treatment system is dependent on the required effluent quality, available surface area and budget. Figure 3.3 illustrates a general flow diagram, utilised in industry, to select the type of passive treatment system best suited to treating a particular ARD stream.

3.1.5 Wheal Jane passive treatment plant

One of the most well-known passive treatment plants in operation is the Wheal Jane Mine treatment plant in the United Kingdom (UK). Numerous studies have been conducted at this site in order to understand the fundamental chemical and biological processes within the treatment system (Whitehead & Prior, 2005; Whitehead et al., 2005; Hall et al., 2005; Hallberg & Johnson, 2005a,b; Barley et al., 2005). The plant consisted of three treatment schemes and only differed in the pre-treatment utilised to modify the pH. The first system was dosed upstream with lime (LD) to increase the pH to pH 5, whilst the second system had an anoxic limestone drain (ALD) and the third system was lime free (LF). Each system had a constructed aerobic reed bed (wetland) designed to remove iron and arsenic, followed by an anaerobic cell (SRBR) to promote sulphate reduction and facilitate the removal of zinc, copper, cadmium and iron as metal sulphides. The final unit consisted of an aerobic rock filter to promote algal growth and precipitation of manganese. The aerobic wetland cells were able to achieve approximately 52%, 90% and 77% removal of Fe (II) in the first cell (of five) for systems LD, ALD and LF respectively. The average removal rates per surface area were 4, 7.6 and 5.8 g/(m^2.day), with the respective surface areas being 187 (LD), 240 (ALD) and 8175 m^2 (LF). The area of the aerobic cells was far in excess of that required to remove iron at the operational flow rates. Therefore, the aerobic wetland cells were over-designed and this could be overcome by distributing flow to different areas of the cells and by having fewer smaller cells. The overall iron removal efficiency of each system was 96.5% (LD), 99.5% (ALD) and 94.8% (LF).

The anaerobic SRBRs were packed with straw, sawdust and cattle manure. They did not perform effectively and showed a lack of alkalinity generation, with no substantial increase in pH (pH rarely exceeded 5.5) (Whitehead et al., 2005). This was largely due to the fact that the SRP were not adapted to the acidic mine water conditions (pH = 2.8). Consequently, little or no metal sulphides were formed and large proportion of the solid suspended Fe (III) was reduced to Fe (II). However, the SRBR in the lime free system did not receive feed for four months and this improved the SRP population as well as the operational efficiency of the unit. Therefore, it was suspected that the continuous flowing

mine water prevented the establishment of a robust, active sulphate reducing microbial community. The performance of the rock filter was largely dependent on the elevated pH of the water out of the anaerobic (SRBR) cells. Hence, performance was poor with regard to manganese removal in the LD and ALD systems. The lime free system performed well after the operational efficiency of the anaerobic cell improved.

Therefore, this project clearly highlighted the challenges faced when designing a passive treatment plant. Furthermore, the relatively limited fundamental understanding of the microbial community structure and chemical processes occurring within the anaerobic SRBR cells, make rational optimisation difficult.

3.2 Sulphide Chemistry

An efficiently operating sulphate reduction bioreactor produces an effluent with an elevated sulphide concentration. The sulphide may be used to effect metal precipitation, either within the reactor or in a subsequent step, but in many cases there is still residual sulphide. Consequently, a sulphide oxidation unit or similar process is required to remove the sulphide. The partial oxidation of sulphide to sulphur, such as in the SULFATEQ™ process. Such a unit is essential due to the toxic and harmful nature of sulphide.

In the following section the chemistry of sulphide oxidation, the mechanisms and conditions affecting chemical and biological sulphide oxidation are discussed, as well as how the processes interact. Thereafter, the biological sulphur cycle is outlined, followed by a review of the impact of pH, temperature and redox potential on chemical and biological sulphide oxidation.

Sulphides are essentially comprised of three chemical species $H_2S_{(aq)}$, HS^- and S^{2-}. The H_2S that will be dealt with within the experimental system will predominantly occur in an aqueous or dissociated state. The following equations represent the equilibrium between the three species and is strongly dependent on pH (pH=pK_i ; i = 1,2) (Kuhn et al., 1983; Chen & Morris, 1972; Broderius & Smith, 1977).

$$H_2S \rightleftharpoons H^+ + HS^-,\ pK_1 = 6.97 - 7.06\ (25^oC) \tag{3.13}$$

$$HS^- \rightleftharpoons H^+ + S^{2-},\ pK_2 = 12.35 - 15\ (25^oC) \tag{3.14}$$

However, the dissociation constant of the second reaction is small (10^{-12}), therefore the possibility of sulphide existing as S^{2-} at the desired pH (7 - 8) is negligible (Broderius & Smith, 1977).

3.3 Chemical sulphide oxidation

Wilmot et al. (1988) showed that chemical oxidation played just as significant a role as biological oxidation in the overall total oxidation of sulphides, within domestic wastewater treatment plants. Chemical oxidation accounted for 44 - 88% of the overall observed sulphide oxidation, with the variations occurring due to the choice of biological substrate influencing biological oxidation. Hence, the following section will highlight the importance of chemical oxidation and how this affects biological sulphide oxidation. The mechanisms of chemical sulphide oxidation have been shown to be dependent on the pH, temperature, sulphide and oxygen concentrations and the presence of neutral salts (Kuhn et al., 1983).

According to the stoichiometry in the following reaction, the required ratio of sulphide to oxygen is 2:1 for chemical sulphide oxidation to produce a sulphur product (Kuhn et al., 1983).

$$2HS^- + O_2 \rightarrow \frac{1}{4}S_8 + 2OH^- \tag{3.15}$$

$$2HS^- + 2O_2 \rightarrow H_2O + S_2O_3^{2-}\ \Delta G^o = -387.35\,kJ/mol \tag{3.16}$$

$$HS^- + 2O_2 \rightarrow SO_4^{2-} + H^+ \tag{3.17}$$

$$HS^- + \frac{3}{2}O_2 \rightarrow HSO_3^- \tag{3.18}$$

$$SO_3^{2-} + \frac{1}{2}O_2 \rightarrow SO_4^{2-} \tag{3.19}$$

However, from reaction 3.16 it is evident that there is the possibility of thiosulphate formation, although this occurs at a low sulphide to oxygen ratio (1:1) and at a neutral or alkaline pH (Janssen et al., 1995; van den Bosch, 2008). The ratio of sulphide to oxygen has to be 2:1 or higher in order to limit sulphate formation via reaction 3.17. Sulfite formation, as an intermediate, is possible from the oxidation of sulphide. However, this is rapidly oxidised to a more stable product such as sulphate (reactions 3.18-3.19). In most chemical studies, thiosulphate and sulphate are the major stable oxidation products (Amend et al., 2004).

3.3.1 Influence of pH

In acidic solutions (pH $<$ 6), H_2S is the dominant sulphide species. However, as the pH increases to 8 so does the solubility of hydrogen sulphide (as per reaction 3.13). Hydrogen

sulphide (H_2S) is not readily oxidised so the rate of chemical oxidation is slow. As the pH increases, to a maximum of 8, so does the oxidation rate due to an increase in HS^- concentration (Mamashela, 2002; Chen & Morris, 1972). Thereafter there is a three-fold decrease in the oxidation rate at pH 9, followed by a further increase to a second maximum, similar to the first, near pH 11(Chen & Morris, 1972).

The pH also plays a role in the disproportionation of S^0 particles as this leads to formation of HS^- and $S_2O_3{}^-$ under alkaline conditions, as per reaction 3.20. Additionally at pH values > 9 more thiosulphate and sulphide are formed, due to the low chemical stability of sulphur in oxidation state (S^0) (Kleinjan et al., 2005a; van den Bosch et al., 2008).

$$4S^0 + 4OH^- \rightarrow S_2O_3^{2-} + 2HS^- + H_2O \tag{3.20}$$

The pH also affects the equilibrium between sulphide and polysulphides. This will be discussed later.

3.3.2 Influence of temperature

Millero et al. (1987) showed that the oxidation of sulphide is a function of temperature at pH 8. The activation energy (ΔH^*) was found to be 56 kJ/mol where, $\Delta H^* = \left(\frac{dlnk}{dT}\right) RT^2$. However, at pH 12 it was (ΔH^*) lower at 46 kJ/mol. Zhang and Millero(1993) found that the rate constant increased with increasing temperature from 25 - 45°C. This is expected, as the Arrhenius equation $\left\{k = k_0 \exp(\frac{-E_a}{RT})\right\}$ is a function of temperature.

3.4 Biological sulphide oxidation

3.4.1 Biological sulphur cycle

In nature sulphur microorganisms play a vital role in the conversion of the various forms of sulphur. Sulphide can be biologically oxidised by denitrifying organisms, colourless bacteria (in the presence of oxygen) or anaerobically by photosynthetic bacteria (Buisman et al., 1989). Sulphide, polysulphides, thiosulphate, elemental sulphur, polythionates, bisulphite and sulphate are all inorganic sulphur compounds that can be utilised within a microbial community as an electron acceptor. This may occur via dissimilatory or assimilatory pathways (Lens et al., 2000). The preferred product is the formation of sulphur and the removal of all dissolved sulphides. The natural sulphur cycle is controlled by heterotrophic bacteria, as well as specialised bacteria such as colourless sulphur bacteria, which interconvert the various forms of the element (Bowker, 2002). Heterotrophic bacteria depend upon organic sources of carbon, whereas autotrophs are able to utilise carbon dioxide from the atmosphere.

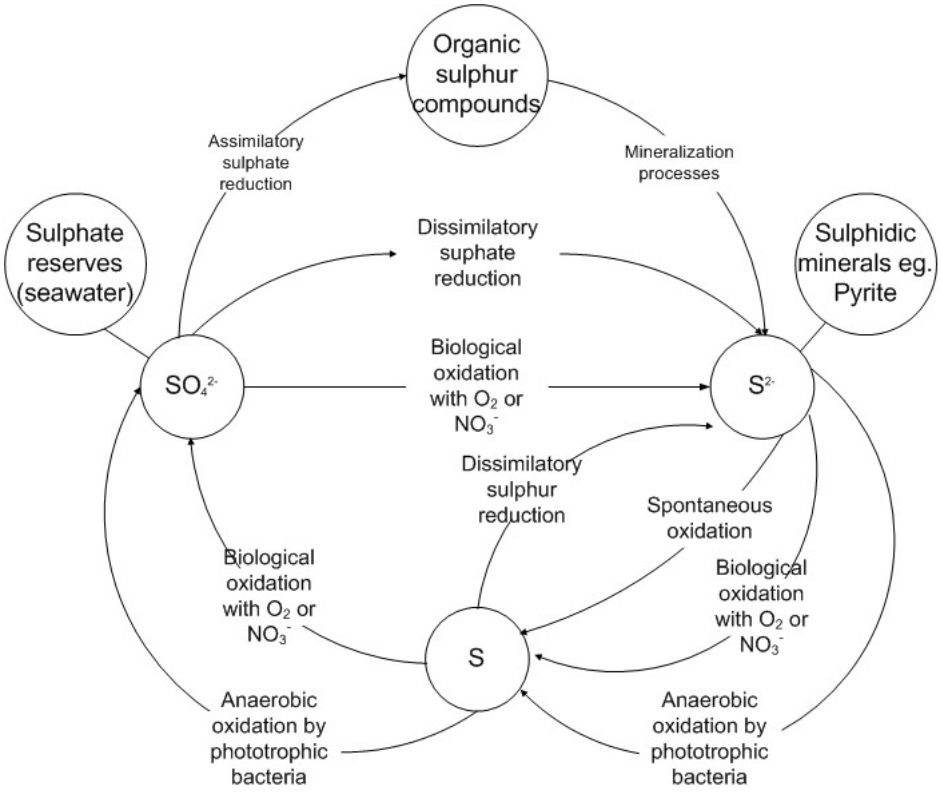


Figure 3.4: The sulphur cycle (Robertson and Kuenen, 1992)

Most sulphide that accumulates within the environment is formed due to sulphate reduction by sulphate reducing prokaryotes. Bacteria such as *Desulfuromonas*, *Desulfovibrio* and *Desulfotomaculum* conduct dissimilatory sulphate reduction using SO_4^{2-}, $S_2O_3^{2-}$, SO_3^{2-}, $S_2O_4^{2-}$ and S^0 as a terminal electron acceptor instead of oxygen. The heterotrophic SRP are obligately anaerobic organisms and derive energy from simple organic compounds such as pyruvate or lactate; whilst the autrotrophic SRP rely on CO_2 and oxidation of H_2 (Oyekola, 2008; Lens & Kuenen, 2001). Thereafter, sulphide oxidising bacteria (SOB) oxidise the sulphides to a range of products.

Sulphide oxidising bacteria are chemoautotrophic and obtain their energy from the oxidation of sulphur compounds. Sulphide oxidising bacteria can be divided into two main groups viz. photosynthetic sulphur bacteria and colourless sulphur bacteria. Photosynthetic sulphur bacteria use sulphide as the electron donor, CO_2 as the carbon source and the reaction is powered by light (Molwantwa, 2008). Colourless sulphur bacteria generally oxidise sulphide to sulphate, generating more metabolically useful energy that is obtained by partial oxidation to S^0 (Lens & Kuenen, 2001). In order to obtain sulphur as a product, sulphide oxidation must occur under stringent conditions, such as high sulphide loads, controlled redox potential and pH. These governing factors will be discussed in depth in the upcoming sections.

3.4.2 Ratio of sulphide to oxygen

In order to suppress sulphate production (reaction 3.22 & 3.23) and promote sulphur formation the ratio of sulphide to oxygen must be strictly controlled. According to reaction stoichiometry two moles of sulphide would be required to one mole of oxygen (reaction 3.21). Sulphate formation is preferred (by SOB) to the formation of elemental sulphur as it yields four times the energy (van den Bosch, 2008).

$$2HS^- + O_2 \rightarrow 2S^0 + 2OH^- \, \Delta G^o = -169.35 \, kJ/mol \tag{3.21}$$

$$2S^0 + 3O_2 \rightarrow 2SO_4^{2-} + 2H^+ \tag{3.22}$$

$$HS^- + 2O_2 \rightarrow SO_4^{2-} + H^+ \Delta G^o = -732.58 \, kJ/mol \tag{3.23}$$

According to Buisman et al. (1990a), in order to minimise sulphate production the sulphide load must be in excess than that of the oxygen concentration. Therefore the ratio of sulphide to oxygen should be 2:1 or higher (reaction 3.21). Janssen et al. (1995) demonstrated that when the oxygen supply was increased four-fold reaction 3.23 was favoured.

Stefess (1993) and the groups of Buisman et al. (1990a) and Janssen et al. (1998) all concurred that the sulphide loading rate is an important factor in determining the sulphur production and sulphide oxidation rate; and that a substantial increase in sulphide concentration would inhibit sulphate formation. Additionally the ratio of sulphide to oxygen should be 2:1 or slightly higher. However, the sulphide loading must be controlled as an excessively high sulphide loading would inhibit microbial activity and thus affect sulphide oxidation(Buisman et al., 1991).

3.4.3 Effect of chemical sulphide oxidation on biological sulphide oxidation

A high sulphide loading rate and high sulphide to oxygen ratio is necessary in order to favour elemental sulphur production . However, this can lead to thiosulphate formation via chemical sulphide oxidation. Under oxygen limited conditions the specific biological activity drops, due to a lack of oxygen. Consequently, chemical sulphide oxidation becomes more prominent, resulting in a large amount of sulphide being converted to thiosulphate (Janssen et al., 1995; Buisman et al., 1990a). Furthermore, the tendency toward thiosulphate formation is increased at low oxygen concentration, exceedingly high sulphide concentration (10 $S_{tot}{}^{2-}$: 1.1 O_2) and a alkaline pH 8 (Buisman et al., 1990a; Janssen et al., 1995; van den Bosch et al., 2008; van den Bosch, 2008). Hence, the formation

of thiosulphate is inevitable, however if the ratio of sulphide to oxygen is maintained between 2:1 to 2.33:1 it can be minimised.

Gonzalez-Sanchez and Revah (2007) showed that the chemical oxidation of sulphide to sulphide intermediates has a positive effect on biological sulphide oxidation, until the sulphide concentration becomes too high ($>$ 3 mM). A high inlet sulphide and low biomass concentration results in the inhibition of biomass growth and biological sulphide oxidation. The formation of polysulphides and sulphide intermediates also increased biological activity by decreasing the sulphide toxicity. Nonetheless, this was for a particular alkaliphilic sulfoxidising bacterial consortium within an alkaline environment (pH $>$ 9) and might not be true at a neutral pH.

3.4.4 Biologically produced sulphur

Elemental sulphur is the element with the largest number of allotropes. Currently there are 30 well characterised sulphur allotropes (Steudel & Eckert, 2003). The most common and stable allotropes are homocyclic non-polar molecules. This also gives sulphur its hydrophobic nature and very low solubility in water (5 μg/L) (van den Bosch, 2008). Biologically produced sulphur can be stored as globules within the cell or excreted as globules. In 1887, Winograndsky detailed how living cells such as *Beggiatoa* could contain amorphous sulphur inclusions, which would then disappear once H_2S became limiting. Furthermore, he postulated how these amorphous inclusions would crystallise once the cells died (Kleinjan & de Keizer, 2003). This was proven via X-ray diffraction (XRD), which showed that fresh sulphur globules were amorphous in nature, existed at the submicron scale and were extremely hydrophilic. It was concluded that the particles have high colloidal stability due to biological surface-active polymers/proteins which are secreted by the bacteria (Janssen et al., 1999; Kleinjan & de Keizer, 2003). It is assumed that these polymers play a role in the formation of larger sulphur aggregates, by sterical and electrical stabilisation of the colloidal particles (van den Bosch, 2008).

3.5 Polysulphide formation and its impact on sulphide oxidation

Inorganic polysulphides ($S_n{}^{2-}$) play an important role in sulphur chemistry. They occur as green-yellowish to orange coloured aqueous solutions and were first described by Carl Scheele in 1777 (Lens & Kuenen, 2001). Polysulphides are produced by the oxidation of aqueous hydrogen sulphide at an alkaline pH. The hydrogen sulphide reacts with inorganic or organic sulphur (Kamyshny et al., 2004; Lens et al., 2000). Polysulphide anions comprise (x-1) zerovalent sulphur atoms (S^0) and one sulphide atom of divalent state (S^{2-}) (x = chain length, 2 $<$ x $\leq$6) (van den Bosch, 2008).

$$HS^- + S_8 \rightleftharpoons HS_9^- \rightleftharpoons S_9^{2-} + H^+ \tag{3.24}$$

$$S_9^{2-} + HS^- \rightleftharpoons 2S_5^{2-} + H^+ \tag{3.25}$$

$$2S_5^{2-} \rightleftharpoons S_4^{2-} + S_6^{2-} \tag{3.26}$$

The reaction of hydrogen sulphide and elemental (S_8) sulphur forms a polysulphane, which may dissociate to form a long chain polysulphide and proton (reaction 3.24). The reaction is initiated by the strong nucleophile (HS^-) which causes the S_8 ring to open and form the polysulphane (Kleinjan et al., 2005b; Steudel, 2003a). The nine 'S' polysulphide chain thereafter reacts further with hydrogen sulphide to form two polysulphides of chain length five which then dissociate into shorter polysulphide ions. van den Bosch (2008) found that under mildly alkaline conditions and in equilibrium with excess inorganic sulphur the average polysulphide chain length (x) varies from 4.39 - 5.5 which corresponds to reactions 3.24-3.26

$$S_2^{2-} + S_8 \rightleftharpoons S_{10}^{2-} \tag{3.27}$$

Polysulphide ions are stronger nucleophiles than HS^- and thus are also capable of opening an S_8 ring. The presence of polysulphides has been found to accelerate the dissolution of elemental sulphur (Kleinjan et al., 2005b). This (reaction 3.27) occurs at a much faster rate than reaction 3.24 (Steudel, 2003b) but only occurs under alkaline conditions (pH > 9.47). Chen and Morris(1972) found that polysulphide ion oxidation occurred more rapidly than sulphide oxidation and therefore polysulphide ions were found to act as a catalyst to sulphide oxidation.

Polysulphides can also be oxidised to thiosulphate and zero-valent sulphur. It was confirmed that the polysulphide oxidation followed the reaction stoichiometry (3.28) in the pH range 7 - 9. Elemental sulphur is sometimes observed, if the average sulphur content x > 2 (as per reaction 3.28) (Kleinjan et al., 2005a).

$$S_x^{2-} + \frac{3}{2}O_2 \rightarrow S_2O_3^{2-} + (x-2)S^0 \tag{3.28}$$

$$HS^- + (x-1)S^0 \rightleftharpoons S_x^{2-} + H^+ \tag{3.29}$$

Lastly, polysulphide formation may also occur via reaction 3.29, under natron-alkaline conditions. Essentially they are formed via the reaction between sulphide and biologically produced sulphur particles (S^0). Kleinjan et al. (2005b) determined that reaction 3.29

occurred at pH 8 and at temperatures 30°C to 50°C. Furthermore, it was determined that polysulphides formed in this reaction have an autocatalytic effect on the reaction rate.

Therefore, sulphide chemistry is extremely complex with the possibility of multiple reactions occurring simultaneously to produce various oxidation products. Nonetheless, these are controlled closely by pH and redox potential.

3.5.1 Redox potential

The oxidation-reduction potential (ORP) of an aqueous solution is determined by its tendency to either accept or donate electrons and is a result of the proportion of the oxidised and reduced forms of all dissolved compounds. Therefore the tendency for a molecule to donate/accept electrons is expressed by its E_h value, which is expressed relative to the standard hydrogen electrode (SHE) (van den Bosch, 2008). Figure 3.5 shows that only -2, 0 and +6 oxidation states are stable in water. The Pourbaix diagram clearly shows the various forms of sulphur species at different pH and redox potentials. From the diagram it's also evident that the possibility of sulphur formation occurs within a very large pH range (0-8) and ORP window (Kelsall & Thompson, 1993). Practically, this window is influenced by the sulphide and polysulphide concentration as well as the sulphide to oxygen ratio. Additionally, the microbial consortia will only be able to oxidise sulphide to sulphur within a narrow pH range.

As stated earlier the pH of the reactor liquid plays a critical role in the distribution of the total sulphide concentration. In a sulphur-producing bioreactor, sulphide and polysulphide concentrations are in equilibrium, or very close to equilibrium. At pH < 9.17 the majority of the sulphide concentration (S^{2-}) is present as HS^-. If the pH > 9.17 majority of the sulphide concentration is present as polysulphides ($S_x{}^{2-}$, x ≥ 2) and S^{2-}. Therefore, there exists an equilibrium at pH $= 9.17$, as described by the following expression (van den Bosch, 2008):

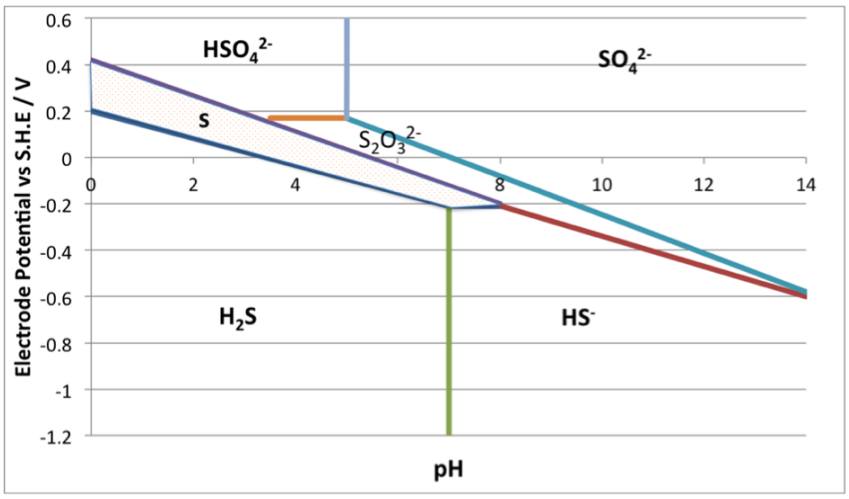


Figure 3.5: Potential-pH diagram for a sulphur/water system at 298.15K

In systems where biologically produced sulphur is present the ORP is primarily a function of the polysulphide concentration, which is determined by the total sulphide concentration and pH. As a result the ORP increases for decreasing pH values, provided the total sulphide concentration remains constant. Therefore the theoretical ORP of a solution versus a standard H_2 electrode potential can be thermodynamically be calculated and related to pH and total sulphide concentration via the following equations (van den Bosch, 2008):

$$S_x^{2-} + xH_2O + (2x-2)e^- \rightleftharpoons xHS^- + xOH^- \tag{3.30}$$

The general equilibrium equation 3.30 and the Nernst equation can be combined to form an electrode potential equation (equation 3.32):

$$E_h = E_h^0 - \frac{R.T}{n.F} \times ln\frac{\Pi_j[red]^{n_j}}{\Pi_i[ox]^{n_i}} \;\; (Nernst - Equation) \tag{3.31}$$

$$E = E^0 - \frac{R.T}{n.F} \times ln\frac{[HS^-]^x[OH^-]^x}{[S_x^{2-}]} \tag{3.32}$$

$$K_x = \frac{[S_x^{2-}][H^+]}{[HS^-]} \times \frac{\gamma_{S_x^{2-}}\gamma_{H^+}}{\gamma_{HS^-}} \; with\, pK_a = 9.17,\; x \geq 1 \tag{3.33}$$

Combining the above equation 3.32 with the equilibrium constant (reaction 3.33), the following equation (3.35) relates ORP to pH and Sulphide_{total} :

$$[Sulphide_{total}] = [HS^-] + [S_x^{2-}] \tag{3.34}$$

$$ORP = E^0 - \frac{R.T}{(2x-2)F} \times ln\left(\frac{10^{-14}}{K_x}\right)^x - (x-1)\frac{R.T}{(2x-2)F} \times ln\left(\frac{[S_{tot}].K_x}{K_x + 10^{-pH}}\right) \tag{3.35}$$

Therefore if there is stringent control on the redox state of the solution, it is possible to oxidise sulfide to elemental sulphur by creating an oxygen-limiting environment and a sulphide to oxygen ratio (2.63 : 1) (Janssen et al., 1998).

3.6 Biofilms

Since the 1980's biofilms have become a focal point in the field of water and wastewater treatment as well as biotechnology. A biofilm is defined as a matrix-enclosed bacterial population adherent to each other and/or to surfaces or interfaces (Costerton et al., 1995). Microbial biofilms are often involved in the biocorrosion of steel piping, due to SRPs and sulphide oxidising bacteria. Localised corrosion is caused by the formation of anaerobic

zones, due to metabolic oxygen consumption, under the biofilm, while the adjacent surface, without a biofilm, remains aerobic. Consequently, an anode is formed under the biofilm and the adjacent area becomes cathodic, resulting in dissolution of the metal (Sand & Gehrke, 2003).

Biofilms have also been identified within bioleaching systems and environments. The attachment process to the mineral sulphide surface is largely mediated by an EPS layer. The chemical reactions occur outside of the cells, but still within the EPS-generated microenvironment. Bioleaching is essentially an interfacial process that takes place within this particular microenvironment, which is created by exopolymers and iron (III) ions to form the EPS layer (Sand & Gehrke, 2006). Bacteria will initiate biofilm development within an aquatic system if there are sufficient nutrients available for cell replication, as well as extracellular polymeric substance (EPS) production (Costerton et al., 1995; Lazarova & Manem, 1995). Thereafter the bacteria adhere to the surface, undergo phenotypic change (which alters many of its structural molecules) and derepress EPS synthesis (Costerton et al., 1995), leading to the development of a microcolony. The microcolony is a basic unit of biofilm growth and these combine to form a biofilm. One of the most important fundamental characteristics of bacterial biofilms is their capacity for focussed and cooperative proliferation. If a particular cell is unable to replicate (due to lack of suitable substrates) it may simply remain dormant, entrapped within the biofilm until conditions improve. Alternatively, if a neighbouring cell is able to provide the substrate, it will utilise the neighbouring cell's by-products. It is these symbiotic relationships and metabolic cooperativity that produces extremely complex and heterogeneous biofilms, with vastly intricate metabolic networks (Lappin-Scott & Costerton, 1995; Costerton, 2000).

Microbial growth and life within a biofilm is very different to that of planktonic life forms. Bacteria may also form biofilms as a stress response to environmental conditions. This stress could be physical forces, such as shear forces produced by water flow, nutrient deprivation or the presence of toxic compounds that are inhibitory to bacterial growth (Jefferson, 2004). Additionally, the biofilm matrix provides a safe-haven from predation, which is a common threat from bacterial predators such as amoebae (Costerton, 2007).

3.6.1 Biofilm structure

Biofilms form intriguing microbial systems within the aquatic environment with characteristic internal architecture. In essence, bacteria produce EPS to facilitate attachment to the substratum, but also the formation and maintenance of the biofilm structure and resistance to environmental stresses. From previous studies (Costerton, 2007; Lawrence et al., 1991; Purevdorj-Gage & Stoodley, 2004; Purevdorj-Gage, 2004; Stoodley et al., 2000) it is shown that biofilms are not flat uniform structures, but rather highly complex heterogenic films; consisting of voids, channels, pores, cell clusters and layers. The biofilm may be made up of thick flat biomasses, organised mushrooms or thin filamentous

streamers. It has been hypothesised and observed that the biofilm structure is not a random formation of bacterial cells, but rather an arrangement determined to maximise the influx of nutrients. It is also influenced by a diverse range of physical, chemical and environmental factors which affect the adaptation and growth of the organisms (Costerton et al., 1995). Studies show that different populations are restricted to well-defined depth intervals within the biofilm (Lappin-Scott & Costerton, 1995; Bowker, 2002). Therefore, the structured distribution of various microbial populations within the biofilm is dependent on their role within the general microbial community. The general principle within a microbial community is that the end products of metabolism by one population are utilised as a resource by another. Biofilms therefore may be considered as micro-ecosystems wherein different microbial strains and species efficiently work together for the general well being of the bacterial community. As mentioned earlier the biofilm does consist of voids and pores which facilitate transport of nutrients and water. Therefore the internal structure of the biofilm plays a key role in the mass transport within the film which shall be explained in section 3.6.2. Biofilms are generally attached to a solid substrate, to provide anchor points and encourage proliferation. However, biofilms may also form on the liquid surface.

3.6.1.1 Extracellular polymeric substance

One of the key factors in the biofilm structure is the extracellular polymeric substance (EPS). Chemically, EPS is composed of a combination of polysaccharides, proteins, lipids, humic and nucleic acids (Purevdorj-Gage, 2004; Stoodley et al., 2002b). Extracellular polymeric substances are essentially the matrix of which the biofilm is comprised and gives a biofilm its structural complexity and integrity. Flemming et al. (2007) described EPS as the "housing of biofilm cells", as it determines the immediate living environment of biofilm cells, by affecting porosity, density, water content and mechanical stability. Hentzer et al. (2001) showed they could induce structural complexity in an otherwise flat undifferentiated wild-type (non-mucoid) *P. aeruginosa* biofilm, by over expression of alginate. Alginate is a principal component of EPS and is required for structural development (Nivens et al., 2001). However, the biofilm structure may also be influenced by hydrodynamics, as unidirectional flow and high shear will cause the biofilm cell clusters to become long and filamentous. Flemming et al. (2000) proposed a possible mechanism behind the increase in mechanical strength due to high shear. They hypothesised that the biofilm stretches at higher shear, causing individual polymer strands to become physically aligned, allowing hydrogen bonding to occur between neighbouring polymer molecules. Additionally, divalent cations (Ca^{2+}, Mg^{2+}) increase the electrostatic forces, which can help maintain and strengthen the biofilm matrix. Nonetheless, it's still unclear if the increased mechanical strength of biofilms exposed to high shear stresses are regulated at the genetic level or are determined by physical mechanisms (Stoodley et al., 2002b). EPS is also produced within biofilms to provide the sessile cells with protection from antimicrobial agents or predators and to cause cell aggregation (Stoodley et al., 2002b; Purevdorj-Gage,



Figure 3.6: Occurrence of a floating sulphur biofilm on a high-organic load sulphidic tannery pond in Wellington, South Africa (Molwantwa, 2007)

2004).

3.6.1.2 Floating biofilms - Formation theory

Most literature has focussed on biofilms which arise from colonisation of solid-liquid interfaces, such as submerged biofilms. However, there are occurrences of floating biofilms in nature. Floating biofilms have been observed on the surface of highly sulphidic tannery wastewater ponds (Figure 3.6) (Molwantwa, 2008).

Floating biofilms are similar in nature to biofilms that are attached to a substrate. The air-liquid interface of an open body of water is an ideal substrate for the development of a biofilm, as there is easy access to gaseous oxygen and nutrients within the liquid medium. The air-liquid interface is an attractive site for aerobic organisms. The biofilms formed by these organisms, remain at the air-liquid interface mainly due to the hydrophobic nature of the organisms rather than their buoyancy (Spiers et al., 2003). All surfaces possess physiochemical characteristics, which may influence the adsorption and attachment of bacteria and inevitably the development of a biofilm. The DLVO theory, originally formulated by Derjaguin & Landau (1941) and Verwey & Overbeek (1948), equates electrostatic forces and London-van der Waals forces active at the surface, with the propensity for colloidal attraction and adhesion (Lappin-Scott & Costerton, 1995). It is generally represented by equation 3.36:

$$V_T(L) = V_A(L) + V_R(L) \tag{3.36}$$

The total interaction energy (V_T) of a particle, as a function of its separation distance (l) from the substrate, is the sum of the van der Waals attraction force (V_A) and the electrostatic interaction (V_R). The theory predicts that there are two regions where particle attraction may occur, when L $\leq$ 1 nm or 10 nm $\geq$ L $\geq$ 5 nm. These points in space are known as the primary and secondary minimum respectively, and between these

two positions, the surfaces (bacterium and substratum) experience maximum repulsion (Lappin-Scott & Costerton, 1995). This electrostatic repulsion is primarily due to the fact that the substratum and bacterial cell surface are negatively charged. In this particular case the water surface is negatively charged, which is further exacerbated by the influence of the electrolytic strength of the aqueous medium. If the medium has a high concentration of cations (sodium, calcium, aluminium) and anions (acetate, sulphate, sulphide); this will cause an increase in the ionic strength of the solution including the surface tension of the water, even though it is still 'dilute'. Weissenborn & Pugh (1996) found that there was a substantial increase in surface tension of water with sodium acetate, magnesium and sodium sulphate (dilute) solutions. This is beneficial as a high surface tension leads to an increase in bacterial adhesion, thus facilitating floating biofilm formation.

The DLVO theory is popular as a theoretical model. However there are discrepancies between observed and predicted results. The most commonly used (alternative) theory is the surface free energy theory, for describing the surface tension of a surface. This theory is best explained in terms of system free energy. If the total free energy of the system is reduced by cell contact with a surface, then adsorption of the cell to the substratum will occur (Absolom et al., 1983; Lappin-Scott & Costerton, 1995). Therefore, if the free energy function (ΔF_{adh}) decreases, then bacterial adhesion will be favoured. A thermodynamic free energy balance may be developed on the basis of interfacial free energies:

$$\Delta F_{adh} = \gamma_{bs} - \gamma_{sl} - \gamma_{bl} \tag{3.37}$$

ΔF_{adh} is the free energy of adhesion, γ_{bs} is the interfacial free energy and γ_{bl} is the bacterial-liquid interfacial free energy. Young's equation (3.38) describes the relationship between contact angle and interfacial energies of the involved phases; therefore if the contact angle is measured then the free energy of adhesion can be determined (Lappin-Scott & Costerton, 1995).

$$\gamma_{sv} - \gamma_{sl} = \gamma_{lv} cos\vartheta \tag{3.38}$$

Absolom et al. (1983) were able to show that the the adhesion of bacteria from aqueous suspensions to polymeric substrata, followed the thermodynamic model to a considerable extent. Furthermore, the determination of the extent of adhesion of bacteria to polymeric substrata provided a method for determination of the surface tension of the various bacterial species. The bacteria studied were hydrophilic with surface tensions in the range of 0.03 - 0.06 N/m. The surface tension of water in contact with air is approximately 0.072 N/m at 25°C (Perry & Green, 2008). Therefore, the greater upward force of the water's surface tension, which is increased due to the high concentration of dissolved ions, should cause the bacterial floating biofilm to be supported at the air-liquid interface.

3.6.2 Mass transport and mass transfer limitations

The mass transport to and within the biofilm, with respect to sulfide and oxygen will play an important role in the biological oxidation of sulfide. In biofilms at steady-state, a continuity equation (3.39) has been found to be a comprehensive model and provide an accurate description of the nutrient concentration profiles within the biofilm. Equation 3.39 equates biofilm activity with internal mass transport, assuming constant effective diffusivity and constant biofilm density (Beyenal & Lewandowski, 2002).

$$D_f \frac{d^2C}{dz^2} = \frac{\mu_{max} C X_f}{Y_{x/s}(K_s + C)} \tag{3.39}$$

However, due to the FSB constantly growing and the diffusivity possibly changing due to the amount of sulphur deposited within the FSB, this equation would not be valid in representing the mass transport through a floating sulphur biofilm. Beyenal & Lewandowski (2002) described the rate of nutrient and sulphide transport to the biofilm may be quantified by linking the convective external mass transfer rate to the diffusive mass transport rate across the biofilm interface. Assuming there is no, or negligible, substrate consumption in the bulk solution, the flux of dissolved substrates must be conserved. Therefore, the external transfer rate ($k_1(C_b - C_s)$) and internal mass transfer rate ($D_f(\frac{dC}{dz}) \mid_{z=L_f}$ must be equal at the biofilm surface. Hence, the flux of substrates into the biofilm at the surface is:

$$N_s = k_1(C_b - C_s) = D_f \frac{dC}{dz} \mid_{z=L_f} \tag{3.40}$$

However, once again this equation is suited to a particular biofilm that is fully submerged and not at an air-liquid interface. Due to the heterogeneous nature of the FSB and the many conduits, the following proposed equation and idealistic model will represent the movement of oxygen downwards into the FSB. However, the concept of equation 3.40 will be followed. The movement of sulphide and nutrients upwards will not be considered. The flux of oxygen through the laminar gas-film is represented by the right-hand side of equation 3.41, which occurs over a distance of δ_G. The flux of oxygen through the FSB is represented by the equation on the left-hand side and occurs over the thickness of the FSB. This is best represented by Figure 3.7, which depicts the mass transport of oxygen through the floating sulphur biofilm and shows how both flux equations are equal.

$$N_{O_2} = -D_f \frac{\partial C_{O_2}}{\partial y} \ldots \{FSB\}; \quad N_{O_2} = (N_{O_2} + N_{N_2})Y_{O_2} - D_f \frac{P}{RT} \frac{\partial Y_{O_2}}{\partial y} \ldots \{Gas - film\} \tag{3.41}$$

Mass transport within a biofilm is greatly affected by the hydrodynamics of the system. According to de Beer et al. (1996) the mass transfer boundary layer was parallel to

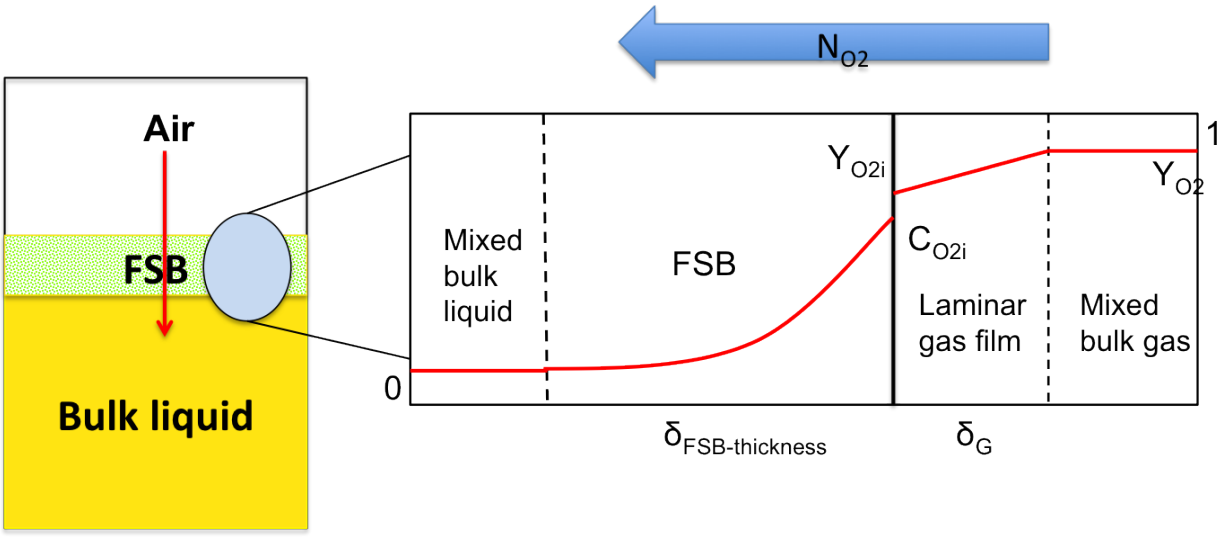


Figure 3.7: Simplified schematic diagram of the LFCR with an FSB and air penetrating the FSB (left-hand side). The right-hand side is an expanded view of the air-liquid interface, rotated 90 degrees to the right. Depicted is the bulk gas layer, laminar gas film, FSB layer and bulk liquid layer. Additionally the change in dissolved oxygen concentration gradient across all layers is shown. The diagram is not to scale and neither is the dissolved oxygen concentration profile.

the substratum at low velocities, however at higher velocities (>0.04 m/s) the boundary layer closely followed the irregular biofilm surface. Moreover the voids within the biofilm enhanced the mass transfer rate and product exchange with the bulk liquid by facilitating convection when the velocity was high to ensure the boundary layer was close to the biofilm surface. It was also demonstrated how an increase in the velocity decreased the mass transfer boundary layer above the voids and cell clusters. The oxygen concentration was much greater within the void at a higher velocity (de Beer et al., 1996).

A biofilm consists of cell clusters and voids which form a network of channels and allows the lateral movement of fluid within the biofilm. The oxygen distribution is strongly associated with the biofilm structure. de Beer et al. (1994b) demonstrated that oxygen was supplied to the cell cluster through the cell cluster-liquid interface. The largest gradient existed at both the cell cluster - pore interface and the cell cluster - bulk liquid interface. It was also determined that the flux from the void to the cell cluster and from the bulk liquid to the cell cluster, was of the same order of magnitude, provided the mass transfer boundary layer was thin. However, the conduits below the cell clusters facilitated oxygen transport in the horizontal direction.

The flow velocity at which the biofilm is cultivated also plays an important role in the internal structure of a biofilm. Beyenal & Lewandowski (2002) determined that the flow velocity affected the nutrient transport rate as well as the mechanical pliability of the biofilm structure. When the velocity was too high the biofilm increased its mechanical

strength to resist shearing. As a result the density increased and ultimately lead to a less porous structure, where the internal mass transfer rate was significantly reduced.

Therefore it will be the aim of this investigation to ascertain to what extent mass transport limitations affect sulphide oxidation within the floating sulphur biofilm.

3.7 Microbial ecology

The Integrated managed passive treatment system is essentially comprised of two units. The first unit the DPBR, has a sulphate reducing microbial community to perform the process of sulphate reduction under anaerobic conditions. Additionally, there is a mixed microbial community capable of anaerobic digestion to hydrolyse and metabolise the organic packing materials. The background and literature to SRPs will be presented in Chapter 9 together with the literature on the sulphate reduction process. The second unit, the LFCR has a sulphur oxidising mixed microbial community capable of converting the dissolved sulphides to sulphur, sulphate or thiosulphate.

3.7.1 Sulphur oxidising Prokaryotes

Reduced inorganic sulphur compounds (HS^-, S^0, ${S_2O_3}^{2-}$, ${SO_3}^{2-}$) are oxidised by prokaryotes and the major oxidation product is sulphate. There are a diverse range of sulphur-oxidising prokayotes, including photoautotrophs such as green sulphur bacteria (GSB) of the genus *Chlorobium* or the purple sulphur bacteria families *Chromatiaceae* or *Ectothiorhodospiraceae* (Syed et al., 2006; Hell et al., 2008) (Table 3.4). These particular species generally inhabit freshwater, marine or hypersaline habitats. Blooms of purple and green sulphur bacteria usually occur several metres below the surface, at the chemocline and are not visible at the water surface. These species are able to oxidise reduced sulphur species as they are able to fix carbon dioxide and perform photosynthesis under anoxygenic conditions (equation 8.2). The green sulphur bacteria contain bacteriochlorophyll c or d, which acts as the light harvesting pigment. They are strictly anaerobic and obligately phototrophic. In the presence of sulfide and CO_2, only acetate and pyruvate are assimilated as organic carbon sources (Imhoff, 2004). Henshaw and Zhu(2001) demonstrated the ability of *Chlorobium thiosulfatophilum* to convert hydrogen sulphide to elemental sulphur in a continuous-flow photobioreactor. The sulphide removal efficiency was found to be 82 - 100% at sulphide loading rates of 111 - 328 mg/L.h. Sulphur globules are formed as the oxidation product which may be stored within the cells (*Chromatiaceae*) or excreted as sulphur globules (*Ectothiorhodospiraceae*). These two particular families are able to grow photoautotrophically or photoheterotrophically.

$$CO_2 + H_2S \rightarrow 2S^0 + H_2O + CH_2O \tag{3.42}$$

Table 3.4: Summary of various sulphur oxidising prokaryotes, both photoautotrophs and chemolithotrophs. (Dworkin et al., 2006a; Imhoff, 2004; Lens et al., 2000)

Proteobacteria	Family	Genus-species	Sulphur species
- - -	Chlorobiaceae*	Chlorobium limicola, Chl. phaeobacteroides, Chl. thiosulfatophilum	HS^- and S^0 to SO_4^{2-}
		Pelodictyon luteolum	HS^- and S^0 to SO_4^{2-}
α	Purple non-sulphur*	Rhodobacter sphaeroides, Rhodospirillum rubrum	HS^- and S^0 to SO_4^{2-}
		Rhodopila palustris	HS^- and $S_2O_3^{2-}$ to SO_4^{2-}
β	Hydrogenophilaceae	Thiobacillus denitrificans, T. thioparus	HS^-, S^0, $S_2O_3^{2-}$, $S_4O_6^{4-}$ to SO_4^{2-}
γ	Chromatiaceae*	Chromatium buderi, Chr. okenii, Chr. weissei, Chr. vinosum	HS^- and S^0 to SO_4^{2-}
		Thiospirillum winogradskyi	HS^- and S^0 to SO_4^{2-}
		Thiocapsa halophila	HS^-, S^0 and $S_2O_3^{2-}$ to SO_4^{2-}
	Ectothiorhodospiraceae	Halorhodospira sp.	HS^-, S^0 and $S_2O_3^{2-}$ to SO_4^{2-}
	Thiotrichaceae	Beggiatoa sp.	HS^- and $S_2O_3^{2-}$ to SO_4^{2-}
		Thioploca sp.	HS^- to SO_4^{2-}
	Acidithiobacillaceae	Acidithiobacillus ferrooxidans	HS^-, S^0, $S_2O_3^{2-}$, $S_4O_6^{4-}$ to SO_4^{2-}
		Acidithiobacillus thiooxidans	HS^-, S^0, $S_2O_3^{2-}$, $S_4O_6^{4-}$ to SO_4^{2-}
		Acidithiobacillus caldus	HS^-, S^0, $S_2O_3^{2-}$, $S_4O_6^{4-}$ to SO_4^{2-}

The second group of sulphur oxidisers are commonly known as colourless sulphur bacteria. These particular prokaryotes are chemolithotrophs and comprise an extremely large, heterogeneous collection of bacteria. These prokaryotes were termed "colourless" due to a lack of photopigment, while still able to oxidise sulphide to sulphur or sulphate. Table 3.4 lists the families and genera which have been traditionally regarded as colourless sulphur bacteria. In addition to inorganic sulphur compounds, some species are able to gain energy from the oxidation of other inorganic compounds, such as ferrous iron (*Acidithiobacillus ferrooxidans*) or hydrogen. Although most sulphur-oxidising bacteria require oxygen, some are able to grow anaerobically and utilise nitrate as an electron acceptor during denitrification (*Thiobacillus denitrificans*) (Dworkin et al., 2006a).

Thiobacillus denitrificans has an optimum temperature of 25 - 30°C and is able to oxidise sulphur species using nitrate as an electron acceptor (facultative anaerobic chemolithotroph). Cardoso et al. (2006) demonstrated that *Thiobacillus denitrificans* was capable of oxidising sulphur, sulphide and thiosulphate to sulphate, whilst degrading nitrate at rates of 0.8, 1.65 and 7.56 mM NO_3^-/day. It was proposed that the slow degradation rate with sulphur was possibly due to the limited mass transfer of substrate from the solid phase (S^0). Furthermore, the addition of acetate (0.5 mM) improved the rate of denitrification and sulphur oxidation.

$$S^0 + 1.2NO_3^- + 0.4H_2O \rightarrow SO_4^{2-} + 0.6N_2 + 0.8H^+ \; \Delta G = -547.6\, kJ/reaction \quad (3.43)$$

$$S_2O_3^{2-} + 1.6NO_3^- + 0.2H_2O \rightarrow 2SO_4^{2-} + 0.8N_2 + 0.4H^+ \; \Delta G = -765.7\, kJ/reaction \quad (3.44)$$

Colourless sulphur bacteria are located in various environments, such as thermal springs, wastewater treatment plants, soda lakes, freshwater or marine sediments. Organisms such as *Beggiatoa sp.* and *Thioploca* have been located in various marine sediments. In general *Beggiatoa* prefer microoxic habitats at the interface of a reduced sulphur source, typically sulphide, and oxygen or nitrate which act as electron acceptors. *Beggiatoa* mats have been shown to develop seasonally and transform the bottom sediment from a nitrate sink to an ammonia source, due to nitrate reduction (Dworkin et al., 2006b). *Beggiatoa* and *Thioploca* both have a filamentous morphology and have been noted to store sulphur as inclusions within the cell, especially in activated sludge systems.

3.8 Research motivation

Numerous passive and semi-passive systems have been designed to treat acid rock drainage. Investigations aimed at improving the efficiency and effectiveness of passive treatment

systems have been performed. The primary areas of concern include: acidity removal (Skousen & Ziemkiewicz, 2005; Whitehead et al., 2005), metal removal (The International Network for Acid Prevention, 2009; Fu & Wang, 2011; Gazea et al., 1996), choice of substrate and choice of reactor configuration (Ziemkiewicz et al., 2003; Skousen & Ziemkiewicz, 2005; Johnson & Hallberg, 2005b).

Due to the broad nature of passive treatment systems, this research will focus primarily on biological sulphate reduction and biological sulphide oxidation reactors. Biological sulphate reduction systems have been well researched with regard to the aforementioned sections. However, this has been done exclusively for batch, continuous stirred tank reactor (CSTR) and upflow anaerobic sludge blanket (UASB) reactors, while for passive treatment systems it has been either an anaerobic wetland or packed bed reactor. The few studies specific to packed bed reactors have not been comprehensive and many unknown variables, with regard to choice of substrate and packing materials still persist. Studies have been inconclusive or unsuccessful with respect to predicting the biodegradability of complex organic substrates, as well as long-term performance of these reactors (Zagury et al., 2007). Therefore, an extensive literature review on these systems, as well as the experimental results will be presented in Chapter 9.

With respect to the sulphide oxidation unit, various studies on biological sulphide oxidation have been conducted, but are largely confined to active treatment systems. These active systems were either up flow channel, membrane or gas-lift reactors (Table 3.5). Hurse and Keller (2004a; 2004b) reported a sulphide removal of 50% at a loading rate up to 1.74 mg/L.h. Similarly, Kobayashi et al. (1983) was able to achieve a sulphide removal efficiency of 95% at a low sulphide loading rate of 1.27 mg/L.h. Henshaw & Zhu (2001) achieved a higher sulphide removal of 100% at a loading rate of 111 mg/L.h and a sulphur recovery of 95%, whilst Basu et al. (1996) achieved results of a similar nature. All these systems were able to remove sulphide efficiently. However they required a large amount of energy in the form of light and a large surface area. Hurse and Keller (2004b), Henshaw & Zhu (2001) and Kobayashi et al. (1983) demonstrated sulphide removal rates of 2.23, 5.1 and 0.5 - 0.8 g/(m^2.day) respectively. The amount of sulphide removed per unit of radiant energy was 1.47 g/(W.day), 0.62 g/(W.day) and not determined (n.d.) respectively. In essence, these systems are able to remove sulphide quite effectively, although they do require a large amount of energy and surface area. Such systems would not be feasible over a long period of time in treating ARD.

Chemotrophic systems were also developed with significantly greater removal rates and efficiencies. Krishnakumar et al. (2005) demonstrated a sulphide removal efficiency of 100% at a sulphide loading rate of 312 mg/(L.hr) in a fluidised bed reactor, whilst Janssen et al. (1997) achieved 90% efficiency at a higher loading rate of 583 mg/(L.hr) within a similar setup. Both systems were able to recover the sulphur product at a yield of 90 and 80% respectively. These active systems are extremely robust as they are able to handle a high sulphide loading rate, however such systems would not be suitable for an ARD long-term

Table 3.5: Performance of different biological sulphide oxidising systems reported in literature

Scale	Sulphide in Wastewater/gas	Reactor Type	Sulphide concentration (mg/L)	Sulphide loading rate (mg/L.h)	Sulphide removal (%)	Sulphur recovery (%)	Reference
Phototrophic systems							
Lab	Wastewater	Fixed film - Continuous flow	154	111	100	95	(Henshaw & Zhu, 2001)
Lab	Wastewater	Fixed film - Upflow	16	0.59 - 1.27	95	n.d.	(Kobayashi et al., 1983)
Lab	Gas	Suspended - CSTR	25000 ppm	94.4	100	99	(Basu et al., 1996)
Lab	Gas	Suspended - CSTR	69.3	61	100	n.d.	(Kim et al., 1991)
Lab	Wastewater	Fixed - Biofilm	2.7 - 24.6	0.191 - 1.74	50	n.d.	(Hurse & Keller, 2004a)
Chemotrophic systems							
Lab	Wastewater	Suspended solids - Upflow	448	9.17	99	52.7	(Mahmood et al., 2008)
Lab	Wastewater	Sludge bed reactor	240	583	90	80	(Janssen et al., 1997)
Pilot	Wastewater	Attached	60 - 240	n.d.	70	60 - 90	(Buisman et al., 1993)
Lab	Gas	Immobilised - Downflow biofilter	100 - 4000 ppm	1500 - 140 000	99	$< 10\%$	(Rattanapan et al., 2009)
Lab	Wastewater	Fluidised bed	240	312 - 1250	100 - 90	90 - 60	(Krishnakumar et al., 2005)
Pilot-scale	Wastewater	Membrane bioreactor	300 - 860	n.d.	n.d.	79	(Vannini et al., 2008)

treatment system. This is due to the fact that ARD streams, or partially treated ARD streams have a low sulphide loading. Additionally, treatment systems will be located in remote (rural) regions, where there is a lack of infrastructure and electricity. The concept of utilising dissolved metals to remove dissolved sulphides from BSR effluent is not possible, due to the low concentration of iron and manganese within the ARD waste streams, there will always be a metal deficit .

Ergo there is a need for investigation into passive sulphide oxidation systems. Pulles, Howard & de Lange conducted a few preliminary studies, however, they were unable to provide the fundamental information with regard to hydrodynamics, residence time, organic loading rate and sulphur speciation from chemical and biological sulphide oxidation in the LFCR. Furthermore, the system was not optimised for sulphur recovery. Additionally there was insufficient data on floating sulphur biofilms with regard to the microbial community, how they are formed and influenced by reactor conditions and the mass transport of oxygen through the biofilm. Therefore, subsequent studies were conducted at EBRU at Rhodes University (Molwantwa, 2008). Following these studies was the preliminary investigation at GARL which, highlighted further deficiencies in the understanding of the fundamental processes occurring within the LFCR.

Due to the LFCR being a new and novel reactor design one cannot utilise kinetic data sets which are obtained within perfectly mixed CSTR/batch reactors. Therefore a comprehensive study is required to understand the fundamental processes, in order to optimise the reactor for an integrated managed passive treatment system for ARD treatment.

3.9 Research Strategy

The research presented in this thesis formed part of a larger study on the IMPI process, funded by the Water research commission (WRC project K5 1834). Initial LFCR and biofilm studies were conducted (Chapter 2) to assess the viability of the technology. Additionally, a basic oxygen mass transport model was developed, to determine the required surface area for a given sulphide removal efficiency, based on simplified assumptions. Therefore, the broad aim of this research was to gain fundamental understanding of this particular ARD passive treatment process and the underlying chemical, biological and physical processes. Additionally, to improve the engineering design of the process, such that it was more efficient with regard to sulphide oxidation and recovery of solid sulphur. This was achieved through a series of experimental studies on the LFCR and the DPBR.

Based on the author's interpretation of the initial work done at GARL, a hydrodynamics study was conducted to determine the mixing patterns within the LFCR (Chapter 6). The analytical methods were developed concurrently with the design and construction of

the improved LFCRs (Chapter 4). Sulphide oxidation kinetics (abiotic and biotic) were investigated under standard conditions (Chapter 7). Biological LFCR experiments were conducted to assess the effect of residence time and organic loading (Chapter 8), based on the biotic experiments in Chapter 7. The findings from the biological LFCR experiments led to the study of the preceding unit, the DPBR (Chapter 9). It was identified that the performance of the LFCR was dependent on the consistent release of soluble organic compounds, in the form of VFAs, from the DPBR. Hence, a study on DPBR performance and organic carbon flux was conducted. In addition, the effect of low molecular weight phenolic compounds was investigated, as it was suspected that the possible release of these compounds during hydrolysis of the complex carbon, could lead to inhibition of biological sulphate reduction. Concurrently, a preliminary study was conducted to assess the microbial diversity within the treatment system described in Chapter 8. The strategy is graphically summarised in Figure 3.8. The research hypotheses are presented in the following section, which will be addressed in the subsequent chapters of this thesis.

3.10 Research hypotheses

1. The linear flow channel reactor has extremely laminar fluid flow with the hydraulic regime being stratified and largely governed by diffusional mass transport.

2. The biofilm structural integrity and sulphur content of the biofilm increases with a decrease in residence time and increase in organic loading to an optimum; above which the biofilm becomes primarily organic and system performance is compromised.

3. The rate of sulphide oxidation within the biofilm is mass transfer controlled with the mass transfer coefficient being controlled by biofilm thickness.

4. A packed bed reactor column, packed primarily with lignocellulosic materials, is less suitable than a mixture primarily of organic waste materials, over a long-term (> 6 months), with regard to sustained release of dissolved organic carbon (volatile fatty acids), for an efficient biological sulphate reduction process.

Key questions will be presented at the beginning of each respective chapter.

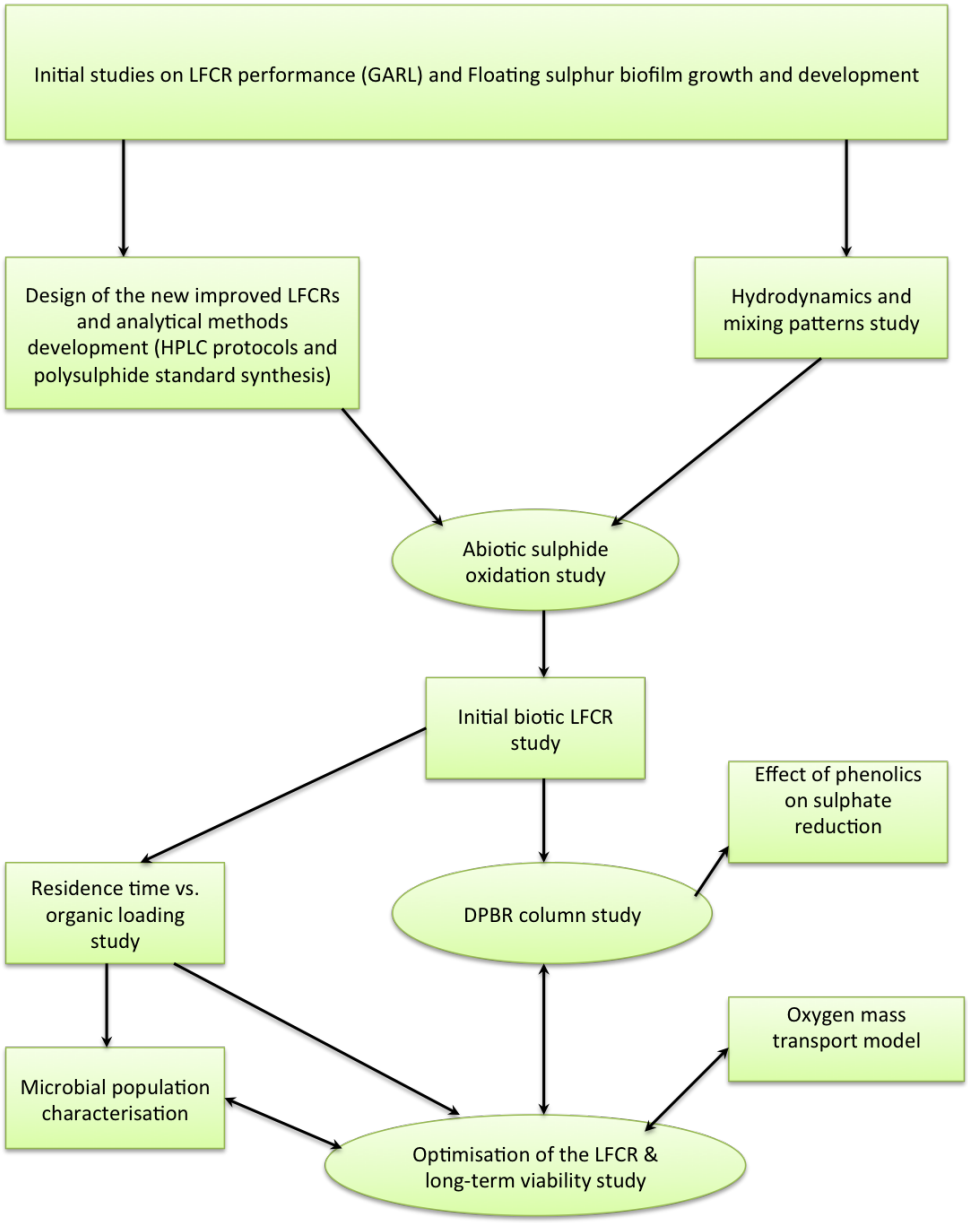


Figure 3.8: Illustration of the research strategy adopted in this work

Chapter 4

Reactor design & Analytical methods development

4.1 Introduction

Following the analysis of the preliminary studies at Golder Associate Research laboratories, the LFCR was redesigned to facilitate a more rigorous monitoring programme and allow the study of hydrodynamics. A further limitation of the work at GARL was the inability to close the sulphur balance, largely due to the inability to quantify the intermediate species. The development of the analytical techniques to achieve this are described in this chapter.

4.2 Linear Flow Channel Reactor Design (LFCR)

The redesigned LFCR reactor is detailed in Figures 4.1-4.4. The entire length (2.5 m) was drawn as three separate sections, in order to accurately show the placement of the holes for the cylindrical baffles. The LFCR had a total volume of 37.5 L. Ideally it was operated with a working liquid volume of 25 L and a headspace of 12.5 L. The LFCR lid was fitted with a silicon gasket to ensure no loss of hydrogen sulphide gas. The reactor was fitted with three inlet and outlet ports to allow for the testing of various liquid depths. The drain valve allowed for easier drainage and cleaning of the reactor. Twenty blind holes were positioned on the the reactor floor to allow for the placement of cylindrical baffles (1 cm and 3 cm diameter). Various configurations were tested to try to increase the mixing and turbulence within the reactor (Chapter 6). Lastly, 15 sampling ports on the right-hand side wall were designed to allow for sampling of the bulk reactor fluid. Each port was fitted with a taper stud and a molded thermogreen LB-2 GC septum (9.5 mm diameter) disc. This ensured multiple samples could be withdrawn using a syringe fitted with a hypodermic needle. The LFCRs were constructed from perspex to allow for easy visualisation of the mixing patterns and subsurface phenomena.

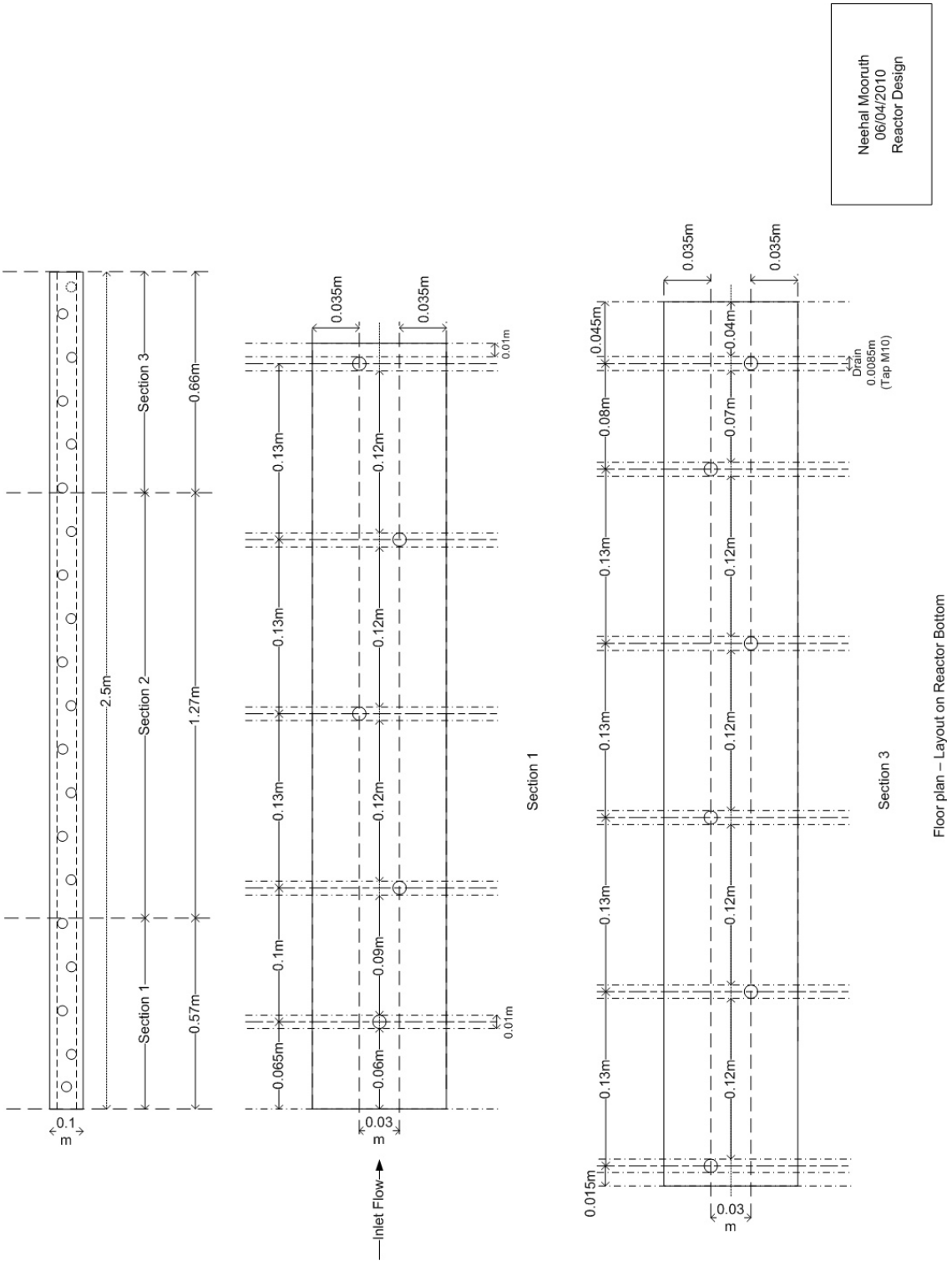


Figure 4.1: Floor plan view of the LFCR unit with the entire length being drawn as three separate sections showing the necessary lengths and spacings of the cylindrical holes for baffle placement

The following figure represents the floor plan view of section 2 of the LFCR unit.

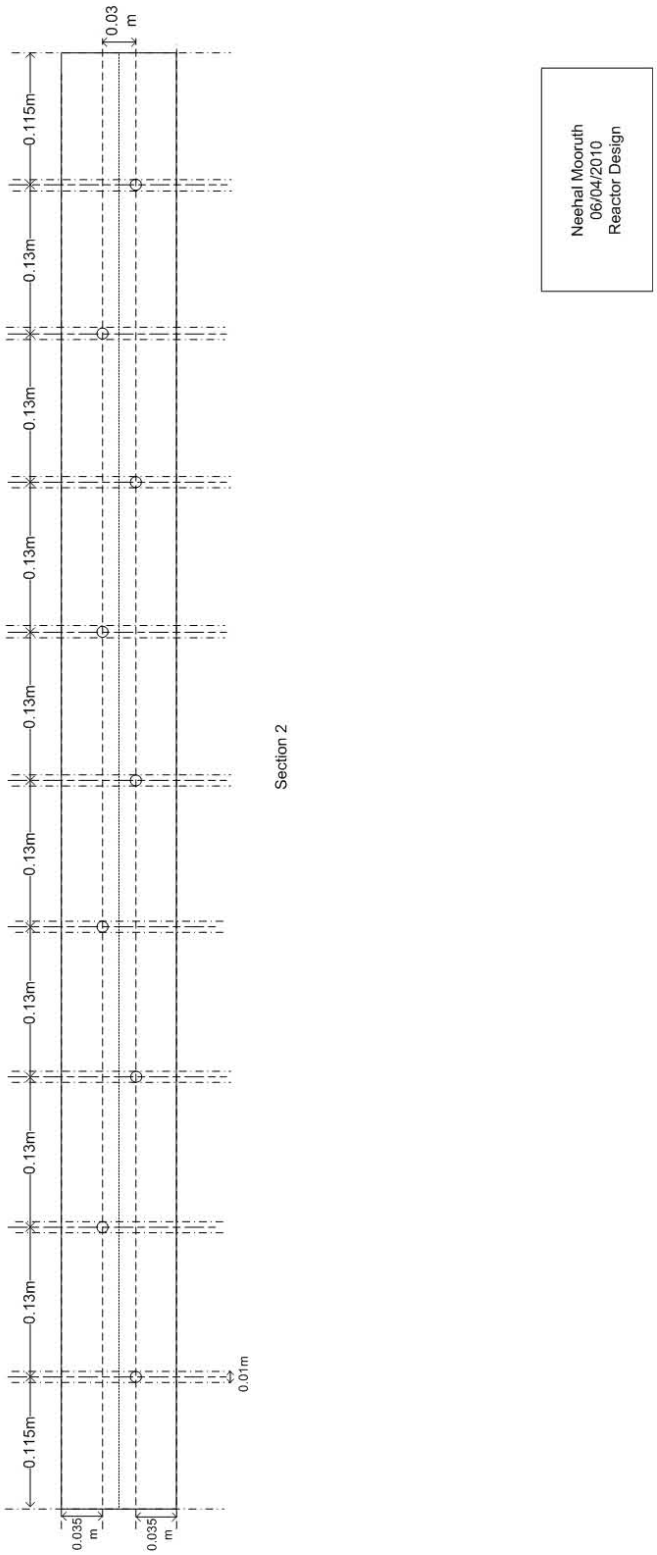


Figure 4.2: Floor plan view of section 2 of the LFCR unit showing the necessary lengths and spacings of the cylindrical holes for baffle placement

The following figure represents the front view of the front and rear wall of the LFCR unit.

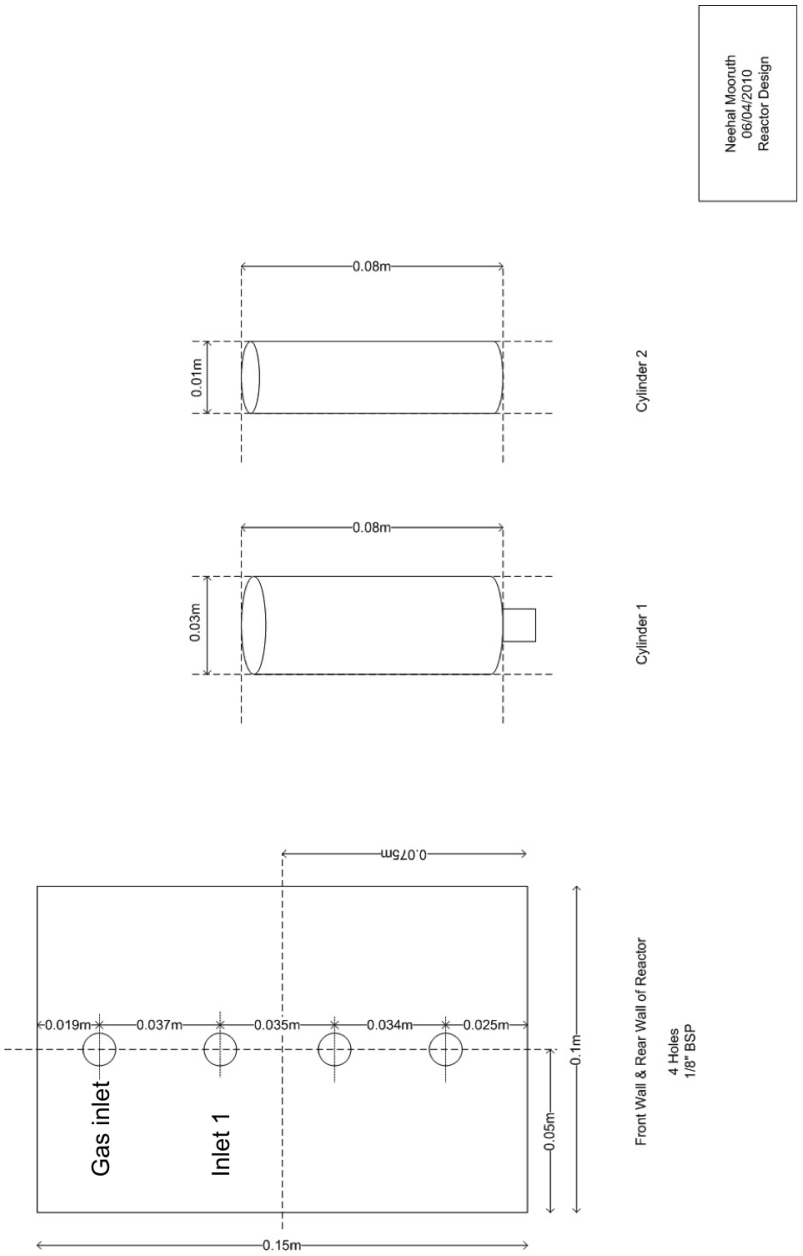


Figure 4.3: Schematic drawing of the front and rear wall of the LFCR with 3 liquid inlet/outlets (Top inlet = Inlet 1) and a gas inlet/outlet; additionally two cylindrical baffles represented.

The following figure represents the front view of the right-side wall of the LFCR unit.

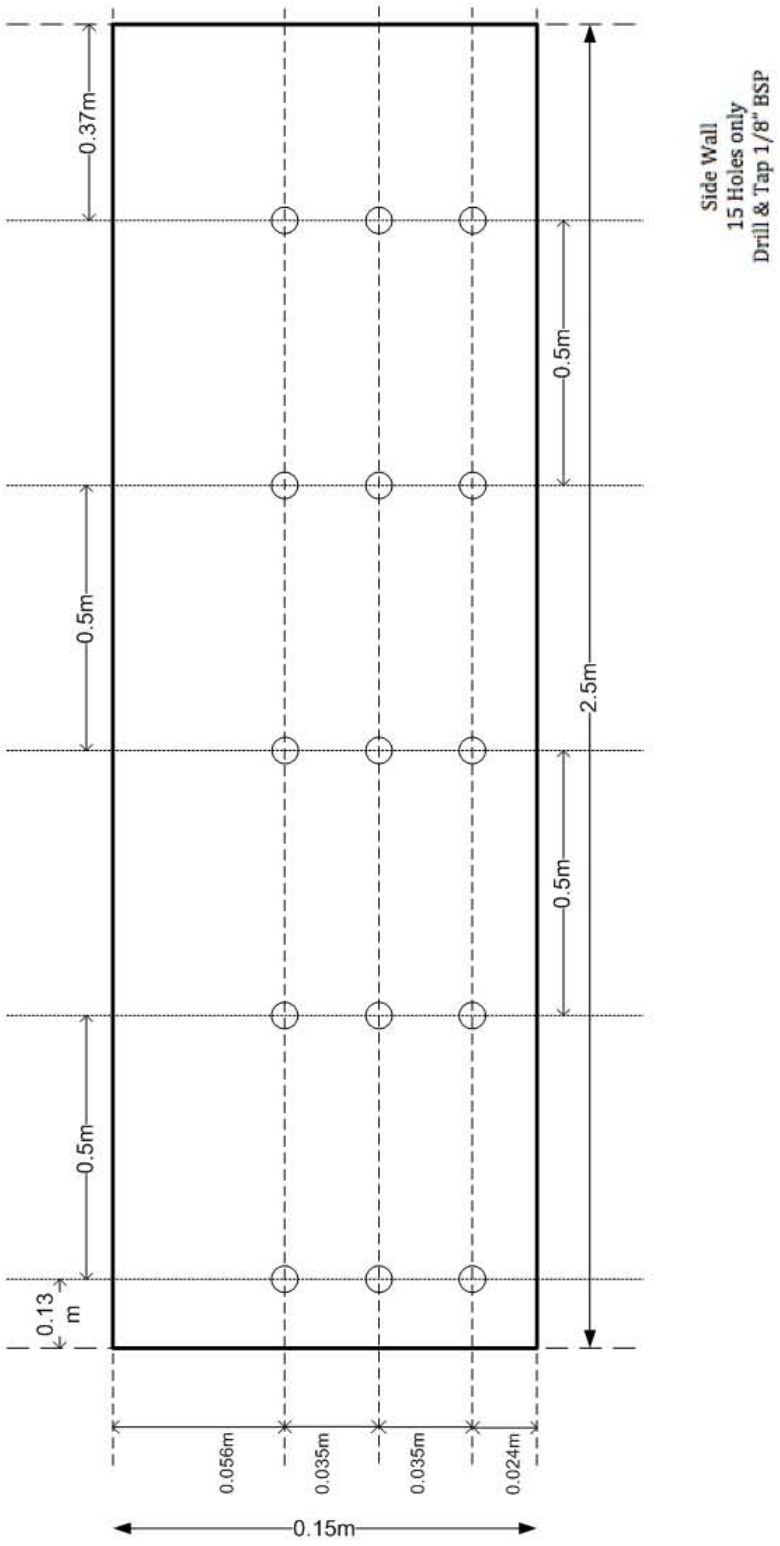


Figure 4.4: Schematic drawing of 15 sampling ports on the sampling side wall of the LFCR

4.3 Polysulphides Assay development

4.3.1 Introduction

Polysulphides occur in the form of a yellowish-green aqueous solution, absorb radiation in the UV region and are produced by the oxidation of hydrogen sulphide solutions at a basic pH. They are represented by the following formula: S_n^{2-}

A number of methods have been developed to determine the order and concentration of polysulphides in solution. Giggenbach (1972) was able to measure absorbance bands in the electronic range over a wide alkaline pH range and concluded that the maximum 'n' is 5. Hence, higher polysulphide chain lengths were not detected. Furthermore, Boulegue and Michard(1978) showed that the maximum average length of a polysulphide chain was 4.86 with a standard deviation of 0.36. Therefore, it was reasoned that a hexasulphide also existed within the aqueous solution but was not measured. Later studies postulated that there were hexasulphide and higher polysulphide chains, however they were unable to measure or show the existence of the compounds. Subsequently, Kamyshny et al. (2004) developed a novel approach to determine inorganic polysulphide disproportionation patterns by rapid one-phase chemical methylation with methyl trifluorromethanesulfonate (methyl triflate). The method was based on the reaction of methyl triflate with polysulphides, much the same way short-life radicals are captured by radical traps and this reaction follows equation 4.1.

$$S_n^{2-} + 2CF_3SO_3CH_3 \rightleftharpoons (CH_3)_2S_n + 2CF_3SO_3^- \tag{4.1}$$

However, methyl triflate is immiscible in water so the rate determining step is the phase transfer of methyl triflate to the aqueous phase. If this step is not sufficiently fast it could allow for the redistribution of the polysulphides prior to the derivatization process completing. Kamyshny et al. (2004) showed that in order to bypass the phase transfer step and increase the available methylating agent for the reaction, it should be carried out in a water-methanol medium. Additionally, it was shown that homogenous derivatization is much faster than disproportionation, thus the dimethylpolysulphide distribution that is formed in this process reflects the initial distribution of polysulphides. Disproportionation reactions (Reaction 4.2) will occur due to the addition of methanol.

$$\sum_{i=1,n} \nu_{i,water} S_{i,water}^{2-} \rightarrow \sum_{i=1,n} \nu_{i,water-methanol}^{w} S_{i,water-methanol}^{2-} + \nu_{S_8}^{w} S_{8,s} \tag{4.2}$$

$$CF_3SO_3CH_3 + H_2O \rightleftharpoons CF_3SO_3^- + CH_3OH + H^+ \tag{4.3}$$

Equation 4.1 is also accompanied by the hydrolysis of methyl triflate (reaction 4.3) which, leads to a pH change and subsequent destruction and disproportionation of polysulphides, especially at pH < 10. Therefore, the water-methanol method preparation strategy, in conjunction with phosphate buffer, was adopted (Kamyshny et al., 2004, 2006).

Due to polysulphides not being commercially available from any manufacturer (Sigma Aldrich, Merck), standards needed to be synthesised according to the following protocol. A list of all the required apparatus can be found in Appendix A. Due to the previous studies not providing an explicitly accurate account of the synthesis procedure, the following protocol was developed via a trial and error approach. It is based on the work done by Kamyshny et al. (2003) and Pearson & Robinson (1931).

4.3.2 Standard synthesis - K_2S_5

4.3.2.1 Experimental Procedure

The following experiment was carried out within a glovebox in order to prevent the oxidation of the potassium hydrosulphide product. The glovebox was flushed with nitrogen three times in order to ensure there was no oxygen present. The absence of oxygen was verified using a Resazurin (1 g/L) solution. Potassium was utilised as the alkali metal and 2 g was weighed out. The liquid paraffin was dried off before adding the metal to Erlenmeyer flask 2 containing 30 mL of absolute dry ethanol.

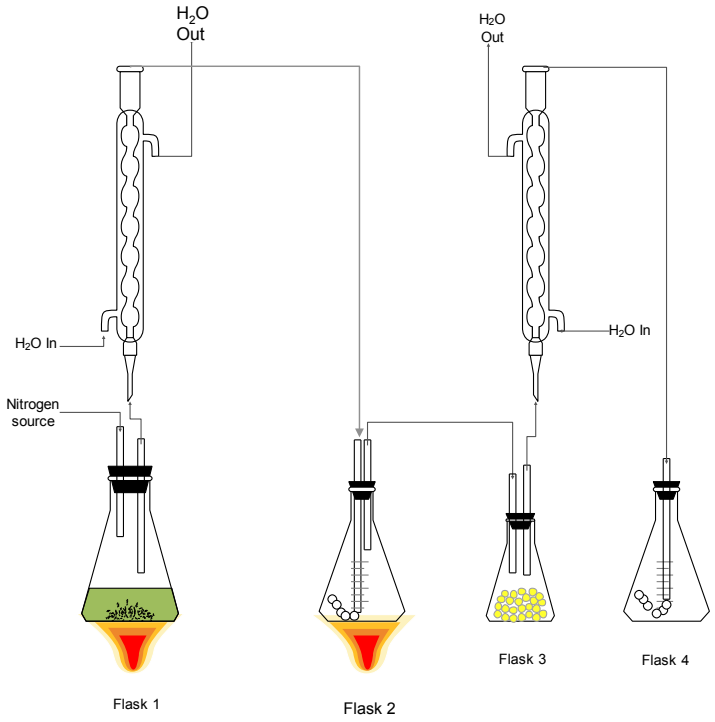


Figure 4.5: Diagrammatical representation of the polysulphide standard synthesis apparatus



Figure 4.6: Photograph of the polysulphide standard synthesis apparatus

Reaction 4.4 occurred in the flask with a large amount of heat being released. The flask

was swirled gently to ensure no potassium particles stuck to the sides.

$$K + C_2H_5OH\,(excess) \rightarrow C_2H_5OK + H^+ + e^- \tag{4.4}$$

Approximately 0.0512 moles of potassium ethylate, (a clear liquid) was formed. It was allowed to cool then the flask was sealed with a stopper and removed from the glove box. Potassium ethylate reacts violently with water and is highly flammable and corrosive. Erlenmeyer flask 2 was attached to the experimental rig (Figure 4.5). Pyrite was added to the concentrated HCl in Erlenmeyer flask 1. Sufficient HCl and pyrite used to ensure the production of enough H_2S (> 0.0512 moles) to fully convert potassium ethylate to potassium hydrosulphide (reaction 4.6).

$$FeS_2 + HCl \rightarrow 2H_2S_{(g)} + FeCl_2 + Fe(OH)_2 \tag{4.5}$$

$$H_2S + C_2H_5OK \rightarrow KHS + C_2H_5OH \tag{4.6}$$

The minimum amount of pyrite required was 3.086 g. However, it was suppled in excess (10X) to ensure rapid production of H_2S (30.86 g). The required amount of HCl was 0.934 g. However, this was also supplied in excess (200 mL, 32%) to produce excess H_2S. Furthermore the HCl was cooled to 5°C (prior to reacting with the pyrite) and thereafter heated to 30°C to prevent the volatilisation of $FeCl_2$ which poisons the product. Condenser 1 ensured that all $FeCl_2$ was condensed out of the vapour emanating from Erlenmeyer flask 1. The water flow rate was 0.67 L/min. The H_2S gas was bubbled into the solution (in flask 2) to convert all ETOK to potassium hydrosulphide (KHS), a white solid. This was achieved by passing nitrogen through erlenmeyer flask 1 and 2 as a carrier gas (450 mL/min). Furthermore, it also ensured that the experiment was conducted under an inert atmosphere. Subsequently, the H_2S supply line was disconnected and replaced with the nitrogen feed in order to ensure the flask (2) headspace remained inert. Thereafter 4 g of pure sulphur powder was added to the solution (reaction 4.7). The solution was boiled for 50 minutes under a nitrogen atmosphere on a heating pad.

$$2KHS + 4S \rightarrow K_2S_5 + H_2S \tag{4.7}$$

The temperature of the heating pad was increased incrementally (5°C) every 10 minutes to ensure that the sulphur did not burn. The solution colour turned from yellow to an orange-red colour at a temperature of 60°C. The longer the solution boils the darker it will become and the longer the polysulphide chain. The water and ethanol from the previous steps were boiled off. These vapours were cooled in the second condenser and trapped in flask 3. This was done to prevent the condensed vapours from re-entering flask 2 and contaminating the product. The cooling water flow rate in condenser 2 was 3 L/min.

Therefore, an intermediate flask (3) with silica gel was necessary, on the vapour outlet. Finally flask (2) was placed in an ice-bath to rapidly cool the solution and precipitate out the K_2S_5 crystals. Vacuum filtration was carried out under a nitrogen atmosphere and the crystals washed with ethanol. The product was dried in a vacuum desiccator with P_2O_5. Subsequently, the product was stored in a vial in the glovebox under a nitrogen atmosphere to prevent degradation.

4.3.3 Standard Synthesis - K_2S_3

4.3.3.1 Experimental Procedure

This was carried out similarly, using the same experimental apparatus described in section 5.2.2, with a few exceptions. Potassium (5 g) was added to the flask with 100 mL of absolute dry ethanol. The potassium was allowed to fully react to form liquid potassium ethylate (ETOK). The solution was halved and each flask (2a and 2b) covered with a rubber stopper. Thereafter flask 2a was connected to the H_2S line. H_2S was bubbled into the solution to convert all ETOK to potassium hydrosulphide (KHS). The H_2S line was disconnected and the nitrogen line connected directly. The solution was boiled for four minutes in order to remove the excess H_2S gas and flask 2a was flushed with nitrogen concurrently. The remaining half of the potassium hydrosulphide solution (flask 2b) was added to flask 2a. Thereafter 4.1 g of pure sulphur powder was added to the solution. The solution was boiled for 30 minutes under a nitrogen atmosphere. The temperature of the heating pad was increased incrementally (5°C) every 10 minutes to ensure that the sulphur did not burn. The solution turned from yellow to an orange colour at the temperature of (50°C). During this time a yellow-orange precipitate (K_2S_3) formed (reaction 4.8). Flask (2a) was placed in an ice-bath to rapidly cool the solution and precipitate the K_2S_3. Thereafter the product was vacuum filtered under a nitrogen atmosphere, washed with ethanol and dried in a vacuum desiccator with P_2O_5.

$$2KHS + 2S \rightarrow K_2S_3 + H_2S \tag{4.8}$$

4.3.4 Polysulphide Standards

The following standard curves were generated using the synthesised standards. Each polysulphide species was quantified by using the internal standard {(1 mM),1,2:5,6-dibenzanthracene ($C_{22}H_{14}$) in 1,4 dioxane}. A range of polysulphide species were detected in each sample. The K_2S_3 sample had predominantly polysulphides of chain length 2 and 3 (Figure 4.7). A possible reason for the higher concentration of S_2 species is the decomposition of S_3 species during the HPLC preparation procedure, which is clearly shown by the outlier at 50% dilution. The K_2S_5 sample had a variety of polysulphides from chain length 5 to 9 (Figure 4.8). However, the most dominant species

was MeS_7. This was probably the most dominant species due to the reaction proceeding for too long at a high temperature of 60°C. However, this analysis clearly shows that a variety of polysulphide species can be formed simultaneously via this synthesis procedure. Furthermore, the retention times (Table 4.1) for polysulphides species of chain length 2 to 11 were plotted and a linear trend was observed. This was not observed by Rizkov et al. (2004) as there was a logarithmic relationship between retention time and chain length. Moreover, the relationship was only applicable for chain lengths two to eight. A possible reason for the difference is that the standard which was synthesised was less prone to disproportionation and more stable with regard to chain lengths greater than eight. The correlation coefficient ($R^2 = 0.978$) indicated an extremely good fit over the range of two to eleven (Figure 4.9), as Rizkov et al. (2004) were only able to achieve an $R^2 = 0.947$. Additionally, the straight line fits for polysulphides of a chain length greater than five have an $R^2 > 0.92$. This clearly shows that the synthesised polysulphide standard was stable even when diluted. A sample HPLC chromatogram showing the polysulphide species is presented in Appendix A.

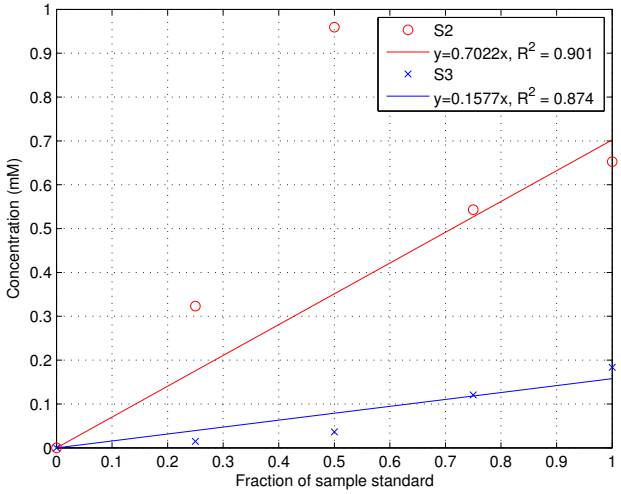


Figure 4.7: Polysulphide sample standard curves for chain length 2 & 3, for a 0%, 25%, 50% and 75% dilution. The S2 50% dilution data point was taken as an outlier.

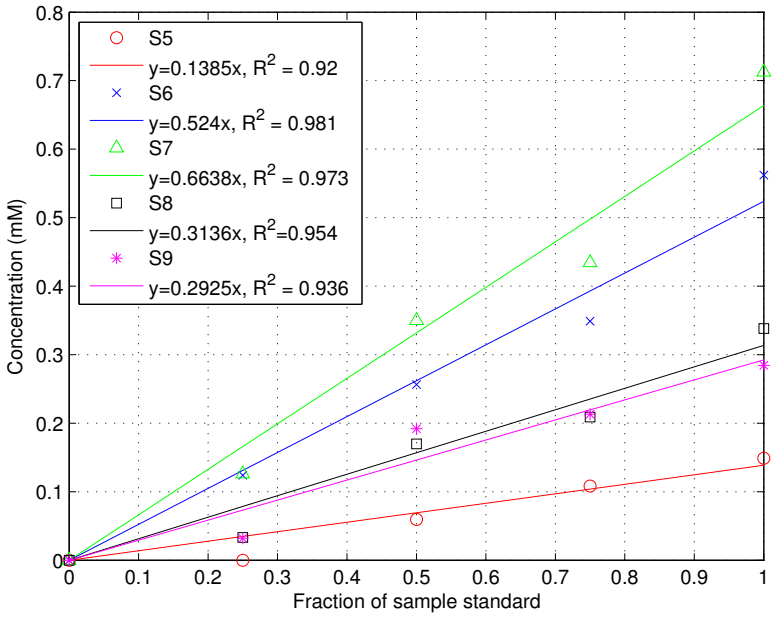


Figure 4.8: Polysulphide sample standard curves for chain length 5-9, for a 0%, 25%, 50% and 75% dilution

Table 4.1: Retention time of each methylated polysulphide species from n = 2 - 11

Species	Retention time (mins)
S_2	5
S_3	9.5
S_4	13
S_5	18
S_6	26
S_7	36
S_8	42.5
S_9	44.5
S_{10}	47
S_{11}	53

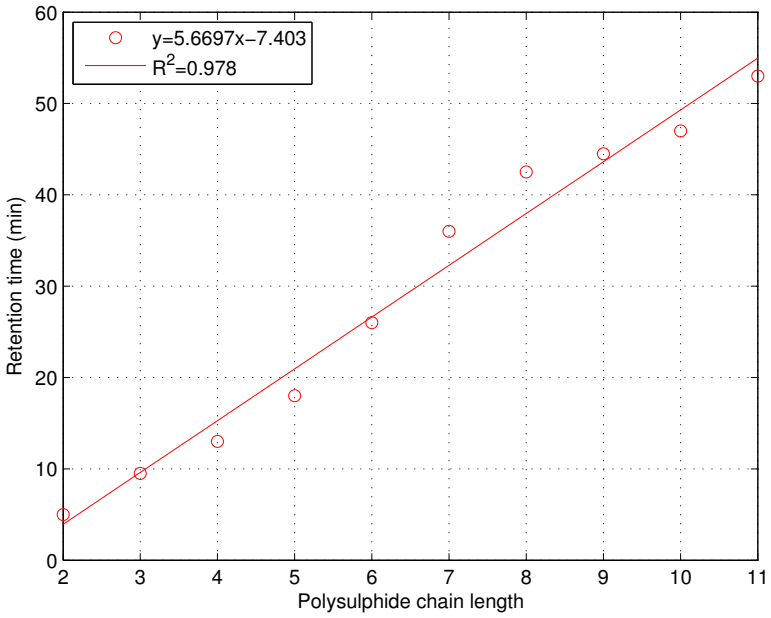


Figure 4.9: Linear trend between polysulphide of chain length (2 - 11) and retention time

4.4 Conclusion

The linear flow channel reactor was redesigned in an effort to improve the hydrodynamic and mixing regime within the reactor. Furthermore, the new design also offered a greater flexibility with regard to sampling and different operating reactor liquid volumes. Perspex was chosen as the material of construction, to gain the ability to observe the biological and chemical phenomena occurring beneath the liquid surface. The 15 sampling ports also allowed for mapping of the various species concentration profiles in the LFCR. Lastly, the improved design also had a sealable gasket lid in order to prevent the escape of H_2S gas to the atmosphere. Therefore, the improved LFCR design should help in determining the viability of the unit with regard to sulphide oxidation in the subsequent chapters. Polysulphides standards were successfully synthesised and a polysulphides synthesis protocol was developed. Together with the HPLC protocol this will provide more information with regard to sulphur speciation following the sulphide oxidation reactions and should facilitate the closure of the sulphur material balance across the LFCR.

Chapter 5

Materials & Methods

Chapter 5 presents the detailed methodologies used during this research. Furthermore the experimental setup and materials will be fully discussed. However, if a particular experiment/study utilised an alternative approach it will be stated at the beginning of its respective chapter.

5.1 Experimental Setup

5.1.1 Degrading Packed Bed Reactor Column

The Degrading Packed Bed Reactor columns were 0.21 m in diameter with a length of 1.0 m. The DPBRs were initially packed by Golder Associates Africa in 2009; and were packed with wattle, blue gum chips, grass and some organic sewage sludge. The columns were repacked in 2011 due to column failure, using a different packing arrangement for column 1 (C1). Column 1 was packed with wood chips, leaf mulch, grass and dry organic activated sewage sludge. Column 2 (C2) was packed with wood chips, grass and wet organic primary sewage sludge (9 g solids/L) The schematic diagrams and preparation protocol are outlined in section 9.9.2. The DPBRs were fed a synthetic AMD feed (Table 5.1) at a flow rate of 3 mL/min:

Table 5.1: Synthetic AMD feed based on Landau colliery effluent after neutralisation with lime. Feed pH was adjusted to pH 6.1 - 6.5.

Component	Concentration (mg/L)	Concentration (mM)
SO_4^{2-}	2000	20.8
Al^{3+}	100	3.7
Ca^{2+}	230	5.8
Fe^{2+}	35	0.6
Mg^{2+}	210	8.6
Mn^{2+}	96	1.7
Na^{+}	8	0.3

5.1.2 Linear Flow Channel Reactor

Studies were carried out using three identical 37.5 L purpose built Perspex reactors. Typically, these were operated with a liquid working volume of 25 L and a headspace of 12.5 L. Air was blown into the headspace at a rate of 48 L/day and exited via the gas outlet port, which then passed through a sodium hydroxide scrubber. Each reactor was sealed with a silicone gasket, which ensured that any sulphide gas liberated was not lost and could be recovered in the sodium hydroxide scrubber. The bio-reactors were operated at room temperature (23 - 25°C) and atmospheric pressure. Two additional, smaller, LFCRs were constructed with a volume 3.75 L. These reactors were primarily utilised for anaerobic studies and for particular biofilm investigations. The reactor drawings are detailed on page 64 - 67. A full layout of the experimental apparatus can be located in Appendix A.

5.1.2.1 Sampling Layout

Figure 5.1 clearly shows all 15 sampling ports and their designated codes. Port number (1,1) is closest to the inlet and is in column 1, row 1, while the port at the back corner (5,3) is in column 5 and row 3. The designated sample port codes are necessary to understand the contour diagrams used throughout the upcoming chapters to show distribution of aqueous species. A 19 gauge needle (8 cm) was utilised to sample the reactor fluid.

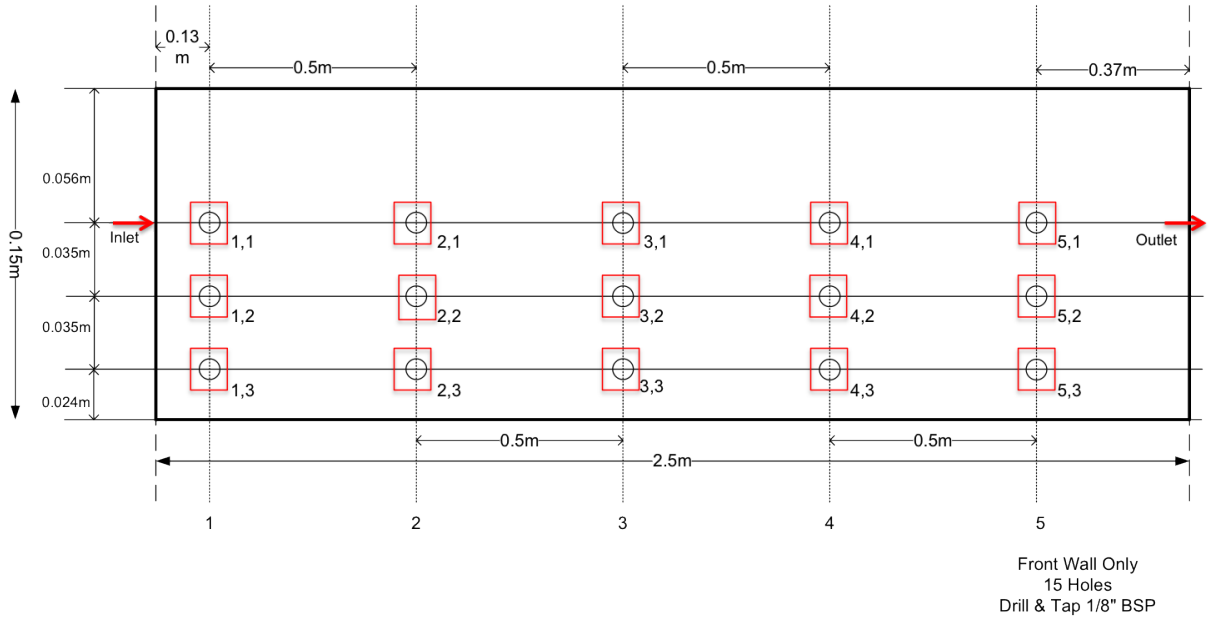


Figure 5.1: Schematic diagram of LFCR front wall with the 15 sampling ports being highlighted & numbered accordingly

5.2 Analytical Methods

5.2.1 Chemical Oxygen Demand (COD)

5.2.1.1 Low concentration range (100 - 1500 mg/L)

Chemical oxygen demand (COD) measurements were carried out using the Merck reagent test protocol. The protocol is based on the oxidation of the sample in a hot sulphuric acid and potassium dichromate solution, containing silver sulphate as a catalyst. Chloride ions are masked by the mercury sulphate in solution A (Merck-Millipore, April 2011). The concentration of residual yellow $Cr_2O_7{}^{2-}$ ions and green Cr^{3+} ions are determined photometrically. In order to determine the COD value of the sample within the low concentration range the following reagents were mixed together within a COD test tube: 0.3 mL COD solution A (Cat No. 114538) 2.3 mL COD solution B (Cat No. 114539) and 3 mL of sample. The cap was screwed on tightly and the solutions mixed by inversion. The COD tube was then heated on a HANNA thermoreactor at 150°C for two hours. After the tube had cooled down (room temperature) the COD concentration was determined spectrophotometrically at 610 nm. A representative COD standard curve was generated using potassium hydrogen phthalate (Appendix A).

5.2.1.2 High concentration range (1500 - 10000 mg/L)

This assay was performed using a similar Merck reagent test protocol. However, COD solution A is manufactured to handle more concentrated samples. In order to determine the COD value of the sample within the high concentration range the following reagents were mixed together within a COD test tube: 2.2 mL COD solution A (Cat No. 114679) , 1.8 mL COD solution B (Cat No. 114680) and 1 mL of sample. The tube was heated as above and the COD determined photometrically.

5.2.1.3 COD - Sulphur

The COD of sulphur (S_8) was determined by adding a known mass of chemical sulphur to the COD test tube in addition to 1 mL of dH_2O and the high concentration range reagents. A standard curve was generated. This assay was conducted to allow the quantification of the contribution of colloidal sulphur in the measured COD values.

5.2.2 pH

All pH testing was conducted using a Cyberscan 2500 micro pH meter. The meter was checked daily and calibrated using Metrohm standard solutions (pH of 4.0, 7.0 & 9.0).

5.2.3 Redox

All redox analyses were done using a Metrohm Redox platinum-ring electrode.

5.2.4 Phenolics - Assay

5.2.4.1 Catechol

The catechol concentration was determined using high performance liquid chromatography (HPLC, Thermo Scientific System). Separation was achieved using an Ascentis RP-Amide (C18) octadecylsilane reverse phase column (15 cm x 4.6 mm, 5 μm), with quantification by UV (210 nm). A mobile phase of 1% glacial acetic acid at a flow rate of 0.5 mL/min was used. The catechol species had a retention time of 11 minutes (Proestos et al., 2006). The sample was centrifuged at 13000 g for 10 minutes. The supernatant was diluted (1:1) with dH_2O and filtered through a 0.22 μm hydrophilic Durapore (PVDF) Millex syringe filter into the HPLC vial. A catechol standard curve (0 - 100 mg/L) was used to calculate the concentration in the experimental samples.

5.2.4.2 Gallic Acid

The gallic acid concentration was determined using high performance liquid chromatography (HPLC, Thermo Scientific System). Separation was achieved using an Ascentis RP-Amide (C18) octadecylsilane reverse phase column (15 cm x 4.6 mm, 5 μm), with quantification by UV (210 nm). A mobile phase of 1% glacial acetic acid at a flow rate of 0.5 mL/min was used. The species had a retention time of 5 minutes (Proestos et al., 2006). The sample was centrifuged at 13000 g for 10 minutes. The supernatant was diluted (1:1) with dH_2O and filtered through a 0.22 μm hydrophilic Durapore (PVDF) Millex syringe filter into the HPLC vial. A gallic acid standard curve (0 - 100 mg/L) was used to calculate the concentration in the experimental samples.

5.2.5 Hydrogen sulphide assay

The soluble dissolved hydrogen sulphide concentration was determined spectrophotometrically at a wavelength of 670 nm (Cline & Richards, 1969). The sample (fully filled tube) was centrifuged at 13000 g for 10 minutes and 20 μL of supernatant was added to 200 μL of zinc acetate (10 g/L) in a test tube. The volume was made up to 5 mL using ultra pure water. Thereafter 500 μL of N,N-dimethyl-p-phenylenediamine hydrochloride solution and 500 μL ferric chloride solution was added consecutively (APHA et al., 2012). This was vortexed for 30 seconds and allowed to fully react in order to produce the methylene blue product. After 10 minutes the absorbance was measured.

The absorbance value was converted to a sulphide concentration using a sulphide standard curve (0 - 1 mg/L).

Standard curve and reagent preparations are shown in Appendix A.

5.2.6 Sulphate assay

The sulphate concentration was determined by HPLC (Waters System), using a Waters IC-Pak HR Anion Column (4.6 x 75 mm, 5 μm) and conductivity detector and. Sodium-borate gluconate was used as the mobile phase at a flow rate of 1 mL/min. A sample injection volume of 50 μL was used. Each sample was run for 12 minutes in order to ensure that the sulphate ion and other ions completely eluted. The samples were prepared by centrifuging at 13000 g for 10 minutes, diluting the supernatant (1:1) with dH_2O and filtering through a 0.22 µm hydrophilic Durapore (PVDF) Millex syringe filter. This ensured the chromatography column was not overloaded due to a high concentration of sulphate (Waters, 2001).

A sulphate concentration standard curve (0 - 10 mM) was generated (Appendix A). The mobile phase preparation procedure is outlined in Appendix A.

5.2.7 Sulphur assay

The sulphur concentration was determined by HPLC (Thermo Scientific System) using a Discovery HS (C18) octadecylsilane reverse phase column (25 cm x 4.6 mm, 5 μm), with detection by UV (263 nm). A sample injection volume of 20 μL was selected. The mobile phase consisted of methanol (95%) and dH_2O (5%) and a flow rate of 2 mL/min for 10 minutes. All samples underwent a rigorous sample preparation. The sample was centrifuged at 13000 g for 10 minutes. A portion of supernatant (200 μL) was dissolved into 1800 μL of chloroform ($CHCl_3$, 100%) in an eppendorf tube. Thereafter it was vortexed for 1 minute in order to mix the colloidal sulphur into the organic chloroform. The eppendorf tube was placed in a water bath (45°C) for 25 minutes to facilitate the dissolution of the colloidal sulphur. Thereafter it was vortexed for an additional 2 minutes. The organic layer was pipetted and filtered through a 0.22 μm Millex nylon syringe filter into the HPLC sample vial (Steudel et al., 1981, 1987; Rethmeier et al., 1997; Bowker, 2002). The samples were kept at a constant 25°C within the HPLC autosampler in order to ensure no chloroform evaporated from the HPLC vial.

A standard curve was generated for the required sulphur range (0 - 7.516 mM). The initial five fold dilution was accounted for within the calculation of the sulphur concentration. It was assumed that all sulphur that dissolved into the chloroform layer was colloidal sulphur. Standard curve and chromatograms are shown Appendix A.

5.2.8 Thiosulphate assay

The thiosulphate concentration was determined by HPLC (Thermo Scientific System) with a UV detector and a Discovery HS (C18) octadecylsilane reverse phase column (25 cm x 4.6 mm, 5 μm). Acetonitrile (20%) and dH_2O (80%) was used as the mobile phase at a flow rate of 1 mL/min for five minutes. A sample injection volume of 20 μL was selected and the thiosulphate species was detected at a wavelength of 230 nm. The sample was centrifuged at 13000 g for 10 minutes and the supernatant diluted (1:1) with dH_2O. The solution was filtered through a 0.22 μm hydrophilic Durapore (PVDF) Millex syringe filter into the HPLC sample vial, which was placed in a glovebox and flushed with nitrogen three times to ensure an inert atmosphere. Tetrapropylammonium (TPA) hydroxide solution (0.005 M) was added (4 μL) and the vial sealed. The vial was removed from the glovebox for immediate HPLC analysis. All samples were kept at a constant 20°C within the HPLC autosampler in order to prevent sample degradation (Steudel et al., 1987; Miura & Kawaoi, 2000).

A standard curve was generated for the required thiosulphate range (0 - 0.1 mM). The initial two fold dilution was accounted for within the calculation of the thiosulphate concentration. Standard curve and chromatograms are shown Appendix A.

5.2.9 Volatile Fatty Acids (VFAs) assay

Acetic, lactic, propionic, butyric, valeric, iso-butyric and iso-valeric acid concentrations were determined by HPLC (Thermo Scientific System). An Ultra-violet (UV) detector and a Biorad organic acids column (Aminex HPX-87H, 30 cm x 7.8 mm, 9 μm) were utilised. Acidified distilled water (0.01 M H_2SO_4) was used as the mobile phase at a flow rate of 0.6 mL/min. A sample injection volume of 100 μL was selected and the VFAs were detected at a wavelength of 210 nm. The sample was centrifuged at 13000 g for 10 minutes and the supernatant filtered through a 0.22 μm hydrophilic Durapore (PVDF) Millex syringe filter. The filtered sample was diluted (1:1) with dH_2O prior to analysis (Biorad, 2012).

A standard curve was generated for the required range (0 - 1 g/L) for each volatile fatty acid. The initial two fold dilution was accounted for within the calculation of the VFA concentration for all samples. Standard curves are shown in Appendix A.

5.2.10 Polysulphides Assay - S_X (x = 2 - 11)

The polysulphide concentration was determined by HPLC (Thermo Scientific System). A UV detector and a Discovery HS (C18) octadecylsilane reverse phase column (25 cm x 4.6 mm, 5 μm) was used. All samples underwent a standard sample preparation procedure. The sample was centrifuged at 13000 g for 10 minutes. Thereafter, 100 μL of

supernatant was mixed with 100 μL (50 mM, same pH as sample) of phosphate buffer, and 800 μL of methanol and filtered through a 0.22 μm hydrophilic Durapore (PVDF) Millex syringe filter into a HPLC sample vial. The vial was placed in a glovebox and flushed with nitrogen three times to ensure an inert atmosphere. An internal standard (10 μL of 1 mM 1,2:5,6-dibenzanthracene ($C_{22}H_{14}$) in 1,4 dioxane) was added along with 4 μL of trifluormethanesulfonate (methyl triflate, CF_3SO_2-OCH_3). The vial was sealed and removed from the glovebox for analysis.

The HPLC separation protocol required a mobile phase flow rate of 0.5 mL/min. Solution A consisted of methanol (100%) that had been filtered (0.22 μm hydrophobic Durapore membrane (PVDF)) and degassed for 20 minutes. Solution B consisted of ultra pure water that was filtered (0.22 μm hydrophilic MF-Millipore membrane) and degassed for 40 minutes. The elution protocol is detailed in Table 5.2

Table 5.2: High performance liquid chromatography elution protocol for the polysulphides assay

Time (minutes)	Concentration (%)
0 - 10	70 $\rightarrow$ 80% A, adjust B accordingly (gradient conditions)
10-25	Isocratic conditions
25-35	80 $\rightarrow$ 100% A, adjust B accordingly (gradient conditions)
35-60	100% A

A sample injection volume of 20 μL was selected and the polysulphide species were detected at a wavelength of 230 nm (Kamyshny et al., 2003, 2004, 2006, 2007; Rizkov et al., 2004). The sample vials were maintained in the HPLC autosampler (AS3000) at 15°C to slow down the rate of degradation and disproportionation of the polysulphide species.

Standard curves are shown and reagent preparations and procedures are outlined in Appendix A.

5.3 Error analysis

Error analysis was conducted on all measurements in order to ensure accurate reporting of the results and observations of all experimental runs, including previous chapters. All HPLC analyses were conducted to an accuracy range of 0 - 0.1%. Standards for the analyte being detected were run at the start, middle and end of the sample set. This allowed for the calculation of the error in the measured concentration. All samples were maintained at a constant temperature within the autosampler, in order to ensure no sample degradation. The HPLC analytical column was conditioned thoroughly before each analytical batch run, and was flushed with mobile phase for 2 minutes between each sample. An example

of a HPLC sulphur standard curve at the start and end of an analytical run is presented in Appendix A (Figure A.14).

5.4 Scanning Electron Microscopy (SEM)

5.4.1 Top-view

All top-view biofilm samples were prepared as follows prior to Scanning Electron Microscopy (SEM). The sample was harvested onto filter paper and fixed using a 1% glutaraldehyde solution for 1 - 2 days, depending on the structural integrity of the biofilm. After fixation the glutaraldehyde solution was removed and the specimen was washed in a 1X phosphate-buffered saline (PBS) solution. The PBS was removed and a dehydration sequence was executed using increasing concentrations of ethanol (30, 50, 75, 90, 95 and 100%). Initially, 3 mL of 30% ethanol was pipetted on top of the filter paper, ensuring the specimen was completely covered and left for 10 minutes. Thereafter the ethanol was removed and the following concentration added. The process was repeated up until a concentration of 100%. The specimen was then placed in a petri dish and completely covered with 100% ethanol. The petri dish was sealed and placed in the refrigerator at 4°C for 2-3 days. This ensured that the biofilm remained fixed and moist to preserve the structure of the biofilm. Prior to analysis a portion of the sample filter paper was cut and mounted onto an aluminium stub with carbon glue. A few drops of hexamethyldisilazane (HMDS) was added on top of the sample and left to dry for 3 hours (Fratesi et al., 2004). Finally the dried sample was coated with carbon using a Balzers evaporation coater and analysed using a FEI NOVA NANOSEM 230 with a field emission gun.

5.4.2 Bottom-view

Bottom-view samples were prepared as above, but in a petri dish in order to preserve the fragile structures, on the undersurface of the floating sulphur biofilm. No filter paper was utilised. Additionally, the sample was stuck to the aluminium stub with carbon tape rather than carbon glue.

5.4.3 Cross-sectional Biofilm analysis

All cross-sectional view biofilm samples were prepared by as follows prior to Scanning Electron Microscopy (SEM). The sample was harvested in a petri dish and fixed using a 1% glutaraldehyde solution for 2 - 3 days, depending on the structural integrity of the biofilm. After fixation the glutaraldehyde was removed and the specimen washed in a 1X phosphate-buffered saline (PBS) solution and subjected to a standard dehydration sequence. After dehydration, the specimen was placed in a clean petri dish and completely

covered with 100% ethanol. The petri dish was sealed and stored at 4°C for 2-3 days. A quickset L.R. White-resin was mixed and used to half fill a rubber mould. Once the lower half of the resin had set the specimen was placed on the resin block. Thereafter the remainder of the resin was poured on top to complete the mould. The resin was left to dry overnight. The block was removed and sanded down to expose the biofilm cross-section. Thereafter it was polished using a 0.1 µm polishing wheel and 0.05 µm silica powder solution in order to obtain a smooth clear finish. The resin block were rinsed with dH_2O and sonicated (10 minutes) in order to remove any debris from the surface. The block was mounted onto an aluminium stub with carbon glue. Lastly, it was coated twice with carbon (using a Balzers evaporation coater) to improve the conductivity of the sample. A silver dag was placed on the resin block to provide a conductive path to the aluminium stub. The sample was analysed using a analysed using a FEI NOVA NANOSEM 230 with a field emission gun.

5.5 Floating sulphur biofilm - Elemental analysis

5.5.1 Sulphur analysis

The sulphur content of the FSB was determined after harvesting the biofilm from the LFCR by skimming the liquid surface with a scoop. The sample was centrifuged to concentrate the solids. The supernatant was discarded and the solids recovered after drying at 37°C overnight. The solids were weighed and added to 1 L of chloroform (100%) in a Schott bottle. The mixture was stirred and heated (50°C) on a magnetic stirrer for 5 days to ensure the maximum sulphur dissolution. The mixture was cooled to room temperature in a water bath and vacuum filtered through a hydrophobic membrane using a Durapore Millipore filtration apparatus. The residual solids were dried at 37°C overnight and the filtrate stored in a clean Schott bottle. The filtrate was diluted as necessary and analysed for sulphur on the HPLC. The residual solids were combusted in the furnace at 450°C to determine if any sulphur remained. The temperature was chosen as the boiling point of amorphous, monoclinic and rhombic sulphur is 444.6 ˚ C (Perry & Green, 2008), so residual sulphur would boil off, (and combust) leaving behind the carbon and inorganic matter. Furthermore, any sulphate salts such as magnesium sulphate (1185°C), calcium sulphate (1193°C) and sodium sulphate (884°C) would remain behind as their melting points are significantly higher than 450°C (Perry & Green, 2008).

5.5.2 Carbon and inorganic analysis

After combustion at 450°C the residual solids were weighed (at room temperature) and used to determine the remaining constituents of the biofilm (carbon and inorganic matter). The solids were combusted at 550°C to remove all organic carbon. The remaining ash was

reweighed to determine the inorganic content. Thereafter it was analysed by SEM-EDS to gain a qualitative analysis of the inorganic salts and metals held within the biofilm matrix.

5.6 Microsensor measurement

Dissolved oxygen (D.O.) and redox microsensors were sourced from Unisense, Denmark. The microsensor apparatus was designed to allow for in-situ measurement at any point along the LFCR.

5.6.1 Dissolved Oxygen

A Clark-type OXY-10 10 μm diameter glass electrode D.O. microsensor was used to measure in-situ dissolved oxygen concentration in the FSB. A manual micromanipulator (MM-33) was used to lower the electrode at 5 μm intervals. A picoammeter (OXY-Meter) was used to detect the signal from the microsensor. The output was sent to a laptop via a USB cable and recorded by Unisense© SensorTrace BASIC 3.0 software.

The microsensor was calibrated in a glove box using degassed dH_2O as a zero solution and saturated dH_2O as the max solution. The zero solution was degassed for one hour and the max solution was aerated for 24 hours.

5.6.2 Redox

A redox microelectrode RD-10 (10 μm) was used in conjunction with a reference electrode (REF-10) to measure the redox potential gradient in the FSB. The reference electrode was placed in a bulk liquid solution sampled from LFCR near the FSB. This allowed for the redox electrode tip to develop an electrical potential relative to the reference electrode. Both electrodes were connected to a high impedance millivolt meter (Unisense© pH/mV-Meter) and the output was sent to a laptop via a USB cable and recorded by Unisense© SensorTrace BASIC 3.0 software. The reference electrode was a simple silver/silver-chloride open-ended electrode with a gel stabilized electrolyte and a tip of diameter 10 μm. The micromanipulator (MM-33) was used to lower the electrode at 5 μm intervals.

5.7 Floating sulphur biofilm harvesting

The floating sulphur biofilm was harvested by two methods.

1. A scoop was used to skim the FSB off the water surface in experimental run 16.

2. The FSB was harvested by initially loosening the FSB from the (2.5 m) wall it was least firmly attached too. Thereafter the bulk fluid was drained allowing the FSB to remain fully intact and hanging on the wall. The FSB was recovered by lifting or scraping it off the reactor wall. This method was performed for experimental runs 8 - 15, as the harvesting was performed at the end of the experiment, hence, the LFCR could be drained.

5.8 Molecular Methods

5.8.1 Nucleic acid extraction

Biofilm samples for nucleic acid extraction were cut into small pieces (0.5 cm^2) using a sterile scalpel. The biomass pieces were placed into a sterile 50 mL falcon tube with 1X PBS buffer (20 mL). The tube was vigorously agitated (10 min) to separate cells from within the biofilm matrix (de Lipthay et al., 2004). The liquid fraction was transferred to a sterile Beckman centrifuge tube and centrifuged at 10 000 g for 10 minutes. The supernatant was discarded and the pellet recovered, and washed with 1X PBS solution (pH 7.0), before being centrifuged again (13 000 g, 5 min). Total DNA from the pellet was extracted using a High Pure PCR Template Preparation Kit (Roche) according to the manufacturer's instructions. The extracted DNA was quantified spectrophotometrically (260 nm) (NanoDrop 2000). The purity and concentration of the DNA was determined using Classic NanoDrop software.

5.8.2 Polymerase chain reaction

Polymerase chain reaction (PCR) was performed on a range of samples, including samples from the DPBRs, LFCRs (floating sulphur biofilm) and the inocula. Each 30 μL PCR reaction contained: 1 μL 10 mM GM5F (5'-CCTACGGGAGGCAGCAG-3') primer solution (Muyzer et al., 1993; Santegoeds et al., 1998), 1 μL 10 mM 907R GC (5'-CGC CCG CCG CGC CCC GCG CCC GTC CCG CCG CCC CCG CCC GCC GTC AAT TCC TTT GAG TTT-3') primer stock solution (Muyzer et al., 1993; Santegoeds et al., 1998), 14 μL KAPA SYBER MasterMix Solution, 1 μL DNA (0-50 ng/μL chromosomal DNA) and 13 μL nuclease free water. The PCR reactions were placed in the G-Storm (GS1) thermocycler and a touchdown thermocycle program was run as per Table 5.3 for 40 cycles.

Table 5.3: Touch-down programme used for PCR amplification (40 cycles)

Reaction	Temperature	Time
Initial Denaturation	95°C	2 minutes
Denaturation	94°C	30 seconds
Annealing	60°C	20 seconds
Extension	72°C	2 minutes

5.8.3 Agarose gel electrophoresis

Amplified PCR products were separated by agarose gel electrophoresis. A 0.8% (w/v) agarose gel was prepared, which consisted of 0.8 g of molecular grade agarose and 100 mL 1X TAE Buffer (Appendix A). The mixture was boiled until the agarose was completely dissolved and then cooled to 40°C. Ethidium bromide stock solution (10 mg/mL, 5 μL) was added and then the gel poured. The gel was placed in the electrophoresis unit containing 1X TAE buffer. The samples were loaded into the wells with 2 μL 6X DNA loading dye (Fermentas). A Generuler™100 bp DNA ladder (Fermentas) was used in order to determine the size of the amplicons. The PCR amplified DNA bands were excised from the gels and purified using the QIAquick Gel Extraction Kit (QIAGEN™), according to the manufacturer's instructions. Thereafter, the DNA was analysed via denaturing gradient gel electrophoresis.

5.8.4 Denaturing gradient gel electrophoresis

The Biorad DCode™ Universal Mutation Detection system was used for denaturing gradient gel electrophoresis (DGGE). The gel plates were cleaned and assembled according to manufacturer's instructions. In order to determine the optimal conditions for the DGGE, an initial broad concentration gradient range was used. The solutions used for the initial DGGE gel were 30 and 80% denaturant (8% gel) (as per manufacturer instructions). These solutions were placed in the Biorad 487 Gradient Delivery System in order to pour the gel between the glass plates for a parallel DGGE. A 15-well comb was inserted in between the glass plates to form the wells. The gel was allowed to set for three hours. Once the gel had set, it was removed from the casting stand and placed in the electrophoresis tank. The tank was filled with 1X TAE buffer and preheated to 60°C. The comb was removed and the wells were flushed of excess acrylamide using a pipette. Approximately 20 μL of PCR product (section 4.7.3) and 2 μL of 6X DNA loading dye were combined and loaded into each well. The gel was run at 60 V for 15 hours. Once complete the gel was removed and stained with ethidium bromide (10 mg/mL, 2 μL) in 1X TAE buffer solution, before being photographed using a UV G-BOX image analyser (Syngene).

The optimised parallel DGGE was run at 30% to 65% denaturant based on the separation achieved in the first DGGE gel. The optimised DGGE run was executed as per the procedure above.

5.8.5 DNA gel extraction

Bands were excised from the DGGE gel under long wavelength UV light and placed into sterile eppendorf tubes with 20 μL of nuclease free water. The samples were placed at 4°C overnight, then vortexed and subsequently heated on a heating block at 37°C for 30 minutes (Sambrook & Russell, 2001). Thereafter, the eppendorf tubes were centrifuged at 13000 *g* for 30 seconds. Approximately 1 μL of the sample was used as the template in a PCR amplification, performed as described in Section 4.7.2.

5.8.6 Ligation

PCR products for cloning were ligated using the PGEM-T Easy vector system (Promega), according to the manufacturers instructions and incubated overnight at 4°C.

5.8.7 Transformation

Competent *E.coli* DH5α was prepared by the $CaCl_2$ method, which was adapted from Sambrook & Russell (2001). Approximately 5 μL of the ligation reaction product was combined competent *E.coli* DH5α (35 μL). The tubes were mixed and left on ice for 20 minutes, after which the cells were heat-shocked at 42°C for 40 seconds. The tubes were then placed on a shaking platform at 37°C for 3 hours. Thereafter 200 μL of the cells were plated onto Luria agar (LA) plates containing 100 μg/mL Ampicillin and spread with 4 μL IPTG stock solution (200mg/ml) and 40 μL X-GAL stock solution (100mg/ml). The plates were left overnight in an incubation chamber at 37°C. E. coli cells habouring the recombinant pGEM-T Easy constructs. Colonies containing the insert appeared white and those that just had the plasmid appeared blue. White colonies were picked off the plate with a sterile loop and used to inoculate 5 mL Luria broth (liquid) reaction tubes. The cultures were grown overnight at 37°C.

5.8.8 Plasmid extraction

Plasmids were extracted from the overnight cultures using the GenElute™HP Plasmid miniprep kit (Sigma Aldrich). They were recovered by centrifuging at 13 000 *g* for 90 seconds in sterile eppendorf tubes (2 mL). The supernatant was discarded and another 2 mL added until all the cells were pelleted. Thereafter the pellet was processed as per the manufacturer's kit instructions.

5.8.9 Sequencing

The plasmids were sequenced at the DNA Sequencer lab at Stellenbosch University. Chromatograms were generated by the genetic analyser data collection system. The sequences were compared to available sequences in the National Centre for Biotechnology information (NCBI) database, using the Basic Local Alignment Search Tool (BLAST) algorithm (Altschul et al., 1990). Thereafter the percentage similarity to an identified species was recorded, also the length of the match and the E value, which is important for determining the accuracy of the result. Subsequently, phylogenetic trees were constructed in order to represent the results graphically.

5.8.10 Quantitative real-time polymerase chain reaction

A plasmid/insert standard was created where a ~600bp 16S fragment was inserted into pGEM-T Easy (Promega) and linearized with ScaI (Fermentas). A 5-point standard series containing 1x10-1-1x10-5ng pDNA was created and used as the standard range. Plasmid copies were calculated based on insert length and content, with approximately 2.5x108 copies of plasmid per nanogram. The KAPA SYBR Fast qPCR kit containing a green dye (KAPA Biosystems) was used as per manufacturer's instructions in qPCR reactions, the final reaction volume was 15 µL. Universal 16S primer sets were used to quantify copies of genes from template added to the reaction. The thermal cycling steps were: 1 x 96°C for 6 min, 40x (96°C for 10 sec, 60°C for 15 sec and 72°C for 20 sec), melt curve analysis from 72 to 95°C with 0.2°C increments. The reaction were transferred to the Corbett Rotorgene 6000 for analysis.

Chapter 6

Fluid dynamics within the LFCR

6.1 Introduction

The analysis of the data from the GARL study identified a large discrepancy between the apparent sulphide oxidation efficiency and sulphur recovery. This, coupled with the inconsistent performance of the demonstration-scale plant suggested some short-circuiting with the feed bypassing the reaction zone (FSB) in the LFCR. The LFCR was originally designed under the assumption of plug flow. However, the reactor geometry and fluid velocities during normal operation made this assumption questionable. Therefore, a hydraulic study on the LFCR was conducted in order to gain a better understanding of the flow patterns within the reactor. The fluid dynamics study aimed to answer the following hypothesis and key questions, to determine the impact hydrodynamics plays in the performance of the LFCR.

- The linear flow channel reactor has laminar fluid flow with the hydraulic regime being stratified and largely governed by diffusional mass transport.

1. What type of hydraulic regime is present within the LFCR, if plug-flow is not present?
2. Is the hydraulic regime laminar or turbulent, and if laminar, is it governed by diffusional transport or advective transport?
3. Is there sulphide oxidation within the bulk-phase of the linear flow channel reactor and is it necessary for the reactor fluid to be perfectly mixed?

This chapter will be arranged as follows, the by-pass study will be discussed first, followed by the tracer and hydraulic density studies. The respective experimental methods, results and discussions pertaining to each study will be presented.

6.2 Bypass study

6.2.1 Test conditions

The experiment was conducted at ambient temperature (23 - 25°C), pressure (1 atm.) and at a steady state flow rate of 25 L/day, to simulate the experimental conditions used at

GARL. The feed sulphide concentration was maintained at 4.55 mM and was pumped in through the top inlet (inlet port 1), while the effluent exited from outlet port 3 (lowest outlet, Figure 4.3). The LFCR was sampled daily from all 15 side sampling ports, as well as the influent and effluent ports. The experiment was conducted over a period of three days.

6.2.2 Results and discussion

A lab-scale study was conducted to simulate the GARL setup and configuration. This was performed to discern what flow pattern was prevalent within the LFCR. From Figures 6.1 and 6.2 it's clear that there was poor mixing in the LFCR. The influent sulphide entered the reactor, crept along the floor of the reactor and exited from outlet port 3. Hence, the highest concentration of sulphide was at the bottom. This configuration is indicative of a inefficient design, as the influent bypassed the reaction zone (FSB) at the surface. The average sulphide oxidation rate was 0.564 mmol/L.day, which equated to an average sulphide removal efficiency of 12.4%. This was similar to the sulphide removal efficiency in the GARL study for experiments number one, two and three (Table 2.2 on page 14), as the average sulphide removal efficiency was 12 - 20% per LFCR channel. Lastly, the residence time was determined to be 0.33 - 1.21 hours, which was extremely short considering the theoretical residence time was 24 hours. This would also explain the poor sulphide oxidation rate per channel, as the feed largely bypassed the FSB. Therefore the LFCR was reconfigured and the outlet port was positioned at the top, at the liquid surface (Figure 6.3). The result was that the incoming sulphide feed would be forced upwards towards the floating sulphur biofilm.

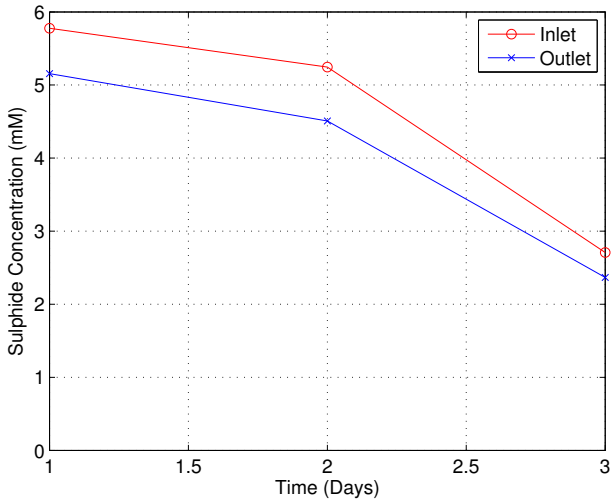


Figure 6.1: Inlet and outlet sulphide concentrations (mM) which were observed during the (LFCR - demonstration-scale plant design) hydraulic regime study

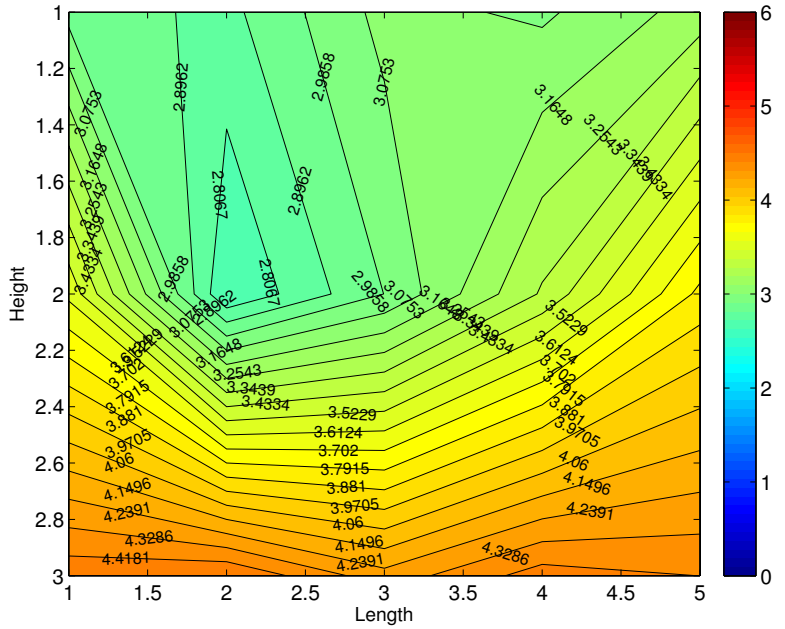


Figure 6.2: Contour map of the sulphide concentration (mM) within the LFCR on day 2, illustrating the hydraulic regime within the original LFCR demonstration-scale plant design

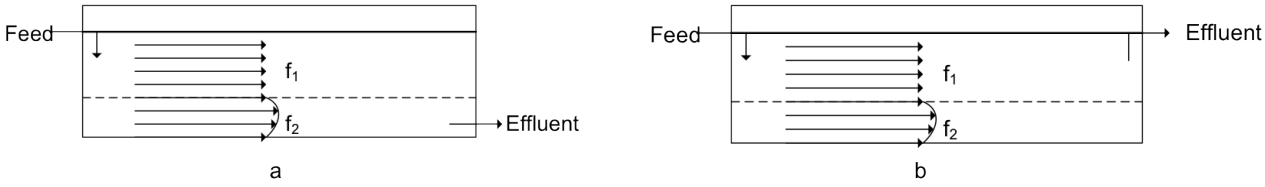


Figure 6.3: Illustration depicting the original LFCR design as per the demonstration-scale plant (a) and the improved LFCR design with the effluent port at the liquid surface (b)

6.3 Dye tracer study

6.3.1 Experimental method

Each study was conducted until sufficient data on the flow regime in the LFCR was obtained. The experiments were visually recorded via time-lapse photography to track the movements of the various dye tracers. A 12 megapixel canon digital camera was mounted on a 1.3 m high tripod, 2 m from the side wall of the LFCR. A photograph was taken every 30s at the start of the experiment for five minutes, thereafter every ten minutes until the end of the experiment. White sheet paper was utilised to block off the surroundings to enhance the contrast of the phenolphthalein pink against the white backdrop. Thereafter all images were digitally analysed in Matlab (image processing toolbox) to determine the velocities and distances covered.

6.3.2 Test conditions

The dye tracer study was conducted firstly to determine the optimal tracer and secondly, the hydraulic regime in the LFCR, whilst utilising that particular tracer. The experiments were conducted under the conditions summarised in Tables 6.1a & 6.1b

6.3.2.1 Phenolphthalein tracer

The reactor was filled with a sodium hydroxide (NaOH) solution (25 L, 0.04±0.002 M), to which ten drops of phenolphthalein were added to achieve a uniform pink colour. Hydrochloric acid (HCl) was pumped into the reactor at a flow rate of 120 L/day. When the neutralisation reaction occurred (Equation 6.1) the liquid within the reactor turned colourless, thus demonstrating the fluid's path. The duration of each experiment varied based on how long it took for the entire reactor fluid volume to turn colourless.

$$NaOH + HCl \rightarrow NaCl + H_2O \tag{6.1}$$

6.3.2.2 Potassium dichromate tracer

The second tracer was investigated by pumping 1 L of potassium dichromate ($K_2Cr_2O_7$, 1.0004 g/cm^3) solution into the reactor containing 25 L of water. This test was conducted in an effort to determine the critical role of the incoming fluid's density within the reactor and if potassium dichromate was a better tracer.

6.3.2.3 Food colouring tracer

The third tracer was green food colouring (0.99991 g/cm^3). A total of 5 mL was added to 1 L of water and pumped into the reactor .

6.3.2.4 Sulphide tracer

Approximately two litres of sulphide solution (6.06 mM) was pumped into the reactor containing a 3.03 mM sulphide solution (25 L). The test run lasted 20 minutes with samples drawn from the sample ports every two minutes. Sample port 1-4 were the first 4 ports on the top row, 5-8 on the second row and 9-12 on the last row. The ports on column 5 at the end were not sampled due to time constraints. Note, this sample port numbering format is only applicable to this experiment and Figure 6.10 on page 102.

Table 6.1: Tables of experimental parameters used in the hydrodynamic study to improve mixing within the LFCR.

(a) Experimental conditions of phenolphthalein mixing tests utilising cylinders of diameter 10 and 30 mm

Test No.	NaOH		HCl			
	Concentration (M)	Density (g/cm^3)	Concentration (M)	Density (g/cm^3)	Cylinder diameter (mm)	Inlet Port
1	0.042	1.000	0.042	1.001	10	1
2	0.040	1.000	0.400	1.003	10	1
3	0.040	1.000	0.420	1.003	30	1
4	0.041	1.000	0.41	1.002	-	1

(b) Experimental conditions of improved mixing tests utilising various tracers and cylinders of diameter 10 and 30 mm

Test No.	Type	Density (g/cm^3)	Cylinder diameter (mm)	Inlet Port	Yellow Layer Volume (m^3)
5	Potassium dichromate	1.0004	10	1	0.00695
6	Green dye	0.99991	30	2	-
7	Sulphide	1.0003	10	1	-

6.4 Results

6.4.1 Phenolphthalein Test

Table 6.2: Results of hydrodynamic experiment tests no. 1 -4. Average velocities, respective reynolds numbers and clear layer volumes are presented.

Test No.	Avg. Velocity (mm/s)	Re	Clear layer volume (m^3)	Pe
1	Inconclusive		0.0047	-
2	6.67	$\leq$160.1	0.0104	165
3	4.52	$41.7 \leq Re \leq 118$	0.00675	112
4	5.2	≤ 130	0.01475	129

6.4.1.1 Test 1

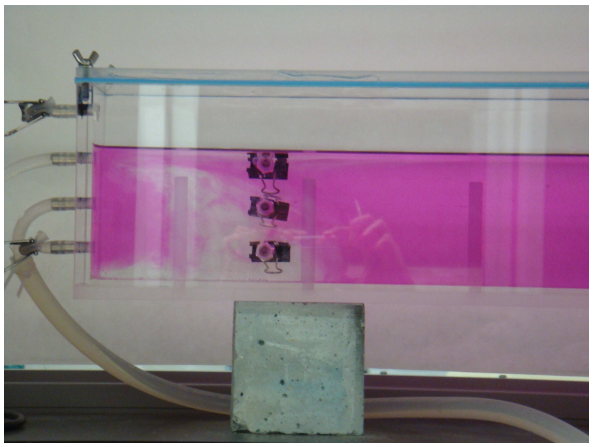
From the experimental calculations it was determined that only 1 L of hydrochloric acid (0.042 M) would be necessary to neutralise the 25 L of sodium hydroxide solution (0.00168 M). So the ratio of acid to base was 1:1. The following pictures show that there was mixing within the first 0.13 m of the channel. Figure 6.4a shows turbulent eddies and back-mixing as the HCl entered the reactor and moved downwards due to gravity. As time progressed the amount of HCl increased and eventually formed a laminar layer on the floor of the reactor (Figure 6.4b). The recirculation regions and turbulent mixing caused by the cylinders became more evident due to the 'wavy' nature of the pink layer (Figure 6.4c). Nonetheless, the entire reactor volume was not neutralised due to the poor mixing and accumulation of the acid solution (1 L) within the first half of the reactor (Figure 6.4d).

6.4.1.2 Test 2

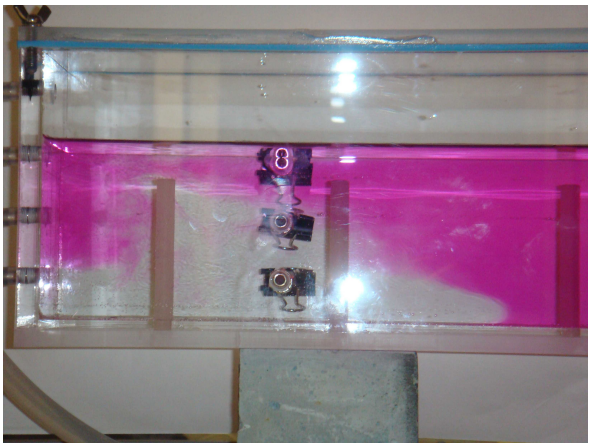
The hydrochloric acid concentration was increased ten fold in order to completely neutralise the entire reactor, at a volumetric flow rate of 120 L/day. The fluid moved faster in the longitudinal direction (z) than in test 1, as the clear laminar layer had an average linear velocity of 6.67 mm/s (Figure 6.5a). Furthermore the turbulent mixing caused by the cylinders is visible in Figure 6.5b. A laminar parabolic profile which occurred in the bottom region of the reactor was also clearly visible. Figure 6.5d shows that the flow within the reactor was stratified. There was a pink layer in the top half of the LFCR and a clear layer in the lower half of the reactor.

6.4.1.3 Test 3

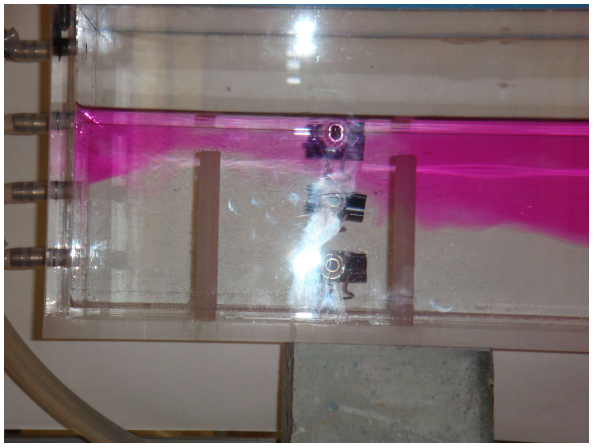
Test 3 was executed in exactly the same manner as test 2 however, 30 mm diameter cylinders were utilised. The larger baffles did cause more turbulent eddies (Figure 6.6a). Each cylinder also acted as a barrier to the laminar flow thus decreasing the linear velocity



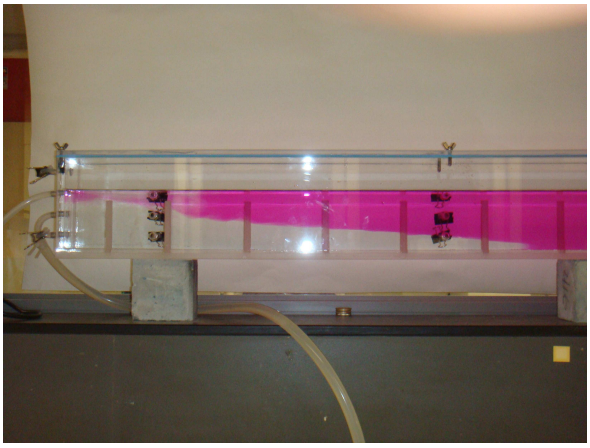
(a) Fluid path at t = 1.5 minutes



(b) Fluid path at t = 3 minutes

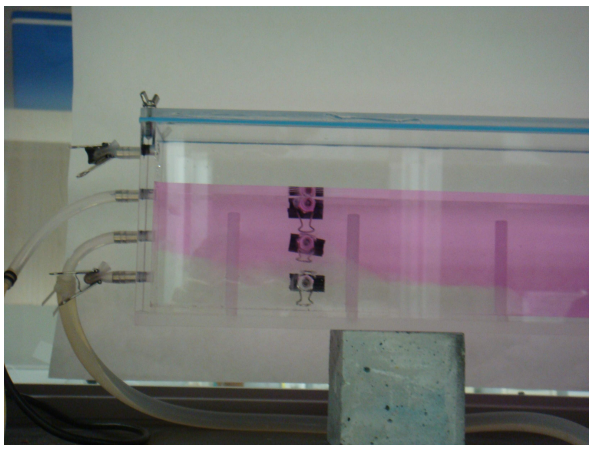


(c) Fluid path at t = 4.5 minutes

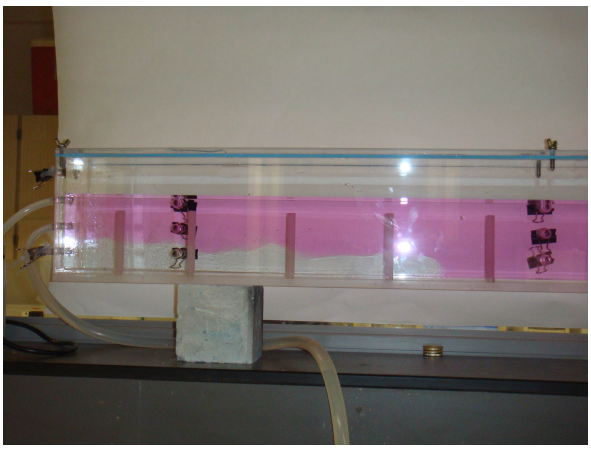


(d) Fluid path at t = 9.5 minutes

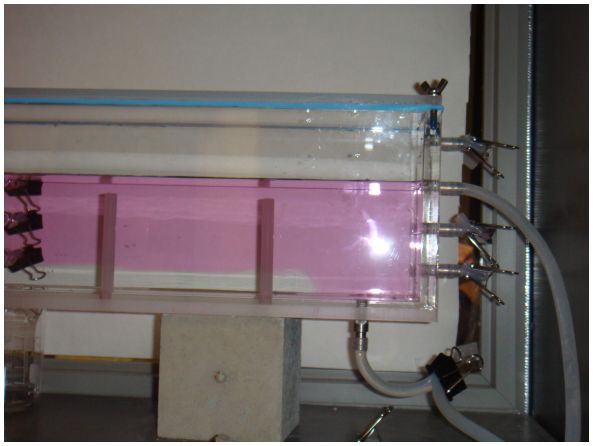
Figure 6.4: The fluid flow path of hydrochloric acid (0.042 M), pumped in at a volumetric flow rate of 120 L/day. Cylindrical baffles (10 mm) were utilised to induce mixing (test 1). All photographs were taken in cross-sectional view of the reactor.



(a) Fluid path at t = 45 seconds



(b) Fluid path at t = 1.5 minutes

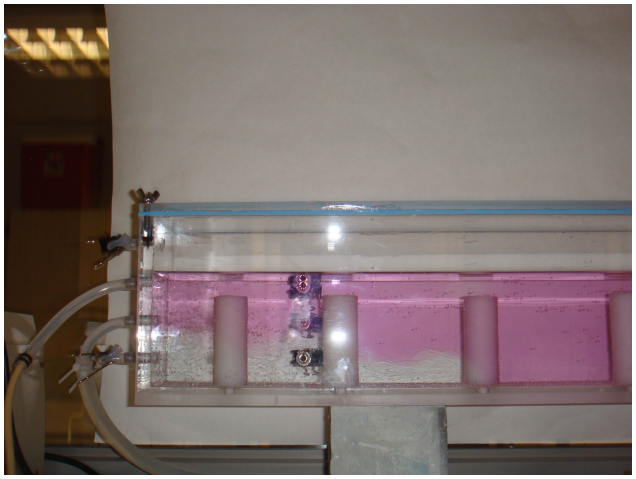


(c) Fluid path at t = 8.5 minutes

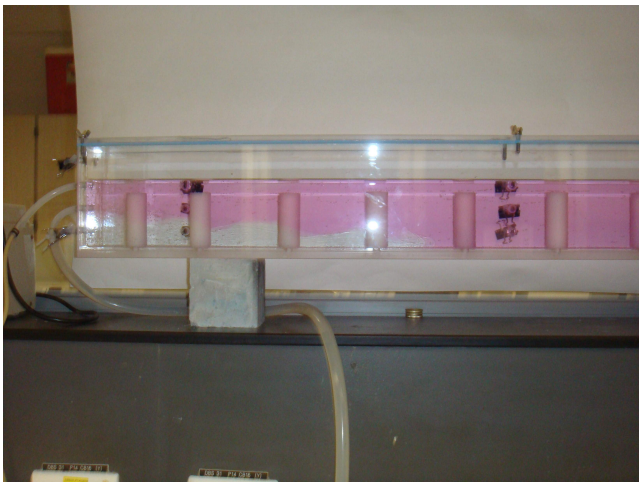


(d) Fluid path at t = 12.5 minutes

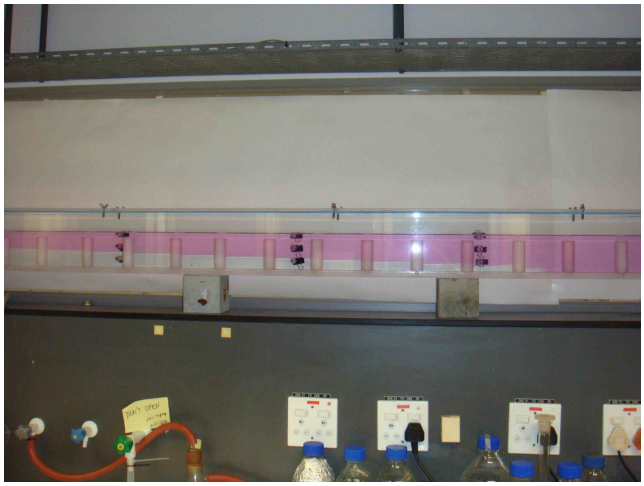
Figure 6.5: The fluid flow path of hydrochloric acid (0.40 M), pumped in at a volumetric flow rate of 120 L/day. Cylindrical baffles (10 mm) were utilised to induce mixing (test 2). All photographs were taken in cross-sectional view of the reactor.



(a) Fluid path at t = 35 seconds



(b) Fluid path at t = 1 minute



(c) Hydrochloric acid path within the reactor at t = 6 minutes

Figure 6.6: The fluid flow path of hydrochloric acid (0.420 M) within the reactor, which was pumped in at a volumetric flow rate of 120 L/day. Cylindrical baffles (30 mm) were utilised to induce mixing (test 3). All photographs were taken in cross-sectional view of the reactor.

resulting in a smaller clear layer on the floor of the reactor (Figure 6.6c) and stratification throughout the y-direction. The cylinders decreased the flow gradually as the bulk fluid velocity was 4.9 mm/s at cylinder 8, 4.5 mm/s at cylinder 15 and finally 4.17 mm/s at the end of the reactor. The larger baffles did not induce mixing, but rather diminished the fluid velocity and promoted stagnation.

6.4.1.4 Test 4

Test 4 was conducted in the same manner as the previous experiments, but no cylinders were used to confirm whether they promoted fluid mixing or caused retardation and stagnation of fluid flow. The similar parabolic velocity profile of laminar flow was observed, with a bulk velocity of 5.2 mm/s. Without baffles, a large amount of mixing was observed by the wavy nature of the pink layer near the entrance. Furthermore, it was evident that the parabolic velocity profile was slightly distorted, as the upper portion was probably experiencing a lower shear stress and so the profile appeared less parabolic (Figure 6.7).

6.4.2 Potassium Dichromate dye tracer - Test 5

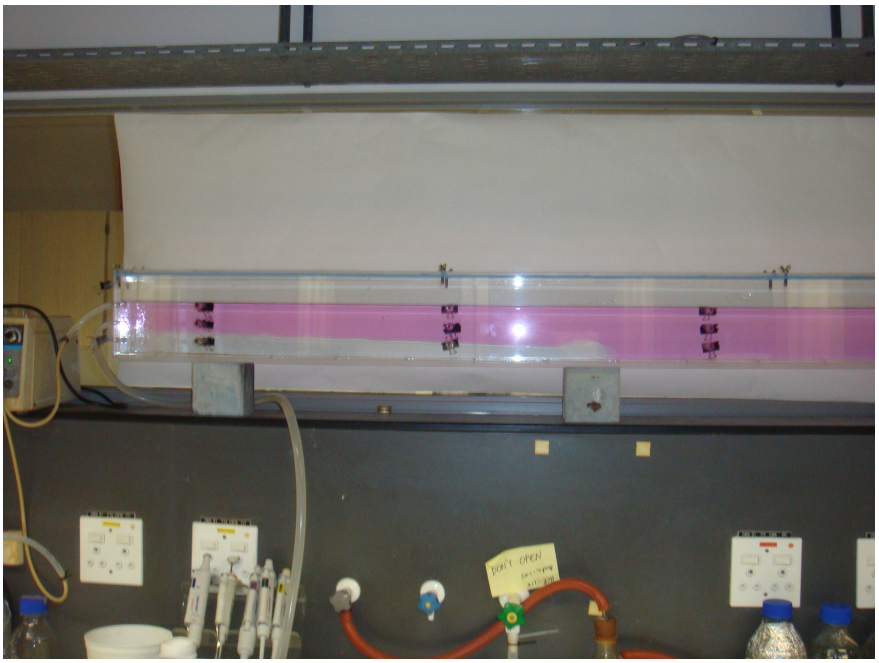
Figure 6.8a shows that density does play a critical role in the fluid flow within the reactor. The potassium dichromate solution seemed to float 0.08 m after entering the reactor before sinking due to the density difference. The initial velocity of the feed fluid allowed it to move horizontally (z-direction), before succumbing to the density difference and lower buoyancy force. Once again a 'yellow' laminar parabolic profile was evident as the solution progressed longitudinally down the reactor (Figure 6.8b). A clear (less dense) layer occurred in the upper half of the reactor, with a yellow (more dense) potassium dichromate layer below.

6.4.3 Green dye tracer - Test 6

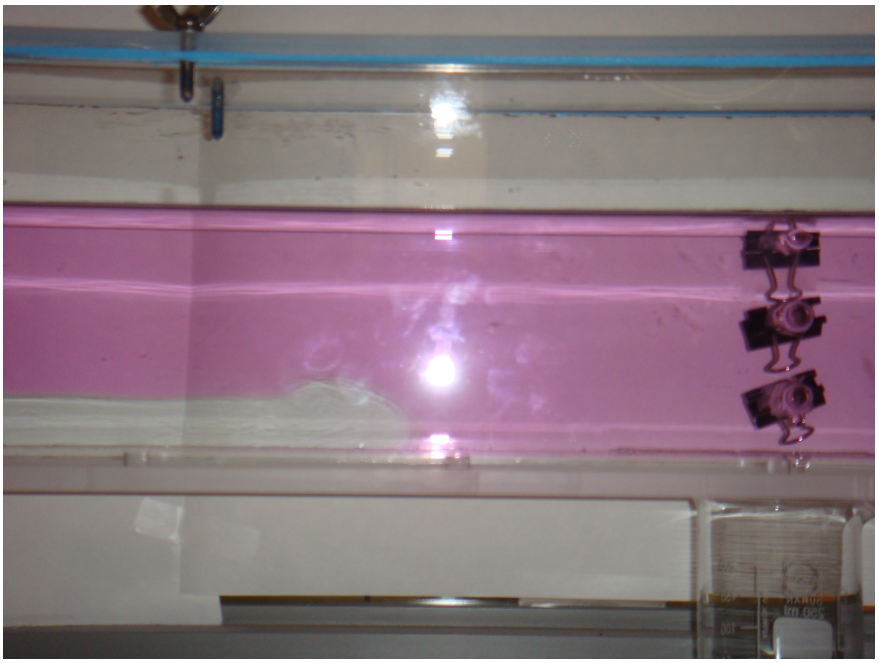
The green dye was pumped in via inlet 2 and rose to the surface of the liquid layer in the reactor (Figure 6.9). No turbulent eddies or mixing occurred in the reactor . The green dye floated on the surface and formed a thick green stagnant fluid layer due to it being less dense than water. The feed was pumped in via a lower inlet in an effort to encourage mixing and cause the fluid to disperse throughout the reactor, however this did not follow the observed regime in previous experiments.

6.4.4 Sulphide tracer - Test 7

Figure 6.10 shows the concentration profile within the reactor as a function of time. The first clear trend was the increase in concentration with an increase in depth. Ports 9 - 12 had the highest concentration of sulphide (80 - 95 mg/L). The second trend was that concentration increased with time at all ports.

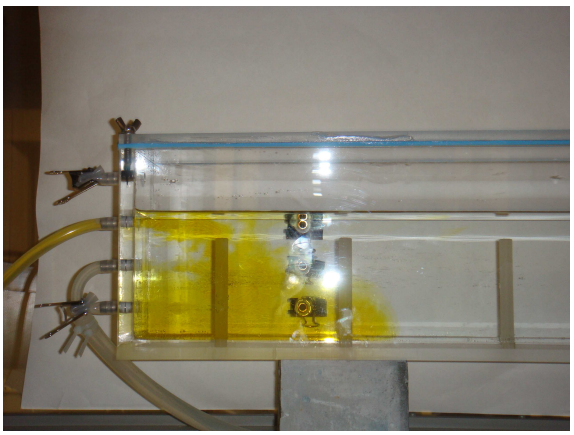


(a) Fluid path at t = 3 minutes

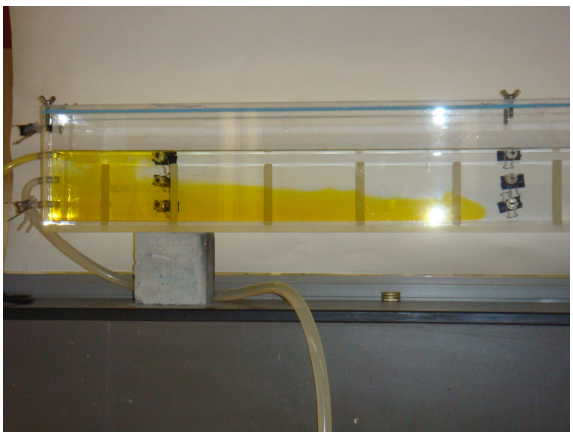


(b) Fluid path (t = 6 minutes) resembling Couette flow with the 'upper plate' being non-stationary

Figure 6.7: Hydrochloric acid path within the reactor with no cylindrical baffles (test 4)

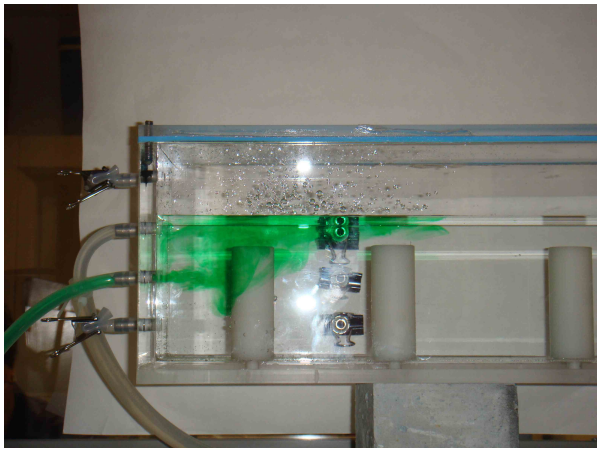


(a) Fluid path at t = 1minute

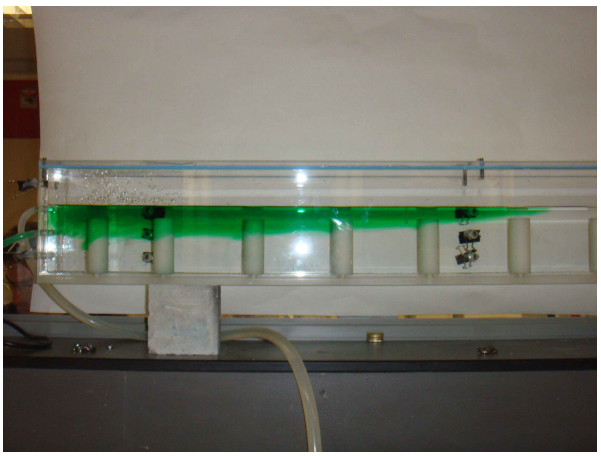


(b) Fluid path at t =3.5minutes

Figure 6.8: The fluid flow path of $K_2Cr_2O_7$ ($\rho = 1.0004$ g/cm^3), pumped in at a volumetric flow rate of 120 L/day. Cylindrical baffles (10 mm) were utilised to induce mixing (test 5). The yellow layer volume occupied was 0.00695 m^3. All photographs were taken in cross-sectional view of the reactor.



(a) Fluid path at t = 30seconds



(b) Fluid path at t = 4minutes

Figure 6.9: The fluid flow path of green dye ($\rho = 0.99991$ g/cm^3), pumped in at a volumetric flow rate of 120 L/day, through inlet port 2. Cylindrical baffles (30 mm) were utilised to induce mixing (test 6). All photographs were taken in cross-sectional view of the reactor.

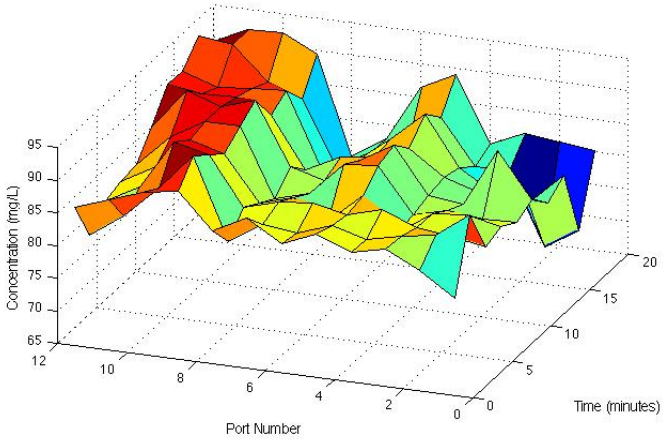


Figure 6.10: Concentration profile of the reactor in the y & z-direction with time. Ports number 1-4 are the top row (1.1 - 4.1), ports number 5-8 (1.2 - 4.2) and 9-12 (1.3 - 4.3) are the second and third rows respectively.

6.5 Discussion

The overall flow regime for the specific operating conditions cannot be determined simply by the Reynolds number *(Re)*. From the hydrodynamic tracer experiments it was determined that there were two discrete flow regimes in the LFCR. The upper portion of the reactor was strictly laminar flow whilst, the lower portion was laminar parabolic profile flow. The requirement for laminar flow in a circular tube is $Re < 2300$. From the tracer experiments it was determined that the reynolds number range was, $0 < Re < 307$, hence the flow was laminar.

The flow pattern was unconventional due to the heterogeneous nature of the fluid movement within the LFCR. The fluid entered the reactor and caused some turbulent eddies in the bulk volume before sinking to the bottom of the channel (Figure 6.4a). There was also some back mixing in the front corner of the reactor, thus confirming it as a dead-zone. The fluid then proceeded to move forward along the floor of the reactor as a laminar parabolic velocity profile (Figure 6.7 b). When it reached the back wall of the reactor, the fluid collided with the wall thus causing the laminar layer of hydrochloric acid to be displaced upwards. There was some mixing in the back corner resulting in a second dead-zone and movement of some of the HCl back towards the entrance. This hydraulic regime is best represented by Figure 6.11. This particular flow pattern is governed by three factors, the first being laminar flow between 'two parallel plates', the second being density and lastly, advective and diffusive mass transport. The first two points will be discussed within this dye tracer study, thereafter the hydraulic density study will discussed and further data presented. The final point will be presented to create cohesion between both studies, in an effort to elucidate the observed hydraulic regime within the LFCR. The green tracer study did not follow this regime due to the tracer being less dense, hence floating

in the reactor. As a result, it was deemed to be a poor tracer as it did not accurately represent the hydrodynamic regime in the LFCR at GARL.

Laminar flow consists of axial stream lines where fluid flows in parallel layers with no bulk flow between layers. A characteristic of laminar flow is the development of a radial velocity profile similar to that of laminar flow between parallel plates or in a pipe (Figure 6.12b) (Bird et al., 2002). This particular flow pattern was observed in the tracer experiments. However, it will be shown that this parabolic profile is not a function of radius (r) but rather the vertical height (y) as this is not a pipe but a channel. The vertical velocity profile developed along the channel length was a result of shear forces exerted on the fluid at the wall (reactor floor) and by the fluid in region 1 (f_1) (Figure 6.12a). Therefore, the Navier Stokes derivation of flow between parallel plates can be utilised.

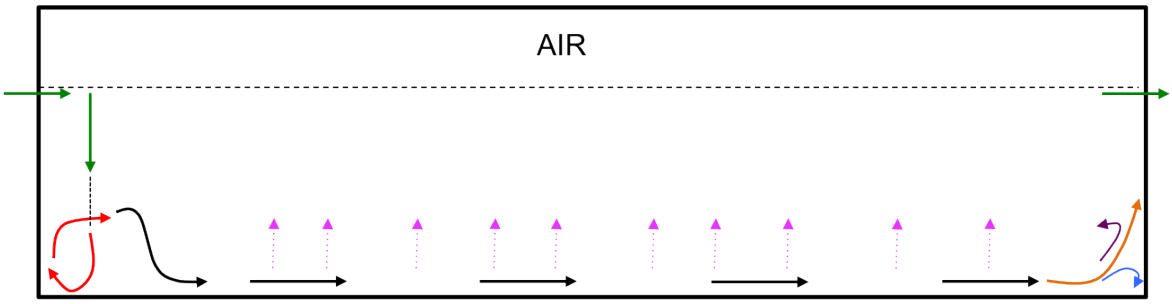
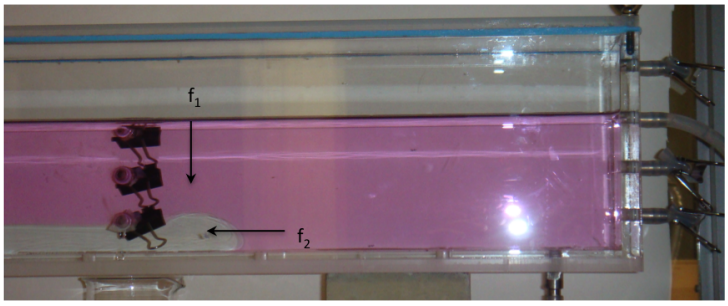
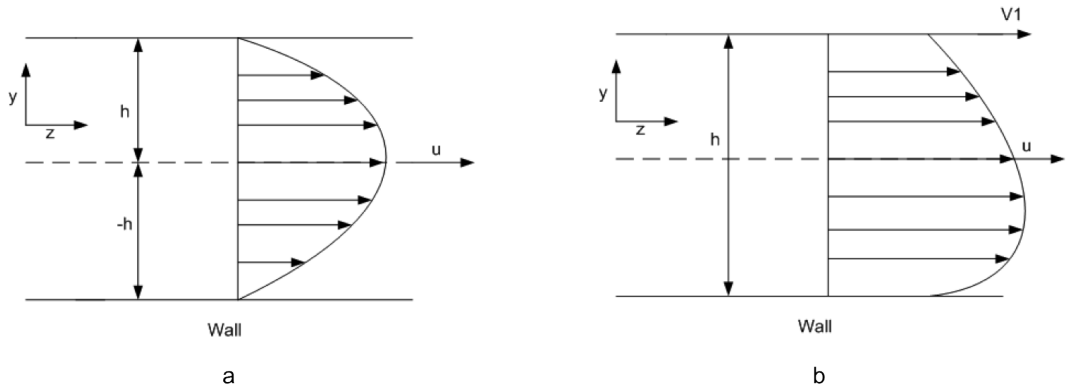


Figure 6.11: Schematic representation of fluid flow regime in the LFCR with various types of flow being displayed accordingly. The sinking influent (green arrows), entrance dead zone (red arrows), laminar parabolic flow (black arrows) and back corner dead zone (orange, maroon, blue arrows) are displayed. The smaller pink arrows represent the movement of fluid in the y-direction due to diffusion.



(a) Tracer experiment depicting a parabolic profile similar to that of Couette flow. Pink fluid in region 1 is represented by f_1 and clear fluid in lower region 2 by f_2.



(b) Illustration depicting laminar flow between two stationary parallel plates (a) and laminar Couette flow between a stationary and an upper moving plate (b)

Figure 6.12: Photograph (a) and illustration (b) depicting Couette flow between parallel plates

Navier Stokes theory may be utilised if specific conditions (1-3 below) are met. The general equation 6.2 can be simplified to equation 6.3 (Bird et al., 2002; Welty et al., 2007).

$$\rho\frac{\partial v_z}{\partial t} = \rho g_z - \frac{\partial P}{\partial z} + \mu\left(\frac{\partial^2 v_z}{\partial x^2} + \frac{\partial^2 v_z}{\partial y^2} + \frac{\partial^2 v_z}{\partial z^2}\right) \tag{6.2}$$

1. Fully developed laminar flow and incompressible flow at a constant density
2. The no-slip condition is valid at the solid boundary (reactor floor)
3. No flow in the x and y directions and the flow is constant across the plate (at steady state). The velocity (v_z) is only a function of y.

$$0 = -\frac{\partial P}{\partial z} + \mu\left(\frac{\partial^2 v_z}{\partial y^2}\right) \tag{6.3}$$

First integration:

$$\int \frac{\partial^2 v_z}{\partial y^2} = \int \frac{1}{\mu}\frac{\partial P}{\partial z}$$

Second integration:

$$\int \frac{\partial v_z}{\partial y} = \int \frac{1}{\mu}\frac{\partial P}{\partial z} y + C_1$$

$$v_z = \frac{1}{2\mu}\frac{\partial P}{\partial z} y^2 + C_1 y + C_2$$

The following boundary conditions are valid, assuming that the no slip condition holds true (Figure 6.12b a).

B.C. 1: At y = h, u = 0

B.C. 2: At y = -h, u = 0

Using the above boundary conditions yields a solution for C_1 and C_2:

$$C_1 = 0 \;\; C_2 = \frac{-1}{2\mu}\frac{\partial P}{\partial z} h^2$$

The velocity profile for flow within two parallel plates can be represented by equation 6.4

$$v = \frac{1}{2\mu}\frac{\partial P}{\partial z}\left(y^2 - h^2\right) \tag{6.4}$$

From the tracer study it was evident that there was a (fully developed) laminar parabolic velocity profile flow. However, the upper part of the parabola was not a mirror image of the lower part. Therefore the shear stress at the reactor floor was greater. This was due to the fact that the fluid (f_1) was a pseudo-wall and experienced a shear stress force due to the faster moving fluid below (f_2). Consequently fluid (f_1) had a velocity. Hence the 'upper plate' in Couette flow is not stationery but moving and equation 6.4 can be adjusted to incorporate this change by changing boundary condition 1 & 2 (Figure 6.12b b).

B.C. 1: At y = h, u = V_1

B.C. 2: At y = 0, u = 0

Using the above boundary conditions yields a solution for C_1 and C_2:

$$C_2 = 0 \;\; C_1 = \frac{V_1}{h} - \frac{1}{2\mu}\frac{\partial P}{\partial z} h$$

Thus the velocity profile for flow within two parallel plates with the upper plate being non-stationary, can be represented by equation 6.5.

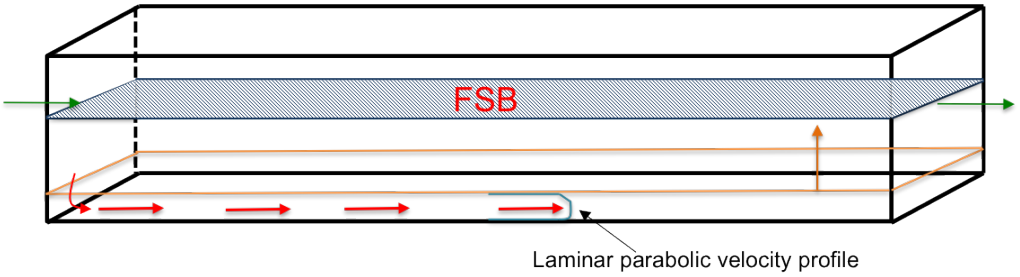


Figure 6.13: Schematic diagram of the flow regime within the LFCR. The incoming influent continually sinks to the bottom thus displacing the previous laminar layer (orange plane) upwards. This happens until that particular plane reaches the top and exits (green arrow) out the LFCR. The FSB floats on top of the liquid surface (blue layer) with the headspace above containing air.

$$v_z = \frac{1}{2\mu}\frac{\partial P}{\partial z}\left(y^2 - hy\right) + \frac{V_1 y}{h} \tag{6.5}$$

As mentioned earlier the 'upper plate', or fluid (f_1), will experience a shear stress force $\tau_{y,z}$. This acts in the longitudinal direction (z) and is exerted on the streamline parallel to it i.e. the y-direction. The magnitude of this force is given by Newton's Law of Viscosity.

$$\tau_{y,z} = \mu\frac{\partial v_z}{\partial y} \tag{6.6}$$

In short, if the reactor liquid volume was divided into infinitely many planes, then the (orange) plane immediately adjacent to the moving parabolic profile will experience a shear force in order to create the profile (Figure 6.13). Thus, this layer would experience a force and hence a forward motion in the direction of the moving fluid. Likewise, this fluid plane would exert a shear force on the plane above it and cause movement. Additionally, the fluid at the uppermost plane at the effluent port will be moving left to right due to the fluid exiting (green arrow). Therefore, this fluid would also exert a shear force on the fluid plane below it, thus causing this plane to move forward (left to right) as well. Hence the f_1 region is not stagnant, but moving slowly.

The observed phenomenon of stratification which occurred throughout all tests (1-7) can also be attributed to the extremely low flow rate (120 L/day) as well as the density differences. The green dye tracer study clearly showed that a small difference of 0.00009 g/cm^3 (0.009%) in the influent density, relative to that of the reactor fluid has profound effects. Even though the green dye was fed through a lower inlet (port 2), it still rose to the surface due to the density difference. The observed sinking of the influent near the entrance in experiments one to five, was simply due to a density difference.

However, in experiment one the influent had a greater density than the reactor fluid, yet it accumulated in the first half of the reactor. In experiment two, on the other hand, the influent had a greater density difference (0.2%) and reached the back of the reactor,

managing to create a larger clear layer (0.0104 m^3). If the continuity equation is applied to both scenarios over the inlet of the reactor, then the following deduction can be made. The area of the pipe and LFCR entrance is the same in each scenario, as is the velocity in the pipe. The density of the fluid in the pipe is identical to the density of the fluid as it exits the pipe into the entrance of the LFCR. However, the density of the fluid in experiment one was lower than that of experiment two ($\rho_{pipe-test1} < \rho_{pipe-test2}$). By equation 6.7, the entrance velocity ($v_{LFCR-entrance}$) is dependent on the influent density. Therefore, the influent in experiment two had a greater velocity and was able to move faster and further into the reactor. This phenomenon will be explored further in the following hydraulic density study, as well as the final aspect of advective and diffusive mass transport and mixing. These final two points will be able to provide the missing link in understanding the hydraulic regime within the LFCR.

$$\rho_{influent} Area_{pipe} v_{pipe} = \rho_{influent} Area_{LFCR-entrance} v_{LFCR-entrance} \tag{6.7}$$

6.6 Hydraulic density study

The purpose of this study was to assess how varying the density of the feed solution relative to the reactor solution impacted the hydraulic regime.

6.6.1 Test conditions

This study was performed by filling the LFCR with a NaOH solution (0.00168 M) and a few drops of phenolphthalein. Thereafter HCl solution was pumped into the LFCR was pumped in at a volumetric flow rate of 12.5 L/day (2 day R.T.).

6.6.2 Results & discussion

The heterogeneous mixing observed in the LFCR was attributed to the extremely low flow rate of 12.5 L/day. The flow within the LFCR was laminar, as the fluid had a maximum linear velocity of 1.05 mm/s ($0 < Re < 26$), on the floor of the reactor at the highest concentration (200X) (Table 6.3). The incoming fluid (HCl) sank to the bottom of the reactor immediately due to a density difference of 0.3% between the feed (ρ_{feed}) and reactor fluid ($\rho_{reactor}$) and moved along the reactor floor. The velocity profile along the reactor floor still resembled that of a laminar parabolic velocity profile (Figure 6.12b). The bulk velocity of the the influent decreased with a decrease in hydrochloric acid concentration and density. Therefore the bulk velocity of the influent is directly proportional to its density. A linear trend between relative density difference (RDD) (ρ_{feed} - $\rho_{reactor}$) and the bulk linear velocity was determined, further supporting the fact that the bulk velocity of the influent was directly proportional to its density (Figure 6.15). The slowest bulk fluid

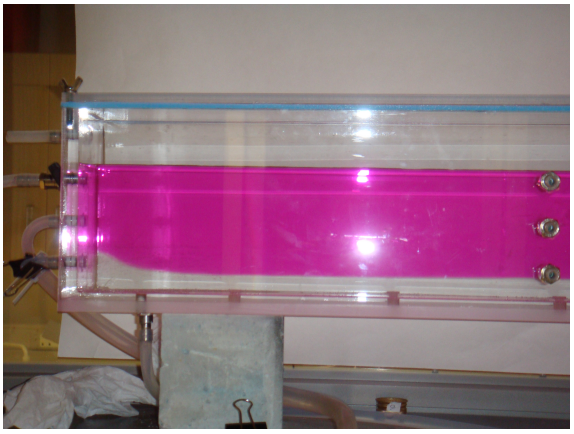
Table 6.3: Hydraulic density study results showing the relative density difference and influent fluid velocities, Reynolds numbers (Re) and Peclet numbers (Pe), as well as the respective measured residence times.

HCl:NaOH	Relative density difference (RDD) (g/cm^3)	Avg. Fluid velocity (mm/s)	Re	Pe	Residence time (h)
200 : 1	0.006383	1.05	< 26	25.98	46.6-48.0
100 : 1	0.003133	0.883	< 21	8.54	47.1-48.0
20 : 1	0.000578	0.622	< 16	2.67	48.0-48.5
10 : 1	0.000154	0.287	< 7	0.6	48.0-49.0
1 : 1	-0.0000354	Inconclusive			

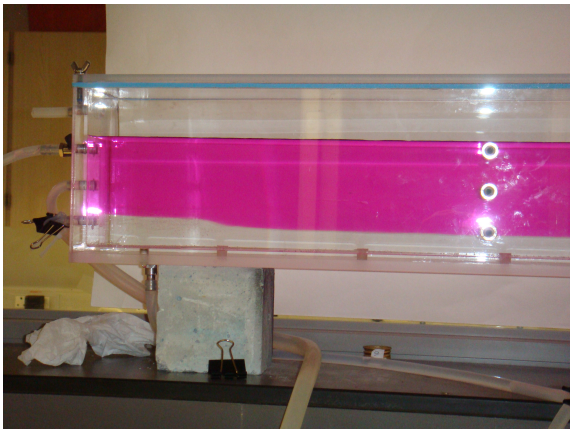
velocity was 0.287 mm/s with a Reynolds number of approximately seven or less, due to the RDD being so small. At an equimolar ratio (0.00168 M) the hydrochloric acid did not sink but floated on the surface before moving downwards to the reactor floor. The hydrochloric acid floated on the surface due to it being less dense, as well as having a low bulk velocity (< 0.287 mm/s). This clearly highlights the importance of the influent density and the relative density difference between the influent and reactor fluid.

The residence time of a fluid element was calculated based on the rate of the rising clear layer. It was determined that the residence for a fluid element at a volumetric flow rate of 12.5 L/day was between 46.6 - 48 hours. This was calculated at the maximum RDD of the study. The theoretical residence time was 48 hours. However, due to transverse dispersion at the back of the reactor, it is possible that a fluid element may spend a shorter time within the reactor. The residence time for a fluid element at a ratio of 10 HCl : 1NaOH was in the range of 48 - 49 hours. This was due to the back-mixing and the dead-zone at the entrance of the reactor. The collision of fluid with the back corner of the reactor also caused some fluid to flow back as a wave above the incoming feed fluid (Figure 6.14).

The final reason for the observed hydrodynamic regime in the LFCR is due to advective as well as diffusive mass transport, more specifically transverse dispersion. When one miscible fluid displaces another miscible fluid there will be mutual spreading and the finite interface width will become a parameter of the instability. If the density of the mixture of miscible fluids depends on concentration, the velocity field is no longer divergence free, even though the fluid is incompressible. As the density of the fluid element changes continuously due to diffusion, the divergence of the velocity field doesn't vanish, thereby giving rise to an additional stress tensor (Chen & Meiburg, 1996). Joseph & Hu (1991) found that under certain conditions these stresses can act in a similar manner to surface tension between two miscible fluids. An in depth analysis considering these factors of the observed flow regime, is beyond the scope of this particular study. Therefore, a more simplified analytical approach



(a) Feed fluid (HCl) colliding with the back corner of the LFCR and rising up the back wall



(b) Feed fluid (HCl) colliding with the back wall and flowing back towards the LFCR entrance

Figure 6.14: Photographs depicting the flow of HCl into the dead-zone (back-corner) of the LFCR

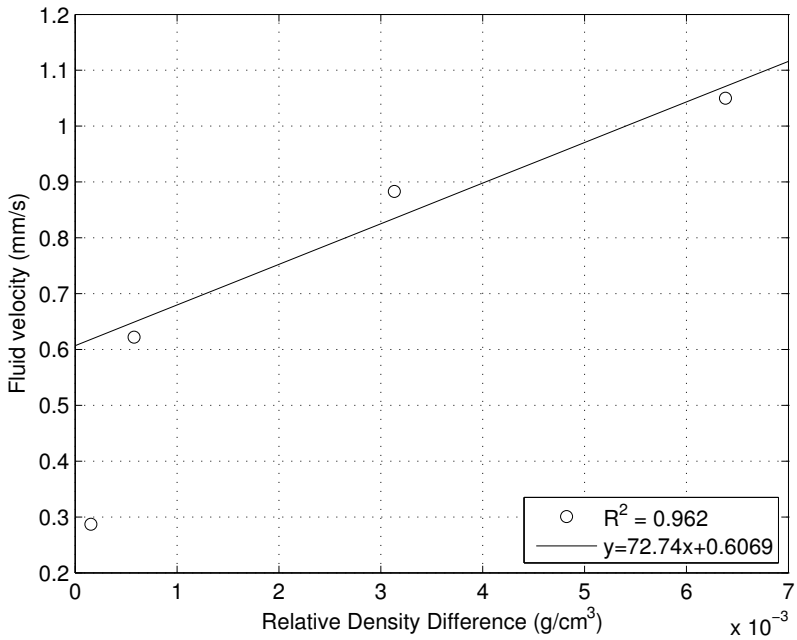


Figure 6.15: Graph of the relationship between linear fluid velocity and relative density difference. Data point 0.287 mm/s was classified as an outlier and ignored due to back-mixing and the hydraulic regime not being observed.

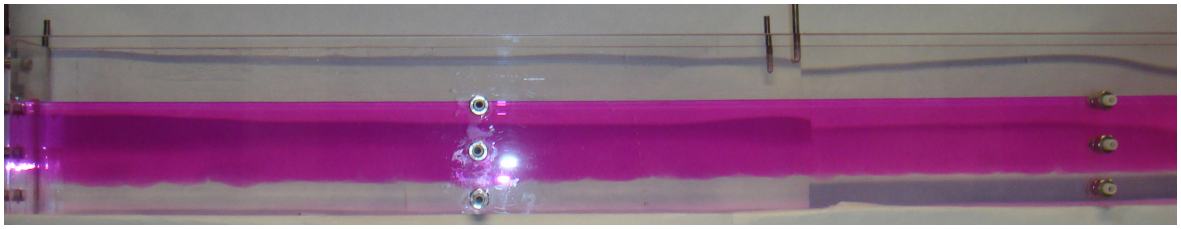
will be conducted, that being the ratio of convective transport to diffusive transport, namely the Peclet number (Pe). Chen and Meiburg(1996) showed that at low Pe, the displacement front between two miscible fluids becomes more diffuse at the tip and the concentration diffuses relatively quickly across the duct. Similarly, Rakotomalala et al. (1997) showed that at Pe of the order 1, mixing involves diffusion and advection in the flow direction. However, at large Pe, the fluids do not mix and there is a well defined interface. This was determined for flow between parallel plates with both fluids having identical viscosities. Their numerical simulation is an ideal and close approximation of the current experimental results, as the conditions are almost identical if the following assumptions are made:

- The floor of the reactor is the bottom plate, whilst the upper plate is the region of fluid (f_1) causing the shear stress similar to that of a wall/plate, hence a parabolic velocity profile.
- The sodium hydroxide reactor solution (1) and hydrochloric acid solutions (2) are dilute, having approximately equal viscosities and that are similar to that of water ($\mu_1 \approx \mu_2 \approx \mu_{H_2O}$).
- The molecular diffusion coefficient of H^+ is an accurate approximation of the overall observed molecular diffusion within the LFCR.

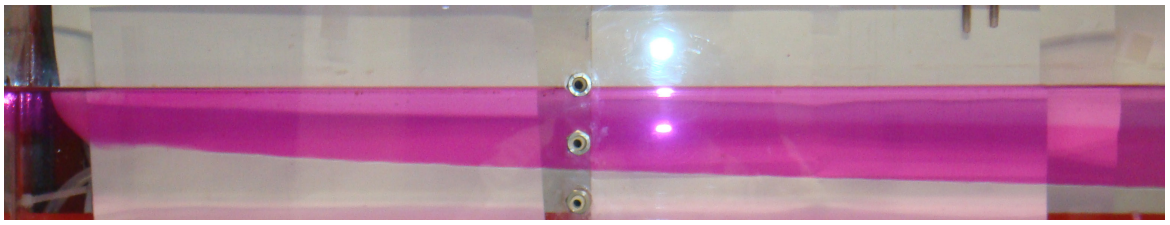
The Peclet number was defined in the same manner as Rakotomalala et al. (1997), where (v) is the linear fluid velocity, (H) is the clear layer height, (L) is the extent of the pumped fluid in the flow direction and (D_m) is the diffusion coefficient of an H^+ ion in water at 25°C ($D_m = 9.31 \times 10^{-5}$ cm^2/s) (Cussler, 2009). The Peclet number is defined in this way as it is the ratio between transverse diffusion time (τ_D) to the advection time (τ_C), which is an appropriate way of analytically describing the amount of transverse diffusion (equation 6.8).

$$Pe = \frac{\tau_D}{\tau_C} = \frac{vH^2}{LD_m} \tag{6.8}$$

There was a decrease in the Peclet number with a decrease in linear fluid velocity, which was expected. The numerical simulation was an accurate approximation of the experimental results. At a high Peclet number (165) there was very little transverse dispersion as there were clear finite boundary lines between the clear and pink layers. The Peclet number is inversely proportional to the advection time ($Pe \propto \frac{1}{\tau_C}$), therefore for a large Peclet number ($>> 1$) the advection time will be significantly smaller than the transverse diffusion time ($\tau_C >> \tau_D$). In essence, the time for advection to occur is much shorter than the diffusion time, therefore dispersion of the fluid elements (or convective mass transport) will be governed primarily by advection. At a much smaller Peclet number (8.54) mass transport of the H^+ ions was still governed by advection, however there was evidence of dispersion



(a) Hydraulic density study with HCl and NaOH at a ratio of 100:1. There is diffusion in the vertical y-direction, indicated by the wavy pink layer.



(b) Hydraulic density study with HCl and NaOH at a ratio of 10:1. There is substantially more diffusion in the vertical y-direction, due to the lower advective transport in the z-direction.

Figure 6.16: Photographs of the clear laminar layer and pink layer interface, depicting the effects of transverse dispersion by increased diffusive transport

by diffusion occurring within the clear laminar layer. The wavy nature of the pink layer at the pink-clear interface was not caused by the velocity of the fluid, as this was not evident at higher velocities (> 0.883 mm/s) (Figure 6.16a). Consequently, the uneven interface was due to increased dispersion by molecular diffusion upwards in the y-direction. Finally at the lowest Peclet number (0.6), there was no laminar parabolic velocity profile front, but a 'clear' wedge, which was predicted by the numerical simulation as well (Figure 6.16b). The lack of a velocity profile front was due to the extremely low fluid velocity. Hence, transverse dispersion was dominated by diffusion in the y-direction (upward), rather than advection in the y and z-directions. In other words transverse dispersion is a function of influent density and therefore the smaller the relative density difference the greater the axial dispersion, with convective mass transport being dominated by molecular diffusion. As a result, the LFCR is not only stratified on the macro-scale, in terms of the entire liquid height (0.1 m), but also has limited diffusion at low linear velocities or relative density differences. For these reasons the Peclet number should be greater than 25, with a minimum linear velocity of 1 mm/s in order to have improved transverse dispersion by advection.

For this purpose a mixing study was also conducted in order to improve the amount of dispersion in the LFCR, due to the slow mass transport of fluid elements and poor homogeneity within the reactor. Due to the extremely slow flow rates and laminar regime, cylindrical baffles were utilised. This was done in an effort to create vortices in the wake of the cylinder, similar to that of the Von Karman vortex sheet. Numerous studies have been conducted on cylinders within a laminar flow regime (Wen & Lin, 2001; Fu &

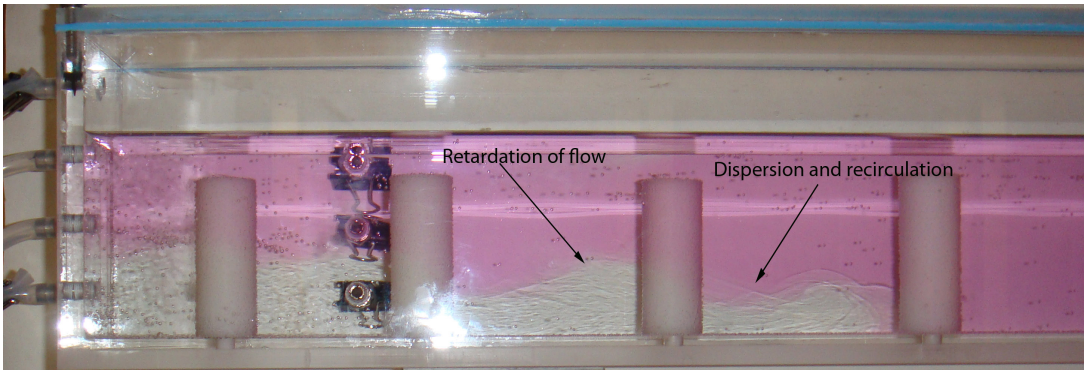


Figure 6.17: Photograph depicting the retardation of fluid flow in the LFCR by 30 mm cylindrical baffles. Additionally, the recirculation and significant increase in mixing and dispersion is clearly illustrated by the uneven clear-pink interface. (Test no. 3, HCl (0.42 M))

Rockwell, 2005; Chen et al., 2007a) as well as within a channel (Zovatto & Pedrizzetti, 2001; Chakraborty et al., 2004; Rehimi et al., 2008). The flow around a circular cylinder in an infinite fluid medium is conditioned by the Reynolds number. When $\mathrm{Re} < 5$, the flow is governed by creeping flow and the effects of viscosity. However when $5 < \mathrm{Re} < 47$, two steady recirculation regions develop behind the cylinder. Furthermore, for $\mathrm{Re} \approx 47$, which is the approximate Reynolds number the LFCR is operated at the wake becomes unstable , creating the appearance of a vortex street (Rehimi et al., 2008). However, the presence of two parallel walls can confine or restrict the vortices that are formed. Due to the unique stratified flow pattern within the LFCR, it can only be approximated to the flow patterns in previous studies and only qualitative deductions can be made. The 30 mm cylinders did cause substantial dispersion and mixing in the LFCR, however it was at the expense of retarding the fluid flow velocity (Figure 6.17). The fluid front passed around the cylinder and was forced upwards due to stagnation at the cylinder surface. There was a large amount of recirculation or stagnation in between the cylinders. Consequently, the 30 mm cylinders functioned more as resistive barriers to the laminar fluid, which was not favourable considering the extremely low flow rate. These particular cylinders would be better suited at a higher flow rate. Instead, a smaller diameter cylinder (10 mm) was utilised, but the dispersion and mixing was drastically reduced due to the cylinder being too thin and the confinement ratio being too small ($\phi = \frac{1}{10}$). On the other hand the larger cylinder created a confinement ratio of ($\phi = \frac{3}{10}$), which was significantly bigger and increased the dispersion.

6.7 Conclusion

The linear flow channel reactor was originally designed under the assumption that there would be plug flow within the bulk liquid volume. However, there was poor mixing with two distinct fluid (laminar) flow regions so plug-flow was not achieved. The reactor was stratified and had a concentration gradient in the y-direction as well as the z-direction. As a result, the original LFCR design allowed the incoming fluid to essentially bypass the FSB reaction zone, by exiting out the effluent port at the bottom back corner of the reactor. This explains the substantial disparity between the 'observed' sulphide oxidation efficiency and sulphur yield in the initial data generated at GARL. For this reason it was redesigned and the effluent port was raised to the height of the bulk liquid, thus forcing the influent upwards towards the reaction zone, and increasing the residence time from 0.33 - 1.21 hours up to 23.3 - 24 hours.

A dye tracer study was performed to accurately determine the hydraulic regime in the reactor. It was determined that an acid/base phenolphthalein dye tracer was the most effective at mapping the fluid flow path, and offered the greatest clarity and resolution in terms of the time lapse photography. A laminar parabolic velocity profile was observed along the floor of the reactor, due to the slower moving bulk liquid above acting as a pseudo-wall. Hence, the observed flow pattern was similar to that of laminar flow between parallel plates, with a moving upper plate boundary. The importance of influent density was determined to be highly significant to the hydraulic regime. The fluid velocity was linearly related to the relative density difference and the influent density not only affected the linear fluid velocity, but also the level of dispersion. At a higher influent density, the fluid velocity was greater and the level of dispersion by diffusion was reduced, but increased by advection. The influent moved consistently along the floor of the reactor to the back wall, then displaced the fluid above it. Moreover, there was a clear well-defined interface between the clear and pink layers. At lower influent densities, the RDD approached zero (or negative), resulting in a lower fluid velocity and greater level of dispersion by molecular diffusion, relative to advection. For this reason, there was a greater mass transport of influent in the vertical y-direction than along the channel length (z-direction). Thus, the clear-pink interface had a wavy uneven nature. Additionally, it was assumed at a flow rate of 12.5 L/day that the residence time of a fluid element was 48 hours. However, it varied from 46.6-49 hours due to a fluid element rising sooner to the exit level port due to the above-mentioned laminar flow mixing pattern. Mixing and dispersion was improved by the implementation of cylindrical baffles, however they promoted stagnation, back mixing and accumulation of the influent in between the cylinders, so were not considered for further application.

In short, the LFCR has a stratified liquid-liquid flow pattern of miscible fluids in the laminar flow regime. There was very little transverse dispersion, hence plug flow is not present within the bulk liquid volume. Nevertheless, the final question of whether the

LFCR should be homogeneously mixed or remain heterogeneous was not answered. This will be covered extensively in Chapter 8. The implications of these hydrodynamics on the sulphide oxidation within a biological system in the LFCR will be explained.

Chapter 7

Abiotic sulphide oxidation and Initial biotic studies

7.1 Introduction

The chapter will be presented as a series of three separate studies under the umbrella of abiotic sulphide oxidation, in order to determine the extent of chemical sulphide oxidation Following this will be a preliminary study on biological sulphide oxidation in the LFCR. A batch reactor experiment was performed in order to determine the nature of chemical sulphide oxidation within a perfectly mixed (ideal) and oxygenated batch reactor system. The primary focus was to determine the sulphur species formed as a result of abiotic sulphide oxidation, and the role of pH as it has been reported (Chapter 3) to be a crucial parameter in sulphide oxidation and sulphur species selectivity. Thereafter, the results of an abiotic LFCR experiment at a natural sulphide pH of 11.6 and 7 will be discussed, highlighting the significant differences between a well-mixed ideal system and that of the LFCR, and the sulphur species formed. Thereafter the results of a preliminary biotic LFCR study will be presented, to contrast the effect of combined chemical and biological sulphide oxidation processes, in an effort to determine the extent to which chemical sulphide oxidation plays a role in the overall process. Please note, all experimental runs from this chapter onwards will be numbered from one onwards. Furthermore, they will be referred to "experimental run no." in the text, and not by the full descriptive headings. The following key questions will be addressed within this chapter:

1. Is sulphide oxidation in the LFCR governed primarily by chemical sulphide oxidation or biological sulphide oxidation, and if a combination to what extent does chemical sulphide oxidation play a role?

2. What are the primary sulphur species formed by abiotic sulphide oxidation and do they differ from a biologically catalysed system?

7.2 Abiotic sulphide oxidation - Batch reactor study

7.2.1 Experimental

Chemical sulphide ($Na_2S.9H_2O$) was utilised and the experiment was run in magnetically stirred batch reactors with a working volume of 200 mL. The reactor was left open and was stirred at 100 rpm. The starting sulphide concentration was 6.061 mM and concentrated hydrochloric acid (32%) was periodically added to adjust the pH, where necessary. The pH was not adjusted in run 1, while in run 2 it was only adjusted down to pH 7.0 twice, and in run 3 pH adjustment to pH 7.0 was continuous. The pH was (manually) adjusted every 30 minutes, except in the final hour of the experiment. The experiments were conducted at atmospheric pressure (101.3 kPa) and ambient temperature (23°C). Samples were analysed for sulphur, sulphate and polysulphides. Thiosulphate and sulfite assays were not developed at the time.

7.2.2 Results & discussion

The results of the batch reactor study are summarised in Table 7.1. The data from the individual experiments will be discussed in detail in the sections below.

Table 7.1: Results of sulphide oxidation and sulphur species formed within the constant-volume batch reactor study at various pH values

Run	Sulphide conversion (%)	Sulphide converted (mmol)	S_X^{2-}	$S_{8,c}$	SO_4^{2-}	Avg. pH	Rate constant (k) ($\frac{1}{hr}$)
1	24.7	0.30	0.074	0	0	11.4	0.0432
2	64.7	0.78	0.154	0.082	0.152	8.43	0.189
3	89.5	1.11	0.345	0.074	0.126	7.0	0.2268 - 1.243

7.2.2.1 Experimental run 1 - pH = 11.6

The sulphide concentration decreased from 6.06 to 4.56 mM over seven hours. However, there was very little change in the pH (Figure 7.1 a). The samples were analysed for sulphide, polysulphides, sulphur and sulphate; and it was determined that the sulphide concentration was 5.5 mM after half an hour. The concentration decreased slowly over the next four hours to 4.56 mM. The sulphide oxidation rate was determined to be 0.214 mmole/L.hr. The rapid decrease in sulphide concentration over the first half an hour can be explained by the formation of colloidal sulphur in extremely low concentrations and thiosulphate ($S_2O_3^{2-}$) or sulfite (HSO_3^-) (reactions 7.1-7.3). While no colloidal sulphur was detected, it is the only known way polysulphides were formed by the reaction of sulphide with free colloidal sulphur (reaction 7.4). Additionally the rapid decrease in sulphide

concentration between 5 - 6 hours can also be explained by the appearance of polysulphides species at a total concentration of 0.079 mM. It is most likely the sulphide oxidised within this experiment was converted to predominantly thiosulphate and sulfite (0.226 mmol), as the final polysulphide concentration was 0.074 mmol and no colloidal sulphur or sulphate was detected (Table 7.1). The pH decrease was negligible as it decreased from 11.6 to 11.2, which was most likely caused by the formation of protons as a by-product of the polysulphide synthesis reaction.

$$2HS^- + O_2 \rightarrow \frac{1}{4}S_8 + 2OH^- \tag{7.1}$$

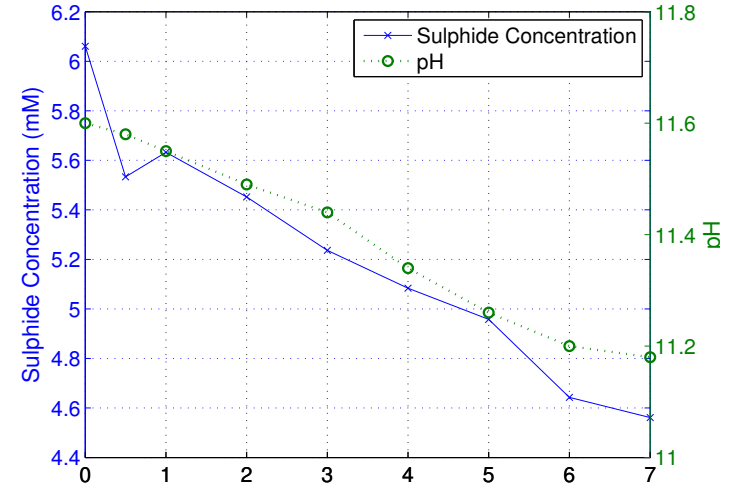
$$2HS^- + 2O_2 \rightarrow H_2O + S_2O_3^{2-}\ \Delta G^o = -387.35\,kJ/mol \tag{7.2}$$

$$HS^- + \frac{3}{2}O_2 \rightarrow HSO_3^- \tag{7.3}$$

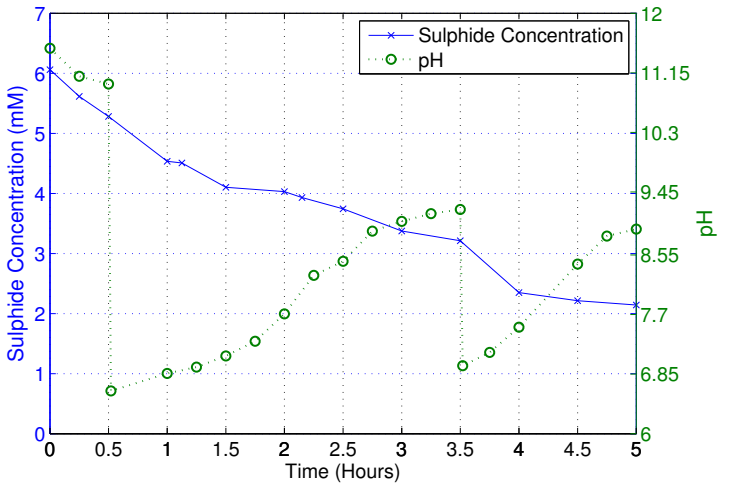
$$HS^- + S_8 \rightleftharpoons HS_9^- \rightleftharpoons S_9^{2-} + H^+ \tag{7.4}$$

7.2.2.2 Experimental run 2 - 11.6 > pH > 6.5

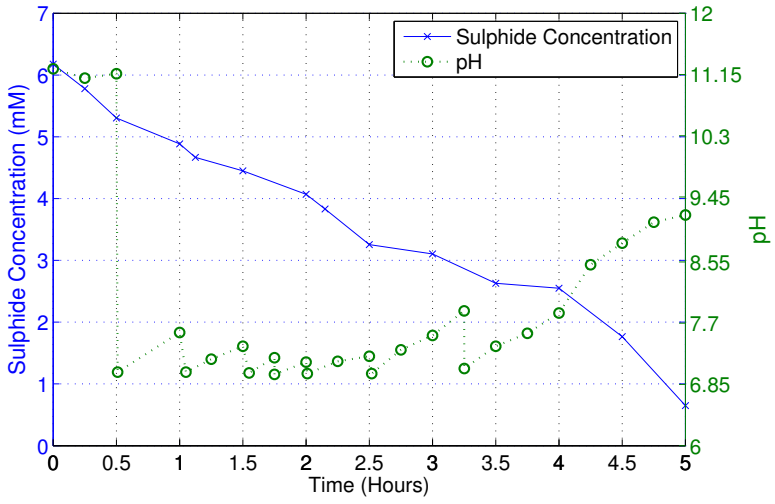
In run 2 the sulphide concentration decreased from 6.06 to 2.14 mM over the duration of the experiment (5 hours) and the pH increased steadily. However, the pH was adjusted down from 11.5 to 6.61 at the 30th minute after the start of the experiment (Figure 7.1b). Thereafter it was adjusted again, to 6.97, after 3.5 hours. The pH was not maintained at pH 7.0, in order to see how it fluctuated as a result of acid addition and the changes in sulphur speciation. Following the initial adjustment to pH 6.61 the pH had increased up to pH 6.85 within 30 minutes. The pH increased further to pH 6.85 accompanied by a decrease in sulphide concentration from 5.3 to 4.89 mM. Therefore, 0.26 mmol of sulphide was oxidised within the first hour and 0.1 and 0.149 mmol of polysulphides and colloidal sulphur respectively were formed (Figure 7.2c). Hence, the predominant species was sulphur and polysulphides as sulphate was detected in trace quantities (0.05 mmol). The pH continued to increase to pH 9.2, with a steady decrease in sulphide concentration after three and a half hours. At 3.5 hours acid was added to reduce the pH to 6.97. Post acid addition a sample was taken to determine the polysulphide and colloidal sulphur concentrations, which were 0.71 and 1.35 mM respectively (Figure 7.2b). The sharp increase in colloidal sulphur concentration was due to the increase in protons causing equilibrium reaction 7.4 to shift towards the left, favouring the decomposition of polysulphides. Thereafter the pH was allowed to increase again from the fourth to fifth hour and there was a slight increase in polysulphide concentration. The final polysulphide and colloidal sulphur concentrations were 0.771 and 0.41 mM, resulting in a final 0.154 and 0.082 mmol respectively (Table 7.1).



(a)

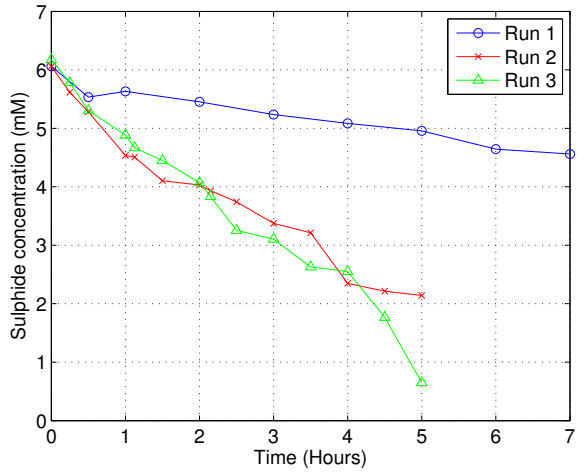


(b)

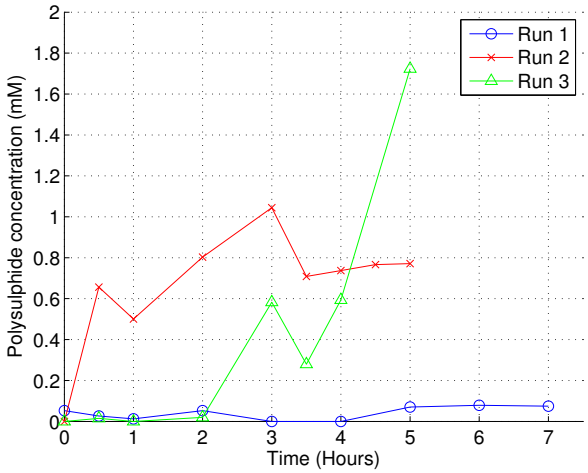


(c)

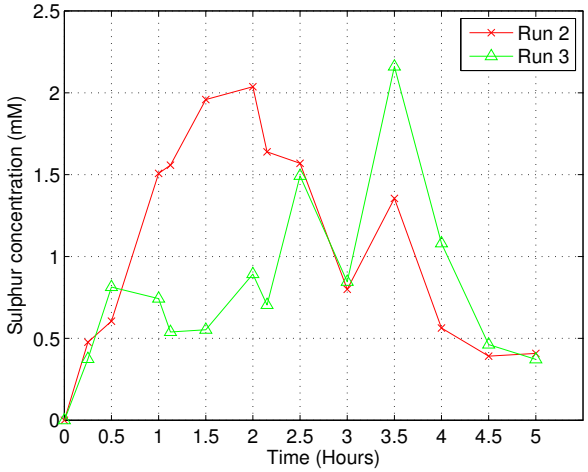
Figure 7.1: Sulphide concentration and pH vs. time for experimental batch-reactor runs 1(a), 2 (b) & 3 (c)



(a) Change in sulphide concentration throughout the duration of experimental runs 1, 2 and 3



(b) Measured polysulphide concentration in experimental runs 1, 2 and 3 throughout the duration of the experiment.



(c) Colloidal sulphur concentration observed in experimental run 2 and 3

Figure 7.2: Sulphur species concentration profiles measured during experimental runs 1 (pH = 11.6), 2 (11.6 > pH > 6.5) and 3 (pH = 7)

7.2.2.3 Experimental run 3 - pH = 7.0

Experimental run 3 was only conducted for five hours due to the rapid decrease (to almost zero) in sulphide concentration in the last hour (Figure 7.1 c). The pH was lowered to 7.0 after 30 minutes and was thereafter regularly maintained at pH 7.0. However, in the final hour the pH was allowed to rise in order to observe changes in sulphur speciation. A sulphide conversion of 89.5% was observed with 0.126 mmol of sulphate being formed. The most dominant species formed as a result of sulphide oxidation over the first three hours was colloidal sulphur (Figure 7.2c). Furthermore, the constant increase in the pH was due to the hydroxyl ions being produced (reaction 7.1). This is the only plausible explanation, as it would also explain the rapid decrease in sulphide concentration in the last hour. The sulphide concentration rapidly decreased due to it reacting with the free colloidal sulphur to form polysulphides (reaction 7.4). Moreover, this reaction was only observed when no pH adjustment occurred and the pH reached an alkaline range (pH $\geq$ 8). as the pH increased due to reaction 7.4. Therefore, the production of polysulphides over the first three hours of the experiment was suppressed due to the addition of acid, favouring the reverse reaction (7.4) . The final amount of polysulphides and colloidal sulphur was 0.345 and 0.074 mmol respectively. The final solution was also a green-yellowish colour clearly suggesting a high concentration of polysulphides.

7.2.2.4 Rate constant

The data was further analysed in order to determine the reaction order (α). The change in concentration as a function of time for a batch reactor can be represented mathematically by equation 7.5. If the reaction is first order, integration of equation 7.5 with the limit $C_A = C_{A0}$ at t = 0, will yield equation 7.6. Consequently, if there is a linear relationship the reaction follows first-order kinetics and the reaction constant (k) is the slope. ($A = HS^-$)

$$-\frac{\partial C_A}{\partial t} = kC_A^{\alpha} \tag{7.5}$$

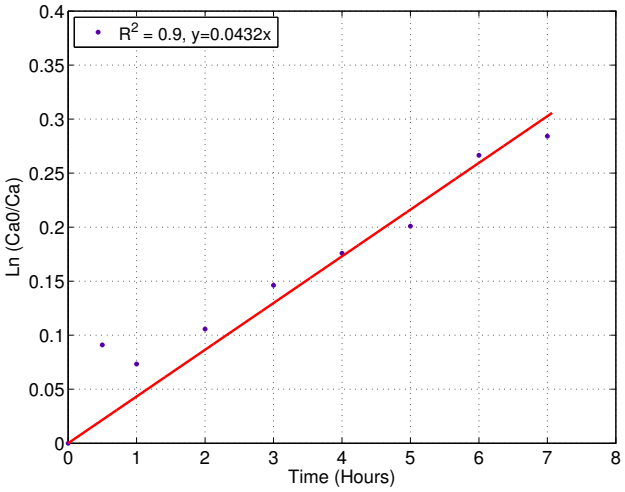
$$ln\frac{C_{A0}}{C_A} = kt \tag{7.6}$$

In all three experiments it was determined that the reactions did follow first order kinetics with respect to total sulfide (HS^-). The reaction rate constant (k) for an alkaline pH of 11.4 (average) was 0.0432 $\frac{1}{hr}$ (Figure 7.3a). The rate constant of experimental run 2 was determined to be 0.189 $\frac{1}{hr}$ (Figure 7.3b). The higher reaction rate did coincide with the findings of Chen & Morris (1972). They observed a maximum specific rate of sulphide oxidation in the pH range 7.7 - 8.34 and a minimum rate in the pH range 8.9 - 9.7. The rate constant was greatest in the final experiment (k = 0.2268 $\frac{1}{hr}$), however only over the first four hours (Figure 7.3c). The reaction rate was first order and the correlation

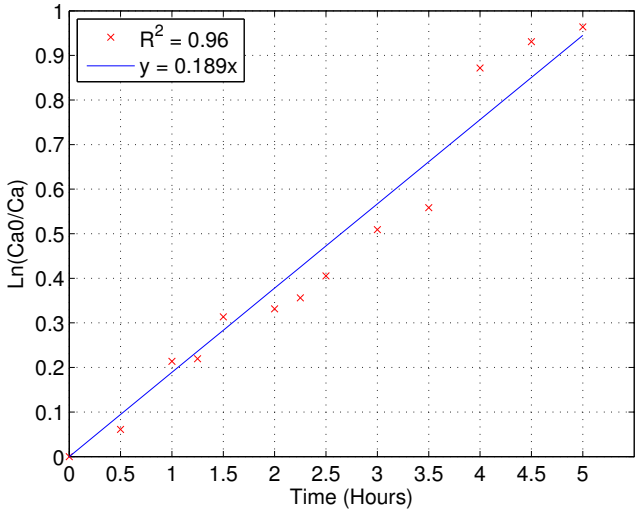
coefficient indicates a good fit ($R^2 = 0.976$). In the final hour the rate constant increased dramatically to k = 1.243 $\frac{1}{hr}$, due to the formation of polysulphides . This clearly shows the disproportionation of sulphur species due to pH and that observed reaction rates can only be clearly determined if the pH is carefully controlled.

7.2.3 Conclusion

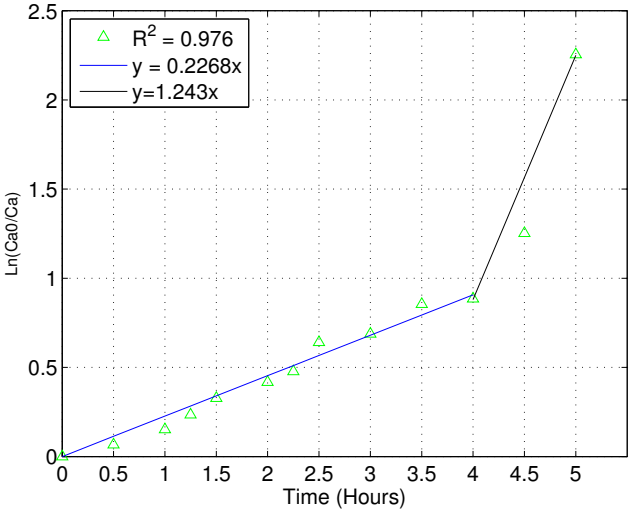
These simple batch reactor experiments showed that abiotic sulphide oxidation is highest in the pH range 7 - 8, which relates closely to Chen and Morris'(1972) observations. Additionally sulphur production is promoted within this pH range as well as the formation of some polysulphides. Even so, polysulphide production is only favoured at a more alkaline pH of 8.1 or greater, in the presence of colloidal sulphur. Moreover, this leads to the complete disproportionation of sulphur species, namely sulphide to polysulphides. This phenomenon was clearly illustrated by van den Bosch (2008) within a fed batch bioreactor, whereby he showed that the formation of polysulphides was contingent on there being colloidal sulphur present at pH 9.17. However, his findings were for a biological system and at an alkaline pH, greater than pH 8.6. No sulphate formation occurred. Therefore, in order to promote sulphur production and minimise unwanted by-products the ideal pH range for abiotic sulphide oxidation would be 7 - 8.3. However, I am of the opinion, that sulphate production within a biological system in this pH range, will be thermodynamically favoured to a certain extent, due to the complete oxidation of sulphide being more energetically favourable to the bateria.



(a)



(b)



(c)

Figure 7.3: Plot of linearised sulphide concentrations as a function of time for constant-volume batch reactor runs 1 (a), 2 (b) & 3 (c). Plots show a first-order relationship

7.3 Abiotic sulphide oxidation - LFCR study

An abiotic sulphide oxidation study was conducted within the LFCR, to observe the effects of hydrodynamics on the chemical system as well as the overall performance of the reactor, to provide additional insight into chemical sulphide oxidation.

7.3.1 Experimental

Two experiments were conducted as detailed in Table 7.2. Experimental run 4 was conducted without pH adjustment (pH 11.6) and experiment 5 was controlled within the pH range 7.0 - 8.3 using hyrochloric acid.

Table 7.2: Summary of operating conditions in the abiotic sulphide oxidation LFCR study. The pH in the LFCRs was not controlled, however the feed pH was maintained in the optimum range for run 5.

Run	Feed pH	Air flow rate (L/day)	Feed flow rate (L/day)	R.T. (Days)	Run time (Days)
4	11.6	48	5	5	10
5	7.0 - 8.3	48	12.5	2	12

7.3.2 Results

The results and sulphur species balance of experimental runs 4 and 5 are presented in Table 7.3.

Table 7.3: Sulphur species balance of abiotic sulphide oxidation LFCR experiments 4 - 5

Run	Feed pH	Sulphide loading rate	Sulphide conversion	Sulphur species (mmol)				
		(mmol/day)	(%)	Sulphide converted	Sulphate	Sulphur	Thiosulphate	Polysulphides
4	11.6	31.5	24.71	77.98	4.61	0	-	33.4
5	7.0 - 8.3	63.25	32.02	256.76	3.0	0	113.52	11.05

7.3.2.1 Experimental run 4 - Five day R.T. and pH 11.6

The inlet and outlet sulphide concentration data for the abiotic control reactor is presented in Figure 7.4. The results showed that the extent of sulphide oxidation was an average of 24.7%. At the feed rate and concentration this equated to an average daily sulphide oxidation rate of 7.8 mmole/day.

The pH of the solution in the reactor was high with an average 11.71 (Figure 7.4), for the duration of the experiment due to the absence of buffering compounds in the system. Bicarbonate is generated in the DPBR as a product of the oxidation of the carbon source and buffers the reactor effluent around pH 8 (normally in a biological system). Elemental sulphur has limited stability when the pH exceeds pH 9 and tends to hydrolyse to form thiosulphate and bisulphide (HS^-) (Kleinjan et al., 2005b; van den Bosch et al., 2008). The hydrodynamic profile in the reactor was similar to that predicted by the tracer studies (reported in Chapter 6), with significant stratification observed on the first day (Figure 7.5). The contour plot represents the sulphide concentration profile within the reactor at the various sampling points as depicted in Figure 4.4. Point 1.1 (1 length, 1 depth) is the sample point closest to the inlet, while point 5.3 represents the sample point closest to the base at the far end of the reactor. The data in Figure 7.5 confirms the laminar flow pattern along the base of the reactor, with the measured sulphide concentration ($>$ 8 mM) being significantly higher than the feed concentration. By day 5 (Figure 7.6) sulphide concentrations throughout the reactor had essentially stabilised around 6 mM. The homogeneous distribution was a consequence of the slow advective transport, and the fact that the denser influent displaced liquid at the bottom upwards. This flow pattern was illustrated during the tracer study. There was no further change in the sulphide distribution pattern for the remainder of the experiment.

Approximately 78 mmol of sulphide was converted and 49% of this has been accounted for, by by-products sulphate and polysulphides. As anticipated very little sulphate was produced (5.9%), due to the extremely high pH, consistent with the batch reactor study. The remainder (51%) was most likely thiosulphate (19.9 mmol) as no elemental sulphur was present. Chen & Morris (1972) demonstrated that the predominant products formed from sulphide oxidation at pH $>$ 8.5 was thiosulphate. Furthermore, sulphite was formed very slowly, but was oxidised to sulphate. The overall measured sulphide conversion (24.7%) and sulphur species formed is similar to what was observed in the batch reactor experiment (1). The average sulphide oxidation rate was 0.013 mmol/L.hr, which was significantly lower than the sulphide oxidation rate within batch reactor run 1. This experiment illustrated the effect of the hydrodynamic regime in the LFCR as well as the implications of limited oxygen diffusion into the bulk liquid volume.

7.3.2.2 Experimental run 5 - Two day R.T. - pH = 7.0

In contrast, the pH controlled system performed very differently. The dissolution of crystalline sodium sulphide produced a clear solution. However, as the pH was reduced to between pH 7 and pH 8.3, in the presence of free dissolved oxygen, polysulphide formation occurred and the solution was characterised by a "strawish-green" colour (Chen & Morris, 1972). The fresh feed pumped into the reactor was initially at a lower pH (pH 7) than the bulk solution ($\pm$ pH 7.8). As a result, the formation of a transient plume of colloidal sulphur was observed (Figure 7.7). The pattern of sulphur formation was consistent with

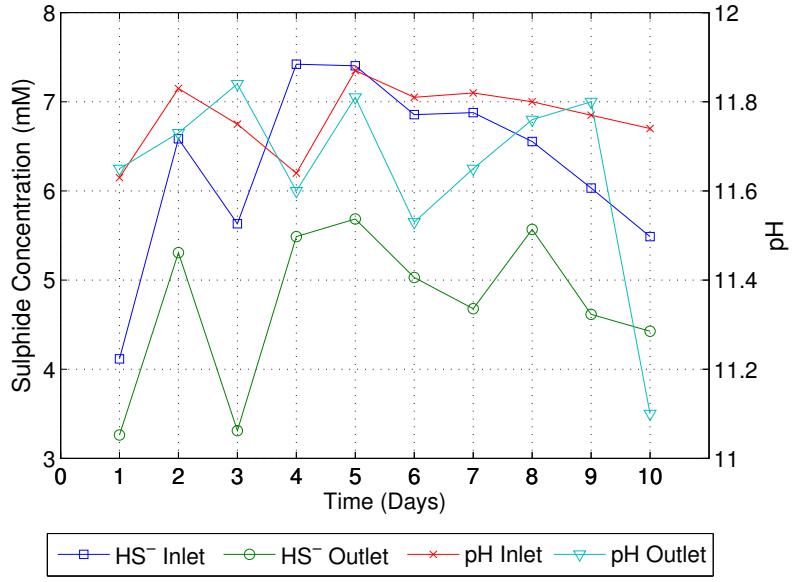


Figure 7.4: Influent an effluent sulphide concentration and pH profile of the LFCR (experimental run 4)

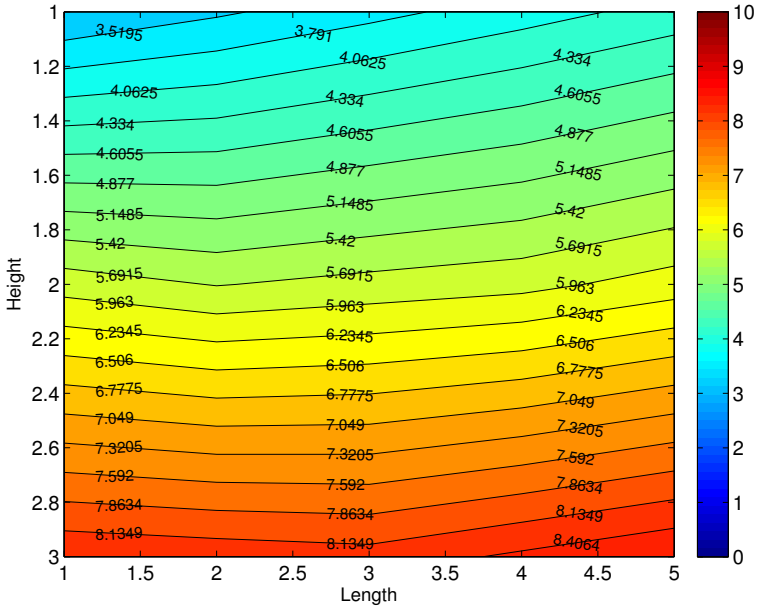


Figure 7.5: Sulphide concentration (mM) contour map of the LFCR on day 1 (experimental run 4). Depth 1 represents the top layer of sample ports and Length 1 the ports closest to the inlet (refer to Figure 5.1)

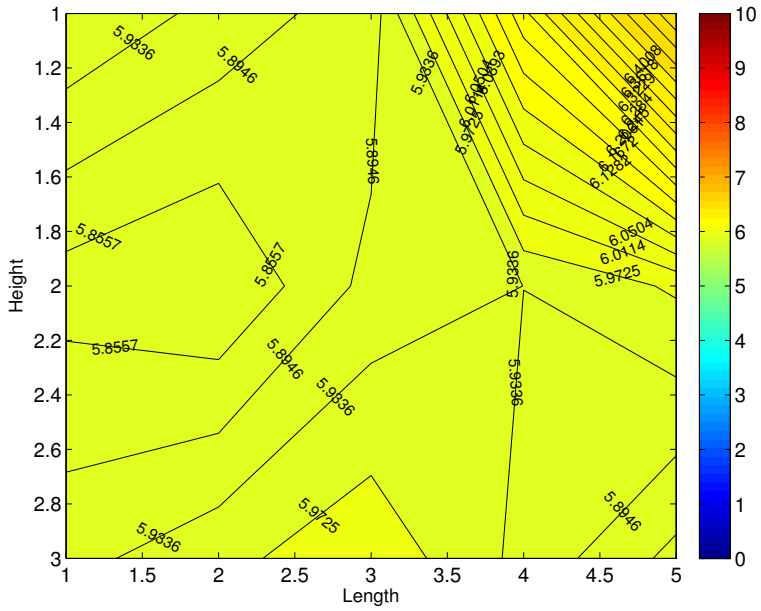


Figure 7.6: Sulphide concentration (mM) contour map of the LFCR on day 5 (experimental run 4)

the previously determined hydrodynamic regime. On day five the measured pH was 11.5 due to the reactor effluent being recycled for the remainder of the experiment, however the pH was lowered to 7.0 after sampling.

The plume of colloidal sulphur was short lived, most likely due the reaction with free sulphide to form polysulphide. The hydrogen ions liberated during this reaction caused the pH to decrease back to around pH 7 (Day 2), and once this had occurred no further colloidal sulphur was observed at the inlet (Figure 7.8). The mass balance data is consistent with this explanation. A total of 256.8 mmol (32.0%) of the influent sulphide was consumed. At steady state no colloidal sulphur was detected and very little sulphate, implying that the sulphide had been converted to polysulphides, thiosulphate and/or sulfite (Figure 7.9). Approximately 88% of the converted sulphide was converted to thiosulphate and 4.3% to polysulphides. This sulphur speciation profile is very different to that of experimental run 2, where colloidal sulphur and polysulphides accounted for the majority of the converted sulphide. The unaccounted converted sulphide species (7.7%) was most likely converted to sulphur, however due to the low concentrations it was most likely below the detection limit. The dissolved oxygen (D.O) concentration through the free liquid surface was determined by utilising a D.O. microprobe. Oxygen only managed to penetrate up to a liquid depth of 2800 μm (Figure 7.10), which equated to 2.8% penetration of the total depth. Furthermore, the low influent flow rate (5 L/day) resulted in the mass transport of the sulphide species to the reaction zone to be largely governed by diffusion. For these reasons, the rate of sulphide oxidation in the LFCR was greatly reduced and thiosulphate formation was favoured, than that was observed in the batch reactor study (2).

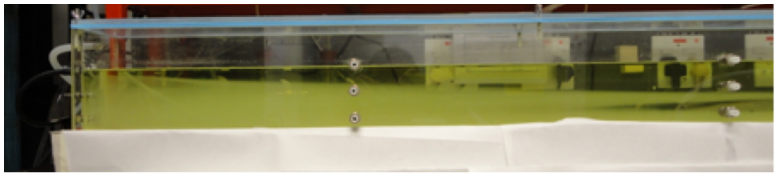


Figure 7.7: Evidence of colloidal sulphur formation during pH-controlled abiotic experimental run 5 (Day 1)

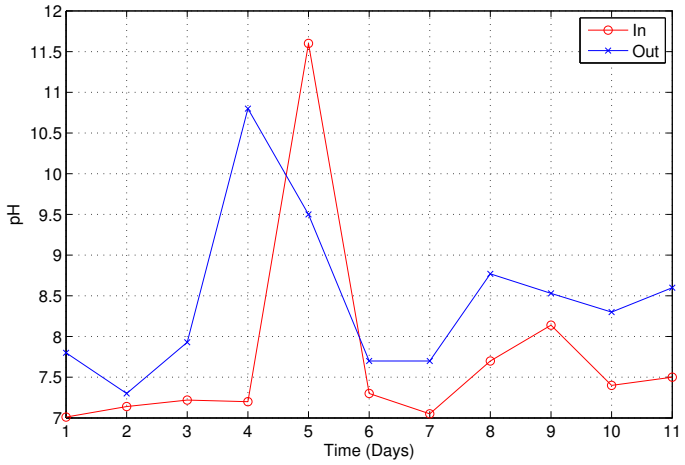


Figure 7.8: pH profiles of influent and effluent of LFCR experimental run 5. The feed pH was controlled within the optimal range of pH 7-8.3. The LFCR bulk-liquid pH was not controlled.

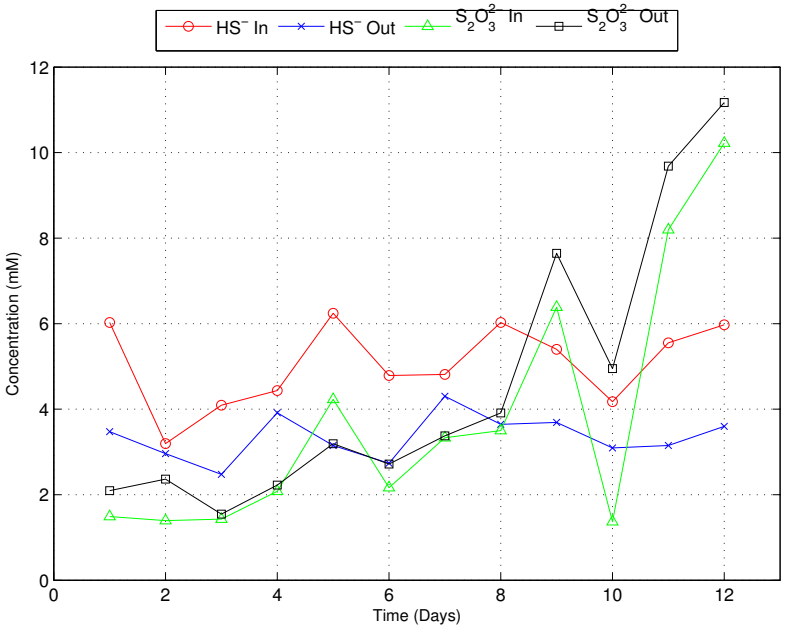


Figure 7.9: Sulphide and thiosulphate inlet and outlet concentrations measured over the duration of LFCR experimental run 5

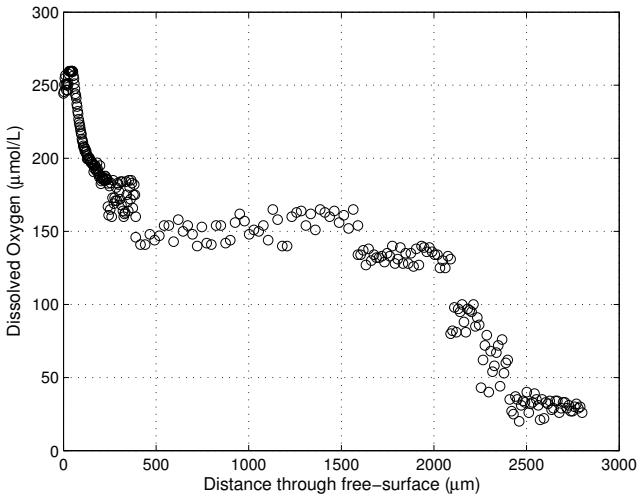


Figure 7.10: Dissolved oxygen concentration profile through the liquid surface for experimental run 5 (pH = 7.0) on day 4.

7.4 Biological sulphide oxidation - Initial LFCR study

7.4.1 Experimental

The experimental parameters for the two initial biological sulphide oxidation runs are summarised in Table 7.4. The LFCRs were fed DPBR effluent, which contained sulphide in addition to some sulphur and sulphate. However, the LFCRs were not supplemented with any carbon source and the pH of the feed stream was not controlled. The LFCRs were operated at a working liquid volume of 25 L and the headspace was provided with an excess of air, at 48 L/day, in order to provide substantially more than the stoichiometric amount of oxygen for biological sulphide oxidation to occur. Therefore the FSB would need to impede the oxygen mass transport in order to ensure the 2:1 sulphide to oxygen ratio. A feed flow rate of 5 L/day was selected, based on the preliminary test work completed at GARL (Chapter 2). The highest sulphur recovery was at a flow rate of 6.6 L/day and an apparent sulphide removal of 100%. Hence, a flow rate of 5 L/day would be an ideal starting point for gaining insight into the biological sulphide oxidation process within the LFCR. Experimental runs 6 and 7 were conducted under the same conditions in order to determine reproducibility.

Table 7.4: Experimental parameters for initial LFCR biological sulphide oxidation study (experimental run 6, 7).

Run	Air flow rate (L/day)	Feed flow rate (L/day)	R.T. (Days)	Run time (Days)	Feed pH
6	48	5	5	14	7.5
7	48	5	5	14	7.8

7.4.2 Results and discussion

The results and full sulphur species material balance of experimental runs 6 and 7 are presented in Table 7.5

Table 7.5: Sulphur species balance across initial biological experimental runs 6 & 7. Biofilm sulphur refers to sulphur in the floating biofilm.

Run	HS^- loading	HS^- converted	Conversion	Sulphur Species (mmol)				
	(mmol/day)	(mmol)	(%)	Biofilm	Colloidal	Sulphate	Polysulphides	$S^{\%}$
6	10.2	130.04	93.02	72.5	34.1	12.42	11.07	-
7	6.45	65.79	72.6	0	0	88.8	0	29.77%

$S^{\%}$ refers to the percent difference. This is the error between the measured HS^- converted and total of measured sulphur species

7.4.2.1 Experimental run 6 - Five Day R.T. - No acetate addition

Experimental run 6 was operated as a biotic system with a five day residence time and was fed sulphide effluent from the DPBR. The LFCR was run for five days, after which pseudo-steady-state (Section 8.3) was established and sulphide removal stabilised. Observation of the LFCR showed the appearance of a cloudy layer below the liquid surface (Figure 7.11). The presence of the colloidal sulphur particles had not been previously noted as the construction materials of the GARL reactors and demonstration scale units did not permit observation of the subsurface. The sulphur species balance was calculated for the steady-state period. The average sulphide loading rate was 10.2 mmol/day with a sulphide conversion of 93.02%. Approximately a third (36.05%) of the incoming sulphide was converted to unwanted products viz. sulphate (9.55%) and colloidal sulphur (26.5%) (Figure 7.12). Colloidal sulphur is difficult to recover, compared to sulphur formed within the FSB. Approximately 3.9 mmol/day of colloidal sulphur was formed due to the FSB not providing a sufficient barrier to oxygen transport into the bulk liquid. The formation of the colloidal sulphur layer was a consequence of the relatively thin and brittle biofilm layer, which did not significantly impede oxygen mass transfer (Figure 7.13). As a consequence the redox zone, where oxidation to elemental sulphur could occur was relatively thicker and sulphur formation was not confined to the biofilm. Colloidal sulphur also promotes the production of unwanted polysulphides. Sulphide oxidation during the unsteady-state period resulted primarily in polysulphide formation, suggested by the yellow colour of the solution and confirmed by removing a small sample and acidifying (polysulphide rapidly converted to elemental sulphur). Further oxidation of polysulphides to sulphur occurred on days 4 and 5. The colloidal sulphur layer was not stable and periodically condensed, with small sulphur particles sinking to the base of the reactor. The colloidal layer then reformed. This can be seen from the contour plots generated using data from the different regions in the reactor (Figure 7.13), which clearly show the formation of colloidal sulphur near the surface. Furthermore, due to poor FSB formation a large amount of colloidal sulphur that formed in the bulk liquid phase, exited from the reactor. This was observed on day 12, when the sulphur concentration in the effluent exceeded 2 mM (Figure 7.14).

The FSB also contained a large amount of inorganic precipitates (43.12 wt%) such as gypsum and calcium carbonate (determined by EDS) and lacked structural integrity, most likely due to the limited organic carbon. As a result, the FSB could not be harvested and the sulphur quantified. Therefore, the sulphur was calculated by measuring the other sulphur species and subtracting it from the total sulphide converted. There was also an increase in the pH of the bulk liquid due to the production of sulphur (Equation 3.21). The primary product was sulphur, hence the formation of hydroxyl ions increased the pH by approximately 0.5 pH units. Even though sulphate ions and polysulphides were formed, which generate protons, these were not sufficient to cause a decrease in pH.

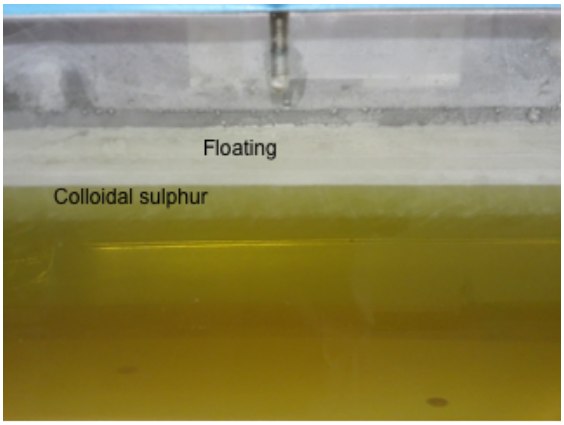
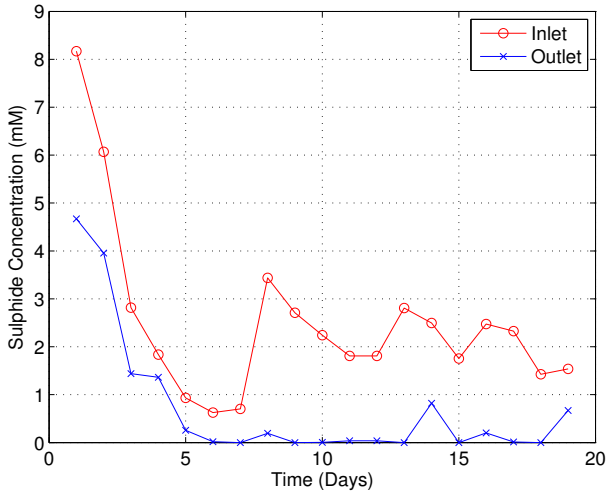


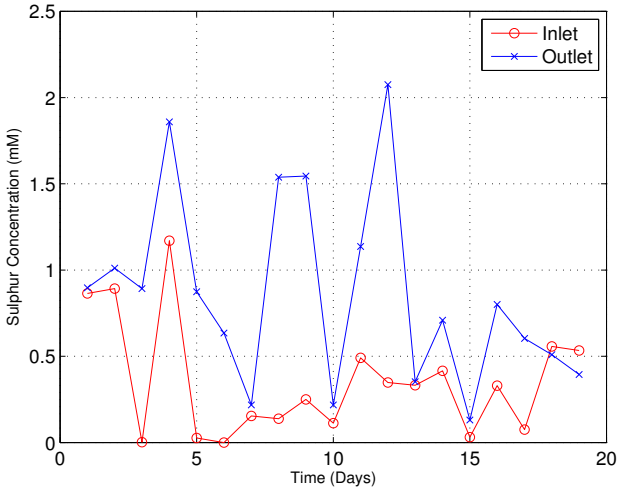
Figure 7.11: Elemental sulphur formation in the LFCR. Both the floating sulphur biofilm and colloidal sulphur particles are visible.

7.4.2.2 Experimental run 7 - Five day R.T. - No acetate addition

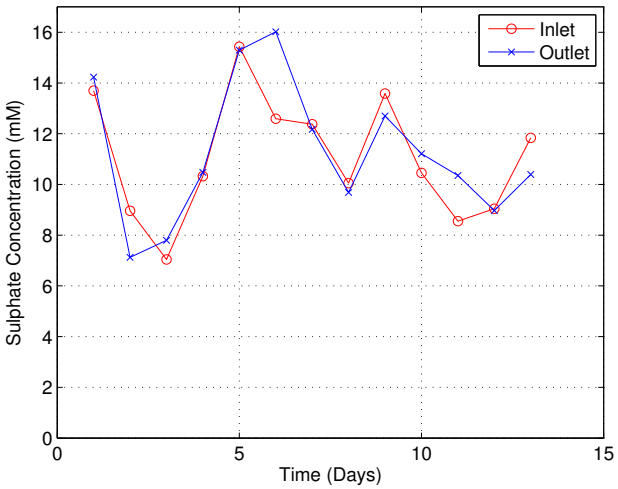
Experimental run 7 was conducted at a five-day residence time. The data from this experiment were characteristic of a poorly performing system. Effluent from the DPBR was fed to the LFCR without the feed sulphide concentration being manipulated, resulting in fluctuations in the feed sulphide concentration. This was due to the DPBR not performing efficiently, demonstrated by the fluctuating sulphide concentration and high sulphate concentration of the effluent. This is clearly illustrated in Figure 7.15a, as the sulphide concentration varied between 0 and 4 mM throughout the duration of the experiment. The high influent sulphate concentration is also indicative of a poor performing DPBR (Figure 7.15c). Only a partial biofilm developed on the liquid surface and as a result the mass transport of oxygen at the interfacial surface was unimpeded. Furthermore, the FSB was very thin and brittle with a large inorganic content in the form of gypsum. This, coupled with the relatively low (< 4 mM)and inconsistent feed sulphide concentration, resulted in a sulphide to oxygen stoichiometry significantly below 2:1 for the duration of the experiment. All the sulphide that reacted was fully oxidised to sulphate (Equation 3.23). Despite the lack of an intact FSB, light microscopy observations confirmed the presence of planktonic microorganisms (Figure 7.16), so the sulphide oxidation reactions were probably biologically catalysed (Buisman et al., 1990b, 1991). In addition, a portion of the elemental sulphur in the reactor was further oxidised to sulphate. This was clearly illustrated on day 9 (Figure 7.18). The sulphate concentration was high near the top back-end of the reactor due to the complete oxidation of sulphide and sulphur to sulphate. This was facilitated by the rapid diffusion of oxygen into the bulk liquid, due to the lack of an FSB, and catalysed by the planktonic population of sulphur-oxidising prokaryotes. The pH in this system fell to below pH 7, confirming the generation of acidity (Equation 3.22). The mass balance information indicated that fewer than 20 mmol of sulphate cannot be accounted for by the oxidation of influent sulphide and sulphur. The most likely explanation is that



(a) Sulphide concentration profiles



(b) Colloidal sulphur concentration profiles



(c) Sulphate concentration profiles for steady-state period

Figure 7.12: Influent and effluent concentration profiles for measured sulphur species in experimental run 6 of the LFCR

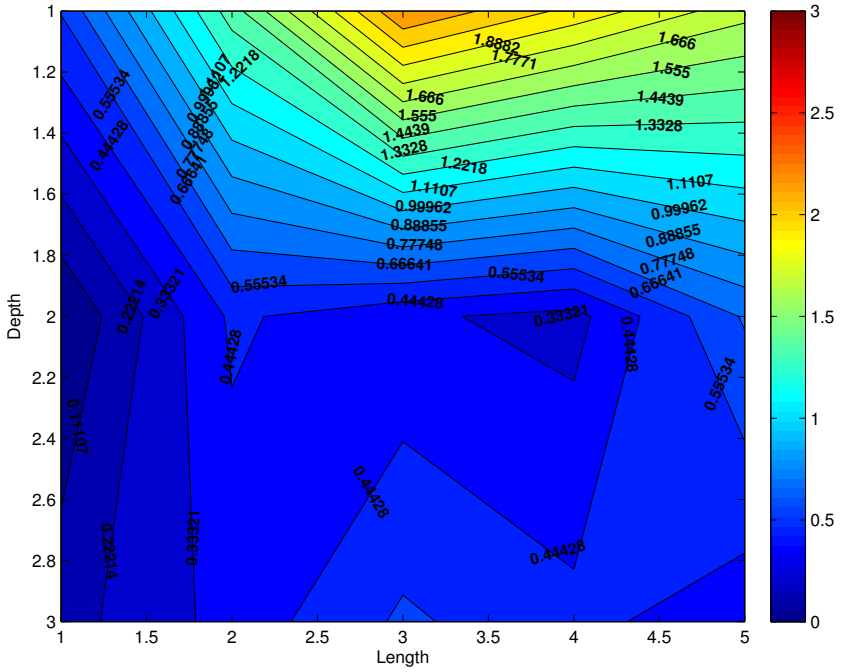


Figure 7.13: Contour plot showing the distribution of colloidal sulphur (mM) through the LFCR on day 2 of experimental run 6

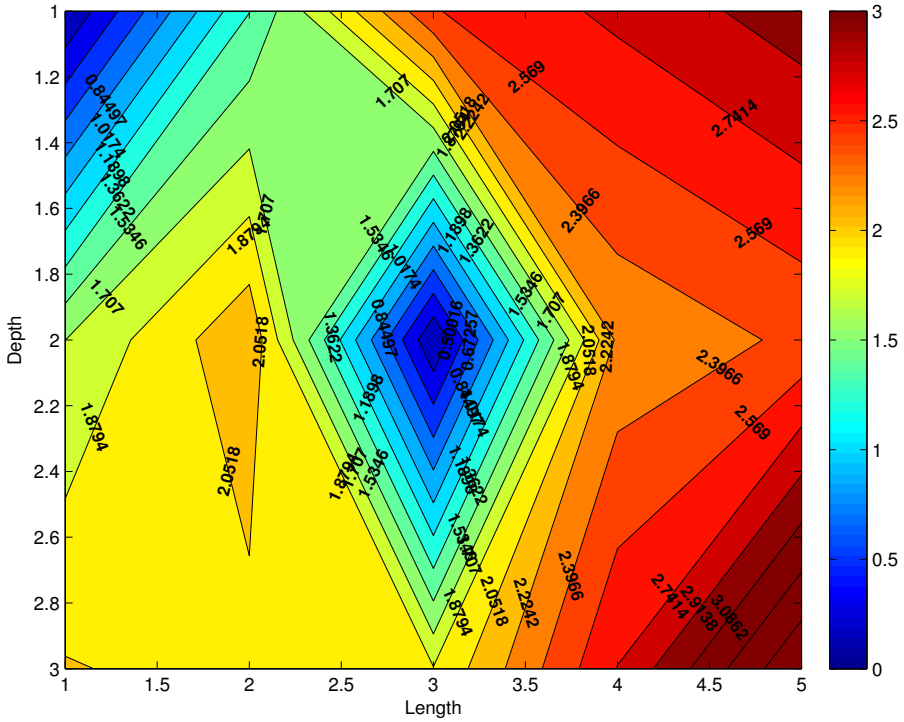
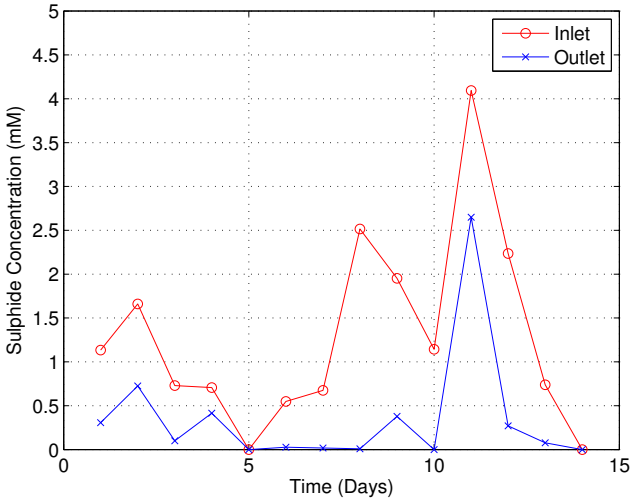


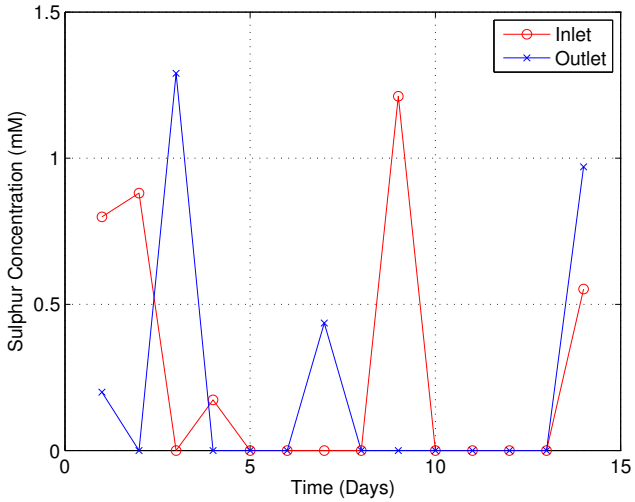
Figure 7.14: Contour plot showing distribution of colloidal sulpur (mM) through the LFCR on day 12

the relatively poor sulphate reduction in the DPBR resulted in calcium and sulphate concentrations being sufficiently high to induce gypsum ($CaSO_4.2H_2O$) precipitation. Due to the high sulphate, magnesium and calcium concentrations in the DPBR influent, it is possible that gypsum was formed within the DPBR. The solubility of gypsum within an aqueous magnesium or sodium sulphate solution (10 - 14 mM) is approximately 12 - 15 mM at 25°C (Tanji, 1969; Wollmann & Voigt, 2008). Therefore, a portion of the gypsum could have re-dissolved in the LFCR thus explaining the surplus sulphate in the effluent over days 1-3.

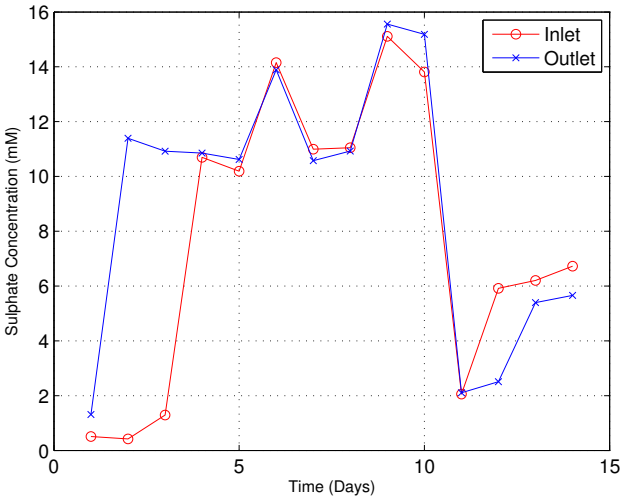
This experiment also clearly illustrated the importance of consistency in the performance of the sulphate reduction step. Inefficient sulphate reduction in the DPBR had a significant effect on the subsequent sulphide oxidation step as a large amount of residual sulphate entered the LFCR, resulting in a high concentration of sulphate in the reactor fluid (at the bottom) due to accumulation. This led to the relative density difference between the feed and reactor fluid being reversed. Consequently, the incoming sulphide didn't sink to the reactor floor but rather floated to the surface as it could not displace the denser sulphate ions. This was clearly observed in the hydraulic study (Chapter 6). The diversion of the sulphide to the air-water interface, where the dissolved oxygen concentraton was greatest, resulted in a sulphide:oxygen ratio below two and complete oxidation to sulphate. This phenomenon whereby the incoming sulphide feed 'floats' on the liquid surface, is clearly illustrated in Figure 7.19. From the sulphide and sulphate concentration data it was determined that the ratio of sulphide to sulphate was 1: 28 (on day 12), and the relative density difference (RDD) was -0.0006113 g/cm^3.



(a) Sulphide concentration profiles



(b) Colloidal sulphur concentration profiles



(c) Sulphate concentration profiles

Figure 7.15: Influent and effluent concentration profiles for measured sulphur species in experimental run 7 of the LFCR

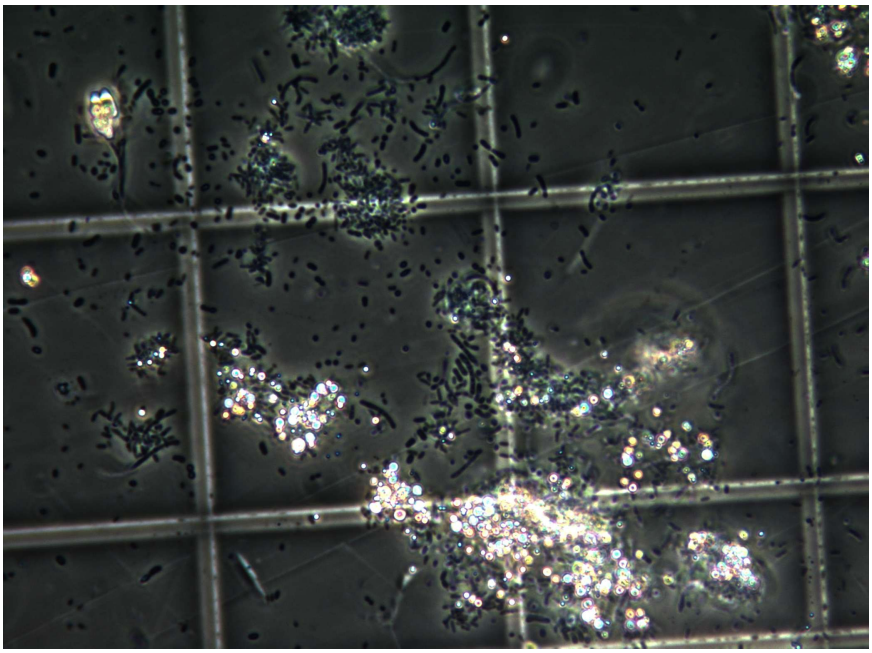


Figure 7.16: Light microscope image at 100X magnification depicting the planktonic population

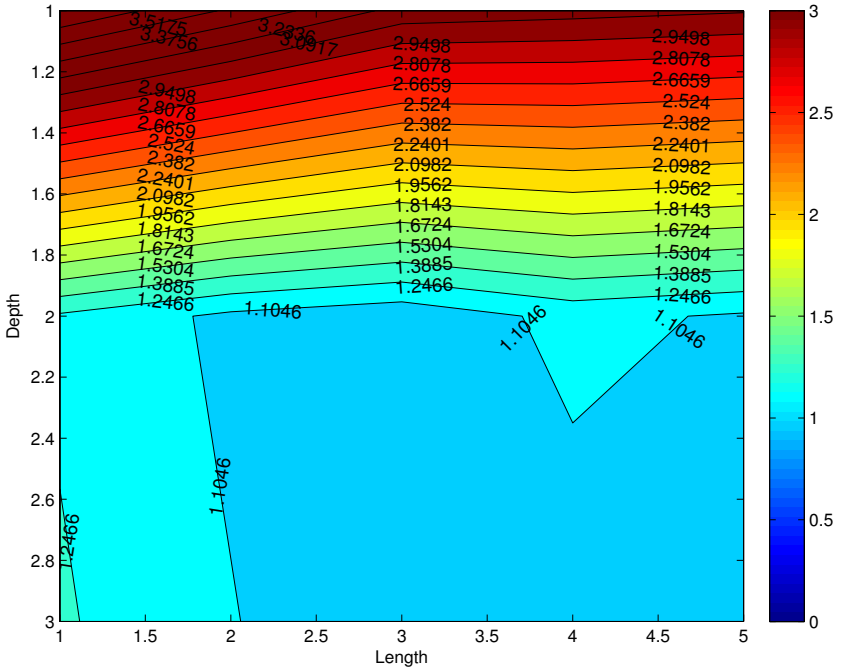


Figure 7.17: Sulphide concentration (mM) contour plot for experimental run 7 on day 10, representing the 'floating' of sulphide.

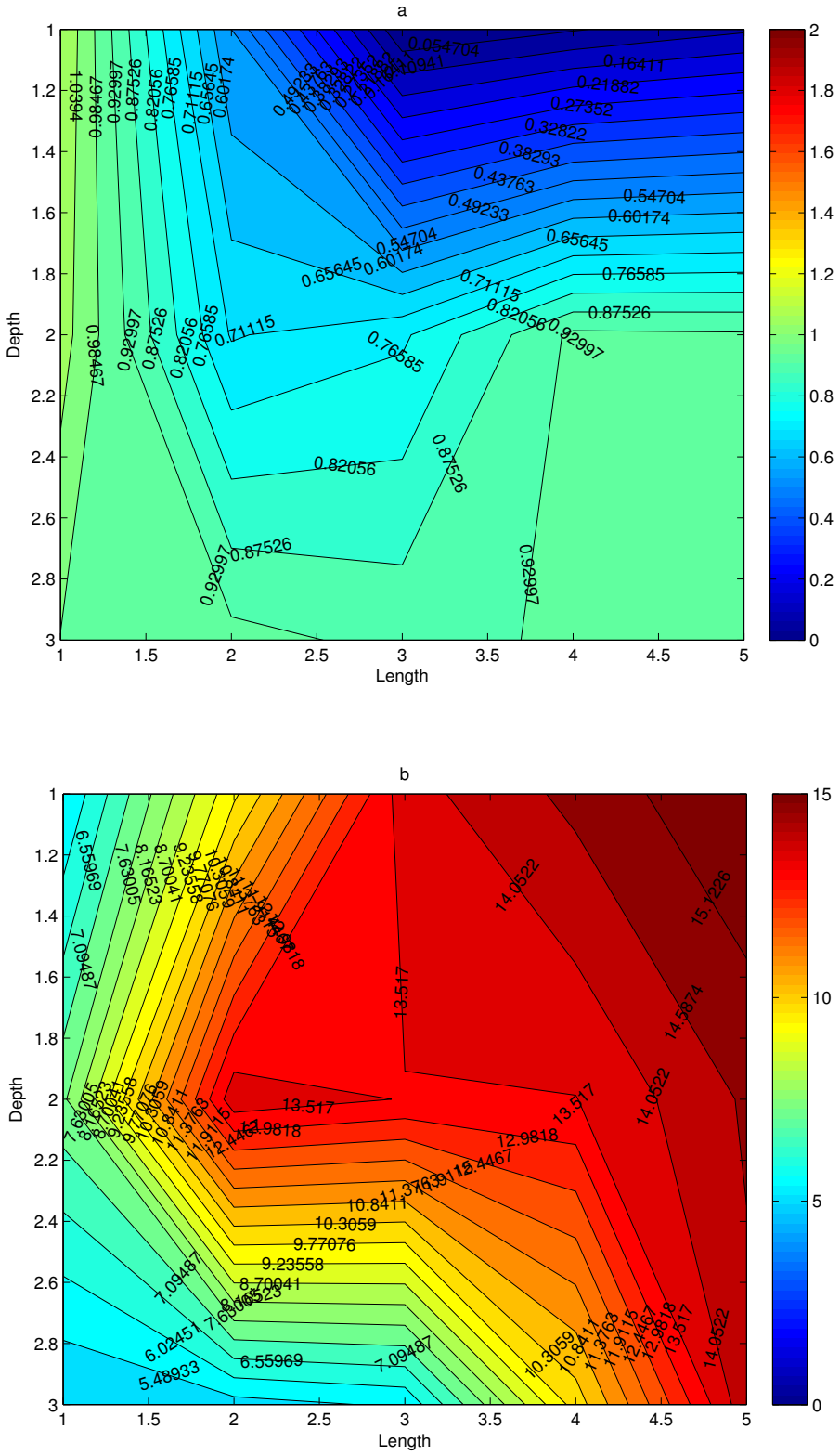


Figure 7.18: Sulphur (a) and sulphate (b) concentration (mM) contour plots for experimental run 7 on day 9

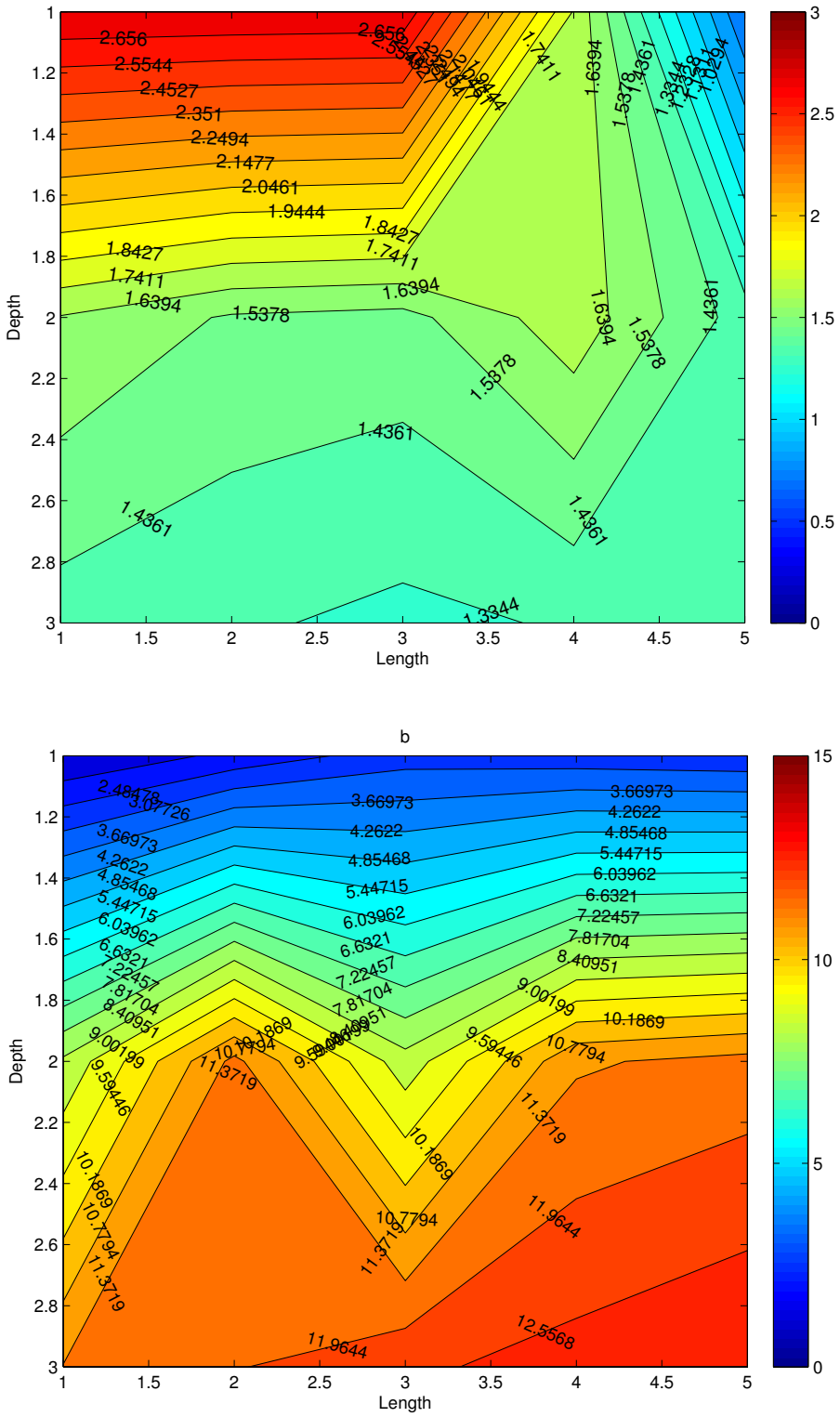


Figure 7.19: Sulphide (a) and sulphate (b) concentration (mM) contour plots for experimental run 7 on day 12

7.5 Final conclusions

The first three experimental runs were conducted in order to determine the rate of chemical sulphide oxidation within an ideally mixed and well oxygenated batch reactor system. It was determined that the reaction rate followed first order kinetics. Additionally, the sulphide oxidation rate was several orders of magnitude greater in the pH range 7 - 8 than the natural pH range of 11 - 11.6. Furthermore, the formation of colloidal sulphur was observed and the rapid formation of polysulphides due to the disproportionation of the sulphur species in an alkaline pH range (> 8). Moreover, the catalytic effect of the colloidal sulphur in the production of polysulphides led to a five-fold increase in the sulphide oxidation rate

Experimental runs 4 and 5 were conducted in order to determine the extent of chemical sulphide oxidation within the LFCR and the effect of the hydraulic regime on the oxidation rate. Once again, the sulphide oxidation rate was much lower at a pH of 11.6 (0.312 mmol/L.day) than 7.0 (0.856 mmol/L.day). Colloidal sulphur was formed at pH 7. However, this was further oxidised and the final sulphur species were primarily thiosulphate and polysulphides. The dissolved oxygen concentration as a function of depth was determined in experimental run 5. Oxygen only managed to penetrate the liquid surface up to a depth of 2.8 mm. Moreover, the poor hydrodynamics, lack of mixing and slow influent velocity exacerbated the poor convective mass transport of sulphide species to the (surface) reaction zone. Hence, the sulphide oxidation rate and sulphide conversion was significantly lower than was observed in the batch reactor study. It was a combination of poor oxygen diffusion, mixing and convective mass transport which resulted in a lower sulphide conversion of 24 - 32%. However, these conditions are necessary for optimal LFCR performance as demonstrated by experimental run 6 and 7.

In contrast, experimental runs 6 and 7 had a higher sulphide conversion of 93% and 72.6% respectively, yet the sulphide oxidation rates were 0.366 and 0.188 mmol/L.day. The lower sulphide oxidation rates (than experimental run 5) was due to the lower sulphide loading. A large amount of sulphate was formed, with possibly very little/no thiosulphate. This was due to the microorganisms favouring complete oxidation, as they derive more energy from the complete oxidation of sulphide to sulphate. Therefore, chemical sulphide oxidation played a smaller role in the overall observed oxidation rate and based on the suplur species formed. However it can greatly affect the sulphur species present and efficiency of the LFCR by formation of polysulphides.

Experiments 6 and 7 demonstrated the consequences of two of the challenges facing the demonstration plant, that of organic carbon flux and efficient and consistent upstream sulphate reduction. Due to the high concentration of sulphates in the feed stream to the LFCR, it led to the vertical displacement of the sulphide species. As a result, the incoming sulphide 'floated' on top, close to the surface and was rapidly oxidised. Therefore, the upstream sulphate reduction unit has to be operate efficiently in order to reduce the

concentration of sulphates in the effluent stream. This is important as the primary aim is to reduce sulphate to acceptable levels, but it also affects the performance of the subsequent oxidation unit.

Biofilm formation was incomplete in both experiments (6 & 7), most likely due to the fact that there was insufficient soluble, readily available carbon (VFAs) to support heterotrophic species involved in biofilm formation. The absence of a biofilm resulted in unimpeded mass flux of oxygen into the bulk liquid, facilitating complete oxidation of the sulphide and colloidal sulphur species.

Partial sulphide oxidation requires the sulphide to oxygen ratio to be 2:1 or greater to reduce sulphate formation. The following chapter will investigate the effect of organic loading on the ability to form a robust, structurally sound floating sulphur biofilm, to sufficiently impede oxygen mass transport and support sulphur deposition. Moreover, the effect of residence time will also be investigated in order to determine the optimal flow conditions for maximum sulphide conversion to sulphur.

Chapter 8

Biological LFCR experiments

8.1 Introduction

In the preceding chapters the hydrodynamics in the LFCR were characterised in order to understand the flow regime within the reactor. This provided insight into the importance of fluid densities and more importantly the relative density difference (RDD). Additionally, the relationship between fluid density and residence time was highlighted. The nature of chemical sulphide oxidation within the LFCR was investigated and the products formed as a result of chemical sulphide oxidation were determined. Moreover, the role of pH on chemical sulphide oxidation was also illustrated.

Therefore, the aim of this chapter is to investigate and describe the LFCR performance as a biological system for the partial oxidation of sulphide to sulphur and the recovery of the sulphur via the floating sulphur biofilm. The performance of the LFCR is heavily reliant on the ratio of sulphide to oxygen being maintained at two to one or greater. However, the amount of oxygen being introduced into the system cannot be controlled as the system has to remain semi-passive. Therefore, the FSB is responsible for regulating the flux of oxygen into the liquid surface in order to maintain this ratio.

The data presented in this chapter will be used to test the following stated hypotheses:

- The biofilm structural integrity and sulphur content of the biofilm increases, with a decrease in residence time and increase in organic loading to an optimum; above which the biofilm becomes primarily organic and system performance is compromised.
- The rate of sulphide oxidation within the FSB is mass transfer controlled with the flux of oxygen being controlled primarily by FSB thickness, density (porosity) and structure.

A number of specific questions are addressed through the data presented in this chapter. These are listed below.

1. Is there a loss of $H_2S_{(g)}$ through the FSB, and is it this missing component what has hindered the ability to close the sulphur material balance across the LFCR ?
2. Does sulphide oxidation occur within the bulk-phase of the linear flow channel reactor and is it necessary for the reactor fluid to be perfectly mixed?

3. Does LFCR performance increase (i.e. sulphur recovery via the FSB) with a decrease in residence time?
4. What is the optimal residence time in the LFCR and what is the best method for sulphur recovery from the floating sulphur biofilm?
5. Does the FSB increase in thickness with a decrease in residence time?
6. Does the structure and porosity of the FSB change with residence time?
7. Data presented in the previous chapter confirmed the LFCR was organic carbon limited and this restricted biofilm formation. Therefore, what is the minimum organic loading rate and is organic carbon utilisation a function of residence time and/or FSB thickness?
8. Does the structure, porosity and thickness of the FSB influence the mass transport of oxygen and if so, to what extent?
9. Is the community structure significantly different in an organic carbon limited LFCR system and one which is not limited?

These questions will be addressed by discussing the results from the biological LFCR residence time study with regard to various measurements/factors. A sulphur material balance and the primary sulphur species formed will be discussed. A carbon species material balance was conducted, in order to determine the amount of organic carbon required for FSB development and its influence on LFCR performance. A microprobe study was performed in order to determine the dissolved oxygen profile through the FSB. Analysis of FSB structure and thickness was also determined via SEM. Lastly, a preliminary microbial ecology characterisation was performed for various LFCR experimental runs including the original inoculums. This study provided valuable information on the change of the microbial population with changing conditions and LFCR performance.

8.2 Experimental Conditions

The LFCRs were operated with a working liquid volume of 25 L, unless otherwise stated. The reactors were closed to the surroundings (gasket sealed lid) creating a headspace of 12.5 L. The headspace was flushed with air at a flow rate of 48 L/day, with the exit gas passing through an alkaline scrubber to recover any H_2S gas. The lid was only removed when microprobe measurements were taken. Unless otherwise stated the reactors were fed, via the uppermost inlet port, at a set flow rate and the effluent exited via the uppermost exit port. For each biological LFCR experiment the reactor was filled with 25 L of sulphide effluent from the DPBR and was allowed to stand for 24 hours. This was

to allow the microbial consortium to acclimatise to the new conditions prior to starting the experiment. The DPBR effluent contained both sulphate reducing and sulphide oxidising bacterial consortia. The FSB was only harvested from the liquid surface at the end of the experiment unless, otherwise stated. The LFCRs were operated according to the conditions in Table 8.1. The LFCRs were dosed with acetate, either at the start of the experiment in the bulk reactor fluid, or were supplemented daily in the feed to the LFCR.

8.3 Pseudo-steady-state

Steady-state is defined as a point in time, when all process variables remain constant, except for minor fluctuations. Conventional ways of declaring steady-state within a chemical or biological system were not applicable, due to the unique characteristics of the LFCR. The primary reasons for not being able to use a conventional method of defining a steady-state are firstly, that the hydrodynamic regime within the reactor is extremely stratified, so process variables would vary with depth and length. Secondly, the flux of oxygen into the system is constantly changing due to the the growth of the FSB, which acts as an impedance to the mass transport of oxygen. Therefore, pseudo-steady-state (PSS) is defined as the condition where the sulphide concentration increases with depth (y-direction) and the gradient is continually maintained. This implies that a stable hydrodynamic regime is in place and there is a constant steady flux of oxygen into the reaction (oxidation) zone.

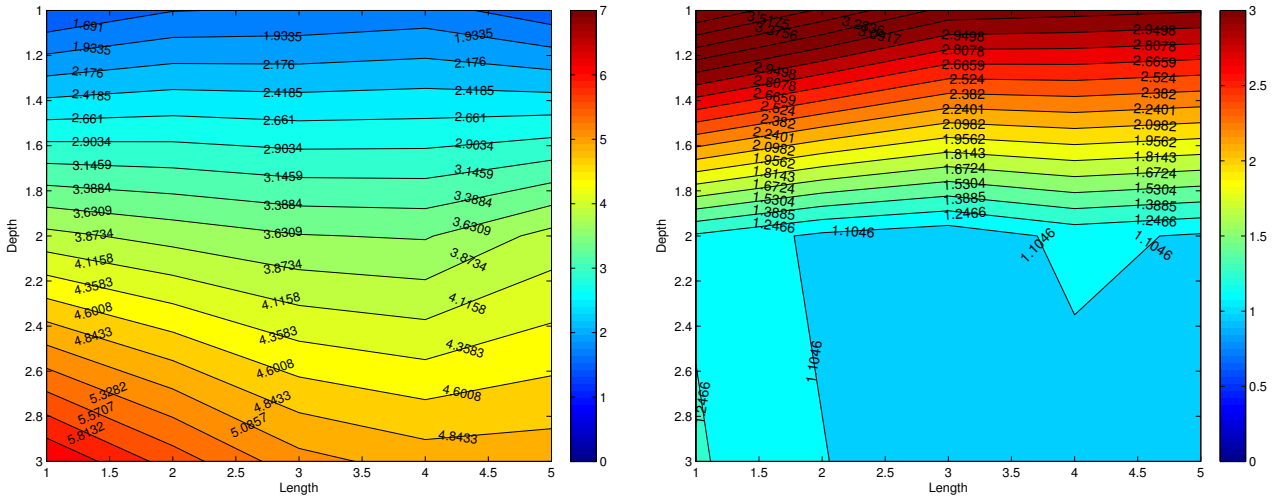
8.3.1 Sulphide depth/length profiling

As stated above, PSS is valid when the sulphide concentration increases with depth. As an example, experimental run 10 (2 day R.T.) reached pseudo-steady state on day five (Figure 8.1 b). Moreover, there was a linear sulphide concentration profile along the length of the reactor, confirming the normal hydraulic regime was present. Unlike experimental run 7 on day 10, where the hydraulic regime was not observed as the influent sulphide floated on the surface (Figure 8.1 a). Hence, all the sulphide was oxidised completely to sulphate, due to the RDD being negative (-6.113×10^{-4} g/cm^3). Lastly, the sulphide concentration profile emphasizes the fact that the reactor was stratified, although it is necessary for the reactor to be stratified, such that the correct sulphide to oxygen ratio is maintained. It was demonstrated in experimental run 11 (day 10) that the hydraulic regime was not observed as the influent floated near the surface and the RDD was -1.3156 $\times 10^{-2}$ g/cm^3 (Figure 8.2). As a result the sulphide was not oxidised to sulphur and stored but rather to sulphate, due to the high concentration of sulphide altering the redox potential and sulphide gradient within the FSB (Figure 8.3). Hence, colloidal sulphur was produced by chemical sulphide oxidation on day 10 and subsequently oxidised further to sulphate on day 11, due to it being more beneficial to the microbial population to oxidise the sulphur

Table 8.1: Summary of experimental conditions throughout all biological LFCR experimental runs 8 -16

Run	Air flow rate (L/day)	Feed flow rate (L/day)	Residence time (Days)	Run Time (Days)	Acetate addition (g/L.day)	Avg.Feed pH
8	48	6.25	4	18	0*	7.80
9	48	6.25	4	18	0*	7.70
10	48	12.5	2	12	0*	7.50
11	48	12.5	2	12	0.99	7.78
12	48	12.5	2	14	2.26	7.79
13	48	25	1	10	1.17	7.67
14	48	25	1	10	2.24	7.89
15**	48	25	0.5	7	0.86	8.05
16-(1)	48	18.75	1.5	7	1.26	7.9
16-(2)	48	18.75	1.5	7	1.77	7.85
16-(3)	48	18.75	1.5	6	n.d.	7.87

* The LFCR was dosed with acetate prior to starting the experiment, thus ensuring the starting bulk-liquid concentration was 1 g/L.
** LFCR was operated at a liquid volume of 12.5 L.
All LFCR's were operated at 1 atm. and room temperature (24 - 25°C)
n.d. = not determined



(a) Experimental run 10 (Day 5)

(b) Experimental run 7 (Day 10)

Figure 8.1: Sulphide concentration contour maps of LFCR experimental runs 7 and 10, depicting the sulphide concentration profiles at unsteady-state and pseudo-steady-state respectively.

to sulphate. Furthermore due to the high influent pH 9.45 on day 10, it is likely that thiosulphate was formed as well.

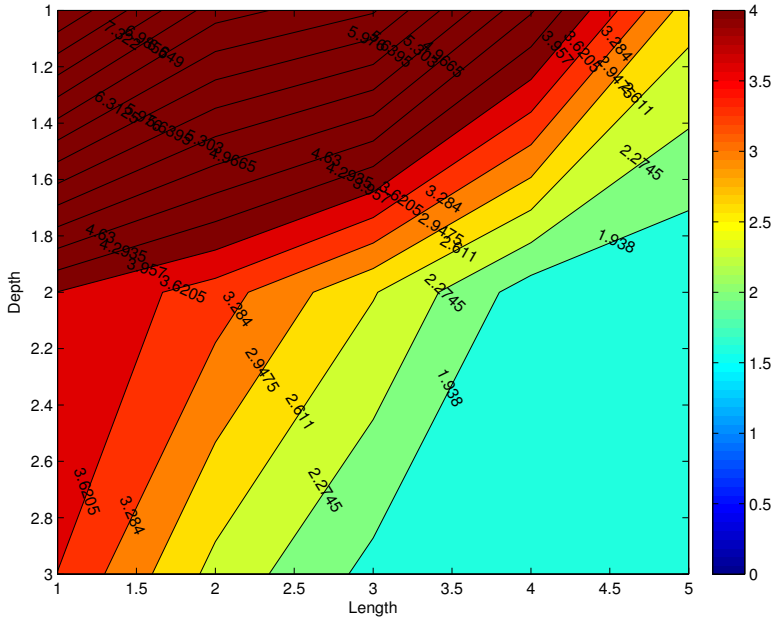


Figure 8.2: Sulphide concentration (mM) contour map of the bulk liquid in the LFCR in experimental run 11 (day 10)

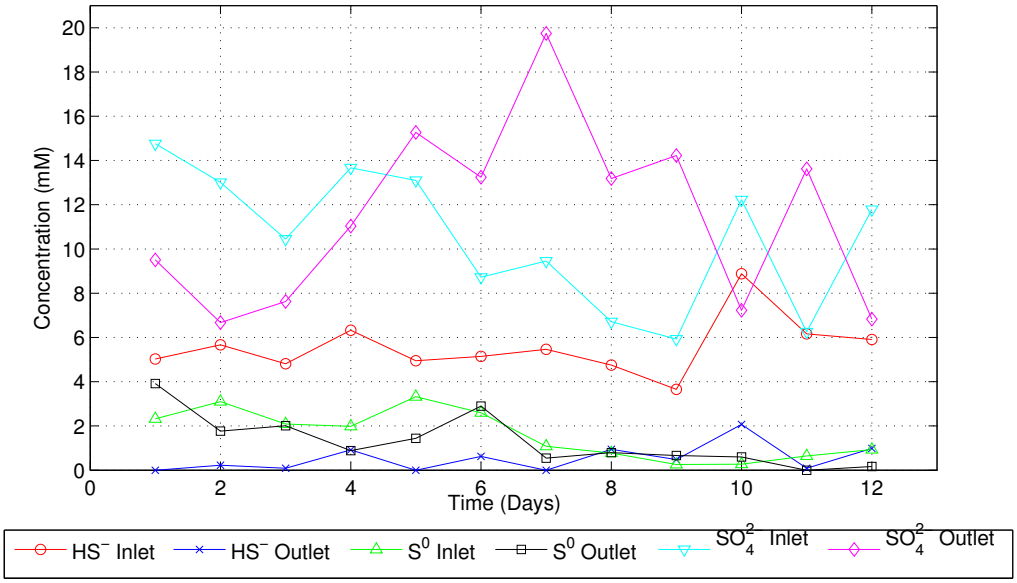


Figure 8.3: Influent and effluent sulphide, colloidal sulphur and sulphate concentrations (mM) throughout the duration of experimental run 11

8.4 Results - Sulphur species material balance

A summary of the results with regard to the sulphur species material balance is presented in Table 8.2 for experimental runs 8 to 16-(3). The performance of the LFCR was judged by various factors, firstly how quickly pseudo-steady-state was established and a complete FSB was formed. Secondly, the sulphide oxidation rate and removal efficiency of the LFCR. Thirdly, the quantity of sulphur that reported to the FSB and if the FSB remained intact over the duration of the experiment. Lastly, the proportion of sulphide that was converted to sulphate and if there was full oxidation of colloidal sulphur. Key observations from the various experiments will be briefly highlighted below, before an in depth discussion of the results in subsequent sections.

Experimental run 8 was conducted at a four day residence time and PSS was established on the fourth day. A floating sulphur biofilm began developing on day one, and a sulphide removal efficiency of 96.1% was attained. However, the LFCR exhibited 'poor performance' due to the collapse of the FSB and loss of the sulphur deposits. The collapse of the FSB was due to numerous factors that will be discussed in Section 8.4.5. On the other hand experimental run 10 was conducted at a two day residence time and PSS was established on the fourth day. Pseudo-steady-state is generally established after one or two residence times have elapsed, as the hydraulic regime would be present throughout the reactor due to the continuous pumping in of influent. The formation of a FSB is also crucial to pseudo-steady-state being maintained. A lower sulphide removal efficiency (82.2%) was achieved as compared to experimental run 8. However, the FSB remained structurally intact over the duration of the experiment and a greater quantity of sulphur reported to the

biofilm, thus exhibiting optimal performance. Lastly, experimental run 15 was conducted at a half day residence time and PSS was established on day one. A floating sulphur biofilm was formed within the first day and a high sulphide removal efficiency of 93.5% was achieved. However, a significant proportion of the deposited sulphur fell into the bulk liquid due to delamination of the FSB lower layers. A portion of this sulphur was oxidised fully to sulphate and a large proportion of sulphide was oxidised completely to sulphate. The sulphur material balance was closed to within 0.36% percent difference ($S^{\%}$) between the measured sulphide converted and sum of the sulphur species products (Table 8.2). This experiment clearly exhibited numerous factors of a 'poor performing' LFCR, which will be discussed in Section 8.4.5.2.

In an effort to close the sulphur species material balance, the exiting headspace gas was passed though a sodium hydroxide (3 M) scrubber, to trap any H_2S gas that may have been liberated. The sulphide concentration in the solution was measured during and at the end of each experimental run. However, no sulphide was detected in the scrubbing solution, therefore there was negligible liberation of H_2S gas from the LFCR surface.

Table 8.2: Sulphur species balance across experimental runs 8 - 16. Solids refers to sulphur recovered from collapsed biofilm, while biofilm refers to sulphur in the floating biofilm.

Run	HS^- Loading (mmol/day)	HS^- Converted (mmol)	HS^- Conversion (%)	Sulphur Species (mmol)					
				Colloidal	Sulphate	Biofilm	Solids	Polysulphides	$S^{\%}$
8	33.56	580.67	96.10	44.94	190.96	144.07	202.8	-	0.36%
9	29.69	498.27	93.30	(79.31)†	317.66	178	83.8	-	0.38%
10	60.46	572.73	82.20	6.65	33.0	527.0	0	4.0	0.36%
11	69.50	754.20	91.0	45.98*	151.72	501.77	0	16.24	5.2%
12	52.75	617.44	84.70	(60.45)† 40.29*	109.85	480.71	0	-	7.9%
13	122.84	1023.7	85.01	(4.95)†	269.83	698.6	0	-	6.06%
14	111.50	879.04	80.74	27.8	113.94	660.1	0	-	9.19%
15‡	56.78	378.79	93.50	(145.29)†	299.76	225.8	0	0	0.39%
16-(1)	98.93	452.62	65.20	119.39	71.66	122.14	0	-	36.41%
16-(2)	111.93	572.06	81.97	185.14	56.84	435.22	0	-	16.83%
16-(3)	100.23	620.82	89.46	414.45	235.33※	135.26	0	-	12.15%

* Colloidal sulphur reacted to form polysulphides and not sulphate.

† Values in brackets must be taken as negative as those species were oxidised to sulphate

$S^{\%}$ refers to the percent difference. This is the error between the measured HS^- converted and total of measured sulphur species. (See Appendix A for formula)

‡ Experimental run 15 was conducted at an operating liquid volume of 12.5 L

※ There was an accumulation of sulphate within the LFCR, hence there was a net 'disappearance' of sulphate. Ignore value in material balance calculation.

8.4.1 Sulphide removal efficiency and oxidation rate

The highest sulphide removal efficiency was achieved in experimental run 8 (96.1%), whilst the lowest was 65.2% in experimental run 16-(1). There was no clear relationship between sulphide conversion and sulphide loading or residence time, however this was due to numerous factors influencing the overall performance of the LFCR. Nevertheless, the sulphur recovery in the LFCR was consistently higher than the GARL study indicating that their measured sulphide removal efficiency was inaccurate. Moreover, these results clearly illustrate the fact that the LFCR reactor is oxygen limited and is unable to achieve a 100% sulphide removal efficiency. However, sulphide conversion to elemental sulphur in the FSB is the true measure of the performance of the LFCR, as it is more beneficial to harvest the sulphur than for it to remain as colloidal sulphur.

The sulphide oxidation rate was measured for all experimental runs. Experimental run 8 and 9 were conducted at a four day residence time with an initial dose of acetate of 14.39 g. Both experiments were at unsteady-state from day one to three, where the sulphide oxidation rate increased linearly to reach a maximum of approximately 1.7 and 2 mmol/(L.day) respectively (Figure 8.4). However, on day four pseudo-steady-state was reached and the sulphide oxidation rate decreased linearly at -0.216 and -0.177 mmol/(L.day^2) respectively, over the subsequent six days. This clearly shows that once a floating sulphur biofilm is established there is an impedance of oxygen mass transport and decrease in the sulphide oxidation rate. The FSB is necessary to ensure that sulphur is the primary product, but the data highlights the need to optimise the harvesting frequency. Similarly, a decreasing trend was observed in the two day residence time studies. Experimental runs 10 and 12 reached pseudo-steady state on day four and six respectively (Figure 8.5a)). Pseudo-steady-state took longer than one residence time to be established, due to the FSB growth taking longer than one residence time to form fully. Consequently, the sulphide oxidation rate increased to a maximum of approximately 2.95 and 2.5 mmol/(L.day) on day five and seven respectively. Correspondingly both decreased the following day at an average rate of -0.268 and -0.117 mmol/(L.day^2) respectively over eight days. On the other hand experimental run 11 reached PSS within the first day and a stable sulphide oxidation rate of approximately 2.54 mmol/(L.day) was maintained for the first seven days. However, on days eight and nine the sulphide oxidation rate drastically declined, indicating the significant decrease in the availability of dissolved oxygen for sulphide oxidation to occur.

The trends for experimental runs conducted at 1.5 (Exp. 16-(1), (2)) and one day residence time (Exp. 13,14) differed slightly from the trends observed previously. Experimental run 13 and 14 were conducted at a one day residence time and were at unsteady-state for the first day (Figure 8.5b). In experimental run 13 the sulphide oxidation rate increased to a maximum of 4.65 mmol/(L.day) (day 3) and subsequently decreased during the PSS phase. The decrease was linear, at an average rate of -0.331 mmol/(L.day^2) and was more

significant than in previous experiments.

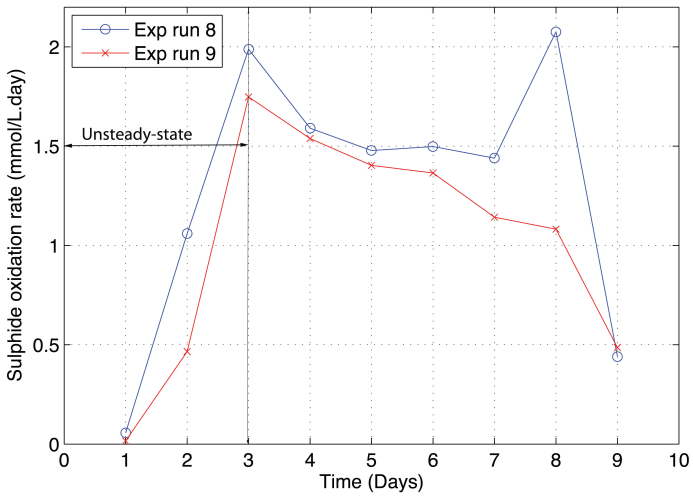
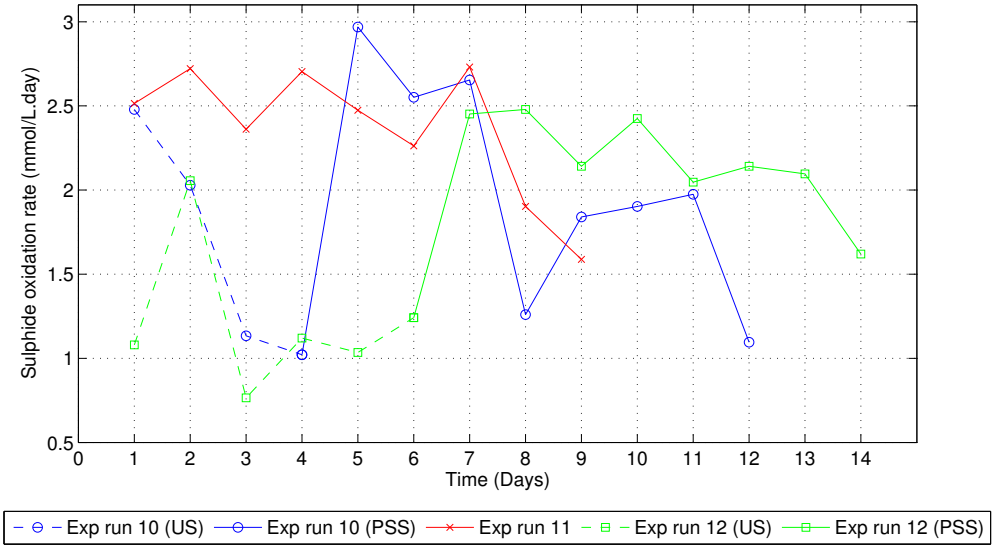


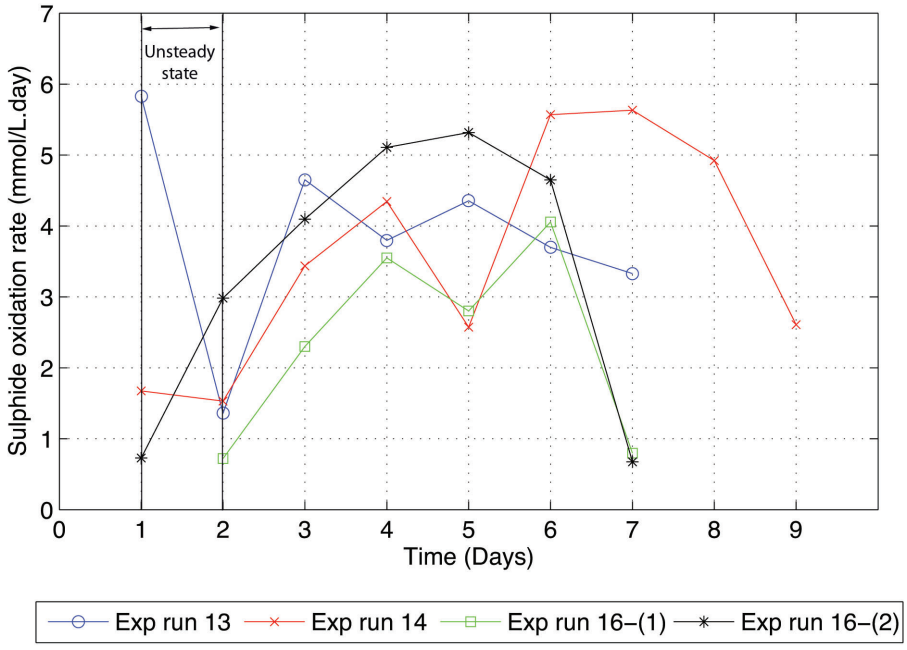
Figure 8.4: Representing the daily sulphide oxidation rate in the LFCR. Experimental run 8 and 9 were conducted at a four day residence time and average sulphide loading of 33.56 and 29.69 mmol/day. Annotated with the unsteady-state phase.

Experimental run 14, 16-(1) and 16 (2) displayed a similar trend of increasing sulphide oxidation rate, to reach a maximum before decreasing. In experiment 14 the sulphide oxidation rate increased by 0.7534 mmol/(L.day) at a decreasing rate, to reach a maximum of 5.57 mmol/(L.day), after which it decreased drastically by -0.959 mmol/(L.day^2) to 2.6 mmol/(L.day). Similarly, the sulphide oxidation rate in experimental run 16-(1) and 16-(2) increased at a rate of 0.717 and 0.789 mmol/(L.day^2) respectively, to reach a maximum and dramatically declined the following day.

These data sets summarise the overall performance of the LFCR. The sulphide oxidation rate fluctuates significantly during an operational cycle, increasing during the unsteady-state phase and steadily decreasing once pseudo-steady-state is established. The decline in the rate was primarily due to the fact that the sulphur content of the FSB was increasing, consequently the oxygen mass flux into the FSB decreased due to increased resistance (will be shown in Section 8.7). It should be noted that the minimum in sulphide oxidation rate was reached after approximately four residence times for experimental runs 10 - 16-(2). Therefore, it would be advantageous to harvest the FSB after approximately three to four residence times to maintain a high sulphur recovery, as was demonstrated in experiment 16. Finally, experiment 15 was discarded due to the fact that the FSB broke and tore continually throughout the experiment. The causes of the FSB failure will be discussed in Section 8.4.5.



(a) Experimental run 10, 11 and 12 were conducted at a two day residence time, and a sulphide loading of 60.46, 69.5 and 52.75 mmol/day respectively. The dashed lines represent the unsteady-state (US) phase and the solid line is the pseudo-steady-state (PSS) phase.Experimental run 11 unsteady-state phase not shown.



(b) Experimental run 13, 14 were conducted at an one day residence time and sulphide loading of 122.84 and 111.5 mmol/day. Experimental run 16-(1) and 16-(2) were run consecutively at an one and a half day residence time and a sulphide loading of 98.9 and 111.9 mmol/day. Annotated with the unsteady phase.

Figure 8.5: Sulphide oxidation rate profiles for experimental runs 10 - 16-(2), except run 15.

8.4.2 Effect of pH and colloidal sulphur

As previously discussed pH plays a critical role in the speciation of the products from the sulphide oxidation process. Thiosulphate and polysulphides are the major products from abiotic sulphide oxidation in an alkaline pH range (Chapter 7). These conditions were observed in experimental runs 11 and 12.

8.4.2.1 Experimental run 11 - 2 day R.T. - 0.99 g/L acetate loading

The mean feed sulphide concentration was 5.56 mM, resulting in a sulphide loading rate of 69.50 mmol/day (Figure 8.3). A sulphide conversion of 91% was attained. The sulphide concentration gradient across the depth of the bulk fluid was pronounced (Figure 8.7), probably due to the conversion of sulphide to polysulphides and oxidation to sulphur within the FSB. The sulphate data showed no net sulphate production or consumption during days 1 - 7. A total of 1039 mmol entered the LFCR and 1038 mmol exited (Figure 8.3). The observed 'production' of sulphate from day 5 - 7 was due to an accumulation of sulphate within the reactor. This is a result of dead-zones at the front and back corner of the LFCR, hence very little mixing occurs within these zones, leading to an accumulation of sulphate ions (Figure 6.11). However, there was a reduction in colloidal sulphur, taken from 3 mM to below 1.5 mM, between days 2 - 5. The colloidal sulphur was not oxidised to sulphate, but rather reacted with free bisulphide ions to form polysulphides (Table 8.3). The production of polysulphides was favoured due to the high inlet pH (8.2 - 9.2) over days 2 - 5 (Figure 8.6). Moreover, the inlet colloidal sulphur concentration was greater than 2 mM over the concerned period and decreased to approximately 0.575 mM over the subsequent days. Therefore, there was sufficient sulphur available for the formation of polysulphides. A total of 16.24 mmol of polysulphides was measured and the polysulphide chain was predominantly nine or ten sulphur atoms long. It was assumed that the polysulphides were produced chemically according to reactions 3.24 and 3.27.

Approximately 54.87 mmol of sulphur reacted with bisulphide and 42.33 mmol of equivalent sulphur in the form of polysulphides was accounted for over the four day period. Some polysulphides may have decomposed during the sample preparation procedure, due to the effluent pH on days two and five being below the optimum range ($\geq$ 8.1).

The portion of converted sulphide that reported to the floating sulphur biofilm as sulphur was 66.53%. This was a significant decrease from run 10, primarily due to the fact that a large proportion (20.11%) of sulphate was formed. As previously mentioned no net sulphate was produced from days 1 -7, therefore there was a net production of 151 mmol over days 8 - 12. The pH within the reactor was not favourable for polysulphide production but sulphate production, as the mean pH (within the bulk fluid) was 7.68 over the five day period. Polysulphide production accounted for 6.1% of the converted sulphide and at a mean pH of 8.3 within the bulk fluid. As mentioned earlier the floating of influent

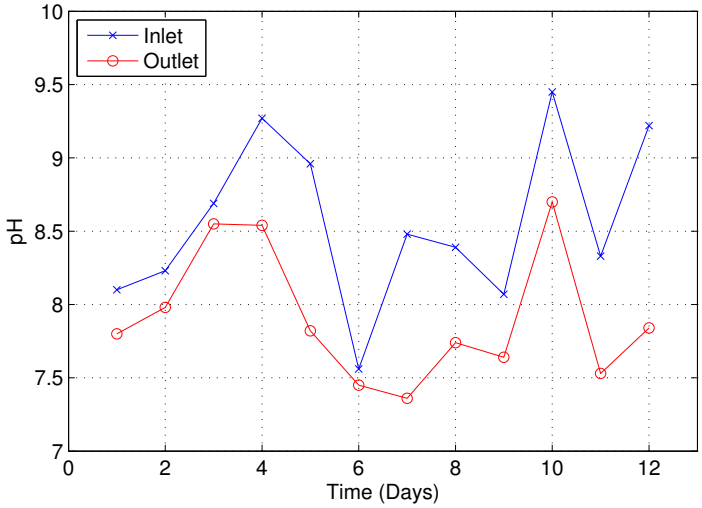


Figure 8.6: Influent and effluent pH profiles for experimental run 11

Table 8.3: The measured amount of colloidal sulphur which was consumed over the period of day 2 - 5, the effluent concentration of polysulphides and the equivalent colloidal sulphur (S_x^{2-}-S_8) that reacted with bisulphide ions to form polysulphides (experimental run 11).

Day	2	3	4	5
Colloidal Sulphur (mmol)	16.67	0.91	13.73	23.56
S_x^{2-} (mM)	1.27	0.54	0.22	0.35
S_x^{2-}-S_8 (mmol)	15.91	0.53	2.75	23.14

sulphide on day 10 was due to displacement by denser bulk reactor fluid (Figure 8.2). This was caused by the accumulation of sulphate ions within the LFCR, hence the less dense influent sulphide was displaced to the surface and oxidised fully. The measured percent difference was 5.17% as 38.04 mmol were not accounted for and the most likely sulphur species that was formed was thiosulphate due to the high pH of the feed.

8.4.2.2 Experimental run 12 - 2 day R.T. - 2.26 g/L acetate loading

Polysulphide production was again significant in experimental run 12. The average sulphide concentration in the feed was 4.22 mM, resulting in a sulphide loading of 52.75 mmol/day. The overall sulphide conversion efficiency was 84.7 % with 77.86% of the converted sulphide recovered as sulphur in the biofilm. Once again sulphate formation was significant. Approximately 60.45 mmol of sulphate was formed by oxidation of colloidal sulphur and 8.0% (49.4 mmol) of the converted sulphide was fully oxidised to sulphate. Colloidal sulphur (40.29 mmol) most likely reacted with free bisulphide ions in the bulk fluid to produce polysulphides (equation (3.29)). A sulphur species balance was performed each day for the entire experiment. The disappearance of colloidal sulphur was accompanied

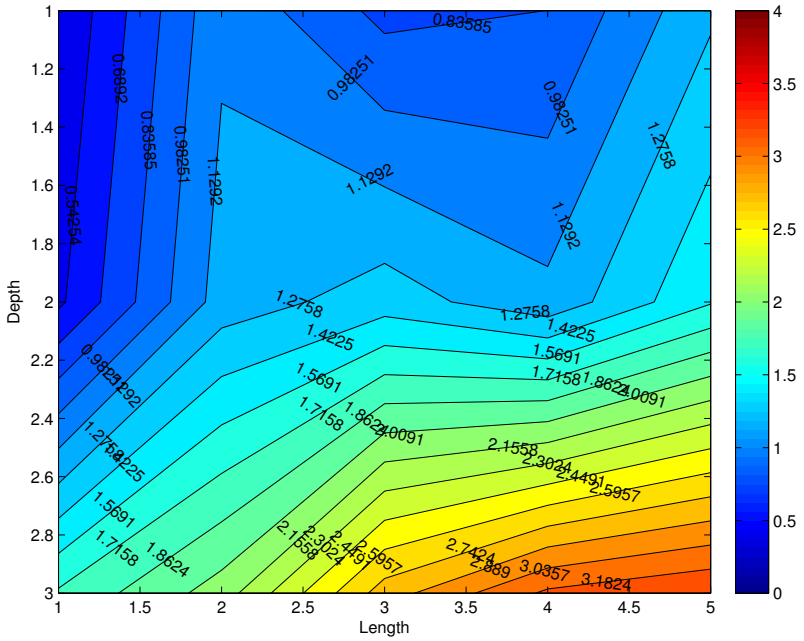


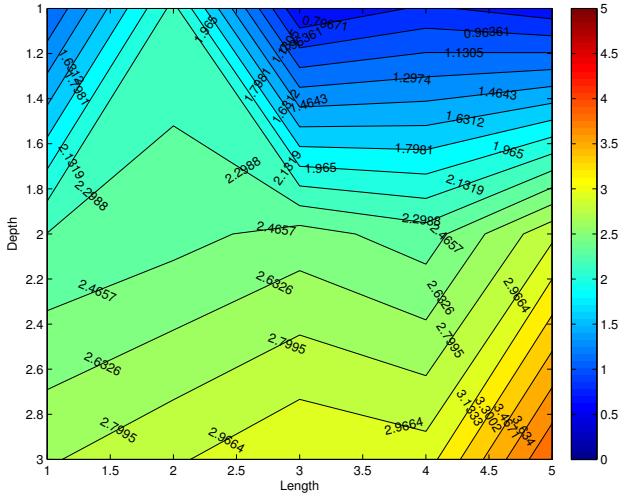
Figure 8.7: Contour plot of sulphide concentration (mM) in the LFCR on day 5 (experimental run 11)

by the appearance of an equal or greater quantity of sulphate, except on day 12, when no sulphate was produced. The inlet colloidal sulphur concentration in the feed was generally high, at 5.93 mM and the inlet pH was 8.77, whilst the outlet pH was 5.41 indicating significant acid production (protons). This explanation was furthered supported by the contour plots (Figure 8.8a,b,c).

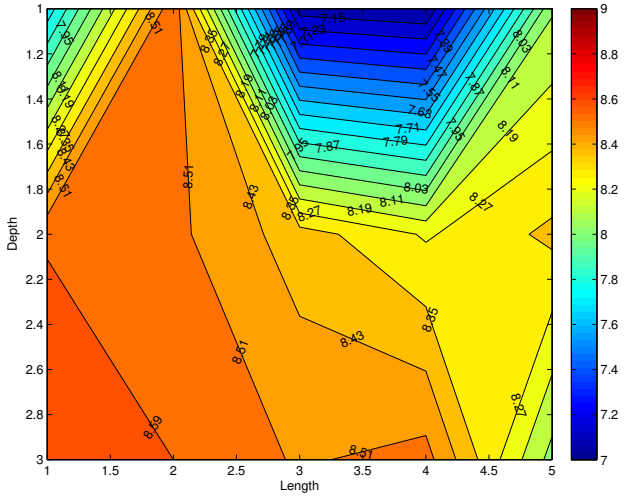
Figure 8.8 shows the relationship between sulphide, colloidal sulphur and pH during experimental run 12. The sulphide profile is consistent with pseudo-steady state, showing the expected vertical and horizontal gradients. The colloidal sulphur concentration in the feed is high, with the highest concentration observed near the feed inlet (port 1,1). The colloidal sulphur concentration rapidly decreases, indicating a reaction rather than dispersion. The low sulphide concentration in that region suggests the reaction between colloidal sulphur and bisulphide, forming polysulphides and acidity (reaction 3.29). This is supported by the pH data. The bulk liquid below the biofilm did not have the characteristic yellow/green colour, suggesting the rapid conversion of polysulphide to thiosulphate (reaction 3.30). The pH of the bulk liquid near the reactor outlet (port 5,5) was still relatively high (pH 8.1), while the pH of the collected effluent had decreased to pH 5.4. This suggests that rapid oxidation of thiosulphate to sulphate occurred in the effluent pipe, where oxygen penetration through the silicon tubing was much greater than through the biofilm.

A percent difference of 7.9% (error) was obtained, as 47.04 mmol was not accounted for, and it was probably thiosulphate due to the production of polysulphides as well as the elevated pH.

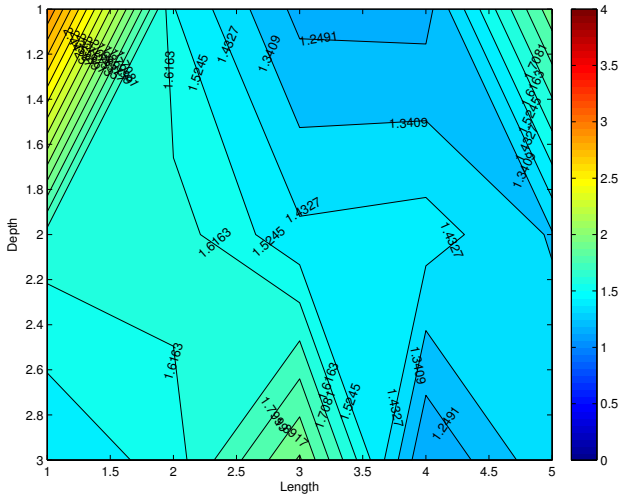
Experiments 11 and 12 highlighted the chemical reactions/processes that determine sulphur speciation and the dependence on pH and colloidal sulphur concentration. If the colloidal sulphur concentration is high ($>$ 2 mM), within the pH range 8.1 - 9.5, then polysulphides will be produced. For this reason the pH should be maintained below pH 8.1 in order to prevent unwanted polysulphide production and promote sulphur formation in the FSB.



(a) Contour plot showing sulphide concentration (mM)



(b) Contour plot of the pH profile



(c) Contour plot of colloidal sulphur concentration (mM) distribution in the LFCR bulk fluid

Figure 8.8: Contour plots of concentration distributions in the LFCR on day 12, illustrating the production of polysulphides (Experimental run 12)

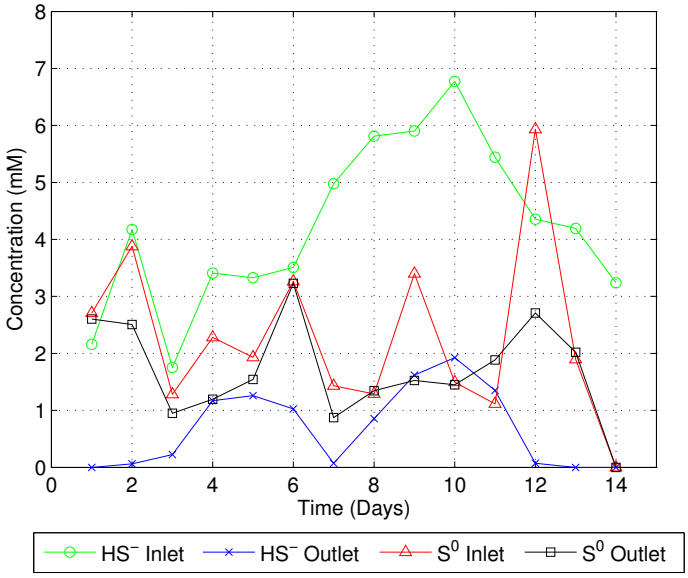


Figure 8.9: Influent and effluent sulphide and colloidal sulphur concentrations (mM) throughout the duration of experimental run 12. The spike of colloidal sulphur on day 12 was due to an inconsistency in the upstream DPBR.

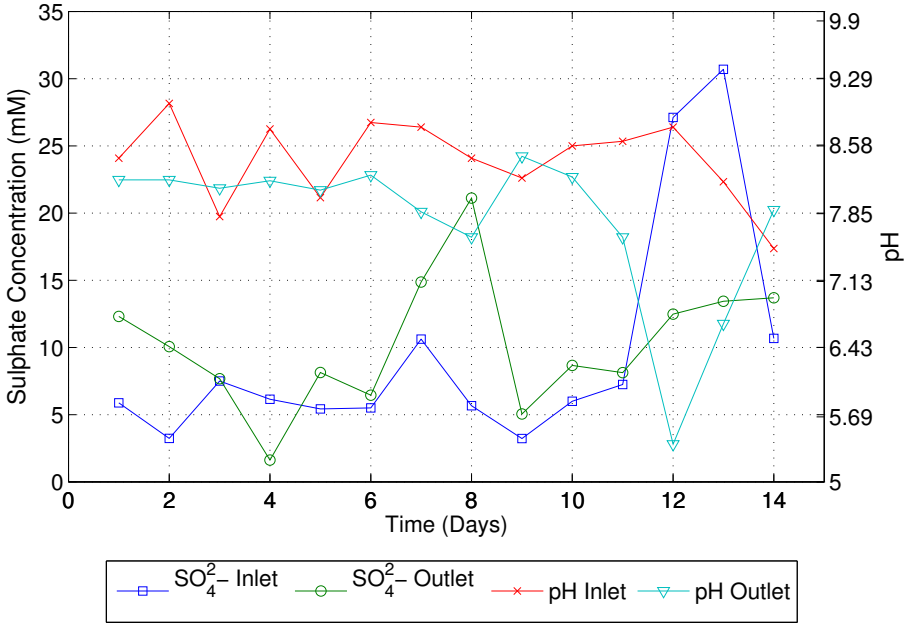


Figure 8.10: Sulphate concentrations (mM) and the associated pH profile of the influent and effluent stream throughout the duration of experimental run 12

8.4.3 Sulphur yield vs. residence time

The sulphur yield is the primary measure of system performance. The two best performing experimental runs were 10 and 14, which showed the highest sulphur yield, with minimal sulphate formation. Sulphate minimisation will be covered in the following section.

Experimental run 10 was operated with a two day residence time and achieved an 82.2% sulphide conversion, with 92% of the converted sulphide reporting as solid sulphur in the FSB. The average sulphide loading rate was 60.46 mmol/day (Table 8.2). While the average sulphide conversion was approximately 10% lower than runs 8 and 9, the overall efficiency of the LFCR was increased three fold, due to the formation of a fully developed FSB, facilitating greater sulphur accumulation. Moreover, a smaller proportion of colloidal sulphur was formed (1.2%) due to the lower residence time impacting the FSB structure. As a result, less oxygen was able to penetrate through the thicker FSB, thus minimising full oxidation of colloidal sulphur particles. The impact of residence time on FSB structure will be explained fully in Section 8.6. The contour plots revealed that a steady sulphide gradient was maintained within the reactor throughout the duration of the experiment (Figure 8.1a). This was achieved by maintaining a high sulphide loading and inlet flow rate. The incoming sulphate concentration remained low (8 - 9 mM) due to the improved efficiency of the upstream DPBR (Figure 8.11). The sulphide concentration was approximately 5.03 mM and sank to the reactor floor, even though the reactor fluid had a greater proportion of sulphates in solution. This was due to the fact that the (mass) ratio of sulphide to sulphate was 1 : 4 hence, the relative density difference (RDD) was 0.00019 g/cm^3. During experiment 9 the (mass) ratio of sulphide to sulphate was 1 : 28, with a RDD of -0.0006113 g/cm^3. In short, the floating sulphur biofilm (of experiment 10) was able to hold 527.0 mmol (67.5 g/m^2) of sulphur, which was substantially higher than previous experiments, whilst minimising unwanted by-product formation.

Similarly, in experimental run 14 pseudo-steady-state was attained on day two and the average sulphide concentration in the feed was 4.46 mM at a loading rate of 111.5 mmol/day (Figure 8.13). The overall sulphide conversion was 80.74% with 75.1% of the converted sulphide reporting to the FSB as sulphur. The amount of sulphate formed (113.94 mmol) was significantly lower than experimental run 13, accounting for 12.96% of the converted sulphide. A small amount (3.16%) of the sulphide was converted to colloidal sulphur as well. A 9.19% error difference was calculated as 77.2 mmol of converted sulphide were not accounted for; it was most likely converted to thiosulphate and polysulphides, as the bulk fluid had a green-yellowish colour just below the surface of the FSB on day one and four. The influent pH was high (9.14 and 8.79) on the respective days, which favoured the production of polysulphides (Figure 8.13). Colloidal sulphur was consistently present in the feed (0.8 - 2.32 mM) and could be converted to polysulphides when the pH was sufficiently high. However, the formation of a robust FSB ensured sulphur was the primary product. The biofilm was able to accumulate 660.1 mmol (84.5 g/m^2) of sulphur. This was

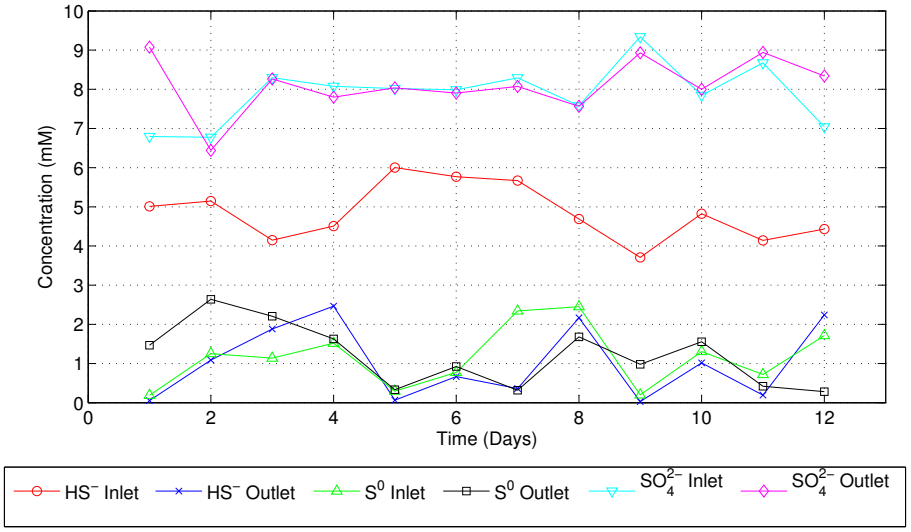


Figure 8.11: Influent and effluent sulphide, colloidal sulphur and sulphate concentrations (mM) throughout the duration of experimental run 10

significantly greater than experimental run 10.

A linear relationship (y=mx+c) between sulphur yield and residence time was determined, which showed that a decrease in residence time, down to 1 day, led to an increase in sulphur recovery (Figure 8.14). The half day and one and half day residence time experiments (15, 16-(1)) were excluded from the calculation, due to poor structural integrity of the biofilm and the poor harvesting strategy respectively. The constant (m) is essentially represented by equation 8.1. Dividing the constant by the reactor volume showed that the sulphur yield decreased by 6.17 mmol/L for each one day increase in residence time. Hence, there is an inverse relationship between residence time and sulphur recovery. While there was a decrease of approximately 10% in sulphide removal at a lower residence time, the associated benefit of increased sulphur recovery is significantly more desirable. The sulphide conversion efficiency could be improved by a small increase in reactor surface area. The linear relationship was only valid down to a one day residence time, due to the drop in sulphur recovery at a shorter residence time. The reasons for this are discussed in Section 8.4.5.

$$m = \dot{V_{S_8}} * V_{reactor} = -154.2\, mmol/day \tag{8.1}$$

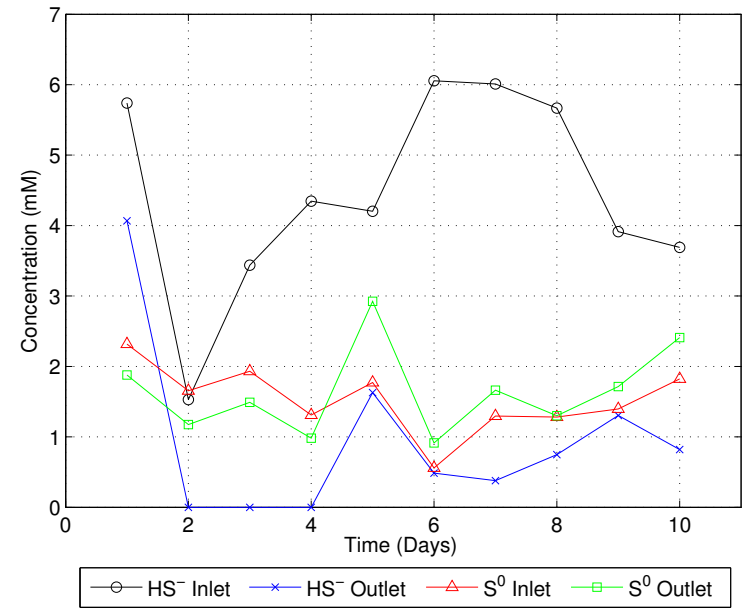


Figure 8.12: Influent and effluent sulphide and colloidal sulphur concentrations (mM) throughout the duration of experimental run 14

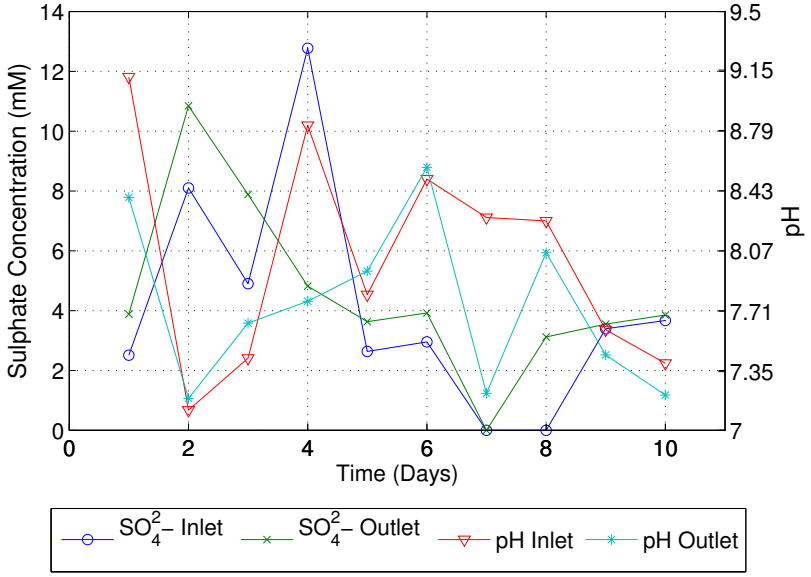


Figure 8.13: Sulphate concentrations (mM) and the associated pH profile of the influent and effluent stream throughout the duration of experimental run 14

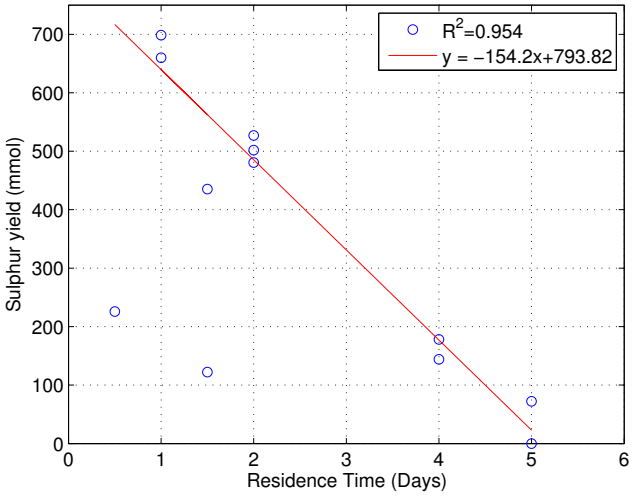


Figure 8.14: Linear relationship between sulphur recovered in the FSB and residence time. Two points were identified as outliers at a sulphur yield of 225.8 and 122.14 mmol. Data from experimental runs 6 - 16-(2).

8.4.4 Sulphate production minimisation

In order to maximise the conversion of sulphide to sulphur, the complete oxidation of sulphide to sulphate, as well as the oxidation of elemental sulphur must be suppressed.The relationship between residence time and sulphate production is presented in Figure 8.15. The data represent the complete oxidation of sulphide to sulphate, as well as the oxidation of sulphur from the FSB to sulphate. It does not include the oxidation of colloidal sulphur in the feed to sulphate. This is primarily due to the fact that colloidal sulphur in the feed could not be controlled, so there was no consistent relationship. It was demonstrated that the optimum residence time in the LFCR was approximately two days (2.18 days), at which less than 8% of the sulphide was fully oxidised. Sulphate production was highest at the higher residence times (4-5 days) and to a large extent was due to the complete oxidation of sulphide to sulphate. The 'poor performance' was attributable to the FSB structure being compromised as a greater mass flux of oxygen was able to penetrate deeper into the bulk liquid. Secondly, the FSB was not sufficiently structurally robust to retain the deposited sulphur, hence the FSB collapsed leaving the surface exposed, resulting in complete oxidation of sulphide in the bulk liquid. At the same time sulphur deposits within the FSB entered the bulk liquid as colloidal sulphur near the surface and were oxidised fully to sulphate. The effect of FSB structure and development with regard to sulphur deposition and sulphate minimisation will be discussed further in the following section.

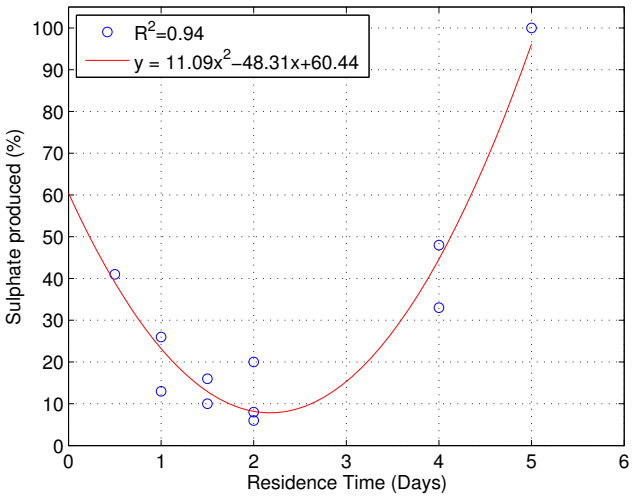


Figure 8.15: Parabolic relationship between sulphate production and residence time. The percentage of sulphate produced does not incorporate the oxidation of influent colloidal sulphur. Data from experimental runs 6 - 16-(2)

8.4.5 Reasons for poor LFCR performance

A number of the experimental runs were characterised by poor performance, for all, or part of, the run. These were characterised by several factors, such as FSB collapse, tearing of the FSB, poor harvesting strategy and colonisation by cyanobacteria and green sulphur bacteria. These causes will be discussed fully in the following section, in addition to the necessary steps to prevent their occurrence.

8.4.5.1 Floating sulphur biofilm collapse

Experimental runs 8 and 9 both experienced FSB collapse, but only run 8 will be discussed in detail. A high sulphide conversion was achieved, with 24.8% of the converted sulphide recovered from the biofilm as sulphur, at an average sulphide loading rate of 33.56 mmol/day (Figure 8.16). Approximately 40.63% of the influent sulphide was converted to unwanted products, sulphate (32.89%) and colloidal sulphur (7.74%). The remaining sulphide was converted to sulphur within the biofilm. The biofilm which formed was not structurally robust, as a result a large proportion of the biofilm and sulphur fell to the reactor floor and was reported as sulphur solids.

The partial break and collapse of the biofilm occurred on day eight. A section (8 x 10 cm) of heavily laden FSB broke off and fell to the reactor floor (Figure 8.18). By day 12 the collapsed biofilm had become thinner and changed colour, becoming more brown and less white. This was due to the reaction of sulphur with bisulphide ions to form polysulphides. Some of the sulphur which fell out of the biofilm formed a cloudy, colloidal sulphur layer in

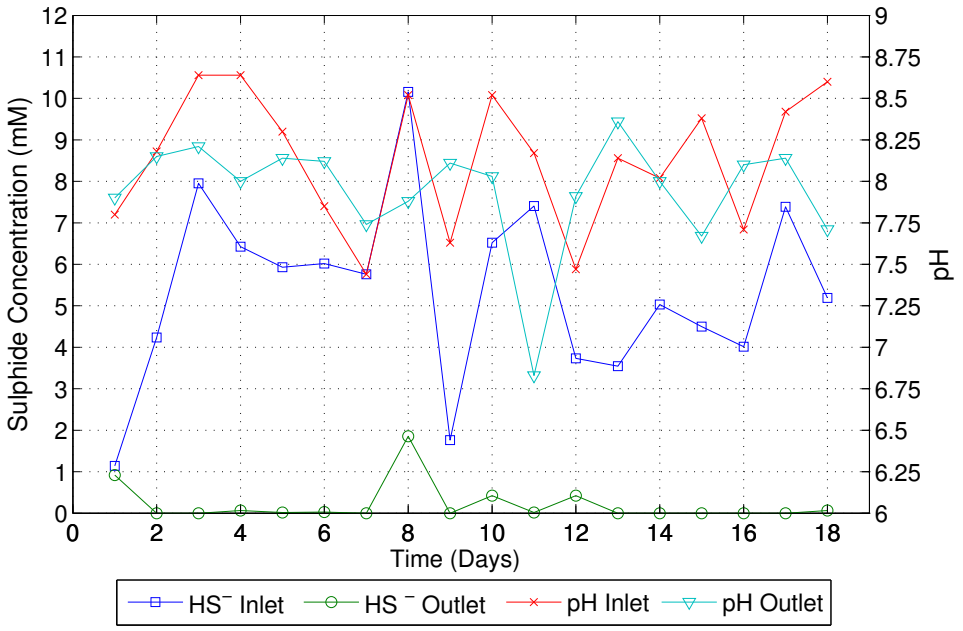


Figure 8.16: Plot of influent and effluent sulphide concentrations and pH over the duration of experimental run 8

the reactor (Figure 8.19a). This was oxidised to sulphate, which contributed to the increase in effluent sulphate concentration on days nine and ten (Figure 8.17). The partial collapse of the FSB also affected the sulphide concentration gradient in the bulk liquid. On day nine the absence of a biofilm resulted in increased oxygen penetration in those areas and the sulphide at the surface was completely oxidised. The two dark blue zones in Figure 8.19b indicate where the FSB partially collapsed. The lack of the FSB barrier enabled a greater mass flux of oxygen into the bulk fluid, resulting in the complete oxidation of colloidal sulphur in those regions.

Experiments 8 and 9 were supplemented with acetate at the beginning (1 g/L), but no further supplementation was provided. The lack of organic carbon in the feed may have contributed to the compromised structural integrity as the experiment progressed. Therefore, no subsequent biofilm layers would have formed. The second factor that may have compromised the FSB structural integrity was residence time. The FSB had no clear defined boundaries or structural layers, hence it was not robust enough to hold all the accumulated sulphur. The effect of residence time on FSB structure will be discussed further in Section 8.6.

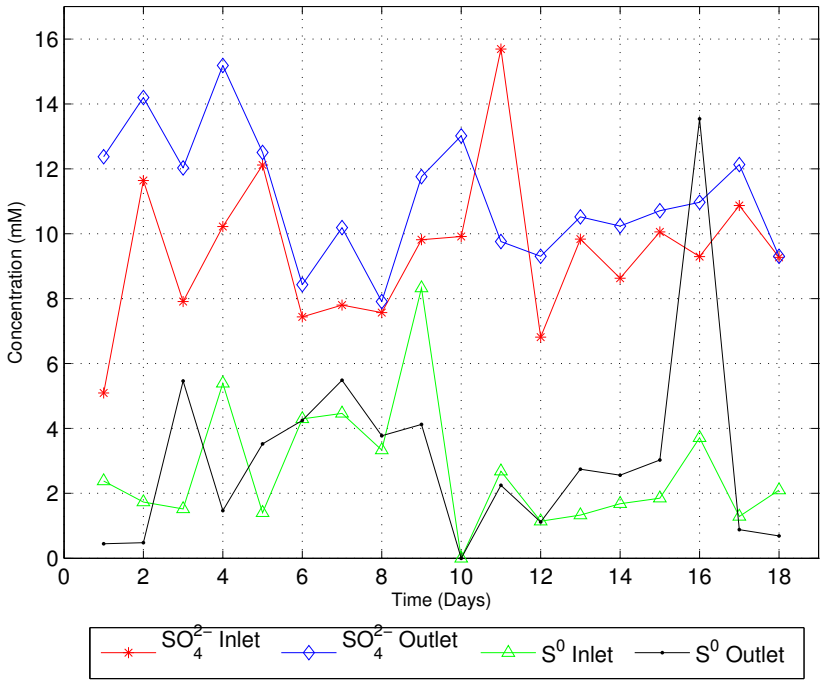


Figure 8.17: Plot of influent and effluent sulphate and colloidal sulphur concentrations over the duration of experimental run 8

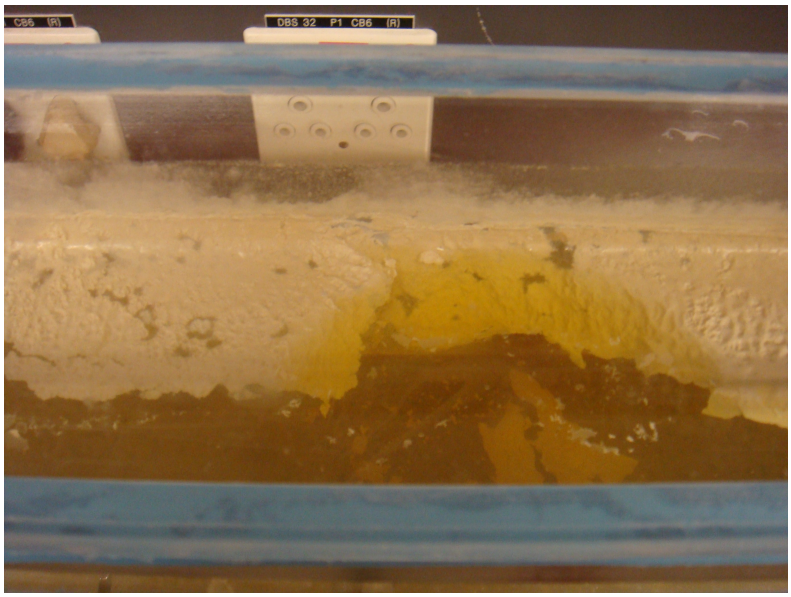
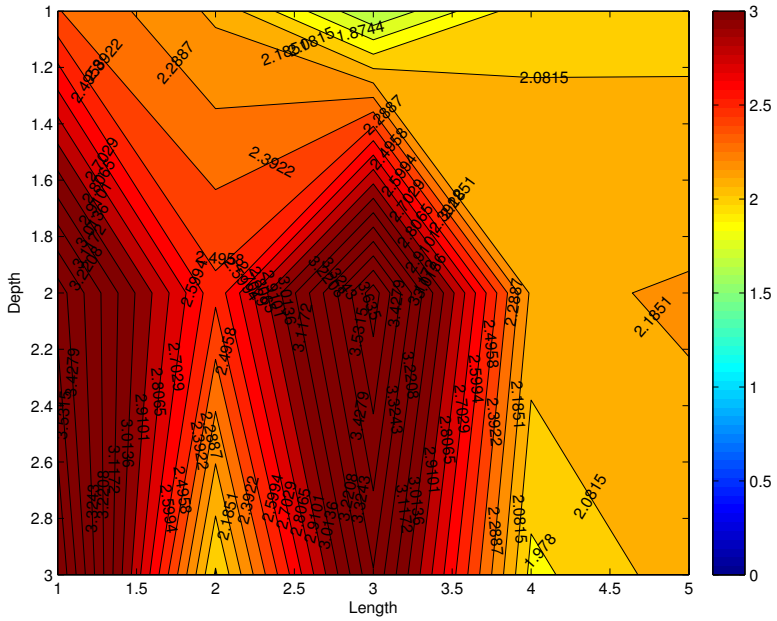
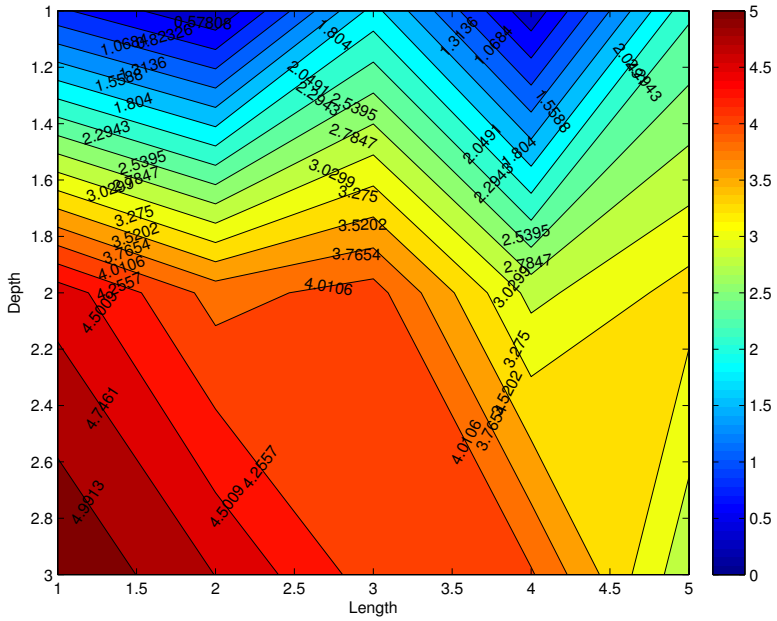


Figure 8.18: Partially broken spongy biofilm grown at a flow rate of 6.25 L/day which, is heavily laden with sulphur particles (Experiment 8, Day 8)



(a) Sulphur concentration (mM) on day 8 after the partial collapse of the FSB and release of colloidal sulphur particles into the bulk liquid



(b) Sulphide concentration (mM) on day 9 after the partial collapse of the FSB

Figure 8.19: Contour plots of sulphide and sulphur concentrations in the LFCR for experimental run 8. Depicting the consequences of FSB collapse.

8.4.5.2 Effect of a short residence time - 0.5 day

Experimental run 15 was conducted at a flow rate of 25 L/day and at an operating liquid volume of 12.5 L, resulting in a 12 hour residence time. This experiment was conducted in order to determine the impact of a short residence time and decreased volume. It was suspected that a decreased residence time would cause wash out of the planktonic population, as well as decreased sulphide removal and shearing of the biofilm structure. Pseudo-steady-state was reached on day one, at an average inlet sulphide concentration of 2.27 mM and loading rate of 56.78 mmol/day (Figure 8.20). A sulphide conversion of 93.5% was achieved, however a substantial amount of sulphate (40.78%) was formed from the complete oxidation of colloidal sulphur and sulphide. The FSB delaminated, as a lower layer heavily laden with sulphur, tore away from the floating sulphur biofilm on day four (sampling port 2.1 & 3.1). Consequently, the layer fell into the bulk fluid leading to the dissolution of the trapped sulphur on days five to seven (reaction 3.24). Additionally the release of the sulphur deposits caused a colloidal sulphur layer below the surface, which was subsequently oxidised. As a result there was an observed increase in the effluent sulphate concentration on day five (Figure 8.21). A considerable amount of colloidal sulphur entered the reactor (day 4-6, Figure 8.20) and was oxidised to sulphate. This is clearly illustrated by Figure 8.22a. This was due to an inconsistency in the feed composition due to poor performance in the upstream unit (DPBR). Coupled with sulphur oxidation, there was complete oxidation of sulphide in the bulk fluid at ports 2.1 and 3.1 (Figure 8.22b). Finally the smaller volume and short residence time ensured the colloidal sulphur reached the oxygen interface rapidly. Moreover, the lack of a complete FSB allowed greater penetration of oxygen into the shallower bulk liquid volume. These three contributing factors lead to a large proportion of colloidal sulphur being oxidised to sulphate.

Nevertheless, 225.8 mmol did report to the FSB as solid sulphur and accounted for 59.61% of the removed sulphide. A larger quantity of sulphur would have been recovered if the lower layer of the FSB had not torn due to the low acetate utilisation rate that was caused by the short-residence time. This will be discussed further in Section 8.5.

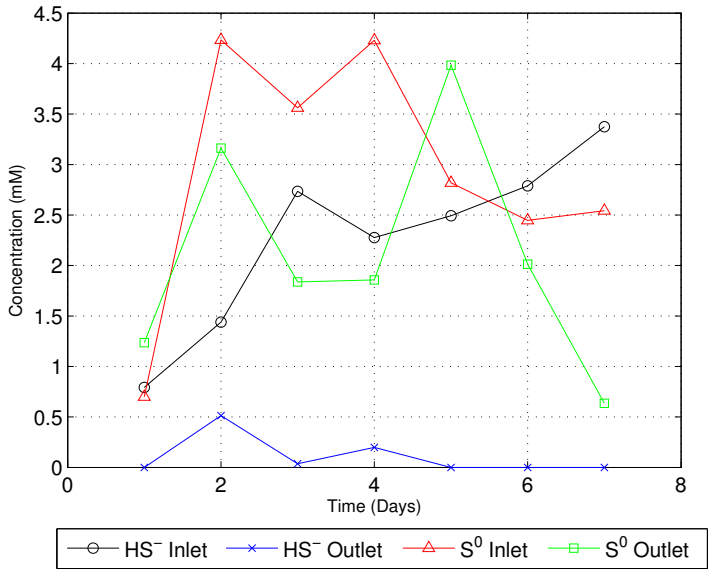


Figure 8.20: Influent and effluent sulphide and colloidal sulphur concentrations (mM) throughout the duration of experimental run 15

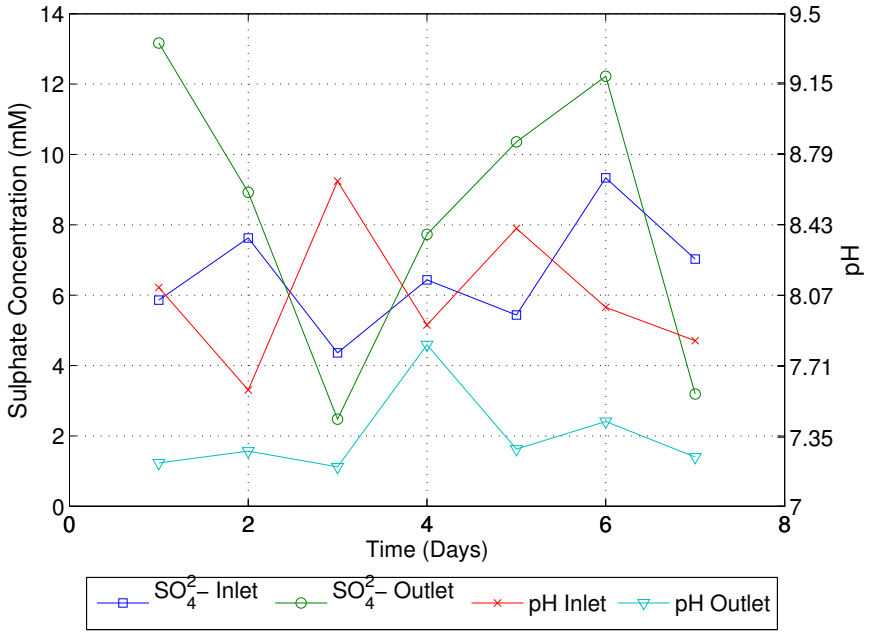
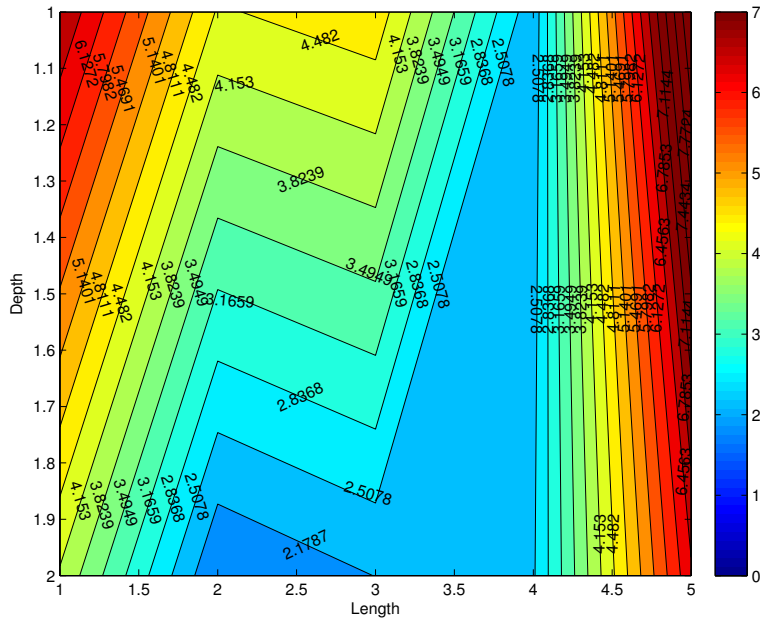
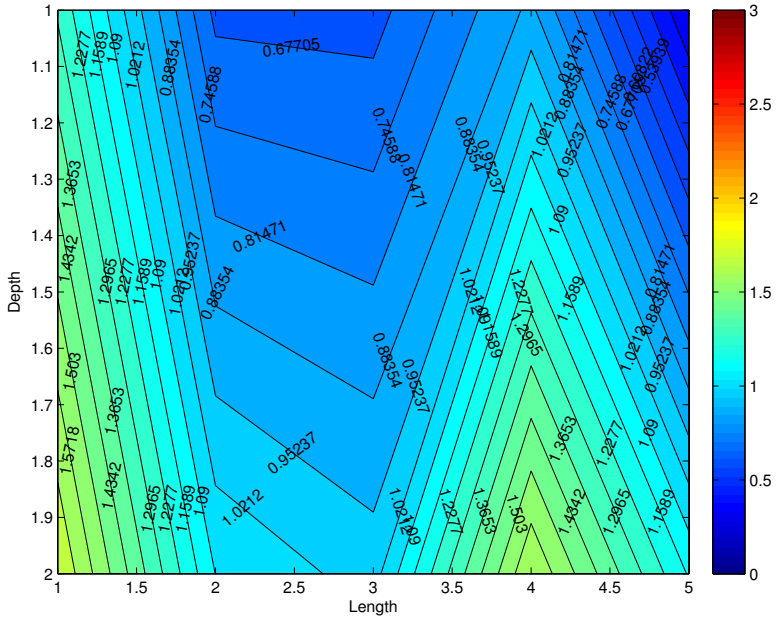


Figure 8.21: Sulphate concentrations (mM) and the associated pH profile of the influent and effluent stream throughout the duration of experimental run 15

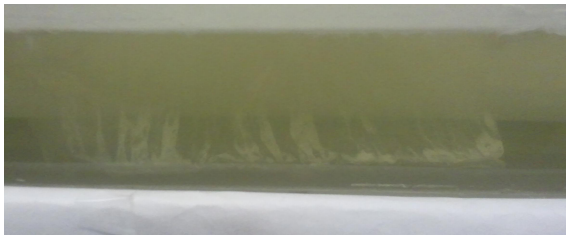


(a) Sulphur concentration contour plot of the colloidal sulphur concentrations in the bulk fluid on day five.

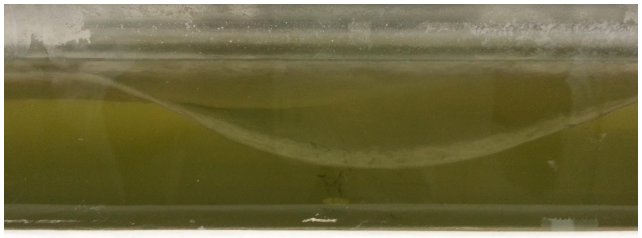


(b) Sulphide concentration contour plot of experimental run 15 (12 hour R.T.) on day four.

Figure 8.22: Contour plots of sulphur species profiles in the LFCR in experimental run 15 ($\frac{1}{2}$ day R.T.). Illustrating the oxidation of colloidal sulphur due to tearing of the FSB.



(a) Lower layer of the FSB that has torn away and dropped the sulphur deposits on the reactor floor. The remaining sulphur (white precipitates) within the FSB matrix was slowly dissolving into the bulk liquid.



(b) Lower layer of the FSB that has partially torn away from an upper layer.

Figure 8.23: Photographs of the FSB (side-view) depicting the tearing of the lower layers due to a high flow rate. (Experimental run 15, 0.5 day R.T.)

8.4.5.3 Poor harvesting method - Experimental run 16 - (1) - 1.5 day R.T.

The original harvesting method developed at GARL was to spray the surface with water and disturb the surface tension. Therefore collapsing the biofilm and collecting the pieces from the bottom of the channel after an extended period of time. However, this method was not adopted for all experiments, due to the dissolution of the sulphur deposits by reacting with bisulphide ions, as observed in experiment 8. Therefore, the strategy of skimming the FSB off the liquid surface was adopted.

Experiment 16 was divided into three phases each lasting approximately four residence times (6 days). Pseudo-steady-state in the LFCR was attained on day 2 with a sulphide gradient ranging from 1.15 to 1.93 mM. The average inlet sulphide concentration was 5.28 mM and the sulphide loading rate was 98.93 mmol/day (Figure 8.24). A sulphide conversion of 65.20% was achieved with 26.38% of that being converted to colloidal sulphur. However, the amount of sulphur recovered in the FSB was only 122.14 mmol (26.99%). This was chiefly a result of two factors. The experiment was designed to optimise the structural integrity of the biofilm and its ability to hold a large amount of sulphur. The LFCR was supplied organic carbon (1.5 g acetate/L) which resulted in an initial biofilm that was carbon rich and thicker. As a consequence there was some attachment to the walls of the LFCR, as well as the floor of the reactor via EPS and biofilm strand networks. This made harvesting of the FSB difficult. The second factor contributing to the poor sulphur recovery in phase one was the method of harvesting. A scoop was used to skim the FSB off the water surface. In previous experiments (8-15) the second method (Chapter 5) was used, which ensured no sulphur was lost as colloidal sulphur in the bulk fluid during the harvesting process.

Therefore, the recovery of the FSB at the end of phase one was poor as the bulk fluid was not drained and the FSB was recovered by skimming. The FSB anchored to the reactor floor and side walls which made recovery particularly more difficult. Hence, a large amount of sulphur fell into the bulk fluid during harvesting (Figure 8.25). Significantly less sulphate (15.83%) was formed due to the high sulphide loading and well-formed thick FSB which

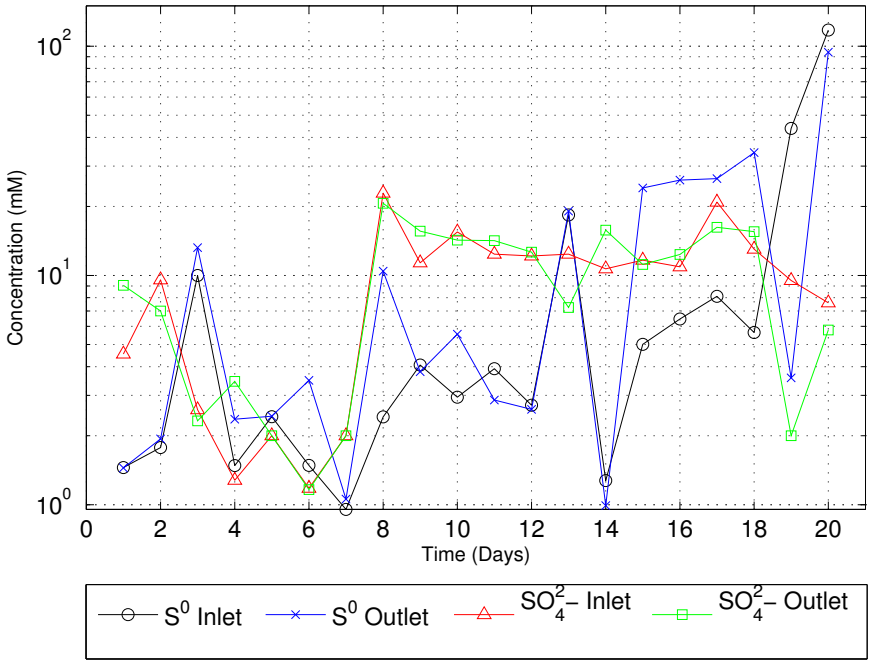


Figure 8.24: Sulphate and colloidal sulphur concentrations (mM) of the influent and effluent stream throughout the duration of experimental run 16, phases 1-3

impeded the flux of oxygen.

During phase two a large amount of colloidal sulphur in the effluent (195.6 mmol) on day eight was observed due to harvesting (Figure 8.24). Therefore, a portion of the colloidal sulphur was from the FSB in phase 1. It was calculated that the amount of sulphur lost was approximately 139.43 - 145.3 mmol. The sulphur material balance would be closed for phase one if this value was incorporated and the amount of sulphur recovered by the FSB would have been a minimum of 261.57 mmol (57.8%). The FSB began to reform four hours after harvesting the phase one FSB. An initial EPS layer formed on the surface together with a cloudy white colloidal sulphur layer (5 mm thick) below (one hour after harvesting). Thereafter a thin white skin layer was formed on the surface, which was the scaffolding and initial structure of the FSB (Figure 8.26). The harvesting in phase two was substantially better due to the FSB being stronger, as significantly less sulphur was lost in the bulk fluid. The increased robustness of the FSB will be discussed in Sections 8.5 and 8.6. An alternative method of FSB harvesting will be proposed in the final recommendations chapter (10).

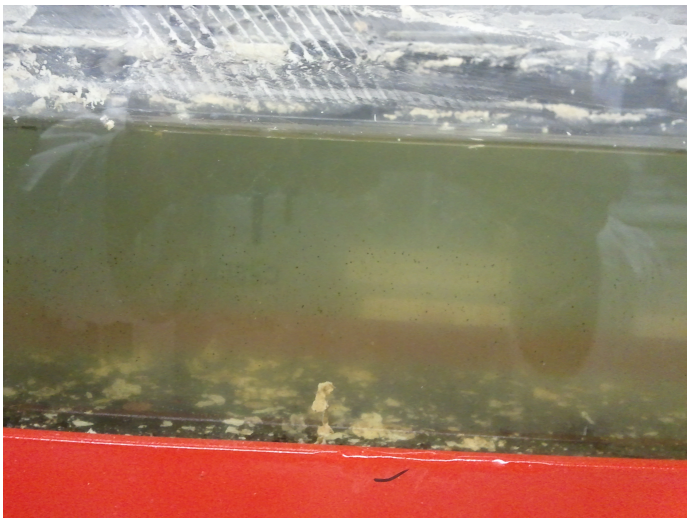


Figure 8.25: Photograph of the LFCR showing the pieces of FSB which, fell to the reactor floor during harvesting in phase one (Experimental run 16).

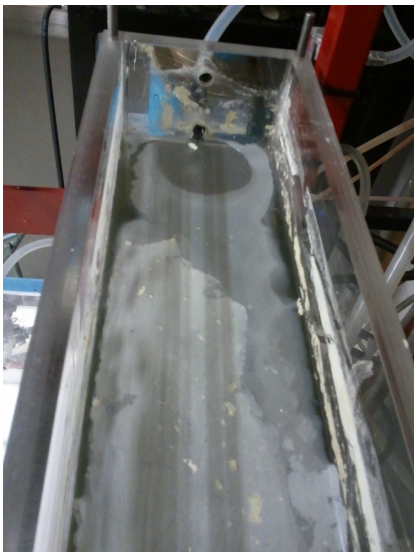


Figure 8.26: Thin white skin layer representing initial biofilm growth four hours after harvesting the previous FSB (Experimental run 16, day 7)

8.4.5.4 Effect of green sulphur bacteria (GSB)

The final cause of poor LFCR performance was the growth of green sulphur bacteria and cyanobacteria, which overwhelmed the other microbial populations. Consequently, the cyanobacteria became the dominant species and compromised the FSB structure, whilst the green sulphur bacteria formed a secondary biofilm along the floor and walls of the reactor.

Experimental run 16-(3) showed the worst performance and clearly illustrated the importance of microbial community structure for LFCR performance. The average sulphide concentration in the feed was 6.08 mM, with a sulphide loading rate of 100.23 mmol/day (Figure 8.24). The sulphide conversion (89.46%) was higher than the previous two phases, however only 21.79% of the converted sulphide was recovered as sulphur in the FSB. Approximately 414.45 mmol of colloidal sulphur was formed, even though a high sulphide loading was maintained throughout the experimental run. The primary cause of the low sulphur recovery was the prevalence of a GSB, which started growing on the reactor walls on day 13 (Figure 8.28). The green sulphur bacteria spread from the back of the channel along the sampling port wall as well as the floor of the reactor. The proliferation of GSB was assisted by the fluorescent laboratory lights, which provided the bacteria with 4.5 - 5 μmol/m^2.s of photon light flux 24 hours a day from day 12 to day 18. The lights were left on at night as part of an unrelated algal growth experiment.

Green sulphur bacteria are obligate anaerobes therefore their growth and proliferation was in the anaerobic zones of the LFCR, the floor and walls of the reactor. Green sulphur bacteria are capable of oxidising sulphide to elemental sulphur, which is deposited extracellularly as sulphur globules when sulphide is in-excess. Complete oxidation to sulphate occurs when the sulphide substrate is limiting (Pringault et al., 1999). In phototrophic organisms the formation of organic carbon material from carbon dioxide may be expressed by reaction 8.2, where CH_2O represents cellular material(Hell et al., 2008). The ATP and reducing power needed to form cell material from CO_2 are produced as a result of electron transport initiated by light reactions. In the case of cyanobacteria or plants the ultimate H-donor in photosynthesis is H_2O, whereas GSB are able to utilise reduced sulphur compounds (HS^-) (Hell et al., 2008). Therefore GSB are able to oxidise sulphur compounds for photoautotrophic growth.

$$CO_2 \overset{4H+ATP+enzymes}{\longrightarrow} CH_2O + H_2O \tag{8.2}$$

—

No sulphate was formed due to the chemical conversion of sulphide to colloidal sulphur, however there was an accumulation of sulphate in the reactor on day 19 and 20 (235.33 mmol), due to the dead-zones in the reactor. Thus the lack of sulphate production is consistent with the observations of green sulphur bacteria.

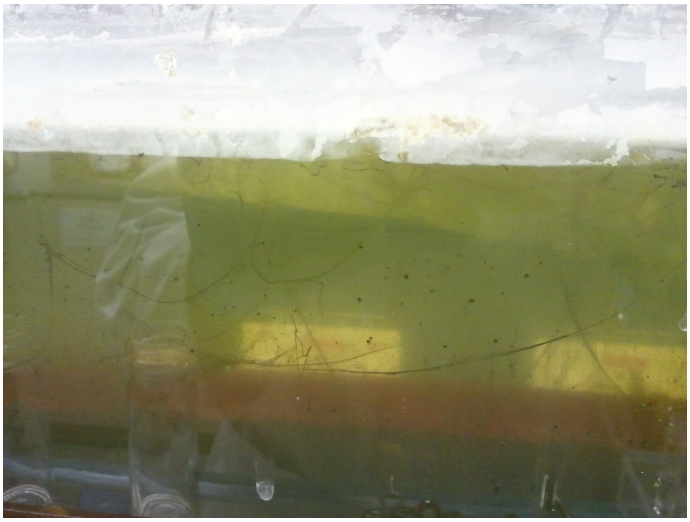
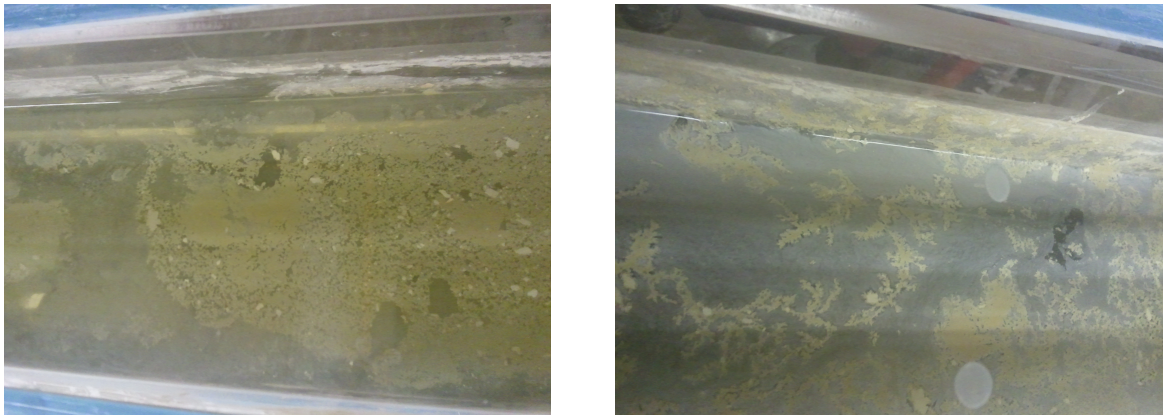


Figure 8.27: Photograph of the underside of the FSB and the EPS strand networks which, are attached to the reactor floor, side walls and other parts of the FSB. Green sulphur bacteria are also present on the wall of the reactor as small green colonies. Additionally, the bulk fluid was a green colour due to the presence of GSB (Day 14, experimental run 16, phase two).

The FSB became less robust as the cyanobacteria became the dominant population. microorganism. It led to the FSB being structurally weakened and unable to hold a large quantity of sulphur deposits. The presence of the cyanobacteria was identified by green patches in the FSB surface (Figure 8.28). Cyanobacteria are able to carry out oxygenic photosynthesis, however they are also capable of anaerobic metabolism. Therefore the cyanobacteria was able to grow in the FSB as an aerobic photoautotroph utilising HS^- as an electron donor, however water may also be utilised thus producing oxygen as a by-product (Dworkin et al., 2006c). Therefore, significant portions of the FSB had been structurally weakened due to the dominance of cyanobacteria and lack of EPS production. For this reason the FSB began to collapse when harvesting commenced and most of the sulphur was lost to the bulk liquid, only 21.8% of converted sulphide reported to the FSB as sulphur.



(a) Photograph of the liquid surface with a considerable amount of green cyanobacteria at the air-liquid interface (Day 15).

(b) Photograph of the FSB with a considerable amount of green cyanobacteria present in structural matrix of the FSB (Day 17).

Figure 8.28: Photographs of the top of the FSB of experimental run 16 - phase 3

8.5 Carbon species material balance

The second major aspect of this chapter is the investigation into the carbon requirement and utilisation in the LFCR. Experimental runs 11 - 16-(2) were supplemented with acetate in the feed to determine the minimum required for optimum LFCR performance. The following section aims to highlight the necessity for a consistent supply of organic carbon to support the formation of a robust and sturdy FSB.

8.5.1 Results

Table 8.4 summarises the average acetate concentration in the feed and the amounts of acetate utilised over the duration of the experiments. The material balances were performed across the LFCR, by measuring inlet and outlet concentrations.

Table 8.4: Acetate material balance across the LFCR for biological experimental runs 11 - 16-(2)

Run	RT (days)	Feed acetate concentration (g/L)	Avg. acetate utilisation (%)	Acetate utilised (g)	Acetate utilisation rate (g/L.day)
11	2	0.99	15.86	15.74	0.0525
12	2	2.26	15.25	99.11	0.2832
13	1	1.17	9.01	26.45	0.1058
14	1	2.24	16.98	115.30	0.4612
15	0.5	0.86	7.39	12.38	0.1414
16-(1)	1.5	1.24	10.31	24.18	0.1228
16-(2)	1.5	1.77	10.50	31.50	0.16

8.5.2 Discussion

The initial experiments 6 and 7 were not provided an organic carbon source, consequently FSB development was hindered and this prevented the recovery of sulphur, as well as the harvesting of the biofilm due to its poor structural integrity. As a result, the subsequent experiments were supplemented with acetate to improve biofilm growth and FSB development.

Experimental run 11 and 12 had an average acetate utilisation of 15.86% and 15.25% respectively for a two day residence time. Whilst, experimental run 13 had a lower average acetate utilisation of 9%. Experimental run 14 was operated at a one day residence time, but had a greater acetate utilisation of 16.98%. The increase was most likely due to the higher organic loading rate. Experimental run 15 had the lowest average acetate utilisation at 7.39%, whilst in experimental run 16-(1) and 16-(2) utilisation was 10.31% and 10.5% respectively. A direct relationship was observed between residence time and the acetate utilisation rate. As the residence time decreased the average acetate utilisation rate increased (Figure 8.29). Therefore the amount of acetate utilised was a function of the period of time the acetate was in contact with the biofilm. The acetate utilisation rate was plotted independent of residence time, as 'concentration of acetate used (g/L)' (Figure 8.30). The concentration of acetate used was approximately 0.1 g/L for residence times 0.5, 1 and 2 days, at an acetate loading rate of approximately 1 g/L. So, the microbial kinetics of acetate utilisation is approximately constant across the different residence times at 0.1 g/L. Experiment 16 was slightly higher at 0.18 and 0.24 g/L. Experimental runs 12 and 14 also had a greater daily acetate utilisation and total acetate used, which was probably due to higher loading rate of acetate being 2.26 and 2.24 g/L respectively. Thus a greater amount of acetate was in contact with the biofilm, hence a larger utilisation rate was observed. For these reasons the minimum organic loading concentration required for optimal LFCR performance was found to be 0.1 g/L.

Upon closer inspection an interesting and dynamic trend was identified with regard to the daily acetate utilisation. In experimental run 11 and 13 the amount of acetate consumed started high and thereafter decreased to 'negative' consumption due to some accumulation of acetate in the reactor (Figure 8.31a). However, the amount of accumulation within the bulk fluid was minimal, as no distinct regions of high acetate concentration were observed (Figure 8.32). The following day the amount of acetate increased to reach a second maximum and decreased again. A similar trend was also observed in experimental run 12 as the amount of acetate utilised decreased to a minimum, thereafter instantaneously increased to maximum and subsequently decreased again. This sinusoidal pattern was extremely interesting especially considering the fact that, not only was it present in the unsteady-state phase, but the pseudo-steady-state phase as well. Therefore, the consumption of acetate was independent of the sulphide oxidation rate, however the varying pattern seems to suggest that acetate was required periodically in greater

quantities. These periods could possibly be the moments when the FSB was expanded structurally by another layer, or the FSB was reinforced to hold the sulphur deposits. This theory will be explored further in the FSB structural analysis section.

Lastly, the initial experiments 6 and 7 were carbon substrate limited and as a result the microbial community was largely composed of photoautotrophic organisms. In the subsequent acetate supplementation experiments a more diverse microbial community structure was established, comprising far more heterotrophic organisms. Hence, the FSB structure and LFCR performance greatly improved, the results of the microbial study will be discussed in Section 8.7.

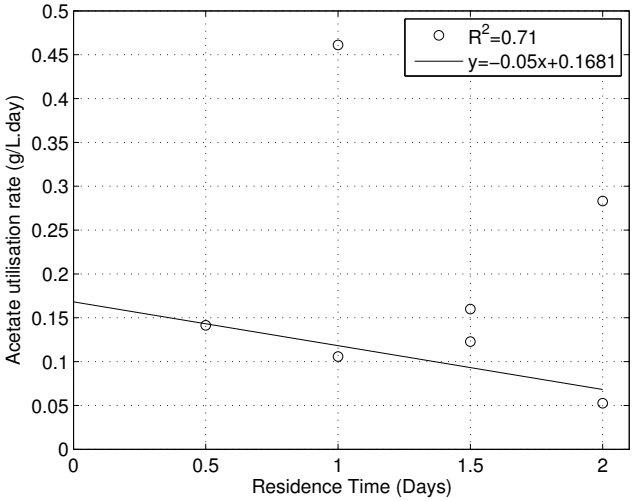


Figure 8.29: Relationship between residence time and acetate utilisation within the LFCR for biological experimental runs. Experimental run 12 and 14 were ignored with regard to the linear plot, due to the higher organic loading rate.

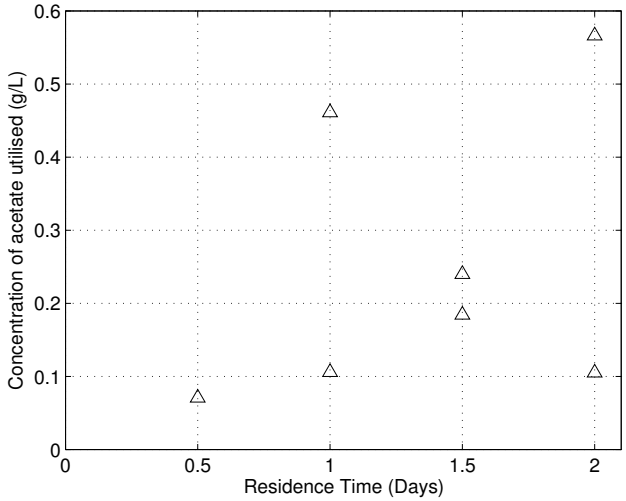


Figure 8.30: Concentration of acetate used for LFCR experimental runs 11 - 16-(2). The scatter-plot shows that the average consumption rate of acetate in the FSB is a constant.

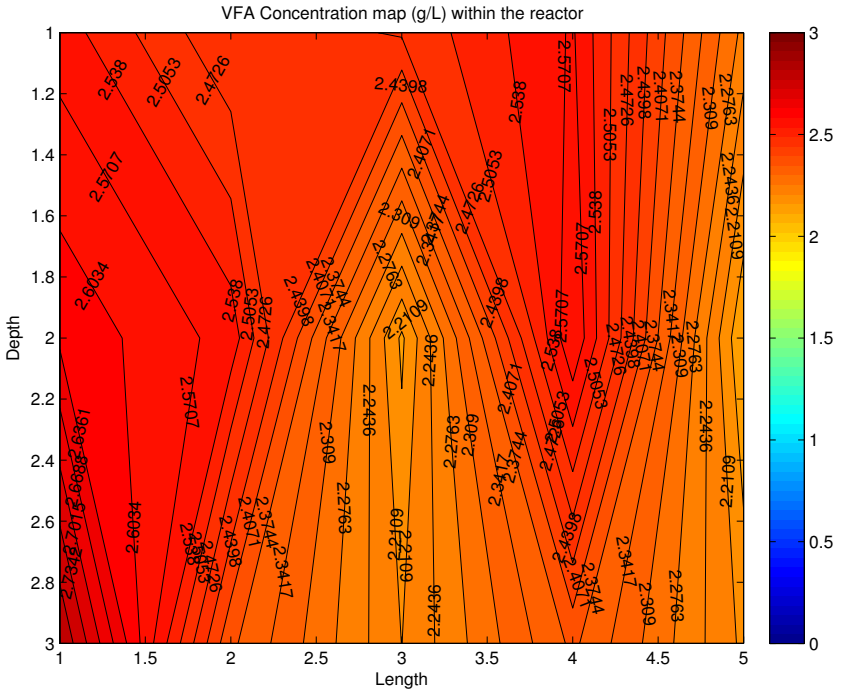
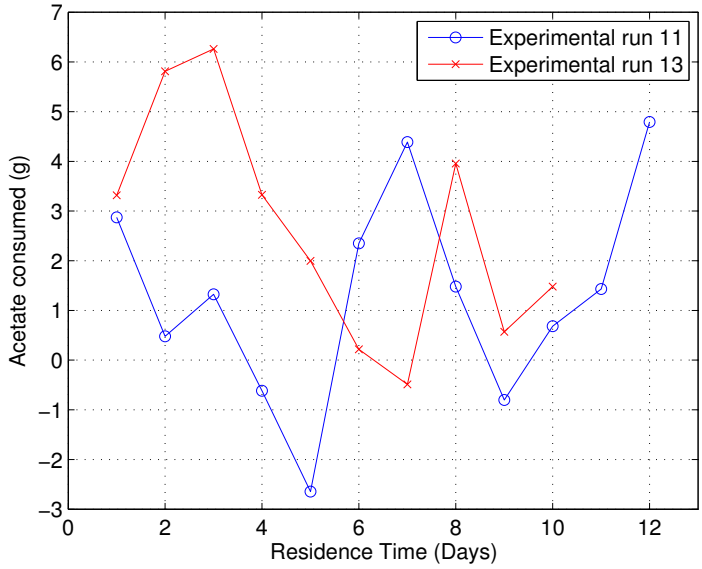
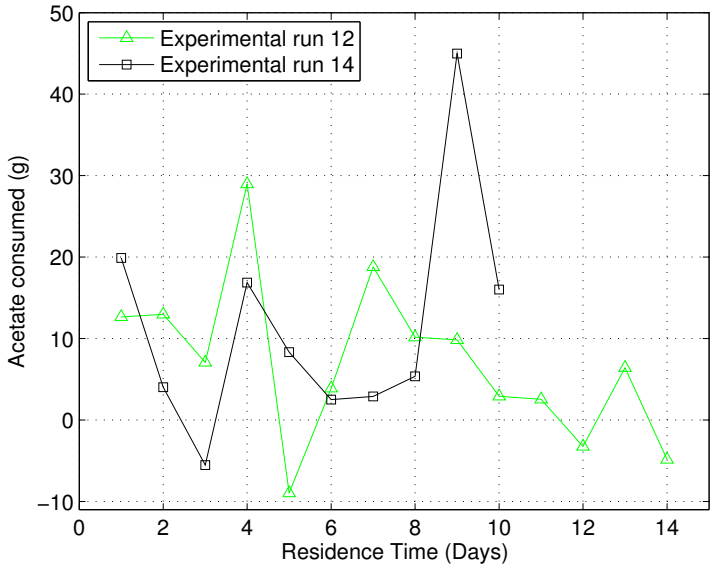


Figure 8.32: Acetate concentration contour plot showing no accumulation of acetate in the dead-zones of the LFCR (Experimental run 12, day 5)



(a) Experimental runs 11 and 13 at a two (0.99 g/L) and one (1.17 g/L) day residence time respectively.



(b) Experimental runs 12 and 14 at a two (2.26 g/L) and one (2.24 g/L) day residence time respectively.

Figure 8.31: Daily acetate utilised for biological LFCR experimental runs 11 - 14.

8.6 Floating sulphur biofilm analysis

8.6.1 Compositional analysis

A compositional analysis was conducted on each floating sulphur biofilm harvested from experimental runs 8 - 16-(2). A decrease in residence time led to an increase in the relative proportion of elemental sulphur in the FSB. However, an increase in the organic (acetate) loading rate did not lead to a proportional increase in the organic content of the FSB. At a four day residence time the average sulphur content was 52.6%, while at a two day residence time it increased to 88% and reached a maximum of 94% at 12 hours (Figure 8.33). Therefore, as residence time decreases there is an increase in the amount of sulphur sequestered to the FSB. As a result the FSB became mainly inorganic, as less carbon was accumulated in the biofilm, due to the shorter contact time between the acetate substrate and biofilm at shorter residence times.

An interesting phenomenon was that experimental run 12 utilised 99 g of acetate (40.3 g carbon), however the FSB was only comprised of approximately 2.1 g of carbon. Therefore, the vast majority of the acetate was consumed for cell metabolism (energy consumption). Heterotrophic organisms are capable of acetate assimilation via the glyoxylate or tricarboxylic acid cycle, thus forming CO_2 as a by-product. Therefore, a more comprehensive carbon balance would be necessary to determine the loss of CO_2 to the atmosphere. Similar trends were observed in the other experimental runs. This would suggest a dynamic system in which a substantial part of the total energy budget is required to maintain the redox gradients that occur within the biofilm.

Further compositional analysis was performed in order to determine what metals and inorganic matter (other than sulphur) were present in the FSB (Table 8.5). Interestingly, the FSB from experimental runs 8 and 9 (4 day R.T.) had no metal precipitates and the fraction of inorganic matter was 0 and 4.5% respectively. Experimental runs 10 - 16-(2) contained significantly less organic carbon and considerably more inorganic salts and metal precipitates. From the weight and atomic percent analyses, it was calculated that the inorganic salts that precipitated due to evaporative crystallisation, on the top surface of the FSB, were calcium, magnesium and sodium sulphate, as well as sodium chloride. These were covered in EPS in some cases (Figure 8.34a & b). The metal precipitates that were enclosed in the FSB matrix, were probably metal sulphide precipitates from the DPBR upstream. Iron and zinc sulphide precipitates were found, in addition to aluminium hydroxide and manganese precipitates. The metal precipitates were 0 - 1 μm with a crystalline shape indicating that they were nano-sized particles, which washed out of the DPBR. However, these particles became trapped within the EPS matrix of the FSB and covered by a layer of bacterial cells (Figure 8.34d).

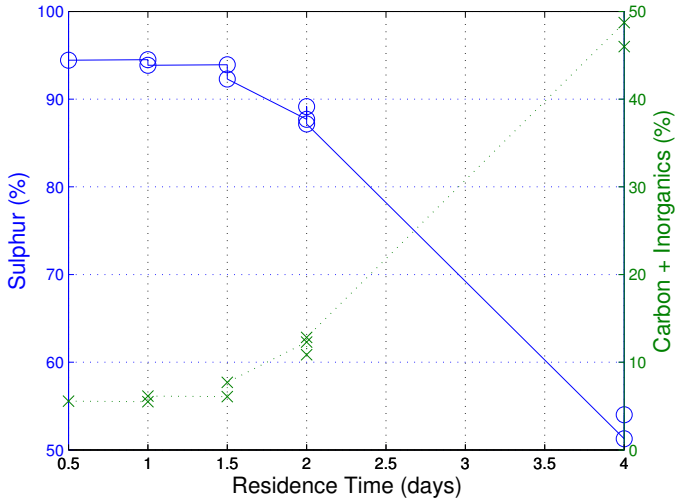
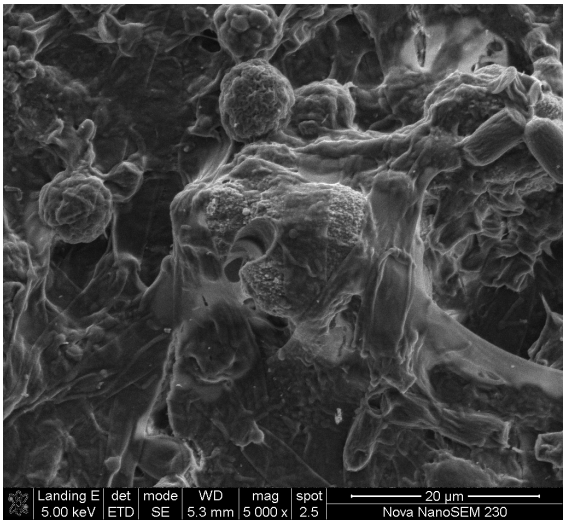


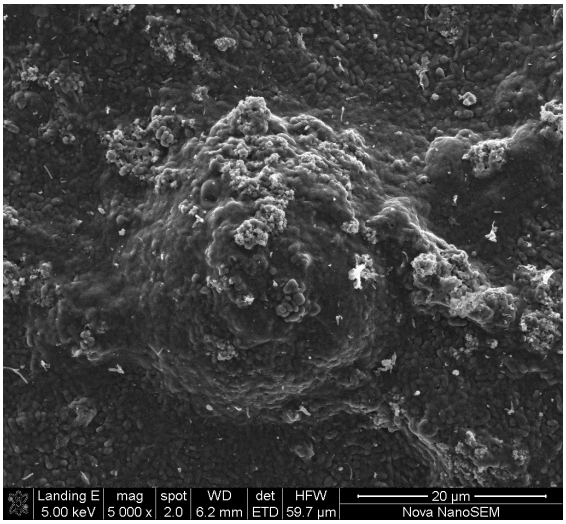
Figure 8.33: Compositional breakdown of the floating sulphur biofilm from experimental runs 8 - 16-(2).

Table 8.5: Elemental compositional analysis of the FSB from experimental runs 8 - 16-(2). The mass of organic carbon (C) and inorganic matter (I) (excluding solid sulphur recovered) is presented. The mass of sulphur recovered is presented as FSB-S*. The compositional break-down of the inorganic fraction is presented as weight percent. The sulphur (%) is due to sulphate salts. Analyses conducted using SEM-EDS.

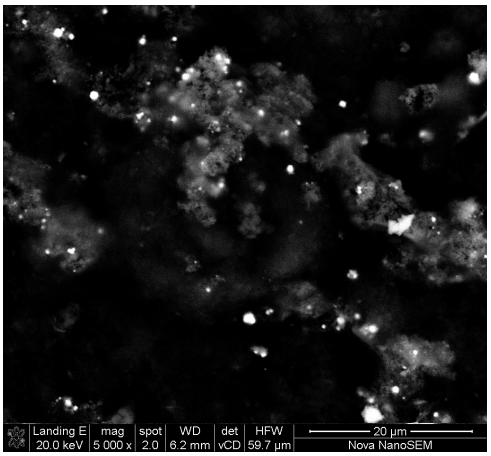
Run no.				Non-metals (%)							Metals (%)					
	FSB-S* (g)	C (g)	I (g)	O	S	Ca	Mg	Si	P	Cl	Na	Fe	Zn	K	Al	Mn
8	4.61	4.382 ±0.088	0	0	0	0	0	0	0	0	0	0	0	0	0	0
9	5.7	4.633 ±0.093	0.219	0	0	0	0	0	0	0	0	0	0	0	0	0
10	16.86	2.237 ±0.045	0.128	43.8	14.6	25.2	1	0	0	12.8	0	0	0	0	0	2.5
11	16.06	1.638 ±0.033	0.318	38.4	9.8	11.3	8.6	0.8	6.1	0	3.9	14.3	2.6	1.5	2.7	0
12	15.38	2.141 ±0.043	0.123	33.6	4.2	8.1	3.6	0.6	8.2	18.5	8.4	4.1	2.8	3.1	2.9	1.8
13	22.36	0.801 ±0.016	0.343	44.8	7.9	18.7	2.2	0	2.8	0.6	4.1	5.8	7.7	1.9	1.3	2.2
14	21.12	1.094 ±0.022	0.288	42.8	8.5	5.2	4	0	7.5	0	12	5.7	4.6	2.1	4.3	3.3
15	7.23	0.164 ±0.003	0.261	46.0	7.8	8.8	4.7	0	8.9	0.6	3.2	4.8	7.5	2.5	5.2	0
16-(1)	3.91	0.422 ±0.008	0.046	65.8	3.3	15	2.3	0	4.8	0	4.9	0	0	4	0	0
16-(2)	13.93	1.109 ±0.022	0.053	39.8	12.7	12.9	1.9	1.2	3.6	0	4.5	16.6	0	1	3.7	2.3



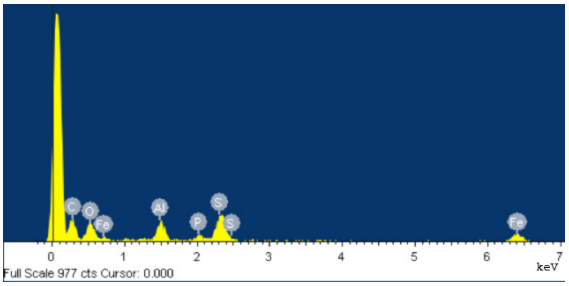
(a) Calcium sulphate precipitate covered in EPS



(b) Topographical image of the FSB underside containing a cell cluster as well as smaller EPS-free cell clusters



(c) Density scatter image of Figure 8.34b depicting the presence of metals and sulphide precipitates within the FSB



(d) SEM-EDS analysis of inorganic precipitates

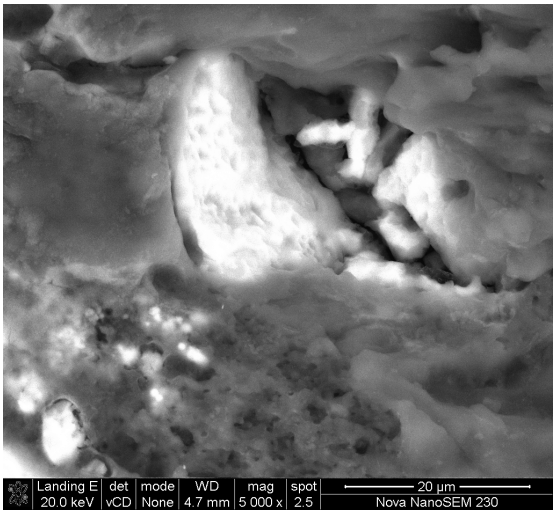
Figure 8.34: Scanning electron microscopy images of inorganic matter in the FSB structure

8.6.2 EPS, strand networks and FSB thickness

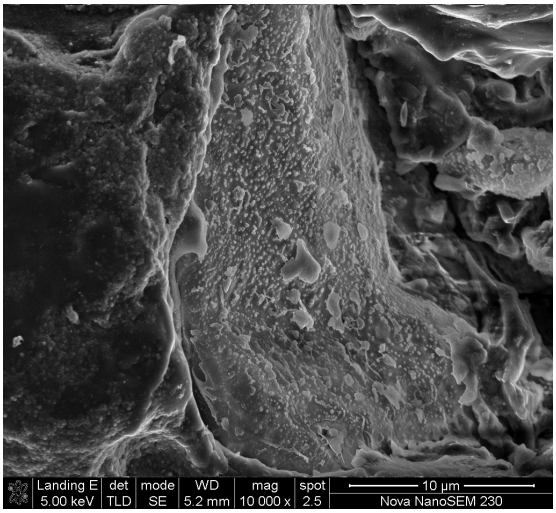
Visual observations and SEM analyses showed that the FSB is an extremely heterogeneous structure, made up of EPS, sulphur, inorganic precipitates, water, cells and cell clusters. Flemming & Wingender (2010) described the EPS matrix as a network providing sufficient mechanical stability to maintain a spatial arrangement for micro-consortia over a prolonged period. This stability is provided by the hydrophobic interactions, cross-linking by multivalent cations and entanglements of the biopolymers. Furthermore, they showed that the presence of Ca^{2+} ions increased the mechanical stability of mucoid *P. aeruginosa* biofilms. This effect was explained by the Ca^{2+} ions cross-linking polyanionic alginate molecules, thereby increasing the mechanical strength of the EPS matrix. Hydrogen bonding and van der Waals interactions between the biopolymers also increase the structural integrity of a biofilm. Furthermore, it has been shown that Ca^{2+} ions influence the hydraulic conductivity of biofilms, and cause increased retention of colloids with an increase in biofilm growth (Morales et al., 2007).

The EPS also did not only form the structural architecture of the floating sulphur biofilm but also covered the sulphur deposits. This is supported by Figure 8.35 a and b, which clearly illustrates that sulphur precipitates are covered in a layer of EPS and become part of the FSB structure. Sulphur was formed by biological sulphide oxidation as well as chemical sulphide oxidation. Evidence of chemical sulphide oxidation is shown in Figure 8.35c, d where large rhombic sulphur crystals (98 μm) were identified on the underside of the FSB. The FSB structural matrix was also influenced by the formation of biofilm strand networks. These strands grew on the underside of the FSB in an effort to anchor the biofilm. In addition to the biofilm strands growing downwards to the reactor floor to provide anchorage and further attachment, there was growth of strands to other parts of the FSB (Figure 8.36a & b). The most likely explanation is to increase the volume of the FSB, as the strands provided ancillary points of attachment to the microbial population, and a 'sticky' web for the deposition of biologically produced sulphur. Smaller EPS strands (1 - 2 μm) were also identified between biofilm layers. These possibly also influenced the structure by initially joining layers of the FSB together, prior to further deposition of EPS and biopolymers to increase the mechanical strength of the biofilm (Figure 8.36c).

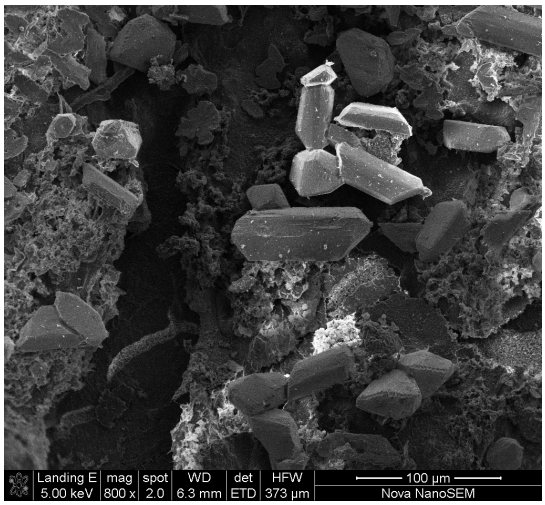
The relationship between residence time and floating sulphur biofilm thickness was also investigated. The thickness of the FSB was determined by SEM analyses. The thickest FSB (407 μm) was generated at a two day residence time, whilst the thinnest FSB (134 μm) was generated at a 6.5 day residence time. At a two day residence time the FSB formed in layers, and had well defined boundary edges. Furthermore, there were clear distinct layers of sulphur deposition, as well as zones of high sulphur concentration (Figure 8.37b). The four day residence time FSB upper surface (exposed to air) was structurally well-defined, however the lower part of the FSB was broken with no clear visible edge (Figure 8.37a). The biofilm was significantly more porous and broken, than the two day residence time FSB. As



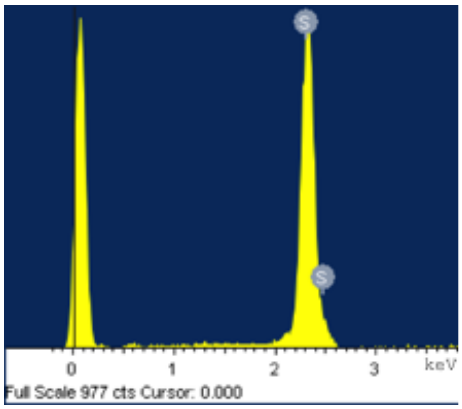
(a) Density scatter image of a sulphur deposit entrapped within the biofilm EPS matrix.



(b) Topographical image of the sulphur deposit (a) covered in EPS and other organic matter forming part of the FSB structural matrix

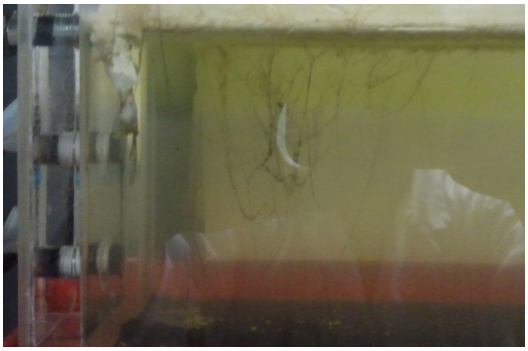


(c) Rhombic sulphur crystals attached to the underside of the FSB

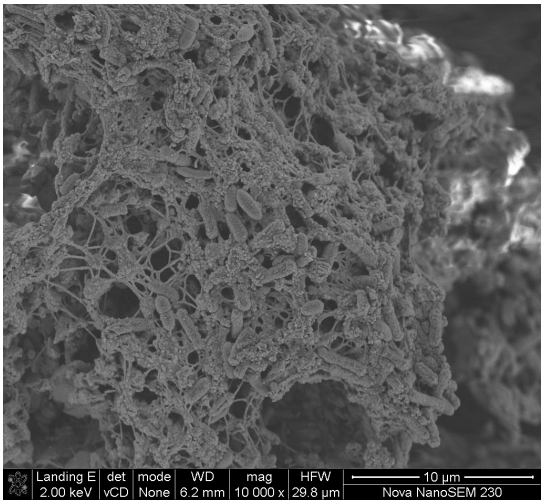


(d) SEM-EDS analysis of rhombic sulphur crystals (100%)

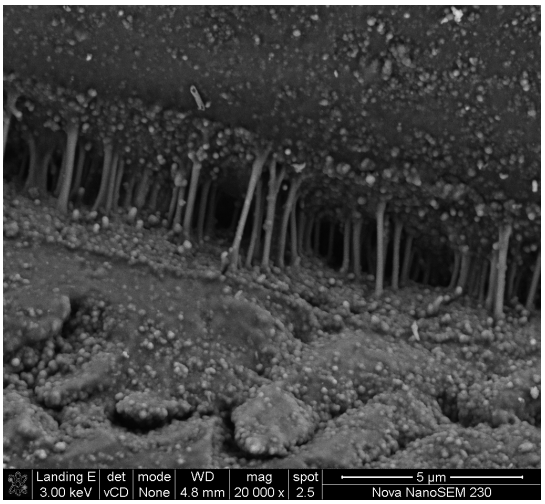
Figure 8.35: Scanning electron microscopy images of sulphur deposits formed within the FSB matrix.



(a) Biofilm strand networks growing downwards to the reactor floor and other parts of the FSB.

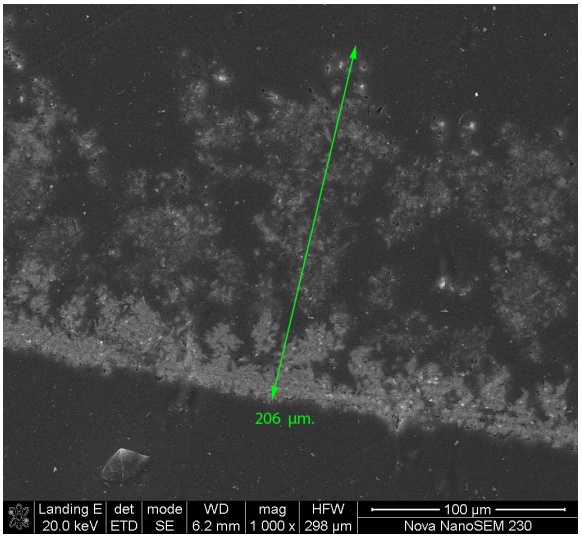


(b) Biofilm strand network increasing the volume of the FSB to allow for attachment of sulphide-oxidising bacteria and biologically produced sulphur.

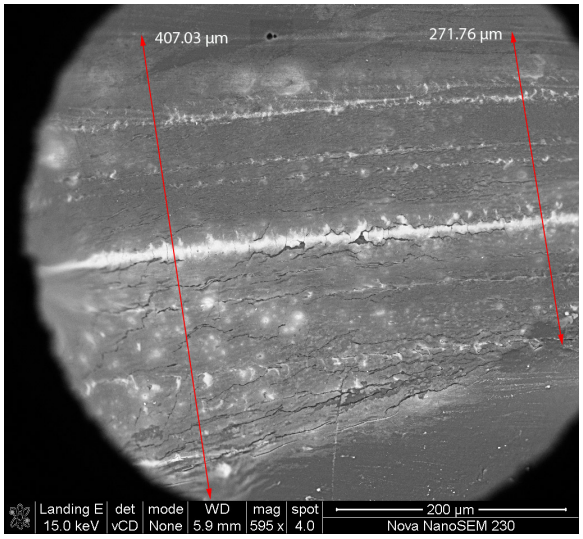


(c) Illustrating the layers of the floating sulphur biofilm which are joined together by EPS strands approximately 1-2 μm long (cross-section view).

Figure 8.36: Photographs and SEM images illustrating the presence of EPS strand networks, anchoring, increasing the surface area and joining layers of the biofilm.



(a) Four-day residence time (206 μm) (Experimental run 8).



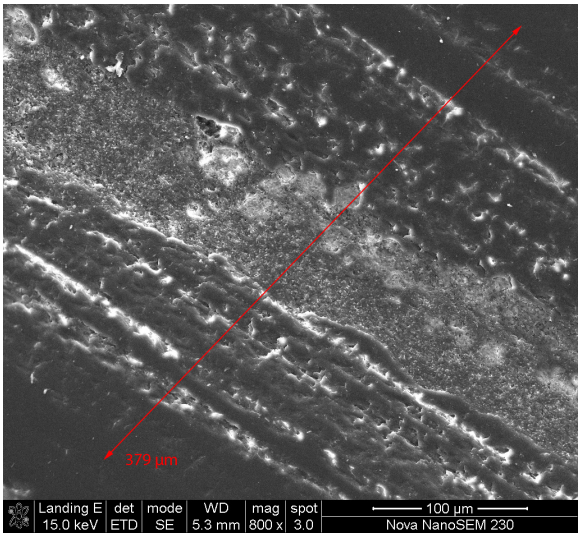
(b) Two-day residence time (407 μm) and harvested from position 3.1. The bright white lines are sulphur layers and areas of high sulphur deposition. (Experimental run 12)

Figure 8.37: Scanning electron microscopy images of FSB samples (4 and 2 day residence time) in cross-sectional view. Each image is annotated with the measured thickness of the FSB.

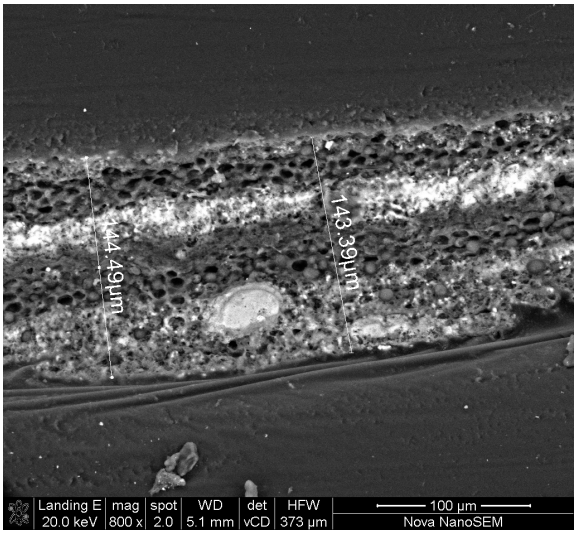
it contained significantly less sulphur and inorganics, with no clear distinct sulphur deposit or organic layers. A similar trend was observed in the 1 and 1.5 and 0.5 day residence time biofilms (Figure 8.38a, b, Figure 8.39), they were extremely dense and rich in sulphur, with a clear defined structure. The thinnest FSB was grown at a residence time of 6.5 days. Biofilm layers were visible, however the structure was significantly less well-defined as the layers were not joined together and delamination was visible. The FSB also had significantly less sulphur deposits.

A linear relationship between residence time and FSB thickness (Figure 8.40) is best represented by equation 8.3, where (x) is residence time (days) and (F) FSB thickness (μm). This equation is only valid for residence times over the range of one to seven days. Due to delamination and tearing of the FSB in experiment 15, the biofilm was significantly thinner. This was largely due to the shorter contact time between the acetate substrate and the biofilm, as a result residence time is not the only factor that could affect FSB thickness.

$$F_{thickness} = -49.27x + 443.5 \tag{8.3}$$

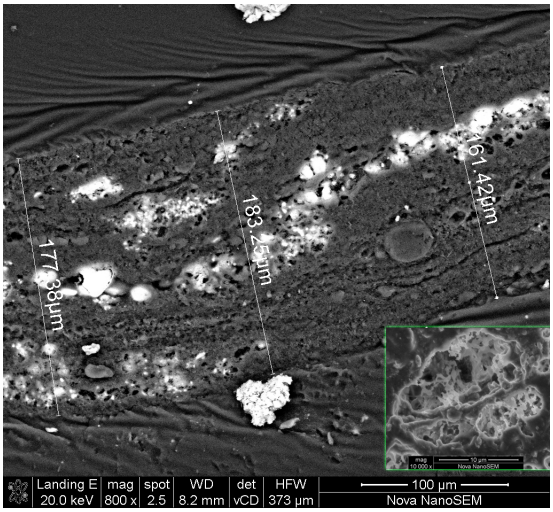


(a) One-day residence time (379 μm) and harvested from position 3.1 (Experimental run 14).

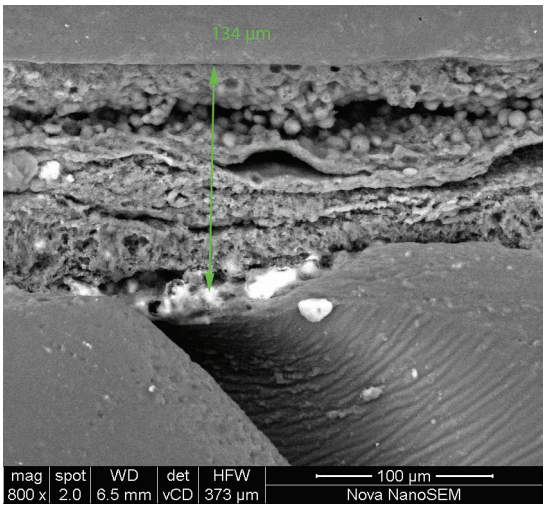


(b) One and a half day residence time (144 μm) (Experimental run 16, phase two) .

Figure 8.38: Scanning electron microscopy images of FSB samples in cross-sectional view. Each image is annotated with the measured thickness of the FSB.



(a) Half day residence time (183 μm) with an enlargement of a conduit in the FSB structure (green-box, right hand corner) (experimental run 15).



(b) FSB grown at 6.5 day residence time. (134 μm)

Figure 8.39: Scanning electron microscopy images of FSB samples in cross-sectional view. Each image is annotated with the measured thickness of the FSB. The bright white zones are high concentrations of sulphur.

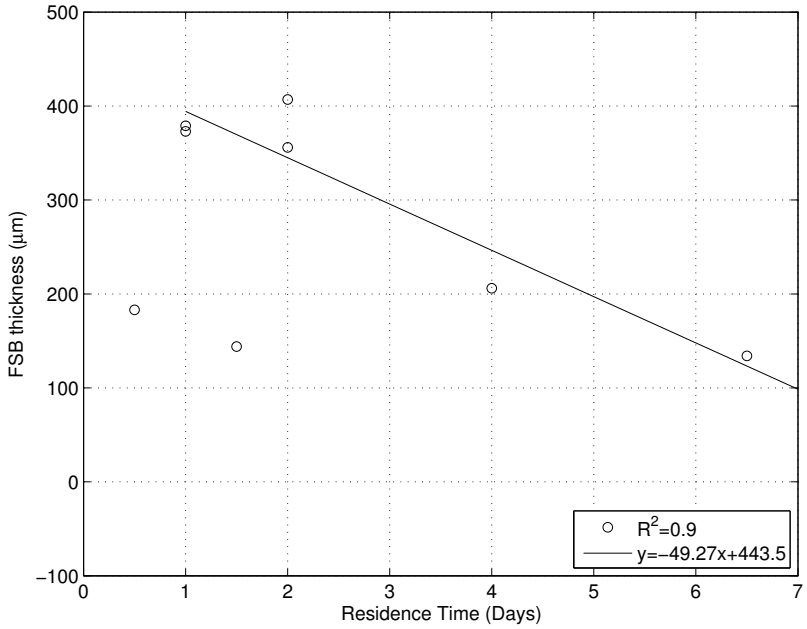


Figure 8.40: Relationship between FSB thickness and residence time, with the maximum thickness being reached at a residence time of 1-2 days. The FSB thickness at a 0.5 and 1.5 day R.T. were classified as outliers.

8.6.3 Conduits and pores

The floating sulphur biofilm was analysed to gain a sense of the structure, porosity, composition and microbial community within the FSB. Numerous voids were identified within the FSB structure by SEM analysis. Vertical (y-direction facing) voids are referred to as pores and horizontal voids are conduits (de Beer et al., 1994b). The conduits allow for the movement of fluid as well as essential nutrients and substrates. The conduit diameter varied between 2 - 60 μm (Figure 8.41). The conduits are primarily formed to channel nutrients towards cell clusters, but more importantly dissolved oxygen for the purpose of sulphide oxidation and respiration. de Beer et al. (1994b) demonstrated that conduits facilitated oxygen mass transport below the cell cluster and that the oxygen distribution in and above the biofilm was strongly correlated with the biofilm structure. Conduits also allowed for the movement of planktonic bacteria in the x and z-direction within the biofilm (Figure 8.42a). Pores also allowed for increased mass transport into the FSB. Pores on the top surface of the FSB (Figure 8.42b) were identified and these allowed for the mass transport of oxygen down through the thick sulphur layer into the FSB. Pores were identified as true structural features and not artifacts of the sample preparation, by viewing the edges and inner surface of the pore (Figure 8.43). A hole or tear on the upper surface would have had sharp, broken edges. The full analysis of the dissolved oxygen concentration profiles with regard to these voids will be presented later in this chapter.

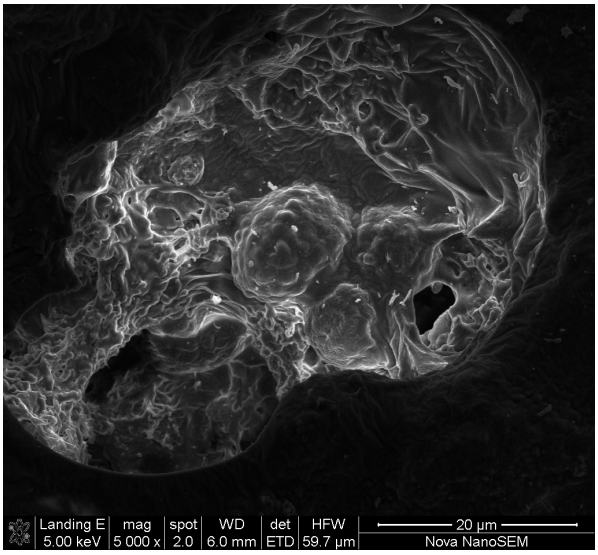
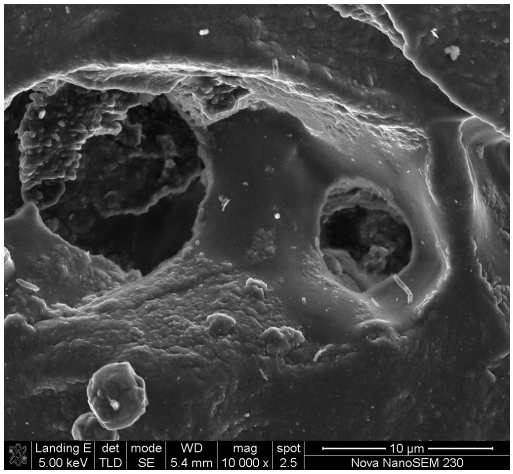
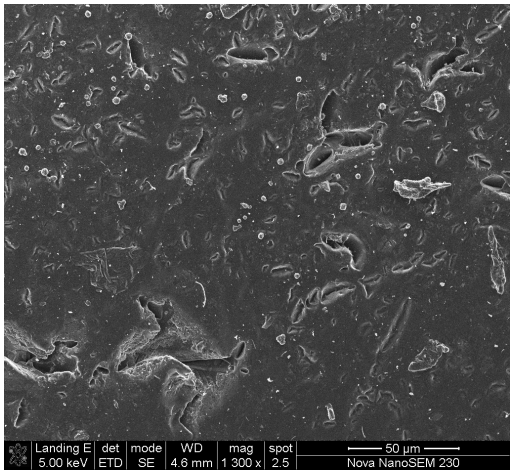


Figure 8.41: Scanning electron microscopy image depicting a conduit within the the FSB structure (cross-sectional view), with a cell cluster in the centre to possibly receive the incoming nutrients. (Experimental run 10)



(a) Conduit within the FSB matrix



(b) Open pores on the top surface of the FSB to allow for the diffusion of oxygen downwards into the FSB.

Figure 8.42: Scanning electron microscopy images of the internal and top surface of the FSB from experimental run 13



Figure 8.43: Scanning electron microscopy image of a pore, showing no sharp broken edges, hence a true structural feature of the FSB.

8.6.4 Spherical and oval-shaped pod macrostructures

An interesting feature of the FSB was the observation of spherical balls and oval-shaped pods. These structures were covered in EPS and had pores/holes on the outer surface. These holes may be used for the movement of not only necessary substrates, but by-products and the resident bacteria. The spherical balls varied in size from 8 - 56 μm in diameter (Figure 8.44). Numerous smaller structures, possibly cell clusters, were attached to the outer surface of the pod, which was covered in a layer of EPS. Similar pods were observed on the top-surface of the FSB, while smaller, spherical shaped pods occurred in the FSB matrix. However, not all bacteria were contained within the pod structures. A substantial number of bacteria were attached to the underside of the FSB and not covered by EPS (Figure 8.45a). Figure 8.45b clearly shows bacteria contained within a spherical pod and small nano-particles of sulphur distributed over the inner surface of the pod. This is further supported by the density scatter image (Figure 8.46), which distinctly shows the inorganic sulphur nano-particles trapped within the EPS matrix and oval-shaped pods.

Pod-like structures were initially observed in *Escherichia coli* urinary tract infections and were believed to protect the bacteria from antibiotics, as well as host inflammatory responses (Anderson et al., 2003). A similar occurrence of pods was observed in a study conducted by Norlund et al. (2009), whereby two species (*Acidiphilium sp.* DBS4-1 and *Acidithiobacillus ferrooxidans*) coexisted within a pod. They proposed that formation of the pod was linked to the co-ordination of their sulphur metabolisms for mutual benefit, as *Acidiphilium sp.* DBS4-1 reduced sulphur to sulphide, which was then oxidised by At. ferrooxidans back to colloidal sulphur. Therefore, the pod was necessary for creating the correct redox conditions for sulphur cycling, these pods however were planktonic and not

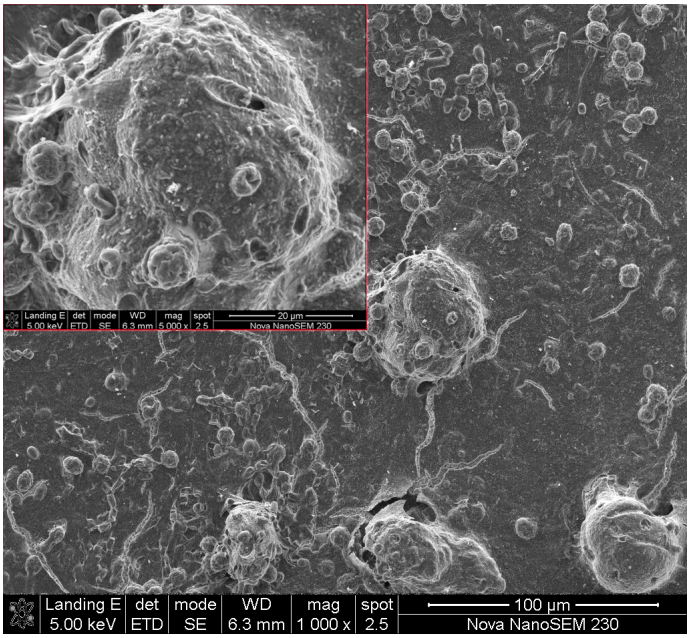
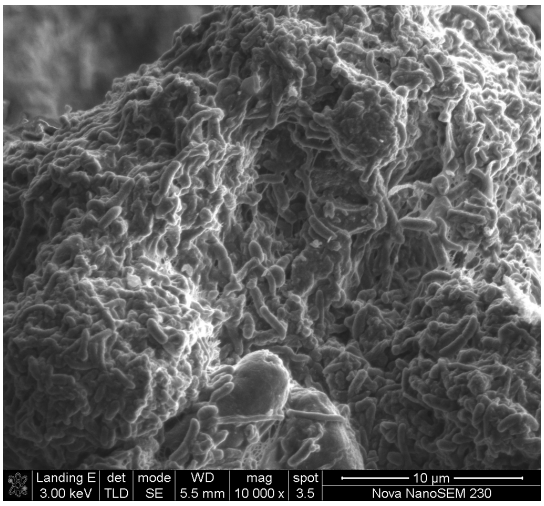


Figure 8.44: Scanning electron microscopy image of the top-side of the floating sulphur biofilm (experimental run 12). Illustrating the formation of large spherical pod structures. An enlarged image of the central pod is displayed in the red box in the top left-hand corner.

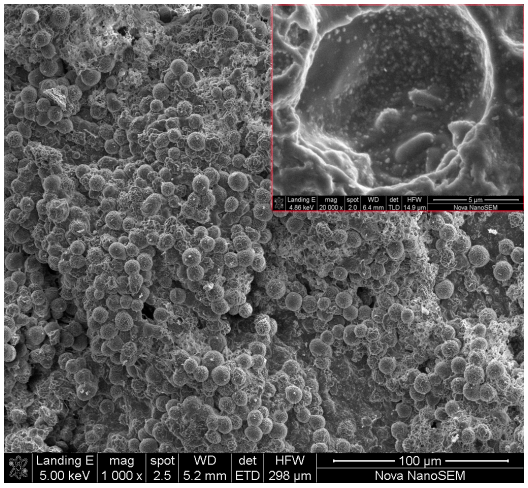
attached to a biofilm. Hence, it is proposed that the bacterial population possibly formed these large macrostructure pods or spherical clusters within the FSB, to create an ideal micro-environment for particular organisms.

8.6.5 Discussion

From the analyses conducted on the FSB samples harvested from experimental runs 8 - 16-(2), it was evident that the FSB formed in a particular manner. The following mechanistic model is proposed to describe FSB formation. At the start of the experiment, during the unsteady-state phase, a colloidal sulphur aqueous layer approximately 0.5 cm deep forms due to the rapid oxidation of the dissolved sulphide (Figure 8.47 (step 1)). This is due to the unimpeded mass flux of oxygen into the bulk liquid. Within this layer is EPS which forms the scaffolding and initial structure of the FSB and assists in the accumulation of cells. As the amount of colloidal sulphur formed increases, just below the surface, the mass flux of oxygen slowly becomes impeded further due to more EPS deposition and accumulation of cells. Consequently, a thin-skin layer of white semi-solid sulphur and EPS forms on the liquid surface (Figure 8.48a). This further promotes oxygen retardation together with the EPS layer forming the initial structure of the FSB. This thin-skin sulphur layer also establishes the optimal redox potential gradient for sulphide oxidation to solid sulphur and allows further deposition. As the concentration of EPS increases, the biofilm matrix of the FSB is formed under the thin-skin layer. Consequently, this provides the



(a) Diverse microbial population on the underside of the FSB at the entrance of the LFCR with very little EPS



(b) Scanning electron microscopy image of the FSB top surface illustrating the presence of spherical 'pods' containing sulphide-oxidising bacteria. An enlarged image of a spherical interior containing four bacteria and sulphur nano-particles is displayed in the top right-hand corner (red box). (experimental run 13)

Figure 8.45: Scanning electron microscopy images of the FSB in experimental run 11 and 13 depicting the diverse microbial population and cell clusters within the FSB

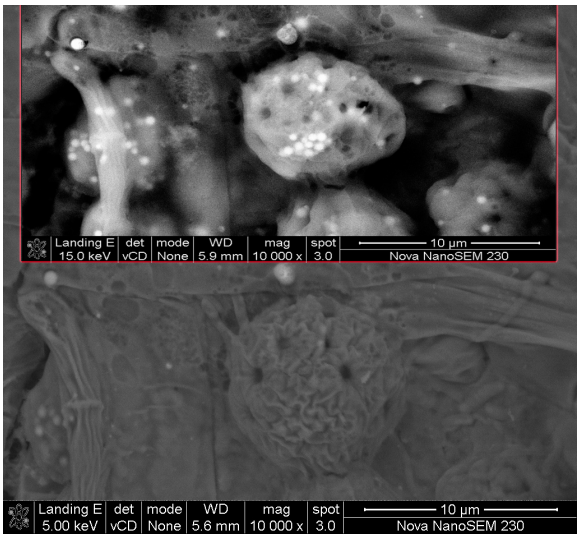


Figure 8.46: Scanning electron microscopy image of the top-side of the floating sulphur biofilm (experimental run 12). Illustrating the topography of the FSB and a spherical pod in the lower half of the image. In the upper half (red box) the density image of the same position clearly showing the presence of sulphur particles within the central spherical pod as well as other pods which are concealed by the EPS layers.

required surface area for the deposition of chemically and biologically produced sulphur on the underside of the FSB (Figure 8.48c). As the underside becomes heavily-laden with sulphur a new biological layer of EPS and cells is formed thus encapsulating the sulphur deposits (Figure 8.48d). This new layer is initially attached to the previous layer by EPS strands, thereafter additional EPS is deposited to increase the mechanical robustness of the FSB and its ability to hold a greater quantity of sulphur (Figure 8.47). This FSB development strategy is further supported by the FSB SEM cross-section images.

An appropriate analogy to describe the floating sulphur biofilm is one which was proposed by Watnick & Kolter (2000) and Flemming et al. (2007). They described a biofilm as a house containing many rooms with bacteria/cell clusters and these houses form a city. The floating sulphur biofilm can be likened to that of a high rise apartment building, which consists of many floors and each floor represents a new layer added to the FSB. Each concrete floor is separated and supported by reinforced concrete pillars, similar to that of the EPS strands and deposits providing mechanical stability. Bacteria and cell clusters live in between the layers in the different apartments. Movement along the corridors of each floor and in between the floors is possible, via the pores and conduits in the structural matrix of the FSB. Sulphur deposits and inorganic precipitates are stored in between the layers in the apartment rooms. This analogy best represents the method and manner in which the various bacteria work together in a symbiotic and cohesive manner. The FSB infrastructure is further supported by the van der Waals forces, hydrogen bonding and physiochemical interactions that improve the mechanical strength of the biofilm.

From the data presented in this section as well as the carbon material balance data, the following conclusions can be drawn. The minimum organic loading required for optimal floating sulphur biofilm development and growth was 0.1 g acetate /L. Moreover, an initial dose of acetate (1 g/L) is sufficient for initial FSB development, however after significant sulphur deposition this initial dose was insufficient. As a result the FSB was not sufficiently structurally robust to withstand the weight of the sulphur deposits, therefore it collapsed. Hence, continuous organic supplementation is required for the development of a robust, well-defined and structurally strong FSB, capable of withstanding the weight of the accumulated sulphur deposits. As residence time decreased there was an observed decrease in the carbon content of the FSB. This was due to the fact that the 'contact time' between the FSB and acetate substrate decreased, so the quantity of acetate assimilated by the microbial population in the FSB decreased. On the other hand, the sulphur content of the FSB increased with a decrease in residence time due to the improved structural integrity of the FSB, hence a greater quantity of sulphur was accumulated. On that account, the LFCR performance did increase as the residence time decreased (up until a 1 day R.T.), due to an increased sulphur yield.

The floating sulphur biofilm structure did change with residence time, as the thickness increased with a decrease in residence time (up until a 1 day R.T.). Moreover the structure improved as there was better cohesion between the organic and sulphur layers. The porosity

of the FSB decreased with decreasing residence times due to the increased deposition of sulphur. There was delamination of the FSB at the shortest residence time of 12 hours, due to the lack of sufficient acetate being assimilated in the FSB within the short period of contact time, hence the FSB failed. The difference between the amount of acetate that was consumed and the carbon content of the FSBs, was extremely high. Thus a significant proportion of the acetate supplemented, was utilised for cell metabolism and proliferation. Therefore, a more rigorous analysis of the carbon species is required. Numerous features such as pores, conduits and pod-shaped macrostructures were identified within the FSB matrix. The pod-shaped macrostructures were possibly created to provide an ideal microenvironment for certain organisms. Pores and conduits most likely improved the transport of necessary substrates and nutrients, this will be explored further in Section 8.7.

For these reasons, the optimal residence time is one to two days, as there is sufficient contact time between the FSB and the acetate substrate to form a robust FSB. Consequently, it will also be able to hold the maximum amount of sulphur deposits within this particular residence time range.

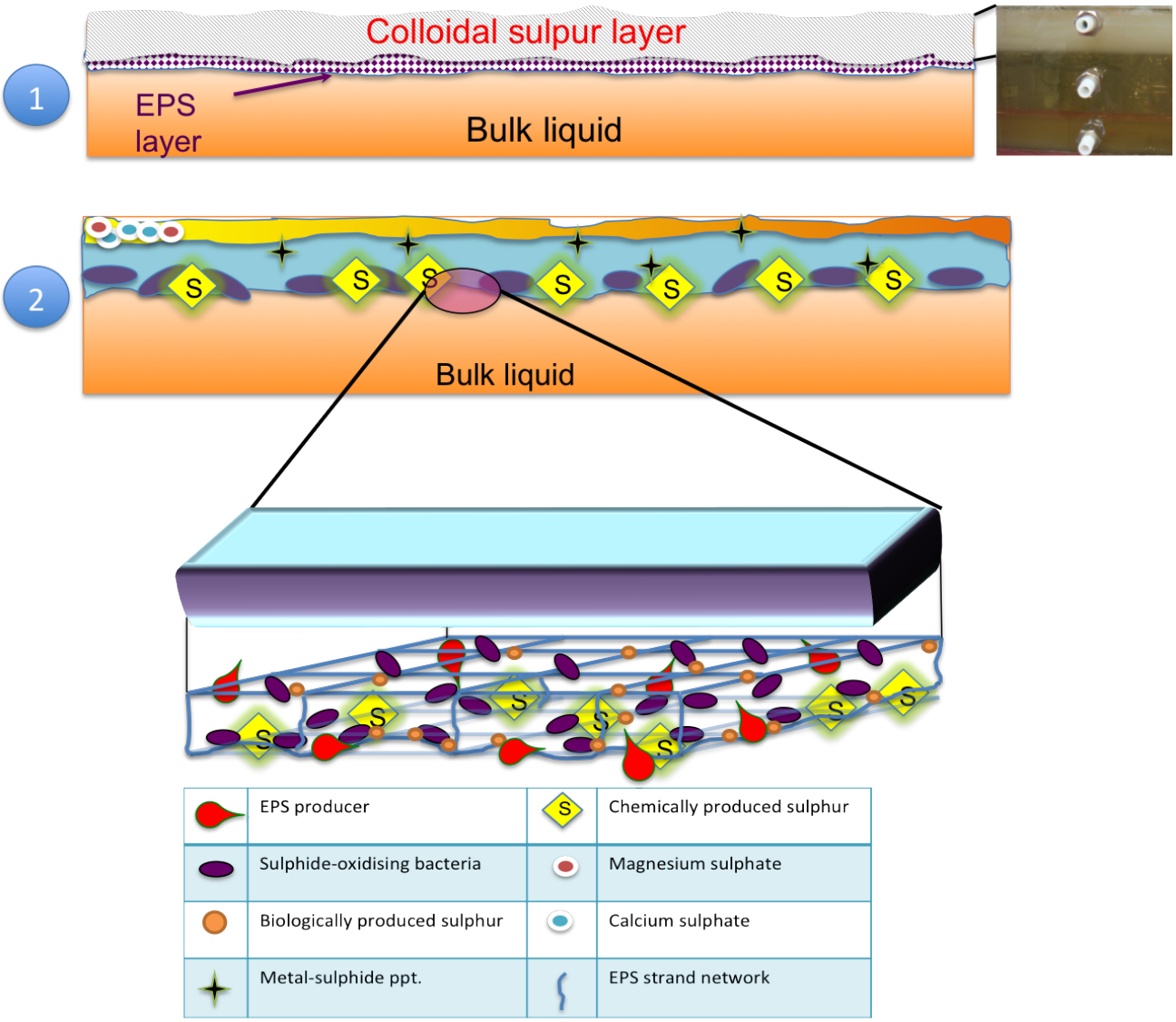
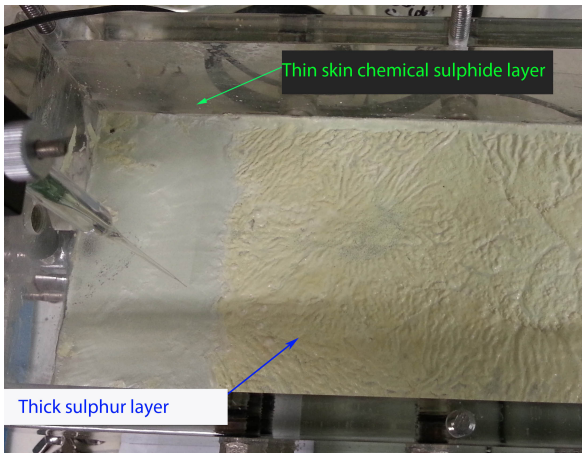
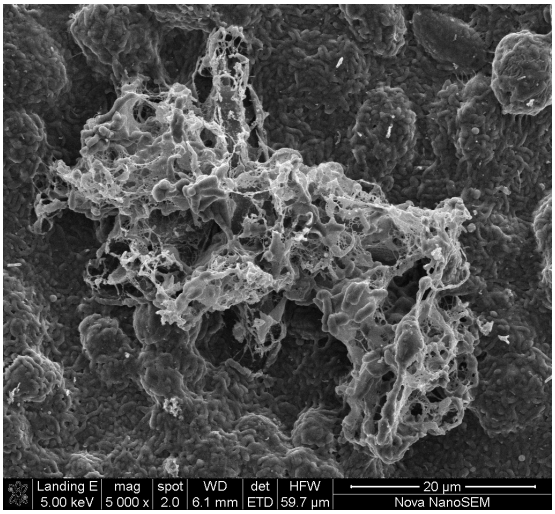


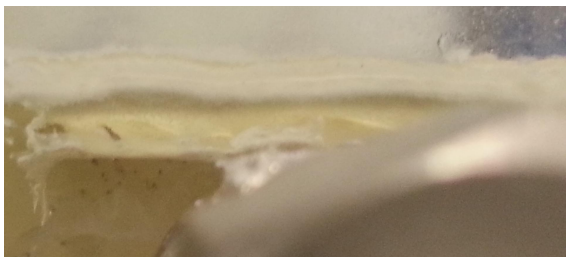
Figure 8.47: Day one of FSB growth (0 - 12 hours) is depicted in step 1. Illustration depicting the colloidal sulphur layer that forms in the bulk liquid at the air-liquid interface. Just below this layer is an EPS layer which forms the framework of the biofilm. On the right-side is a photograph of the colloidal sulphur layer. Day two to three of FSB growth (step 2). A thick (yellow/orange) sulphur layer develops on the top surface of the FSB, due to deposition of sulphur. In addition to the sulphur there are other inorganic precipitates such as magnesium and calcium sulphate close to the entrance of the LFCR. These are formed by evaporative crystallisation. The newly formed biofilm (blue) layer contains the sulphur-oxidising consortia, sulphur deposits and metal sulphide precipitates. The underside of the FSB which sits in the bulk liquid (faded orange) layer, is enlarged below. The light blue/purple layer is the structural matrix of the FSB. Attached below it is a newly formed EPS strand network containing sulphide-oxidising bacteria, EPS producers and sulphur deposits produced both chemically and biologically. This will form the new scaffolding for the subsequent biofilm layer.



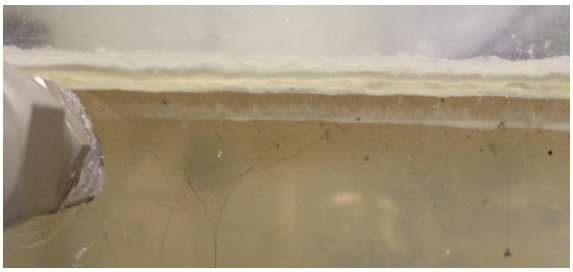
(a) Photograph depicting an one day old thin-skin chemical sulphur film on the left, and a thicker, older (5 day old) heavily laden FSB on the right



(b) Scanning electron microscopy image of the underside of the FSB, clearly illustrating the formation of new EPS strand networks and attachment of bacteria and sulphur deposits. This will form the infrastructure and skeleton of the new biofilm layer.



(c) Photograph of a four day old FSB (side-view). Clearly illustrating the biofilm-sulphur layer which has formed under the thin-skin chemical sulphur layer.



(d) Photograph of a five day old FSB (side view). Illustrating the first layer of the FSB that is heavily laden with sulphur and a new EPS biofilm, which has formed underneath to allow for further deposition of solid sulphur. There are also EPS strands present to increase the mechanical strength of the FSB and to allow for further attachment of the microbial population.

Figure 8.48: Photographs and SEM images illustrating the different stages of FSB development from day 1 - 5 for a one day residence time study.

8.7 Results - Dissolved oxygen profiling - LFCR experimental runs

8.7.1 Introduction

The dissolved oxygen (D.O.) profile through the FSB was measured as a function of depth, position and time. This was performed to determine the mass flux of oxygen through the FSB. These analyses were conducted during experimental runs 8 - 16-(2), however only selected data will be presented to highlight the relevant phenomena. Additionally, the SEM analyses (Section 8.6) were conducted in order to characterise the biofilm structure, porosity and composition. The results of the dissolved oxygen profiling study will be divided into three major sections, FSB structural heterogeneity, the effect of FSB age and lastly the oxygen mass transfer coefficient in the FSB.

8.7.2 Floating sulphur biofilm structural heterogeneity

The D.O. concentration profile through the biofilm during operation at a 1 day residence time was measured at the inlet port and one (1.1) and three quarters along the length of the LFCR (Figure 8.49a). The D.O. concentration on day five at position 1.1 was at a maximum concentration of 225 μmol/L 9 μm below the surface and decreased to 150 μmol/L within the next 15 μm. The D.O. concentration in the FSB only decreased after passing a depth of 9 μm, because the layer of inorganic sulphur and calcium sulphate deposits was uneven and highly porous. Furthermore, there was a thin liquid film, as a result of the evaporation from the surface and condensation on the LFCR channel lid and FSB surface. Consequently, this particular upper layer was saturated with oxygen. However, from 10 - 15 μm there was a sharp decline in concentration to 150 μmol/L due to a film layer below the inorganic sulphur layer. It is likely this was an interstitial liquid film or resistance film approximately 5 μm thick, as the decline in the dissolved oxygen concentration was immediate. Therefore, this film offers substantial resistance to the mass transport of oxygen through the FSB. Subsequently, the concentration continued to decrease to 80 μmol/L till a depth of 35 μm. The concentration decreased to zero over the remaining 75 μm, however, there were three sharp increases in concentration by 20, 40 and 70 μmol/L respectively. These increases were probably produced by the presence of conduits within the biofilm matrix, which allowed for the lateral movement of fluid containing dissolved oxygen. The rapid decrease in D.O. concentration at 60 μm was a zone of high biological activity, possibly due to a cell cluster or pod, as the decrease occurred over 10 μm. A similar profile was observed at the inlet port, which was a thin, white, 'skin' chemical sulphur layer. The initial D.O. concentration was 190 μmol/L that subsequently increased to 240 μmol/L at 15 μm. The lower starting concentration was caused by the lack of a liquid film on top of the inorganic layer. As a result the D.O. concentration

was substantially lower, due to there being very little liquid in/on the inorganic layer, to facilitate the diffusion of oxygen from the headspace into the FSB. Similarly, a single conduit or break in the FSB matrix was identified at 70 μm. The average decrease in D.O. concentration on day five at both positions was 1.9 - 2.0 μmol/(L.μm).

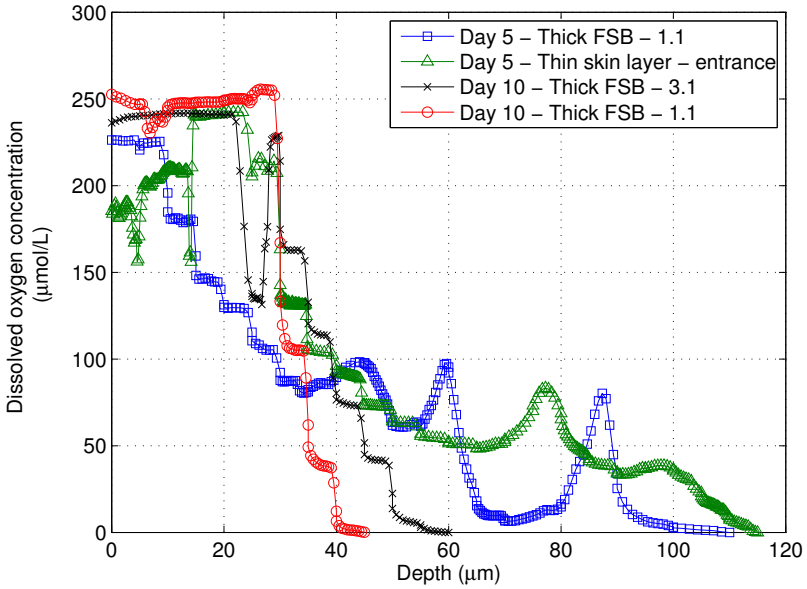
8.7.3 Effect of FSB age

The D.O. concentration was measured at different time points during experimental runs 13 and 15. The average feed sulphide concentration during experiment 13 was 5.5 and 5.2 mM on days 5 and 10 respectively. In addition, the sulphide oxidation rate was 4.3 and 5 mmol/(L.day).

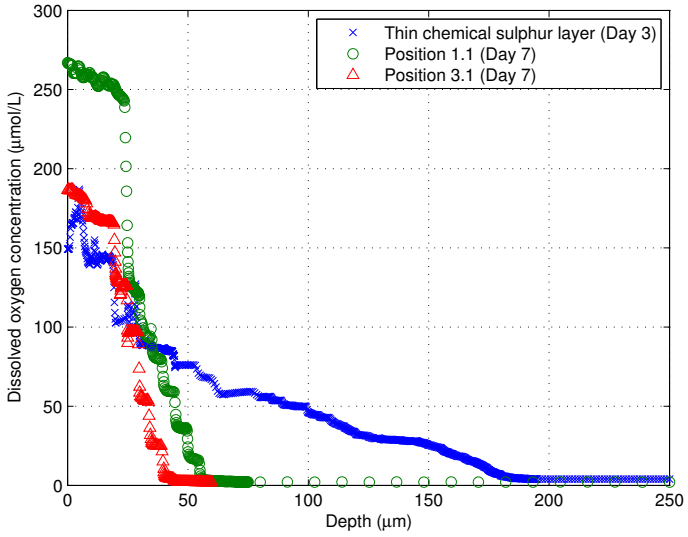
The D.O. concentration was measured on day 10 at position 1.1 and 3.1. The maximum concentration was 250 μmol/L that rapidly decreased to zero within 40 μm at an average rate of 6.5 μmol/(L.μm) (Figure 8.49a). A similar trend was observed at position 3.1, as the D.O. concentration decreased at an average rate of 5 μmol/(L.μm) over 60 μm. This stark contrast in dissolved oxygen profiles five days later, was primarily due to the increase in sulphur content and thickness of the FSB. This is supported by the data as the initial 29 and 20 μm was saturated with oxygen at positions 1.1 and 3.1 respectively. The inorganic sulphur layer had increased from approximately 9 - 15 μm on day five to 20 - 29 μm, as a result of sulphur deposition. Consequently, the interstitial film was located further down at approximately 25 - 30 μm, and was the start of the reaction zone as the D.O. concentration rapidly decreased. These factors contributed to the significant decrease in porosity of the FSB, hence the mass transfer resistance of the FSB was greatly increased. Nevertheless, oxygen was still able to diffuse downwards due to pores in the FSB structure (Figure 8.43b). The final thickness of the FSB on day 10 was 373 μm.

The D.O. concentration was measured on day three and seven of experimental run 15 to determine the effect of FSB age at a residence time of 12 hours (Figure 8.49b). On day three the FSB was a thin skin primarily composed of sulphur, for this reason there was a greater penetration of oxygen up to a depth of 180 μm. The maximum D.O. concentration at the surface was approximately 185 μmol/L, as there was no thin liquid film present (from condensation). The D.O. concentration was measured on day seven at position 1.1 and 3.1. The profile differed significantly due to the FSB being older and inevitably thicker and less porous due to increased sulphur deposits. The maximum D.O. concentration was 260 μmol/L for the initial 25 μm (at position 1.1) and thereafter rapidly decreased to zero at a depth of 56 μm. The rapid decrease was due to the interstitial film below the inorganic layer and thereafter the dissolved oxygen was consumed in the subsequent reaction zone. The amount of dissolved oxygen was rapidly depleted due to the increased resistance from the upper inorganic and interstitial film layers. A similar trend was observed at position 3.1, however the maximum D.O. concentration was 185 μmol/L.

Therefore, as time progressed and the FSB grew older and there was a change in the



(a) Dissolved oxygen profile through a floating sulphur biofilm grown at an one day residence time (Experimental run 13) and dosed with acetate at loading rate of 1.17 g/L.day.



(b) Dissolved oxygen profile through a floating sulphur biofilm grown at half day residence time (Experimental run 15) and dosed with acetate at loading rate of 1.26 g/L.day

Figure 8.49: Dissolved oxygen concentration profiles through a FSB grown at an one day and half day residence time.

porosity, thickness and quantity of sulphur deposits. The resistance of the FSB increased due to an increase in thickness and sulphur deposits, resulting in reduced porosity. A more detailed study to determine the oxygen mass transfer coefficient in the floating sulphur biofilm was conducted. This was performed in order to investigate the relationship between the observed decrease in sulphide oxidation rates (Section 8.4.1) and the oxygen transfer through the maturing biofilm.

8.7.4 The oxygen mass transfer coefficient in the FSB

8.7.4.1 Experimental

In order to determine the change in dissolved oxygen concentration with depth and time the smaller LFCR (2.5 L) apparatus was utilised. The D.O. profile was measured daily for five consecutive days, to determine the change with time. The LFCR was operated at a one day residence time with an average organic loading rate of 1.77 g/(L.day) and sulphide loading rate of approximately 11.36 mmol/day.

Following the measurement of the D.O. profile, the headspace (1.25 L) was flushed with nitrogen for 40 minutes at 400 mL/min, to deoxygenate the FSB. Thereafter the D.O. microprobe was lowered to a predetermined depth, to measure the rate of change of the D.O. concentration. The working principle of the D.O. microprobe is based on the diffusion of oxygen through a silicone membrane to an oxygen reducing cathode. The reducing cathode is polarised against a Ag/AgCl anode. Therefore, the change in the oxygen concentration that diffused through a particular distance over a certain time period was measured. Together with the D.O. profile, the local oxygen mass transfer coefficient (k_f) was determined by equation 8.4. The diffusivity of oxygen within the biofilm (D_f) was determined and thereafter (k_f). The depth (F_{depth}) was chosen such that the D.O. concentration profile decreased consistently, thus ensuring there were few or no pores or conduits to influence or bias the movement of oxygen through the FSB. The measurements were conducted in order to determine the mass transport of oxygen from the atmosphere downwards into the FSB.

$$\frac{\partial C_{O_2}}{\partial t} = D_f \frac{\partial^2 C_{O_2}}{\partial y^2} \qquad where\, D_f = k_f.F_{depth} \tag{8.4}$$

Rasmussen & Lewandowski (1998b) proposed an alternative method to measuring the local mass transfer coefficient, utilising ferricyanide and measuring the amount of ferricyanide that has diffused to the tip and been reduced to ferrocyanide. This particular method is dependent on the fact that the ferricyanide is able to diffuse freely within the biofilm structure and that there is movement of water and pore water. Hence, it is particularly useful in determining the mass transfer coefficient of water and dissolved substrates within the FSB. However, within this particular system, the fluid velocities are significantly lower,

by orders of magnitude. Furthermore, the diffusion coefficient of ferricyanide (7.35×10^{-10} m^2/s) in water is an order of magnitude different to that of oxygen in water (2.38×10^{-9} m^2/s). Therefore, the actual molecular diffusional movements of the ion will be significantly slower than that of oxygen. In addition, the movement of oxygen is primarily in the y-direction, from the atmosphere downwards, while the ferricyanide method relies upon the lateral and upward movement of the ferricyanide ions from the bulk solution below. Therefore, the D.O. microprobe method was considered more appropriate to determine the mass transfer coefficient of oxygen. Measurements were conducted in triplicate in order to obtain an accurate measurement of the mass transfer coefficient. Furthermore, Rasmussen & Lewandowski (1998a) demonstrated that the D.O. microprobe method is accurate within the concerned flow range of 0 - 4.1 mm/s, as the average deviation as percentage of average flux was 16 - 19%.

8.7.4.2 Results & discussion

The FSB was thin and incomplete at the start of the experiment (0 - 16 hours) and as time progressed, the FSB became much thicker and heavily laden with sulphur (Figure 8.48). As the FSB aged the D.O. concentration profile changed accordingly (Figure 8.50). On day one, the D.O. concentration was 'scattered' with no discernible profile (Figure 8.50a), due to the FSB being extremely thin, incomplete and the reaction zone most likely occurring within the first 60 μm. The D.O. profile became more defined and the D.O. concentration decreased much sooner due to the retardation and consumption of oxygen.

The D.O. concentration profile on day one was at a maximum of 250 μmol/L and subsequently decreased to 40 μmol/L at a depth of 200 μm (Figure 8.50a). On day two the rate at which D.O. decreased was similar and reached 0 μmol/L at a depth of 100 μm. A similar trend was observed on day three however, the initial decrease in concentration was significantly steeper. By day four the average D.O. concentration was 40 μmol/L up to a depth of 75 μm, whilst on day five the concentration reached zero much sooner at a shallow depth of 55 μm (Figure 8.50b). Therefore, as time progressed the FSB became thicker and the depth to which oxygen could penetrate became shorter. On day one oxygen had penetrated to a depth of 200 μm and by day five it had reduced four-fold to a maximum depth of 55 μm. This was due to the upper inorganic and biofilm layers which increased the resistance of the FSB, hence significantly less oxygen was able to penetrate the lower layers, and was consumed rapidly due to the high concentration of sulphide within the reaction zone and limiting oxygen.

Each dissolved oxygen concentration profile was fitted with an exponential curve ($C(y) = ae^{by}$) in order to determine the rate at which the concentration was decreasing with depth (y) (Table 8.6). The coefficients 'a' and 'b' increased as time progressed, thereby indicating an increase in the steepness of the curve. The calculated derivatives showed that the rate of change of D.O. concentration with depth increased greatly within the first

Table 8.6: Exponential functions which were fitted to the dissolved oxygen concentration data for days 1 - 5. Additionally the goodness of fit and the respective functions' derivatives is presented. The calculated diffusion and local mass transfer coefficient of oxygen in the FSB is presented as well.

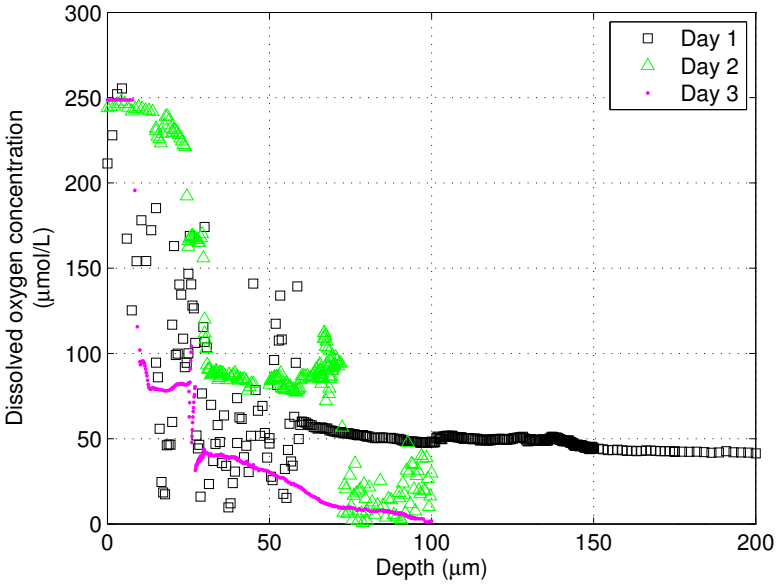
Day	Function	Max. Depth (μm)	R^2	Derivative (C'(y))	D_f (m^2/s)	k_f (m/s)
1	$C_1(y) = 109.1\ e^{-0.007y}$	200	0.320	$C_1'(y) = -0.763\ e^{-0.007y}$	4.131×10^{-8}	1.65×10^{-4}
2	$C_2(y) = 295.7\ e^{-0.0236y}$	100	0.811	$C_2'(y) = -6.973\ e^{-0.0236y}$	3.940×10^{-10}	2.345×10^{-6}
3	$C_3(y) = 240.9\ e^{-0.0541y}$	100	0.855	$C_3'(y) = -13.038\ e^{-0.0541y}$	9.340×10^{-11}	1.868×10^{-6}
4	$C_4(y) = 220.1\ e^{-0.070y}$	75	0.865	$C_4'(y) = -15.396\ e^{-0.070y}$	1.508×10^{-11}	2.154×10^{-7}
5	$C_5(y) = 350\ e^{-0.0703y}$	55	0.953	$C_5'(y) = -24.609\ e^{-0.0703y}$	1.090×10^{-11}	3.634×10^{-7}

50 μm but then became less severe up to a depth of 200 μm. Likewise, the rate of change of concentration with depth increased greatly with time.

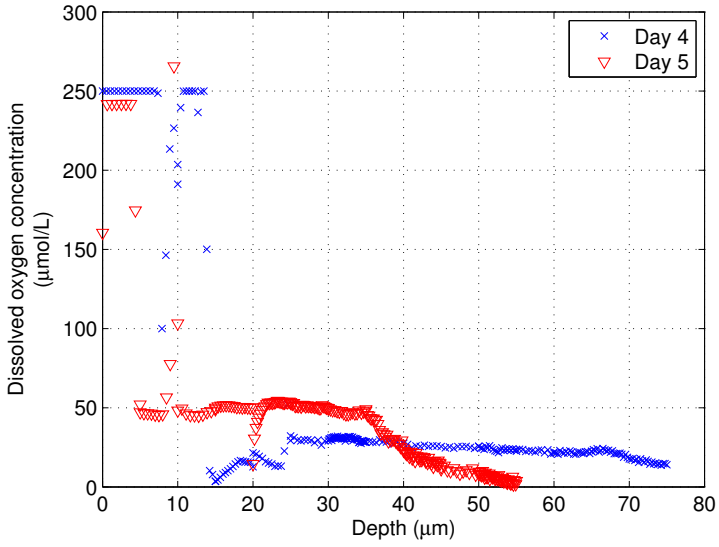
From the analyses and examination of the results together with the D.O. profiles, it was evident that the diffusion coefficient of oxygen (D_f) within the biofilm decreased with time. This decrease was by orders of magnitude, as D_f in the FSB at the start of the experiment was 4.131×10^{-8} m^2/s, and subsequently decreased to 1.09×10^{-11} m^2/s on day five. The principal cause behind the rapid change was the deposition of sulphur. As the biofilm grew older, it became thicker, more dense and heavily loaded with sulphur and inorganic particles. The top upper layer was asymmetrically crammed with sulphur and inorganic deposits, with a thin liquid film, hence saturated with oxygen due to its uneven nature. Furthermore, this layer increased in thickness as the FSB grew, which resulted in the interstitial liquid film and reaction zone moving downwards. The lower organic biofilm layers were more structured, yet still heavily laden with sulphur precipitates. This inevitably caused the resistance of the FSB to increase. The local oxygen mass transfer coefficient in the FSB was calculated, and decreased accordingly with age of the FSB. At the start of the experiment it was 1.65×10^{-4} m/s and on day five it had declined to 3.634×10^{-7} m/s (Table 8.6).

The diffusion coefficient of oxygen in the FSB, in experimental runs 11 - 15 was calculated, by firstly determining the amount of oxygen that was required for the observed sulphide oxidation rates. Thereafter the daily change in FSB thickness that contained available dissolved oxygen was assumed. This was performed by assuming the maximum thickness with available dissolved oxygen on day 1 (the measured FSB thickness by SEM), which subsequently decreased to the final depth with available D.O. (measured by D.O. probe). Moreover, a sensitivity analysis was conducted by varying the interim FSB thickness to ensure the D.O. profile trends were still valid. It was not possible to harvest a FSB sample everyday to determine the interim thickness, without compromising the experiments.

Figure 8.51 clearly shows that the (theoretically calculated) diffusion coefficient of oxygen in the FSB, decreased with time by an order of magnitude in experiments 11 - 15.



(a) Day 1, 2 and 3



(b) Day 4 and day 5

Figure 8.50: Dissolved oxygen profiles through the FSB grown at a 1 day residence time and measured on days 1-5.

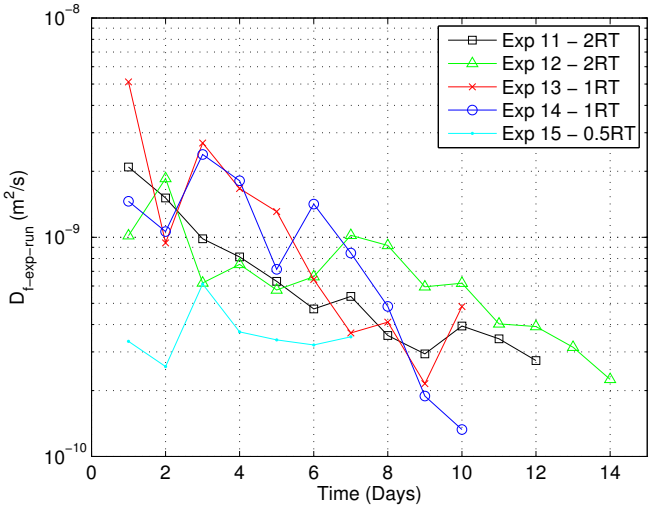


Figure 8.51: Calculated diffusional coefficient of oxygen in the FSB for experimental runs 11 - 16-(2).

Correspondingly, this trend was observed in the oxygen mass transport coefficient study, and similarly the D.O. profiles did become steeper due to less oxygen penetration into the FSB. However, the diffusion coefficients (D_f) were an order of magnitude smaller than what was calculated for experimental runs 11 - 15 ($D_{f-exp-run}$). The only plausible explanation for the discrepancy between the D.O. profiling data and the calculated diffusion coefficients, is the experimental data. It is likely the FSB in the D.O. profiling study was more heavily laden with sulphur deposits, consequently the diffusion coefficient was inaccurate. However, the difference between $D_f = 1 \times 10^{-11}$ m^2/s and $D_{f-exp-run} = 1 \times 10^{-10}$ m^2/s, may also be due to a porosity factor. The FSB has a certain amount of porosity that is determined by the manner in which the FSB is formed, in addition to arrangement of the sulphur and inorganic deposits. Moreover, the FSB is extremely heterogeneous, resulting in varying resistances to oxygen penetration in the FSB. For these reasons further study would be necessary to determine the porosity factor.

A biofilm is comprised to a large extent of water, therefore one could assume that the diffusion coefficient of oxygen in a biofilm is similar to that in water. Picioreanu et al. (2000a,b) proposed that the oxygen substrate diffusion coefficient was 2.3×10^{-9} m^2/s, when modeling mass transport phenomena within a biofilm. On the other hand Fu et al. (1994) showed that the effective diffusivity of oxygen in different biofilm layers was 25-90% lower, than the diffusivity of oxygen in water. The data illustrate that the concepts and assumptions generally applied to the modeling, and determination of mass transport coefficients of attached biofilms in previous studies, will not always be true, or applicable to this particular floating sulphur biofilm (Picioreanu et al., 2000a,b; Wanner et al., 2006; Zhang & Bishop, 1994).

8.7.5 Conclusions - Dissolved oxygen profiling

In order to understand the D.O. profile consider all the experimental runs. At a R.T. of 4, 2 and 1.5 days, the FSB had a residual D.O. concentration of 50, 40 and 17 μmol/L respectively. The FSB thickness of these experimental runs was 206, 407 and 144 μm respectively. However these D.O. concentrations were reached at a depth significantly sooner and persisted till the bottom of the FSB. At a R.T. of 1 and 0.5 days, the residual D.O. concentration was 0 μmol/L and this occurred at an average depth of 40 - 60 μm. The FSB thickness was 377 and 183 μm respectively. Therefore, the decrease in D.O. concentration to zero or almost zero, is not strongly related to R.T. as it is to porosity of the FSB. As the R.T. decreases the FSB becomes significantly more compact, layered and dense due to the deposition of sulphur and precipitates in and between the organic layers. Additionally, the structural matrix of the FSB becomes thicker, less porous and comprised of large macrostructure pods. Inevitably all these factors lead to decreased porosity and increased net resistance to the mass flux of oxygen into the FSB.

8.8 Microbial ecology

8.8.1 Introduction

The isolation of pure cultures has traditionally been the first step in identifying and characterising the microbial community in a wastewater treatment system. However, typical culturing methods only account for 1% or less of the available bacterial diversity in environmental samples, as most natural populations are not amenable to pure-culture isolation (Riesenfeld et al., 2004; Amann et al., 1992). This has been the primary reason for the relatively limited progress in the identification and characterisation of microbial biofilm communities. A structured natural biofilm ecosystem is a mix of microorganisms that function as a cooperative consortium in a complex and symbiotic manner (Davey & O'Toole, 2000). Therefore, the availability of molecular tools has significantly improved our ability to characterise the community structure in the biofilm.

A preliminary study into the microbial diversity of the floating sulphur biofilm was conducted in an effort to gain a greater understanding of the observed LFCR performance. In addition, it was hoped that this information would also provide crucial information with regard to process optimisation of the LFCR. A sample of the original LFCR inoculum (no. 10), prior to carbon amendment was analysed, to gain insight into the change of the microbial community due to acetate addition. Furthermore, FSBs developed under carbon limitations (no. 11) and acetate supplementation were also analysed (no. 1-9).

Table 8.7: Extracted DNA concentrations from various sampling points of the LFCR FSB for experimental runs 14, 15, 16-(2) and 16-(3). DPBR 2 effluent and the DPBR inoculum - Rumen fluid was analysed. The LFCR stock culture inoculum from the demonstration-scale plant and LFCR experimental run 6 FSB was analysed as well.

No.	Source - Experimental run - Position	Extracted DNA (ng/μL)
1	LFCR - 14 - Effluent liquid	34.3
2	LFCR - 15 - 0.13 m	26
3	LFCR - 15 - 2.5 m	104.6
4	LFCR - 16-(3) - 0.13 m	97
5	LFCR - 16-(3) - 1.13 m	98
6	LFCR - 16-(3) - 2.40 m	136
7	LFCR - 16-(2) - 0.13 m	18
8	DPBR 2 - Effluent liquid	61
9	Rumen fluid inoculum	345
10	LFCR stock culture inoculum	101.8
11	LFCR - 6 - 0.13m	87.61

8.8.2 Experimental

Eleven samples were taken and DNA extraction was performed as described in Chapter 5. Sufficient DNA was extracted from all samples in order to perform PCR (Table 8.7). The PCR conditions were optimised with respect to annealing temperature and it was determined that the ideal temperature was 60°C (Figure B.1). The subsequent PCR reactions were conducted at 60°C for samples one to nine (as per Chapter 5). The PCR primers amplified up a 586bp fragment and thereafter DGGE was used to separate some of the unique fragments (Figure 8.52,8.53,8.54) (Chapter 5). Each DGGE band was excised and PCR was subsequently performed to obtain a single PCR product. These were validated on an agarose gel. The bands were excised, ligated into a vector, transformed extracted and sequenced as described in Chapter 5.

The DGGE method was adopted as it has been successfully employed to gain a qualitative insight into community richness. Numerous studies of eukaryotic, archaeal and eubacterial communities in freshwater have been conducted. These studies have shown positive results in trying to assess biodiversity (Dorigo et al., 2005) (Figure 8.52, 8.53 & 8.54). A quantitative real-time polymerase chain reaction (qPCR) analysis was conducted on sample 10 and 11 from the LFCR. The method which was followed is presented Chapter 5.

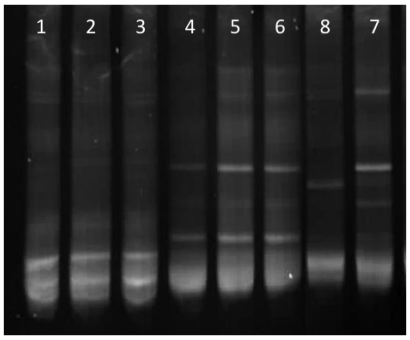


Figure 8.53: A 30 to 80% gradient denaturing gradient gel showing separation of various bands for samples 1-8. Similar bands were identified across the samples.

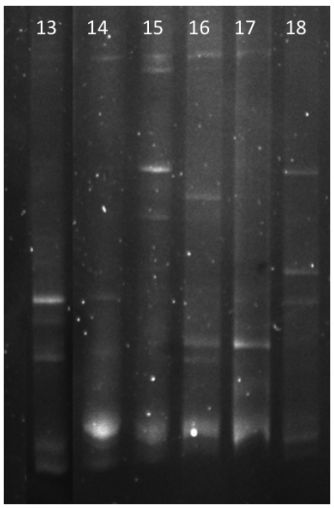


Figure 8.54: A 30 to 60% gradient denaturing gradient gel of showing separation of various bands for samples 1-6. Due to the feint nature of the bands they are not all clearly visible in the photograph.

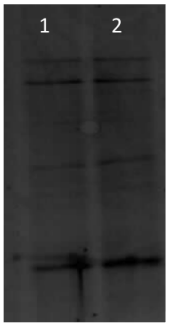


Figure 8.52: A 30 to 80% gradient denaturing gradient gel showing separation of four bands (A-D) from sample no. 9.

8.8.3 Results - Comparison of microbial populations

A number (34) of plasmid inserts from each of the different samples were sequenced and compared to sequences in the National Centre for Biotechnology Information (NCBI) database, using the Basic Local Alignment Search Tool (BLAST). The sequence matches are presented in Tables B.1, B.2 and B.3. The results were then used for the preparation of three phylogenetic trees (Figure 8.55, 8.56 and 8.57), the first representing the inocula used, the second is the LFCR system with no carbon (acetate) supplementation and the final phylogenetic tree representing the microbial community structure after acetate supplementation.

Most of the isolated bacterial sequences were > 97% similar to sequences in the NCBI database and could be identified to species level (> 97% homology), although few of these were cultured isolates. From Figure 8.55 it is clear that far fewer unique clones (9) were identified and the microbial community structure was not as diverse as the acetate supplemented system. The rumen fluid inoculum yielded four unique clones, two that were closely related to organisms of the genus *Pseudomonas* (9A,9D). The other two clones were closely related to a rumen bacterium and organism of the *Prevotella* species. The *Prevotella spp.* is a moderately saccharolytic species which, is obligately anaerobic and is able to ferment basal medium to produce acetic and succinic acids (Shah & Collins, 1990). The sequencing results of sample 10 and 11 also showed numerous similarities to photolithotrophic organisms.

Clones 10A, B and C had a >97% similarity to *Thiomonas intermedia* K12, *Chlorobium limicola* and *Chromatium okenii* respectively, with all three organisms capable of photolithotrophic growth. *Thiomonas intermedia* was found within the initial inoculum, which is capable of oxidising thiosulphate and possibly tetrathionate, as demonstrated by Wentzien & Sand (2004) with strain K12. *Chlorobium limicola* is a green sulphur bacteria that is obligately anaerobic and photolithotrophic. It is capable oxidising sulphide or sulphur, as it has been previously used in a suspended-growth CSTR for sulphide oxidation by Henshaw et al. (1998) and was able to achieve 90% sulphide conversion to elemental sulphur. *Chromatium okenii* is a purple sulphur bacterium capable of growing anaerobically in light, whilst utilising sulphide or sulphur as an electron donor (Dworkin et al., 2006d). All the above species are capable of autotrophic sulphide oxidation, therefore this would explain the poor performance exhibited in the initial biological LFCR experiments (6 & 7). Furthermore, many of these organisms are obligately anaerobic, therefore this would explain the limited biofilm development.

The remaining species that were identified with a high similarity to the bacterial clones, were *Desulfovibrio sulfodismutans* and *Cupriavidus metallidurans. Desulfovibrio sulfodismutans* is an obligately anaerobic sulphate reducing bacterium capable of heterolithotrophic growth by disproportionation of thiosulphate or sulphite to sulphate and sulphide (Bak & Pfennig, 1987). Likewise, *Cupriavidus metallidurans* is capable of

chemolithotrophic growth as it is able to fix carbon dioxide.

An analysis of the carbon limited LFCR experiment 6 was conducted (Figure 8.56), by sampling the FSB and liquid just below the biofilm. Only three unique clones were able to be identified. *Geobacter lovleyi* and *Sphaerochaeta globosa* were identified, and are able to grow autotrophically. Many of the isolates in the inocula which were identified, was with a high similarity to autotrophic organisms. Therefore, the lack of carbon supplementation and availability to sunlight in the LFCR system, would explain the particular reduction in the microbial community structure. There were numerous autophototrophic organisms in the inocula, due to them being obtained from the demonstration-scale plant in Middelburg, which is exposed to sunlight. An archaeon *Methanomethylovorans sp.* was identified with high similarity as well, and is capable of metabolising methane.

A microbial diversity study was conducted on the LFCR system after acetate supplementation and a much greater microbial diversity of heterotrophic organisms was identified. A total of 24 unique clones were identified, however not all isolates had a $> 97\%$ similarity to specific species in the NCBI database. *Geobacter lovleyi, Geobacter thiogenes* and *Desulfovibrio sp.* were identified again. Various sulphur-oxidising bacteria were identified, such as *Thiobacillus sp.* and/or *Halothiobacillus sp.* were identified with 95% similarity to isolate 15A and 15B. *Thiobacillus sp.* are colourless sulphur bacteria which are able to derive energy chemolithotrophically from reduced sulphur compounds. Therefore an electron donor (reduced sulphur compound e.g. H_2S) and electron acceptor (i.e. oxygen) is necessary for proliferation. Therefore, the FSB would be the ideal environment for such an organism. *Halothiobacillus sp.* has been identified in a hypersaline Siberian soda lake, as well as in a microbial mat within an anaerobic digester employing biological desulphurisation (Banciu et al., 2008; Kobayashi et al., 2012).

A larger number of the unique bacterial clones had a high similarity (>97%) to heterotrophic organisms that were identified, such as *Haematobacter sp.*, *Herbaspirillum huttiense subsp. putei*, *Spirochaete sp.*, *Paludibacter propionicigenes* (Ueki et al., 2006) and *Cloacibacillus sp. Herbaspirillum huttiense subsp. putei* is able to utilise acetic acid as a substrate (Dobritsa et al., 2010). The presence of a *spirochaete* species within the microbial population was also visually confirmed by SEM. Dubinina et al. (2011) identified a new novel spirocheata strain (*Spirochaeta perfilievii sp.* nov.) capable of oxidising sulphide to elemental sulphur under micro-oxic conditions. The strain was an aerotolerant anaerobe with fermentative metabolism. The photoautotrophic organism *Chlorobium limicola* was only identified in the compromised LFCR experiment 16-(3). Therefore, the microbial community structure was greatly altered by the supplementation of acetate to the LFCR, as no photoautotrophic organisms were detected in the LFCR under optimal conditions. Furthermore, there was a more diverse microbial community structure, with a large number of heterotrophic and chemolithotrophic organisms.

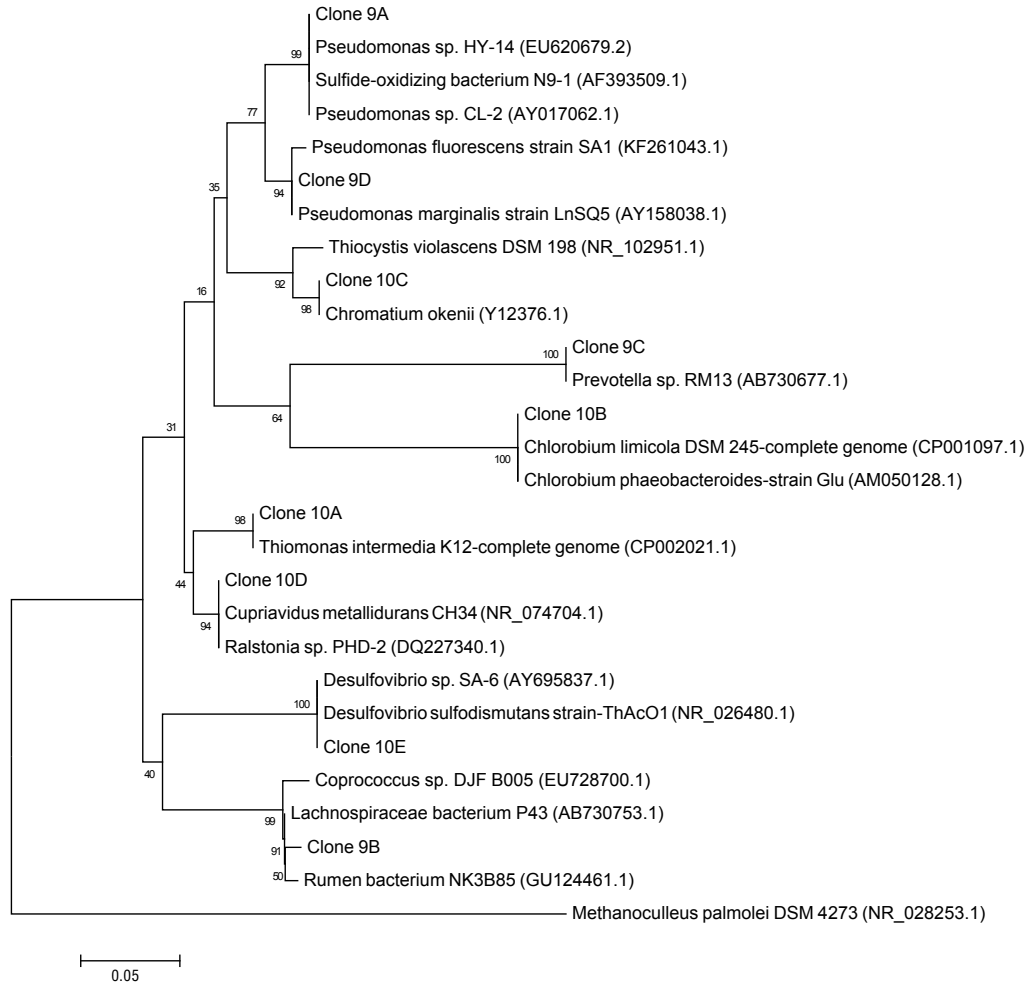


Figure 8.55: Overall Phylogenetic tree relating the rumen fluid and LFCR inoculum sample (9,10) sequences to known species from the National Centre for Biotechnology Information database.

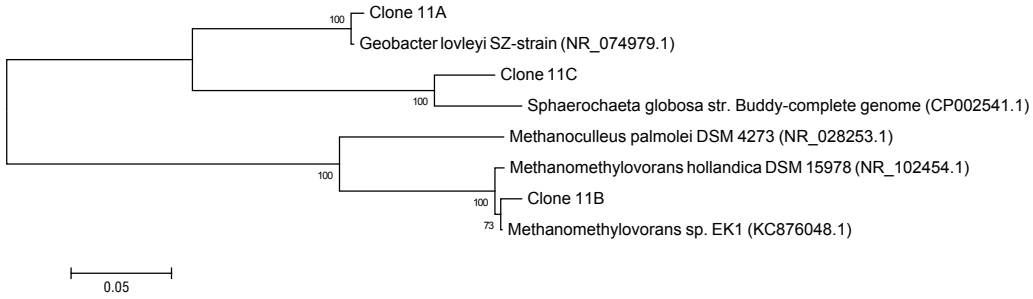


Figure 8.56: Phylogenetic tree of sample 11 from a non-acetate supplemented LFCR experiment (6). The sequences were compared to known species from the National Centre for Biotechnology Information database. This tree represents an overall picture of the populations present prior to LFCR acetate supplementation and post inoculation.

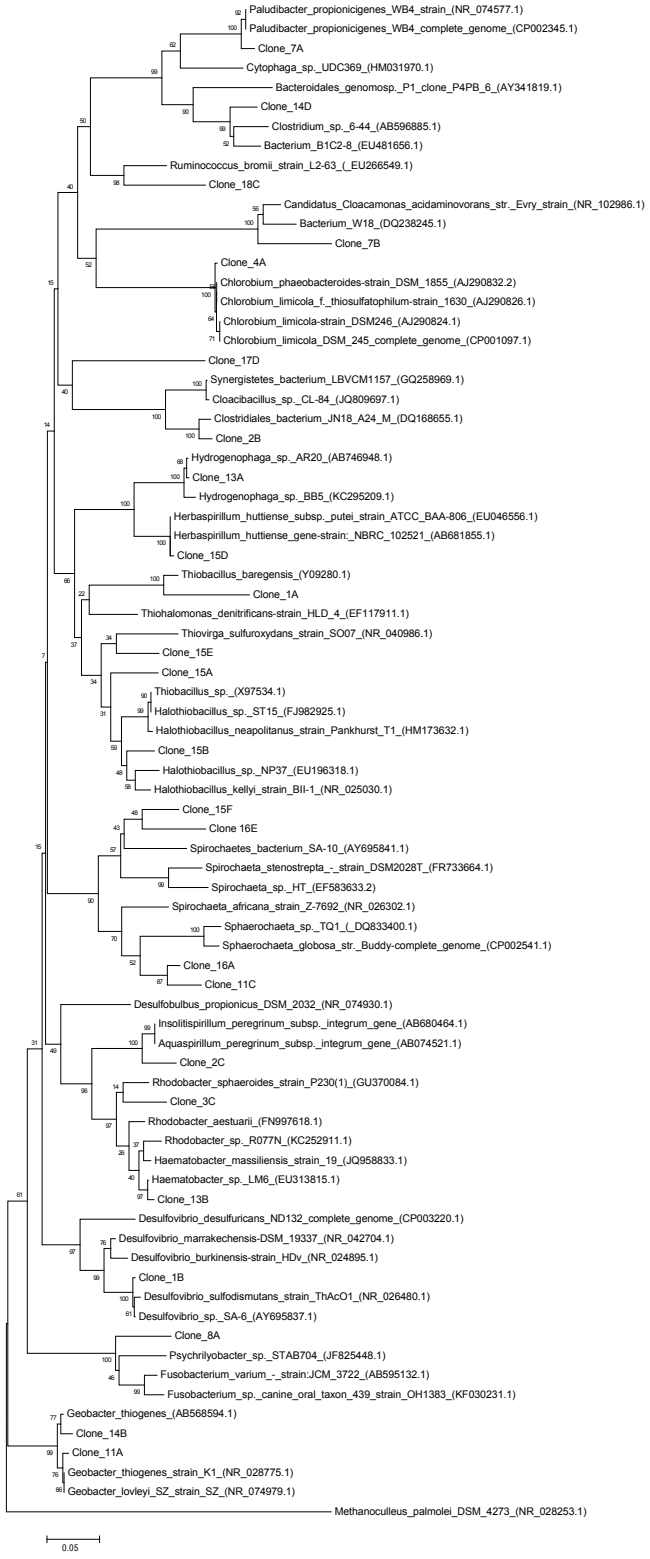


Figure 8.57: Overall Phylogenetic tree relating the floating sulphur biofilm sample (1-7, 11) sequences to known species from the National Centre for Biotechnology Information database. This tree includes isolates for the study and represents an overall picture of the populations present during LFCR acetate supplementation. Sample 8 was DPBR 2 effluent liquid. The inoculation samples were not included (9, 10).

8.9 Final discussion & conclusions

Due to the length of this chapter and numerous topics and issues which were discussed, the discussion and conclusions related to each objective/key question and hypothesis, will be presented in the same order as laid out at the start of the chapter.

There was no loss of sulphide in the form of $H_2S_{(g)}$ to the atmosphere, as all the scrubbing solutions were tested and had negligible or no sulphide. Moreover, from the error analysis of each experimental run with regard to the sulphur material balance (Table 8.2), it was clear that the material balances were closed to within a 10% error. Experimental run 16 was an exception due to the harvesting issue and loss of FSB sulphur. Furthermore, the error (0 - 10%) in some of the material balances, was also high due to the fact that thiosulphate was not measured in all cases and was most likely a product of chemical sulphide oxidation.

The abiotic sulphide oxidation study showed that it is not ideal to have a well-mixed, homogeneous bulk liquid layer. A higher sulphide concentration at the surface, as compared to the bulk liquid, will ultimately result in the formation of colloidal sulphur and sulphate. Therefore, the slow gradual displacement of sulphide upwards to the FSB reaction zone is favoured, as the correct sulphide to oxygen ratio is maintained. As a result the production and deposition of sulphur in the FSB is favoured. The slow gradual displacement of the incoming sulphide is heavily dependent on the relative density difference being positive and the ratio of sulphide to sulphate being maintained at approximately 1:4. Therefore, the performance of the LFCR is strongly governed by the composition of the feed and that it be maintained consistently, without great fluctuations in the sulphide or sulphate concentrations, as demonstrated in experiment 10.

There was an improvement in LFCR performance with a corresponding decrease in R.T.. The amount of sulphur recovered in the FSB increased with a decrease in R.T., reaching a maximum at a one day R.T.. However, when the R.T. was decreased further to 12 hours, less sulphur was recovered due to delamination of the FSB and structural degradation, with the sulphur deposits lost to the bulk liquid in the reactor. The linear relationship between R.T. and sulphur recovered is best illustrated in Figure 8.14. The optimal R.T. was identified as 1 - 2 days. The harvesting strategy of skimming the FSB of the surface was not favourable.

The floating sulphur biofilm increased in thickness with a decrease in R.T.. The thickest FSB was measured at a 1 day R.T. and the thinnest was at a 6.5 day R.T. However, the sudden drop off in thickness at a half day R.T. was due to the inability of the microbial community to lay down a sufficiently strong organic 'backbone' to support the amount of sulphur being deposited, resulting in the FSB structural integrity failing. The lack of sufficient acetate assimilation and EPS formation was supported by the extremely low carbon content (2.1%) of the FSB. The lower layers tore away due to a lack of EPS

deposition to strengthen and join the lower layers of the FSB together. For these reasons it is believed that FSB thickness and composition is not only a function of R.T., but also the relative rates of EPS production and sulphur deposition.

There was a change in structure and porosity of the FSB with R.T. and biofilm age. These changes influenced the dissolved oxygen profiles and diffusion coefficient in the FSB. The FSB became more highly structured as the R.T. decreased. At a four day R.T. there were significant open spaces within the FSB structure and the irregular undersurface of the biofilm indicated a lack of well structured organisation (Figure 8.37a). The lack of structure was a contributing factor to the FSB collapse, as it was not capable of withstanding the weight of the sulphur deposits. The LFCR was not continuously supplemented with acetate and this may have contributed to the poor structural integrity of the FSB.

As R.T. was decreased the manner in which the FSB formed became more structured. The FSB formed by a method of 'layering' that was evident in the SEM cross-sectional images. An initial EPS layer formed with colloidal sulphur (0-12 hours) formed on the surface, followed by an inorganic layer just below and then an organic layer and thereafter another sulphur deposit layer. This mechanism of alternating organic biofilm and sulphur deposits continued further down into the FSB. This particular occurrence was observed at the two, one and half day residence times. The presence of divalent ions (Ca^{2+}) could have increased the mechanical strength of the EPS matrix, by cross-linking polyanionic alginate molecules. Additionally, hydrogen bonding and van der Waals forces between the layers of biopolymers may have increased the strength of the FSB. At almost 'stagnant' conditions, (6.5 day R.T., 1 g acetate /L.day) the layering effect was observed, however the layers were not well attached to each other. Therefore, FSB structure is strongly related to the R.T., as well as the availability of sufficient organic carbon. Poor FSB development was observed in the initial LFCR experimental runs (7 & 8) due to a lack of sufficient organic carbon to develop a robust biofilm. The minimum organic loading in the current study was determined to be 0.1 g/L of acetate, provided continuously.

Pores and conduits were observed within the biofilm matrix, suggesting that there was transport and lateral movement of substrates, nutrients and fluids within the FSB. Large pod-like macrostructures containing microbial organisms were identified within the biofilm. It is believed these macrostructures were created to provide the ideal micro-environment for certain microorganisms.

The dissolved oxygen profiles were also found to be a function of structure, porosity and biofilm age. Pores assisted in the movement of oxygen downwards (y-direction) from the atmosphere into the bulk of the FSB. On the other hand conduits allowed for the lateral movement of dissolved oxygen in the x and z-directions. These two structural features were found to be essential in improving the diffusional mass transport of oxygen within the FSB. However, there was a highly resistive interstitial film in between the top inorganic layer and the biofilm layer below. This layer varied in thickness (5-10 μm) and severely hampered the oxygen mass transport, by lowering the maximum D.O. concentration from

150 μmol/L. The D.O. concentration did decrease with age of the FSB, as less oxygen was able to penetrate a more heavily laden sulphur biofilm. Consequently, as the FSB aged and sulphur deposits increased, there was a corresponding decrease in porosity, thus increasing the resistance to oxygen penetration.

The D.O. profile was not necessarily affected by the thickness of the FSB, but more so the matter contained within the FSB, the sulphur deposits. On day one the maximum flux of oxygen was possible and the FSB was constructed just below the inorganic colloidal sulphur layer. Thereafter, layer upon layer was built below the initial organic biofilm layer. As a result less oxygen was able to penetrate further into the FSB, due to all the sulphur and organic matter occupying the FSB. Hence, the porosity of the FSB severely diminished. This was illustrated in the D.O. profiling study where a one day R.T. floating sulphur biofilm with an average thickness of 379 μm had dissolved oxygen up to a depth of 115 μm (day 5), however this severely decreased to 40 μm on day 10. The half day residence time FSB had a thickness of 183 μm, yet the D.O. concentration had decreased to zero at a depth of approximately 45 μm (day 7). For this reason, it is proposed that the dissolved oxygen concentration profile is affected more by porosity and structure of the FSB rather than thickness of the FSB.

The structural integrity of the biofilm improved with a decrease in R.T., provided sufficient acetate was available. However, the organic content of the biofilm did not increase with increased organic supplementation, but remained comprised primarily of sulphur ($> 88\%$). The increase in soluble organic carbon provided the necessary carbon substrate for the structural improvement of the FSB, hence a greater proportion of sulphur was sequestered. However, only a small amount of the acetate utilised was deposited in the biofilm as biomass or EPS. This suggests that carbon assimilation was independent of loading. The amount of carbon utilised in experimental runs 12 and 14 was 95% and 98% greater than carbon composition of the FSB. Therefore the majority of the acetate was most likely used for cell metabolism and oxidised fully to CO_2.

The microbial community structure analysis revealed that the LFCR system was severely carbon limited by the lack of soluble organic carbon. Only nine species were identified in the inocula and three in the initial FSB sample. Following acetate supplementation there was a substantial increase in diversity, as an additional 23 species were identified. Moreover, there were more heterotrophic organisms as opposed to the photoautotrophs, which dominated the carbon-limited system. Numerous organisms were identified as sulphur-oxidisers. The increase in microbial diversity following acetate supplementation could also explain the observed improvement in the FSB structure and integrity. Only 35 unique clones were identified and this is most likely not the complete microbial population due to limitations of DGGE.

Finally, and most importantly, the rate of sulphide oxidation was mass transfer controlled. The oxidation rate declined substantially after four residence times due to the poor diffusion of oxygen through the FSB. This was primarily due to a significant decrease in

the diffusion coefficient of oxygen through the FSB, due to a rapid decline in porosity as a result of sulphur deposition. Thus the mass transport of oxygen is controlled to a greater extent by the structure and porosity of the FSB rather than its thickness. The theoretically calculated diffusion coefficient of oxygen ($D_{f-exp-run} = 1 \times 10^{-10}$ m^2/s) for experimental runs 11-15 did not correlate with the measured diffusion coefficient of oxygen in the FSB ($D_f = 1 \times 10^{-11}$ m^2/s). There was approximately one order of magnitude difference between the figures, which may have been caused by the porosity of the FSB. Therefore further investigation and analysis is required to adequately correlate the measured sulphide oxidation rate, to the mass flux of oxygen into the FSB and accurately determine the diffusion coefficient of oxygen in the FSB.

Chapter 9

Packed bed column studies

9.1 Background - Research motivation

The degrading packed bed reactor (DPBR) is essentially a packed bed reactor that is packed with a large amount of lignocellulosic materials as the organic carbon substrate. There is limited literature covering the fundamental chemical, biochemical and microbiological reactions that occur within the anaerobic reactor. In addition the break-down and hydrolysis of complex organic substrates for biological sulphate reduction over the long-term (> 6 months) has not been studied extensively. Moreover, each investigation has been unique with respect to the substrates utilised and the ARD waters treated. Therefore, investigating the hydrolysis and release of soluble organic carbon, in the form of VFAs, over the long-term is essential to adequately assess the stability of semi-passive processes. The preceding chapters have highlighted the importance of a consistent feed to the sulphide oxidation unit, both in terms of sulphide and organic carbon.

9.2 Introduction - Biological sulphate reduction

For many years sulphate reducing bioreactors (SRBRs) have been treated as black boxes, with limited fundamental understanding of the complex chemical and biological processes which occur within the reactor. This began to change in the late 20th century (Sheoran et al. (2010)). Hence, a better understanding of the effect of pH, redox, metal concentration, sulphate concentration, hydraulic residence time, organic substrate loading and most importantly microbial community structure and activity, have been investigated. Sulphate reducing prokaryotes inhabit a variety of environments, such as wetland sediments, cattle rumens and geothermal vents. Sulphate reducing prokaryotes are either heterotrophic or autotrophic and reduce a sulphate ion to sulphide if there is a suitable electron donor available. The organic substrate (electron donor) is oxidised and the sulphate ion (electron acceptor) is reduced (equation 9.1) . The resulting energy released is used by the microbe for metabolic activity, growth and development (Sheoran et al., 2010). The sulphide can react with dissolved metals to form metal sulphides or remain in solution. Active sulphate reduction bioreactors (SRBRs) will be discussed, followed by passive SRBRs and the crucial parameters which have substantial implications for the performance of the reactor.

$$2CH_2O + SO_4^{2-} \rightarrow H_2S + 2HCO_3^- \quad (9.1)$$

9.2.1 Sulphate reduction bioreactor configurations

A variety of reactor configurations have been studied for active systems, such as CSTRs, upflow anaerobic sludge bed reactors (UASBs) and upflow or down flow packed bed reactors (Table 9.1). The most common passive reactor configuration is an upflow or down flow packed bed reactor (UF/DF-PBR). A CSTR has advantages for biological sulphate reduction, as it is well mixed with the potential for temperature control. The major difference between passive treatment systems and active treatment systems is that passive systems have no mixing or temperature control. However, due to the cells being freely suspended and growing relatively slowly, it is essential that a long residence time be used to prevent cell washout. Boshoff et al. (2004) and Moosa et al. (2002) showed that a sulphate removal of 60-80% and 80-90% respectively could be achieved, but at a residence time of 4 and 2.5 days respectively (Table 9.1). A shorter residence time and higher conversion was achieved by Moosa et al. (2002) due to the reactor being heated and run on a monomer substrate (acetate). Consequently, the biological sulphate reduction (BSR) process was not limited by the hydrolysis of the organic substrate. Therefore, in order to have a continuous reactor system with a low residence time, an immobilised cell bioreactor such as a UASB is required.

An upflow anaerobic sludge bed reactor facilitates biomass retention in sludge granules, allowing the biomass residence time to be decoupled from the hydraulic residence time, permitting high flow rates without cell washout (Sheoran et al., 2010). The SRPs form a biofilm on the the sludge or carrier matrix particles thus immobilising themselves and also providing themselves with protection from harmful conditions or toxic agents. The primary difference between these systems (Table 9.1) with regard to performance is the organic substrate utilised and the COD:SO_4^{2-} ratio. Poinapen et al. (2009) was able to achieve a higher sulphate conversion where primary sewage sludge was utilised which is significantly more hydrolysable than tannery effluent. A significant proportion of the substrate was composed of VFAs and easily biodegradable organic matter which have provided the necessary supply of SCOD for the removal of sulphate, therefore the BSR process is limited by the hydrolysis step of complex substrates.

The recent studies on passive treatment systems have mainly used a packed bed reactor configuration. Accordingly, the performance in passive systems is orders of magnitude lower with the maximum sulphate reduction rate being 0.31 g/L.day (Table 9.1). The performance of passive treatment systems is heavily reliant on the following parameters, organic substrate and sulphate loading rates, pH/redox potential, metal concentration, temperature and residence time. These parameters will be discussed in this chapter prior to presentation of the upflow packed bed reactor studies.

Table 9.1: Comparison of active and passive sulphate reduction bioreactor systems.

	Reactor type	T (°C)	Carbon Source	SO_4^{2-} Feed concentration (g/L.day)	SO_4^{2-} Reduction rate (g/L.day)	Conversion (%)	COD : SO_4^{2-}	Reference
	CSTR	35	Acetate	1	0.768	80-90	n.d.	Moosa et al. (2002)
A	CSTR	-	Tannery effluent	1.8	0.25	60-80	0.1	Boshoff et al. (2004)
C	UASB	-	Tannery effluent	1.8	0.6	80	0.56	Boshoff et al. (2004)
T	UASB	30	Acetate, Propionate & Butyrate	1.195	0.805	68	0.5	Omil et al. (1996)
I	UASB	20	Primary sewage sludge	1.5	1.74	93	1.75	Poinapen et al. (2009)
V	UASB	35	Primary sewage sludge	1.8	2.42	92	1.45	Poinapen et al. (2009)
E	UASB	35	Molasses	2.2	1.86	80	15	Annachhatre & Suktrakoolvait (2001)
	UF-PBR	25	Lactate	3.77	0.46	82	1.88	Jong & Parry (2003)
P	PBR	25	Whey, cow manure	0.896	0.003	27	n.d.	Christensen et al. (1996)
A	UF-PBR	25	Spent mushroom compost, wastepaper sludge, spent oak chips	0.129	0.102	78.7	n.d.	Chang et al. (2000)
S	UF-PBR	25	Wood chips, sawdust	0.243	0.12	31.6	n.d.	Waybrant et al. (2002)
S	DF-PBR	25	Wood chips, manure, primary sewage sludge	1.09	0.013	1.8	n.d.	Molwantwa et al. (2010)
I	Batch	-	Wood chips, leaf compost, poultry manure	3.39 g	0.06	> 95	n.d.	(Zagury et al., 2006)
V	DF-PBR	-	Wood chips, manure, primary sewage sludge & molasses	1.73	0.31	23.5	0.75 (SCOD)	(Coetser et al., 2005)
E								

9.3 Effect of pH, redox potential and temperature on BSR process

The correct environmental conditions, such as pH, redox potential and temperature are necessary for the biological sulphate reduction process to occur effectively. The majority of sulphate reducing strains that have been identified are inhibited at low pH. Fortin et al. (1996) isolated a strain from an abandoned mine at acidic and slightly oxidising conditions, however no growth has been recorded below pH 5.5. It was concluded that SRP make the oxidising conditions favourable by reducing sulphate to sulphide which inevitably generates an alkaline environment. Elliot et al. (1998) showed that SRPs are capable of biological sulphate reduction under acidic conditions (pH 3.25) as a sulphate removal of 38.3% was achieved, although at pH 3 the sulphate removal fell to 14.4%. On the other hand, Johnson & Hallberg (2003) and Dopson & Johnson (2012) have conducted various studies into the microbial diversity of acidophilic microorganisms, as well as SRPs in extremely acidic conditions. They described an acidophilic SRP consortia capable of sulphide generation under low pH conditions in a bio-sulphidogenic reactor. These studies represent the exception and for the majority of SRP to thrive, they require a pH in the range of 5 - 8. Outside this range the rate of microbial sulphate reduction and metal removal decreases rapidly (Sheoran et al., 2010).

A negative redox potential is as important as optimum pH in ensuring the optimal conditions for BSR to occur. An anoxic environment, with a redox potential lower than -100 mV is essential for treating sulphate rich waters (Sheoran et al., 2010; Cocos et al., 2002). Once sulphate reduction is initiated, the sulphide products helps to drive the redox potential down further, with efficiently operating systems typically showing a redox potential below -350 mV.

Temperature plays a critical role with regard to biological sulphate reduction, as SRPs can be classified as mesophiles ($< 40°C$), thermophiles (40-60°C) and extreme thermophiles ($> 60°C$) based on optimum growth temperatures. Sulphate reducing prokaryotes have been identified in environments experiencing temperatures from -5 to 75°C.Typically, the rate of sulphate reduction increases with temperature to a maximum, then decreases rapidly once the optimum is exceeded. Moosa et al. (2002) reported an increase in sulphate reduction rate with an increase in temperature from 20 to 35°C while a further increase to 40°C resulted in inactivity in the mixed SRP culture. At low temperature ($< 10°C$) the BSR rate decreases by 50% from an optimum temperature of 20°C. However, some passive bioreactors have been operated successfully between 2°C and 16°C over a period of 32 months (Sheoran et al., 2010). In general the performance of a passive sulphate reducing bioreactor is reduced at low temperatures. However the sub-optimum temperature also affects the rate of hydrolysis of the organic substrates. Therefore, the BSR process could be further hampered by lack of available SCOD due to the hydrolysis reactions being extremely slow.

9.4 Direct organic substrates

Direct organic substrates are compounds that do not require degradation/break-down by other microorganisms and can be utilised immediately by SRP. These substrates are generally alcohols (ethanol and methanol), organic acids (acetate, lactate, formate) or sugars (glucose and sucrose) (Sheoran et al., 2010). Lactate is theoretically the superior electron donor with respect to its thermodynamic, kinetic properties and amount of biomass and energy produced, as compared to acetate, ethanol or methanol. The complete oxidation of one mole of lactate results in the production of three moles of bicarbonate alkalinity (equations 9.2, 9.3) compared to other simple molecules, such as ethanol (equation 9.4), which yields two moles of bicarbonate, with concomitant reduction of 3 moles of sulphate (Tsukamoto & Miller, 1999; Sheoran et al., 2010; Nagpal et al., 2000; Liamleam & Annachhatre, 2007).

$$\overset{lactate}{CH_3CH(OH)COOH} + \frac{1}{2}H_2SO_4 \rightarrow CH_3COOH + CO_2 + \frac{1}{2}H_2S + H_2O \ \Delta\text{G=-34.2 kJ/mol} \tag{9.2}$$

$$CH_3COO^-(acetic\,acid) + SO_4^{2-} \rightarrow 2HCO_3^- + HS^- \Delta G = -47.6kJ/mol \tag{9.3}$$

$$2C_2H_5OH\,(ethanol) + SO_4^{2-} \rightarrow 2CH_3COO^- + HS^- + H^+ + 2H_2O \tag{9.4}$$

The major disadvantages of utilising lactate or ethanol are firstly, SRPs can only partially oxidise the C_2-C_4 molecules to acetate and very few SRPs are capable of utilising acetate alone (Sheoran et al., 2010). Another major disadvantage with lactate are fermentation reactions (Oyekola, 2008). The most significant disadvantage of direct organic substrates is the cost of the electron donor, and BSR treatment processes have been largely confined to niche applications as a consequence (Hulshoff et al., 1998).

Tsukamoto & Miller (1999) found that methanol was a more efficient electron donor than lactate in the bioreactor column setup. However, methanol is considerably more expensive than lactate. The choice of organic substrates is of critical importance in a sulphate reduction bioreactor. Hence, many passive SRBRs are designed to utilise indirect, waste organic substrates that are cheap, easily accessible and can be broken down into VFAs. In order for passive treatment to be a viable long-term sustainable solution for ARD treatment, the organic substrate has to be a readily available waste material.

9.5 Indirect organic substrates

Sulphate reducing prokaryotes are unable to obtain the necessary nutrients from indirect (complex) organic substrates, hence prior decomposition by other microorganisms is required. There is a wide variety of substrates that can be utilised, such as composts (spent mushroom/leaf compost), agricultural byproducts (cow, horse, poultry, sheep manure or molasses), cellulosic wastes (grass cuttings, wood chips, straw, hay, sawdust or leaf mulch) and sewage waste (sewage sludge or digested sludge). In order to sustain a SRP population there has to be a sustained release of organic acids from the degrading complex substrates, hence a proper selection and characterisation of substrates is critical.

9.5.1 Characterisation of organic wastes

A number of studies(Christensen et al., 1996; Gibert et al., 2004; Cocos et al., 2002; Sheoran et al., 2010) concluded that these substrates (listed above) individually do not promote significant activity of SRP. As a result, a more reactive mixture containing more than one organic carbon source is preferred. Cocos et al. (2002) found that the most reactive mixture in terms of sulphate reduction was wood chips (3%), leaf compost (30%), poultry manure (20%), support material (10%) and bacterial source (37%); achieving a sulphate reduction rate of approximately 71 mg/L.day. On the other hand Waybrant et al. (1998) achieved a sulphate reduction of 160 mg/L.day with a reactive mixture of sewage sludge (20%), leaf mulch (10%), wood chips (25%), sheep manure (20%) and sawdust (25%). However, Waybrant et al. (2002) showed that a column packed with cellulosic wastes achieved a higher (19.2 mg/L.day) sulphate reduction rate than one packed with cellulosic and organic waste materials (sewage sludge). This may have been due to several factors, such as a greater liberation of dissolved organic carbon (DOC) and nutrients (N, P). Chang et al. (2000) showed better sulphate reduction in reactors packed with spent mushroom compost, spent oak from shiitake farms and wastepaper sludge, than those packed with oak chips or organic rich soil. Their results showed that raw oak contained chemicals that inhibited sulphate reduction. These were hydrophobic in nature and degraded over time. Furthermore, it was determined that biologically or chemically treated/degraded organic substrates are better electron donors for sulphidogenesis than unaltered substrates such as oak chips or organic rich soil.

Gibert et al. (2004) characterised the composition of lignocellulosic and organic wastes and found that sheep manure had a greater biodegradable fraction (by 20%) than oak leaves. Moreover, sheep manure had a lower lignin and cellulose content by 7% and 33% respectively. While lignocellulosic wastes (oak leaves) have a greater carbon content and volatile solids fraction, the carbon to nitrogen ratio is lower than organic waste (sheep and poultry manure), which is preferable for long-term BSR. Similarly, compost has a higher lignin and and cellulose content with an extremely low biodegradable faction. As

a result, biological sulphate reduction was only observed after the addition of a soluble carbon source such as sodium acetate.

Therefore, waste organic substrates such as sewage sludge, manure or digested sludge are ideal for biological sulphate reduction due to the large amount of labile and easily biodegradable carbon. Moreover, these substrates have a higher nitrogen and phosphorus content than lignocellulosic wastes, which is preferable for long term operation of SRBR. However, only a fraction of organic wastes is bioavailable for the process of biological sulphate reduction, consequently they are depleted fairly rapidly. Therefore lignocellulosic wastes need to be utilised for long term operation (> 1 year) in a passive SRBR, as they generally have a higher carbon content and the potential to release DOC over a longer period (Waybrant et al., 2002; Cocos et al., 2002; Gibert et al., 2004). However, the primary disadvantage of lignocellulosic wastes is the high lignin, cellulose and hemicellulose content. These are not easily hydrolysable and needs to undergo pretreatment via biological or chemical methods.

Some studies have shown promise of supporting sulphidogenesis on cellulosic wastes in conjunction with supplementation of easily assimiable electron donors (Christensen et al., 1996; Nagpal et al., 2000; Dvorak et al., 1992; Coetser et al., 2005; Molwantwa et al., 2010). Hence, hydrolysis of lignocellulosic material is the rate limiting step with regard to biological sulphate reduction. Therefore, if the rate of hydrolysis is improved it would greatly improve the performance of a passive SRBR. Nevertheless, all lignocellulosic wastes are not all the same, so the data and observations are specific to to the substrates utilised and sulphate loading fed to the reactor.

9.5.2 Indirect substrate - Hydrolysis

9.5.2.1 Organic wastes - Sewage sludge / manure

Anaerobic digestion is comprised of four sequential bio-chemical processes, that is hydrolysis followed by acidogenesis, acetogenesis and methanogenesis. Many studies have concluded that the hydrolysis step is the least well defined and generally also the rate limiting step (Vavilin et al., 2008; Appels et al., 2008). The hydrolysis step breaks down insoluble organic material and high molecular weight compounds, such as carbohydrates, polysaccharides, lipids and proteins into soluble monosaccharides and long chain fatty acids. Thereafter these components are further metabolised into VFAs, by the process of acidogenesis, performed by acidogenic (fermentative) bacteria. This is generally considered the quickest step in the AD process (Vavilin et al., 2008). The third stage, acetogenesis, is where the VFAs and alcohols are digested further by acetogens to produce acetic acid, CO_2 and H_2. The final stage, methanogenesis results in methane production. This is accomplished by two groups of methanogens. The first group utilises CO_2 as the electron acceptor and H_2 as the electron donor. The second group acetoclastic methanogens, split acetate into methane and carbon dioxide.

Therefore, in order to promote biological sulphate reduction using indirect substrates the time required to hydrolyse these materials needs to be shortened. First-order kinetics can only be applied when the rate-limiting factor (in hydrolysis) is the surface area of the particulate substrate and biodegradability phenomena don't interfere. Vavilin et al. (2008) found kinetic coefficients of the first-order rate hydrolysis to vary greatly amongst various substrates. For crop residues it was 0.094 day^{-1}, whilst for forest soil, pig manure and cattle manure were 0.54, 0.1 and 0.13 day^{-1} respectively. The highest was primary sludge at 0.99 day^{-1}. While these values are highly dependent on the experimental conditions, inoculum utilised and enzyme concentrations they clearly show the stark contrast between lignocellulosic wastes and organic waste materials with primary sludge being the most ideal. Furthermore, cattle manure and pig manure contain a large proportion of lignocellulosic material, as opposed to primary sludge which has a greater carbohydrate, lipid and protein content.

The hydrolysis of primary sewage sludge and activated sewage sludge has been investigated by several researchers. Andreasen et al. (1997) observed that 9 - 16% of the total COD (TCOD) could be released as soluble COD (SCOD) during primary sludge fermentation, but this dropped to 2.5% for activated sludge. Similarly, Ucisik & Henze (2008) found that the hydrolysis of primary sewage sludge yielded approximately 16% SCOD, but only between 1.93 - 5.6% for activated sludge, in a semi-continuous reactor over a period of five days. Furthermore, there was a 4.4 fold increase in the production of VFAs from primary sewage sludge relative to activated sludge, with a higher proportion of acetate being formed from primary sewage sludge hydrolysis (50%), whilst a greater proportion of propionate (35%), butyrate (10%) and larger chain VFAs (25%) was formed from activated sludge hydrolysis. Ucisik & Henze (2008) proposed that the higher production of VFAs from primary sewage sludge was due to the higher proportion of organic constituents, in the form of proteins and carbohydrates. Additionally, the higher organic matter content gave rise to a higher bacterial activity and consequently a higher concentration of hydrolytic enzymes. Conversely most of the TCOD in activated sludge is in the form of polymers or large organic compounds. However, the primary reason for low SCOD liberation is the inaccessibility of the organic material due to the accumulation of cellular residues and inert materials within the activated sludge matrix. These are generally regarded as non-biodegradable. Anaerobic digestion of sewage sludge is also affected by pH, with the optimal pH range being 7 - 11 in order to promote hydrolysis of proteins, carbohydrates and lipids to form VFAs. The alkaline pH results in the dissociation of acidic groups in EPS and repulsions between the negatively charged EPS. Extracellular polymeric substances are largely composed of proteins and carbohydrates and thus the solubility of proteins and carbohydrates is increased due to the repulsive forces (Chen et al., 2007b).

Therefore, a study comparing a passive SRBR packed with more organic waste versus one with lignocellulosic wastes, is required in order to adequately evaluate the performance a SRBR over the long term. Furthermore, primary sewage sludge will be compared to

activated sewage sludge to determine the biodegradability and liberation of VFAs.

9.5.2.2 Lignocellulosic wastes - Wood chips / grass / leaves

There has been recent interest into converting cellulosic biomass to alternative organic compounds, such as ethanol for transportation fuel or VFAs for bioreactor processes, as they are relatively cheap and abundant. The overriding impediment to a more widespread utilisation of this natural sustainable resource is the inability to overcome the recalcitrance of cellulosic materials (Lynd et al., 2002; Weimer et al., 2009). Considerable effort has been directed toward understanding the rumen ecosystem of ruminant animals, which is arguably the most elegant system able to effectively hydrolyse and ferment cellulosic matter to produce predominantly VFAs. This is performed by the complex rumen community that has been shown to consist of bacteria, fungi and protozoa (Lee et al., 2000). However, bacteria are believed to play the major role because of their numerical predominance and metabolic diversity, with fermentative bacteria being responsible for hydrolysis and acidogenesis. These bacteria produce the necessary enzymes to hydrolyse organic compounds such as cellulose, hemicellulose and others into smaller molecular carbon chain compounds (Roman, 2004).

Lignocellulosic materials are composed of lignin, cellulose and hemicellulose that forms a three dimensional structure that renders cellulose and hemicellulose less accessible to microbial attack due to the physical barrier imparted by the lignin. Lignin is an aromatic polymer that provides cell walls with rigidity in addition to making the plant resistant to enzyme, microbial or mechanical stresses.

To achieve the complete degradation of these polysaccharides a suite of (bacterial) hydrolytic enzymes, which have been shown to target different linkages in the molecules are required (Roman, 2004). There is a distinct difference between aerobic and anaerobic microorganisms in their strategy to hydrolyse cellulose (Table 9.2). Aerobic celluloytic bacteria (e.g. *Cellulomonas, Cytophaga* and most fungi) can generally utilise a variety of carbohydrates, proteins, lipids and cellulose. On the other hand anaerobic cellulolytic species (e.g. *Clostridium, Ruminococcus* and *Fibrobacter)* are more limited and are only able to grow on cellulose and its hydrolytic products. Aerobic organisms produce a large amount of individual enzymes that have a strong synergy in the hydrolysis of cellulose. Conversely, anaerobes don't release a large amount of extracellular cellulase, but instead have a localised multi-enzyme cellulase complex on the surface of the cell or the cell-glycocalyx matrix (Lynd et al., 2002). Therefore, cell attachment and adhesion to the substrate is necessary. Due to the crystalline nature of cellulose, attachment is only possible at an irregularity in the structure, where amorphous cellulose is present. This allows the adhesion and penetration of cellulolytic enzymes. There are three major types of enzymatic activities which occur synergistically and simultaneously. Endoglucanases, which hydrolyse β-1,4-bonds randomly within the cellulose molecule, producing reducing and non-reducing

Table 9.2: Morphological features of cellulolytic bacteria (Lynd et al., 2002; Roman, 2004)

Genus	Growth (T)	Morphology	Features of cellulases
Acetovibrio	Meso	Curved rod	Complexed
Anearocellum	Thermo	Rod	Noncomplexed/cell free
Butyrivibrio	Meso	Curved rod	Noncomplexed
Caldicellulosiruptor	Thermo	Rod	Noncomplexed/cell free
Clostridium	Meso/thermo	Rod	Complexed
Eubacterium	Meso	Rod	
Fibrobacter	Meso	Rod	Complexed
Halocella	Meso	Rod	Noncomplexed
Ruminococcus	Meso	Coccus	Complexed
Spirochaeta	Thermo	Spiral	Noncomplexed
Thermotoga	Thero	Rod	

ends; exoglucanases, which cleave cellobiose from the non-reducing ends of the polymer and β-glucosidases, which hydrolyse cellobiose producing glucose monomers (Roman, 2004). Anaerobic cellulotyic bacteria follow a similar process except that a cellulosome allows close proximity to the bacterial cell wall and cellulose substrate to be constantly maintained during the enzymatic process.

Anaerobic (cellulolytic) microorganisms possessing this cellulosome are generally found within a complex community of interacting (fermentative) anaerobic microorganisms. In an anaerobic, sulphidogenic environment with inorganic electron acceptors (Fe^{3+}, SO_4^{2-}), cellulose is degraded to ultimately form CO_2, H_2O and CH_4. However, within a sulphidogenic environment methanogenesis can be inhibited by a high sulphide concentration and SRPs would be able to dominate the methanogens. Furthermore, it has been shown that the degradation of lignocellulosic materials under sulphidogenic conditions is twice as fast than under methanogenic conditions (Pareek et al., 1998). Therefore, it would seem that from a fundamental perspective the degradation of lignocellulosic materials within a passive sulphate reducing bioreactor would be possible, with VFAs being generated for the BSR reaction. While this would occur at a significantly lower rate than for organic waste substrates, VFA production would last considerably longer.

9.6 Sulphate reducing prokaryotes

Until the early 1980s, it was believed that sulphate reducers were only able to utilise organic compounds such as hydrogen, ethanol, formate, lactate, pyruvate, malate and succinate for growth. These particular organisms were able to incompletely oxidise these compounds to acetate. However, Widdel (1980) isolated and characterised a large number of sulphate reducers that were able to grow on short-chain fatty acids (acetate), long-chain fatty acids

and aromatic compounds such as phenol. As a result currently there are two main groups of sulphate reducing organisms, those that degrade organic compounds incompletely to acetate and those that completely metabolise them to carbon dioxide. Sulphate reducers use sulphate as the terminal electron acceptor and an organic compound (or H_2) as the electron donor. However, SRPs are also able to reduce other compounds such as SO_3^{2-}, $S_2O_3^{2-}$, Fe (III), Cr (VI), Se (VI) and As (VI). Based on comparative 16S rRNA sequences most sulphate reducers belong to 23 genera within the deltaproteobacterium class, followed by gram-positive SRP within Clostridia (Muyzer & Stams, 2008). The most well characterised sulphate reducers along with their morphological and physiological characteristics are summarised in Table 9.3. It is evident that the average optimum temperature is 30°C and almost every organism is able to utilise sulphate, sulphite and thiosulphate as an electron acceptor. *Desulfovibrio* and *Desulfobulbus* are unable to utilise acetate however, are able to use lactate for BSR. *Desulfovibrio sulfodismutans* is also able to grow by disproportionation of a sulphur species. It's able to utilise thiosulphate, sulphite, and elemental sulphur (reaction 9.5, 9.6) (Dworkin et al., 2006a).

$$4S + 4H_2O \rightarrow SO_4^{2-} + 3HS^- + 5H^+ \, \Delta G = 10.2 kJ/mol\, sulphur \tag{9.5}$$

$$S_2O_3^{2-} + H_2O \rightarrow SO_4^{2-} + HS^- + H^+ \, \Delta G = -21.9 kJ/mol\, thiosulphate \tag{9.6}$$

Desulfobacterium, Desulfococcus, Desulfosarcina and Desulfotomaculum are able to use almost all organic compounds especially large chain fatty acids greater than three carbons. The incomplete oxidation of even C-fatty acids yields only acetate. The odd C-fatty acids yield acetate and propionate ((9.8)), this is explained by β-oxidation. In the case of odd C-fatty acids, propionyl-CoA and acetyl-CoA is produced, however propionyl CoA cannot be metabolised by an incomplete SRP oxidisier and therefore is excreted. If 2-methylbutyrate is used by an incomplete oxidiser, propionate is formed as well. Most complete oxidisers can degrade the propionyl residue; therefore also C-odd fatty acids. Therefore SRPs are able to utilise a variety of organic compounds in addition to phenyl substituted organic acids and phenolics (Dworkin et al., 2006a).

Lignin is an aromatic polymer with the substituents being connected by both ether and carbon-carbon linkages. It's essentially composed of three building blocks: p-coumaryl alcohol, coniferyl alcohol and sinapyl alcohol. Recent years have witnessed an increasing interest in the enzymatic biodegradation of lignin, hemicellulose and cellulose. The most common enzymes associated with the degradation of these compounds are lignin perioxidase, endo-xylanase and cellobiohydrolase respectively (van Dyk & Pletschke, 2012). These enzymes are generally found in white-rot fungi such as *Phaenerochaete chrysosporium* or *Coriolus versicolor,* or in ruminant bacteria (Wan & Li, 2012). However, the biodegradation of lignin compounds also results in the production of phenolic compounds such as catechol, phenol, gallic acid and ferulic acid, which are toxic to ruminal

Table 9.3: Morphological and physiological properties of the genera of sulphate reducing bacteria (Adapted from(Dworkin et al., 2006a))

Genus	Morphology	Optimum Temp (°C)	e^- Acceptor*	Acetate	Propionate	Lactate	C_x (x > 3)	Phenyl organic acid
Desulfovibrio	Vibrio	30 - 38	SO_3^{2-}, $S_2O_3^{2-}$	-	-	+	-	-
Desulfobulbus	Oval / rod	28 - 39	SO_3^{2-}, $S_2O_3^{2-}$	-	+	+	-	-
Desulfobacter	Oval / vibrio	28 - 32	SO_3^{2-}, $S_2O_3^{2-}$	+	-	-	-	-
Desulfobacterium	Oval	20 - 35	$S_2O_3^{2-}$	+	+	+	+	+
Desulfococcus	Sphere	28 - 36	SO_3^{2-}, $S_2O_3^{2-}$	+	+	+	+	+
Desulfosarcina	Oval	33	SO_3^{2-}, $S_2O_3^{2-}$	+	+	+	+	+
Desulfotomaculum	Straight, curved rod	30 - 38	$S_2O_3^{2-}$	+	+	+	+	+
Desulfospira	Curved rod	26 - 30	SO_3^{2-}, $S_2O_3^{2-}$, S^0	-	-	+	+	+
Desulfobacula	Rod	28	n.d.	+	-	-	+	+ Toluene, p-cresol, benzoate
mXyS1	Rod	30	n.d.					m-Xylene, Toluene
oXyS1	Rod	32	n.d.					o-Xylene, Toluene
Cat2	Rod	28	n.d.					Phenol, catechol, m-cresol, p-cresol

*Species other than sulphate that can be utilised as an electron acceptor. (+) Positive, (-) Negative, (n.d.) not determined.

bacteria (Jeffries, 1994; Roman, 2004). Various sulphate reducing prokaryotes are able to utilise phenolic compounds as an electron donor for BSR. Harms et al. (1999) identified two strains m-XyS1 and o-XyS1,which showed highest similarity to *Desulfococcus multivorans* (86.9%) and *Desulfosarcina variabilis* (98.7%) respectively. Strain m-XyS1 was able to utilise m-xylene, toluene, m-methylbenzoate, benzoate and m-ethyltoluene. Strain o-XyS1 was able to degrade o-xylene, toluene, o-methylbenzoate, benzoate and o-ethyltoluene. These studies were conducted up to a loading concentration of approximately 100 mg/L of each aromatic compound and showed positive biological sulphide generation. Likewise, Schnell et al. (1989) showed that strain Cat2 was capable of degrading phenol, catechol, m-cresol, p-cresol and many others. However, these studies did not determine the maximum inhibitory concentration for SRPs and the process of biological sulphate reduction. This information is crucial to the performance of a SRBR which is composed primarily of lignocellulosic materials as organic substrates. If sufficient quantities of phenolic and aromatic compounds are produced via hydrolysis then it could inhibit the BSR process.

$$CH_3(CH_2)_{2n}COO^- + \frac{n}{2}SO_4^{2-} \rightarrow (n+1)CH_3COO^- + \frac{n}{2}H_2S \tag{9.7}$$

$$CH_3(CH_2)_{2n+1}COO^- + \frac{n}{2}SO_4^{2-} \rightarrow nCH_3COO^- + CH_3CH_2COO^- + \frac{n}{2}H_2S \tag{9.8}$$

9.7 Objectives

Therefore the primary purpose of the DPBR column study was to answer the following hypothesis and objective:

- A packed bed reactor column, packed primarily with lignocellulosic materials, is less suitable than a mixture primarily of organic waste materials, over a long-term (> 6 months), with regard to sustained release of dissolved organic carbon (volatile fatty acids), for an efficient biological sulphate reduction process.

1. Which packing strategy offers efficient biological sulphate reduction conditions consistently, as well as the correct effluent composition for optimal LFCR performance.

9.8 Initial BSR column studies

9.8.1 Introduction

A pilot plant study was conducted on passive sulphate reducing bioreactor technology at the Vryheid Coronation Colliery (Molwantwa et al., 2010; Coetser et al., 2005). This

investigation was performed in an effort to determine the optimal reactive mixture for sustained VFA and soluble COD release for the BSR process. The pilot plant was designed, constructed and operated by Pulles, Howard and de Lange (environmental consultants). Various small sulphate reducing units (SSRUs) were constructed and operated, though for the purposes of this discussion, the performance of SSRU2, DPBR and SSRU4 will be addressed. The DPBR was originally SSRU3, however the SSRU3 failed, therefore it was repacked and renamed the DPBR. For the purposes of this discussion to prevent confusion it will be referred to the DPBR-SSRU3. The units were packed with 18 m^3 of organic carbon made up of organic and lignocellulosic wastes. The SSRU2 unit contained more of lignocellulosic waste (83%) relative to SSRU4, which contained a greater proportion of organic waste (55.6%), in the form of sewage sludge, chicken litter and manure. The DPBR-SSRU3 had less organic matter (33.3%) and more lignocellulosic wastes in the form of hay, sawdust and wood chips. Additionally, all reactors were dosed with molasses at concentration of 1.411 g/L (Coetser et al., 2005). The molasses addition resulted in a feed soluble COD to sulphate ratio of 0.74. The reactors SSRU2, DPBR-SSRU3 and SSRU4 were fed at a volumetric flow rate of 1.72, 2.11 and 1.6 m^3/day respectively and an average sulphate concentration of 1.4 g/L. The sulphate removal efficiency of each reactor was recorded, with SSRU2 being tracked before molasses dosing commenced and after the dosing strategy was employed. The performance of DPBR-SSRU3 and SSRU4 was only evaluated in the dosing period. The SSRU2 reactor achieved a sulphate removal efficiency of 11.1% before dosing, which increased significantly to 33.2% after the dosing strategy was implemented. This clearly showed that the reactor was carbon substrate limited. The DPBR-SSRU3 reactor achieved a higher removal efficiency of 35.7 %, and the SSRU4 unit achieved a sulphate removal efficiency of 27% as it had a greater proportion of organic wastes. However, the extent of molasses dosing makes these data very difficult to interpret. The observed sulphate reduction can be fully accounted for by the COD added as molasses. Therefore the aim of the PBR column studies was to gain a greater fundamental understanding on the hydrolysis of the organic substrates and the rate of VFA liberation.

9.8.2 Experimental

The Degrading Packed Bed Reactor (DPBR) columns were initially shipped from Golder Associates Research Laboratories (GARL). The columns were packed in a similar manner to that of the 250 L DPBR (Chapter 2). The columns were packed with wattle chips, blue gum chips, dried grass and sewage sludge. The bottom of the column was packed with a 15 cm layer of glass beads followed by wattle chips, blue gum chips and grass according to the following ratio 1:1:0.5. Unfortunately the exact mass of each component was unknown, due to no records being kept at GARL. The sewage sludge was packed in between the layers. The columns were operated at GARL for a period of approximately two years, before being shipped to UCT. The columns were then operated at UCT unmodified, over the period

of 133 days (9/11/2010 to 9/03/2011) and fed the synthetic AMD stream according to the forumulation described in chapter 5 at a flow rate of 2 mL/min. Additionally each column was fed molasses at 1.5 g/(L.day) as suggested by GARL. These two columns were operated in order to provide the sulphide effluent necessary for the initial LFCR biological study.

9.8.3 Preliminary results and discussion

The sulphate reduction process within DPBR column A was efficient and was only able to achieve an average sulphide concentration of 2.42 mM (79.9 mg/L). DPBR column B produced an effluent with a sulphide concentration in the range of 3.03 - 7.58 mM, the mean value was 5.73 mM (189.1 mg/L). The fluctuations in the sulphide concentration was probably due to two factors. The first being possibly a lack of readily available organic carbon for the sulphate reduction process (Figure 9.1). The molasses would have been easily hydrolyzed and converted to volatile fatty acids for BSR.

The second factor may have been due to the pH and sulphide chemistry. The pH of DPBR columns A & B was in the range of 6 - 9 (Figure 9.2). There was a dynamic relationship between the pH and sulphide concentration. When the pH of column B increased there was a corresponding decrease in sulphide concentration. Subsequently, there was a decrease in pH, hence production of protons (H^+). It's most likely that the sulphide was converted to colloidal sulphur as well as to polysulphides at the higher pH, hence the sulphide concentration decreased. Moreover, this process caused the production of protons as a by-product, as observed in the biological LFCR experimental runs. So, this lead to a large drop in the pH and reappearance of sulphide (reaction 3.29) .

The molasses feed concentration was increased from 1.5 to 2.5 g/L on the 109th day. Initially this had a positive impact, with the sulphide concentration in both columns increasing (Figure 9.1). However, after one week the pH of the effluent decreased significantly (Figure 9.2). This was accompanied by a rapid decrease in the sulphate reduction efficiency. Between days 127 and 129 the sulphide concentration in the effluent from DPBR column A decreased from 2.91 to 0 mM, while for DPBR column B the decrease was 9.27 to 1.85 mM. HPLC analysis of the effluent from the columns at this stage showed that the VFA concentrations had increased significantly from an average effluent concentration of 5.2 mg acetic acid/L. Acetic and iso-valeric acids were the two major constituents. The acetic acid values were similar for the two columns (157 and 173 mg/L), but the iso-valeric acid concentration was significantly higher in DPBR column B (661 mg/L) than column A (173 mg/L).

This initial trial showed that the DPBR columns contained a fermentative bacterial population that rapidly converted molasses to VFAs and this population was either significantly larger or more active than the sulphate reducing population. This would explain the response of the columns to the increase in molasses load. The ultimate

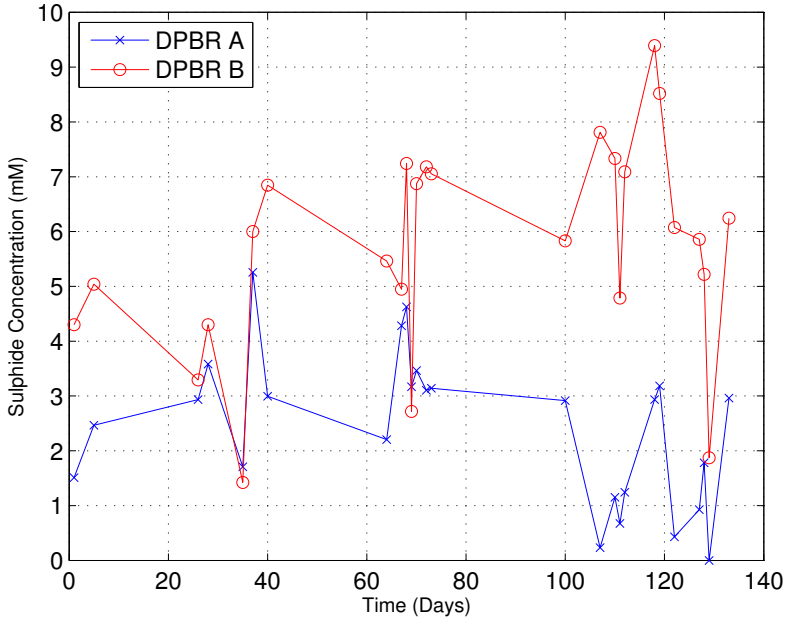


Figure 9.1: Effluent sulphide concentration (mM) of DPBR columns A & B

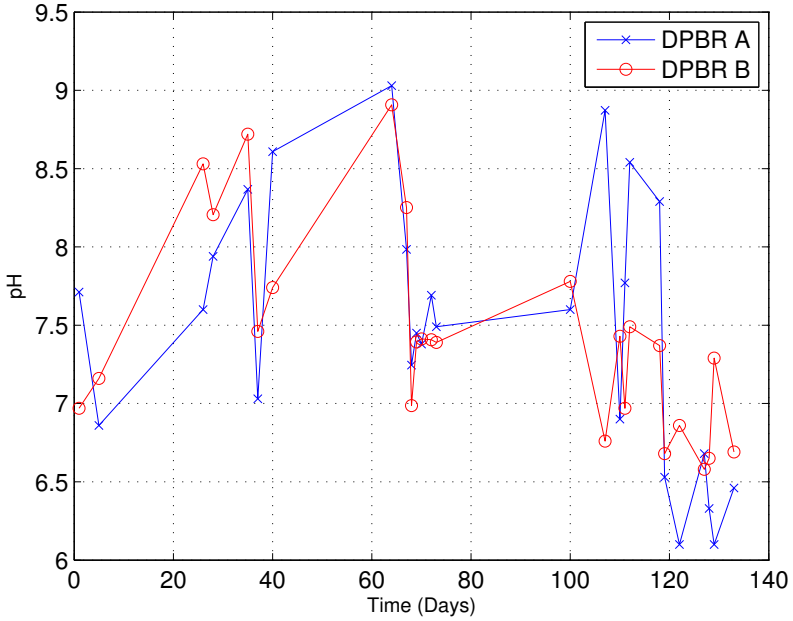


Figure 9.2: pH of DPBR columns A & B effluent stream

consequence of the increased molasses dosing was the inhibition of the SRP population. The fermentative bacteria produced a large amount of VFAs, which substantially lowered the operating pH of the columns to a range of 6-6.5. The increased accumulation in VFA concentration and lower pH was inhibitory to the sulphate reducing population and despite efforts to neutralise the pH and kick-start the BSR process, it was not possible. An inhibitory effect of a pH < 7 on the sulphate reduction rate and SRP growth rate has been shown in previous studies (Al-Zuhair et al., 2008; Fortin et al., 1996; Koschorreck, 2008). Therefore, this is the most likely cause of column failure, as well as a shift in the microbial community structure to due the increased molasses addition.

Both columns were subsequently decommissioned and thereafter repacked according to a different regime. One column was packed primarily with lignocellulosic materials and the other with more organic waste.

9.9 DPBR column study

9.9.1 Introduction

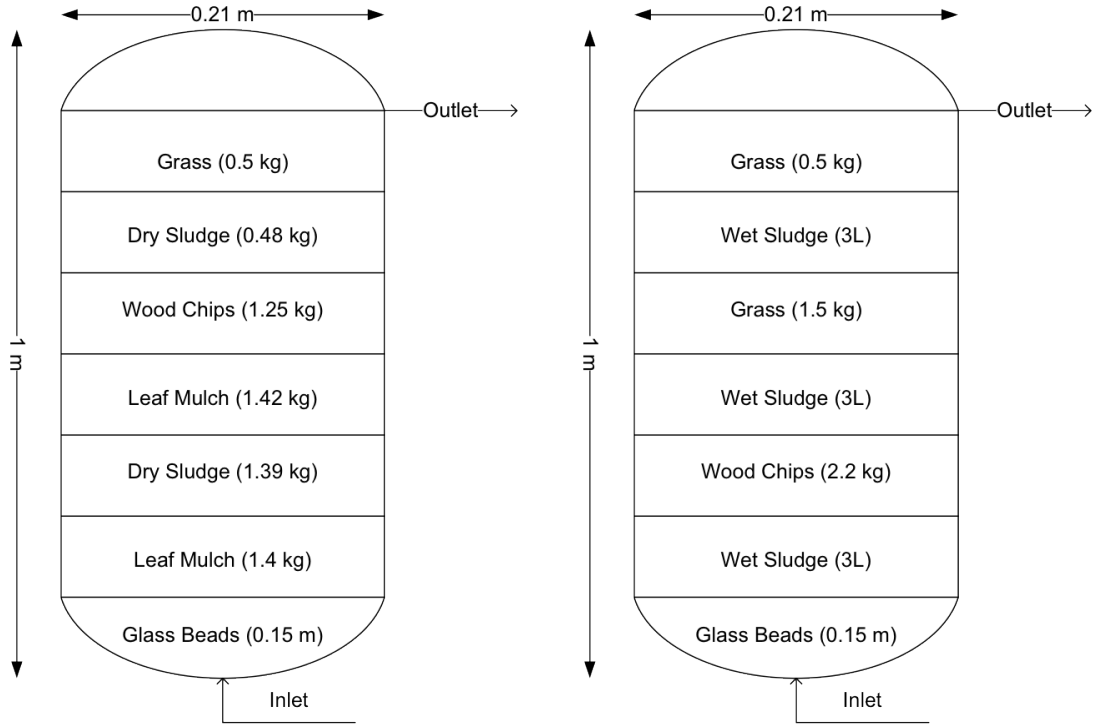
Due to the failure of the sulphate reducing bioreactor columns two new columns were started up to further investigate the BSR process, specifically with respect to sulphur speciation and the release of DOC. In order to adequately, design and optimise a passive SRBR unit, one needs to understand the conditions affecting the rate limiting step. From the previous study it was suspected that the hydrolysis of the complex substrates was the rate limiting step. The addition of more molasses to the feed was used to circumvent this problem, but the success was short-lived, as acidity (from acidogenesis and acetogenesis steps) was produced more rapidly than could be neutralised by the bicarbonate ion formed during the sulphate reduction process.

9.9.2 Experimental setup

9.9.2.1 Characterisation of packing materials

A number of complex organic carbon sources were used to pack the column reactors. To assess their potential to provide organic carbon to the sulphate reducing and sulphide oxidising communities they were characterised to determine their COD and the ease with which they could be hydrolysed under anaerobic conditions.

The four solid complex carbon sources used in the study were wood chips (wattle and bluegum), grass, dry activated sewage sludge and leaf mulch. The leaf mulch had already undergone partial decomposition so it was not possible to obtain a representative sample for the COD analysis. Representative samples of the other materials were dried at 80°C for 48 hours and then homogenised in a laboratory mill. The density of the material was



(a) DPBR column 1 (b) DPBR column 2

Figure 9.3: Layout of organic packing materials with respective masses within DPBR columns 1 & 2, including column dimensions and inlet/outlet configuration

recorded and a small fraction subjected to a COD assay using the standard assay (high range).

9.9.2.2 Packing regime

Two packed bed reactors were prepared with different packing regimes. The packing in the first column consisted of a smaller proportion of lignocellulosic material (Figure 9.3a), while the second was packed according to a traditional degrading packed bed reactor design (Figure 9.3b).

DPBR Column 1 was packed with significantly more easily hydrolyzable and degradable organic matter, with less lignocellulosic materials. The total organic carbon loading was 7.39 kg. The lower section of Column 1 was packed with more organic waste material whilst, the upper section had more lignocellulosic organic matter. This configuration was selected in order to ensure a greater release of volatile fatty acids for the sulphate reduction process.

DPBR column 2 was packed with more cellulosic materials in the form of wood chips and grass. In addition, 9 L of wet primary sewage sludge was utilised with solids concentration of 9 g/L, resulting in a total mass loading of 4.281 kg.

9.9.2.3 Inoculation protocol

The packed columns were inoculated with a mixture of three microbial consortia, rumen fluid, sludge from a batch sulphate reducing reactor and cells detached from the packing material of a previous packed column (Section 9.8). The columns were first inoculated with 15 L of rumen fluid, pumped in at a rate of 1.5 L/hr. The column effluent was recycled for a period of three days. All grass particles and partially digested grass were removed by filtering the fluid through a linen cloth to ensure that the mass of organic packing was not changed. The second inoculum was prepared by agitating 50 mL of sludge from a BSR batch reactor in 50 mL of the bulk reactor fluid. This was mixed with 5 L of detached cell suspension, prepared by agitated washing of packing material (wood chips) from the previous DPBR column. This was pumped into the column at a rate of 1.5 L/hr, after which the columns were sealed and allowed to acclimatise for five days prior to the initiation of feeding.

9.9.2.4 Methane inhibition

Each column was dosed with 1 L (5 mM) 2-Bromoethanesulfonic acid (BESA) post-inoculation in order to inhibit methanogenesis.

9.9.2.5 Feed stream composition

Each column was fed an ARD synthetic stream at a flow rate of 3 mL/min (Table 5.1), additionally column 1 was fed 1 g/L sodium acetate (CH_3COONa). Column 2 was dosed with molasses in order to provide some soluble organic carbon for the BSR process. The column was dosed at a rate of 0.075 g/L over the period 100 - 200 days. The columns were fed by an upflow regime in order to minimise channeling within the packing. The pH of the feed stream was adjusted within the range of 6.0 - 6.5 with NaOH (3 M), unless otherwise stated.

9.9.3 Hydraulic residence time (HRT)

The hydraulic residence time (HRT) was calculated for each column as well as the void volume. This was achieved by pumping in dH_2O until water exited out the top outlet (prior to inoculation). Column 1 had a significantly smaller void volume of 7.58 L due to the fine/small particle size of the leaf mulch and dry sewage sludge (Table 9.4). Hence, a greater proportion of mass could fit in the limited volume. Column 2 had a void volume of 14.38 L due to the uneven wood chips as well as the 9L of water in the form of primary sewage sludge. Hence, column 1 and 2 had a HRT of 1.75 and 3.33 days respectively. The HRT was determined by assuming that the feed rate was 3 mL/min. Therefore the residence time in column 2 was almost double that of column 1. A faster feed rate (than

initial study) was chosen in order to meet the demands of producing sufficient sulphide effluent for the biological LFCR experiments.

Table 9.4: Void volume and hydraulic residence times of DPBR columns 1 and 2

	Column 1	Column 2
Void volume (L)	7.58	14.38
Hydraulic residence time (days)	1.75	3.33

9.9.4 Unsteady-state

Unsteady-state for this particular system was defined as the operating pH not being within the optimal range of 7 - 8.5, as well as the redox potential being greater than -300 mV. Additionally, if the sulphide concentration in the effluent was less than 1 mM for two consecutive residence times, then the reactor was no longer at steady-state. The columns were at unsteady-state during the first month of operation. During the first month sulphate reduction was erratic and a stable redox potential was not observed, particularly for Column 1. To accelerate the transition to steady state operation the columns were supplemented with additional inoculum, consisting of cell suspension from a stock sulphate reducing reactor. Column 2 received a single dose of 4 L on the 13th day, while Column 1 received 6.2 L, in smaller doses, between the 13th and 28th day. Column 2 required less re-inoculation possibly due to the longer hydraulic residence time, therefore there was less wash out of the sulphate reducing bacteria.

The pH of column 1 was initially unstable, however after a few weeks of operation it stabilised within the range of pH 6.5 - 7.5. During the unsteady-state phase, column 1 was re-inoculated multiple times in order to promote sulphate reduction and lower the redox potential. This was done throughout the first month of operation until the redox potential was lowered to below -300 mV and sulphide was being produced. Column 2 was much more stable and was given a 10 mL dose of sodium carbonate solution (200 g/L , pH = 11.16) on the 15th day as well as on the 55th day in order to increase the pH. Although, the pH remained relatively stable during the first month of operation (Figure 9.4).

9.9.5 Results & discussion

9.9.5.1 Characterisation of packing materials

The density and COD of the three packing materials tested are summarised in the Table 9.5. Wood had the highest COD concentration per cm^3, while grass was the lowest.

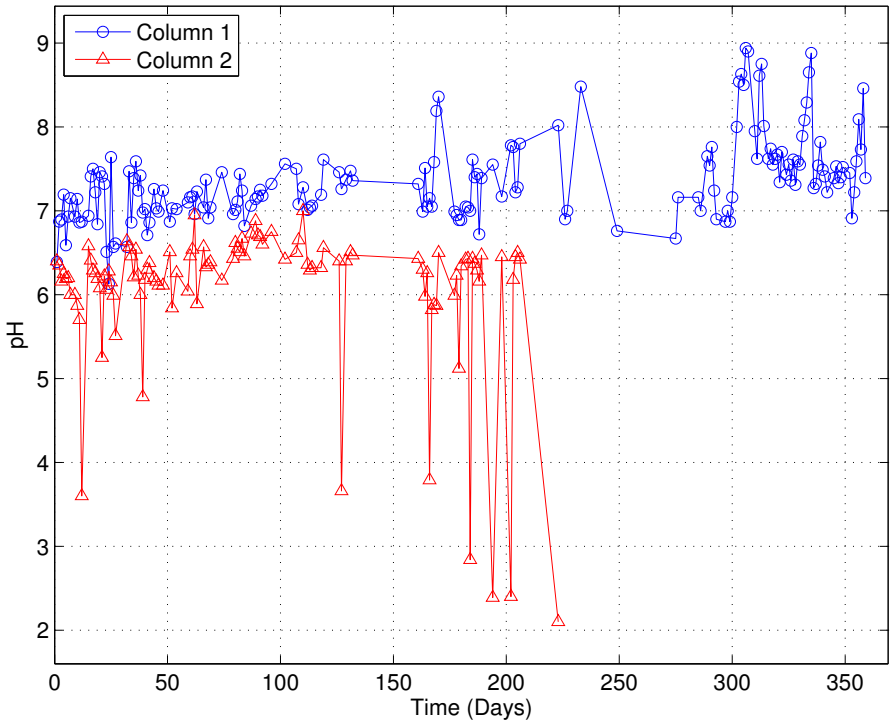


Figure 9.4: pH data of DPBR columns 1 and 2 effluent

Table 9.5: Chemical oxygen demand of each organic packing material

Organic material	Density (g/cm^3)	g COD / cm^3 of organic matter
Wood chips	0.506	902.79
Grass	0.817	685.99
Dry activated sewage sludge	1.375	752.63

9.9.5.2 Packed bed reactor column performance

During the initial phase of the experiment the performance of the columns was unstable. No sulphide was detected in the effluent from Column 1 for the first month (Figure 9.5) and the redox potential fluctuated between -350 mV and -100 mV. With regard to sulphate removal efficiency both columns performed almost identically at start-up. Both column 1 and 2 attained an average sulphate removal efficiency of 59% during the unsteady-state phase (Figure 9.6). Although it did fluctuate tremendously due to the columns not being able to maintain a stable pH/redox potential. Column 1 fluctuated from 21 - 94%, whilst column 2 varied from 27 - 77%.

During the first month of operation the evolution of gas from Column 1 was observed. The gas was collected and analysed by gas chromatography, which confirmed a mixture of methane (70%) and carbon dioxide (30%). In an attempt to inhibit methanogenesis

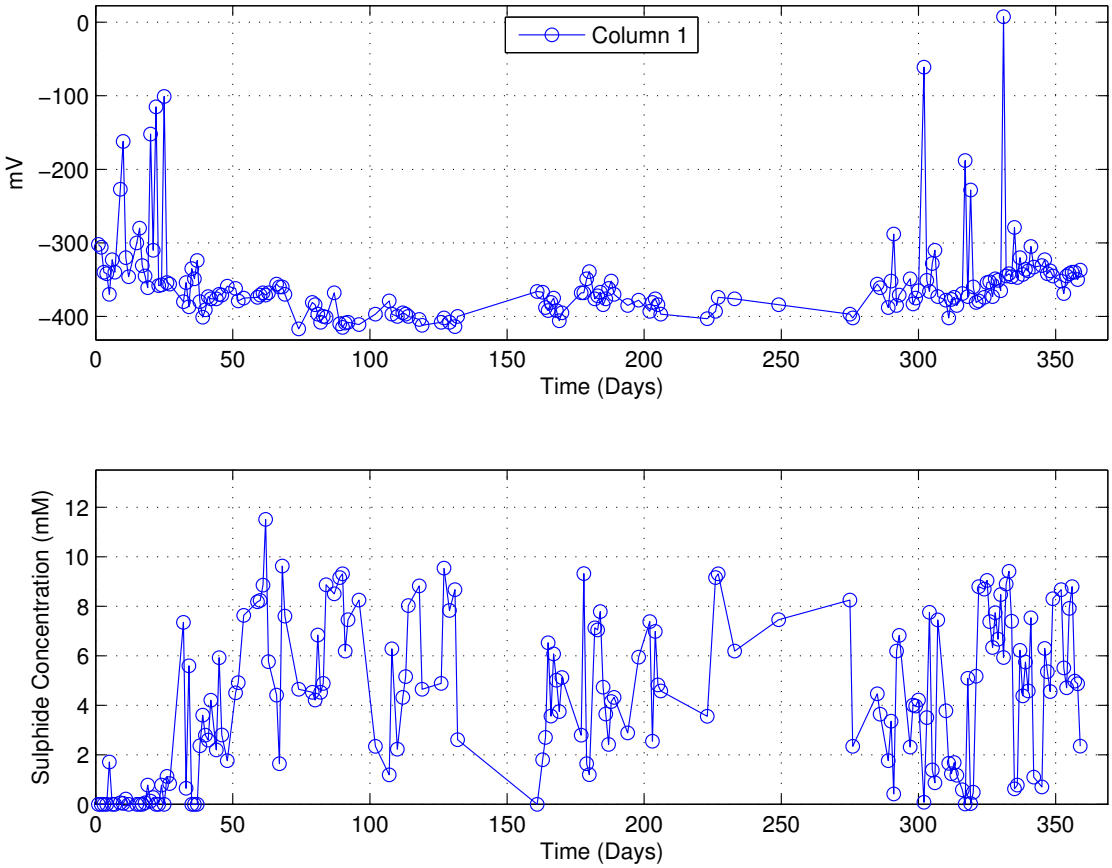


Figure 9.5: DPBR Column 1 redox & sulphide concentration (mM) data over a period of 359 days

the sulphate concentration in the feed to Column 1 was increased to 5 g/L (on day 38) in an attempt to increase the sulphide concentration. Methanogenic organisms are more susceptible to sulphide inhibition than sulphate reducers. The increased feed concentration was maintained for one month and accounts for the significant increase in effluent sulphate concentration (Figure 9.7). The sulphate removal efficiency within column 1 increased to 66.2% due to some inhibition of methanogenesis. One litre of 2-bromoethanesulfonic acid (BESA) solution (10 mM) was pumped into column 1 to inhibit the process of methanogenesis (62nd day) and the feed sulphate concentration was reduced back to 2 g/L.

The pH of DPBR column 1 was erratic during the first month of operation (unsteady-state phase) as the pH fluctuated between 6.2 and 7.6. Thereafter the pH in the effluent stabilised within the range of pH 7.2-7.4 (Figure 9.4). However, on day 118 the pH increased to 7.5, following a period of two weeks during which the column was not fed or sampled, after which it was less stable and fluctuated till reaching a maximum of 8.9 on the 302nd day. Thereafter, the feed pH was decreased from 6.5 to 5.0 - 5.1 in order to prevent the outlet pH from rising above 7.5. This, clearly illustrated that the sulphate reduction process improved slowly over the duration of the experiment as more sulphate was reduced resulting in a

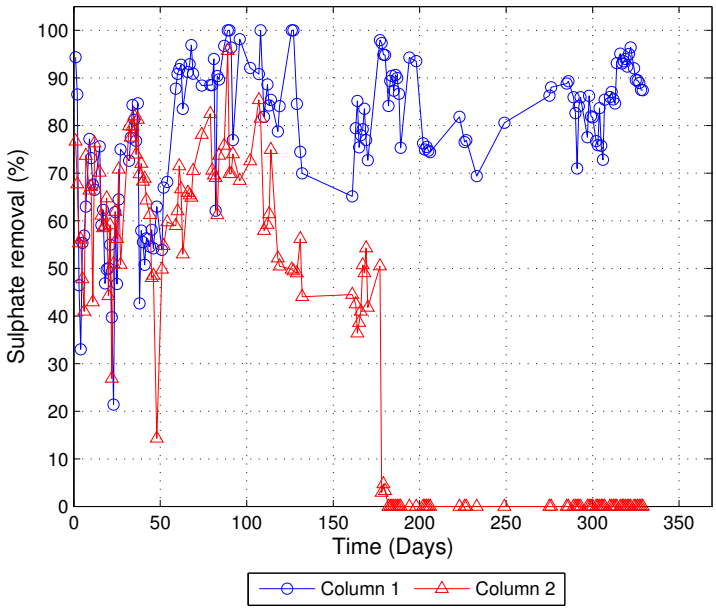


Figure 9.6: Sulphate removal efficiency for DPBR columns 1 and 2, based on measurement of effluent sulphate concentration.

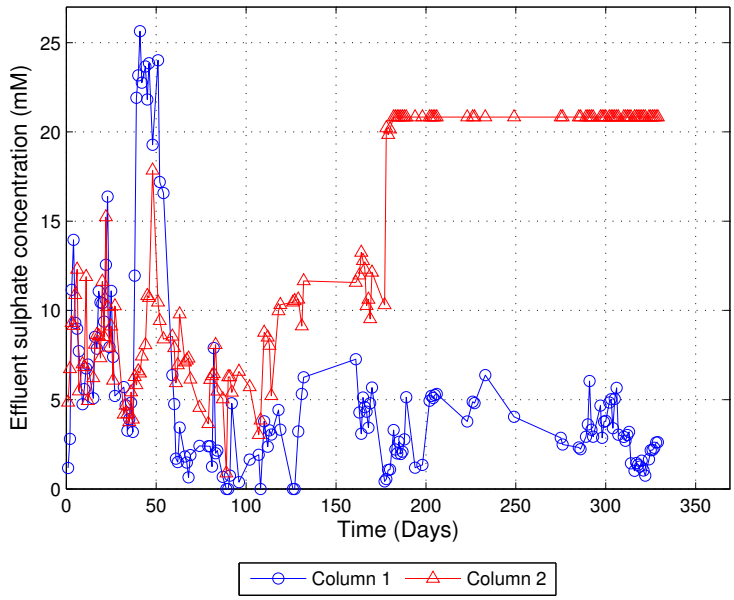


Figure 9.7: Effluent sulphate concentrations from DPBR column 1 and 2

greater generation of alkalinity. This is ideal for a passive treatment system with a lifetime of more than five years. Moreover, it shows that the reactor is able to handle a more acidic ARD stream.

The feed to Column 1 was supplemented with sodium acetate at a concentration of 1 g/L, so the residual acetate detected initially does not necessarily represent metabolism of the complex carbon. Similarly, as the acetate was already in the feed, rather than generated in the column, it would not further influence that pH.

Column 1 maintained a steady sulphate reduction process after the first month and produced an average effluent sulphide concentration of 5.13 mM (Figure 9.5). The sulphate removal efficiency was high at an average 79% which, equated to a volumetric removal rate of 9.40 mmol/L.day (902.86 mg/L.day). In figure 9.7 it seems the sulphate effluent concentration increased on day 120. Though this simply was due to the column not being fed or sampled during the period of 131 - 161 days, hence there was probably a small decrease in the SRP activity. Column 1 returned to steady-state and a high sulphate removal efficiency after day 163.

On the other hand column 2 began generating sulphide much sooner with a sulphide concentration of 1.76 mM after the first week of start-up (Figure 9.8). However, column 2 was only able to maintain a stable redox potential just below -300 mV until day 140 and the average effluent sulphide concentration was 1.71 mM. Furthermore, DPBR column 2 was unable to consistently maintain an outlet pH greater than 6.5 over the first two months of operation (Figure 9.4). The pH did occasionally drop below 6.0 indicating that there was active generation of acidity rather than alkalinity by microbial sulphate reduction. Acidity was generated by the hydrolysis of the primary sewage sludge that was added to the column. This was due to the primary sewage sludge having a greater quantity of labile carbon than the dry activated sludge which was added to DPBR column 1. The dry activated sludge had a lower concentration of labile carbon as it had been collected after two aeration and two dewatering stages. This is clearly illustrated in Figures 9.9 and 9.10, as there was a greater concentration ($>$ 200 mg/L) of VFAs in the column 2 effluent. Hence, there was a greater accumulation of acidity within the column, resulting in a lower effluent pH. DPBR column 2 was not able to attain a high sulphate removal efficiency as the average removal rate after the acclimitisation was 63.7%, with a volumetric sulphate removal rate of 3.99 mmol/L.day. The removal rate decreased further on day 79 to 50.6% (3.45 mmol/L.day). This decrease was probably due to the fact that all the easily degradable labile carbon was consumed and the hydrolysis of the organic substrates was limiting the process of sulphate reduction. This is evinced by the lack of VFAs in the effluent (Figure 9.10).

Column 2 was also not fed over the period 131 - 161 days, in an effort to improve the sulphate reduction efficiency by allowing the SRP population to acclimatise further. The lack of sulphate feed was evident by the constant pH and decrease in sulphide concentration, and corresponding increase in redox potential. Unfortunately, DPBR

column 2 did not perform in the same manner as column 1. The pH began to fluctuate drastically to below pH 6, after four days of feeding. Due to their being no VFAs in the column 2 effluent over the concerned period of days 162 to 223 (Figure 9.10) and low molasses dosing, the previous explanation of column failure is not valid. Therefore the observed instability (low pH) and poor sulphate reduction, was not due to the production and accumulation of VFAs.

The most plausible explanation is that the onset of organic carbon limitation, resulted in reduced sulphate reduction efficiency, thereby reducing the amount of sulphide and bicarbonate generated. The presence of colloidal sulphur was detected, even in efficiently functioning reactors, indicating that sufficient oxygen was available for partial sulphide oxidation. As the sulphide concentration decreased the likelihood of complete sulphide oxidation to sulphate, with the associated proton generation, would have increased. The significant increase in redox potential observed (Figure 9.8) is consistent with this.

Furthermore, as the pH decreased (< 6.5) the speciation of aqueous sulphide would have shifted to the more toxic $H_2S_{(aq)}$ (reaction 3.13). As a result, this would have caused further inhibition of the BSR process. Koschorreck (2008) reported 50% inhibition of the biological sulphate reduction process was possible at low $H_2S_{(g)}$ concentrations of 1.8 mM (61 mg/L). Finally, as the redox potential became positive the ferrous iron in the feed could undergo oxidation, hydrolysis and ultimately precipitation as ferric hydroxide, with the release of three protons.

The column was re-inoculated with 50 mL of SRBR sludge on the 170th day however, this failed to kickstart the BSR process. Furthermore, due to the poor performance over the preceding six months and low sulphide generation it was assumed that the sulphate reducing prokaryotes were unable to perform the BSR reaction due to a lack of freely available soluble organic carbon. Hence, the column was decommissioned after day 233.

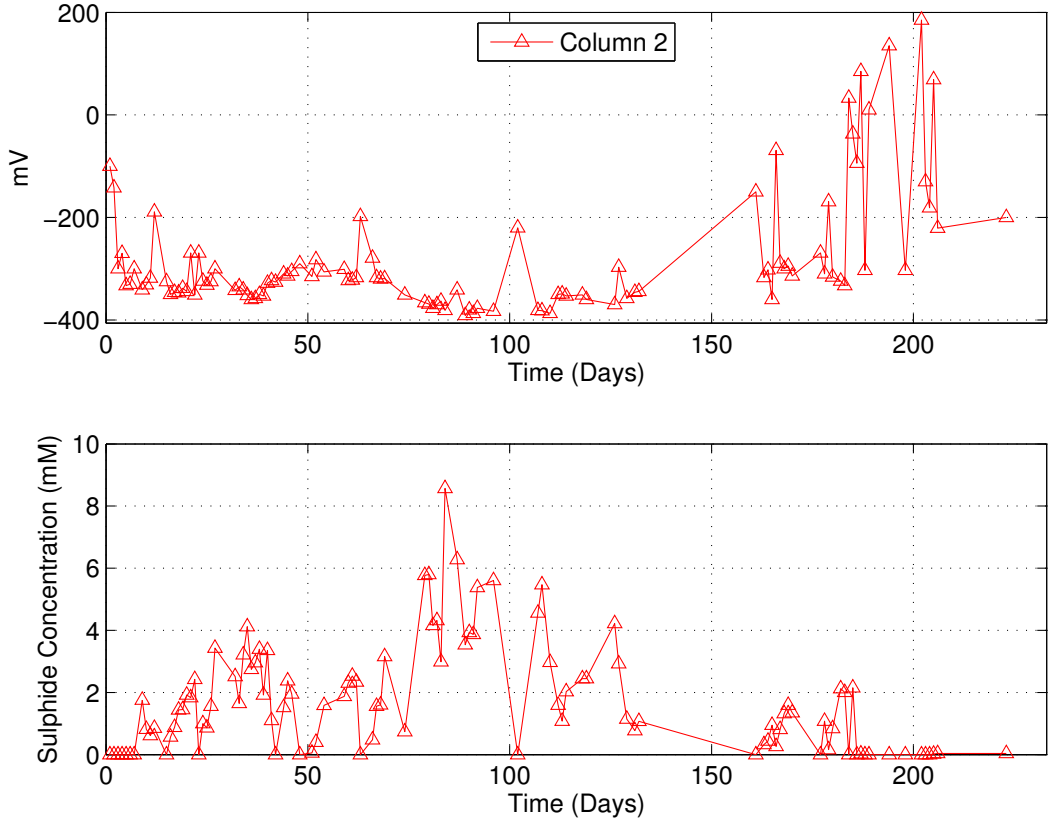


Figure 9.8: DPBR Column 2 redox & sulphide concentration (mM) data over a period of 233 days.

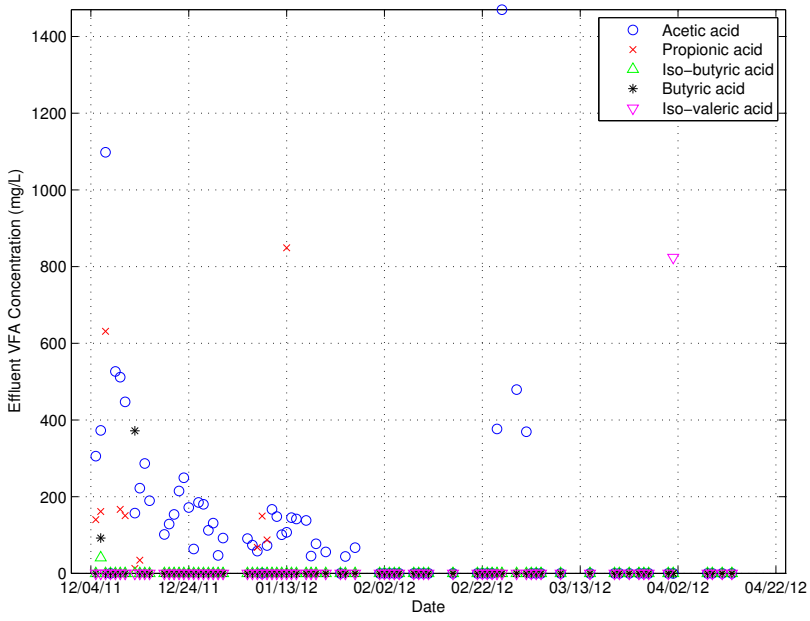


Figure 9.9: Volatile fatty acids concentrations in DPBR column 1 effluent stream. No VFAs were detected after day 120 (data not shown).

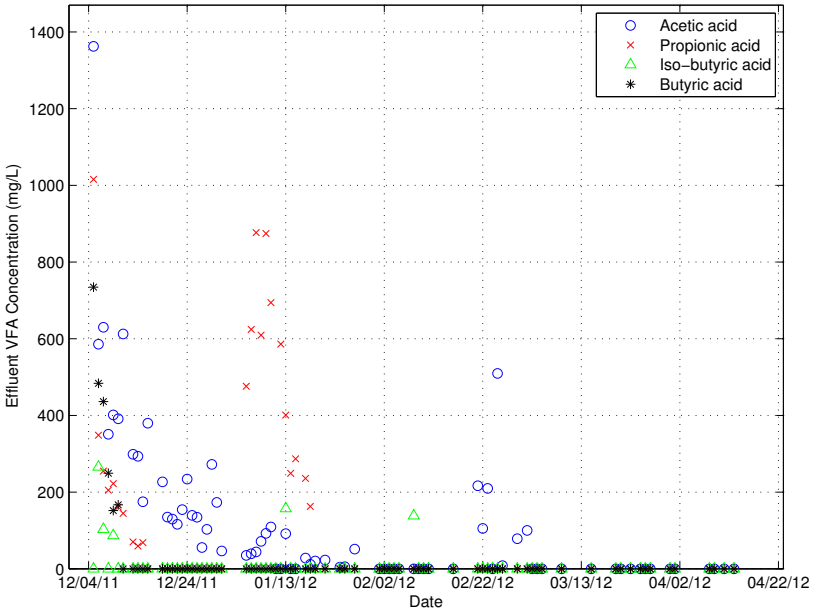


Figure 9.10: Volatile fatty acids concentrations in DPBR column 2 effluent stream (1 - 137 day). No VFAs were detected in the effluent stream after day 137 (data not shown).

9.9.5.3 Relationship between pH and sulphur speciation

There was also a dynamic relationship between pH and the observed sulphide concentration in the effluent (Figure 9.11), as mentioned earlier. When the pH increased to above pH 8 there was an associated decrease in sulphide on the same particular day or following day. On the 289th day the pH reached pH 8.5 and the sulphide concentration dropped to 1.3 mM. Likewise on the 315th day the pH reached a maximum of pH 8.9 and the sulphide concentration was correspondingly reduced to 0 mM. However, the following day the pH decreased to 7.65 and the sulphide concentration increased to 5 mM. This is simply due to the equilibrium reactions between the sulphur species generated and the protons. Due to the presence of a small amount of dissolved oxygen some of the sulphide was partially oxidised to elemental sulphur. As a result biologically produced colloidal sulphur was produced within column 1 (Figure 9.12). Under alkaline conditions (pH $>$ 8) the free bisulphide ions reacted with the colloidal sulphur to produce polysulphides of chain length (x) provided x $\geqslant$ 2 (reaction 9.10). However, there was further reduction of the bisulphide ion as it was able to react with a free hydroxyl group to produce a polysulphide of chain length 2 (reaction 9.11). As a result, the sulphide concentration on various days did appear to be almost zero due to all free bisulphide ions being converted to polysulphides. The polysulphide concentration was measured on day 316, yielding an S_2^{2-} concentration of 10.33 mM. Kamyshny et al. (2006) showed that it is possible to form polysulphides of chain length two and three at a pH of 8.5. The effluent was also tested for the presence of colloidal sulphur over the (steady-state) period of the 60th till the 302nd day. Colloidal sulphur was present in varying concentrations from 0 to 18.3 mM (Figure 9.12). DPBR

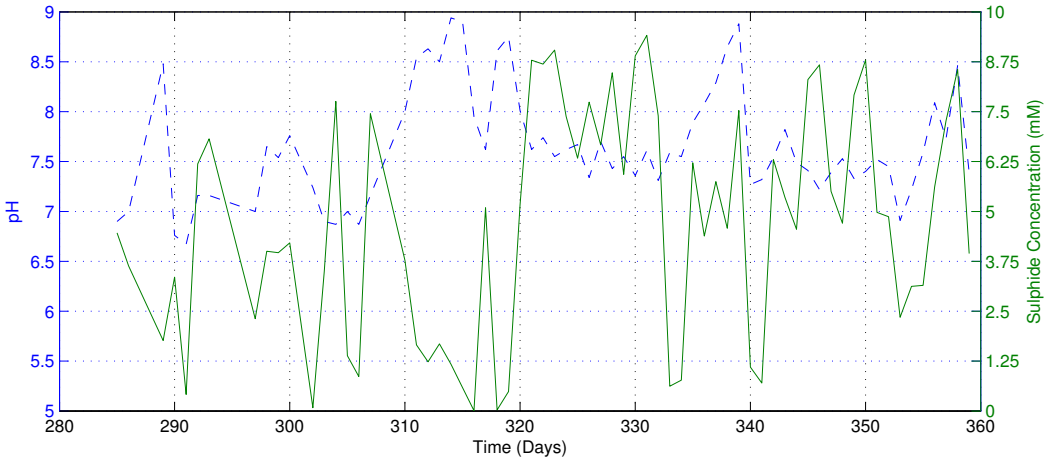


Figure 9.11: Sulphide concentration (mM) and pH data for DPBR column 1 over a period of 75 days. Depicting the relationship between pH and sulphide concentration.

column 1 had a substantially greater proportion of colloidal sulphur simply due to the higher pH. The mean colloidal sulphur concentrations were 6.85 and 2.13 mM for columns 1 and 2 respectively. On the 290th day the colloidal sulphur concentration was 18 mM following the decrease in pH, which caused majority of the polysulphides to decompose back to the constituents, of bisulphide and colloidal sulphur. Correspondingly, there was an increase in the bisulphide concentration. Therefore, the sulphur species formed as a result of the BSR process is also crucially dependent on the pH, colloidal sulphur concentration and hydroxyl ion concentration.

$$HS^- + \frac{1}{2}O_2 \rightarrow S^0 + OH^- \tag{9.9}$$

$$HS^- + (x-1)S^0 \rightleftharpoons S_x^{2-} + H^+ \tag{9.10}$$

$$S_x^{2-} + xH_2O + (2x-2)e^- \rightleftharpoons xHS^- + xOH^- \tag{9.11}$$

9.9.5.4 Hydrolysis of organic packing to volatile fatty acids

The reduction in sulphate removal efficiency coincided with no VFAs exiting DPBR column 2 (Figure 9.10), indicating the onset of carbon substrate limitation. In the column the easily accessible labile carbon lasted for approximately four months, releasing acetic, propionic and iso-butyric acid. This was predominantly from the primary sewage sludge. A similar trend occurred within DPBR column 1 (Figure 9.9) as there were no VFAs in the effluent

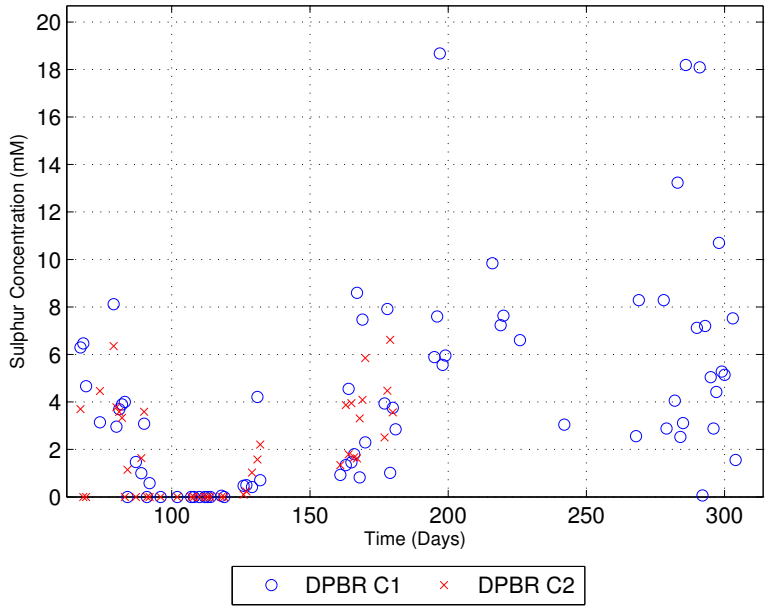


Figure 9.12: Colloidal sulphur concentration (mM) in effluent samples from DPBR columns 1 & 2, over the period of 241 days (69 - 310 days).

stream after the first four months. However, column 1 was supplemented with sodium acetate and this ensured there was a continuous supply of DOC for biological sulphate reduction to occur effectively.

In order to gain a better understanding of the hydrolysis process occurring within both DPBR columns, a reverse calculation was conducted. The theoretical amount of acetic acid required for the measured sulphate reduction was calculated. From Figures 9.13, 9.14 it is evident that the amount of acetic acid supplied in the feed was significantly less than required, while no acetic acid supplementation occurred in Column 2. Hence, it can be concluded that break-down of the organic complex substrates was occurring within the columns. DPBR column 1 required an average concentration of 1100 mg/L (628.57 mg/L.day) of acetic acid to perform the BSR reaction, to reduce the sulphate that was supplied at a rate of 1142.9 mg/L.day. Therefore 291.17 mg/L.day of acetic acid was produced by hydrolysis of the organic packing material. On the other hand column 2 required 216.74 mg/L.day of acetic acid which was obtained from hydrolysing the packing material.

During the initial phase of operation the effluent from Column 2 contained an appreciable amount of VFAs, despite no supplementation of the feed. This suggests that the wet primary sludge provided the necessary DOC and was a better organic waste material than dry activated sewage sludge. Therefore, a column packed primarily with lignocellulosic wastes will not be ideal for a passive treatment BSR unit, due to the relatively slow hydrolysis rate. Additionally, primary sewage sludge would be a more ideal organic waste material than activated sewage sludge. The composition of column 1 packing material was

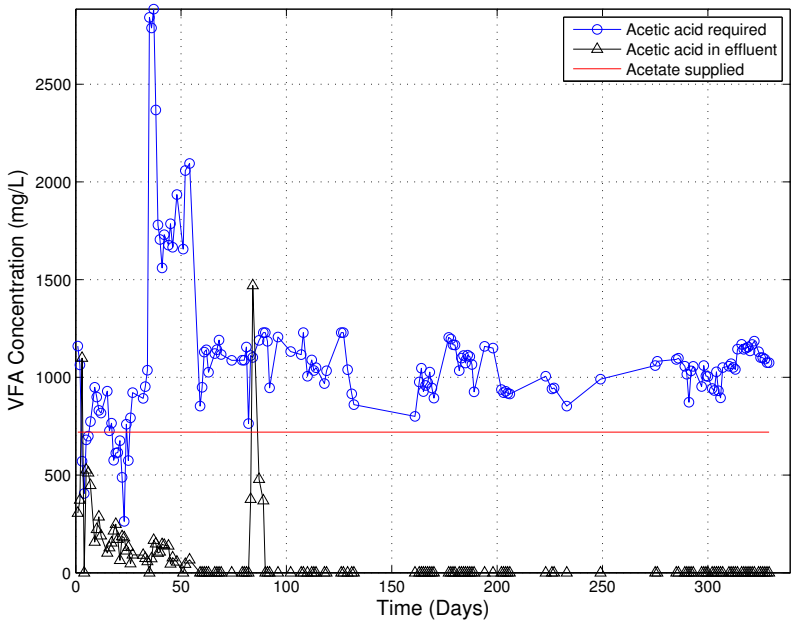


Figure 9.13: The required theoretical amount of acetic acid for given sulphate reduction in DPBR column 1

25% organic waste and 75% lignocellulosic wastes whereas, column 2 was 1.89% organic waste and the remainder lignocellulosic wastes. Based on the amount of required acetic acid for the BSR reaction, the corresponding amount of COD was calculated to be 1044.07 and 685.03 mg/L for column 1 & 2 respectively. As previously mentioned, activated sludge has a lower quantity of SCOD and is less susceptible to microbial attack due to the accumulation of cellular residues. The performance of the DPBR columns was ultimately dictated by the rate of VFA liberation. Based on the measured data, the mean COD:SO_4^{2-} was 0.52 and 0.34 for columns 1 & 2 respectively. In essence this clearly shows that there was insufficient carbon as the theoretical ratio is 0.67, consequently complete sulphate removal was not possible. For this reason a VFA liberation study was conducted in parallel, to gain a better understanding of the hydrolysis occurring within the BSR columns.

A greater quantity of organic waste materials is necessary in order to provide the necessary DOC.

A chemical oxygen demand (COD) analysis was conducted on DPBR column 1 and 2 effluent samples (Figure 9.15). Filtered and unfiltered samples were tested. From the COD analysis it was evident that there were possibly large carbohydrate molecules within the effluent from the process of hydrolysis, in addition to the VFAs over the first four months of operation. The COD concentration in DPBR column 1 effluent was analysed in order to determine if there were still large carbohydrate molecules, indicative of active hydrolysis. The COD concentration varied over a range of 0 - 1400 mg/L over a one month time period (Figure 9.16). Please note, the colloidal sulphur concentration and corresponding

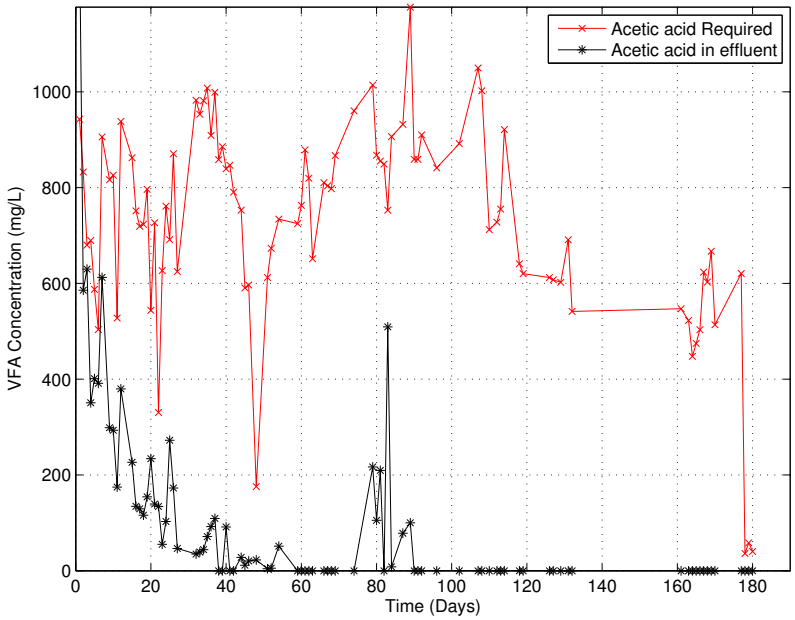


Figure 9.14: The required theoretical amount of acetic acid for given sulphate reduction in DPBR column 2

COD of sulphur was determined and subtracted from the measured effluent COD. This is due to the fact that colloidal sulphur contributes to the measured COD.

9.9.6 Conclusions

In essence the DPBR column study highlighted a significant issue that has been the failure of many passive BSR systems, and that is the organic packing. A system packed primarily with lignocellulosic wastes and very little organic carbon waste materials ($< 2\%$) will not be able to perform efficiently for an extended period of time (> 6 months). The average sulphate removal efficiency achieved in DPBR column 2 was approximately 57.5% This was primarily due to the fact that there was no soluble organic carbon in the form of VFAs for the biological sulphate reduction reaction to proceed. The DPBR Column 1 performed significantly better achieving an average sulphate removal efficiency of 79%, due to the acetate that was supplied at a feed concentration of 719 mg/L. Hence, in order to have a highly efficient passive BSR system, it is crucial that there is soluble COD within the system. In short, the performance of the biological sulphate reduction passive reactors was controlled by the rate of release of soluble dissolved organic carbons via hydrolysis. Furthermore, the primary sulphur species formed was sulphide, however this varied according to pH due to the presence of biologically produced sulphur, causing the formation of polysulphides. A residence time of 3.33 days is sufficient to achieve a 57.5% sulphate removal efficiency by hydrolysing the packing materials. Therefore, if a higher removal efficiency is required then the residence time would have to be increased,

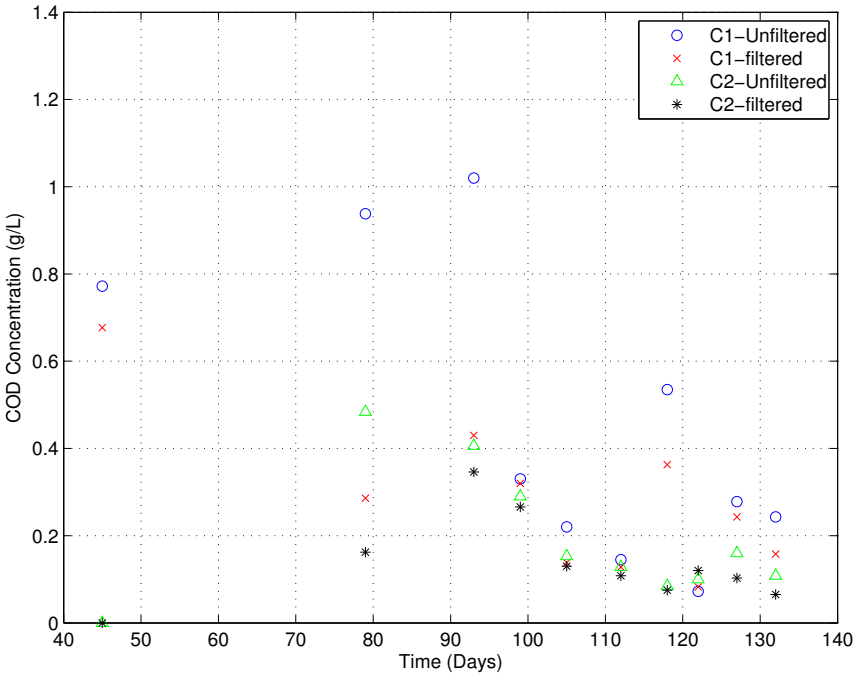


Figure 9.15: Chemical oxygen demand concentrations (mg COD/L) of DPBR column 1 & 2 effluent over the period Jan - April 2012. Filtered and unfiltered samples were analysed.

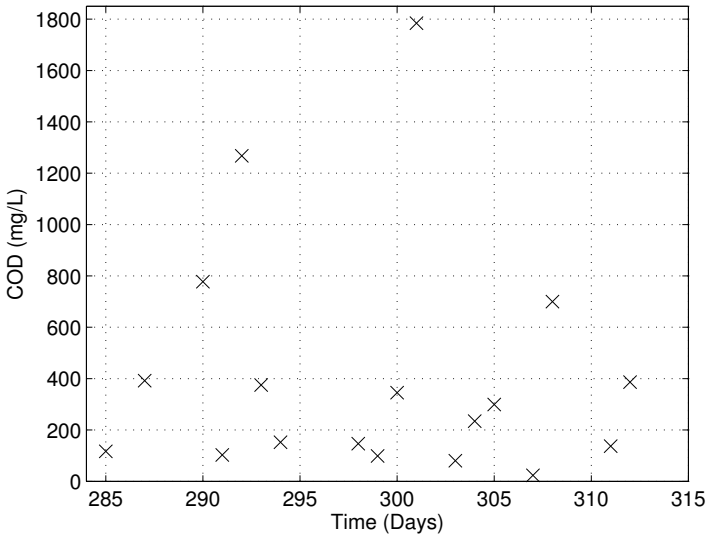


Figure 9.16: DPBR column 1 effluent COD concentrations (mg/L) over approximately a one month time period (285 - 312 days).

or the SRBR has to be supplemented with an additional (soluble) organic carbon source such as acetate. Due to the dynamic relationship between pH and sulphide, the pH will naturally fluctuate based on the concentration of sulphide, colloidal sulphur, polysulphides and bicarbonate ions. Unfortunately an optimum ratio of lignocellulosic wastes to organic wastes was not determined, however, the reactor packing material should have an organic carbon waste composition greater than 25%, to ensure prolonged liberation of soluble COD. The DPBR columns performed significantly better than passive bioreactors run in various other studies (Table 9.1), a higher sulphate removal efficiency and conversion was achieved, even in the none supplemented column.

Table 9.6: Summary of DPBR column 1 & 2 study findings, with regard to sulphate removal and VFA liberation

Parameter	C1	C2
Sulphate removal (%)	75	57.5
Sulphate removal (g/L.day)	0.85	0.22
Acetate supplied (g/day)	0.411	-
Avg. acetic acid required (g/L.day)	0.63	0.22

9.10 VFA release study

A volatile fatty acids release study was conducted concurrently, to better understand the kinetics of hydrolysis for each organic packing material. Each packing material was tested except for the leaf mulch, due to the material being in a decomposition state, it would not have been possible to obtain a representative sample or set of data. Additionally, spent brew malt was tested as an alternative lignocellulosic carbon source.

9.10.1 Experimental Procedure

Each packing material was tested within a magnetically stirred sealed Schott bottle (1L), fitted with a custom designed lid with ports for sampling and gas analysis. This was to simulate the anaerobic environment within the column and to promote a well-mixed system. Chemical sulphide was added to each reactor in order to create a negative redox potential environment similar to that in the DPBR columns. Furthermore, it was added to improve lignocellulose degradation, as it has been shown that the hydrolysis rate is higher under sulphidogenic conditions, rather than methanogenic (Roman et al., 2008). Bioreactors one to three were operated for a period of 36 days whilst, bioreactor four was run for 31 days. All bioreactors were operated at 37°C in order to determine the maximum amount of VFA liberation in an ideal optimum well-mixed system. The reactors were sampled daily. BESA solution (5 mM) was added as well in order to inhibit methanogenesis. This was performed in order to create an environment to promote hydrolysis, acidogenesis

and acetogenesis, resulting in VFA accumulation. The following inoculation and setup protocol was followed for each packing material:

Table 9.7: Inoculation and experimental protocol followed in setting up a batch bioreactor

Mass of organic packing	20 g
Rumen fluid	10 mL
SRBR effluent	10 mL
Sulphide solution (151.52 mM)	10 mL
BESA Solution (5 mM)	10 mL
dH_2O	940 mL

9.10.2 Results & Discussion

Each batch reactor was sampled and analysed for volatile fatty acids and pH. From figures 9.17- 9.20 it is clear that the greatest amount of VFA liberation occurred in the spent brew malt bioreactor (3.777 g/L) with dry activated sewage sludge producing only 1.96 g/L (Table 9.8).

Table 9.8: Summary of the results from VFA liberation kinetics study. Total VFA and soluble COD data represent final values at the end of the experiment.

	B1-Wood chips	B2-Grass	B3-Dry sludge	B4-Spent brew malt
Total VFAs (g/L)	1.570	0	1.960	3.777
SCOD (g/L)	2.096	1.211	2.0	3.167
Avg. VFA release rate (mg/L.day.{g of substrate})	2.18	0	2.72	6.09

It was evident across all organic materials except grass that the hydrolysis process followed linear first order kinetics over the duration of the experiment with regard to acetic acid production. The acetic acid liberation rate in the wood-chips bioreactor was 66.13 mg/L.day over the first 10 days (Figure 9.17). Thereafter the concentration of acetic acid decreased and the formation of iso-butyric acid and valeric acid took place. The initial release of acetic acid was probably the readily hydrolysable organics and thereafter the microorganisms began to breakdown the more complex cellulose. Hydrolysis also did occur within the first six days in the grass bioreactor, at a rate of 134.56 mg/L.day whereby valeric acid was produced. However, the process of hydrolysis seemed to cease after day six.

The dry-sludge bioreactor performed significantly better as acetic acid was produced at a rate of 131.22 mg/L.day whilst, propionic and iso-valeric acid were produced at a rate of 52.88 and 62.94 mg/L.day respectively. Thereafter there appeared to be a decrease in VFA

concentrations till the 1st of June where all VFAs increased rapidly and reached a stable constant value. Between 22nd May and the 1st of June there seemed to be a 'lag-phase'. The most likely cause was that all readily hydrolysable matter was consumed, thereafter there was a lack of the necessary enzymes needed to hydrolyse the more complex solid organic matter. As a result there was an observed decrease in VFAs of chain length greater than two as they were broken down to acetic acid.

The final bioreactor of spent brew malt also followed classic linear first order hydrolysis kinetics. Acetic acid was produced at a rate of 57.62 mg/L.day. However, the butyric and iso-butyric acid liberation did not follow any trend. The spent brew malt had greater liberation simply due to the mashing process of beer brewing. The malt was crushed prior to mashing and thereafter stirred within a mash tun at 60°C for one hour. A large proportion of the sugars and complex carbohydrates would have been removed from the solids during the mash process, although some residual would remain, while the remaining complex carbohydrates could have been partially hydrolrolysed. Furthermore, the wood chips, grass and dry sludge did not undergo any mechanical preparation procedure.

The pH in the reactors initially increased as a consequence of the addition of sulphide (Figure 9.21). The extent of the increase was greatest in the reactors where the initial VFA production was lowest. This was followed by a period during which the pH decreased due to VFA generation and some oxidation of the sulphide. This was followed by a period of stability for approximately two weeks. During this period further oxidation of the sulphide was observed, so a second spike of sodium sulphide was added, increasing the concentration to 1.52 mM (50 mg/L). This resulted in a further increase in pH across all reactors, although the extent of the increase was lower in the reactors with the highest VFA concentrations.

Therefore, in order to have an optimally performing passive sulphate reduction unit there has to be continuous generation of soluble organic carbon in the form of VFAs greater than 1200 mg/L.day. Moreover, the waste organic materials have to be easily hydrolysable, such as in primary or activated sewage sludge. Dry activated sewage sludge is less favourable due to it having a lower content of labile carbon. The average VFA liberation rate of the dry activated sludge was 54.44 mg/L.day, whilst the wood chips was 43.61 mg/L.day. Grass performed the most poorly as it was the least hydrolysable. Spent brew malt was the most labile substrate, as volatile fatty acids were liberated at a rate of 121.84 mg/L.day. Although, the brew malt had undergone a mechanical crushing and a heat activation process to liberate the carbohydrates.

The reactor loaded with dry activated sewage sludge managed to liberate a total VFA concentration of 1.96 g/L, which was significantly higher (10X) than the study conducted by Chen et al. (2007b). They showed that hydrolysis occurs at a faster rate under alkaline conditions, with the optimum pH being pH 10. However, no improvement was observed when the pH was increased. A similar trend of acetic and iso-valeric acid being the major products of hydrolysis was observed in their study, but under methanogenic conditions.

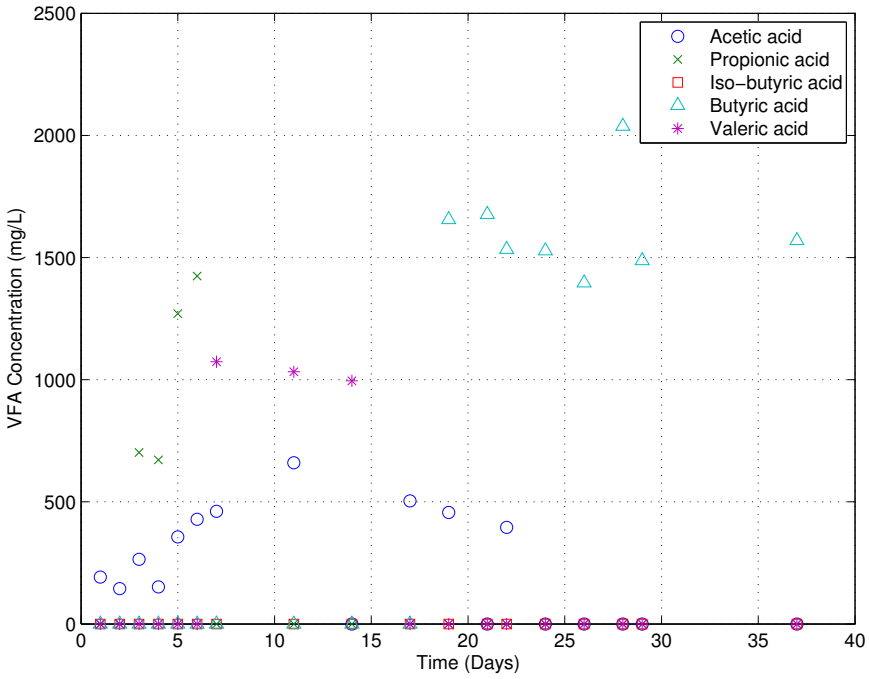


Figure 9.17: Volatile fatty acids cumulative concentration within bioreactor 1 containing 20 g of wood chips

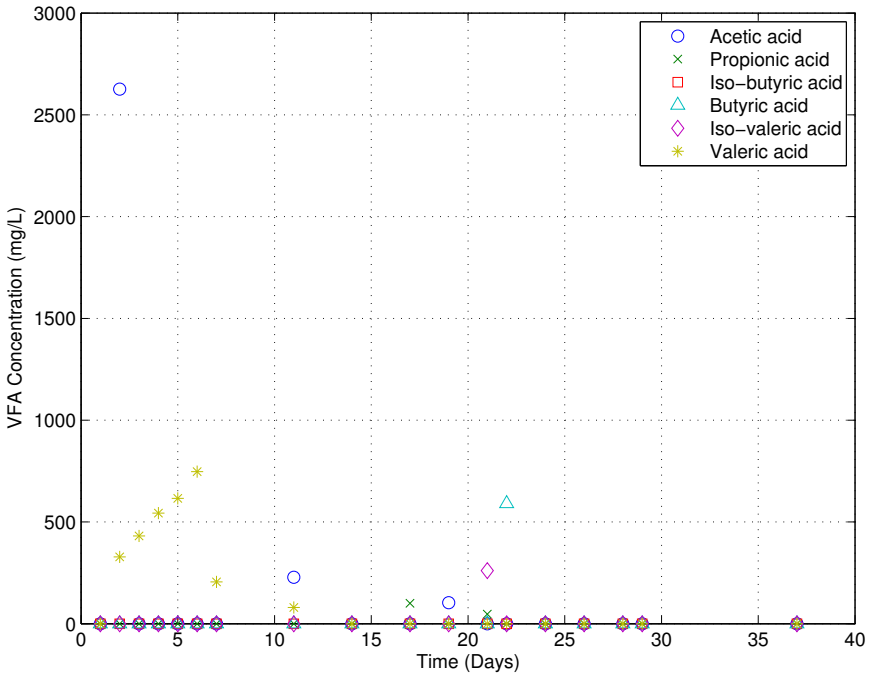


Figure 9.18: Volatile fatty acids cumulative concentration within bioreactor 2 containing 20 g of grass

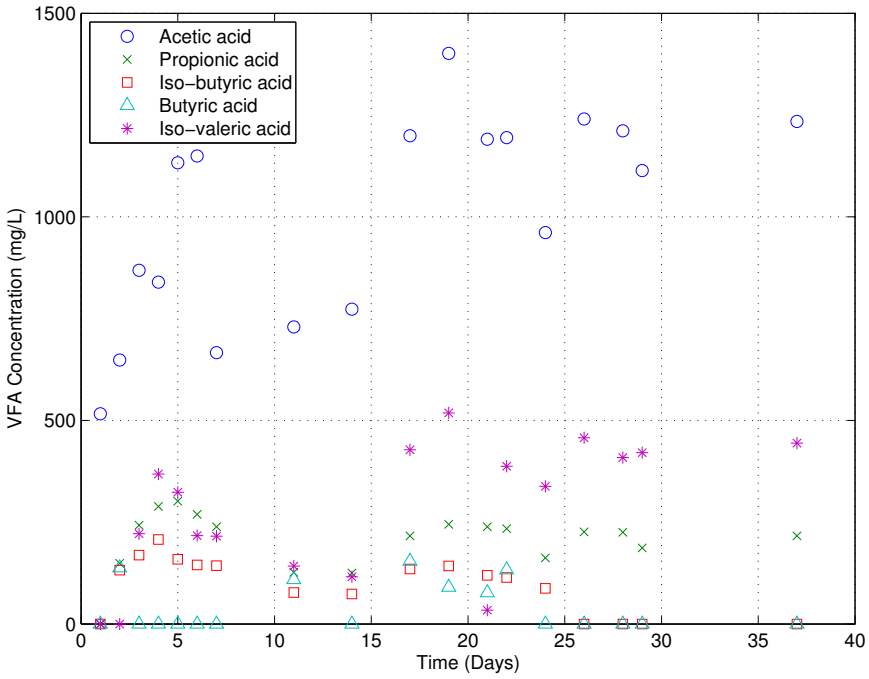


Figure 9.19: Volatile fatty acids cumulative concentration within bioreactor 3 containing 20 g of dry sewage sludge

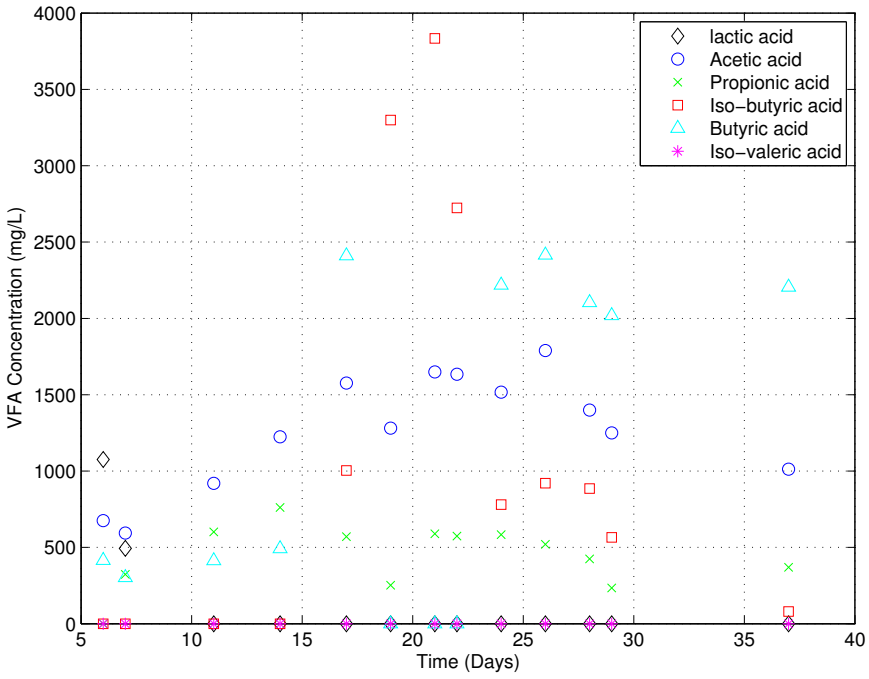


Figure 9.20: Volatile fatty acids cumulative concentration within bioreactor 4 containing 20 g of spent brew malt

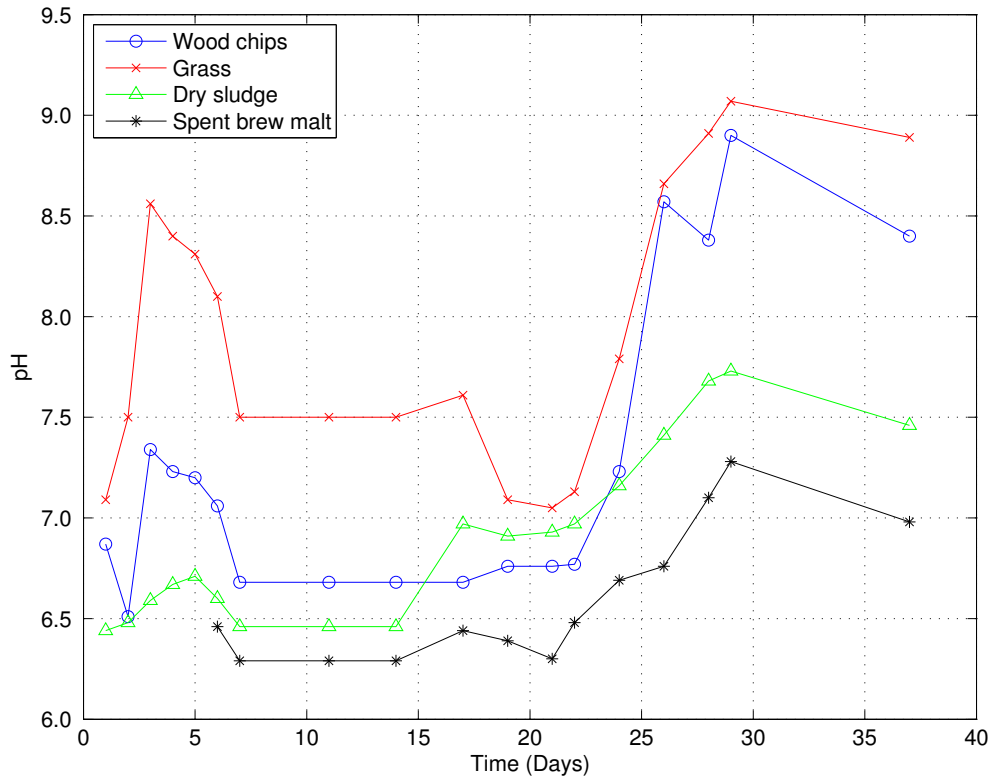


Figure 9.21: pH data of batch bioreactors in VFA liberation kinetics study

Whittington-Jones et al. (2006) demonstrated that hydrolysis and VFA production was enhanced under sulphidogenic conditions and managed to achieve a maximum hydrolysis rate of 4 g/L.day. However, primary sewage sludge was utilised, which has a significantly greater labile organic carbon fraction. Additionally, the experiment was only conducted for eight hours, so the rate of hydrolysis cannot be considered an accurate representation of long-term sewage sludge degradation.

The grass bioreactor reached a maximum degradation rate of 123.11 mg/L.hr within 24 hours, and subsequently decreased until no VFAs were present. This was indicative of the easily hydrolysable fraction being metabolised and the more complex lignocellulose not being degraded. The average total VFA concentration production rate was 49 mg/L.day. Greben et al. (2009) demonstrated a substantially higher VFA production rate at 112.2 mg/L.day, however this was within a reactor that was supplied 1 kg of grass cuttings and received an additional daily 20 g of grass. When there was a reduction in the amount of grass supplied, there was a significant decline in VFA production and sulphate reduction. The system utilised within the study was an 'active' CSTR (with recycle). Therefore, grass is a non-ideal substrate simply due to its recalcitrant nature and low rate of hydrolysis.

The reactor loaded with wood chips showed slightly lower rates, as the average total VFA liberation rate was 43.61 mg/L.day. A study conducted by Yamashita et al. (2011) showed that hydrolysis of wood was slow and limiting, as the sulphate reduction rate was 0.47

g/kg wood.day. On the other hand Roman et al. (2008) managed to achieve a sulphate reduction rate of 0.243 g/kg wood.day. Assuming the VFAs liberated in the wood chips loaded reactor were metabolised completely to acetate and utilised for BSR, the theoretical sulphate reduction rate would be 3.55 g/kg wood.day. The theoretical sulphate reduction rate is significantly higher probably due to the higher temperature (37°C), as it has been shown that hydrolysis is significantly faster at a higher temperature. Yamashita et al. (2011) and Roman et al. (2008) conducted their studies at 20°C and 25°C respectively.

The batch reactor tests showed that the complex carbon sources used to pack the columns could be partially hydrolysed under sulphidogenic conditions and that volatile fatty acids, including acetate, were liberated. However, the rate of VFA liberation was substantially slower than that required to sustain the integrated semi-passive system. A comparison of the COD liberated in the batch tests against the inherent COD of the packing materials demonstrates the very low extent of hydrolysis achieved. The data support the rationale of adding molasses or a similar simple carbon source to the system.

9.11 Effect of phenolic compounds on sulphate-reducing process

9.11.1 Introduction

It has not been conclusively determined whether the low molecular weight phenolic compounds that are produced, as a result of the hydrolysis process of lignin, are inhibitory to sulphate reducing prokaryotes. Roman et al. (2008) demonstrated that the hydrolysis of lignocellulosic materials releases aromatic compounds under methanogenic and sulphidogenic conditions. From the literature review it was shown that SRPs are able to hydrolyse and breakdown phenolic compounds, however the impact of the compound on the BSR process has not been definitively studied. Additionally, the inhibitory (IC_{50}) toxic concentration of catechol to a microbial population can vary from 3 - 2200 mg/L, depending on the microbial species and environmental conditions (Park et al., 2001; Blum & Speece, 1991). The following study was conducted to determine if catechol (1,2-Dihydroxybenzene) and gallic acid (3,4,5-trihydroxybenzoate) are inhibitory to the process of biological sulphate reduction. Gallic acid was tested, due to it being a product of wattle degradation by wattle-tannin-degrading bacteria (*Enterobacter aerogenes* or *Celluomonas*)

9.11.2 Experimental procedure

The study was conducted in magnetically stirred anaerobic Schott bottles (1L). Each bottle was prepared according to Table 9.9. Bottle one was the control whilst, bottles two to five were dosed with either catechol or gallic acid in increasing concentrations of 10, 50,

100 and 1000 mg/L. The experiment was conducted at 37°C, 1 atm. in order to determine if phenolics are inhibitory under ideal BSR conditions.

Table 9.9: Individual components of the batch bioreactor mixture to determine the effect of a phenolic compound on the BSR process.

SRBR sludge	30 mL
Sodium sulphate	2 g
Sodium acetate	2 g
Sulphide solution (1g/L)	20 mL
Phenolic compound	x mg

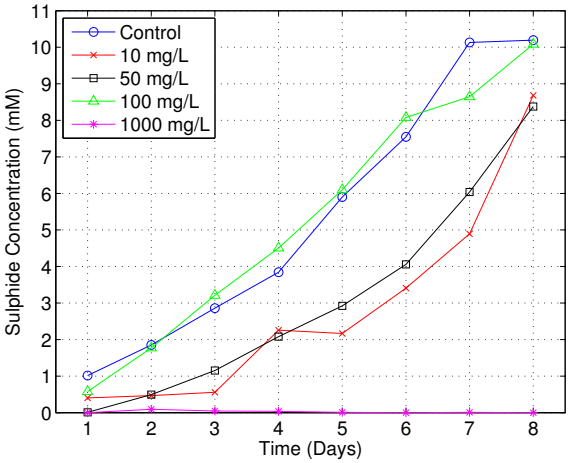
9.11.3 Results and Discussion - Catechol

Sulphide was generated in the control reactor at a rate of 1.45 mmol/L.day to reach a maximum concentration of 10.19 mM. The 10, 50 and 100 mg/L reactors achieved a generation rate of 1.05, 1.14 and 1.39 mmol/L.day respectively (Figure 9.22a). Surprisingly there was an increase in the biological sulphate reduction rate with an increase in catechol. However, at a loading rate of 1000 mg/L no BSR was observed, indicating that the tolerance of the microbial community is between 100 and 1000 mg/L. A volatile fatty acids analysis was conducted in order to understand the observed trends. Based on the amount of sulphide that was generated the theoretical amount of acetic acid consumed was calculated. The analyses showed a greater than expected residual acetate concentration, suggesting that the microbial population either hydrolysed the phenolic compound and utilised the resulting monomers as an organic substrate for the BSR process, or converted the catechol to acetate. No VFAs other than acetic acid were detected. Schink et al. (2000) and Zeyaullah et al. (2009) both presented metabolic pathways for the degradation of catechol, resulting in the formation of benzoyl-CoA or pyruvate/succinate respectively. Pyruvate is only formed in the presence of magnesium ions, and these metabolic pathways have been observed to occur in the presence of SRPs (*Desulfobacterium*) (Harms et al., 1999; Schink et al., 2000). Therefore it is likely the pyruvate was reduced to lactate, by lactate dehydrogenase, for the purposes of biological sulphate reduction.

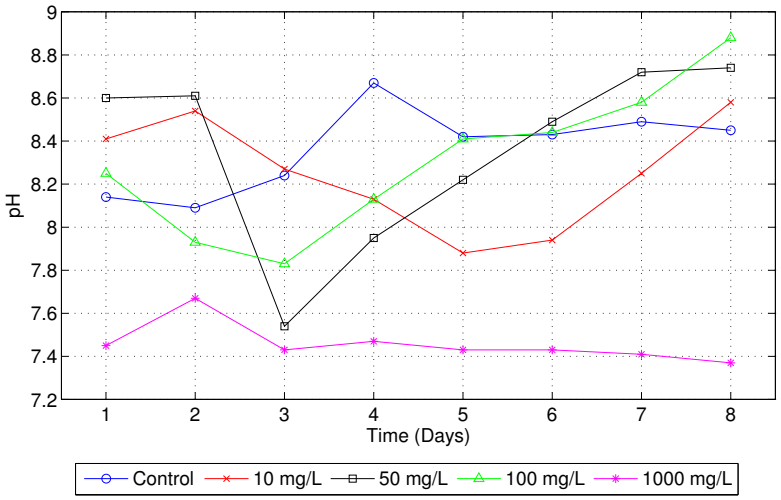
There was an increase in pH, as well as a decrease in redox potential across all bioreactors, except the reactor dosed at 1000 mg/L (Figure 9.22b). No pH increase was observed due to a lack of alkalinity generation from the process of biological sulphate reduction.

9.11.4 Results and discussion - Gallic acid

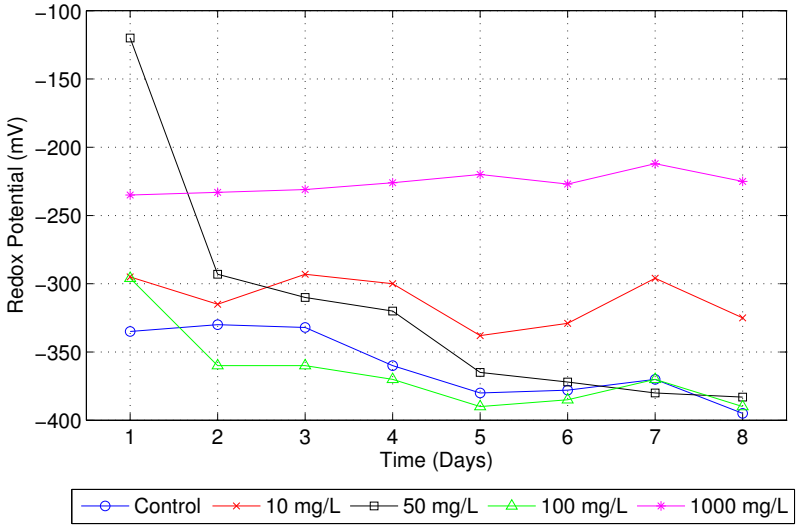
The results for the gallic acid tests showed a similar trend to those for catechol. Sulphide was generated in the control reactor at a rate of 1.59 mmol/L.day to reach a maximum concentration of 4.68 mM within four days. The 10, 50 and 100 mg/L reactors achieved significantly higher rates of 1.45, 2.11 and 2.14 mmol/L.day. This was unexpected as it was



(a) Sulphide concentration (mM) generated

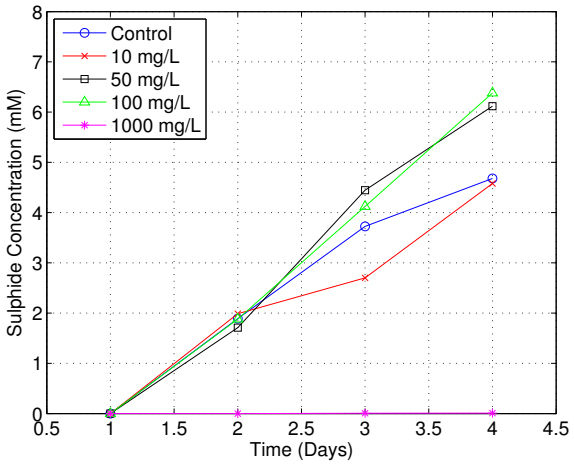


(b) pH of the batch bioreactor fluid

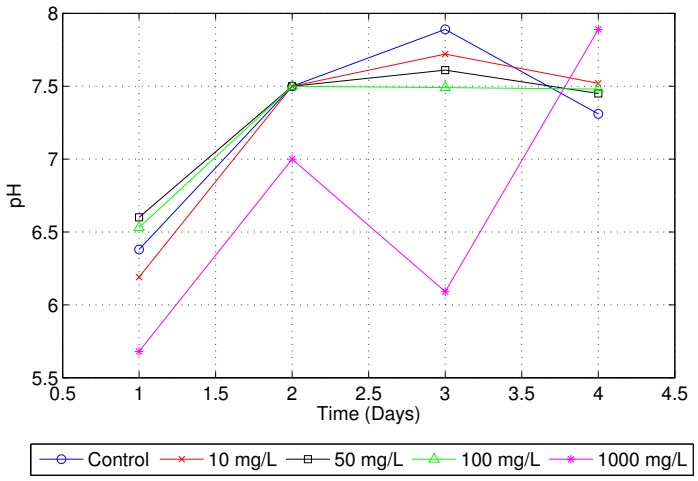


(c) Redox potential (mV) of the batch bioreactor fluid

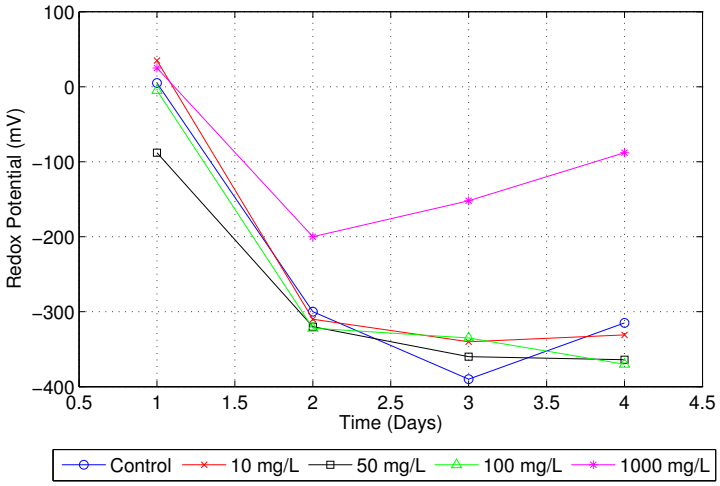
Figure 9.22: Batch bioreactors 1 - 5, with 1 being the control and the rest dosed with catechol at varying concentrations and run for a period of eight days.



(a) Sulphide concentration (mM) generated



(b) pH of the batch bioreactor fluid



(c) Redox potential (mV) of the batch bioreactor fluid

Figure 9.23: Batch bioreactors 1 - 5, with 1 being the control and the rest dosed with gallic acid at varying concentrations and run for a period of four days.

assumed that gallic acid would be more inhibitory than catechol. Once again at a loading rate of 1000 mg/L there was no observed biological sulphate reduction. Therefore, gallic acid at this concentration was inhibitory to the sulphate-reducing microbial population.

The analysis of residual fatty acids again showed that less acetate was consumed than was expected, based on the sulphide generation. Therefore, the only plausible explanation is that the gallic acid was degraded to VFAs to sustain the BSR process. The HPLC analysis indicated the presence of butyric and valeric acids on day 2 (100 mg/L) and 3 (10 mg/L) respectively. Acetic acid was the only VFA added to the reactors initially and no other VFA peaks were observed in the catechol experiment, suggesting that the butyric and valeric acid peaks were products of gallic acid metabolism. Bhat et al. (1998) compiled a comprehensive review of tannin degradation, illustrating a five step metabolic pathway under anaerobic conditions. Gallic acid is firstly decarboxylated to form pyrogallol and thereafter isomerised to phloroglucinol by pyrogallol-phloroglucinol isomerase. Subsequently it is converted to dihydrophloroglucinol, followed by 3-hydroxy-5-oxohexanoate that is degraded further to 3 molecules of Acetyl CoA, or utilised directly in the citric acid cycle. In earlier studies it was shown that rumen bacteria are able to degrade gallic acid to acetate and butyrate.

The study has shown that the microbial consortium present in this study was tolerant of low molecular weight phenolic compounds, such as catechol and gallic acid, to concentrations of at least 100 mg/L. In addition, there is strong evidence to suggest that these compounds were metabolised and the products utilised as electron donors for biological sulphate reduction. While BSR was completely inhibited at 1000 mg/L with both phenolic compounds the concentration of such compounds originating from the degradation of lignocellulosic packing material is likely to be low, due to the slow kinetics and the fact that the phenolics can be degraded. Therefore, it can be concluded that inhibition of sulphate reduction due to phenolic compounds in the packed bed reactors is highly unlikely.

9.12 Final conclusions

From the initial BSR tests, DPBR column study, VFA study and phenolics study, the following conclusions can be drawn. The long-term performance of a passive biological sulphate reduction unit, is dependent on the availability and steady release of soluble dissolved organic carbon, in the form of VFAs. Therefore, the BSR unit would require a substantially greater portion of organic wastes than lignocellulosic wastes. The ideal substrates would be primary sewage sludge and wood chips. If carbon is supplemented via another organic carbon source such as molasses, it must be added so as to not change the operating pH or microbial population. Although, organic carbon supplementation in the form of volatile fatty acids would be far more preferable. This will ensure the pH within the column is reduced, thus preventing the formation of polysulphides at an elevated pH.

Consequently, this could result in the effluent sulphide concentration being more stable and consistent for optimal LFCR performance. The release of aromatic and inhibitory phenolic compounds will occur from the break down of lignin. However, the concentrations necessary for inhibition are extremely high and unlikely (1 g/L). Furthermore, the metabolic products from aromatic degradation can be utilised, by sulphate reducing prokaryotes for BSR.

Chapter 10

Conclusions & recommendations

The primary aim of this investigation was to develop a deeper understanding of the fundamental physical and biochemical processes occurring within the LFCR and to use that to interpret previous research and inform process optimisation. However, it soon became clear that the composition and consistency of the feed to the LFCR were critical factors affecting the hydrodynamics, biofilm formation and consequently LFCR performance. Therefore, a significant amount of work was performed to assess carbon liberation and overall performance of the packed column sulphate reducing reactors. This was done in an effort to provide information that could be used to improve the performance and feasibility of the integrated treatment system.

Initial studies and research on the LFCR were conducted at Golder Associates Research Laboratories (GARL). The data showed efficient sulphide oxidation, but limited recovery of sulphur from the biofilm. It was suggested that loss of sulphide as gaseous hydrogen sulphide could partly account for this. It was determined that the inter-harvest period was influenced by the feed sulphide concentration and that the optimal inter-harvest period was 24 hours. In addition, a longer inter-harvest period allowed for a thicker sticky FSB to develop, whilst a low feed sulphide concentration prevented FSB development.

Critical assessment of the GARL data suggested that vertical stratification of the bulk fluid and subsequent short-circuiting was the most likely explanation for the difference between apparent sulphide oxidation and sulphur recovery. The limited sampling regime contributed to this. The short-circuiting, with a significant portion of the sulphide not being delivered to the biofilm, resulted in the FSB being more organic (brown in colour) and containing significantly less sulphur deposits. For this reason, a study to investigate the relationship between residence time, organic loading rate, FSB development and sulphur yield was performed.

The tools required to analyse the system in greater detail were developed as part of this research. These included an improved LFCR, constructed from Perspex, with multiple (15) sampling ports and inlet/outlet ports to enable the assessment of spatial variation and the visualisation of the bulk liquid. The LFCR lid was fitted with a gasket seal to create a contained system and offgas was passed through a sulphide scrubber, allowing quantification of any sulphide lost as H_2S gas. In addition, analytical techniques were designed and optimised to quantify polysulphides, so that the sulphur balance could be closed. This was achieved within a 10% error during the experimental runs.

The reactors were used to investigate the hydraulic regime in the LFCR using the GARL configuration. Tracer studies confirmed there was significant stratification and plug-flow did not occur. The incoming feed solution sank to the bottom and largely bypassed the reaction zone. As a result, at a theoretical two day residence time, the fluid only resided within the LFCR for a period of 0.33 - 1.21 hours. The LFCR was reconfigured with the outlet port being in line with the inlet port (at position 1 at the liquid surface). This eliminated fluid short-circuiting and at a theoretical two day residence time the fluid resided within the reactor for a period of 48 - 49 hours.

A more rigorous hydrodynamic study was conducted and it was determined that the flow was extremely laminar, more specifically, resembling a stratified liquid-liquid flow pattern of miscible fluids in the laminar regime. The laminar flow on the floor of the reactor was characteristic of laminar-parabolic flow between two parallel plates, as the upper liquid portion was moving slower, hence acting as plate. It was determined that the maximum Reynolds number (Re) was 160 at a volumetric flow rate of 120 L/day, with a corresponding Peclet number (Pe) of 165. Hence, there was significant stratification within the LFCR. The impact of influent density and relative density difference (RDD) on influent velocity, mixing and the maintenance of the correct hydraulic regime was demonstrated. There was an increase in transverse dispersion by diffusion with a decrease in the relative density difference. The use of cylindrical baffles to improve mixing was unsuccessful, as they promoted stagnation and retardation of the laminar liquid flow. The ideal hydraulic regime is one where the incoming sulphide feed sinks to the floor of the channel, creeps along the base of the reactor to the back corner and thereafter rises vertically due to displacement of the denser influent. This hydraulic regime is only present if the RDD is positive. It is necessary as the slow, but consistent delivery of sulphide to the reaction zone ensures that the correct ratio of sulphide to oxygen is maintained, to minimise the formation of sulphate or polysulphides. The lack of this hydraulic regime was demonstrated within a biological system and resulted in the formation of suphate, colloidal sulphur and polysulphides.

An abiotic sulphide oxidation study was conducted to determine the extent of chemical sulphide oxidation. The well-mixed (batch-reactor) abiotic sulphide oxidation study illustrated first order reaction kinetics with regard to sulphide oxidation. The reaction rate constant was substantially lower at pH 11.6 than when the pH was controlled within the range typical of LFCR operation (pH 7 - 8.1). The primary sulphur species formed under abiotic conditions were thiosulphate, polysulphides and colloidal sulphur. The sulphide conversion in the abiotic LFCR was low (24 - 32%) due to the unique hydrodynamics, with little transport of oxygen beyond the interfacial region. Therefore, the presence of a microbial population significantly increased the overall sulphide oxidation efficiency, which was in the range of 80 - 100%. Moreover, chemical sulphide oxidation resulted in different sulphur species-products, such as thiosulphate and polysulphides, whereas a biological system promoted sulphur and sulphate production. This was consistent with published

literature.

The initial biological LFCR experiments confirmed the increased sulphide oxidation rate catalysed by the presence of a microbial population. However, these studies were characterised by poor FSB development, which was attributed to the absence of soluble organic carbon in the SRBR column effluent. The ratio of sulphate to sulphide in the feed was critical as it determined the relative density difference between the feed and bulk liquid. Therefore, efficient performance of the sulphate reduction unit is required to ensure a high sulphide loading and low sulphate concentration and prevent 'floating' of the incoming sulphide feed. Efficient performance would also reduce fluctuations in the ratio of sulphide to sulphate. The microbial ecology study revealed that the FSB was dominated by photoautotrophic organisms, which was consistent with the absence of organic carbon in the feed. The low population of heterotrophic organisms reduced the efficiency of biofilm formation, so performance was compromised. Therefore, subsequent LFCR experiments were supplemented with carbon in the form of acetate.

The bulk of the experimental work assessed the relationship between residence time and LFCR performance with specific regard to sulphur recovery and FSB development. There was a linear increase in LFCR performance (i.e. sulphur recovery) with a corresponding decrease in residence time, down to one day. At a 12 hour residence time delamination and tearing of the lower FSB layers was observed, most likely due to sulphur accumulating faster than the organic backbone of the biofilm was able to support it. The relatively low carbon to sulphur ratio in the biofilm supported this assertion.

The optimal residence time was 1-2 days, characterised by increased sulphur recovery and minimal sulphate production. On average 7.7% of the influent sulphide was converted to sulphate, an unwanted by-product. Additionally, the occurrence of polysulphides was observed when the pH increased above pH 8.1 in the presence of colloidal sulphur.

A change in FSB structure was observed, thickness and porosity with residence time. As residence time decreased there was an observed increase in FSB thickness. At the lower residence times (2, 1.5, 1 & 0.5 days) the FSB formed in layers that were held together by a matrix of organic extracellular polymeric substances. The FSB was constructed in such a manner that an inorganic sulphur layer alternated with an organic layer. Consequently, there was also a decrease in porosity, which inevitably impacted the diffusion of oxygen within the FSB.

Large pod-shaped macrostructures were identified within the FSB matrix and are thought to provide an ideal micro-environment for the sulphide oxidising prokaryotes. Bacteria and nano particles of sulphur were identified within these structures.

The composition of the FSB was not significantly affected by an increase in organic loading and the rate of acetate consumption (0.1-0.5 g/(L.day)) was relatively independent of loading. The carbon content of the recovered biofilm suggested that only 2 - 5% of the consumed acetate was utilised for FSB formation and construction, with the

majority used for cellular metabolism or consumed by cell division in the bulk liquid. The acetate supplementation resulted in a significant increase in microbial diversity, with an additional 32 species identified. These included a large number of chemoheterotrophic and heterotrophic organisms, which positively affected FSB development and structural integrity.

The sulphide oxidation rate decreased with time as the FSB grew thicker and less porous. The sulphide oxidation rate initially increased to reach a maximum before decreasing to zero or an absolute minimum, after approximately four to five residence times. Therefore it would be advantageous to operate the LFCR for three to four residence times followed by FSB harvesting. The dissolved oxygen profiles were observed to be a function of FSB age, spatial variation and porosity. There was greater penetration of oxygen into the FSB (1200 μm depth) at the start of the experiment due to there being less resistance in the form of sulphur deposits and organic biofilm layers. As the FSB grew older there was greater deposition of sulphur and attachment of more layers. Consequently, there was a decrease in porosity and less oxygen was able to penetrate deeper into the FSB, causing a decrease in the oxygen diffusion coefficient and local mass transfer coefficient. The decrease in the oxygen diffusion coefficient was by an order of magnitude, indicating the high resistance to oxygen flux caused by the FSB. Pores and conduits did improve the movement of dissolved oxygen. The dissolved oxygen concentrations varied spatially, due to the heterogeneous nature of the FSB. The theoretically calculated diffusion coefficient of oxygen ($D_{f-exp-run} = 1 \times 10^{-10}$ m^2/s) for the observed sulphide oxidation rate in experimental runs 11-15, did not correlate with the measured diffusion coefficient of oxygen in the FSB ($D_f = 1 \times 10^{-11}$ m^2/s). There was approximately one order of magnitude difference between the figures, which may have been caused by the porosity of the FSB. Therefore, further analysis is required in order to determine the cause for the discrepancy between the diffusion coefficient and that calculated from the observed sulphide oxidation rate.

The packed bed columns received from GARL had been previously operating for almost two years and data from this study indicated relatively limited hydrolysis of the packing material and poor release of VFAs. This resulted in inefficient sulphate reduction and no organic carbon in the effluent. When the columns were unpacked the lignocellulosic material was largely intact, suggesting limited hydrolysis had occurred. This led to the conclusion that a BSR unit packed predominantly with lignocellulosic wastes will not offer reasonable sulphate reduction performance for an extended period of time ($>$ 6 months). The data suggested that the primary sewage sludge will provide the necessary organic substrate for a reasonable sulphate reduction efficiency of approximately 60% during the initial phase. Thereafter, the reactor will fail due to labile organic carbon depletion and the fact that the hydrolysis of the lignocellulosic materials, is not kinetically fast. Therefore, the use of activated sludge or primary sewage sludge in conjunction with lignocellulosic wastes, will be far better suited for a passive sulphate reduction unit. Furthermore, the ratio of organic wastes to lignocellulosic wastes must be greater than 0.33 : 1, to ensure

adequate supply of VFAs for the BSR process. During the current study the packed column containing less lignocellulosic wastes was supplemented with acetate to ensure that suitable feed for the LFCR experiments was generated, but acetate supplementation is not a sustainable nor economically viable solution.

Batch-reactor tests were conducted under sulphidogenic conditions, in the absence of sulphate and with BESA to inhibit methanogenesis, showed that some hydrolysis of the packing materials occurred, resulting in the liberation of VFAs. However, the rate of liberation from cellulosic and lignocellulosic material was significantly slower than from activated sewage sludge.

Batch sulphate reduction tests in the presence of low molecular weight phenolic compounds showed that significant inhibition of sulphate reduction only occurred at high concentrations (>1 g/L). The degradation of lignin in the packed bed reactors was extremely slow, so it is highly unlikely that low molecular weight products could accumulate to inhibitory concentrations. In addition, biodegradation of the phenolic compounds and their utilisation in the BSR process was observed.

In conclusion, the overall semi-passive treatment system can be summarised by a simplified process flow diagram (Figure 10.1). This semi-passive ARD treatment system should be able to achieve 80% or higher sulphate removal efficiency in the sulphate reduction unit, provided there is sufficient soluble organic carbon substrate available ($\geq$1100 mg/L). The LFCR could achieve a sulphide conversion in excess of 85%, with a 7.7% sulphate generation possible at a two-day residence time, with a sulphur recovery varying from 67 - 92%. Therefore, there would an average sulphate conversion of 79.5% across both units. However, due to the production of colloidal sulphur within the SRBR column, the maximum net removal of sulphur species possible was 66% across both units. An inter-harvest period after 3-4 residence times will ensure optimum sulphur recovery. Moreover, the FSB should not be harvested by skimming off the surface. There is a substantial loss of sulphur to the bulk liquid if skimming is conducted. A thin net/mesh (10-20 μm aperture size) suspended in the bulk liquid should be raised upwards to capture the entire FSB. This will ensure all sulphur is captured and not lost, thereafter the FSB can be scraped off the net and reseated within the LFCR. This will also ensure all EPS strand networks anchoring the FSB are broken.

Based on the outcomes of the current study, the following areas of work are recommended for further study, to generate additional data that can be used to improve the LFCR and treatment system:

1. Investigate the effect of temperature on LFCR performance, as the plant will be outdoors and seasonal variation will possibly affect the sulphide oxidation rate.

2. Modify the large-scale LFCR units for a pilot plant, such that sunlight may be minimised to prevent the growth of photoautotrophic organisms. This may be

achieved by covering the top of the LFCR units with a black plastic sheeting, such that it prevents direct sunlight and rain from damaging the FSB.

3. A detailed study of the microbial ecology using FISH/qPCR to assess the distribution of the microbial species within the biofilm and their relative abundance. Additionally, look at the microbial population within the pod macrostructures, so one can speculate on their function.

4. An assessment of the sulphur product is necessary, to determine the potential uses of this valuable product.

5. Design a filter to capture the colloidal sulphur exiting the LFCR in an effort to increase the removal of sulphur species from the effluent water.

6. Conduct a more rigorous carbon balance across the LFCR in order to determine the fate of organic carbon.

7. Conduct an additional carbon balance study utilising a more economical and easily available soluble organic carbon source at various organic loadings.

8. Conduct the abiotic sulphide oxidation experiments in triplicate in order to provide further validation of chapter 7. Additionally, it would be advantageous to further investigate the rate constant with regard to sulphide oxidation, as well as the equilibrium constant with respect to polysulphide speciation.

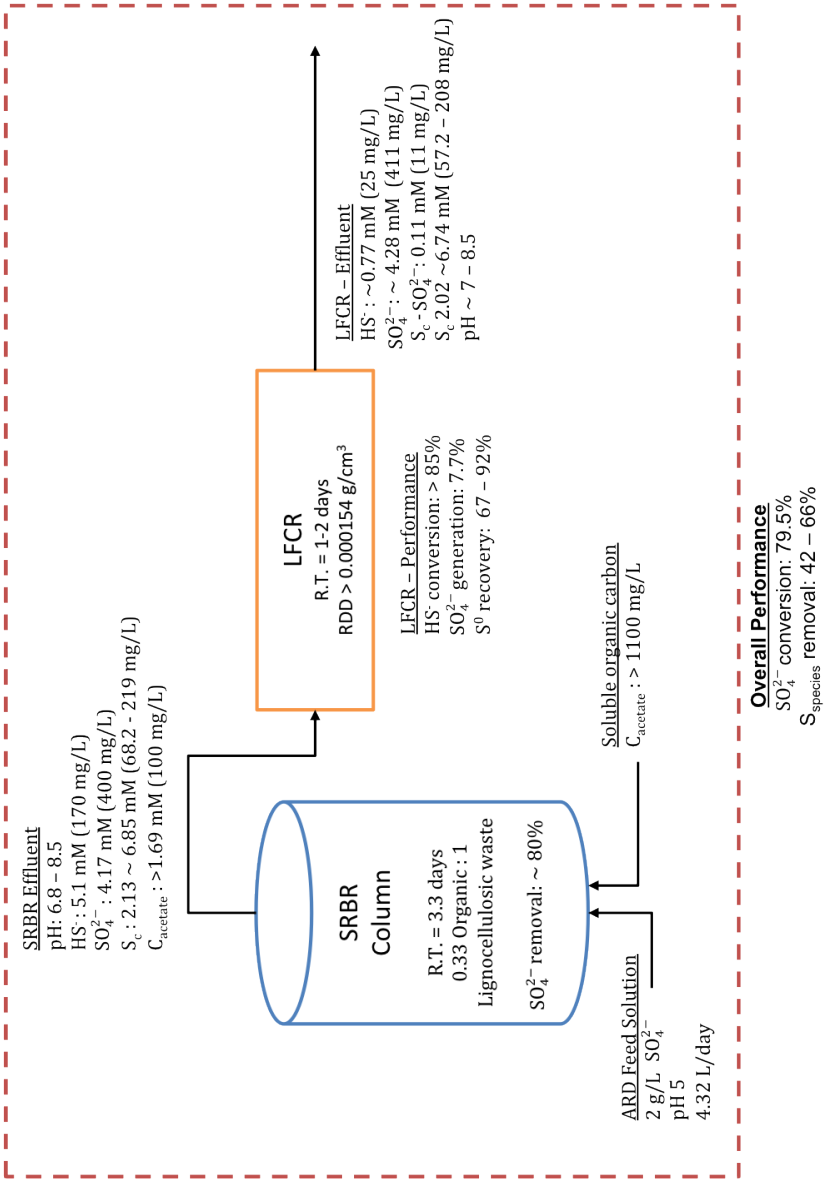


Figure 10.1: Simplified process flow diagram of an optimised Integrated managed passive treatment system. The sulphate conversion efficiency of the first unit (SRBR column) is 80%, with the generation of sulphate within the second unit (LFCR). Hence, the overall sulphate conversion efficiency was 79.5%, with a maximum removal of sulphur species from the ARD being 66%. S_c: Colloidal sulphur, S_c-SO_4^{2-}: Colloidal sulphur which was oxidised to sulphate within the LFCR.

Appendix A

Analytical methods

A.1 Polysulphides assay protocol

A.1.1 Experimental Apparatus

Erlenmeyer Flask (x5)	H_2S gas scrubber
2 Magnetic Stirrers (including heating pads)	Dessicator
Nitrogen source and necessary tubing	Condensor (x2)
Ice Water bath	Vacuum filter unit

$M_{Potassium}$= 39.0983 g/mol and $M_{ethanol}$ = 46.08 g/mol. $n_{potassium}$ = 0.0512 mols and $n_{ethanol}$ = 0.514 mols. $\rho_{ethanol}$ = 0.789 g/cm^3.

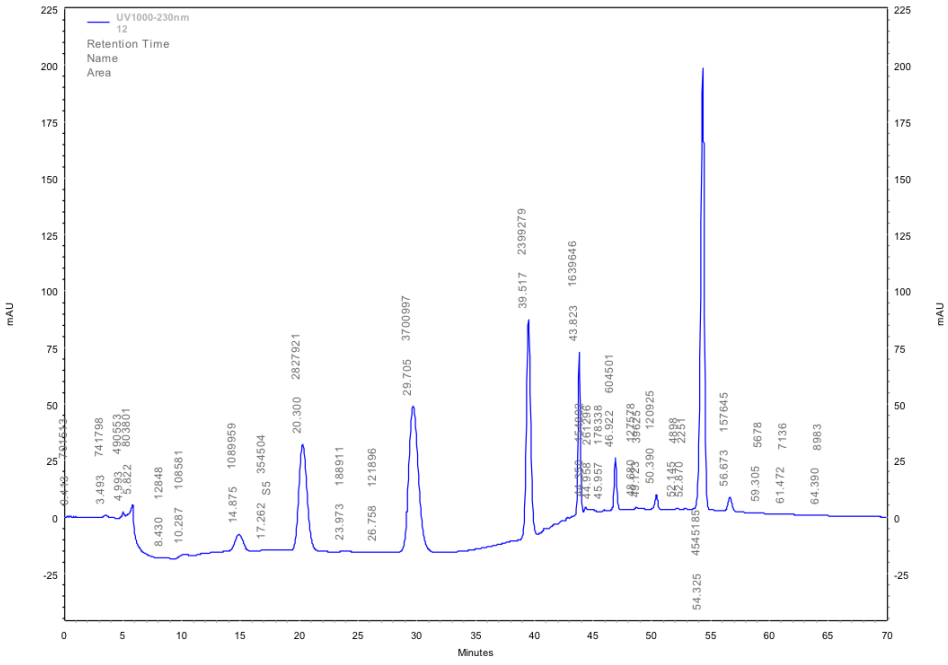


Figure A.1: High performance liquid chromatography analysis of polysulphide standard, illustrating species of chain length 3-11 and the internal standard at a retention time of 54 minutes.

A.2 Hydrogen sulphide assay

A.2.1 Reagent preparation

A.2.1.1 N,N-dimethyl-p-phenylene diamine dihydrochloride solution

1. 2 g N,N-dimethyl-p-phenylene diamine dihydrochloride
2. 267 mL concentrated hydrochloric acid (32 wt%)
3. 233 mL dH_2O

A.2.1.2 Ferric chloride solution

1. 8 g Ferric chloride
2. 267 mL concentrated hydrochloric acid (32 wt%)
3. 233 mL dH_2O

A.2.2 Hydrogen sulphide standard curve

The following curve was generated by diluting a 250 mg/L hydrogen sulphide standard solution down to 1 mg/L. This is due to the fact that the ideal range for determining sulphide concentrations is 0 - 1 mg/L.

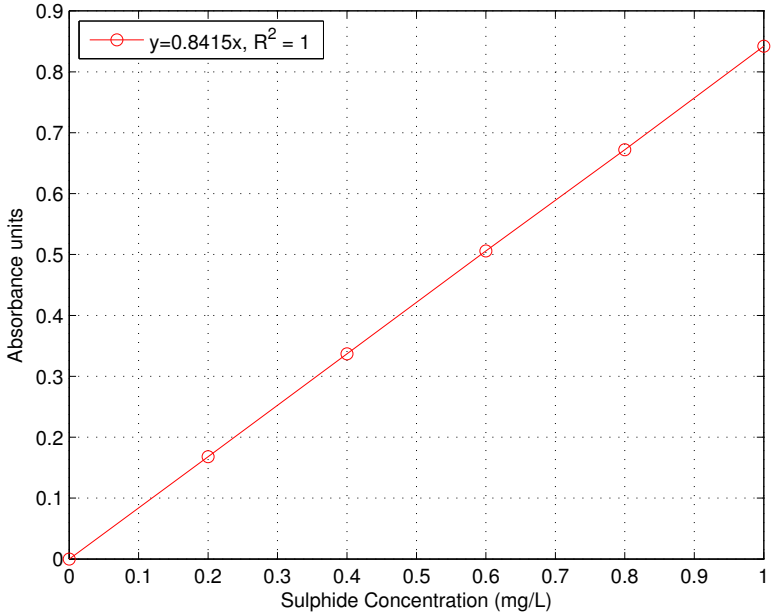


Figure A.2: Hydrogen sulphide standard curve for the concentration range 0 - 1 mg/L

A.3 Sulphate assay

A.3.1 Mobile phase preparation

A.3.1.1 Sodium Borate-Gluconate stock solution (1L)

1. 16g Sodium gluconate
2. 18g Boric acid
3. 25g sodium tetraborate decahydrate
4. Add 750 mL dH_2O and mix until the above salts dissolve
5. Add 250 mL glycerol and mix throughly
6. Thereafter filter solution and autoclave in order to prevent the growth of fungus

A.3.1.2 Moblie phase solution (1L)

1. 500 mL of dH_2O to a schott bottle
2. 20 mL Sodium borate-gluconate stock solution
3. 20 mL 1-Butanol (HPLC grade)
4. 120 mL Acetonitrile (HPLC grade)
5. 340 mL dH_2O

A.3.2 Sulphate standard curve

The following standard curve was generated by running a set of sulphate standards at the beginning and end of each sample sequence.

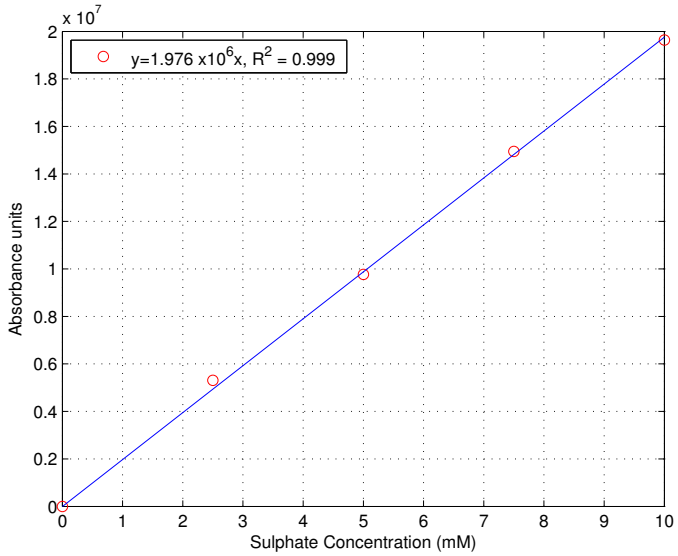


Figure A.3: Sulphate standard curve for the concentration range 0-10 mM

A.4 Sulphur assay standard curve

The following standard curve was generated by running a set of sulphur standards at the beginning and end of each sample sequence. The sulphur standard solution was created by dissolving 240.5 mg of S_8 sulphur into 1L of chloroform (100%). This was achieved by stirring the solution continously on a heated magnetic stirrer (45 $^\circ$C) for 5 days. Thereafter the solution was vacuum filtered through 0.22 μm Millipore hydrophobic filtration membrane and stored within a schott bottle.

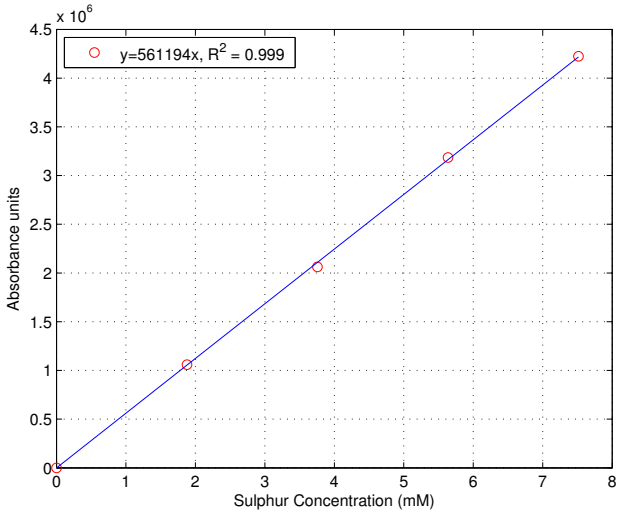


Figure A.4: Sulphur standard curve for the concentration range 0 - 7.516 mM

A.5 Thiosulphate assay standard curve

The following standard curve was generated by running a set of thiosulphate standards at the beginning and end of each sample sequence. Sodium thiosulphate was used to make up a standard solution.

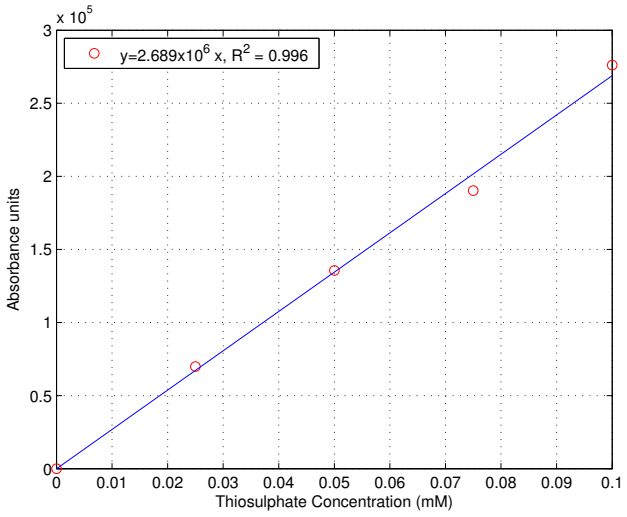


Figure A.5: Thiosulphate standard curve for the concentration range 0-0.1 mM

A.6 Volatile Fatty acids (VFAs) assay

The following standard curves were generated by running a set of VFA standards at the beginning and end of each sample sequence. Sodium lactate was utilised to make up a standard solution.

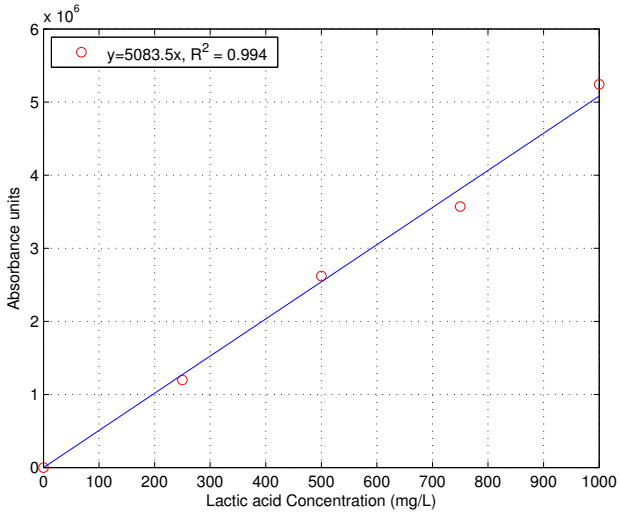


Figure A.6: Lactic acid standard curve for the concentration range 0 - 1000 mg/L

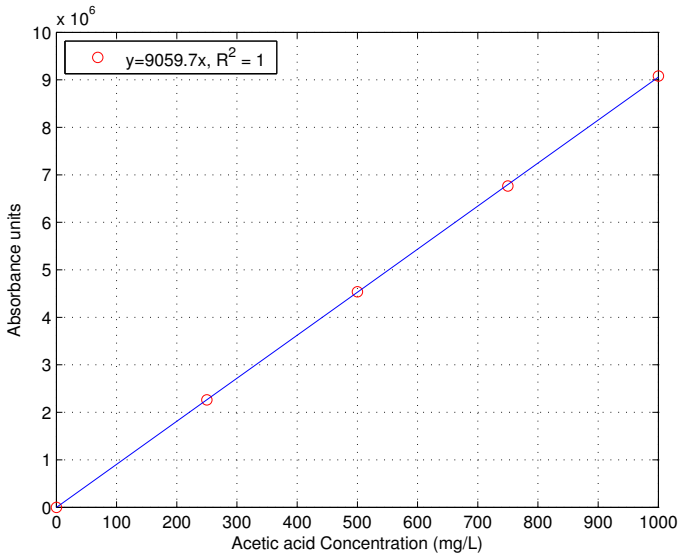


Figure A.7: Acetic acid standard curve for the concentration range 0 - 1000 mg/L

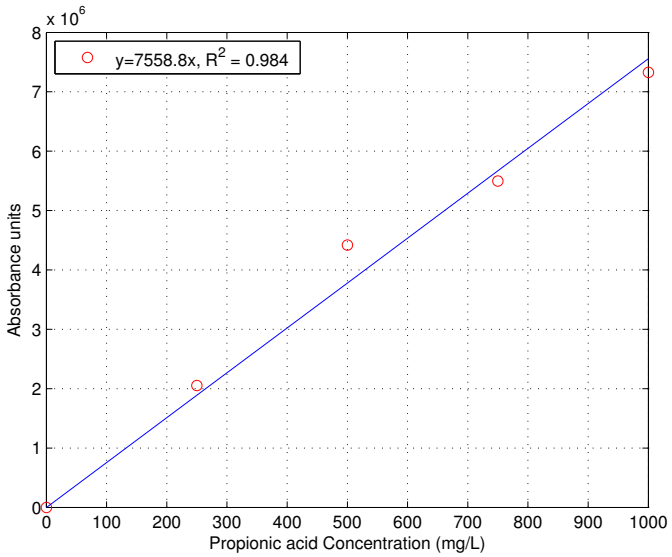


Figure A.8: Propionic acid standard curve for the concentration range 0 - 1000 mg/L

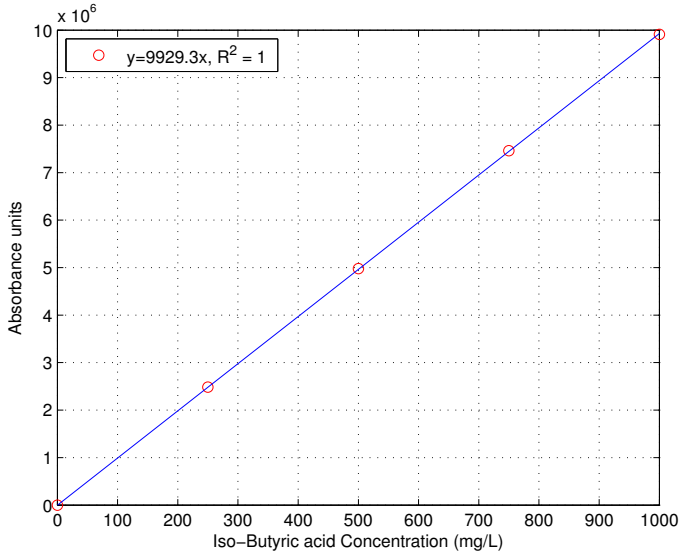


Figure A.9: Iso-butyric acid standard curve for the concentration range 0 - 1000 mg/L

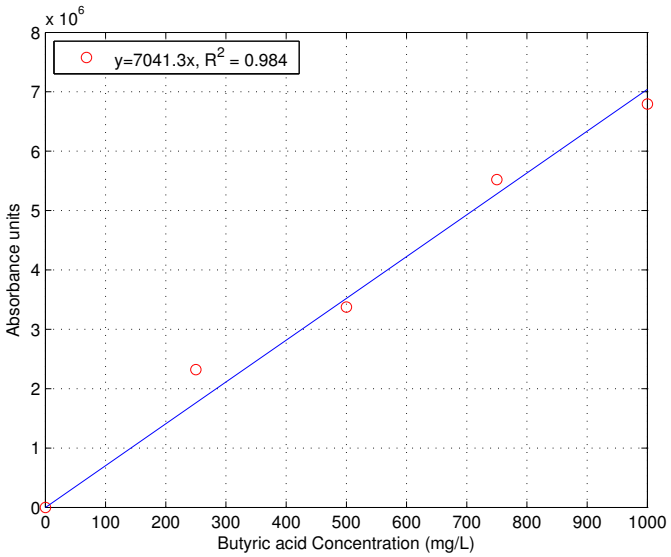


Figure A.10: Butyric acid standard curve for the concentration range 0 - 1000 mg/L

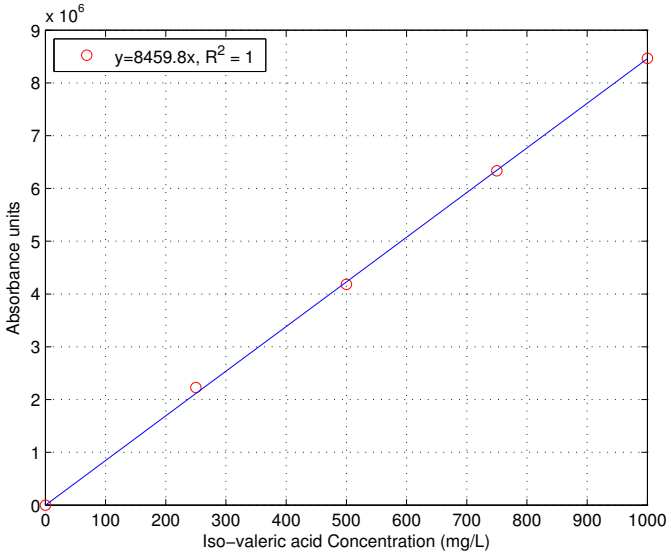


Figure A.11: Iso-valeric acid standard curve for the concentration range 0 - 1000 mg/L

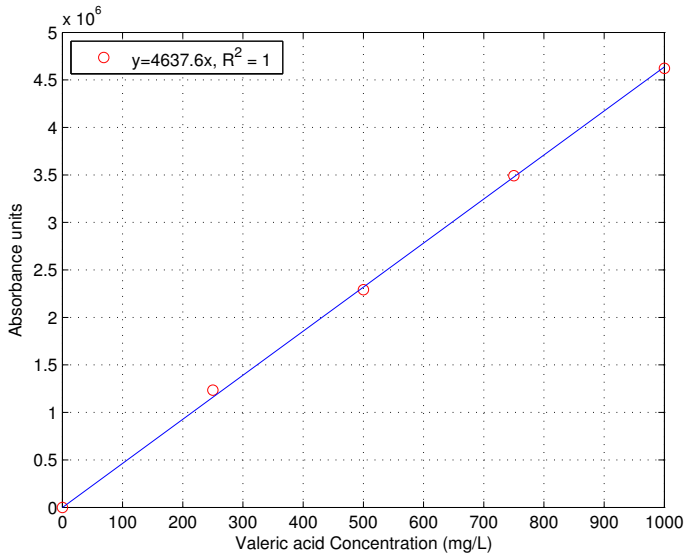


Figure A.12: Valeric acid standard curve for the concentration range 0 - 1000 mg/L

A.6.1 VFAs chromatogram

Each VFA compound elutes at a specific time provided the HPLC is operated as described in chapter 3.

Table A.1: Elution times of all seven volatile fatty acid compounds

Compound	Elution time (mins)
Lactic acid	13.1
Acetic acid	15.79
Propionic acid	18.67
Iso-butyric acid	20.97
Butyric acid	23.18
Iso-valeric acid	26.77
Valeric acid	34.03

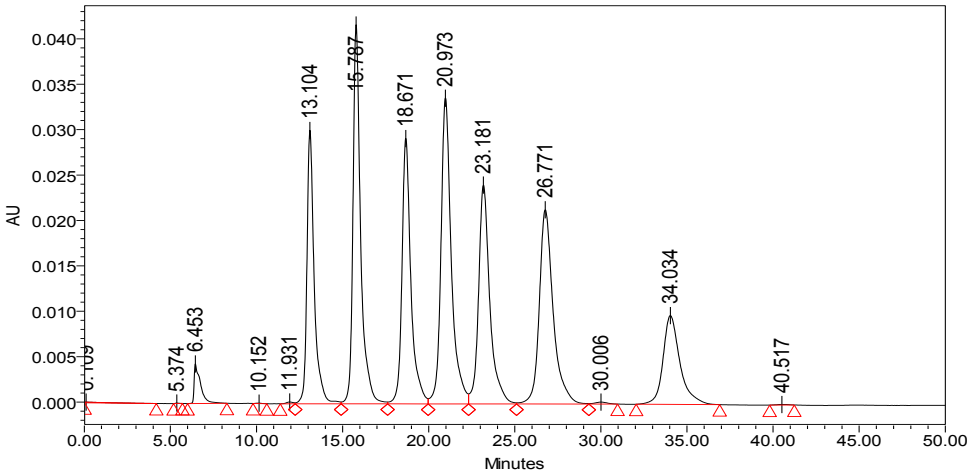


Figure A.13: High performance liquid chromatography chromatogram of volatile fatty acid compounds

A.7 Error analysis

An error analysis was conducted on all samples that were analysed by HPLC. All HPLC analyses were conducted to an accuracy range of 0 - 0.1% (Chapter 3).

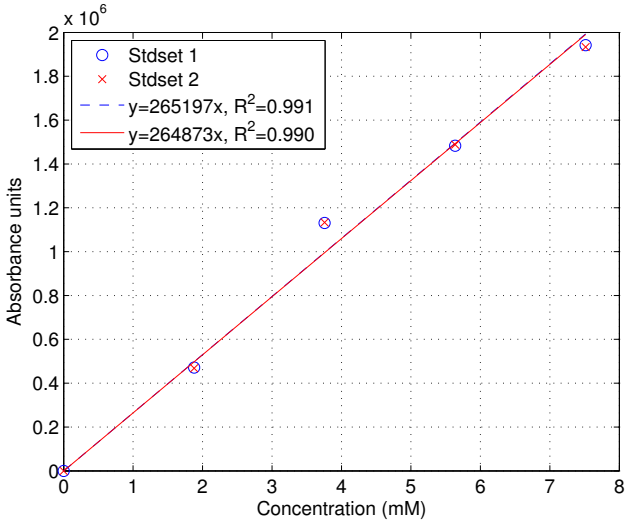


Figure A.14: HPLC sulphur concentration standard curve, for a set of standards at the start (1) and end (2) of an analytical run. The error between the two standards is 0.1 %.

A.8 Molecular methods

A.8.1 50X TAE Buffer

1. 242 g Tris
2. 57.1 mL Glacial acetic acid
3. 10 mL 0.5M EDTA
4. 932.9 mL dH_2O

A.9 Sulphur material balance formula

The following formula was utilised in determining the percent difference (error) between measured sulphide converted and the sum of all the sulphur species products (in mmol).

$$S^{\%} = \frac{HS^-_{converted} - \left\{S_{colloidal} + SO_4^{2-} + S_{Biofilm} + S_{solids} + S_x^{2-}\right\}}{\frac{HS^-_{converted} + \left[S_{colloidal} + SO_4^{2-} + S_{Biofilm} + S_{solids} + S_x^{2-}\right]}{2}} * 100$$

Appendix B

Microbial community structure study

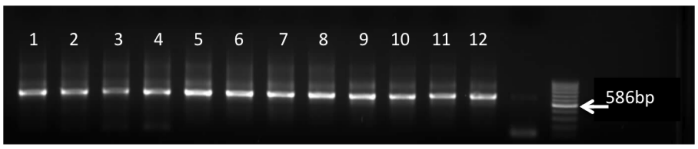


Figure B.1: A 0.8% agarose gel showing 586bp amplified polymerase chain reaction products of samples 1-4 at three different temperatures 55 (lanes 1-4), 60 (5-8) and 65°C (9-12).

Table B.1: Summary of the floating sulphur biofilm samples from experimental runs 14 and 15, identified in the National Centre for Biotechnology Information database. Showing the sample number, clone number, family, genus and the one/two closest species identified and associated percentage similarities to isolate. The percentages given are the percentage homology between the sequence sent in for BLAST and the actual species listed on the NCBI database.

No.	Clone No.	Family; Genus	Closest species	Percentage similarity of isolate
1	1A	Uncultured bacteria	Uncultured bacterium clone 4-109	92%
		Epsilonproteobacteria	Uncultured bacterium clone MS 11-87	92%
	1B	*Desulfovibrionaceae; Desulfovibrio*	Uncultured *Desulfovibrio sp.*	98%
	1C	*Synergistetes; Cloacibacillus*	Uncultured *Cloacibacillus sp.*	99%
		Uncultured bacteria	Uncultured *Synergistetes* bacterium	99%
	13A	Uncultured bacterium	Uncultured bacterium clone BicL_E08	99%
		Comanoadaceae; Hydrogenophaga	*Hydrogenophaga sp.* TR7-01	99%
	13B	*Rhodobacteraceae; Haematobacter*	*Haematobacter sp.* LM6	99%
			Haematobacter massiliensis strain 19	98%
2	2B	Uncultured *Cloacibacillus sp.*	Uncultured *Cloacibacillus sp.* clone	99%
		Uncultured bacteria	Uncultured *Synergistetes* bacterium	99%
	2C	*Rhodospirillaceae; Insolitispirillum*	*Insolitispirillum peregrinum subsp. integrum*	93%
	14B	*Geobacteraceae; Geobacter*	*Geobacter thiogenes*	99%
		Uncultured bacterium	Uncultured bacterium clone NK-M22	99%
	14D	Uncultured bacterium	Uncultured bacterium clone B15	99%
		Bacteroidaceae; Bacteroides	Uncultured *Bacteroides sp.* clone MDAF2	99%
3	3C	*Rhodobacteraceae; Rhodobacter*	*Rhodobacter sphaeroides* strain P230(1)	92%
		Uncultured bacterium	Uncultured Alphaproteobacterium clone	92%
	15A	*Hydrogenophilaceae; Thiobacillus*	*Thiobacillus sp.*	95%
		Halothiobacillaceae; Halothiobacillus	*Halothiobacillus sp.* ST15	95%
	15B	*Halothiobacillaceae; Halothiobacillus*	*Halothiobacillus sp.* NP37	96%
	15D	*Oxalobacteraceae; Herbaspirillum*	*Herbaspirillum huttiense subsp. putei*	99%
			Herbaspirillum huttiense strain RS116	99%
	15E	Uncultured bacterium	Uncultured bacterium clone T14	94%
	15F	Uncultured bacterium	Uncultured Spirochaetes bacterium	93%

Table B.2: Summary of the floating sulphur biofilm samples from experimental runs 16-(2) and 16-(3), identified in the National Centre for Biotechnology Information database. Showing the sample number, clone number, family, genus and the one/two most likely species identified and associated percentage similarities to isolate.

No.	Clone No.	Family; Genus	Closest species	Percentage similarity of isolate
4,5,6	4A, 5A, 6A	*Chlorobiaceae; Chlorobium*	*Chlorobium phaeobacteroides*	99%
	4B, 5B, 6B		*Chlorobium limicola*	99%
4	16A	Uncultured bacterium	Uncultured bacterium clone EMIRGE_OTU_s7t4e_459	92%
		Spirochaetaceae; Spirochaeta	*Spirochaeta africana* strain Z-7692	91%
4	16E	Uncultured bacterium	Uncultured Spirochaetes bacterium	98%
5	17D	Deltaproteobacteria	Uncultured bacterium clone MS4-91	97%
6	18C	Uncultured bacterium	Uncultured bacterium clone RL202_aai49f01	92%
7	7A	Uncultured Bacteroidetes bacterium	Uncultured *Bacteroidetes* bacterium clone S6B_88	99%
		Porphyromonadaceae; Paludibacter	*Paludibacter propionicigenes* WB4	97%
	7B	Uncultured bacterium	Uncultured bacterium clone B16_B10	91%
8	8A	Uncultured bacterium	Uncultured bacterium clone SYNH02_C3-07B-065	99%
		Fusobacteria	Uncultured *Fusobacterium* clone 2-F6	99%
9	9A	*Pseudomonadaceae; Pseudomonas*	Pseudomonas sp. HY-14	100%
			Sulfide-oxidizing bacterium N9-1	100%
	9B	Uncultured bacterium	Uncultured rumen bacterium clone	99%
			Uncultured Firmicutes bacterium clone p1k06cow63	98%
	9C	*Prevotellaceae; Prevotella*	*Prevotella sp.* RM13	100%
		Uncultured bacterium	Uncultured rumen bacterium clone L406RC-1-E02	100%
	9D	*Pseudomonadaceae; Pseudomonas*	*Pseudomonas marginalis* strain LnSQ5	100%

Table B.3: Summary of the LFCR stock culture inoculum and experimental run 6 FSB samples, identified in the National Centre for Biotechnology Information database. Showing the sample number, clone number, and the most likely species identified and associated percentage similarities to isolate.

No.	Clone No.	Closest species	Percentage similarity of isolate
10	10A	*Thiomonas intermedia*	99%
	10B	*Chlorobium limicola*	99%
	10C	*Chromatium okenii*	97%
	10D	*Cupriavidus metallidurans*	99%
	10E	*Desulfovibrio sulfodismutans*	94%
	10F	*Spirochaeta sp.*	99%
11	11A	*Geobacter thiogenes*	97%
	11B*	*Methanomethylovorans sp.*	99%
	11C*	*Spirochaeta sp.*	94%

* qPCR (16S bact. primer)

Bibliography

Absolom, D., Lamberti, F., Policova, Z., Zingg, W., van Oss, C. & Neumann, A. (1983). 'Surface thermodynamics of bacterial adhesion'. *Applied and Environmental Microbiology* **46**(1):90–97.

Akcil, A. & Koldas, S. (2006). 'Acid Mine Drainage (AMD): causes, treatment and case studies'. *Journal of Cleaner Production* **14**(12-13):1139–1145.

Al-Zuhair, S., El-Naas, M. & Al-Hassani, H. (2008). 'Sulfate inhibition effect on sulfate reducing bacteria'. *Journal of biochemical technology* **1**(2):39–44.

Altschul, S., Gish, W., Miller, W., Myers, E. & Lipman, D. (1990). 'Basic local alignment search tool'. *Journal of molecular biology* **215**:403–410.

Amann, R., Stromley, J., Devereux, R., Key, R. & Stahl, D. (1992). 'Molecular and microscopic identification of sulfate-reducing bacteria in multispecies biofilms'. *Applied and Environmental Microbiology* **58**(2):614–623.

Amend, J., Edwards, K. & Lyons, T. (2004). *Sulfur Biogeochemistry: Past and Present*. The Geological Society of America.

Anderson, G., Palermo, J., Schilling, J., Roth, R., Heuser, J. & Hultgren, S. (2003). 'Intracellular bacterial biofilm-like pods in urinary tract infections'. *Science* **301**(105):105–107.

Andreasen, K., Petersen, G., Thomsen, H. & Strube, R. (1997). 'Reduction of nutrient emission by sludge hydrolysis'. *Water Science and Technology* **35**:79–85.

Anglo Coal (2009). 'eMalahleni water reclamation plant - Towards zero disposal'. Tech. rep., Anglo Coal.

Annachhatre, A. & Suktrakoolvait, S. (2001). 'Biological sulfate reduction using molasses as a carbon source'. *Water Environment research* **73**:118–125.

APHA, Rice, E., Water Works Association, A., Baird, R., Eaton, A., Wef & Clesceri, L. (2012). *Standard methods for examination of water and wastewater*. American Public Health Association, 22 edn.

Appels, L., Baeyens, J., Degreve, J. & Dewil, R. (2008). 'Principles and potential of the anaerobic digestion of waste-activated sludge'. *Progress in energy and combustion science* **34**:755–781.

Ashton, P. & Dabrowski, J. (2011). 'An overview of surface water quality in the Olifants River catchment'. Wrc report no. kv293/11, Water Research Commission.

ATSDR (2006). 'Toxicological profile for hydrogen sulfide'. Tech. rep., U.S. Department of health and human services.

Azrina, M., Yap, C., Ismail, A. & Tan, S. (2006). 'Anthropogenic impacts on the distributiom and biodiversity of benthic macroinvertebrates and water quality of the Langat River, Peninsular Malaysia'. *Ecotoxicology and environmental safety* **64**(1):337–347.

Bae, D., Kumar, H., Han, J., Kim, J., Kim, K., Kwon, Y. & An, K. (2010). 'Integrative ecological health assessments of an acid mine stream and in situ pilot tests for wastewater treatments'. *Ecological Engineering* **36**(1).

Bak, F. & Pfennig, N. (1987). 'Chemolithotrophic growth of Desulfovibrio sulfodismutans sp. nov. by disproportionation of inorganic sulphur compounds'. *Archives of microbiology* **147**:184–189.

Banciu, H., Sorokin, D., Tourova, T., Galinski, E., Muntyan, M., Kuenen, J. & Muyzer, G. (2008). 'Influence of salts and pH on growth and activity of a novel facultatively alkaliphilic, extremely salt-tolerant, obligately chemolithoautotrophic sulfur-oxidizing Gammaproteobacterium Thioalkalibacter halophilus gen. nov., sp. from South-Western Siberian soda lakes'. *Extremophiles* **12**:391–404.

Barley, R., Hutton, C., Brown, M., Cusworth, J. & Hamilton, T. (2005). 'Trends in biomass and metal sequestration associated with reeds and algae at Wheal Jane Biorem pilot passive treatment plant'. *Science of the total environment* **338**:107–114.

Basu, R., Clausen, E. & Gaddy, J. (1996). 'Biological conversion of hydrogen sulphide into elemental sulphur'. *Environmental progress* **15**(2):234–238.

Beauchamp, R., Bus, J. & Popp, J. (1984). 'A critical review of literature on hydrogen sulfide toxicity'. *Critical review of toxicology* **13**:25–97.

Bell, F., Bullock, S., Halbich, T. & Lindsay, P. (2001). 'Environmental impacts associated with an abandoned mine in the Witbank Coalfield, South Africa'. *International journal of coal geology* **45**:195–216.

Benschop, A., Ghonim, Z., Wolschlag, L. & van Heeringen, G. (2004). 'Biological process removes sulphur from three refinery streams'. In *ERTC 9th annual meeting*.

Beyenal, H. & Lewandowski, Z. (2000). 'Combined effect of substrate concentration and flow velocity on effective diffusivity in biofilms'. *Water Research* **34**(2):528–538.

Beyenal, H. & Lewandowski, Z. (2002). 'Internal and external mass transfer in biofilms grown at various flow velocities'. *Biotechnology Progress* **18**(1):55–61.

Bhat, T., Singh, B. & Sharma, O. (1998). 'Microbial degradation of tannins - a current perspective'. *Biodegradation* **9**:343–357.

Biorad (2012). 'Guide to Aminex HPLC columns'.

Bird, R. B., Stewart, W. & Lightfoot, E. (2002). *Transport Phenomena*. John Wiley & Sons Limited, 2nd edn.

Blum, D. & Speece, R. (1991). 'A database of chemical toxicity to environmental bacteria and its use in interspecies comparisons and correlations'. *Research journal of the water pollution control federation* **63**(3):198–207.

Boshoff, G., Duncan, J. & Rose, P. (2004). 'Tannery effluent as a carbon source for biological sulphate reduction'. *Water Research* **38**:2651–2658.

Boulegue, J. & Michard, G. (1978). 'Constantes de formation des ions polysulfures S6, S5 et S4 en phase aqueuese'. *Journal of Hydrology* **9**:27–33.

Bouwer, E. & McCarty, P. (1983). 'Effects of 2-Bromoethanesulfonic acid and 2-Chloroethanesulfonic acid on acetate utilization in a continuous-flow methanogenic fixed-film column'. *Applied and Environmental Microbiology* **45**(4):1408–1410.

Bowker, M. (2002). 'The biology and molecular ecology of floating sulphur biofilms'. Master's thesis, Rhodes University.

Brenner, D., Krieg, N. & Staley, J. (2004). *Bergey's manual of Systematic bacteriology*. Springer.

Broderius, S. & Smith, Jr, L. (1977). 'Direct determination and calculation of aqueous hydrogen sulfide'. *Analytical Chemistry* **49**(3):424–428.

Buisman, C., Bloembergen, J. & Paalvast, C. (1993). 'Biological sulphur recovery from paper mill effluent'. In *TAAPI proceedings*, p. 841.

Buisman, C. J., Geraats, B. G., Ijspeert, P. & Lettinga, G. (1990a). 'Optimization of sulphur production in a biotechnological sulphide-removing reactor'. *Biotechnology and Bioengineering* **35**(1):50–56.

Buisman, C. J., Ijspeert, P., Hof, A. & Janssen, A. J. (1991). 'Kinetic parameters of a mixed culture oxidizing sulfide and sulfur with oxygen'. *Biotechnology and Bioengineering* **38**(1):813–820.

Buisman, C. J., Janssen, A. J. & Lettinga, G. (1990b). 'Kinetics of chemical and biological sulphide oxidation in aqueous solutions'. *Water Research* **24**(5):667–671.

Buisman, C. J., Post, R., Ijspeert, P., Geraats, G. & Lettinga, G. (1989). 'Biotechnological process for sulphide removal with sulphur reclamation'. *Acta Biotechnology* **3**(1):255–267.

Cardoso, R., Alvarez, R., Rowlette, P., Flores, E., Gomez, J. & Field, J. (2006). 'Sulfide oxidation under chemolithoautotrophic conditions'. *Biotechnology and Bioengineering* **95**(6):1148–1157.

Chakraborty, J., Verma, N. & Chhabra, R. (2004). 'Wall effects in flow past a circular cylinder in a plane channel: a numerical study'. *Chemical engineering and processing* **43**:1529–1537.

Chang, I., Shin, P. & Kim, B. (2000). 'Biological treatment of acid mine drainage under sulphate reducing conditions with solid waste materials as substrate'. *Water Research* **34**(4):1269–1277.

Chatwin, P. & Sullivan, P. (1982). 'The effect of aspect ratio on the longitudinal diffusivity in rectangular channels'. *Fluid Mechanics* **120**:347–358.

Chen, C. & Meiburg, E. (1996). 'Miscible displacements in capillary tubes. Part 2. Numerical simulations'. *Journal of fluid mechanics* **326**:57–90.

Chen, K. & Morris, J. (1972). 'Kinetics of oxidation of aqueous sulfide by oxygen'. *Environmental Science and Technology* **6**(6):529–537.

Chen, L., Tu, J. & Yeoh, G. (2007a). 'Numerical simulation of turbulent wake flows behind two side-by-side cylinders'. *Journal of fluids and structures* **18**:387–403.

Chen, Y., Jiang, S., Yuan, H., Zhou, Q. & Gu, G. (2007b). 'Hydrolysis and acidification of waste activated sludge at different pHs'. *Water Research* **41**:683–689.

Cheng, S., Grosse, W., Karrenbrock, F. & Thoennessen, M. (2002). 'Efficiency of constructed wetlands in decontamination of water polluted by heavy metals'. *Ecological Engineering* **18**(1):317–325.

Cheong, Y., Min, J. & Kwon, K. (1998). 'Metal removal efficiencies of substrates for treating acid mine drainage of the Dalsung mine, South Korea'. *Journal of Geochemical Exploration* **64**:147–152.

Christensen, B., Laake, M. & Lien, T. (1996). 'Treatment of acid mine water by sulphate-reducing bacteria; Results from a bench scale experiment'. *Water Research* **30**(7):1617–1624.

Cline, J. & Richards, F. (1969). 'Oxygenation of hydrogen sulfide in seawater at constant salinity, temperature and pH'. *Environmental Science and Technology* **3**(9):838–843.

Cocos, I., Zagury, G. J., Clement, B. & Samson, R. (2002). 'Multiple factor design for reactive mixture selection for use in reactive walls in mine drainage treatment'. *Water Research* **32**(1):167–177.

Coetser, S., Heath, R., Molwantwa, J., Rose, P. & Pulles, W. (2005). 'Implementing the degrading packed bed reactor technology and verifying the longterm performance of passive treatment plants at Vryheid Coronation Colliery'. Report no. 1348/1/05, Water Research Commission.

Cooper, C., Bury, N. & Grosell, M. (2006). 'The effects of pH and iron redox state on iron uptake in the intestine of a marine teleost fish, gulf toadfish (Opsanus beta)'. *Comparative biochemistry and physiology, Part A* **143**(1):292–298.

Costerton, J. (2000). 'Biofilms in the new millennium: musings from a peak in Xanadu'. In Press, C. U. (ed.), *Community structure and cooperation in biofilms*, vol. 59, pp. 329–360.

Costerton, J. (2007). *The biofilm primer*. Springer.

Costerton, J., Lewandowski, Z., Caldwell, D., Korber, D. & Lappin-Scott, H. (1995). 'Microbial biofilms'. *Annual Review of Microbiology* **47**(1):711–745.

Cunningham, A., Visser, E., Lewandowski, Z. & Abrahamson, M. (1995). 'Evaluation of a Coupled Mass Transport-Biofilm Process Model using Dissolved Oxygen Microsensors'. *Water Science and Technology* **32**(8):107–114.

Cussler, E. (2009). *Diffusion: Mass transfer in fluid systems*. Cambridge University Press, 3rd edn.

Davey, M. & O'Toole, G. A. (2000). 'Microbial biofilms: from ecology to molecular genetics'. *Microbiology and molecular biology reviews* **64**(4):847–867.

de Beer, D., Stoodley, P. & Lewandowski, Z. (1994a). 'Liquid flow in heterogenous biofilms'. *Biotechnology and Bioengineering* **44**(1):636–641.

de Beer, D., Stoodley, P. & Lewandowski, Z. (1996). 'Liquid flow and mass transport in heterogeneous biofilms'. *Water Research* **30**(11):2761–2765.

de Beer, D., Stoodley, P., Roe, F. & Lewandowski, Z. (1994b). 'Effects of biofilm structures on oxygen distribution and mass transport'. *Biotechnology and Bioengineering* **43**(1):1131–1138.

de Lipthay, J., Enzinger, C., Johnsen, K., Aamand, J. & Sorensen, S. (2004). 'Impact of DNA extraction method on bacterial community composition measured by denaturing gradient gel electrophoresis'. *Soil biology and biochemistry* **36**:1607–1614.

Deng, J. (1992). *Hazardous materials toxicology, clinical principles of environmental health*, pp. 711–717. Williams anf Wilkins.

Dobritsa, A., Reddy, M. & Samadpour, M. (2010). 'Reclassification of Herbaspirillum putei as a later heterotypic synonym of Herbaspirillum huttiense, with the description

of H. huttiense subsp. huttiense subsp. nov. and H. huttiense subsp. putei subsp. nov., comb. nov., and description of Herbaspirillum aquaticum sp. nov.'. *International Journal of systematic and evolutionary microbiology* **60**:1418–1426.

Dopson, M., et al. (2007). 'Mineral and iron oxidation at low temperatures by pure and mixed cultures of acidophilic microorganisms'. *Biotechnology and Bioengineering* **97**(5):1205–1215.

Dopson, M. & Johnson, D. B. (2012). 'Biodiversity, metabolism and applications of acidophilic sulfur-metabolizing microorganisms'. *Environmental microbiology* **14**(10):2620–2631.

Dorigo, U., Volatier, L. & Humbert, J. (2005). 'Molecular approaches to the assessment of biodiversity in aquatic microbial communities'. *Water Research* **39**:2207–2218.

Doshi, M., Daiya, P. & Gill, W. (1978). 'Three dimensional laminar dispersion in open and closed rectangular conduits'. *Chemical Engineering Science* **33**:795–804.

Downing, B. & Mills, C. (2012). 'Natural acid rock drainage and its impact on background metal concentrations'.

Dubinina, G., Grabovich, M., Rainey, N. L. F. & Gavrish, E. (2011). 'Spirochaeta perfilievii sp. nov., an oxygen-tolerant, sulfide-oxidizing, sulfur- and thiosulfate-reducing spirochaete isolated from a saline spring'. *International Journal of systematic and evolutionary microbiology* **61**:110–117.

Dvorak, D., Hedin, R., Edenborn, H. & McIntire, P. (1992). 'Treatment of metal-contaminated water using bacterial sulphate reduction: results from pilot-scale reactors'. *Biotechnology and Bioengineering* **40**(1):609.

DWAF (1996). 'South African Water Quality Guidelines'. Tech. Rep. For Domestic Use, Department of Water Affairs and Forestry.

Dworkin, M., Falkow, S., Rosenberg, E., Schleifer, K. & Stackebrandt, E. (2006a). *The Prokaryotes*, vol. 2. Springer.

Dworkin, M., Falkow, S., Rosenberg, E., Schleifer, K. & Stackebrandt, E. (2006b). *The Prokaryotes*, vol. 6. Springer, third edn.

Dworkin, M., Falkow, S., Rosenberg, E., Schleifer, K. & Stackebrandt, E. (2006c). *The Prokaryotes*, vol. 4. Springer.

Dworkin, M., Falkow, S., Rosenberg, E., Schleifer, K. & Stackebrandt, E. (2006d). *The Prokaryotes*, vol. 5. Springer, third edn.

Dworkin, M., Falkow, S., Rosenberg, E., Schleifer, K. & Stackebrandt, E. (2006e). *The Prokaryotes*, vol. 7. Springer, third edn.

Elliot, P., Ragusa, S. & Catcheside, D. (1998). 'Growth of sulphate reducing bacteria under acidic conditions in an upflow anaerobic bioreactor as a treatment system for acid mine drainage'. *Water resources* **32**(12):3724–3730.

EPA (2003). 'Toxicological review of hydrogen sulfide'. Tech. rep., U.S. Environmental Protection Agency.

Ferris, M., Muyzer, G. & Ward, D. (1996). 'Denaturing gradient gel electrophoresis profiles of 16S rRNA-defined populations inhabiting a hot spring microbial mat community'. *Applied and Environmental Microbiology* **62**(2):340–346.

Flemming, H., Wingender, J., Mayer, C., Korstgens, V. & Borchard, W. (2000). 'Cohesiveness in biofilm matrix polymers'. In Press, C. U. (ed.), *Community structure and cooperation in biofilms*, vol. 59, pp. 87–105.

Flemming, H.-C., Neu, T. & Wozniak, D. (2007). 'The EPS matrix: The "House of biofilm cells"'. *Journal of Bacteriology* **189**(22):7945–7947.

Flemming, H.-C. & Wingender, J. (2003). *Biofilms in Wastewater Treatment - An Interdisciplinary Approach*, chap. 8, pp. 178–210. IWA Publishing.

Flemming, H.-C. & Wingender, J. (2010). 'The biofilm matrix'. *Nature reviews microbiology* **8**:623–633.

Fogler, H. S. (2006). *Elements of chemical reaction engineering*. Pearson, 4 edn.

Fortin, D., Davis, B. & Beveridge, T. (1996). 'Role of Thiobacillus and sulphate-reducing bacteria in iron biocycling in oxic and acidic mine tailings'. *FEMS Microbiology Ecology* **21**:11–14.

Fratesi, S., Lynch, F., Kirkland, B. & Brown, L. (2004). 'Effects of SEM preparation techniques on the appearance of bacteria and biofilms in the carter sandstone'. *Journal of Sedimentary Research* **74**(6):858–867.

Friedrich, C., Rother, D., Bardischewsky, F., Quentmeier, A. & Fischer, J. (2001). 'Oxidation of reduced inorganic sulfur compounds by bacteria: Emergence of a common mechanism?'. *Applied and Environmental Microbiology* **67**(7):2873–2882.

Fu, F. & Wang, Q. (2011). 'Removal of heavy metal ions from wastewaters: A review'. *Journal of Environmental Management* **92**(1):407–418.

Fu, H. & Rockwell, D. (2005). 'Shallow flow past a cylinder: transition phenomena at low Reynolds number'. *Journal of fluid mechanics* **540**:75–97.

Fu, Y., Zhang, T. & Bishop, P. (1994). 'Determination of effective oxygen diffusivity in biofilm grown in a completely mixed biodrum reactor'. *Water Science and Technology* **29**:455–462.

Ganesan, A., et al. (2008). 'Cloacibacillus evryensis gen. nov., sp. nov., a novel asaccharolytic, mesophilic amino-acid-degrading bacterium within the phylum 'Synergistetes', isolated from an anaerobic sludge digester'. *International Journal of systematic and evolutionary microbiology* **58**(9):2003–2012.

Gazea, B., Adam, K. & Kontopoulos, A. (1996). 'A review of passive systems for the treatment of acid mine drainage'. *Minerals Engineering* **9**(1):23 – 42.

Gibert, O., de Pablo, J., Cortina, J. & Ayora, C. (2004). 'Chemical characterisation of natural organic substrates for biological mitigation of acid mine drainage'. *Water Research* **38**(1):4186–4196.

Giggenbach, W. (1972). 'Optical spectra and equilibrium distribution of polysulfide ions in aqueous solutions at 20C'. *Journal of Inorganic Chemistry* **11**(1):1201–1207.

Glover, C. & Hogstrand, C. (2003). 'Effects of dissolved metals and other hydrominerals on in vivo intestinal zinc uptake in freshwater rainbow trout'. *Aquatic toxicology* **62**(1):281–293.

Gonzalez-Sanchez, A. & Revah, S. (2007). 'The effect of chemical oxidation on the biological sulfide oxidation by an alkaliphilic sulfoxidizing bacterial consortium'. *Enzyme and Microbial Technology* **40**(1):292–298.

Gonzalias, A., Kuschk, P., Wiessner, A., Jank, M., Kastner, M. & Koser, H. (2007). 'Treatment of an artificial sulphide containing wastewater in subsurface horizontal flow laboratory-scale constructed wetlands'. *Ecological Engineering* **31**(1):259–268.

Greben, H., Baloyi, J., Sigama, J. & Venter, S. (2009). 'Bioremediation of sulphate rich mine effluents using grass cuttings and rumen fluid microorganisms'. *Journal of Geochemical Exploration* **100**:163–168.

Gunther, P. & Mey, W. (2006). 'SELECTION OF MINE WATER TREATMENT TECHNOLOGIES FOR THE EMALAHLENI (WITBANK) WATER RECLAMATION PROJECT'. Tech. rep., WISA.

Haghsheno, R., Mohebbi, A., Hashemipour, H. & Sarrafi, A. (2009). 'Study of kinetic and fixed bed operation of removal of sulfate anions from an industrial wastewater by an anion exchange resin'. *Journal of Hazardous Materials* **166**(1):961–966.

Hall, G., Swash, P. & Kotilainen, S. (2005). 'The importance of biological oxidation of iron in the aerobic cells of the Wheal Jane pilot passive treatment system'. *Science of the total environment* **338**:67–72.

Hallberg, K. B. & Johnson, D. B. (2005a). 'Biological manganese removal from acid mine drainage in constructed wetlands and prototype bioreactors'. *Science of the total environment* **338**:115–124.

Hallberg, K. B. & Johnson, D. B. (2005b). 'Microbiology of a wetland ecosystem constructed to remediate mine drainage from a heavy metal mine'. *Science of the total environment* **338**(1):53–66.

Harms, G., Zengler, K., Rabus, R., Aeckersberg, F., Minz, D., Mora, R. & Widdel, F. (1999). 'Anaerobic oxidation of o-Xylene, m-Xylene and homologous alkylbenzenes by new types of sulfate-reducing bacteria'. *Applied and Environmental Microbiology* **65**(3):999–1004.

Heath, R., Coleman, T. & Engelbrecht, J. (2010). 'Water quality overview and literature review of the ecology of the Olifants River'. Wrc report no. tt452/10, Water Research Commission.

Hedin, R., Narin, R. & Kleinmann, R. (1994). 'Passive treatment of coal mine drainage'. Circular 9389, US Bureau of Mines.

Hell, R., Dahl, C., Knaff, D. & Leustek, T. (2008). *Sulfur metabolism in phototrophic organisms*. Springer.

Helsel, L., et al. (2007). 'Identification of "Haematobactor", a New Genus of Aerobic gram-negative rods isolated from clinical specimens, and reclassifcation of Rhodobacter massiliensis as "Haematobacter massiliensis comb. nov"'. *Journal of clinical microbiology* **45**(4):1238–1243.

Henshaw, P., Bewtra, J. & Biswas, N. (1998). 'Hydrogen sulphide conversion to elemental sulphur in a suspended-growth continuous stirred tank reactor using Chlorobium limicola'. *Water Research* **32**(6):1769–1778.

Henshaw, P. & Zhu, W. (2001). 'Biological conversion of hydrogen sulphide to elemental sulphur in a fixed-film continuous flow photo-reactor'. *Water Research* **35**(15):3605–3610.

Hentzer, M., Balzer, G., Teitzel, G., Heydorn, A. & Molin, S. (2001). 'Alginate overproduction affects Pseudomonas Aeruginosa biofilm structure and function'. *Journal of Bacteriology* **183**:5395–5401.

Hilton, B. & Oleszkiewicz, J. (1988). 'Sulfide-induced inhibition of anaerobic digestion'. *Journal of Environmental engineering* **114**(6):1377–1391.

Hogg, S. (2005). *Essential Micorbiology*. John Wiley & Sons Limited.

Hogsden, K. & Harding, J. (2012). 'Anthropogenic and natural sources of acidity and metals and their influence on the structure of stream food webs'. *Environmental Pollution* **1**(162):466–474.

Holmer, M. & Storkholm, P. (2001). 'Sulphate reduction and sulphur cycling in lake sediments: a review'. *Freshwater Biology* **46**(1):431–451.

Horn, H. & Hempel, D. (1995). 'Mass Transfer Coefficients for an autotrophic and a heterotrophic biofilm system'. *Water Science and Technology* **32**(8):199–204.

Hulshoff, L., Lens, P., Stams, A. & Lettinga, G. (1998). 'Anaerobic treatment of sulphate-rich wastewaters'. *Biodegradation* **9**:213–224.

Hurse, T. & Keller, J. (2004a). 'Performance of a substratum-irradiated photosynthetic biofilm reactor for the removal of sulfide from wastewater'. *Biotechnology and Bioengineering* **87**(1):14–22.

Hurse, T. & Keller, J. (2004b). 'Reconsidering the use of Photosynthetic bacteria for removal of sulfide from wastewater'. *Biotechnology and Bioengineering* **85**(1):47–55.

Hutton, B., Kahan, I., Naidu, T. & Gunther, P. (2009). 'Operating and maintenance experience at the eMalahleni water reclamation plant'. In *IMWA 2009 - Conference proceedings*. International Mine Water Association.

Imhoff, J. (2004). *Anoxygenic photosynthetic bacteria*, vol. 2. Kluwer academic publishers.

Imhoff, J. (2006). 'The Chromatiaceae'. *Prokaryotes* **6**(1):846–873.

International Energy Agency (2009). 'World Energy Outlook, 2008'. Blue map scenario, International Energy Agency.

Janssen, A., Ma, S., Lens, P. & Lettinga, G. (1997). 'Performance of a sulphide oxidizing expanded bed reactor supplied with dissolved oxygen'. *Biotechnology and Bioengineering* **53**(1):32–40.

Janssen, A., Sleyster, R., van der Kaa, C. & Jochemsen, A. (1995). 'Biological sulphide oxidation in a fed-batch reactor'. *Biotechnology and Bioengineering* **47**:327–333.

Janssen, A. J., Lettinga, G. & de Keizer, A. (1999). 'Removal of hydrogen sulphide from wastewater and waste gases by biological conversion to elemental sulphur. Colloidal and interfacial aspects ofbiologically produced sulphur particles'. *Colloids and Surfaces A: Physiochemical and Engineering Aspects* **151**(1):389–397.

Janssen, A. J., Meijer, S., Bontsema, J. & Lettinga, G. (1998). 'Application of the redox potential for controlling a sulfide oxidizing bioreactor'. *Biotechnology and Bioengineering* **60**(2):147–155.

Jefferson, K. (2004). 'What drives bacteria to produce a biofilm?'. *FEMS Microbiology letters* **236**:163–173.

Jeffries, T. (1994). *Biodegradation of lignin and hemicelluloses*, chap. 8, pp. 233–277. Kluwer academic publishers.

Johnson, D. B. & Hallberg, K. B. (2003). 'The microbiology of acidic mine waters'. *Research in Microbiology* **154**(7):466 – 473.

Johnson, D. B. & Hallberg, K. B. (2005a). 'Acid mine drainage remediation options: a review.'. *The Science of the total environment* **338**(1-2):3–14.

Johnson, D. B. & Hallberg, K. B. (2005b). 'Biogeochemistry of the compost bioreactor components of a composite acid mine drainage passive remediation system'. *Science of the total environment* **338**:81–93.

Jong, T. & Parry, D. (2003). 'Removal of sulfate and heavy metals by sulfate reducing bacteria in short-term bench scale upflow anaerobic packed bed reactor runs'. *Water Research* **37**:3379–3389.

Joseph, D. & Hu, H. (1991). 'Interfacial tension between miscible liquids'. Tech. rep., University of Minnesota.

Kaksonen, A., Franzmann, P. & Puhakka, J. (2004a). 'Effects of hydraulic rentention time and sulfide toxicity on ethanol and acetate oxidation in sulfate-reducing metal-precipitating fluidized-bed reactor'. *Biotechnology and Bioengineering* **86**(3):332–343.

Kaksonen, A., Plumb, J., Franzmann, P. & Puhakka, J. (2004b). 'Simple organic electron donors support diverse sulfate-reducing communities in fluidized-bed reactors treating acidic metal- and sulfate-containing wastewater'. *FEMS Microbiology Ecology* **47**(1):279–289.

Kamyshny, Jr., A., Ekeltchik, I., Gun, J. & Lev, O. (2006). 'Method for the determination of inorganic polysulfide distribution in aquatic systems'. *Analytical Chemistry* **78**(1):2631–2639.

Kamyshny, Jr., A., Goifman, A., Gun, J., Rizkov, D. & Lev, O. (2004). 'Equilibrium distribution of polysulfide ions in aqueous solutions at 25C: A new approach for the study of polysulfides' equilibria'. *Environmental Science and Technology* **38**(1):6633–6644.

Kamyshny, Jr., A., Goifman, A., Rizkov, D. & Lev, O. (2003). 'Formation of Carbonyl Sulfide by the reaction of Carbon Monoxide and inorganic polysulfides'. *Environmental Science and Technology* **37**(1):1865–1872.

Kamyshny, Jr., A., Gun, J., Rizkov, D., Voitsekovski, T. & Lev, O. (2007). 'Equilibrium distribution of polysulfide ions in aqueous solutions at different temperatures by rapid single phase derivatization'. *Environmental Science and Technology* **41**(1):2395–2400.

Keinanen, M., Tigerstedt, C., Peuranen, S. & Vuorinen, P. (2004). 'The susceptibility of early developmental phases of an acid-tolerant and acid-sensitive fish species to acidity and aluminium'. *Ecotoxicology and environmental safety* **58**(1):160–172.

Kelsall, G. & Thompson, I. (1993). 'Redox chemistry of H2S oxidation in the British Gas Stretford Process Part I: Thermodynamics of sulphur-water systems at 298K'. *Applied Electrochemistry* **23**(1):279–286.

Kim, B., Kim, E. & Chang, H. (1991). 'Application of light emitting diodes as a light source to a photosynthetic culture of Chlorobium thiosulfatophilum'. *Biotechnology techniques* **5**(5):343–348.

Kim, D. (2011). 'A review of desalting process techniques and economic analysis of the recovery of salts from retentates'. *Desalination* **270**(1):1–8.

Kleinjan, W. & de Keizer, A. (2003). 'Biologically produced sulfur'. *Topics in current chemistry* **230**(1):167–188.

Kleinjan, W., de Keizer, A. & Janssen, A. (2005a). 'Kinetics of the chemical oxidation of polysulphide anions in aqueous solution'. *Water Research* **39**(1):4093–4100.

Kleinjan, W., de Keizer, A. & Janssen, A. J. (2005b). 'Kinetics of the reaction between dissolved sodium sulfide and biologically produced sulfur'. *Industrial engineering and chemical research* **44**(1):309–317.

Kobayashi, H., Stenstrom, M. & Mah, R. (1983). 'Use of photosynthetic bacteria for H2S removal from anaerobic'. *Water Research* **17**(8):579–587.

Kobayashi, T., Li, Y., Kubota, K., Harada, H., Maeda, T. & Yu, H. (2012). 'Characterization of sulfide-oxidizing microbial mats developed inside a full-scale anaerobic digester employing biological desulfurization'. *Applied microbial biotechnology* **93**:847–857.

Koschorreck, M. (2008). 'Microbial sulphate reduction at a low pH'. *FEMS Microbiology Ecology* **64**:329–342.

Krishnakumar, B., Majumdar, S., Manilal, V. & Haridas, A. (2005). 'Treatment of sulphide containing wastewater with sulphur recovery in a novel reverse fluidized loop reactor (RFLR)'. *Water Research* **39**:639–647.

Kuhn, A., Kelsall, G. & Chana, M. (1983). 'A review of the air oxidation of aqueous sulphide solutions'. *Journal of Chemical Technology and Biotechnology* **33A**(1):406–414.

Kupka, D., Liljeqvist, M., Nurmi, P., Puhakka, J., Tuovinen, O. & Dopson, M. (2009). 'Oxidation of elemental sulfur, tetrathionate and ferrous iron by the psychrotolerant Acidithiobacillus strain SS3'. *Research in Microbiology* **160**:767–774.

Lappin-Scott, H. & Costerton, J. (1995). *Microbial Biofilms*. Cambridge University Press.

Lawrence, J., Korber, D., Hoyle, B. & Costerton, J. (1991). 'Optical sectioning of microbial biofilms'. *Journal of Bacteriology* **173**:6558–6567.

Lazarova, V. & Manem, J. (1995). 'Review Paper: Biofilm characterization and activity analysis in water and wastewater treatment'. *Water Research* **29**(10):2227–2245.

Ledin, M. & Pedersen, K. (1996). 'The environmental impact of mine wastes – Roles of microorganisms and their significance in treatment of mine wastes'. *Earth-Science Reviews* **41**(1-2):67 – 108.

Lee, S., Ha, J. & Cheng, K.-J. (2000). 'Relative contributions of bacteria, protozoa and fungi to in vitro degradation of Orchard grass cell walls and their interactions'. *Applied and Environmental Microbiology* **66**(9):3807–3813.

Lens, P. & Kuenen, J. (2001). 'The biological sulphur cycle: novel opportunities for environmental biotechnology'. *Water Science and Technology* **44**(8):57–66.

Lens, P., Truper, H. & Steudel, R. (2000). *Environmental technologies to treat sulfur pollution*. IWA Publishing, 1st edn.

Lens, P., Vallero, M., Esposito, G. & Zandvoort, M. (2003). 'Perspectives of sulfate reducing bioreactors in environmental biotechnology'. *Reviews in environmental science and biotechnology* **1**(4):311–325.

Leroy, P., Lassin, A., Azaroual, M. & Andre, L. (2010). 'Predicting the surface tension of aqueous 1:1 electrolyte solutions at high salinity'. *Geochemica et Cosmochimica Acta* **74**:5427–5442.

Liamleam, W. & Annachhatre, A. (2007). 'Electron donors for biological sulfate reduction'. *Biotechnology advances* **25**:452–463.

Lindsay, M., Blowes, D., Condon, P. & Ptacek, C. (2011). 'Organic carrbon amendments for passive in situ treatment of mine drainage: Field experiments'. *Applied geochemistry* **26**:1169–1183.

Lorax-International (2003). 'Treatment of Sulphate Mine Effluents'. Tech. rep., International Network for Acid Prevention.

Lynd, L., Weimer, P., van Zyl, W. & Isak, S. (2002). 'Microbial cellulose utilization: Fundamentals and biotechnology'. *Microbiology and molecular biology reviews* **66**(3):506–577.

MacCausland, A. & McTammany, M. (2007). 'The impact of episodic coal mine drainage pollution on benthic macroinvertebrates in streams in the Anthracite region of Pennsylvania'. *Environmental Pollution* **149**(1).

Mack, C.-L., Raja, S., Pulles, W., Muhlbauer, R. & Heath, R. (2009). 'Application of the linear flow channel reactor (LFCR) for the removal of sulphide from semi-treated acid mine drainge (AMD)'. In *International Mine Water Conference IMWA Proceedings*.

Mahmood, Q., Zheng, P., Hayat, Y., Islam, E., Wu, D. & Ren-cun, J. (2008). 'Effect of pH on anoxic sulfide oxidizing reactor performance'. *Bioresource Technology* **99**:3291–3296.

Mamashela, M. (2002). 'Biological sulphide oxidation to elemental sulphur using mixed culture'. Master's thesis, University of Cape Town.

Marsden, D. (1986). 'The current limited impact of Witwatersrand gold mine residues on water pollution in the Vaal river system'. *Journal of South African Institute of Mining and Metallurgy* **86**:481–504.

McKinsey & Company (2009). 'Charting our water future'. Tech. rep.

Merck-Millipore (April 2011). 'COD solutions A+B - Instructions for use'. Tech. rep., Merck Millipore.

Millero, F. (1986). 'The thermodynamics and kinetics of the hydrogen sulfide system in natural waters'. *Marine chemistry* **18**(1):121–147.

Millero, F., Hubinger, S., Fernandez, M. & Garnett, S. (1987). 'Oxidation of H2S in seawater as a function of temperature, pH and ionic strength'. *Environmental Science and Technology* **21**(1):439–443.

Miura, Y. & Kawaoi, A. (2000). 'Determination of thiosulfate, thiocyanate and polythionates in a mixture by ion-pair chromatography with ultraviolet absorbance detection'. *Journal of Chromatography A* **884**(1):81–87.

Molwantwa, J. (2008). *Floating sulphur biofilms: Structure, function and biotechnology.* Ph.D. thesis, Rhodes University.

Molwantwa, J., Coetser, S., Heath, R. & Pulles, W. (2010). 'Monitoring, evaluation and verification of long-term performance of the passive water treatment plant at Vryheid Coronation Colliery'. Tech. rep., Water Research Commission.

Molwantwa, J., Coetser, S., Heath, R. & Rose, P. (2007). 'Development of the floating sulphur biofilm reactor for sulphide oxidation in biological water treatment systems'. *Water SA* **30**(5):655–657.

Moosa, S., Nemati, M. & Harrison, S. (2002). 'A kinetic study of anaerobic reduction of sulphate, Part I: Effect of sulphate concentration'. *Chemical Engineering Science* **57**:2773–2780.

Morales, C., Strathmann, M. & Flemming, H.-C. (2007). 'Influence of biofilms on the movement of colloids in porous media. Implications for colloid facilitated transport in subsurface environments'. *Water Research* **41**:2059–2068.

Morales, T., Dopson, M., Athar, R. & Herbert, R. (2005). 'Analysis of bacterial diversity in acidic pond water and compost after treatment of artificial acid mine drainage for metal removal'. *Biotechnology and Bioengineering* **90**(5):543–551.

Morton, K. (1993). 'A phased approach to mine dewatering'. *Mine Water and Environment* **12**:27–34.

Motsi, T., Rowson, N. & Simmons, M. (2009). 'Adsorption of heavy metals from acid mine drainage by natural zeolite'. *International journal of mineral processing* **92**(1):42–48.

Muhlbauer, R., Raja, S., de Villiers, D., Pulles, W., Clark, S. & Heath, R. (2010). 'Implementation of a demonstration scale integrated managed passive (IMPI) process'. In Wolkersdorfer & Freund (eds.), *Mine Water and Innovative Thinking*. International Mine Water Association.

Muller, M. (2009). 'Water security in South Africa'. Tech. rep., Development Bank of Southern Africa.

Muyzer, G., de Waal, E. & Uitterlinden, A. (1993). 'Profiling of complex micorbial populations by denaturing gel electrophoresis analysis of polymerase chain reaction-amplified genes coding for 16S rRNA'. *Applied and Environmental Microbiology* **59**(3):695–700.

Muyzer, G. & Stams, A. (2008). 'The ecology and biotechnology of sulphate-reducing bacteria'. *Nature reviews microbiology* **6**(6):441–454.

Nagpal, S., Chuichulcherm, S., Livingston, A. & Peeva, L. (2000). 'Ethanol utilization by sulfate-reducing bacteria: An experimental and modeling study'. *Biotechnology and Bioengineering* **70**(5):533–543.

Naicker, K., Cukrowska, E. & McCarthy, T. (2003). 'Acid mine drainage arising from gold mining activity in Johannesburg, South Africa and environs'. *Environmental Pollution* **122**(1):29–40.

Neba, A., Whittington-Jones, K. & Rose, P. (2007). 'The Rhodes BioSURE Process - Part 4: Process scale-up in the treatment of mine drainage wastewaters and the disposal of sewage sludge'. Tech. rep., Water Research Commission.

Neculita, C. & Zagury, G. (2008). 'Biological treatment of highly contaminated acid mine drainage in batch reactors: Long-term treatment and reactive mixture characterization.'. *Journal of hazardous materials* **157**(2-3):358–66.

Neculita, C.-M., Zagury, G. J. & Bussière, B. (2007). 'Passive biological treatment of acid mine drainage: challenges of the 21'. *Challenges* pp. 1–22.

Nevin, K., Holmes, D., Woodard, T., Covalla, S. & Lovley, D. (2007). 'Reclassification of Trichlorobacter thiogenes as Geobacter thiogenes comb. nov.'. *International Journal of systematic and evolutionary microbiology* **57**:463–466.

Nicola, D. & Stapleton, M. (2002). 'Impact of acid mine drainage on benthic communities in streams: the relative roles of substratum vs. aqueous effects'. *Environmental Pollution* **119**(1):303–315.

NIOSH (2005). 'Hydrogen sulfide. NIOSH pocket guide to chemical hazards, Washington DC.'. Tech. rep., National Institute for Occupational Safety and Health.

Nivens, D., Ohman, D., Williams, J. & Franklin, M. (2001). 'Role of alginate and its O acetylation in formation of Pseudomonas Aeruginosa microcolonies and biofilms'. *Journal of Bacteriology* **183**:1047–1057.

Norlund, K., et al. (2009). 'Microbial architecture of environmental sulfur processes: A novel syntrophic sulfur-metabolizing consortia'. *Environmental Science and Technology* **43**:8781–8786.

NRC (2010). 'Acute exposure guideline levels for selected airborne chemicals'. Tech. rep., National Research Council, Washington DC.

Omil, F., Lens, P., Hulshoff, P. & Lettinga, G. (1996). 'Effect of upward velocity and sulphide concentration on volatile fatty acid degradation in a sulphidogenic granular sludge reactor'. *Process biochemistry* **31**(7):699–710.

Omil, F., Lens, P., Visser, A., Hulshoff, P. & Lettinga, G. (1998). 'Long term competition between sulfate reducing and methanogenic bacteria in UASB reactors treating volatile fatty acids'. *Biotechnology and Bioengineering* **57**:676–685.

OSHA (2006). 'Limits of air contaminants. Occupational safety and health standards. Washington DC.'. Tech. rep., Occupational Safety and Health Administration.

O'Toole, G., Kaplan, H. & Kotler, R. (2000). 'Biofilm formation as microbial development'. *Annual Review of Microbiology* **54**:49–79.

Oyekola, O. O. (2008). *An investigation into the relationship between process kinetics and microbial community dynamics in a lactate-fed sulphidogenic CSTR as a function of residence time and sulphate loading.* Ph.D. thesis, University of Cape Town.

Paques (2013). 'SULFATEQ'. Tech. rep., http://en.paques.nl/pageid=64/SULFATEQ™.html.

Pareek, S., Kim, S., Matsui, S. & Shimizu, Y. (1998). 'Hydrolysis of (ligno)cellulosic materials under sulfidogenic and methanogenic conditions'. *Water Science and Technology* **38**(2):193–200.

Park, S., Ko, Y. & Kim, C. (2001). 'Toxic effects of catechol and 4-chlorobenzoate stresses on bacterial cells'. *The journal of microbiology* **39**(3):206–212.

Pearson, T. G. & Robinson, P. L. (1930). 'CLXXXIX-The Polysulfides of Alkali metals(I) - Sodium'. *Journal of the Chemical Society* (1):1473–1497.

Pearson, T. G. & Robinson, P. L. (1931). 'CLXXIII-The Polysulfides of Alkali metals(III) - Potassium'. *Journal of the Chemical Society* (1):1304–1314.

Perez-Gonzalez, A., Urtiaga, A., Ibanez, R. & Ortiz, I. (2012). 'State of the art and review on the treatment technologies of water reverse osmosis concentrates'. *Water Research* **46**(1):267–283.

Perry, R. & Green, D. (2008). *Perry's Chemical Engineers' Handbook*. McGraw-Hill Handbooks, 8th edn.

Picioreanu, C., van Loosdrecht, M. & Heijnen, J. (2000a). 'Effect of diffusive and convective substrate transport on biofilm structure formation: A two-dimensional modeling study'. *Biotechnology and Bioengineering* **69**(5):504–515.

Picioreanu, C., van Loosdrecht, M. & Heijnen, J. (2000b). 'A Theoretical study on the effect of surface roughness on mass transport and transformation in biofilms'. *Biotechnology and Bioengineering* **68**(4):355–369.

Pinetown, K., Ward, C. & van der Westhuizen, W. (2007). 'Quantitative evaluation of minerals in coal deposits in the Witbank and Highveld Coalfields, and the potential impact on acid mine drainage'. *International journal of coal geology* **70**:166–183.

Poinapen, J., Ekama, G. & Wentzel, M. (2009). 'Biological sulphate reduction with primary sewage sludge in an upflow anaerobic sludge (UASB) reactor - Part 3: Performance at 20C and 35C'. *Water SA* **35**(5):543–552.

Pringault, O., Epping, E., Guyoneaud, R., Khalili, A. & Kuhl, M. (1999). 'Dynamics of anoxygenic photosynthesis in an experimental green sulphur bacteria biofilm'. *Environmental microbiology* **1**(4):295–305.

Proestos, C., Sereli, D. & Komaitis, M. (2006). 'Determination of phenolic compounds in aromatic plants by RP-HPLC and GC-MS'. *Food Chemistry* **95**:44–52.

Purevdorj-Gage & Stoodley (2004). *Microbial Biofilms*, chap. 9, pp. 160–173. ASM Press.

Purevdorj-Gage, B. (2004). *Pseudomonas Areuginosa biofilm structure, behaviour and hydrodynamics*. Ph.D. thesis, Montana State University.

Rakotomalala, N., Salin, D. & Watzky, P. (1997). 'Miscible displacement between two parallel plates: BGK lattice gas simulations'. *Journal of fluid mechanics* **338**:277–297.

Ramontja, T., et al. (2010). 'Mine water management in the Witwatersrand gold fields with special emphasis on acid mine drainage'. South African government, Inter-ministerial committee on acid mine drainage.

Rasmussen, K. & Lewandowski, Z. (1998a). 'The accuracy of oxygen flux measurements using microelectrodes'. *Water Research* **32**(12):3747–3755.

Rasmussen, K. & Lewandowski, Z. (1998b). 'Microelectrode Measurements of Local Mass Transport Rates in Heterogeneous Biofilms'. *Biotechnology and Bioengineering* **59**(3):302–309.

Rattanapan, C., Boonsawang, P. & Kantachote, D. (2009). 'Removal of H2S in down-flow GAC biofiltration using sulfide oxidizing bacteria from concentrated latex wastewater'. *Bioresource Technology* **100**(1):125–130.

Rauch, W., Vanhooren, H. & Vanrolleghem, P. (1999). 'A Simplified mixed-culture biofilm model'. *Water Research* **33**(9):2148–2162.

Rehimi, F., Aloui, F., Nasrallah, S., Doubliez, L. & Legrand, J. (2008). 'Experimental investigation of a confined flow downstream of a circular cylinder centred between two parallel plates'. *Fluids and Structures* **24**:855–882.

Rethmeier, J., Rabenstein, A., Langer, M. & Fischer, U. (1997). 'Detection of traces of oxidized and reduced sulfur compounds in small samples by combination of different high-performance liquid chromatography methods'. *Journal of Chromatography A* **760**(1):295–302.

Riesenfeld, C., Schloss, P. D. & Handelsman, J. (2004). 'Metagenomics: Genomic analysis of microbial communities'. *Annual review of Genetics* **38**:525–552.

Rizkov, D., Lev, O., Gun, J., Anisimov, B. & Kuselman, I. (2004). 'Development of in-house reference materials for the determination of inorganic polysulfides in water'. *Accredited Quality Assurance* (9):399–403.

Roman, H. (2004). *The degradation of lignocellulose in a biologically-generated sulphidic environment*. Ph.D. thesis, Rhodes University.

Roman, H., Madikane, M., Pletschke, B. & Rose, P. (2008). 'The degradation of lignocellulose in a chemically and biologically generated sulphidic environment'. *Bioresource Technology* **99**:2333–2339.

Rose, P. (2013). 'Long-term sustainability in the management of acid mine drainage wastewaters. Development of the Rhodes BioSURE Process: A review'. *Water SA* **39**(5):583–592.

Rouault, M. & Richard, Y. (2003). 'Intensity and spatial extension of drought in South Africa at different time scales'. *Water SA* **29**(4):489–500.

Sambrook, J. & Russell, D. (2001). *Molecular Cloning - A laboratory Manual*, vol. 1-3. Cold Spring Harbour Laboratory Press, 3rd edn.

Sand, W. & Gehrke, T. (2003). 'Microbially influenced corrosion of steel in aqueous environments'. *Reviews in environmental science and biotechnology* **2**:169–176.

Sand, W. & Gehrke, T. (2006). 'Extracellular polymeric substances mediate bioleaching/biocorrosion via interfacial processes involving iron(III) ions and acidophlic bacteria'. *Research in Microbiology* **157**:49–56.

Santegoeds, C., Ferdelman, T., Muyzer, G. & de Beer, D. (1998). 'Structural and functional dynamics of sulfate-reducing populations in bacterial biofilms'. *Applied and Environmental Microbiology* **64**(10):3731–3739.

Schink, B., Philipp, B. & Muller, J. (2000). 'Anaerobic degradation of phenolic compounds'. *Naturwissenschaften* **87**:12–23.

Schnell, S., Bak, F. & Pfennig, N. (1989). 'Anaerobic degradation of aniline and dihydroxybenzene by newly isolated sulfate-reducing bacteria and description of Desulfobacterium anilini'. *Archives of microbiology* **152**:556–563.

Scott, R. (1995). 'Flooding of the Central and East Rand gold mines: An investigation into controls over the inflow rate, water quality and the predicted impacts of flooded mines'. Tech. rep., Water Research Commission.

Shah, H. & Collins, D. (1990). 'Prevotella, a new genus to include Bacteroidetes melaninogenicus and related species formerly classified in the genus Bacteroides'. *International Journal of systematic and evolutionary microbiology* **40**(2):205–208.

Sheoran, A. & Sheoran, V. (2006). 'Heavy metal removal mechanism of acid mine drainage in wetlands: A critical review'. *Minerals Engineering* **19**(2):105 – 116.

Sheoran, A., Sheoran, V. & Choudhary, R. (2010). 'Bioremediation of Acid-Rock Drainage by Sulphate-Reducing Prokaryotes: A Review'. *Minerals Engineering* **23**(1):1073–1100.

Sinicrope, T., Langis, R., Gersberg, R., Busanardo, M. & Zedler, J. (1992). 'Metal removal by wetland mesocosms subjected to different hydroperiods'. *Ecological Engineering* **1**(4):309–322.

Skousen, J. & Ziemkiewicz, P. (2005). 'Performance of 116 Passive Treatment Systems for Acid Mine Drainage'. In *Proceedings in the American Society of Mining and Reclamation*, pp. 1100–1133, Breckenridge, Colorado.

South Africa, W. (2012). 'http://www.info.gov.za/aboutsa/geography.html'.

Spiers, A., Bohannon, J., Gehrig, S. & Rainey, P. (2003). 'Biofilm formation at the air-liquid interface by the Pseudomonas fluorescens SBW25 wrinkly spreader requires an acetylated form of cellulose'. *Molecular microbiology* **50**(1):15–27.

Stefess, G. C. (1993). *Oxidation of sulphide to elemental sulphur by Aerobic Thiobacilli*. Ph.D. thesis, Department of Microbiology and Enzymology, University of Technology Delft.

Steudel, R. (2003a). 'Inorganic polysulfanes'. *Topics in current chemistry* **231**(1):99–125.

Steudel, R. (2003b). 'Inorganic polysulfides and radical anions'. *Topics in current chemistry* **231**(1):127–152.

Steudel, R. & Eckert, B. (2003). 'Solid Sulfur Allotropes'. *Topics in current chemistry* **230**(1):1–79.

Steudel, R., Holdt, G., Gobel, T. & Hazeu, W. (1987). 'Chromatographic separation of higher polythionates SnO6 (n=3...22) and their detection in cultures of thiobacillus ferrooxidans; Molecular composition of bacterial sulfur'. *Angewandte Chemie International Edition* **26**(2):151–153.

Steudel, R., Mausle, H., Rosenbauer, D., Mockel, H. & Freyholdt, T. (1981). 'Separation and determination of sulfur homocycles by High Pressure Liquid Chromatography - Detection of novel sulfur rings'. *Angewandte Chemie International Edition* **20**(4):394–395.

Stoodley, P., Cargo, R., Rupp, C., Wilson, S. & Klapper, I. (2002a). 'Biofilm material properties as erlated to shear-induced deformation and detachment phenomena'. *Journal of industrial microbiology and biotechnology* **29**:361–367.

Stoodley, P., Sauer, K., Davies, D. & Costerton, J. (2002b). 'Biofilms as complex differentiated communities'. *Annual Review of Microbiology* **56**:187–209.

Stoodley, P., Stoodley, L., Boyle, J., Jorgensen, F. & Lappin-Scott, H. (2000). 'Environmental and genetic factors influencing biofilm structure'. In Press, C. U. (ed.), *Community structure and cooperation in biofilms*.

Stumm, W. & Morgan, J. (1996). *Aquatic Chemistry: Chemical equilibria and rates in natural waters*. Wiley-Interscience.

Syed, M., Soreanu, G., Falletta, P. & Beland, M. (2006). 'Removal of hydrogen sulfide from gas streams using biological processes - A review'. *Canadian Biosystems Engineering* **48**(2.1-2.14).

Tanji, K. (1969). 'Solubility of gypsum in aqueous electrolytes as affected by ion association and ionic strengths up to 0.15M and 25C'. *Environmental Science and Technology* **3**(7):656–661.

Taylor, G. (1953). 'Dispersion of soluble matter in solvent flowing slowly through a tube'. *Proceedings of the Royal Society A* **219**(1137):186–203.

Taylor, G. (1954). 'Conditions under which dispersion of a solute in a stream of solvent can be used to measure molecular diffusion'. *Proceedings of the Royal Society A* **225**(1163):473–477.

The International Network for Acid Prevention (2009). 'Global Acid Rock Drainage Guide (GARD Guide)'. Tech. rep.

The Water Resources Group 2030 (2012). 'The Water Resources Group - Background, impact and the way forward'. Briefing report, Water Resources Group - World Economic Forum.

The World Economic Forum Water Initiative (2011). *Water Security - The water-food-energy-climate Nexus*. Island Press.

Tsukamoto, T. & Miller, G. (1999). 'Methanol as a carbon source for microbiological treatment for acid mine drainage'. *Water Research* **33**(6):1365–1370.

Ucisik, A. & Henze, M. (2008). 'Biological hydrolysis and acidification of sludge under anaerobic conditions: The effect of sludge type and origin on the production and composition of volatile fatty acids'. *Water Research* **42**:3729–3738.

Ueki, A., Akasaka, H., Suzuki, D. & Ueki, K. (2006). 'Paludibacter propionicigenes gen. nov., sp. nov., a strictly anaerobic, Gram-negative, propionate-producing bacterium isolated from plant residue in irrigated rice-field soil in Japan'. *International Journal of systematic and evolutionary microbiology* **56**(1):39–44.

USDA (2004). 'Dietary Reference Intakes for Water, Potassium, Sodium, Chloride, and Sulfate'. National agriculture library 7, National Academy of Sciences - Institute of Medicine - Food and Nutrition Board.

van den Bosch, P. (2008). *Biological sulfide oxidation by natron-alkaliphilic bacteria. Application in gas desulfurization*. Ph.D. thesis, Wageningen University.

van den Bosch, P., Sorokin, D., Buisman, C. J. & Janssen, A. (2008). 'The effect of pH on thiosulfate formation in a biotechnological process for the removal of hydrogen sulfide from gas streams'. *Environmental Science and Technology* **42**(1):2637–2642.

van Dyk, J. & Pletschke, B. (2012). 'A review of lignocellulose bioconversion using enzymatic hydrolysis and synergistic cooperation between enzymes-Factors affecting enzymes, conversion and synergy'. *Biotechnology advances* **30**:1458–1480.

van Ende, F. P. & van Gemerden, H. (1993). 'Sulfide oxidation under oxygen limitation by a Thiobacillus thioparus isolated from a marine microbial mat'. *FEMS Microbiology Ecology* **13**(1):69–78.

van Hille, R., Mooruth, N., Raja, S. & Heath, R. (2012). 'Towards passive treatment solutions for the oxidation of sulphide and subsequent sulphur removal from acid mine water'. Tech. rep., Water Research Commission.

Vannini, C., Munz, G., Mori, G., Lubello, C., Verni, F. & Petroni, G. (2008). 'Sulphide oxidation to elemental sulphur in a membrane bioreactor: Performance and characterization of the selected microbial sulphur-oxidizing community'. *Systematic and Applied microbiology* **31**:461–473.

Vavilin, V., Fernandez, B., Palatsi, J. & Flotats, X. (2008). 'Hydrolysis kinetics in anaerobic degradation of particulate organic material: An overview'. *Waste management* **28**:939–951.

Wan, C. & Li, Y. (2012). 'Fungal pretreatment of lignocellulosic biomass'. *Biotechnology advances* **30**:1447–1457.

Wanner, O., Eberl, H., Noguera, D., Picioreanu, C. & van Loosdrecht and, M. (2006). *Mathematical modeling of biofilms*. IWA Publishing.

Wasche, S., Horn, H. & Hempel, D. (2000). 'Mass Transfer Phenomena in biofilm systems'. *Water Science and Technology* **41**(5):357–360.

Wäsche, S., Horn, H. & Hempel, D. C. (2002). 'Influence of growth conditions on biofilm development and mass transfer at the bulk/biofilm interface'. *Water Research* **36**(19):4775–4784.

Waters (2001). *Waters Alliance systems for ion chromatography (IC) analysis - Manual*. Alliance Waters.

Watnick, P. & Kolter, R. (2000). 'Biofilm, city of microbes'. *Journal of Bacteriology* **182**(10):2675–2679.

Watson, S., Akhurst, T., Whiteley, C., Rose, P. & Pletschke, B. (2004). 'Primary sludge floc degradation is accelerated under biosulphidogenic conditions: Enzymological aspects'. *Enzyme and Microbial Technology* **34**:595–602.

Watzlaf, G., Schroeder, K. & Kairies, C. (2000). 'Long-term performance of anoxic limestone drains'. *Mine Water and Environment* **19**(1):98–110.

Waybrant, K., Blowes, D. & Ptacek, C. (1998). 'Selection of reactive mixtures for use in permeable reactive walls for treatment of mine drainage'. *Environmental Science and Technology* **32**(1):1972–1979.

Waybrant, K., Ptacek, C. & Blowes, D. (2002). 'Treatment of mine drainage using permeable reactive barriers: Column experiments'. *Environmental Science and Technology* **36**(1):1349–1356.

Wei, L., Ma, F. & Zhao, G. (2010). 'Composition and dynamics of sulfate-reducing bacteria during the waterflooding process in the oil field application'. *Bioresource Technology* **101**:2643–2650.

Weimer, P., Russell, J. & Muck, R. (2009). 'Lessons from the cow: What the ruminant animal can teach us about consolidated bioprocessing of cellulosic biomass'. *Bioresource Technology* **100**:5323–5331.

Weissenborn, P. & Pugh, R. (1996). 'Surface tension of aqueous solutions of electrolytes: Relationship with ion hydration, oxygen solubility, and bubble coalescence'. *Journal of colloid and interface science* **184**:550–563.

Welty, J., Wicks, C., Wilson, R. & Rorrer, G. (2007). *Fundamentals of momentum, heat, and mass transfer*. John Wiley & Sons Limited, 5th edn.

Wen, C.-Y. & Lin, C.-Y. (2001). 'Two-dimensional vortex shedding of a circular cylinder'. *Physics of fluids* **13**(3):557–560.

Wentzien, S. & Sand, W. (2004). 'Tetrathionate disproportionation by Thiomonas intermdia K12'. *Engineering life sciences* **4**(1):25–30.

Whitehead, P., Hall, G., Neal, C. & Prior, H. (2005). 'Chemical behaviour of the Wheal Jane bioremediation system'. *Science of the total environment* **338**:41–51.

Whitehead, P. & Prior, H. (2005). 'Bioremediation of acid mine drainage: an introduction to the Wheal Jane wetlands project'. *Science of the total environment* **338**:15–21.

Whittington-Jones, K., Corbett, C. & Rose, P. (2002). 'The Rhodes BioSURE Process - Part 2: Enhanced hydrolysis of organic organic substrates - Development of the recycling sludge bed reactor'. Tech. rep., Water Research Commission.

Whittington-Jones, K., Molwantwa, J. & Rose, P. (2006). 'Enhanced hydrolysis of carbohydrates in primary sludge under biosulfidogenic conditions'. *Water Research* **40**:1577–1582.

WHO (1996). 'Hydrogen Sulfide in drinking-water'. Tech. rep., World Health Organisation, Geneva.

WHO (2000). 'Hydrogen sulfide. Air quality guidelines: Part II. Evaluation of human health risks'. Tech. rep., World Health Organisation.

WHO (2003). 'WHO Guidelines for Drinking-water Quality'. Tech. Rep. 2, World Health Organisation.

WHO (2004). 'Sulfate in drinking water'. Background document for the development of WHO guidelines for drinking-water quality WHO/SDE/WSH/03.04/114, World Health Organisation.

Wiessner, A., Rahman, K., Kuschk, P., Kastner, M. & Jechorek, M. (2010). 'Dynamics of sulphur compoundsin horizontal sub-surface flow laboratory-scale constructed wetlands treating artificial sewage'. *Water Research* **44**(1):6175–6185.

Wildeman, T. & Schmiermund, R. (2006). 'Mining influenced waters: Their chemistry and methods of treatment'. In *6th International conference on Acid Rock Drainage*.

Wilmot, P., Cadee, K., Katinic, J. & Kavanagh, B. (1988). 'Kinetics of sulfide oxidation by dissolved oxygen'. *Water Pollution Control Federation* **60**(7):1264–1270.

Wolkersdorfer, C. (2008). *Water management at abandoned flooded underground mines.* Springer.

Wollmann, G. & Voigt, W. (2008). 'Solubility of gypsum in MSO4 solutions (M = Mg, Mn, Co, Ni, Cu, Zn) at 298.15 K and 313.15 K'. *Journal of chemical and engineering data* **53**(6):1375–1380.

Wu, S., Kuschk, P., Wiessner, A., Muller, J., Saad, R. & Dong, R. (2012). 'Sulphur transformations in constructed wetlands for wastewater treatment: A review'. *Ecological Engineering* .

Yamashita, T., Yamamoto-Ilkemoto, R. & Zhu, J. (2011). 'Sulfate-reducing bacteria in a denitrification reactor packed with wood as a carbon source'. *Bioresource Technology* **102**:2235–2241.

Yoon, J., Kang, S., Park, S., Lee, S. & Oh, T. (2007). 'Reclassification of Aquaspirillum itersonii and Aquaspirillum peregrinum as Novispirillum itersonii gen. nov., comb. nov. and Insolitispirillum peregrinum gen. nov., comb. nov.'. *International Journal of systematic and evolutionary microbiology* **57**:2830–2835.

Zagury, G. J., Kulnieks, V. & Neculita, C. (2006). 'Characterization and reactivity assessment of organic substrates for sulphate-reducing bacteria in acid mine drainage treatment'. *Chemosphere* **64**:944–954.

Zagury, G. J., Neculita, C. M. & Bussière, B. (2007). 'Passive treatment of acid mine drainage in bioreactors using sulfate-reducing bacteria: critical review and research needs'. *Journal of Environmental Quality* **36**:1–16.

Zeyaullah, M., Abdelkafe, A., Zabya, W. & Ali, A. (2009). 'Biodegradation of catechols by micro-organisms - A short review'. *African journal of biotechnology* **8**(13):2916–2922.

Zhang, J.-Z. & Millero, F. (1993). 'The products from oxidation of H2S in seawater'. *Geochemica et Cosmochimica Acta* **57**(1):1705–1718.

Zhang, T. & Bishop, P. (1994). 'Density, porosity and pore structure of biofilms'. *Water Research* **28**:2267–2277.

Ziemkiewicz, P., Skousen, J. & Lovett, R. (1994). 'Open limestone channels for treating acid mine drainage: A new look at an old idea'. *Green Lands* **24**(4):36–41.

Ziemkiewicz, P., Skousen, J. & Simmons, J. (2003). 'Long-term Performance of Passive Acid Mine Drainage Treatment Systems'. *Mine Water and Environment* **22**(1):118–129.

Zovatto, L. & Pedrizzetti, G. (2001). 'Flow about a circular cylinder between parallel walls'. *Journal of fluid mechanics* **440**:1–25.